EXPERIMENTAL EVALUATION AND COMPUTER SIMULATION

OF POST TENSIONED PRECAST INFILL WALL SYSTEM

Approved by
Dissertation Committee:

James O. Jirsa, Supervisor

Michael E. Kreger, Supervisor

Ned H. Burns

Michael D. Engelhardt

Stelios Kyriakides

EXPERIMENTAL EVALUATION AND COMPUTER SIMULATION OF POST TENSIONED PRECAST INFILL WALL SYSTEM

by

Wanzhi Li, B.S.E, M.S.E.

Dissertation

Presented to the Faculty of the Graduate School of

The University of Texas at Austin

in Partial Fulfillment

of the Requirements

for the Degree of

Doctor of Philosophy

The University of Texas at Austin

December 1997

To:

Mam, Dad

and Xiaomin

ACKNOWLEDGMENTS

Heartfelt thanks to Dr. James O. Jirsa, dissertation supervisor, for his guidance and assistance, especially, for his support and tolerance of my willingness to develop IDARC-PT for foundation simulation which delayed this dissertation. He has been a dedicated teacher, an earnest scholar, especially, an honest friend and an invaluable source of motivation. It is grateful that I have had the fortune of working under him. The consciousness of creation, the discernment of reality, and the methodology of research that I learned from him are the roots of this dissertation.

Sincere thanks to Dr. Michael E. Kreger for his contributions to the project and for serving on my co-supervisor and dissertation committee. He is a trustworthy gentleman from whom I always get help when I need it.

I would also like to extend my sincere thanks to Dr. Ned H. Burns, Dr. Michael D. Engelhardt, and Dr. Stelios Kyriakides for their advice and assistance and for serving on my dissertation committee.

Faithful thanks to Dr. He Guangqian and Prof. Wei Lian, China Academy of Building Research, for their motivation and support. It's my great fortune of working with them. In the past ten years, they passed on their knowledge to me to take up and provided their shoulders to support me. All I had learned from them, the theories of science, the perception of initiation, the judgment of engineering and the arts of study benefit every step of my career in mechanics and engineering.

I would like to send my special thanks to Dr. Jose M. Roesset for his advice and support with the studies on foundation model development. I would also like to thank Dr. Sashi K. Kunnath, University of Central Florida, and Prof. A. M. Reinhorn, University of New York at Buffalo, for providing the source code of IDARC that made it possible for me to develop IDARC-PT in a limited time.

Special thanks to Mr. Frank Carmichael, Maxim Technologies, Inc., for offering me a position that provided a basic support necessary for my family and my dissertation in the special period.

I would like to thank Loring Wyllie, Jr., Degenkolb Engineers, and Tom Sabol, Englekirk and Sabol Consulting Engineers, for their cooperation and advice with the design and detailing of the structural experiment specimens.

Thanks to all my fellow graduate students at the Ferguson Laboratory for their assistance and support. I also want to thank Robert J. Frosch and Michael Brack for their cooperation and assistance throughout the experiment. Also, the assistance of the entire staff of the Ferguson Laboratory is greatly appreciated.

Ardent thanks to my parents, Guoxiang Li and Zhenling Duan for their love and encouragement. They have taught me the moral of life, the joy of learning, and the pursuit of excellence. Thanks to my wife, Yumin Guan, my daughter, Luanyi Li, and all of my family for their support throughout the years. No part of this dissertation would be possible without love and support from my family. Their encouragement is the source of momentum and spirit of my drive and perseverence which helped my dreams come true.

This study was conducted at the Phil M. Ferguson Structural Engineering Laboratory and was sponsored by the National Science Foundation. I want to extend my gratitude to the sponsor for making this study possible.

Wanzhi Li

October 15, 1997

EXPERIMENTAL EVALUATION AND COMPUTER SIMULATION OF POST TENSIONED PRECAST INFILL WALL SYSTEM

Publication No. _____

Wanzhi Li, Ph.D.
The University of Texas at Austin, 1997

Supervisor: James O. Jirsa, Michael E. Kreger

In seismic zones, many reinforced concrete moment resisting frame structures are non-ductile systems. They do not have sufficient strength and deformation tolerance capacity to tolerate earthquake motions. Several currently used seismic rehabilitation techniques have proven to be constructible and feasible for many structures. However, the cost of such rehabilitation projects remains a major problem for many owners. The costs may involve not only the actual construction, but the expenses associated with relocation of operations and loss of revenue or production during the period of construction.

A post tensioned precast infill wall (PTPW) system was developed that takes advantage of the shear strength of an infill wall to increase the shear capacity and the tensile strength of post-tensioning tendons to increase the flexural capacity of the frame systems. Through the use of precast wall panels to build up infill walls, PTPW rehabilitation permits facilitates construction and may eliminate time and space consuming procedures required for cast-in-place construction. PTPW retrofitting techniques can be used to correct defects and weak links in a nonductile frame system, and to simplify the construction process. Such technique may reduce the inconvenience of construction and may allow the structure to continue functioning during construction.

The project focused on studying the feasibility and methodology of PTPW system implementation and involved three phases of research: experimental investigation, computer analysis program modification and development, and foundation simulation. Based on experimental evaluation and computer simulation, design and detailing guidelines were developed for PTPW retrofitting systems.

The first phase, experimental research, consisted of two stages of structural laboratory tests. In the first stage, structural connection tests were investigated. In the second stage, the overall behavior of a PTPW system and connection details and schemes developed in the first stage were assessed.

The second phase, computer program development, included non-linear structural analyses program modification and computer simulation of structural experiments. Special analytical models of post tensioning and non-linear elastic hysteretic response (loops) were developed. A computer program IDARC-PT was developed for PTPW systems and it was demonstrated through structural experiment simulations.

In the third phase, foundation simulation, foundation performance and effects on PTPW systems were investigated. A mechanical model of the foundation was established to simulate the behavior of foundations subjected to uplifting force under earthquakes. A foundation structural model was also developed for foundation simulation using IDARC-PT. Effects of different soil properties and earthquake behaviors were studied through computer simulations. Foundation/post-tensioning and foundation/infill-wall interactions were also investigated by selecting different post tensioning levels in the simulations.

Design procedures and various schemes for PTPW system implementation were studied through structural retrofitting examples. Guidelines were developed for PTPW system analysis and detail design. Topics were recommended for future studies related to the PTPW retrofitting technique.

TABLE OF CONTENTS

CHAPTER I INTRODUCTION

1.1 Statement of Problem 1

1.2 Objective of Project 3

1.3 Scope of Project 4

1.3.1 Experimental Investigations 4

1.3.1.1 Connection Specimen Test 4

1.3.1.2 Large Scale Model Structure Test 5

1.3.2 Analytical Studies 6

1.3.2.1 Analysis Modeling and Programming 6

1.3.2.2 Experimental Simulation 6

1.3.2.3 Foundation Simulation 6

1.3.3 PTPW System Design Guidelines 6

CHAPTER II DEVELOPMENT OF TECHNIQUES

2.1 Requirements of Earthquake Resistance 7

2.1.1 Earthquake Load 7

2.1.2 Review of Structural Seismic Design 9

2.1.3 Seismic Behavior of Concrete Structure 11

2.2 Features of Existing Frame Structures 13

2.2.1 Ductile Defects 14

2.2.2 System Mechanical Defects 15

2.2.2.1 Lack of Lateral Capacity 15

2.2.2.2 Lack of Redundancy 16

2.2.3 System configuration Defects 18

2.2.3.1 Lack of Regularity 18
2.2.3.2 Lack of Continuity 19
2.2.4 Structural Member Defects 21
2.2.4.1 Insufficient Strength 21
2.2.4.2 Inadequate Detail 22
2.3 Development of Rehabilitation Techniques 23
2.3.1 Encasement or Jacketing of Frame elements 24
2.3.2 Application of Steel Bracing 26
2.3.3 Addition of Shear Walls 28
2.4 Infill Wall Practice 30
2.4.1 Reinforced Masonry Infills 30
2.4.2 Cast-in-Place Reinforced Concrete Walls 31
2.4.3 Precast Reinforced Concrete Panels 33
2.5 Precast Infill Wall with Post Tensioning System 34
2.5.1 Closure Strips 35
2.5.2 Shear Lugs 36
2.5.3 Post Tensioning 37
2.5.4 Structural Analysis of PTPW System 37
2.5.5 Foundation Performance of PTPW System 38

CHAPTER III CONNECTION TESTS

3.1 Introduction 39
3.2 Connection Test Variables 39
3.2.1 Closure Strip Variables 42
3.2.1.1 Strip Dimension 42
3.2.1.2 Shear Key Size, Pattern and Configuration 43

3.2.1.3 Strip Reinforcement 46
3.2.1.4 Panel and Grout Strength 48
3.2.2 Shear Lug Variables 48
3.2.2.1 Width of Strip 49
3.2.2.2 Size of Steel Pipe 49
3.2.2.3 Length of Pipe Embedment 50
3.3 Specimen Construction 50
3.3.1 Specimen Design 50
3.3.2 Panel and Frame Segment Construction 50
3.3.3 Construction of Closure Strip Specimen 52
3.3.3.1 Reinforcement and Anchorage 52
3.3.3.2 Supporting and Formwork 53
3.3.3.3 Grouting and Vibration 54
3.3.4 Construction of Shear Lug Specimen 56
3.4 Material Properties 58
3.4.1 Concrete Aggregate 58
3.4.2 Concrete Strength 58
3.4.3 Concrete Admixtures 59
3.4.4 Material Strength 60
3.5 Test Process and Results 61
3.5.1 Test Setup and Instrumentation 61
3.5.2 Test Procedure 63
3.5.3 Test Results 64
3.6 Summary 67

CHAPTER IV ANALYSIS OF CONNECTION TEST RESULTS

4.1 Introduction 68

4.2 Closure Strip Behavior 58

4.2.1 Test Variable Effects 68

4.2.1.1 Shear Keys 68

4.2.1.2 Strip Size 71

4.2.1.3 Reinforcement 72

4.2.1.4 Grout Strength 76

4.2.1.5 Normal Force 76

4.2.1.6 Operation Errors 77

4.2.2 Capacity Evaluation 78

4.2.2.1 Cracking Capacity Estimate 78

4.2.2.2 Ultimate Capacity Estimate 83

4.2.2.3 Residual Capacity Estimate 90

4.3 Shear Lug Performance 96

4.3.1 Variable Effects 96

4.3.1.1 Pipe Size 96

4.3.1.2 Pipe Embedment Length 97

4.3.1.3 Panel Thickness 98

4.3.2 Capacity Evaluation 99

4.3.2.1 Cohesion Strength 100

4.3.2.2 Ultimate Strength 102

4.3.2.3 Residual Strength 105

4.4 Design Recommendations 106

CHAPTER V MODEL STRUCTURAL TEST

5.1 Introduction 108

5.2 Model Structure Design 108

5.2.1 Existing Frame Simulation 108

5.2.1.1 Non-Ductile Features 110

5.2.1.2 Rigid Base Mode 110

5.2.1.3 Lateral Load Mode 111

5.2.2 Structural Retrofitting Simulation 111

5.2.2.1 Closure strip Test Application 113

5.2.2.2 Shear Lug Test Application 115

5.2.2.3 Post Tensioning Implementation 118

5.3 Model Structure Construction 120

5.3.1 Frame Construction 120

5.3.1.1 Base Footing Casting 120

5.3.1.2 Frame Casting 122

5.3.2 Retrofitting Construction 123

5.3.2.1 Precast Panel Construction 123

5.3.2.2 Panel Placing 123

5.3.2.3 Supporting and Bracing 124

5.3.2.4 Infill Grouting 125

5.3.3 Post-Tensioning Tendons 128

5.3.3.1 Tendon Installation 128

5.3.3.2 Tendon Tensioning 129

5.3.4 Material Demonstration 130

5.3.4.1 Concrete Mixture and Strength 130

5.3.4.2 Steel Strength 130

5.4 Model Structure Tests 131
5.4.1 Test Setup and Instrumentation 132
5.4.1.1 Loading Mode and Device 132
5.4.1.2 Specimen Bracing 133
5.4.1.3 Instrumentation 133
5.4.2 Frame Test 135
5.4.2.1 Test Results 135
5.4.3 Retrofitted Structure Tests 138
5.4.3.1 Test Results 138
5.5 Summary 142

CHAPTER VI ANALYSIS OF MODEL STRUCTURE TEST RESULTS

6.1 Introduction 144
6.2 Structural Response 144
6.2.1 Flexural Response 144
6.2.2 Infill Shear Response 158
6.2.3 System Shear Response 151
6.3 Element Performance 153
6.3.1 Column Performance 153
6.3.2 Post Tensioning Response 156
6.3.3 Infill Wall Performance 158
6.3.4 Closure Strip Performance 160
6.3.5 Shear Lug Performance 161
6.4 Structural Capacity Evaluation 175
6.4.1 Flexural Capacity 176
6.4.2 Shear Capacity 171

6.4.2.1 Infill Shear Capacity 171
6.4.2.2 System Shear Capacity (strut) 171
6.4.2.3 Base Shear Capacity (residual) 173
6.4.3 Retrofitting Effectiveness Evaluation 175
6.4.3.1 Frame Retrofitting 175
6.4.3.2 System Retrofitting 176
6.5 Design Comments 178
6.5.1 Flexure Capacity Design 179
6.5.2 Shear Capacity Design 181
6.5.2.1 Infill Wall Design 181
6.5.2.2 Base Shear Capacity / Shear Lug Design 182

CHAPTER VII COMPUTER DESIGN OF EXPERIMENT

7.1 Introduction 184
7.2 Time History Analysis of Structural Response 185
7.2.1 Random Vibration of Non- Linear Systems 185
7.2.2 Linear Acceleration Method 187
7.3 Non-linear Program Demonstration 190
7.3.1 Calculation Model 190
7.3.2 Element Involvement 192
7.3.3 Mechanical Properties 193
7.4 IDARC Demonstration And IDARC-PT Development 196
7.4.1 Program Correction 196
7.4.2 Addition OF New Analytical Model 197
7.4.2.1 Truss (tendon) member Modeling 198
7.4.2.2 Inelastic Axial Spring Modeling 198

7.4.2.3 Post Tensioning 201
7.4.2.4 New Hysteretic Model Creation 201
7.4.2.5 Damping Property Modification 205
7.4.3 Debug of Program IDARC-PT 205
7.5 Simulation of Specimen Tests 206
7.5.1 Input Data Preparation 206
7.5.2 Simulation of Frame Test 206
7.5.3 Simulation of Retrofitted Model Structure Test 209
7.5.3.1 Simulation of Test I (Flexure Model) 210
7.5.3.2 Simulation of Test II (Shear Model) 213
7.5 Summary 215

CHAPTER VIII ANALYTICAL MODEL OF FOUNDATION

8.1 Introduction 217
8.2 Analytical Model of Foundation 220
8.2.1 Foundation Types 221
8.2.2 Uplift Resistance Capacity 223
8.2.2.1 Static Loads on Footing 224
8.2.2.1 Shear Capacity of Soil 225
8.2.2.1 Neighboring Footing Assistance 227
8.2.3 Stiffness and Mechanical Model 229
8.2.3.1 Compression Capacity 230
8.2.3.2 Tension Capacity 232
8.2.4 Structural Model of Foundation 239
8.3 Summary 241

CHAPTER IX FOUNDATION SIMULATION

9.1 Introduction 242

9.2 Foundation-Infill Connection Scheme 245

9.3 Foundation Performance 246

9.4 Soil Property Effects 250

9.5 Earthquake Behavior Effects 253

9.5.1 Long Period Earthquake with High Peak Acceleration 253

9.5.2 Long Period Earthquake with Low Peak Acceleration 256

9.5.3 General Effects of Soil and Earthquake Properties 258

9.6 Interaction Analysis 259

9.6.1 Response of Foundation 260

9.6.2 Foundation/Post Tension Interaction 262

9.6.2.1 Tension Force .vs. Foundation Property 262

9.6.2.2 Effects of Initial Post Tensioning 264

9.6.2 Foundation-Infill Wall Interaction 267

9.6.3.1 Interaction with Base Soil 269

9.6.3.2 Interaction with Earthquake Period 269

9.6.3.3 Interaction with Post Tensioning 270

9.7 Design Comments 271

9.7.1 Proper Location of Infills 272

9.7.2 Adding More Infills 273

9.7.3 Enhancing Infill Flexural Capacity 275

9.8 Summary 276

9.8.1 Soil and Earthquake Effects 277

9.8.2 Soil-Post Tensioning Interaction 278

9.8.3 Soil -Infill Interaction 278

CHAPTER X DESIGN GUIDELINES

10.1 Introduction 281

10.2 Principle of Retrofitting 281

10.2.1 Philosophy of Seismic Design 281

10.2.2 Targets of Retrofitting 283

10.2.2.1 Increasing Structural Strength 283

10.2.2.2 Proving Ductility 284

10.2.2.3 Correcting Structural Defects 284

10.2.2.4 Preventing New Defects 285

10.2.3 Strategy of PTPW system Design 285

10.2.3.1 Retrofitting Schemes 285

10.2.3.2 Mechanical Behavior 286

10.3 Structural Capacity Design 286

10.3.1 Foundation Uplift Capacity Evaluation 287

10.3.2 Flexural Capacity Design 288

10.3.2.1 Overall Structural Flexural Capacity 288

10.3.2.2 Infill Number and Location 290

10.3.3 Shear Capacity Design 291

10.3.3.1 Infill Wall Design 291

10.3.3.2 System Shear Strength 291

10.3.3.3 Base Shear Capacity Design 292

10.4 Structural Detail 292

10.4.1 Infill Wall 292

10.4.1.1 Precast Panel 292

10.4.1.2 Closure Strip 293

10.4.2 Shear Lug 294

10.4.3 Post-Tensioning Details 295
10.5 Summary 296

CHAPTER XI CONCLUSION

11.1 Introduction 297
11.2 Experimental Investigation 299
11.2.1 Structural Connection Tests 299
11.2.1.1 Panel-Panel Connection 299
11.2.1.2 Infill-Frame Connection 300
11.2.2 Model Structural Tests 302
11.2.2.1 Existing Frame Test 302
11.2.2.2 Model Structure Tests 302
11.3 IDARC-PI Development and Test Simulation 305
11.3.1 Analytical Model of PTPW System 305
11.3.2 Structural Test Simulation 306
11.4 Foundation Simulation 307
11.4.1 Analytical Model of Foundation 307
11.4.2 Foundation Effects 308
11.5 Design Guidelines 310
11.6 Future Research 311
11.6.1 Post Tensioning Tendon Anchorage 311
11.6.2 Upgrading Post Tensioning Model 311
11.6.3 Application of Post Tensioning Model 312
11.6.4 Application of Foundation Simulation 313
11.7 Conclusion 314

Appendix A Connection Test Data 315

Appendix B Model Structural Test Data 329

Appendix C Manual of Program IDARC-PT 357

Appendix D Foundation Simulation Data 388

Bibliography 404

Vita 410

CHAPTER I
INTRODUCTION

1.1 STATEMENT OF PROBLEM

A large number of existing reinforced concrete frame structures built in the 1960's or earlier do not have the strength, stiffness and ductility required for adequate earthquake performance. The correction of such deficiencies is of concern to the structural and earthquake engineering profession[48]. In many major earthquake zones, the most urgent problem to be solved is the evaluation and rehabilitation of structures built without sufficient earthquake resistance. Realizing the devastating effects of a major earthquake that may destroy structures and injure or kill the occupants, owners are beginning to consider rehabilitation to provide a safe building for occupants and to protect their investment.

To strengthen existing structures or rehabilitate damaged structures, various methods have been developed[16, 17, 18]. However, some techniques such as element encasement or jacketing, steel bracing and infill walls for retrofitting reinforced concrete frame structures may be time consuming and expensive. In order to investigate economic and constructible techniques for correcting weak links and deficiencies in existing structures, the feasibility and behavior of a vertically post tensioned pre-cast infill wall (PTPW) system, as shown in Figure 1.1, was studied through experimental investigations and theoretical analysis.

Two critical defects in many existing reinforced concrete frame structures are low lateral capacity and inadequate reinforcement details. Because of such defects, structures may fail in a brittle mode under earthquake excitations. To increase shear capacity, adding infill walls to the frame may be an optimum solution. However, the

use of traditional infill walls, may not sufficiently increase the lateral capacity. A precast infill wall coupled with vertical post tensioning is an attractive alternative. Using a PTPW system, frame systems can be converted to frame-shear-wall systems to provide increased shear capacity through added infill walls, and moment capacity of the wall is increased by post tensioning tendons added to boundary columns.

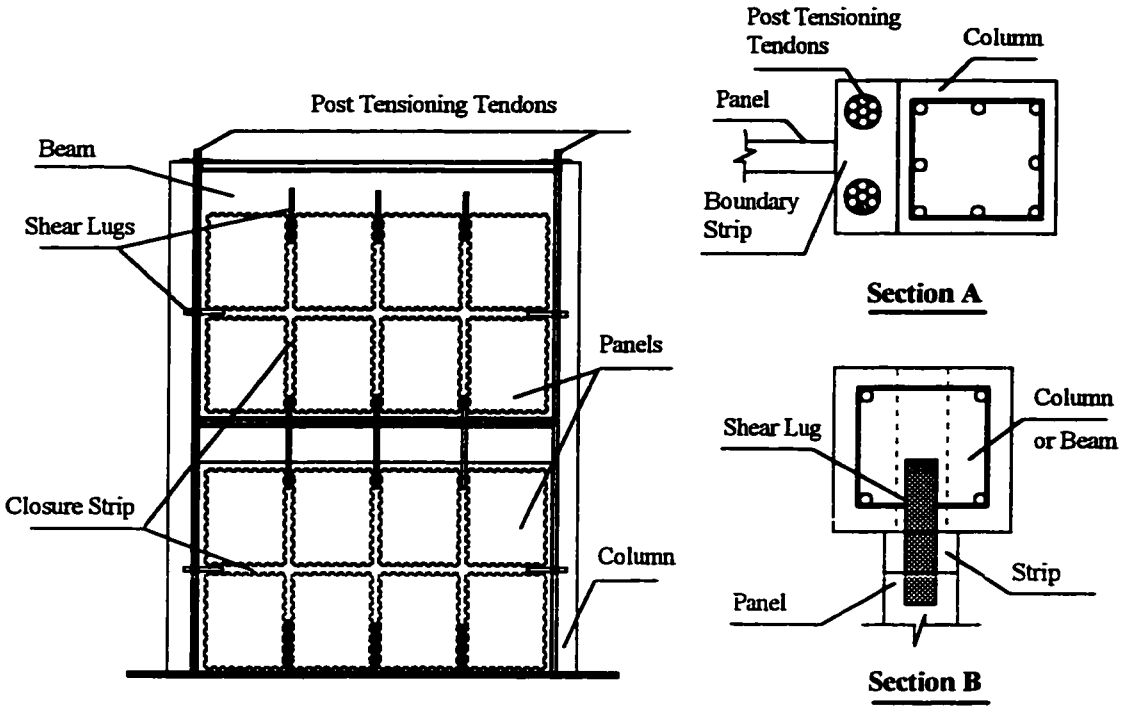

Figure 1.1 Precast Infill Wall With Post Tension System

Figure 1.1 shows a PTPW system. Precast panels used to build the infill walls may shorten construction time and may eliminate the need to evacuate occupants during construction. Closure strips connecting panels with keys along the boundaries were designed to transfer shear between panels. Shear dowels or lugs made of steel

pipes can be used along interface connections to permit shear transfer between existing structural components and infill walls. Post-tensioning tendons were provided vertically next to boundary columns to increase overall flexural capacity of the system.

Experiments have shown that ordinary structural analysis models and computer programs do not reflect the special behavior of post-tensioned reinforcement concrete structures [55]. An analysis model and the associated computer program are needed for PTPW system design and implementation in retrofitting projects.

For any rehabilitation technique, foundation performance is always an important factor[29, 51]. It is a critical issue in using the PTPW system as a retrofitting method because the foundation must provide anchorages for post-tensioning tendons and resist forces transmitted to the soil during an earthquake. Variations in soil properties and ground motions may affect seismic rehabilitation strategy for certain structures. Normally, foundation behavior may dominate the structural rehabilitation decisions regarding placement of infill walls and may control the level of force developed in post-tensioning tendons.

1.2 OBJECTIVE OF PROJECT

Objective of the study was to evaluate the system behavior so that detailed construction schemes and realistic analytical models can be developed. The intent was to carry the PTPW system from concept to practice. Construction and behavior of closure strips, shear lugs and tendon fabrication details were studied experimentally. Response of the PTPW system including foundation response were studied analytically. Finally, design schemes for PTPW systems were developed.

1.3 SCOPE OF PROJECT

The experimental investigations were performed in two stages: panel-to-panel and panel-to-existing frame connections were first studied. Once desired performance for connection details was established, a large-scale model structure was tested. Shear transfer tests of closure strips and infill-to-frame shear lugs provided connection response data. Subsequently, tests of a reinforced concrete frame and a frame-infill-wall and boundary column post-tensioned rehabilitation system provided existing frame and PTPW system response behavior. The analytical studies consist of two phases: development of analytical models and simulations of retrofitted structure and foundation-structural interaction.

1.3.1 Experimental Investigation

1.3.1.1 Connection Specimen Test

Connection construction schemes and details for panel-to-panel connections and panel-to-frame connections were tested. The panel-to-panel connection tests referred to hereafter as closure strip tests were conducted to evaluate the panel-to-panel connection strength and identify the effects of variables including,

1) Materials
2) Closure strip/panel dimensions
3) Shear key size and patterns
4) Closure strip reinforcement

Panel-to-frame connection tests referred to as shear-lug tests were conducted to estimate the interface shear strength and to identify the effects of,

1) Materials
2) Shear lug sections
3) Shear lug embedment lengths
4) Closure strip dimensions

1.3.1.2 large-scale Model Structure Tests

A reinforced concrete existing-frame structure was tested to identify existing weak links related to splice defects and to determine its lateral capacity. The structure with a precast infill wall and boundary post tensioning was tested to evaluate PTPW system efficiency in increasing structural lateral capacity and to identify global as well as local PTPW system behavior including,

1) Total capacity increase
2) Connection performance
3) Effectiveness of post tensioning
4) Hysteretic behavior

1.3.2 Analytical Studies

The analytical studies were performed in two stages: a) PTPW system simulation and computer structural programming; b) foundation simulation and time history analysis of structural seismic response. The analysis procedure was calibrated using tested connection behavior and retrofitted system characteristics. A non-linear structural analysis program IDARC-PT was developed from IDARC-2D to include a post tensioning model and a foundation model. Using IDARC-PT, foundation performance was studied by means of time-history analysis of PTPW systems with varying foundation behavior and different earthquake excitations.

1.3.2.1 Analytical Modeling and Programming

To reflect post-tensioning effects on structural response, analytical models for the PTPW system were established using test results. The analytical models consist of a post-tensioning element and non-linear hysteretic response simulating observed response under cyclic load. Adding models for post-tensioning and hysteretic

response to the non-linear structural analysis computer program IDARC-2D led to a new program IDARC-PT.

1.3.2.2 Experimental Simulation

The simulations of observed response were conducted using IDARC-PT. The existing frame and retrofitted model structure were analyzed with cyclic load input identical to that applied experimentally. The IDARC-PT was efficient and accurate in reflecting observed PTPW system response.

1.3.2.3 Foundation Simulation

The foundation model was based on soil properties and on foundation and structural system behavior. A non-linear foundation response model was included in IDARC-PT. Variables studied include foundation soil properties and ground motion characteristics. Foundation/post-tensioning and foundation/infill interactions were included in simulations.

1.3.3 PTPW System Design Guidelines

Using experimental and analytical results, approaches for implementing the PTPW system in seismic rehabilitation of reinforced concrete frame structures were proposed. Design recommendations were provided for closure strip reinforcement and connection details, for infill walls/panels and post-tensioning, and system capacity design as demonstrated through connection and model structural tests. The influence of the foundation condition on the infill wall and post-tensioning was studied through foundation simulation using program IDARC-PT. A process and scheme for PTPW system analysis and design was proposed.

CHAPTER II

DEVELOPMENT OF TECHNIQUES

2.1 REQUIREMENTS OF EARTHQUAKE RESISTANCE

2.1.1 Earthquake Load

An earthquake produces sudden shaking or vibration of the earth's surface due to movement along geologic faults. Although thousands of earthquakes occur every year, only a few major earthquakes cause damage to structures. Such events are usually the most severe loading a structure is called on to withstand and will generally have long recurrence periods. The ground motion may cause damage or collapse of structures and may endanger the life of building occupants.

Records of major earthquakes date back two thousand years ago, but the science of engineering seismology is only 60 years old[24]. The major cause of earthquake is tectonic movement of crustal plates supporting continents and oceans on the earth's surface. Tectonic movement is caused by convection of molten rocks in the interior of the earth. As the plate movement occurs, stress builds up in the rock. When stresses are sufficient to cause rock fracture, the result is relative motion between fault surfaces. A sudden movement, fracture, or rupture initiates vibrations that propagate as seismic waves --- random vibration processes. The seismic waves, which have frequency content and carry energy, vibrate structures located in the region of faults. Structural vibration produces structural displacement and causes force to develop in elements of the structure. These actions are often referred to earthquake or seismic loads.

Unlike other kinds of loads normally considered in structural design such as gravity load and pressure load, earthquake loads produce vibrations or dynamic displacements rather than forces. Earthquake excited vibrations are time and frequency (or period) dependent and therefore the structural response is also time, mass and frequency (or period) dependent. The equivalent force induced by earthquake to the structure equals:

$$L_{EQ} = M Y_{AC} \qquad (2\text{-}1)$$

where M ... structural mass

Y_{AC} ... structural acceleration under earthquake

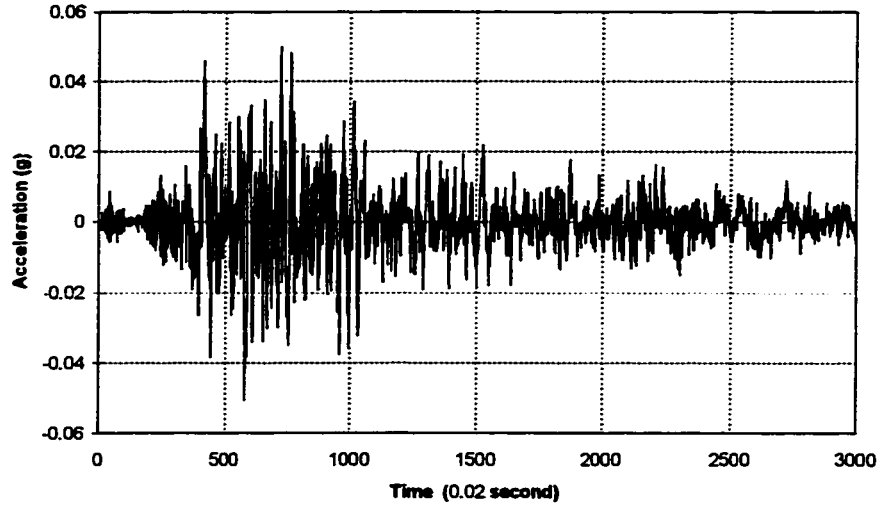

Figure 2.1 Earthquake Wave of Ground Acceleration

Earthquakes can be recorded as seismic waves by means of a seismograph. The propagation of ground motion acceleration waves are used as input to structural dynamic analyses as earthquake excitation[24]. A great number of earthquakes records from all over the world are available for use in structural

seismic analysis. Figure 2.1 shows an example of earthquake records. For design convenience, earthquake load is often simplified as an equivalent static force applied to a structure[10,49]. Another alternate method to describe earthquake excitations is to construct a response spectrum[23, 37, 49].

2.1.2 Review of Structural Seismic Design

Engineers used to apply so called dynamic safety factors for earthquake design[51]. A factor greater than 1.0 might be used to enlarge the gravity load effects on structures, and another factor less than 0.3 might be applied to the structural mass to estimate lateral load effects induced by vibration. A few classical structures have survived past major earthquakes in China because this simple design technique was used. However, most ancient structures designed under this scheme have disappeared.

Earthquake engineering is based on an understanding of structural dynamics and engineering seismology and has resulted in better structural seismic design schemes. Through consideration of earthquake actions on structures, the behavior of structures has rapidly improved in the first half of this century. In this period, the structures were designed as elastic response systems[1, 2]. However, it is often impossible and generally uneconomical to design a structure to remain in the elastic range under major earthquakes.

Based on a better understanding of inelastic and energy dissipation properties of engineering materials, inelastic structural design was developed in the early 1950's. In inelastic design, materials used in structural members must have the ability to withstand deformations beyond yielding.

The energy imported to a structure by external dynamic action is dissipated by viscous damping and through inelastic strain or deformation developing in the structure. The stiffness and vibration frequency of the structure decline. Earthquake load is time and period dependent. For a given earthquake record, the structural response spectra shown in Figure 2.2 indicates the relationship between acceleration Y_{ac} and period T of the structure.

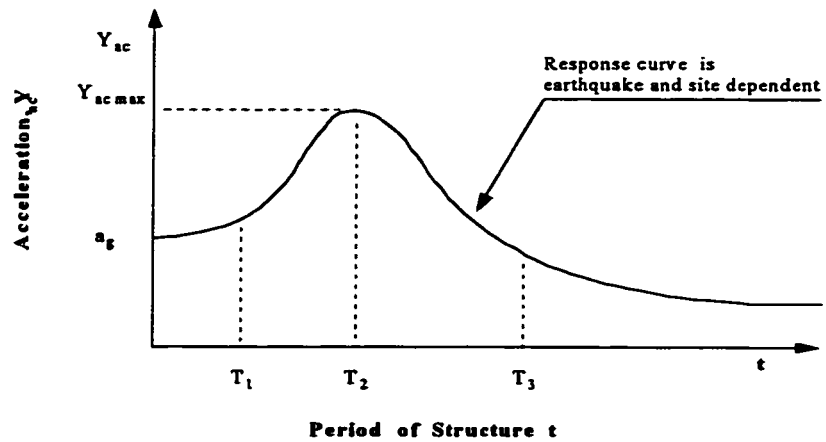

Figure 2.2 Structural Response Spectrum

As structural stiffness declines, the structural period increases, and structural acceleration Y_{ac} decreases after reaching the peak acceleration. Consequently, force L_{EQ} in equation (2-1) reduces. Development of inelastic deformation always reduces structural stiffness. By taking advantages of these properties, the structure can be designed as an inelastic system or ductile system. An ideal ductile structural system is required to have sufficient inelastic deformation while maintaining an acceptable level of strength. The theory of inelastic design has been well accepted and used in structural seismic design [51] since the later 1960's.

Structural seismic design strategies have been established using three limit states, service limit, damage limit and collapse limit.

1. Resist a minor level earthquake ground motion without damage (Service Limit, or Immediate Occupancy Performance);
2. Resist a moderate level of earthquake ground motion without structural damage, but possibly experience some nonstructural damage (Damage Limit, or Life Safety Performance);
3. Resist a major level of earthquake ground motion having an intensity equal to the strongest either experienced or forecast for the building site, without collapse, but possibly with some structural as well as nonstructural damage (Collapse limit, or Collapse Prevention Performance).

. Computer programs reflecting inelastic behavior have developed rapidly in recent years. Among them, step by step integration or time history analysis theory represents a great achievement in seismic structural analysis. Applying step by step integration, the analysis follows inelastic load-deformation response of materials and elements to calculate response to specific earthquake ground motion. Earthquake records are used as excitation input to the structure. Artificial earthquake waves[51] can also be used to simulate intensity, frequency and related foundation soil conditions in an idealized earthquake. With the development of such computational tools, many load-deformation algorithms have been developed for different structures and elements to represent inelastic hysteretic responses.

2.1.3 Seismic Behavior of Concrete Structures

Reinforced concrete structures can be designed as ductile systems by means of effective reinforcement schemes and details. Force-deformation

envelopes for reinforced concrete structures exhibit three distinct stages; an initial elastic stage, cracking to first yielding, yielding to ultimate. It may also be necessary to model strength and stiffness degradation after the ultimate stage is reached. For cyclic loading, different reinforcement ratios and fabrication details result in different properties of the load-deformation response for the structure. Under cyclic loading, stiffness and strength may degrade with different inelastic deformations in different loading directions. Figure 2.3 shows an example of strength and stiffness degradation and pinching behavior in reinforced concrete structures.

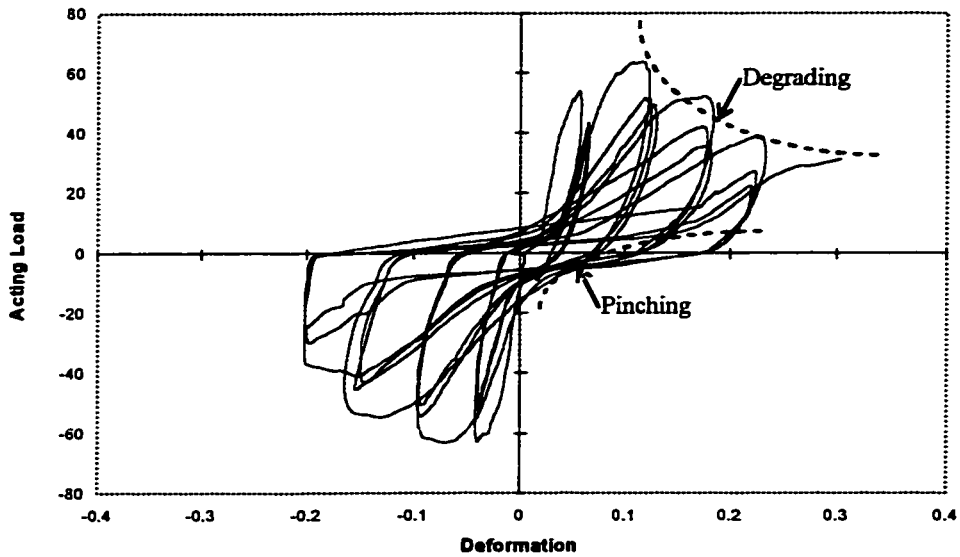

Figure 2.3 Inelastic Behavior of Reinforced Concrete Structure

Structural analysis and design depend on the frequency characteristics of earthquake excitation, stiffness and strength degradation characteristics of the structure. Generally, a reinforced concrete structure should be designed to have:

1) *Well-conceived layout, continuous structural system in horizontal and vertical directions.*

2) *Adequate system lateral capacity, sufficient member strength under all load combinations and deformations.*

3) *Appropriate ductility through proper reinforcement detailing.*

2.2 FEATURES OF EXISTING FRAME STRUCTURES

Reinforced concrete frame structures built in the 1960's, or earlier often had little consideration of earthquake effects in their design. The primary consideration may have been static or vertical gravity loads. Although earthquake load may have been considered, the structural design was often based on elastic stresses. In the design codes of ACI 318-56 and ACI 318-63, the only seismic design guidelines mentioned were:

1) *Elements required to resist wind and earthquake forces shall be limited to those comprising on integral structural system.*

2) *The moment, shear, and direct stresses resulting from wind or earthquake forces determined in accordance with recognized methods shall be added to the maximum stresses which exist at any section for dead and live load*

3) *Members subject to stresses produced by wind or earthquake forces combined with other loads may be proportioned for unit stresses 33-1/3 percent greater than those specified...., provided that the section thus required is not less than that required for the combination of dead and live loads..*

Under such guidelines, detailing requirements to achieve inelastic deformation capacity were not specified indicating structural inelastic action and ductile responses were not recognized as they are today. Structures designed using these early guidelines generally do not have sufficient lateral strength or deformation capacity.

2.2.1 Ductility

In order to reduce the force levels generated in structures responding elastically to earthquake motion, energy must be dissipated through inelastic action in the structures. However, it is expected that large plastic deformations can be developed with sufficient lateral capacity and full gravity loading capacity maintained. Structural behavior can be characterized using a ductility factor μ defined as the ratio of available inelastic deformation capacity to the elastic deformation of the structure.

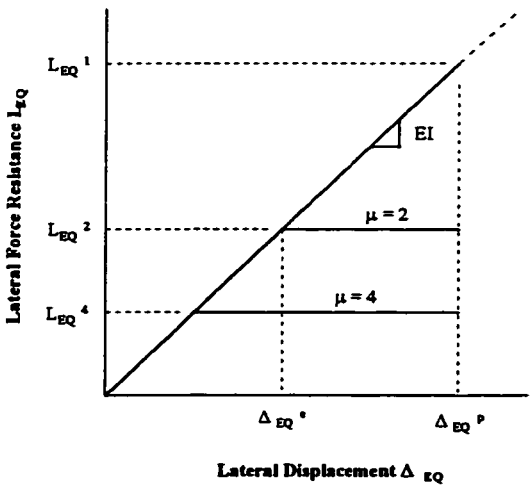

Figure 2.4 Ductile Behavior

Figure 2.4 shows the difference in required force levels to be used in elastic and inelastic design. Based on elastic design, a structure reaches the maximum elastic deformation Δ_{EQ}^{e} under earthquake load intensity L_{EQ}^{1}. By permitting inelastic deformation, the earthquake load intensity is reduced when the same numerical plastic deformation Δ_{EQ}^{p} is reacted.

Assuming equal displacement, which is approximately correct for structures with periods longer than T_2 shown in Figure 2.2, on the descending

branch of amplification curve[37], it can be shown that $\Delta_{EQ}{}^{e}$ almost equals $\Delta_{EQ}{}^{p}$. The design earthquake load intensity can be reduced to,

$$L_{EQ}{}^{x}. = L_{EQ}{}^{I}. / \mu_x \qquad (2\text{-}2)$$

where μ_x is the ductility factor the system provided.

Proper reinforcement details provide structures with the capacity to develop inelastic deformation. Most existing reinforced concrete frame structures, however, have neither adequate strength and stiffness nor reinforcement details required for ductility. Such structures are labeled as non-ductile systems.

2.2.2 System Mechanical Defects

Non-ductile frame structures generally have weak links in the lateral loading resisting system and in addition they may have configuration problems. Such defects may lead to structural failure and create unacceptable risks to occupants and to the owner.

2.2.2.1 Lack of Lateral Capacity

Most structure are designed following a strong-column and weak-beam philosophy. In a system with weak-columns and strong-beams, hinges will form in the columns before those form in beams and result in an unacceptable mechanism. Figure 2.5 shows a weak beam-strong column and a strong beam-weak column system. If plastic hinges are formed in columns before beam hinges form, gravity load capacity may reduced or lost.

Under earthquake excitation, even for an acceptable mechanism, large lateral displacement could also occur due to low stiffness. Large lateral drift could produce P-δ effects which induce extra forces in the elements. The lateral force

system must have adequate stiffness and strength to limit lateral deformations and sufficient moment and shear capacities at all critical locations.

Generally, insufficient lateral resistance is the primary problem existing in reinforced concrete frame structures built in the 1960's or earlier. Increasing their lateral capacity is thus an important target in structural retrofitting.

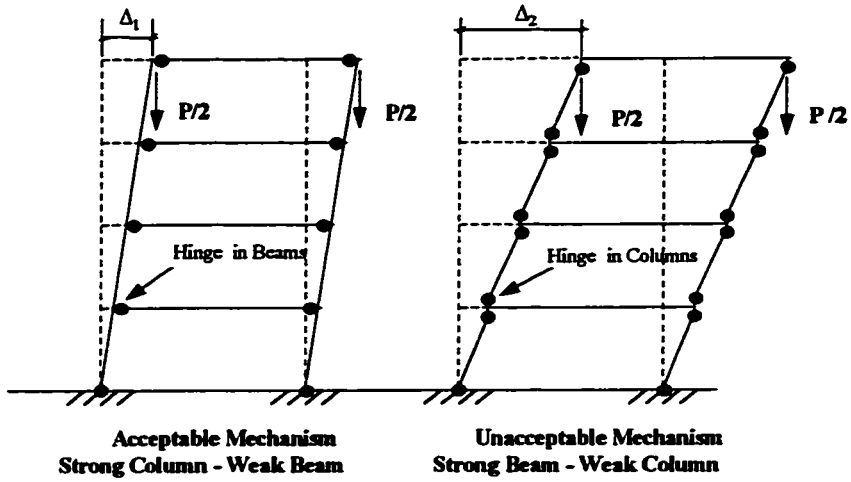

Figure 2.5 Plastic Hinged Mechanisms

2.2.2.2 Lack of Redundancy

A structure must have adequate redundancies to permit development of an acceptable plastic mechanism and to continue sustaining lateral load. Lack of redundancy can result in a plastic hinged mechanism forming in the columns under earthquake load which either be an unstable mechanism or a lower lateral capacity mechanism.

This type of defect may exist in some frame systems as shown in Figure 2.6. The structure in Figure 2.6a represents a pre-cast frame structure in which joints are generally recognized as hinges. While Figure 2.6 b illustrates a rigid

frame structure with hinges connecting the roof truss and the adjunctive frame. Weak links associated with these types of structures may also be categorized as deficiencies related to construction schemes. Without adequate redundancy, a structure possesses low lateral resistance capacity. Figure 2.6c shows an example of precast frame which collapsed under an earthquake.

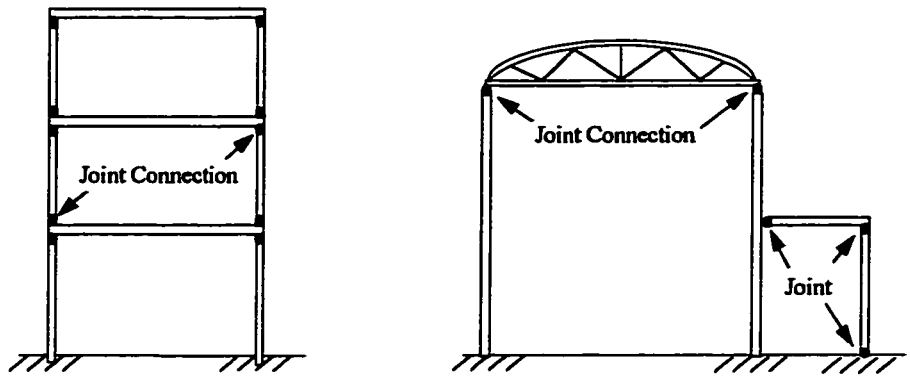

a) Hinged Frame
Built Up with Precast Elements

b) Rigid Frame
Hinge Connected with Roof & Adjunctive

Figure 2.6 Structures Lack of Redundancy

Figure 2.6c Precast Frame Collapse

2.2.3 System Configuration Defects

A desirable lateral force resisting system should allow earthquake load to be evenly distributed throughout the lateral resisting elements of the system and to transfer clearly and directly over the height of the structure. Otherwise, there will be system configuration problems which jeopardize the seismic resistance.

2.2.3.1 Lack of Regularity

Horizontal distribution of earthquake loads depends on the distribution of structural mass and lateral stiffness over the plane. If structural mass and stiffness are uniform, the earthquake load will be distributed evenly. Unfortunately, this is not the case for many structures because of architectural and functional characteristics. In general, it is desired that the centroid of overall system stiffness should coincide the centroid of total mass or as close to the centroid of overall system mass as possible[28,51]. If not, a twisting response will occur under lateral earthquake load which induces torsion moment as shown in Figure 2.7.

$$M_T^e = L_{EQ} \times D_T \qquad (2-3)$$

where L_{EQ} is earthquake load

D_T is the distance between centroids of mass and stiffness

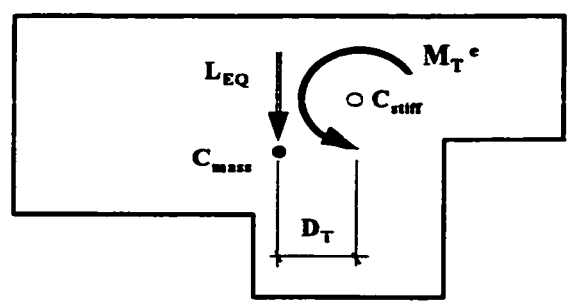

Fig. 2.7 Structural Torsion (plan view)

The torsional moment M_T^e induces additional shear in the frame columns in proportion to their distance from the center of resistance. Structures built with highly irregular plan configurations may develop brittle shear failure in columns

due to torsion effects. Figure 2.7c shows an example of a structure which collapsed because of severe torsional response under earthquake excitation.

Structures with a symmetrical architectural plan may also have torsion problems due to eccentricities between the centroids of total structural mass and stiffness. It is one of the important targets of rehabilitation to correct or eliminate possible torsion effects.

Figure 2.7c Collapse of a Theater

2.2.3.2 Lack of Continuity

A continuous load path must be provided for earthquake load transfer from the roof to the base [28, 51]. The continuous load path refers not only to the continuity of transferring forces but also to the continuity of lateral resisting stiffness. Lack of continuity often result in serious damage to critical elements which may cause collapse of the whole structure.

Figure 2.8 shows some examples of frame structures with discontinuity defects. The structure shown in Figure 2.8a is an example of a structure with

severe stiffness discontinuity as well as force discontinuity. These structures are often built as multipurpose buildings with public services such as parking or commercial stores at the first floor and apartments or offices at the upper floors. The perimeter frame shown in Figure 2.8b is a typical structure having force discontinuity. Observed earthquake damages indicate that most structures possessing discontinuity defects collapsed or seriously damaged as shown in Figures 2.8c and 2.8d. In structural retrofitting, existing discontinuities should be corrected and new discontinuities must be avoided.

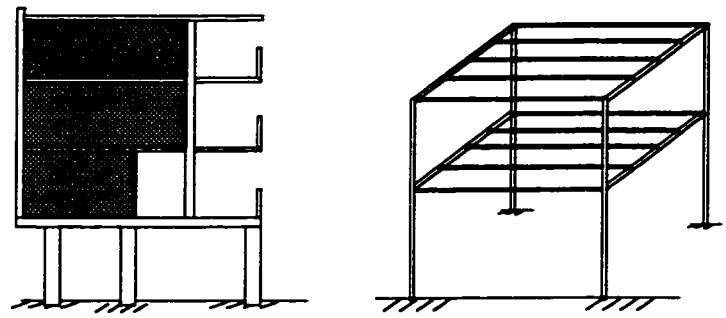

Figure 2.8 Structures Lack of Continuity

Figure 2.8c Stiffness Discontinuity

Figure 2.8d Force Discontinuity

2.2.4 Structural Member Defects

The structural system lateral capacity is made up of the capacities of individual structural members. The element defects create weak links within the structural system. The strength of a structural system is often dominated by the critical weak elements.

2.2.4.1 Insufficient Strength

Elements in older moment-frame structures were often proportioned to resist gravity loads only. The resulting reinforcement ratios and dimensions of elements may be lower than the minimum values required by earthquake resistance in current codes.

The shear resistance of moment-frame structures is often the primarily problem. The lack of transverse reinforcement for confinement and shear capacity in beams and columns create structural weak links which may result in brittle shear failure.

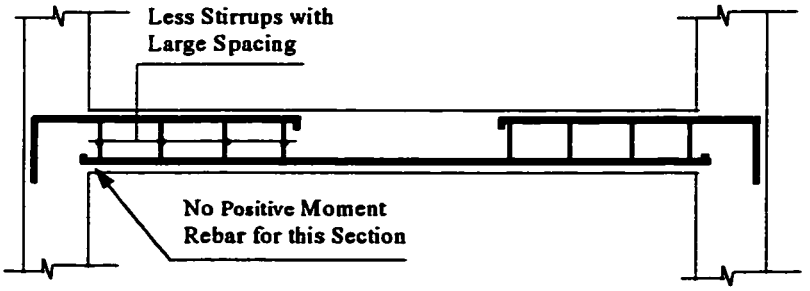

Figure 2.9 Typical Non-ductile Frame Beam Reinforcement

The beam elements may not have sufficient moment capacity at critical sections to withstand moments induced by earthquake load. Beams designed for

supporting gravity loads may have no positive moment capacity because no positive reinforcement was provided at the ends as shown in Figure 2.9. However, due to cyclic earthquake motions, moments of the beams at the column face change from negative to positive, alternatively. The positive moment created by earthquake damages the beams as a result of poor detailing.

For all beam and column elements, sections and reinforcement designed to carry gravity load are often inadequate to resist both gravity and earthquake loads. Therefore, though the non-ductile frame structures may work normally under gravity load, they will be damaged or collapsed under strong earthquake excitation.

2.2.4.2 Inadequate Details

To prevent brittle failure, to provide confinement, and to prevent compression and shear failure in column/beam joints, adequate transverse reinforcement is required.

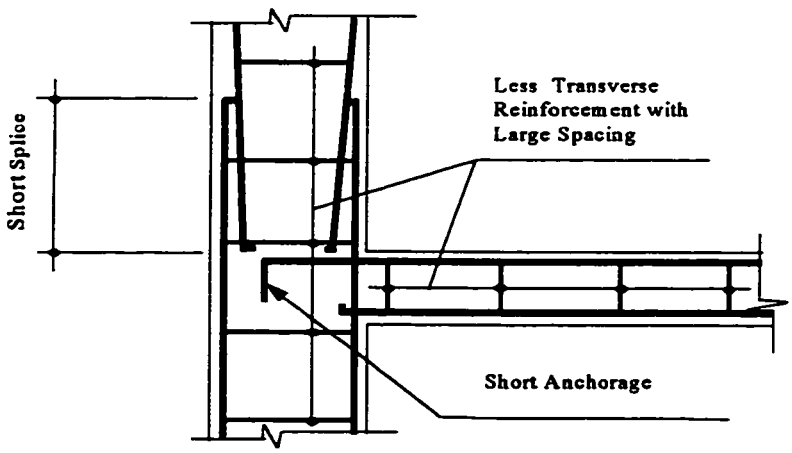

Figure 2.10 Typical Non-ductile Frame Joint Detail

Effective reinforcement details including anchorages, splices and transverse reinforcement must be provided to obtain structural ductile behavior. However, reinforcement details in many existing frames do not meet these requirements. The anchorage length for bars are too short, the splices are not sufficient, and the transverse reinforcement spacings are large which result in structural non-ductile behavior. Examples of inadequate splice and anchorage defects are shown in Figure 2.10.

2.3 DEVELOPMENT OF REHABILITATION TECHNIQUES

To maintain operation in non-ductile moment-frame buildings and to prevent failure under a major earthquake, modifying, rehabilitating or strengthening such structures is needed. The principal strategy for rehabilitating or strengthening frame structures is to modify the load carrying system or correct the problems that are detriments to seismic behavior. This is often done in different ways according to specific structural characteristics and seismic demands. One approach is to stiffen and strengthen the system to resist lateral drift. Another is to modify the lateral capacity to tolerate significant drift and to avoid brittle failure. Combinations of both approaches may be used for structural retrofitting.

The first approach intends to increase the system stiffness and shorten the system period. It may be done by adding new structural elements such as braces and infill walls. The second approach, on the other hand, focuses on improving the system ductility or softening the system. Ductility may be improved by modifying the structural joints to have ductile behavior. For an example, encasing beam/column joints by steel plates can prevent splice failure. Brittle non-structural

infill walls may be removed, in association with modification of the structural joints, to increase the system period.

Both of the approaches will reduce earthquake load to the structure by either shortening or increasing the structural period beyond T_2 as shown in Figure 2.2. If the structural period T is shorter or longer than T_2, the structural acceleration response Y_{ac}, as well as earthquake load L_{EQ}, reduces (equation 2-1).

Based on engineering practice and research results, guidelines for Seismic Rehabilitation of Existing Buildings are being developed by FEMA[56] . For strengthening non-ductile reinforced concrete structures, existing elements may be modified, new elements may be added to the structure and the lateral resisting system may be improved. In retrofitting, the following techniques[16] are most commonly accepted:

1) *Jacketing elements to increasing ductility and capacity of structural members.*

2) *Reducing forces in existing frames by providing supplemental (lateral-resisting) elements.*

3) *Changing the lateral force-resisting system by adding shear wall or infilling selected bays in frames with reinforced concrete, or by introducing bracing systems to carry all the lateral forces.*

2.3.1 Encasement or Jacketing of Frame Elements

By adding reinforcement [12] with new cast-in-place concrete to encase critical existing elements and joints as shown in Figure 2.11, moment and shear strength of the elements will be increased. This will result in improvement of element ductility and eventually system ductility. Through jacketing, defects of

individual elements and joints such as inadequate strength and insufficient details can be corrected, and consequently, the system lateral capacity and ductility can be improved.

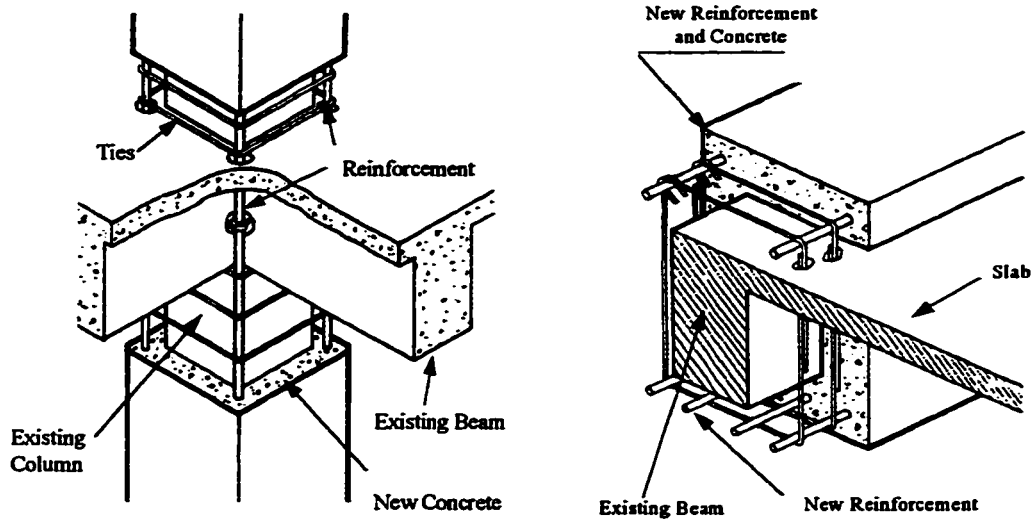

a) Column Jacketing b) Beam Jacketing

Figure 2.11 Encasement /Jacketing Technique

Element jacketing may not significantly influence structural system stiffness or dynamic characteristics. Structural system defects may not be corrected and earthquake load distribution may not be modified by this retrofitting method. Meanwhile, most structural elements may need to be jacketed so that construction may be expensive. Additionally, relocation of building occupants and operation during jacketing may be too costly.

Furthermore, a major deficiency of the jacketing method is the difficulty with strengthening the joints between beams and columns. As shown in Figure 2.12, though the beams and columns can be jacketed, it is very difficult to gain

access to the beam-column joint zone to provide necessary shear or confinement reinforcement to correct joint defects.

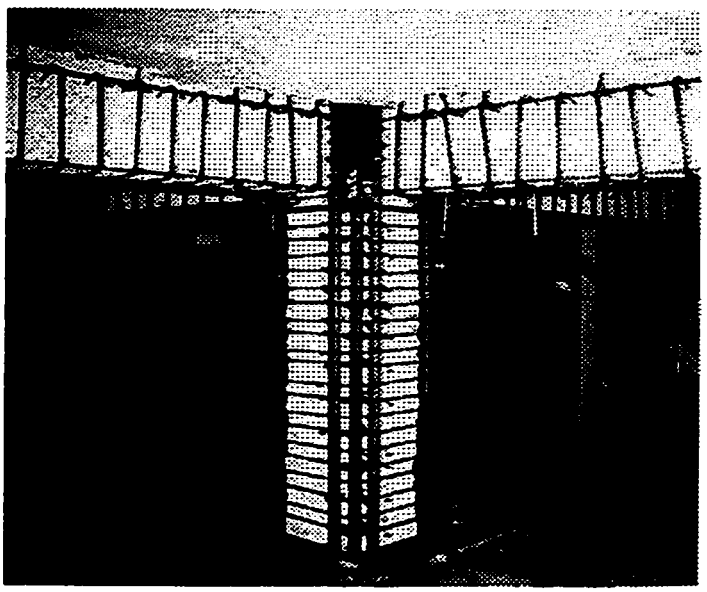

Figure 2.12 Example of Frame Jacketing

2.3.2 Application of Steel Bracing

A structure can be converted from an ordinary frame to a braced-frame system with addition of steel braces [11, 12]. Steel braces provide higher lateral stiffness and reduce the displacement and forces in frame elements. The lateral forces or frame shear forces induced by earthquake are to be mainly resisted by added braces.

Steel braces may be installed in interior frames of the building, as shown in Figure 2.13, to maintain the building appearance and accessibility. However, if multiple frames must be braced, the braces may impair building function. Under such conditions, braces may be added to exterior frames. Figure 2.14 shows an example which took advantage of the column protrusions from the building curtain

wall to connect the exterior braces. Steel pipe lugs were used to anchor the braces at the column connections.

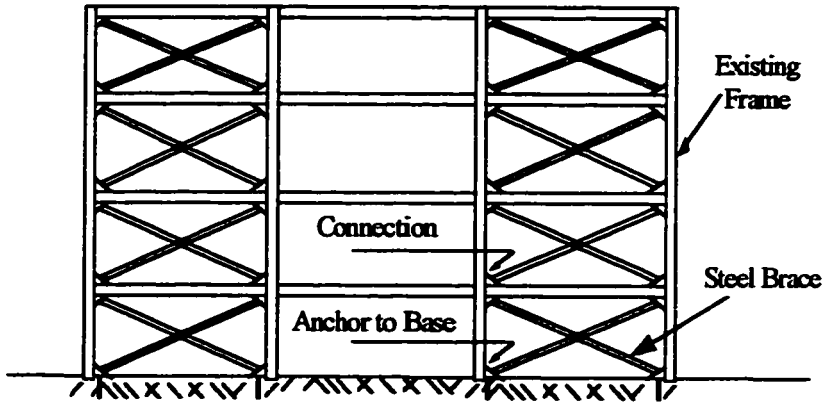

Figure 2.13 Inside Steel Brace Application

Bracing may be used to correct some system defects such as increasing system stiffness and modifying earthquake load distributions to gain advantages over the jacketing method. However, connecting braces to the existing frames may be difficult and construction is time consuming.

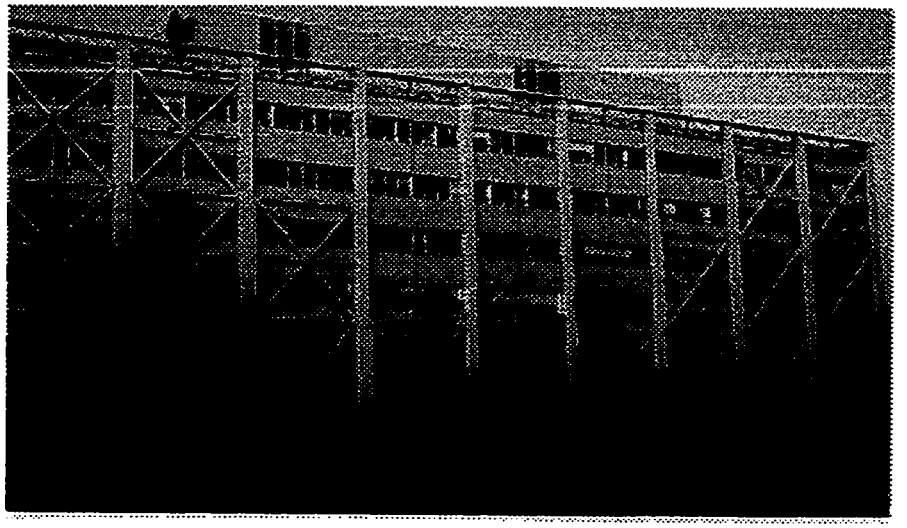

Figure 2.14 Outside Steel Brace Application

2.3.3 Addition of Shear Walls

Adding infill walls to a frame structure will convert the frame system to a totally different (frame/shear-wall) system [22,47,50]. It dramatically increases the structural lateral stiffness and shear strength. In many cases, it is the most efficient method for seismic rehabilitation.

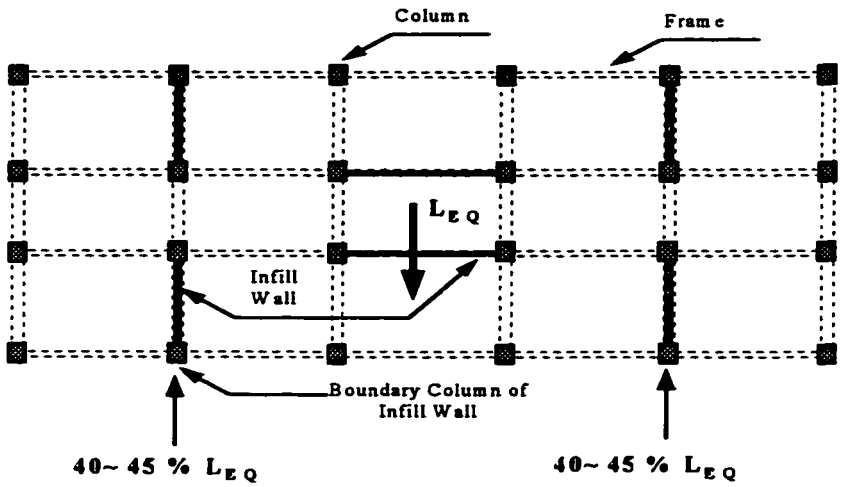

Figure 2.15 Earthquake Load Distribution Over Plan

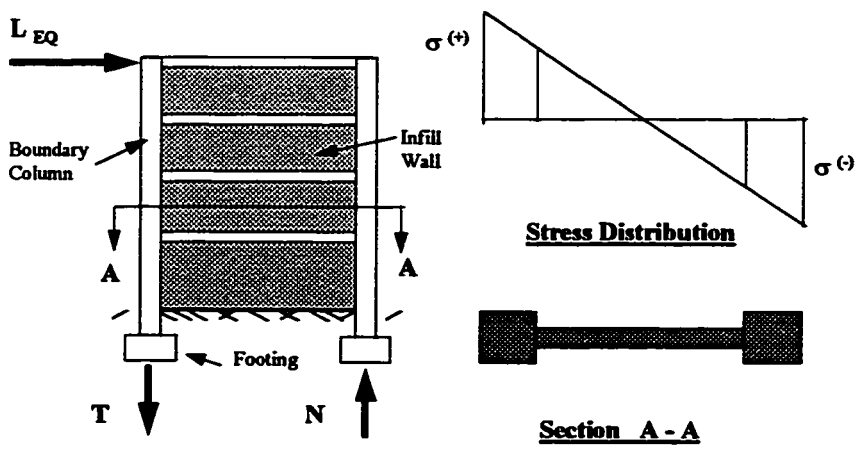

Figure 2.16 Mechanical Behavior of Boundary Column

By selecting the numbers and locations of infill walls, it is possible to change or adjust the earthquake load distributions over the structural system. It is also an efficient scheme to solve structural system configuration defects such as irregularity and discontinuity. Because of the high shear capacity and lateral stiffness, the infill-walls are expected to resist about 80 -90% of the earthquake load of the structure.

Nevertheless, there are some negative aspects of infill or shear wall rehabilitation schemes. The fact that the infill-walls sustain almost all earthquake load creates two problems -- boundary member strength and forces transferred to the foundations. Because earthquake loads are concentrated the frames retrofitted with infills, large forces will be induced to the columns and foundations of corresponding frames as shown in Figure 2.15.

An infill-wall primarily withstanding large earthquake shear force is forced simultaneously to sustain large moment associated with the shear force. Consequently, the moment creates large compression on one end and tension on the other end of the infilled frame as shown in Figure 2.16. Unlike a cast-in-place, monolithic shear-wall, an infill-wall may not be able to carry large moment due to inadequate connections to the structural floors and the base. The function of frame boundary columns where infill-walls are added is to change from a moment-resisting element to an axial force-resisting element.

. As discussed earlier, columns in many existing frames do not have adequate tension capacity due to low longitudinal reinforcement ratios and, especially, short splices and anchorages. Insufficient ties and large tie spacing result in inadequate confinement of the column. On the other hand, concrete compression capacity of the columns may be sufficient. Though the boundary column can be jacketed to

increase its axial load capacity, it is often difficult to meet the demand because the required axial strength may be extremely high.

Moreover, foundation problems faced with any rehabilitation method are generally worse with infill-walls. The problem is not the soil pressure requirements due to infill wall weight in addition to the dead load, rather, the problem is the axial force levels in boundary columns. A foundation designed primarily to sustain forces from gravity loads must now support the large force transferred from wall boundary elements. It may be impossible or uneconomical to strengthen foundations to meet such high force requirements.

2.4 USE OF INFILL-WALLS

Because of its efficiency in increasing system lateral capacity, infill-wall retrofitting method has been popular for frame structures that require large additional lateral capacity. Three different infill-wall construction procedures, reinforced masonry, cast-in-place reinforced concrete and pre-cast reinforced concrete, can be used to provide the infills to strengthen frame structures.

2.4.1 Reinforced Masonry Infills

Reinforced masonry infills have been used routinely and historically to stiffen frame structures [41,52]. Masonry infills provide lateral shear capacity. However, it may not be able to improve lateral deformation capacity. Failure of masonry infills may be brittle and sudden. To improve deformation capacity and to prevent brittle failure, reinforcement can be placed in the grout between masonry layers or to the

wall surfaces as shown in Figure 2.17. Reinforced masonry infills are economical and easy to construct to serve a variety of functional needs.

Because the shear strength of masonry is lower than concrete, more masonry than concrete infill-walls may be needed in a frame structure to provide the same level of lateral shear capacity. In addition, it is often difficult to provide continuity between masonry infills and the surrounding frame elements such as beams, columns and floors.

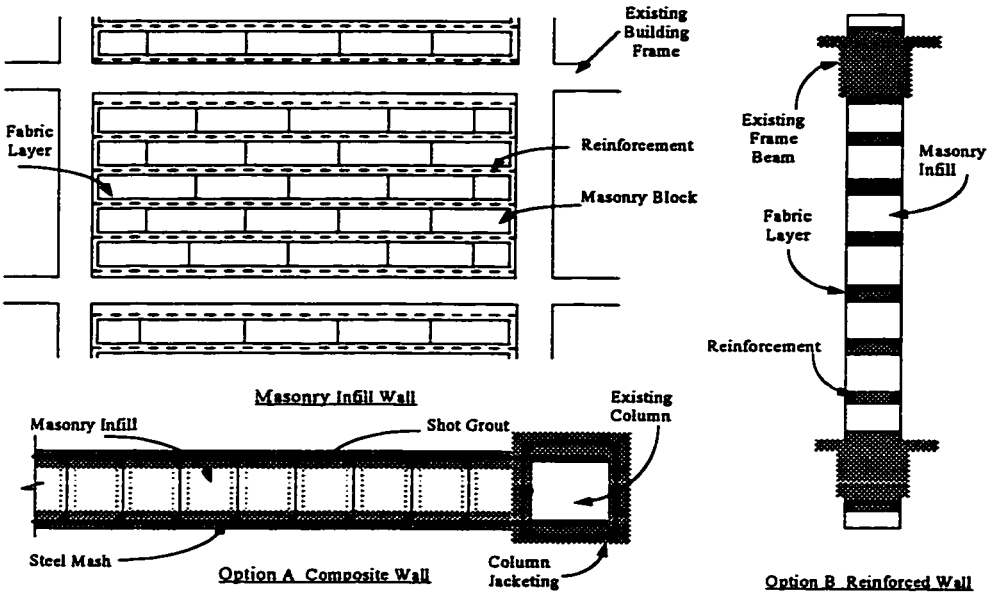

Figure 2.17 Reinforced Masonry Infill Wall

2.4.2 Cast in Place Reinforced Concrete Walls

Adding few reinforced concrete infill-walls to a frame system will convert it from a frame structure into a frame-shear-wall system[47,50,22,40]. The new infill wall system can be designed to carry all the lateral forces to correct the inadequate lateral load capacity of an existing structure. The infill wall is so stiff and strong that many

problems associated with inadequate deformation capacity can be eliminated. Boundary columns or beams can be modified simultaneously with infill wall construction. Connections between infill-walls and original frame elements can be provided as shown in Figure 2.18 .

Cast-in-place concrete can be well consolidated at the interface between columns and infills but it is difficult to consolidate concrete against an overhead surface such as the interface between the infills and the bottom of beams or floors. Shot crest casting may be a good alternative for these locations but it may not efficiently solve the problem of concrete slump or shrinkage. The principal shortcoming of cast-in-place procedures is that they may require a long period of construction. Relocation of building operations may reduce revenues to add to the rehabilitation cost.

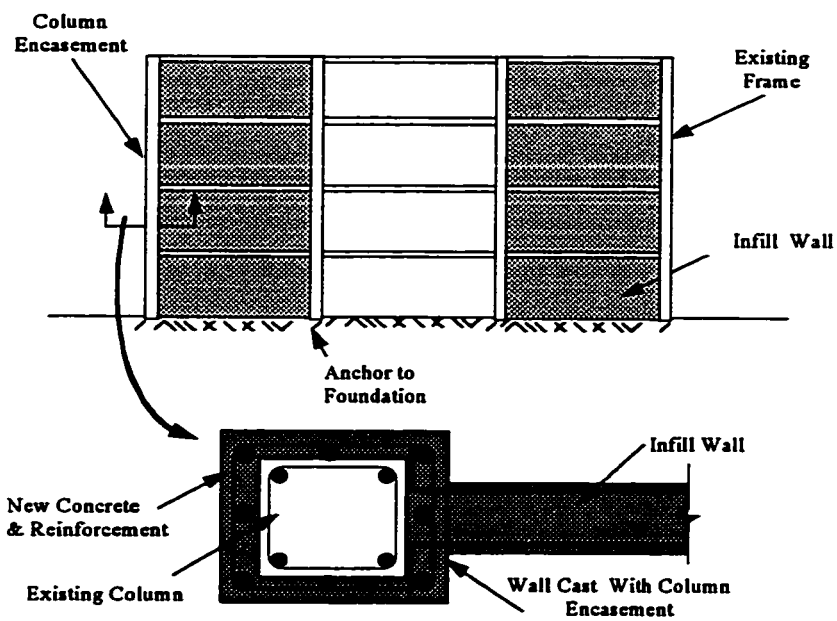

Figure 2.18 Cast-in-place Concrete Infill Wall

2.4.3 Precast Reinforced Concrete Infill Panels

To eliminate the shortcomings of cast-in-place methods and still take advantage of improved shear performance of reinforced concrete infills, pre-cast reinforced concrete panels may provide an alternative for strengthening frame structures[7,53]. Precasting can greatly shorten the construction time[57] and therefore reduce revenue loss.

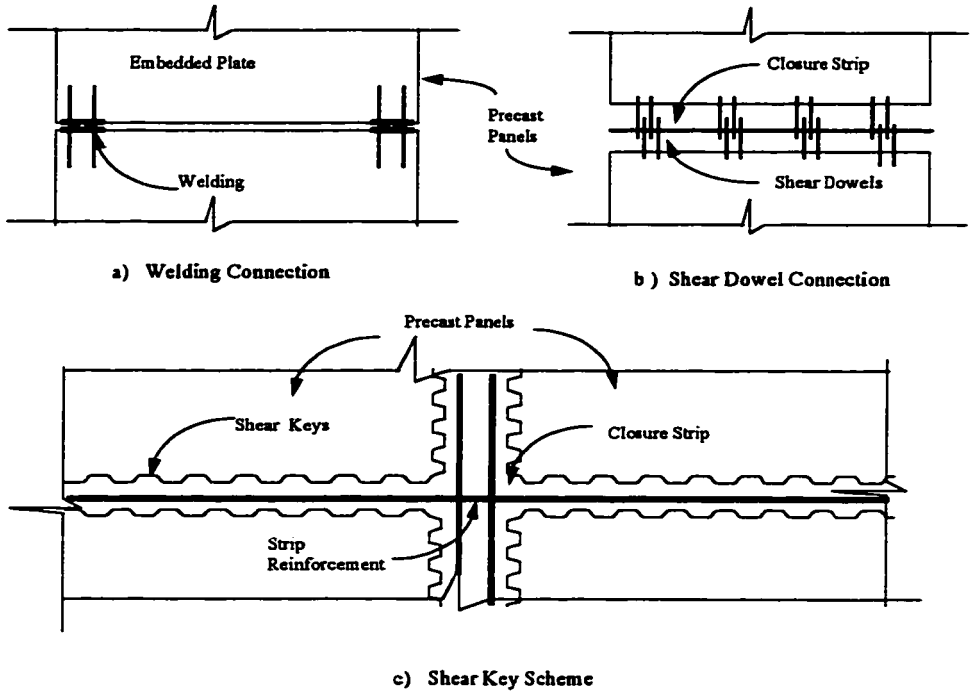

Figure 2.19 Infill Wall Connection Schemes

Several methods have been developed[13,33,34]. Some examples for providing continuity and connection between panels are shown in Figure 2.19. By embedding steel plates, pre-cast panels can be welded to each other. By providing projected reinforcement as shear dowels at panel edges, panels can be grouted with closure

strips to produce a solid wall. By providing shear keys along the panel edges, panels can be grouted with closure strips. Nevertheless, connections between panels and existing frame elements remain a major problem for using precast infill techniques. Grout alone may not develop sufficient shear transfer at the interface between infill-wall panels and frame elements. It is also difficult or costly to connect the infills with the frame through the use of welded panels or shear dowels along a panel-frame element surface.

Currently used infill-wall techniques suffer from two difficulties --- the boundary element (column) strength inadequacy and interface force transfer. A scheme which can minimize these difficulties is desired for frame structural rehabilitation with infills.

2.5 VERTICALLY POST TENSIONED PRE-CAST INFILL WALL

In this project, a vertically Post Tensioned Pre-cast-infill-Wall (PTPW) system was investigated. The intent was to reduce strengthening construction time, to provide the potential to reduce cost, and to solve connection and boundary column strength problems associated with pre-cast infill-wall techniques. Using precast concrete infill walls and post tensioning boundary columns, as shown in Figure 2.20 and Figure 1.1, to strengthen and repair nonductile reinforced concrete frame structures result in a technique that takes the advantage of the shear capacity of infill walls and the moment capacity afforded by post-tensioning tendons adjacent to the boundary columns. In this project, model structural experiments of PTPW system were conducted, analysis models of PTPW system were developed, and foundation effects associated with infill-wall and post tensioning were studied.

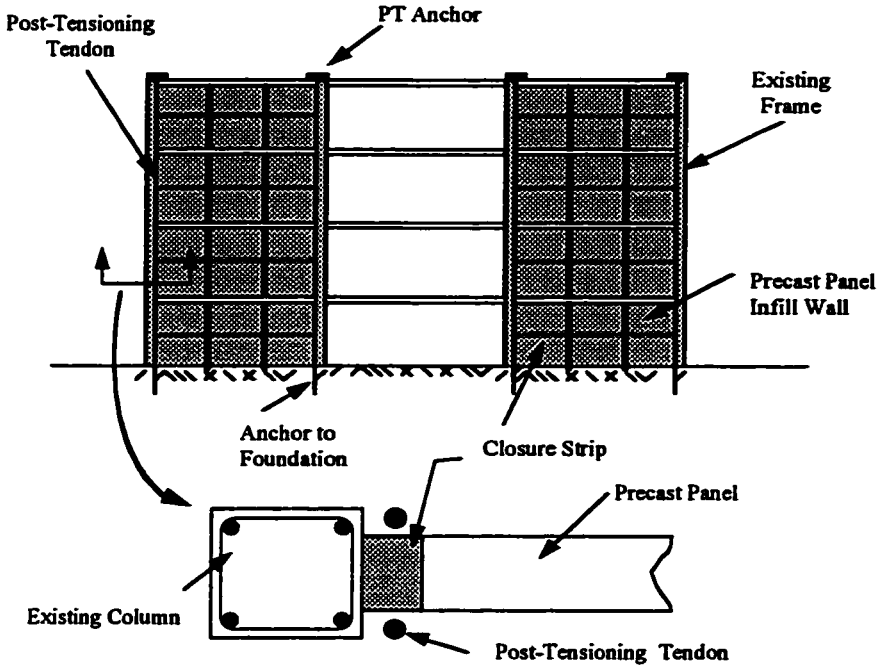

Figure 2.20 Precast Infill Wall with Post Tension System

2.5.1 Closure Strips

Reinforced concrete closure strips, as shown in Figure 2.21, are used to connect pre-cast infill panels. The closure strips are designed to have the following five functions:

1) unite the precast reinforced concrete panels as a solid wall.

2) provide enough reinforcement within the closure strip to compensate for the reinforcement discontinuity between precast reinforced concrete panels.

3) provide space for embedding shear lugs (dowels) between infill-walls and existing frame elements,

4) provide out-of-plane resistance for the infill wall system.

5) provide access for grouting closure strips through shear lug holes across the frame beams between stories.

2.5.2 Shear Lugs

A concept using shear lugs to connect retrofitting elements and existing frame elements, shown in Figure 2.21, was applied in the PTPW system. Steel pipes were used as shear lugs to provide shear transfer at the interface between infill-walls and frame elements.

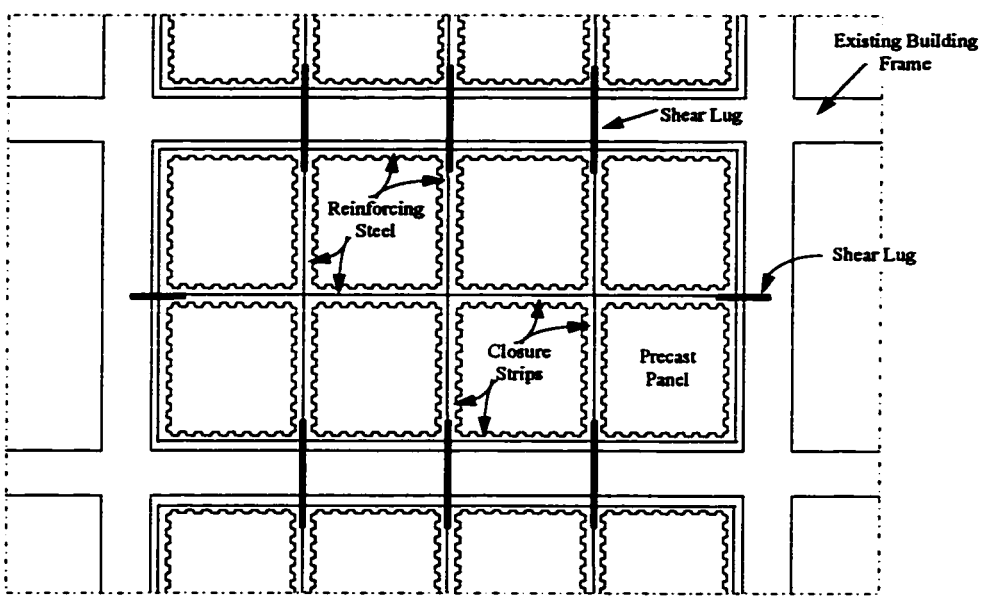

Figure 2.21 Closure Strip and Shear Lug in Precast Infill Wall

One end of the shear lug was embedded in the closure strips and the other end in the holes cored in frame columns or beams as shown in Figure 2.21. Holes cored through beams provided the space to embed the shear lugs, to continue closure strip reinforcement from one level to the next, and to provide access for grouting closure stripe from upper level down to the lower level.

2.5.3 Post Tensioning

As mentioned earlier, frame boundary column strength is a problem in any infill-wall technique. The post tensioning used in the PTPW system is to solve this problem. High strength (Grade 150 DYWIDAG) threaded bars were used as post tensioning tendons in this project.

The tendons were placed adjacent to the frame boundary columns and prestress was provided in the tendons. The prestress in tendons produced pre-compression in the columns to prevent early reinforcement splice failure or column tensile failure subject to lateral load. The tendons were designed to carry the exterior tensile force induced by earthquake load at the frame boundary and made it unnecessary to jacket the boundary columns. The column and infill wall together carried the compression force at the other side to provide the moment capacity in the PTPW system.

2.5.4 Structural Analysis of PTPW System

Due to the unique aspects of PTPW system behavior, no suitable non-linear computer program was available for use to analyze earthquake response of PTPW systems. A post tensioning element model was created. Non-linear elastic models of structural hysteretic response were developed based on structural test results. A computer program IDARC-PT was developed through modification of existing

program IDARC. Simulations were conducted using IDARC-PT and calibrated to give results that matched the experiment very well.

2.5.5 Foundation Performance of PTPW System

A critical problem associated with infill-wall techniques is the foundation performance. An experimental investigation of foundation effects is too costly and beyond the scope of this project. Analytical models of foundations were established. Foundation simulations were conducted using program IDARC-PT. Foundation behavior and foundation effects on a PTPW system were studied. Foundation-post tensioning and foundation-infill wall interactions were investigated through foundation simulation.

Experiments and analyses showed that the PTPW system has great potential for strengthening or rehabilitating reinforced concrete frame structures. In the following chapters, the experimental and computer simulation results are discussed, and proposals for design, analysis, and construction are provided.

CHAPTER III
CONNECTION TESTS

3.1 INTRODUCTION

To understand PTPW system behavior under earthquake excitation, laboratory experiments were conducted. The experiments included structural connection tests and a large scale model structure test. In the structural connection tests, performances of infill panel to panel connections and infill panel to existing structural element connections were investigated. In the model structure tests, characteristics of an existing reinforced concrete frame structure retrofitted with a pre-cast infill-wall and boundary column post tensioning system was studied. A cyclic loading history was used for all the tests to simulate earthquake loading.

3.2 CONNECTION TEST VARIABLES

A PTPW system is intended to take advantages of pre-casting method to reduce structural retrofitting time and cost. An infill wall can be built up with multiple pre-cast panels connected to each other through the use of closure strips and connected to the existing frame by means of shear lugs. Details of the closure strip and the shear lug are the key features in developing pre-cast infill walls for retrofitting concrete frame structures. Whether a structure can be effectively retrofitted with pre-cast units depends on the performances of closure strips and shear lugs. The connection experiments focused on studying the behavior of closure strips and shear lugs.

The connection test specimens were designed to conform with typical infill wall construction procedures and structural details. During retrofitting construction, it was anticipated that pre-cast reinforced concrete panels would be moved horizontally and vertically by a forklift or other lifting equipment within a building. The panel size and panel weight were selected for facility of movement during the construction process. Considering forklift capability, manual operations and building accessibility, a panel with a weight of around 1,000 pounds and longest dimension of about 5 feet was considered suitable for a PTPW system. It was considered that panels with plan dimension of 40" x 40" and a thickness of 6 in. or 4 in. as shown in Figure 3.1 were appropriate for retrofitting a 2/3 scale model structure.

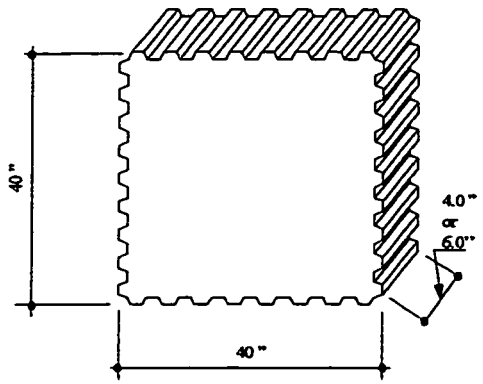

Figure 3.1 Panel Dimension

The connection specimen was designed to represent a subassembly containing a panel to panel or panel to frame connection. Final specimen dimensions shown in Figure 3.2 was selected with a size of 42 in. x 36 in. to fit the dimensions of a shear load test setup available in the Ferguson Structural Engineering Laboratory, at the University of Texas at Austin. The subassembly of a closure strip specimen consisted of four small panel segments and the subassembly of a shear lug specimen consisted of an existing frame segment and two small panel segments as shown in Figure 3.3. The panel segments were constructed with a thickness of 6" or 4" and the frame segments were constructed with a 18"x18" section. All pre-cast segments were united by closure strips.

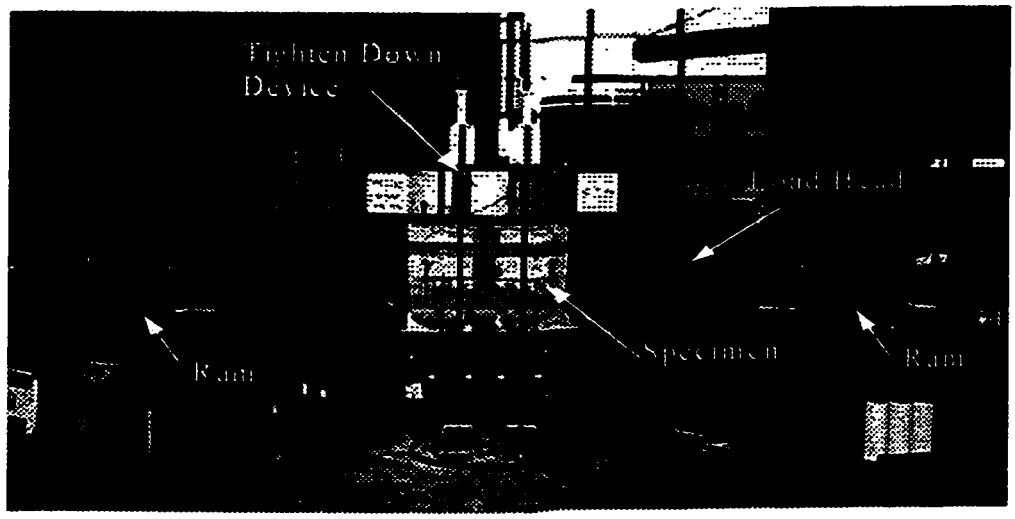

Finger 3.2 Connection Specimen Test Setup

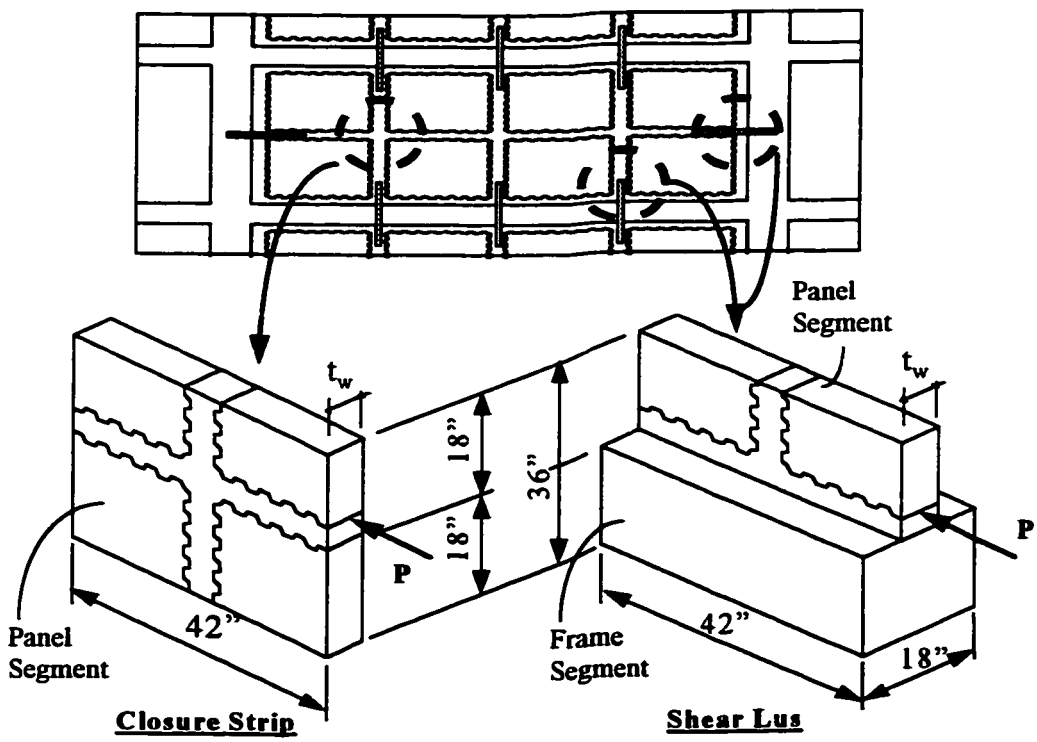

Figure 3.3 Connection Specimen Dimension

The panel segments were reinforced with two layers of 4x4 - w2.9 x w2.9 welded wire fabric which met the minimum requirement of current code of ACI-318-89. The frame segments were reinforced with 4-#7 (one at each corner) to represent existing frame beams or columns. A total of fourteen closure strip specimens and four shear lug specimens were constructed and tested under direct shear loading. The term "direct shear" describes loading behavior under the setup in which large shear can be produced along the critical interface. However, in the tests, both shear and moment were produced under testing load and their effects on the specimen behavior which will be discussed in Chapter IV.

Though an infill wall would never be subjected to only direct shear under lateral load, the direct shear test is convenient for examining the influence of various detailing options on shear transfer between panels or between panels and frame elements.

3.2.1 Closure Strip Variables

Building up an infill wall with precast units is realized through the use of closure strips. The effectiveness of closure strips is dependent on meeting five specific functions as described in Chapter II and also on reducing construction time and effort. The tests focused on an investigation of the design effectiveness and the construction convenience of closure strips. Several factors that might affect closure strip performance were considered in selecting the following variables.

3.2.1.1 Strip Dimension

The most direct factor influencing closure strip function and construction is its size. The closure strip must large enough to permit placement of continuous reinforcement along the closure strip to compensate for the reinforcement discontinuity between pre-cast panels, to provide enough space for embedding shear

lugs in the closure strip to connect infill-walls and existing frame elements, and to provide necessary access for grouting the infill through shear lug holes in the frame beams.

Construction operations and minimum construction time and cost will be. optimized by reducing the amount of cast-in-place concrete or grout used in the retrofitting construction. Obviously, the smaller the closure strip size designed, the less the on site operation required. The closure strip width will be the same as the pre-cast panel thickness for architectural appearance and construction convenience. The height of the closure strip must be determined based on the space needed for strip reinforcement, shear key and shear lug dimensions, and grout placement.

Closure strip width was either 6 in. or 4 in. in accordance with panel thickness. Closure strip height of 4 in. or 2 in. were considered. Closure strips having a height of 4" could be grouted easily and performed very well. The 2 in. height was abandoned due to insufficient room for reinforcing, shear lug embedding and especially the difficulties in concrete grout placement and consolidation.

3.2.1.2 Shear Key Size, Pattern and Configuration

The function of the closure strips is to transfer shear between panels. An effective technique to provide a sound shear transfer mechanism is to roughen the surface, or to provide shear keys or dowels along the interface. Shear key geometry could be easily constructed by forming the desired keys in pre-cast panel construction. Shear key technology has been developed in the pre-cast concrete industry and provided significant background for the key geometry design used in this project. From experimental studies and engineering practice[5,6,10,26], the size and configuration of shear key should be determined by the function of keys, dimension of element, material and method of grouting.

If high strength grout is used and reinforcement is not placed in the closure strips, the shear key along with the strip can be quite small. However, if concrete with coarse aggregate is used as grout for the strip or if reinforcement is placed in the strip, the strip and shear key have to be large enough to permit grout or concrete placement and reinforcement placement. The shear key behavior is determined by the ratios of the height to the base width and the head width to the base width of the key. To preclude crushing of the key, a ratio of height to base width less than 0.5 is desired. To prevent dislocation or overriding of the key, it is reasonable to choose a ratio of head width to base width less than 1.0 or to incline the key edge greater than 45 degree as shown in Figure 3.4.

As mentioned earlier, the panel thickness was chosen as 6" or 4" and this set the closure strip width. Concrete with small aggregate was used to grout the closure strips. Two sets of shear key dimensions shown in Figure 3.4 were used. Table 3.1 listed the key size and panel dimension for the closure strip specimens.

The key dimensions are:

H_k = 1.0" or 1.5"

W_h = 1.5" or 2.25"

W_b = 2.5 or 3.75"

$\phi = 63.4^\circ > 45^\circ$

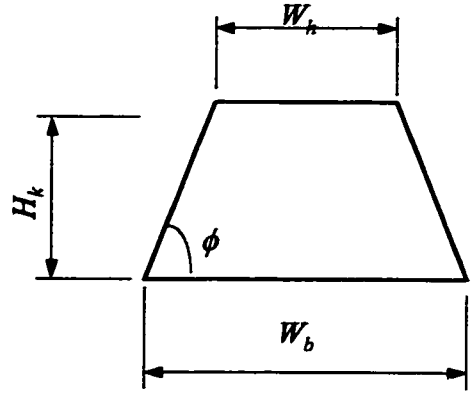

Fig. 3.4 Shear Key Geometry

Table 3.1 Connection Specimen Test Details

Series No.	Specimen No.	Geometric Variables					Material Variables			
		Closure Strip		Shear Key			Concrete Strength			Reinforc.
		Width (in.)	Height (in.)	Height (in.)	Spacing (unit)	Pattern or Embed.	Panel (psi)	Strip (psi)	Strength Ratio	Rebar or Pipe
I	PC-1	6.0	2.0	1.0	1.0	Align	4000	5000	1.250	2-#3
	PC-2	6.0	2.0	1.0	1.5	Align	4000	5000	1.250	2-#3
	PC-3	6.0	2.0	1.0	1.0	Stagger	4000	5000	1.250	2-#3
	PC-4	6.0	2.0	1.0	1.5	Stagger	4000	5000	1.250	2-#3
II	PC-5	6.0	4.0	1.0	1.0	Align	4000	5000	1.250	2-#3
	PC-6	6.0	4.0	1.0	1.0	Align	4000	5000	1.250	4-#4
	PC-7	6.0	4.0	1.0	1.0	Align	4000	3000	0.750	4-#4
	PC-8	6.0	4.0	1.5	1.0	Align	4000	5000	1.250	4-#4
	PC-12	6.0	4.0	1.0	1.0	Align	4000	5000	1.250	6-#5
III	PC-9	6.0	4.0	1.0	1.0	Align	4000	5000	1.250	4-#3
	PC-10	6.0	4.0	1.0	1.0	Align	4000	5000	1.250	2-#4
	PC-11	6.0	4.0	1.5	1.0	Align	4000	5000	1.250	4-#3
IV	FC-3	6.0	4.0	1.0	1.0	Align	4000	5000	1.250	2-#3
	FC-4	4.0	4.0	1.0	1.0	Align	4000	5000	1.250	4-#4
II	FC-1	6.0	4.0	1.0	1.0	F9/W4	4000	5000	1.250	2.5"ϕ
	FC-2	6.0	4.0	1.0	1.0	F9/W9	4000	5000	1.250	2.5"ϕ
	FC-3	6.0	4.0	1.0	1.0	F4/W9	4000	5000	1.250	2.5"ϕ
IV	FC-4	4.0	4.0	1.0	1.0	F4/W9	4000	5000	1.250	2.0"ϕ

* Where Fx/Wy means pipe embedment lengths are x in. into the Frame and y in. into the infill Wall

Keys can be placed along opposite panels to engage each other with a small gap, as shown in Figure 3.5a provided a flowing grout is used. Unfortunately, such an ideal key pattern was impossible for the closure strip in this project, not only because concrete grout was selected but also to accommodate five-function requirement discussed in Chapter II for the closure strips.

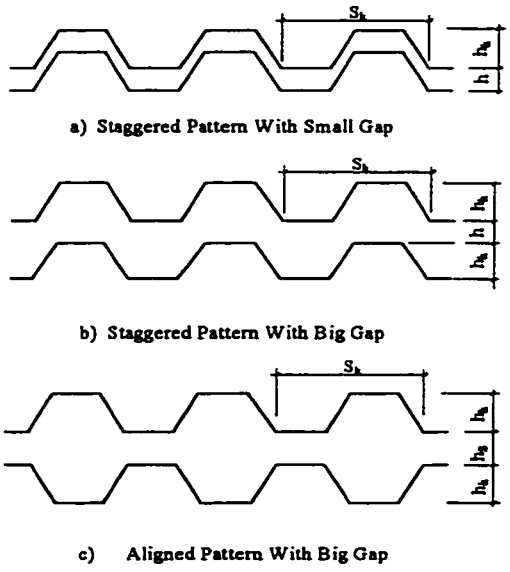

a) Staggered Pattern With Small Gap

b) Staggered Pattern With Big Gap

c) Aligned Pattern With Big Gap

Fig. 3.5 Shear Key Patterns

To meet all the designed functions, the gap between the panels could be enlarged and a staggered key pattern was used as shown in Figure 3.5 b. However, this staggered key pattern was inconvenient for pre-casting operation and for closure strip grouting. Therefore, another option, an aligned key pattern, was adopted for ease of fabrication and construction. Both staggered and aligned key patterns were adopted in closure strip specimen tests and their performance is discussed in Chapter IV.

3.2.1.3 Strip Reinforcement

As mentioned earlier, panels were reinforced with two layers of 4x4-w2.9xw2.9 welded wire mats as shown in Figure 3.6. The panel reinforcement did not protrude from the panel nor extend into the shear keys to eliminate fabrication difficulties and to reduce construction time and cost. For connecting panels, continuous reinforcement was placed in the closure strip, especially in the vertical strip.

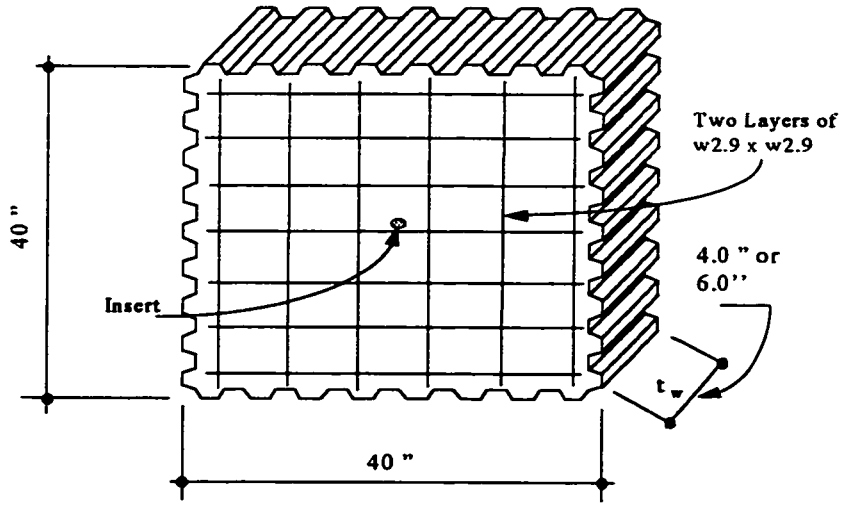

Figure 3.6 Precast Panel Reinforcement

Closure strip reinforcement plays multiple roles in a PTPW system. Continuous reinforcement through vertical closure strips compensates for reinforcement discontinuity between panels. Closure strip reinforcement can be extended through cored holes in existing frame beams and columns to connect infill walls between stories and to attach the infill to the existing frame structure. Moreover, closure strip reinforcement is also the key anchorage to resist out-of-plane actions under an earthquake excitation normal to the wall.

Additionally, closure strip reinforcement should meet the minimum requirements for shrinkage and temperature effects. In the tests, 2-#3 bars were placed in all horizontal and vertical strips. The bars were anchored at the ends of bars with steel plates welded to the bars as shown in Figure 3.7. To investigate vertical reinforcement effects on shear transfer along the horizontal plane (interface), different amounts of vertical reinforcement were studied.

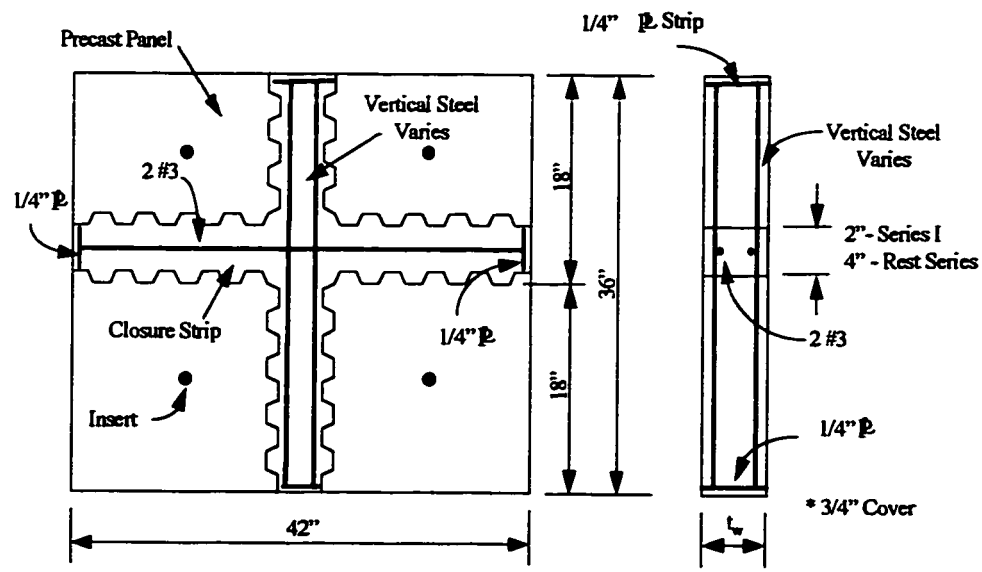

Figure 3.7 Closure Strip Specimen Fabric Details

3.2.1.4 Panel and Grout Strength

An infill wall is constructed by completing the closure strips with on-site grouting (casting) operations. To preclude failure in the closure strips, the grout is generally designed to have a strength higher than the panel strength. However, the quality and strength of the closure strip concrete may depend on consolidation as well. It is desirable to have similar panel strength and grout strength for compatible performance. If the materials have similar characteristics, it is likely that good bond and adhesion will develop and stress concentration at material boundaries will be reduced. Therefore, the ratios of grout (closure strip concrete) strength and panel strength were chosen to be greater than 0.7 and less than 1.5. Different strength ratios were considered by changing grout strength to demonstrate the grouting quality and to investigate the grout effect on the specimen behavior.

All factors including panel dimension, shear key geometry, strip reinforcement, grout strength and strength ratio of strip and panel concrete were set as variables in the closure specimen tests. The effects of these variables on specimen behavior will be discussed in detail in the next chapter.

3.2.2 Shear Lug Variables

Since the existing frame element had a smooth surface and it was decided that the surfaces would not be roughened, mechanical shear dowels were needed. To facilitate shear transfer along the interface between the precast infill wall and existing frame, a special shear dowel or shear lug made of a steel pipe was embedded in the interface between infill and existing frame elements as shown in Figure 3.8. Steel pipe shear lugs were placed in the closure strip and anchored into the frame elements through holes cored (or formed) in the elements representing existing columns or

beams. To investigate the shear lug performance, several variables were studied in the tests.

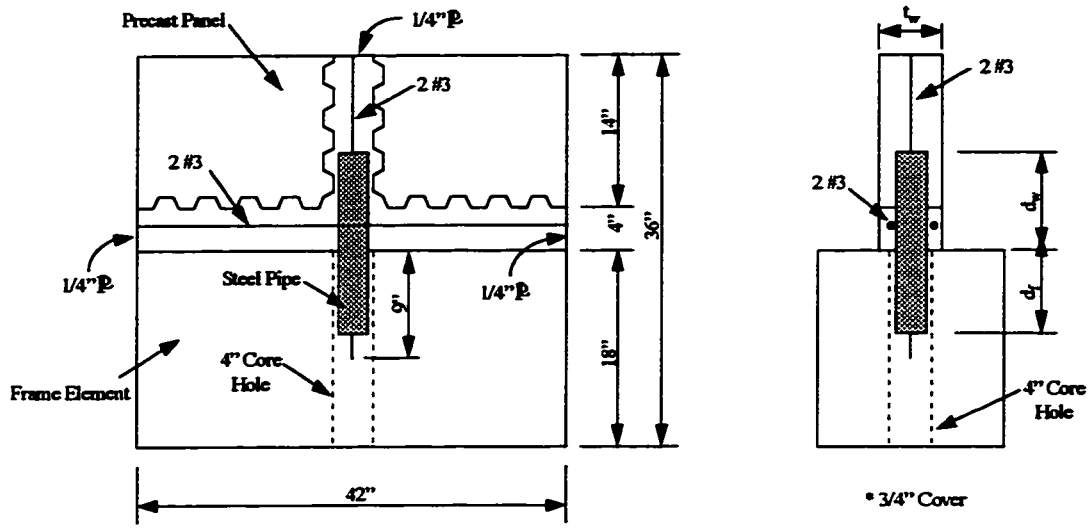

Figure 3.8 Shear Lug Specimen Fabric Details

3.2.2.1 Width of Strip

As mentioned, closure strips must provide embedment space for shear lug placement. Since the strip height was set as 4 in. to provide space for reinforcement placement and grouting operation, the strip width was the only dimension that was varied in the shear lug tests. Strip width corresponding to the panel segment thickness of 6 in. or 4 in. was considered in the shear lug tests.

3.2.2.2 Size of Steel Pipe

A short segment of steel pipe was used as a shear lug for shear transfer along the infill-frame interface. The pipe size had to fit in the infill thickness and the space provided by the closure strip. The pipe shear capacity was designed to provide shear transfer consistent with the infill and frame concrete bearing capacity. Considering

all factors, extra strong pipes with outside diameters of 2 in. and 2-1/2 in. were used as shear lugs in the investigation.

3.2.2.3 Length of Pipe Embedment

Considering shear lug fabrication convenience and infill and frame concrete bearing capabilities, the embedment length of the pipe into the existing frame or into the infill side was designed to prevent concrete bearing failure before shear lug yielding. Different embedment lengths were examined as shown in Table 3.1.

3.3 SPECIMEN CONSTRUCTION

Fourteen closure specimens and four shear lug specimens were designed and constructed in four series or groups as shown in Table 3.1. In each series, variables were changed according to construction experience and test results from the previous series.

3.3.1 Specimen Design

The variables were classified into two categories as geometric variables and material variables. As shown in Table 3.1, geometry variables include panel thickness, closure strip height, shear key size and patterns, and material variables consist of closure strip reinforcement, concrete strength ratio of panel or frame segment to grout, shear lug size and embedment length.

3.3.2 Panel and Frame Segment Construction

Following fabrication of forms with the desired geometry and preparation of reinforcing, the panel segments were cast in a flat position while the frame segments were cast vertically as shown in Figure 3.9a and 3.9b.

Figure 3.9a Precast Panel Formwork and Reinforcement

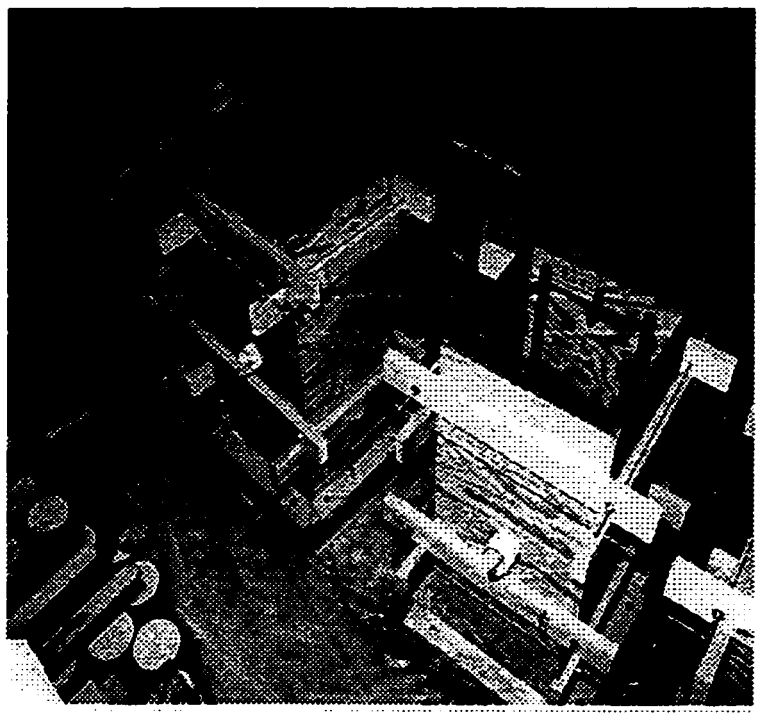

Figure 3.9b Frame Segment Formwork and Reinforcement

Each panel segment had two smooth edges and two keyed edges. The keys were formed using fabric form-keys (inserts) along the specified edges of the formwork. The form-keys (inserts) were made of hard wood lumber and attached with screws to the formwork. As shown in Table 3.1 and Figure 3.4, key heights of 1.0 in. and 1.5 in. were used.

After the segments were cast, they were cured with wet burlap for seven days and then were removed from the formwork and stored. Lifting inserts were placed in every panel and frame segment for ease of lifting and support during construction of the test specimens. Companion concrete cylinders for use in determination of concrete strength were cast and cured with the same manner.

3.3.3 Construction of Closure Strip Specimens

A closure strip specimen was assembled with four concrete panel segments joined by horizontal and vertical strips (grout). The closure strip specimen was grouted in an upright or vertical position, as shown in Figure 3.10, to simulate infill wall assembly construction in frame retrofitting.

3.3.3.1 Reinforcing and Anchorage

Reinforcement was placed through the closure strips. 2-#3 were used in all horizontal strips for all closure strip specimens. Vertical reinforcement was varied among specimens as indicated in Table 3.1. Steel plates were welded to both ends of the bars to provide anchorage. Meanwhile, the anchorage plate dimensions were designed to coincide with the height of the horizontal strip or the width of the vertical strip. The top anchorage plates for vertical rebars were narrow plates to leave an opening for placing grout.

3.3.3.2 Supporting and Formwork

Steel angles (L3x3x3/8) were used to support panel segments during assembly. As shown in Figure 3.11, the steel angle with required core dimension was tightened to the bottom panel segment insert on one end and to the top panel segment insert on the other. Plywood washers were used to enlarge the friction surface. The bottom panel held the top panel in position without any other support. The horizontal strip height was formed by the location of holes cores in the angle. The vertical strip width was formed by the dimension of vertical bar anchorage plates which were designed with the same dimension as the strip width as mentioned earlier. The strip dimension and panel alignment were finally adjusted by using the strip formwork.

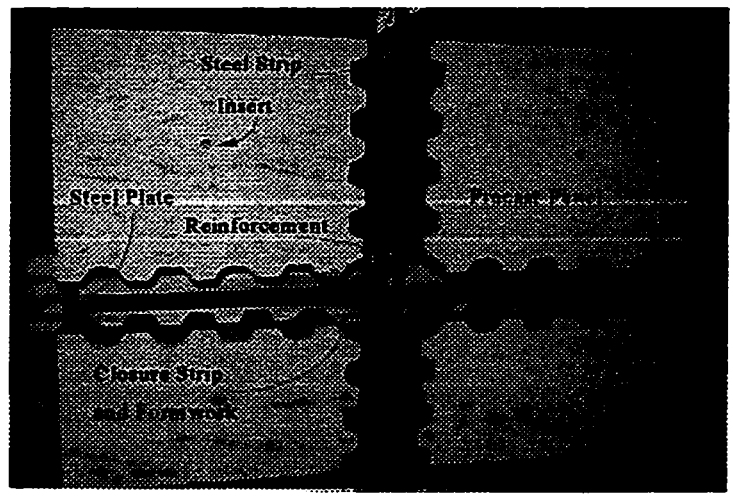

Figure 3.10 Closure Specimen Grouting Scheme

Plywood was used on both sides of strips and secured with all-thread bolts. After final strip dimensions and panel alignments were made, the formwork was tightened from both sides to hold the panel in position.

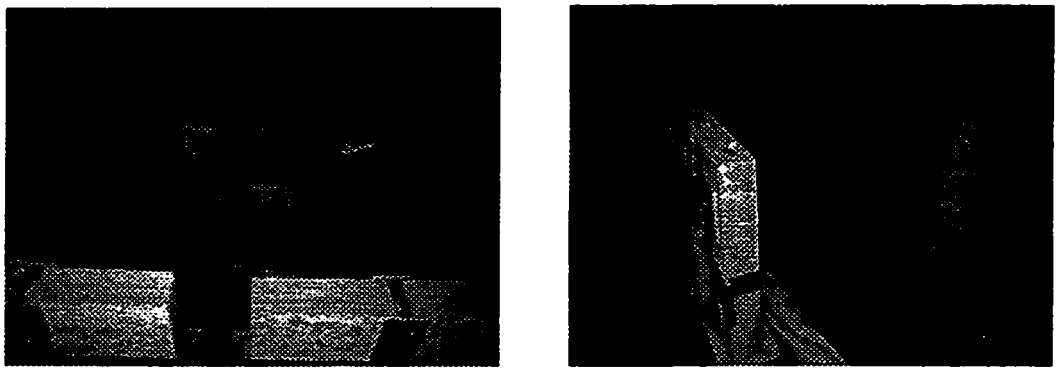

Figure 3.11 Closure Specimen Assembly Supporting

3.3.3.3 Grouting and Vibration

Concrete grout could be placed from the top of the vertical strip to fill both the vertical and horizontal strips. As mentioned earlier, narrow anchorage plates were used to leave an opening in the top of vertical strip. The vertical strip could be well consolidated by direct insertion of the vibrator to the bottom of specimen. However, this method was not acceptable for horizontal strips with a small height. Trial grouting using this method failed for a strip with a height of 2.0 in.. Therefore, another option, using a plywood trough shown in Figure 3.12a, was adopted for specimens PC-1 through PC-4 (Series I) which had 2.0 in. strip heights. The trough permitted easy vibrator access through the key openings and allowed visual monitoring of grouting operations and consolidation. However, the trough method wasted concrete, labor, and time because concrete that projected from the panel surface had to be removed and the surface had to be finished before concrete hardened.

To alleviate difficulties in grouting the horizontal strip, the strip heights were enlarged. Specimens PC-5 through PC-14 were designed with horizontal strip

heights and vertical strip widths of 4.0 in.. To consolidate horizontal strips, air bubbles trapped at the top of keys in the horizontal strips had to be avoided.

Figure 3.12a Trough Method of Strip Grouting

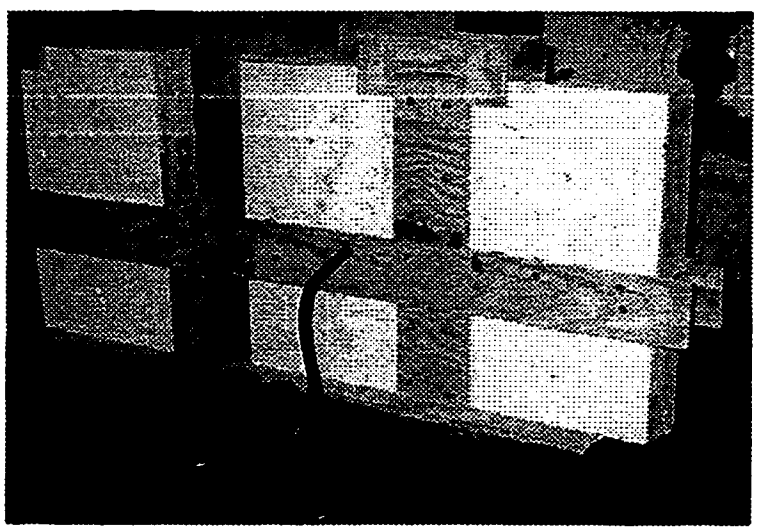

Figure 3.12b Direct Pouring Method of Strip Grouting

In order to displace the air and to vibrate the horizontal strip, small holes with a diameter slightly greater than the vibrator head were drilled along the horizontal strip forms as shown in Fig 3.12b. A plywood lid pinned with a nail was provided for each hole. The lid permits the hole to be opened when the vibrator is inserted and to be blocked after consolidation is achieved and the vibrator is removed. The larger the hole, the easier it is to insert the vibrator and the larger the volume of concrete that is vibrated. However, if the holes were too large, there was a back flow of concrete through the space around the vibrator head. Though the smaller hole prevented concrete backflow, it reduced the volume of grout that could be effectively vibrated and the hole often clogged with aggregate which delayed the vibration. In any case, the insertion of vibrators into the grout strips worked well and proper grout consolidation was achieved for horizontal strip.

3.3.4 Construction of Shear Lug Specimens

At the intersection of the closure strip with the frame segment, the shear lug was positioned so that it was embedded into a hole in the frame segment as shown in Figure 3.13. The holes cored or formed in frame segments had three functions:

1) to embed the shear lug,

2) to anchor vertical closure strip reinforcement,

3) to facilitate placement of closure strip concrete.

The size of the hole was determined based on the width of the beam, the size of the shear lug pipe, and the number of closure strip bars. A 4.0 in. diameter hole was reasonable and functioned well with 2-1/2 in. pipes.

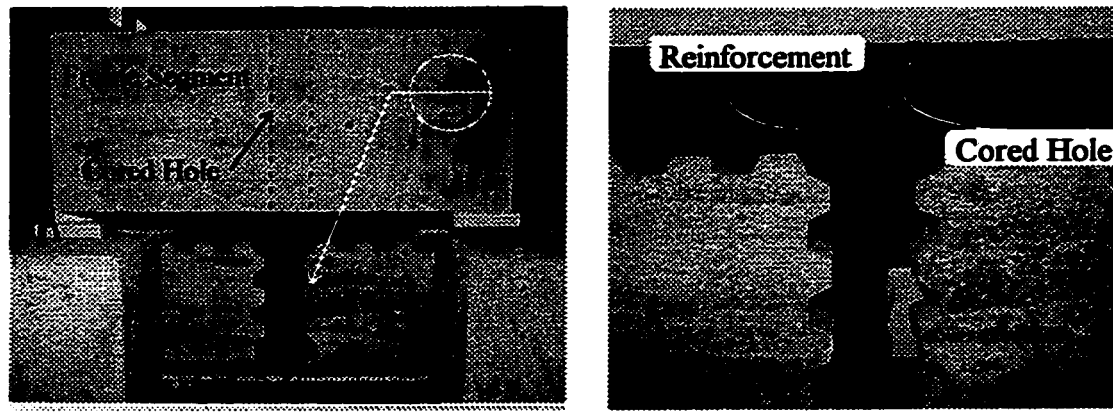

a) Assembly and Support b) Detail A

Figure 3.13 Shear Lug Specimen Assembly Scheme

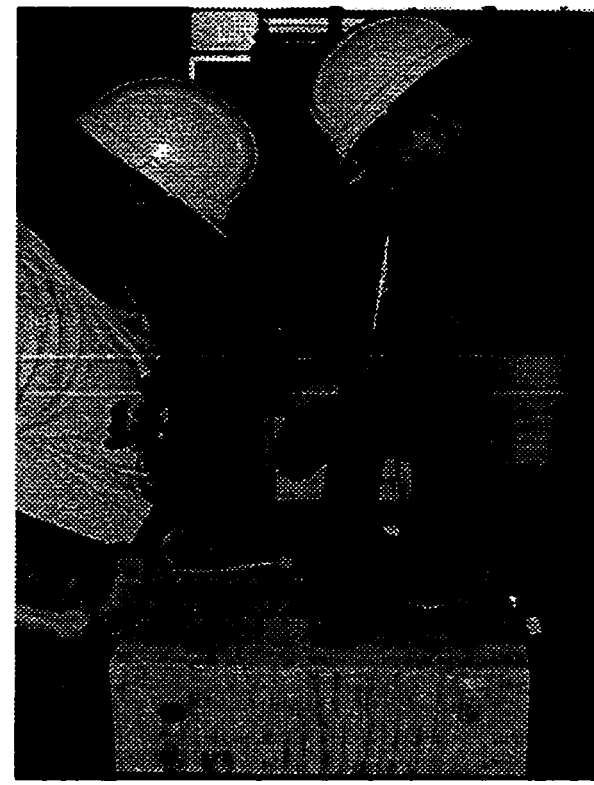

Figure 3.14 Steel Pipe Embedding Scheme

A steel pipe with a 2.0 in. or 2-1/2 in. outside diameter was embedded in the 4.0 in. hole in the concrete frame segment. Prior to embedding the pipe into the interface, concrete was cast from above through the cored hole into the closure strips to simulating casting through a floor beam. Before the grout concrete set, the pipe was inserted into the closure strip through the hole as shown in Figure 3.14. While the concrete was being vibrated, the pipe settled into the grout and stopped at the designed position at where threaded bars were placed across the strip forms.

3.4 MATERIAL PROPERTIES

For cost reduction and for operation convenience, normal concrete and steel should be used as retrofitting materials. To simulate field construction, structural connection specimens were constructed using normal Portland Cement for concrete mixtures and Grade 60 steel was used as reinforcement.

3.4.1 Concrete Aggregate

A 3/8 in. coarse aggregate was used for all concrete and grout mixtures[25,36,39]. This relatively small coarse aggregate was needed to facilitate placement of concrete in congested shear key regions of panel segments, and to promote workability and flowability for concrete. The 3/8 in. aggregate worked very well for both panel and frame segment concrete and for the strip grout.

3.4.2 Concrete Strengths

As mentioned earlier, the strength ratio of grout to panel or frame segment was desired to be in a range of 0.75 to 1.50. For example, panels of PC-1 through PC-4 were designed with a nominal strength of 4,000 psi and the grout concrete had a

nominal strength of 5,000 psi. For each series of connection specimens, panel and grout concrete mixtures are shown in Table 3.2.

Table 3.2 Concrete and Grout Mixtures

Mixture Batch	Segment Concrete		Closure Strip Concrete Grout				
	Panel Segment	Frame Segment	Series I	Series II	Series III	Series IV	Low Strength
Design Strength f'_c (psi)	4000	3000	5000	5000	5000	5000	3000
Cement (pcy)	470.0	400	564	693	564	693	425
Coarse Aggregate (pcy)	1625.0	1625	1625	1167	1625	1167	1167
Fine Aggregate (pcy)	1655.0	1619	1469	1755	1469	1755	1945
Water (pcy)	250.0	275	280	325	280	325	325
Admixture (ozcy)	20.0	12.0	16.8	27.6	16.8	27.6	-
Superplasticizer (ozcy)	-	-	25.0	25.0	25.0	25.0	-
Nominal Slump (in)	6.0	1.5	4.0	4.0	4.0	4.0	6.0
On Site Slump (in)	6.0	1.0	8.0	8.0	8.0	8.0	9.0
Days to Test	111-136	64-184	57-82	37-163	57-82	37-163	125.0
Tested Strength f'_c (psi)	4000-5100	39000	7200	6900	6000	6600	2650

3.4.3 Concrete Admixtures

As listed in Table 3.2, certain admixtures were used including water reducers and retarders[3,25,36]. All admixture applications met the requirement set by ASTM C494 depending on ambient temperatures. Superplasticizer was used to improve workability characteristics and consolidation for strip grout. In order to maintain concrete strength and improve slump simultaneously, adding superplasticizer to the original mixture at the job site may be necessary. Using a suitable amount of superplasticizer, as shown in Table 3.2, the slump was increased from 4 in. to 8 in. or higher. With a 8 in. slump, the concrete mixture possessed very good workability, and shrinkage and strength characteristics were satisfactory.

3.4.4 Material Strength

The strength of the mixtures at the time of test were higher than designed values. The concrete and grout strengths were determined through corresponding concrete cylinder tests at seven and 28 days after casting. Type I cement was used and Figure 3.15 shows concrete strength gain with time for precast panels and frame segments. At the time the specimens were tested, the last group of companion cylinders were tested and the strengths were listed as tested strength in Table 3.2.

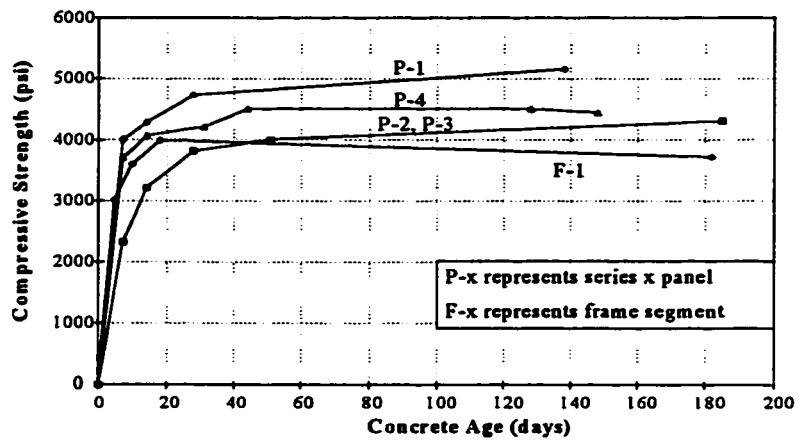

a) Panel Concrete

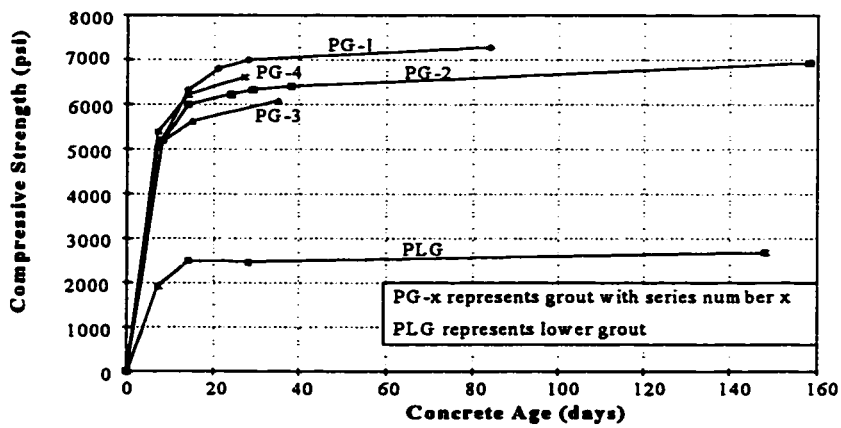

b) Grout Concrete

Figure 3.15 Concrete Strength Gain with Time

The reinforcement and shear lug pipe strength were tested according to ASTM A370-94 specifications. The welded wire fabric had a fracture strength of 72.2 ksi and had no well-defined yield. Closure strip reinforcement yielded at stresses ranging from 63.6 ksi to 73 ksi with ultimate tensile strengths of 101.6 ksi to 112.8 ksi. The shear lug pipe strength had different values according to the pipe size. The pipe with 2.0 in. diameter had a yielding strength of 40.4 ksi and tensile strength of 55.7 ksi. The pipe with 2-1/2 in. diameter had a yield and tensile strengths as high as 53.6 ksi and 71.6 ksi respectively. All the reinforcement and steel strengths are presented in Table 3.3.

Table 3.3 Reinforcement and Pipe Strength

Strength	Material Item					
(ksi)	Wire Fabric	Rebar #3	Raber #4	Rebar #5	2.0" Pipe	2-1/2" Pipe
Yielding	-	63.6	73.0	61.9	40.4	53.6
Ultimate	72.2	101.6	128.8	102.3	55.7	71.6
Fracture	72.2	-	-	-	-	-

3.5 TEST PROCESS AND RESULTS

As indicated in Table 3.1, The specimens were constructed in four groups. Corresponding to the construction time, tests also followed in four series. Table 3.4 outlines the age of each specimen at date of testing. All closure strip specimens as well as shear lug specimens were tested using a test setup available in The Phil Ferguson Structural Engineering Laboratory, The University of Texas at Austin, built in a previous research study.

3.5.1 Test Set-up and Instrumentation

The setup, shown in Figure 3.2, was designed for direct shear testing of concrete interfaces. Two 400-kip hydraulic rams were positioned at both ends of the

setup to provide cyclic load simulation in each directions. A specimen was held in such a way that the bottom portion was held by the base and the top portion was held by a head block. Loading was applied through the head block to impose direct shear to the interface between the two portions. To prevent uplift or restrain vertical dislocation, vertical load can be applied through a vertical tightening device available with the setup.

All specimens were constructed to have an exact dimension to fit the setup. Specimens were seated with a high-strength gypsum (hydro-stone). The interface, either the base line or the top surface of the panel keys, was at the level of applied direct shear. Vertical loading was applied for some specimens as shown in Table 3.4 to restrict uplift.

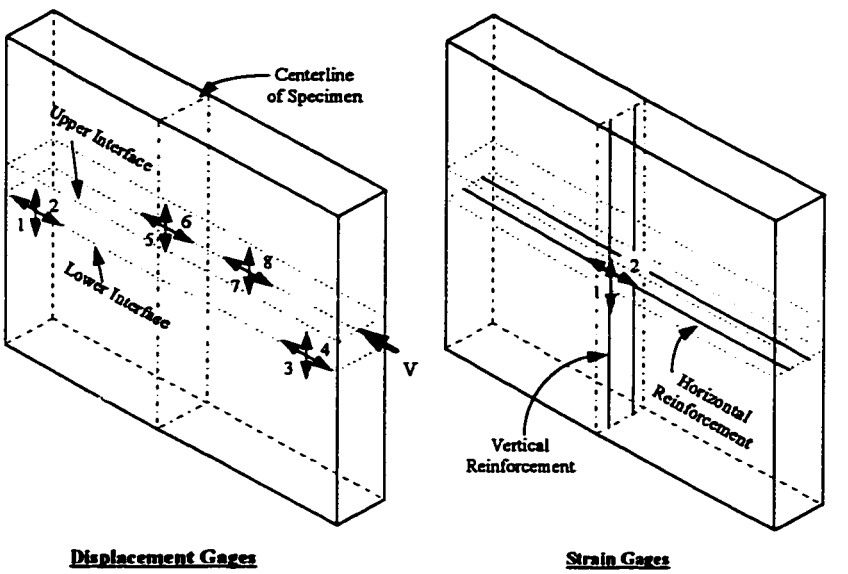

Figure 3.16a Closure Strip Specimen Instrumentation

Response of specimens was monitored through data acquisition devices as shown in Figure 3.16a and Figure 3.16b. Pressure transducers were used in the hydraulic system to monitor test load. Linear displacement transducers were mounted

horizontally and vertically along and above the shear interface to observe and record

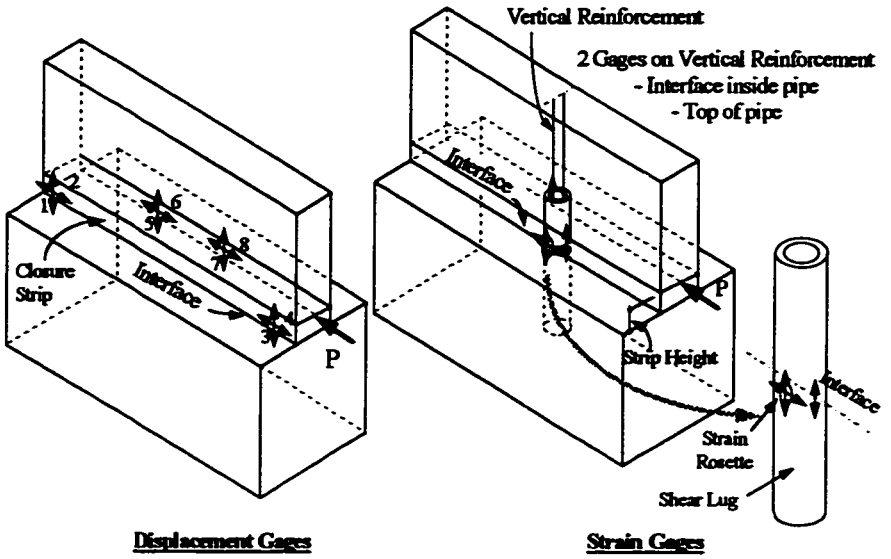

Figure 3.16b Shear Lug Specimen Instrumentation

specimen displacement. Strain gauges were attached to closure strip reinforcement and shear lug pipes. All monitoring devices were connected to a computer data acquisition system.

3.5.2 Test Procedure

The test specimens were subjected to direct shear along the horizontal closure strip. In order to simulate earthquake cyclic load, rams applied loads in alternating directions. The loading process was monitored through pressure transducers, load-displacement plots and computer outputs simultaneously.

The loading history was conducted in two stages of load and displacement control. Before initial cracking occurred, the loading was increased in steps with three cycles at each load levels of 5, 10 and 20 kips. After the specimen cracked and

softened considerably, loading was controlled using horizontal displacement with three more cycles at displacement increments of 0.025, 0.05 and 0.10 in. up to a total displacement of at least 0.4 in..

Because of the loading eccentricities induced due to specimen alignment and deflections of the test setup under load, specimen uplift and dislocation occurred in several tests. To prevent such movement and possible damage to the specimen leading to shear failure at locations other than the critical interface, vertical rods were used to control vertical movement. With the use of the vertical rods, specimen uplift was eliminated.

3.5.3 Test Results

Figure. 3.17 illustrates the load-displacement history for closure strip specimen PC-5 and shear lug specimen FC-3. Similar diagrams for all other specimens are presented in Appendix A. The key values and test results are listed in Table 3.4. The results shown in Figures 3.17a and 3.17b illustrate specimen behavior typical of that was observed in all connection specimens.

From the response diagrams and recorded test data, it was noted that the connection specimens exhibited three distinct stages of behavior - cracking (cohesion for shear lug specimens), ultimate and residual shear strength. The word "strength" denotes the value of lateral load or direct shear reached in each stage in the test.

The three strength levels describe a specimen failure mechanism. Cracking strength represents the range of elastic behavior. Ultimate strength indicates the peak lateral force capacity in the inelastic range. Residual strength indicates the shear capacity maintained through large displacements. Each strength behavior is significant for structural seismic design and retrofitting.

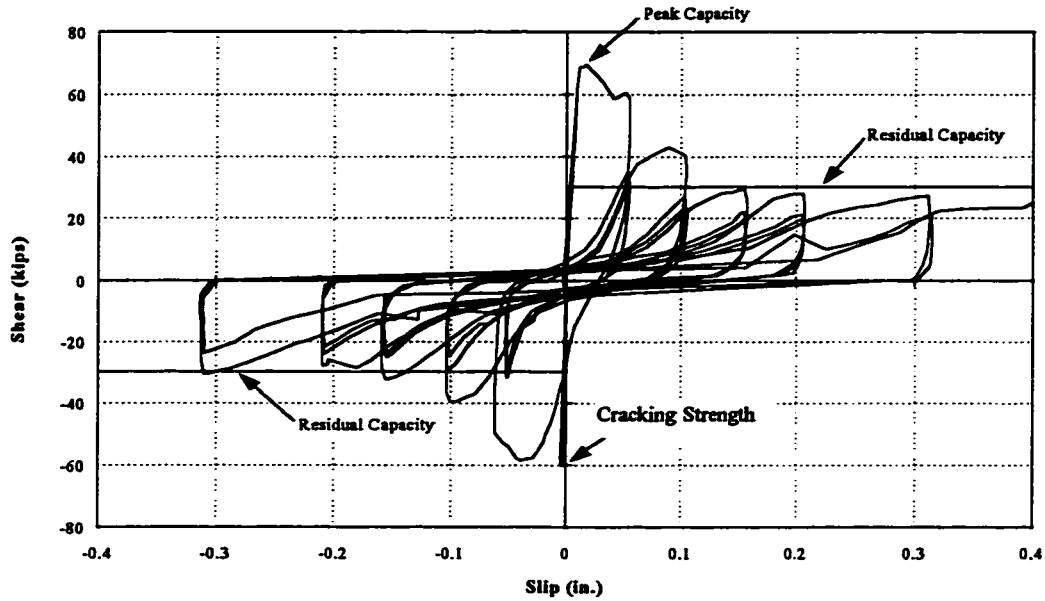

Figure 3.17a Closure Strip Specimen Test Result (PC-5)

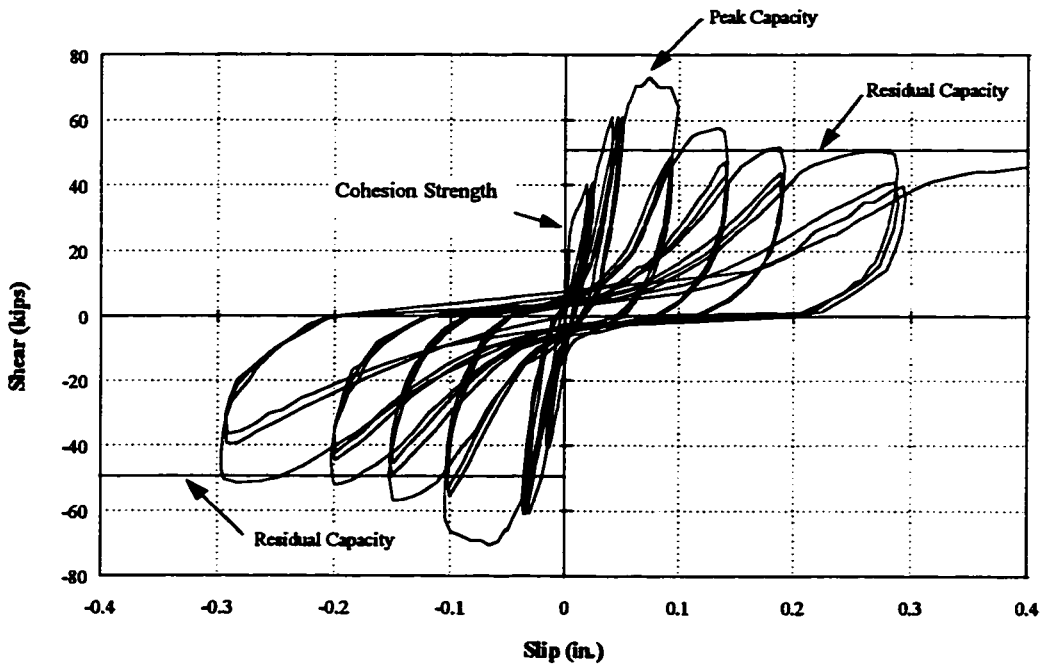

Figure 3.17b Shear Lug Specimen Test Result (FC-3)

The three strength stages coincide with commonly accepted limit states [46] in structural seismic design. Cracking strength is of concern at service limit state under frequent earthquake excitations. Under major earthquakes, the ultimate or peak strength can be used to represent the damage limit state. Residual strength reflects structural ductility and force available at the collapse limit state.

Table 3.4 Connection Specimen Test Results

Specimen Number	Testing Feature				Materia Property				Test Results		
	Test Age		Vertical Load		Rebar or Pipe		Concrete Strength		Specimen Strength (kips)		
	Panel (days)	Strip (days)	Peak (kips)	Residual (kips)	Bar/Pipe Size	A_s (in_2)	Panel f_c' (psi)	Strip f_c' (psi)	Cracking P_c	Ultimate P_u	Residual P_r
PC-1	136	82	-	-	2-#3	0.221	5100	7200	81.0	84.0	30.0
PC-2	125	71	-	-	2-#3	0.221	5100	7200	59.0	62.0	29.0
PC-3	119	65	-	-	2-#3	0.221	5100	7200	69.0	73.0	27.0
PC-4	111	57	-	-	2-#3	0.221	5100	7200	50.0	70.0	28.0
PC-5	64	37	-	-	2-#3	0.221	4000	6400	60.0	70.0	27.0
PC-6	188	161	63	18	4-#4	0.785	4300	6900	60.0	179.0	-
PC-7	162	125	-	-	4-#4	0.785	4300	2650	40.0	102.0	58.0
PC-8	170	143	-	-	4-#4	0.785	4300	6900	60.0	153.0	54.0
PC-9	190	27	-	-	4-#3	0.442	4300	6900	80.0	103.0	45.0
PC-10	175	33	24	8	2-#4	0.393	4300	6000	80.0	109.0	45.0
PC-11	181	36	42	16	4-#3	0.442	4300	6000	84.0	157.0	60.0
PC-12	184	163	82	-	6-#5	1.840	4300	6000	70.0	202.0	-
PC-13	41	24	-	-	2-#3	0.221	4500	6600	55.0	63.0	20.0
PC-14	42	25	-	-	4-#4	0.785	4500	6600	25.0	74.0	25.0
FC-1	50	23	-	-	2.5x9x4	2.250	4000	6300	30.0	62.0	34.0
FC-2	60	29	-	-	2.5x9x9	2.250	4000	6300	35.0	71.0	48.0
FC-3	62	35	-	-	2.5x4x9	2.250	4000	6300	30.0	73.0	50.0
FC-4	45	28	-	-	2x4x9	1.480	4500	6600	25.0	55.0	31.0

It was noted that ultimate and residual strengths were almost directly proportional to the vertical strip reinforcement ratio for the closure strip specimen and steel pipe dimension for the shear lug specimen. However, when the closure strip reinforcement ratio was extremely high, the residual strength was not developed. With very large vertical reinforcement, ultimate strength was reached followed by concrete bearing failure and no yielding of vertical reinforcement. Specimen PC-12 and PC-14 are the examples of concrete bearing failure caused by very high reinforcement ratios.

Further analysis of material and geometry effects on specimen strength behavior will be discussed in Chapter IV.

3.6 SUMMARY

In this chapter, connection specimen details including selection of test variables, design and construction, and test procedures were discussed. The experimental data from these tests provided information essential to design of a PTPW system for retrofitting concrete frame structures. The closure strip designed with 4.0 in. height functioned very well in providing adequate room for reinforcement, shear lug embedment and grouting operations. An easily fabricated shear key played a significant role in forming shear transfer mechanism along the interface between panels. Superplasticized concrete grout with 3/8 in. coarse aggregate worked amazingly well for direct placement of grout from the vertical closure strip to horizontal strips. Consolidation of grout in horizontal closure strips was facilitated very well by vibrating grout through holes in the forms over the closure strip. The insertion of shear lug into the grout prior to concrete setting worked very well. These experiences provided feasible and effective schemes for PTPW system construction.

Connections between elements are the key links to realizing a practical and efficient PTPW system. The response of the connection specimens was characterized by cracking (or cohesion for shear lug specimen), ultimate and residual strength levels. The three strength levels reflect the overall infill wall behavior under cyclic lateral load. Such behavior is vital for structural seismic design for service, damage and collapse limit states.

CHAPTER IV

ANALYSIS OF CONNECTION TESTS

4.1 INTRODUCTION

To investigate the behavior of panel-to-panel and panel-to-frame connections, eighteen specimens were constructed and tested. The specimens were subjected to reversed cyclic loads which were initially applied in a load-control mode. When the stiffness of the specimen decreased considerably, displacement control was used. All joint specimens were tested using the setup shown in Fig. 3.2. This Chapter focuses on the evaluation of connection specimen test results.

4.2 CLOSURE STRIP BEHAVIOR

4.2.1 Test Variable Effects

Test variables considered for closure strip specimens are dimensions of shear keys, size of closure strips, reinforcement of the vertical strip, strength of concrete, and vertical force applied on specimens.

4.2.1.1 Shear Keys

Three dimensions governing key height, spacing and geometry were considered in closure strip tests. Series I specimens were cast initially with different key patterns, either aligned or staggered. Different key spacing in terms of 1 or 1-1/2 unit key lengths were used. The remainder of the specimens were designed using aligned key

patterns but different key heights. Studying the test results shown in Table 3.4, it can be seen that none of the shear key variables significantly affected the residual strength.

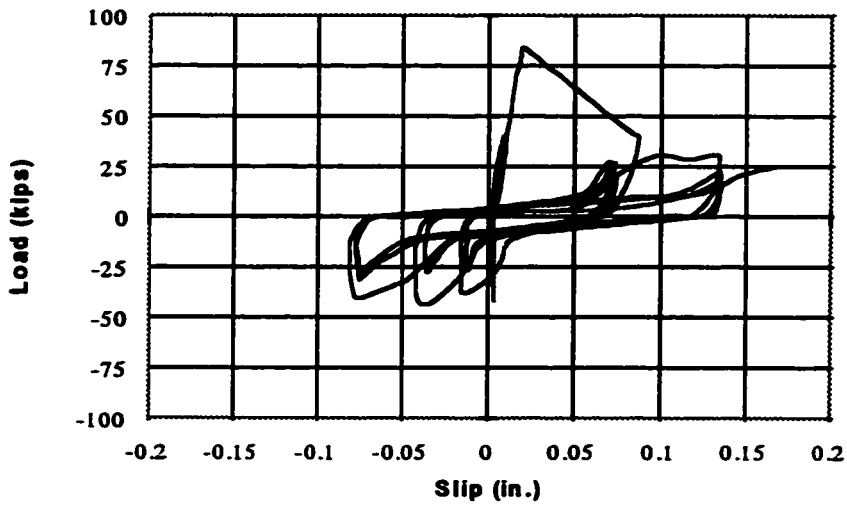

a) Aligned Key Pattern PC-1

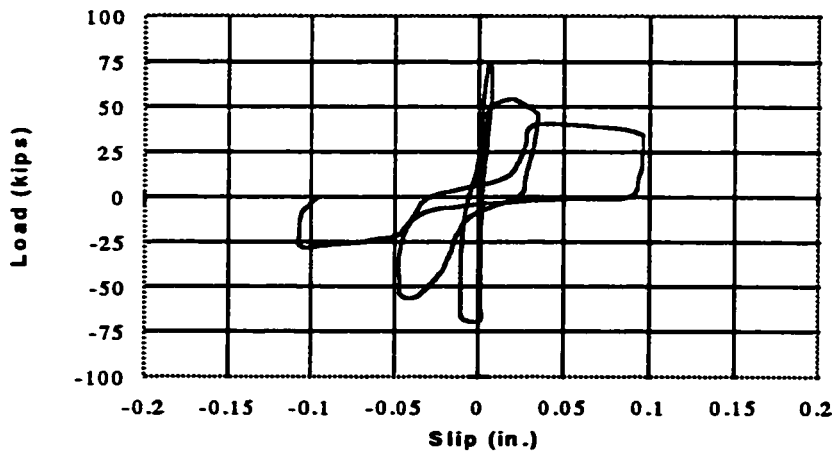

b) Staggered Key Pattern PC-3

Figure 4.1 Comparison of Shear Key Pattern Effects

Comparing the results of specimens PC-1 and PC-3, shown in Figure 4.1, cracking and ultimate strengths were quite similar. Staggered patterns were not used after the series I tests because it was felt that aligned keys would permit more standardization of panel construction and placement and these would be more economical.

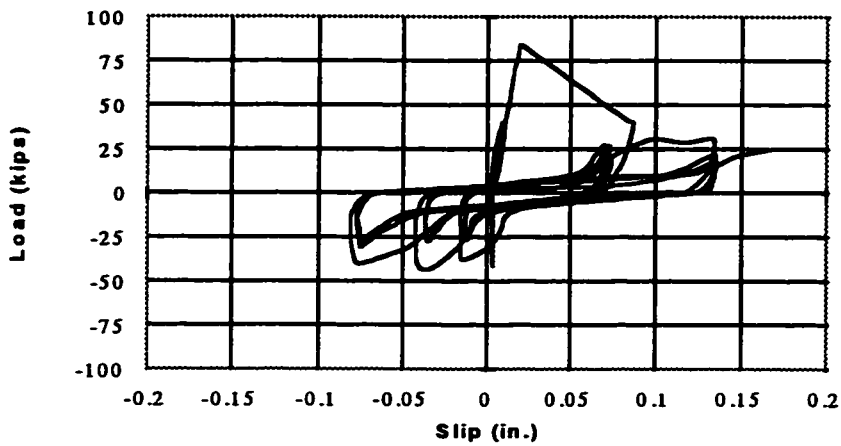

b) Small Spacing PC-1

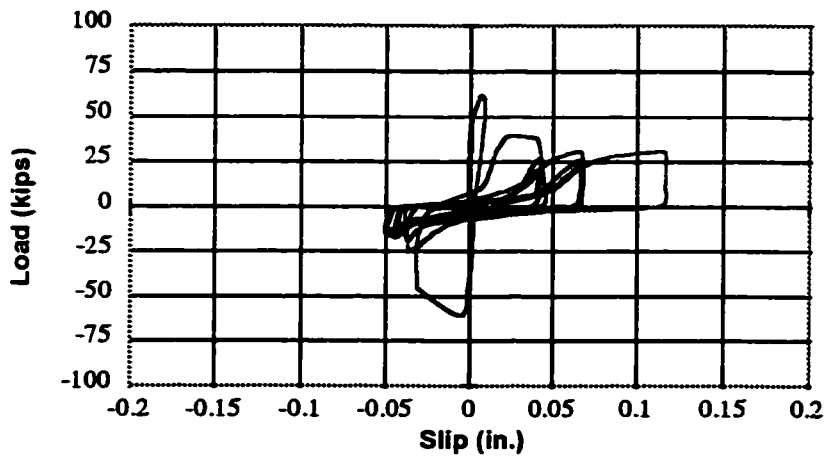

b) Large Spacing PC-2

Figure 4.2 Comparison of Shear Key Spacing Effects

Key spacing affected cracking strength as can be seen in Figure 4.2 by comparing PC-1 with PC-2 (or PC-3 with PC-4). With larger key spacing, PC-2 (or PC-4) had less shear area within the keys along the interface than PC-1 (or PC-3). Because the panel concrete had lower strength than the closure strip grout, the panel keys crushed when the cracking strength was reached. This confirmed the fact that the cracking strength was dependent primarily on the concrete strength and net shear area of panel keys along the interface.

Finally, the key height seemed to affect ultimate strength. Only two specimens, PC-8 and PC-11 were designed using keys with a height of 1.5 in. but with other variables identical to PC-6 and PC-9, respectively. The results indicated that PC-11 reached a much higher ultimate strength than PC-9 even though PC-9 had higher grout strength. However, PC-6 with lower key height than PC-8 reached a slightly higher ultimate strength than PC-8. This may have been the result of other factors or operational errors which will be discussed later. A greater key height should provide a relatively larger space for better consolidation of grouting around keys and sufficient material for good bond of the closure strip reinforcement. Key height is taken into account in evaluating ultimate strength in the next section.

4.2.1.2 Strip Size

The strip width coincided with the panel thickness. In most tests, the panel thickness was 6 in.. Only two specimens, PC-13 and PC-14, were designed with a smaller strip or panel width of 4 in.. Reviewing the results listed in Table 3.4, cracking, ultimate and residual strengths of those two were much lower than PC-5 and PC-6 which were identical except for the panel thickness.

As discussed previously, smaller closure strip heights required a smaller volume of concrete grout but resulted in difficulties for placing strip reinforcement,

embedding shear lugs and especially grouting horizontal closure strips. A strip height of 4 in. was selected over the 2 in. height. On the other hand, the use of a higher strip produced undesired behavior because the distance d_c between the point of load application and the weak interface was increased as shown in Fig. 4.3. Under the same level of direct shear, the interface moment is proportional to d_c. Greater interface moment is imposed on the section as d_c increases. The influence of moment was also considered in ultimate strength evaluation.

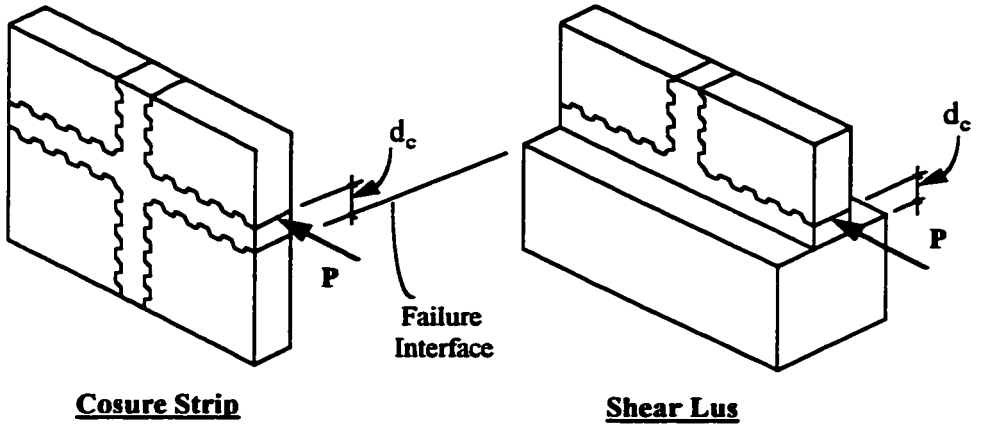

Figure 4.3 Distance (gap) Between Loading-Failure Interface

4.2.1.3 Reinforcement

The test results showed that reinforcement in the vertical closure strips played an important role in determining the ultimate and shear friction strength. Within a certain range, more vertical strip reinforcement resulted in higher ultimate and residual strength. The load-interface slip responses of specimen PC-5 and PC-8 are shown in Figure 4.4. When the vertical closure strip reinforcement was increased from two #3 to four #4 bars, the ultimate strength increased from 70 kips to 153 kips and the residual strength increased from 30 kips to 50 kips. Results of other tests

showed similar ultimate and residual strength increases as vertical strip reinforcement increased.

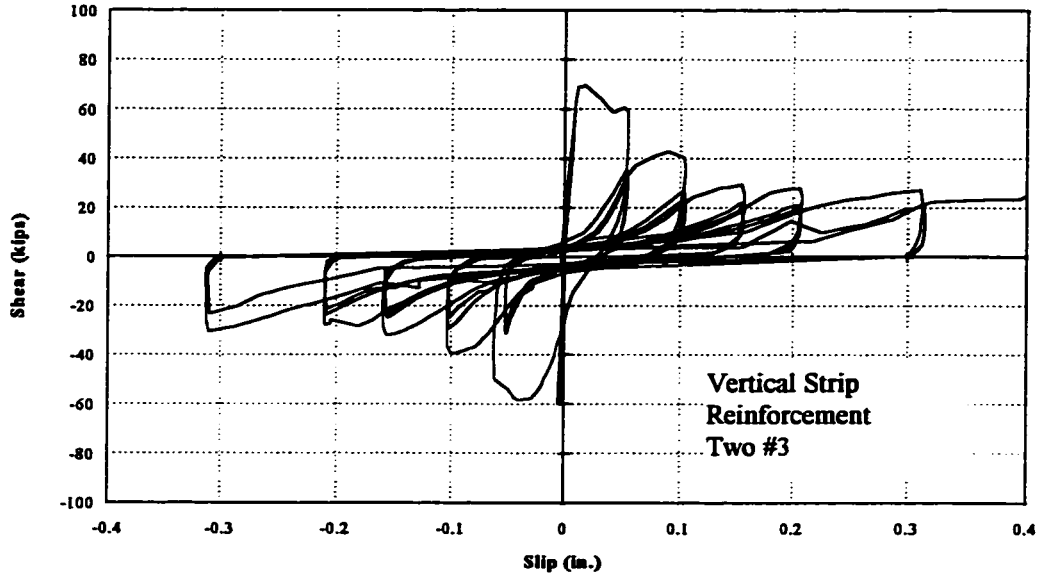

a) Test of Closure Strip PC-5

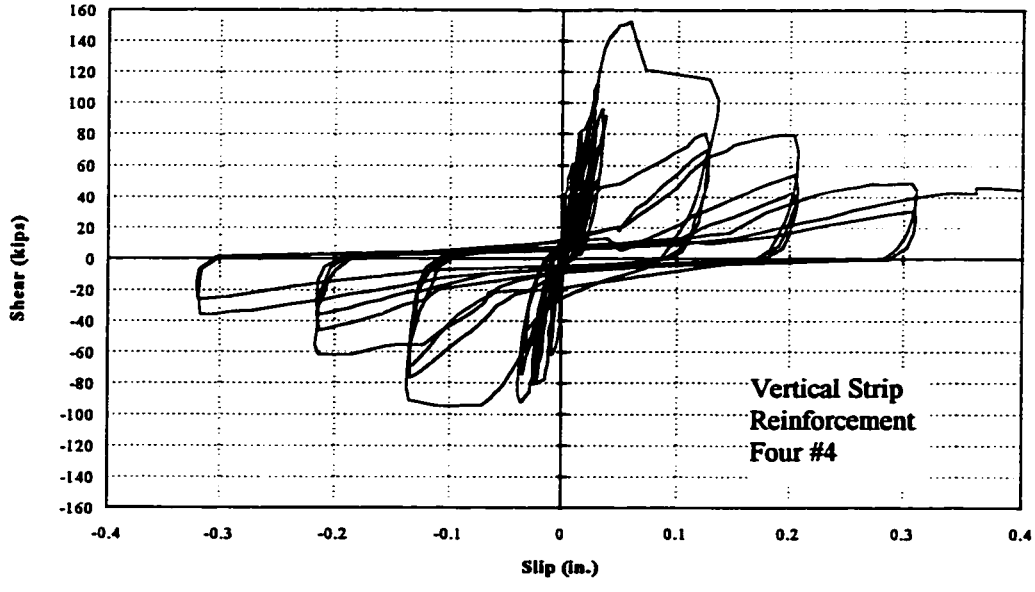

b) Test of Closure Strip PC-8

Figure 4.4 Comparison of Reinforcement Effects

As the direct shear load **P** was applied, an overturning moment was produced as induced by a gap d_c that was observed between loaded panel and the weak-joint interface. The overturning moment produced compression on one side and tension on the other side of the specimen.

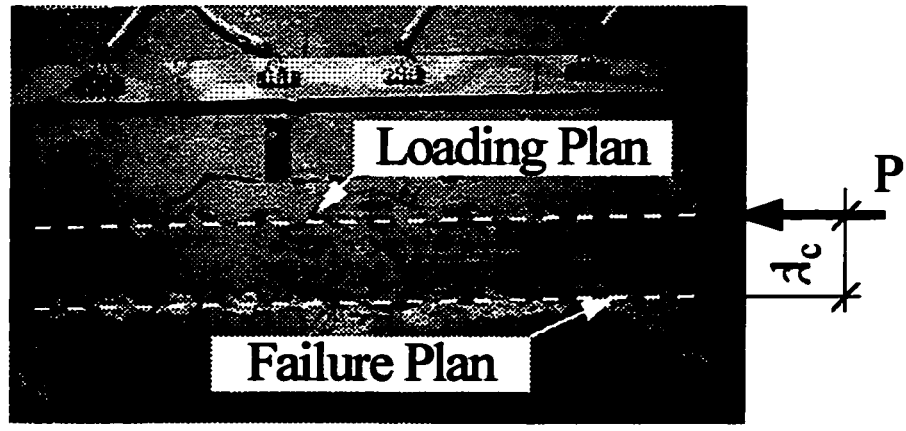

a) Location of Failure Plane and Loading Plane

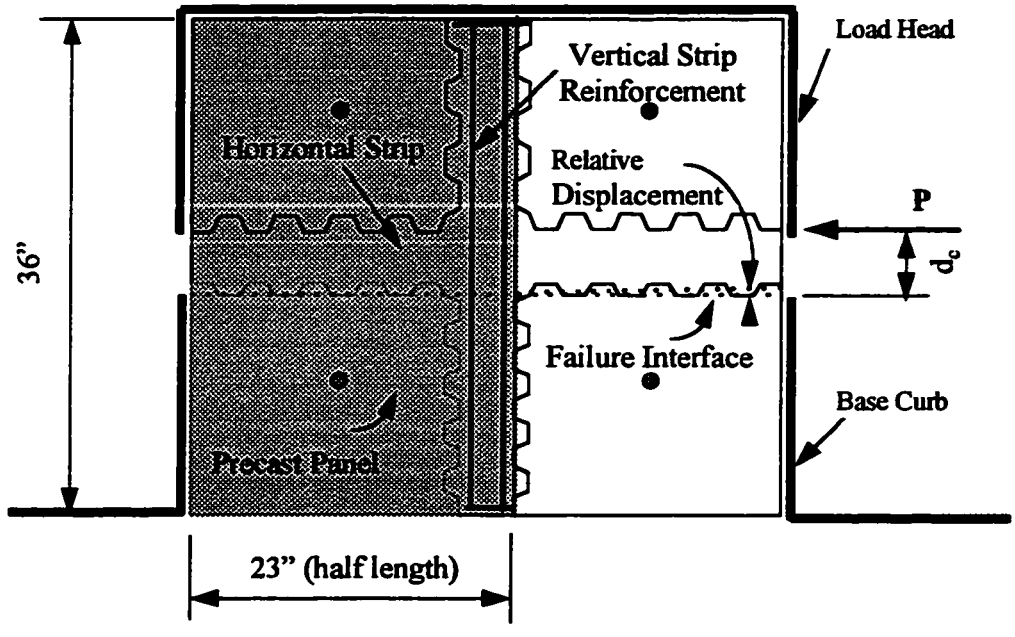

b) Portion of Specimen Resisting Moment

Figure 4.5 Failure Mechanism Under Exterior Moment

However, because the load and resulting overturning moment was relatively low prior to reaching cracking strength, no distress was observed on the interface in a region where tension developed. Therefore, the vertical strip reinforcement was not greatly stressed.

After cracking, a vertical gap between top and bottom panels developed on the interface at the tension side because there was no reinforcement between the panels. The vertical strip reinforcement was called upon to withstand the tension produced by the overturning moment. Half of the specimen, shaded in Figure 4.5, responded as a flexural member with the vertical strip reinforcement resisting tension as shown in Figure 4.5. As load increased, larger forces were developed in the vertical strip reinforcement to resist the moment ($M_e = P \; x \; d_c$). When load increased to a level at which the reinforcement yielded, ultimate strength of the specimen was reached.

The concrete along the interface crushed when the ultimate load was reached. Under continuing load, larger deformations were developed in the vertical strip reinforcement, interface slip was observed, and the specimen capacity decreased. The force in the yielded reinforcement acted as a normal force on the crushed interface and permitted shear friction to develop and it is referred to as residual strength.

It was observed that the ultimate and residual strengths were primarily dependent on the ratio of vertical strip reinforcement to the half section of the specimen. In a certain range, the higher the reinforcement ratio, the higher the moment capacity and ultimate strength. However, if the reinforcement ratio is too high, the reinforcement may not yield before the concrete crushes under bearing. Specimen PC-12 with six #5 bars (ratio of $\rho = 1.8$ %) in the vertical strip exhibited bearing failure mode which precluded yielding of the vertical strip reinforcement.

4.2.1.4 Grout Strength

All specimens except PC-7 were grouted with closure strip concrete having a strength of 6000 - 7200 psi while the concrete strength of all panels was 4300 - 5100 psi. Because the grout strength was about 1.4 to 1.6 times of the panel concrete strength, panel keys were crushed in all specimens except PC-7. The failure interface was typically along the base of the panel keys as shown in Figure 4.5a. On the other hand, PC-7 was grouted with concrete having a strength of 2650 psi. Crush was observed in the strip and a failure surface developed along the base of the closure strip keys in PC-7. The tests indicated that the cracking and ultimate strength was dependent on the panel concrete or grout strength whichever is lower. However, residual strength was not significantly affected by change of grout strength.

4.2.1.5 Normal Force

Although specimens were tested under direct shear, a direct-shear load between panels would not exist in actual precast infill walls. Though the test setup was designed to produce pure shear across the interface, exterior moment was produced because of the existence of gap d_c between the load and weak interface plane as described earlier. The exterior moment produced relative (vertical) displacement between the top and bottom panels at the two sides of the specimen as shown in Figure 4.6. In tests PC-7 through PC-9, the specimens lifted from the setup before ultimate strength was reached.

In order to prevent specimen uplift, a vertical load was applied to the specimen by tying the loading head to the base as shown in Figure 4.7. Unlike the specimens tested without vertical load, specimens PC-6, PC-10, PC-11 and PC-12

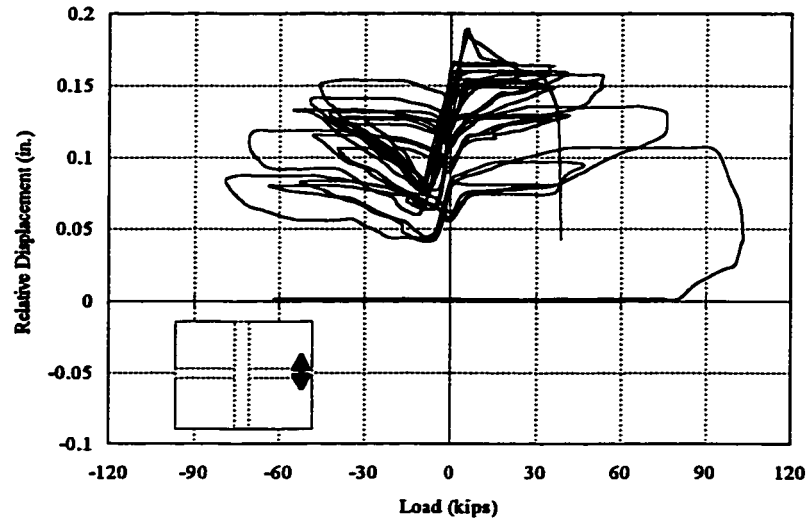

Figure 4.6 Relative Displacement of Top and Bottom Panels (PC-9)

were tested.under combination of direct shear and vertical load. Diagonal cracks were observed in the horizontal closure strips in specimens PC-6, PC-7 and PC-12. The diagonal cracking mode more closely represents infill wall behavior because vertical load is likely in infill walls. The increase in ultimate and residual strengths observed for specimens on with vertical load was applied is shown in Table 3.4.

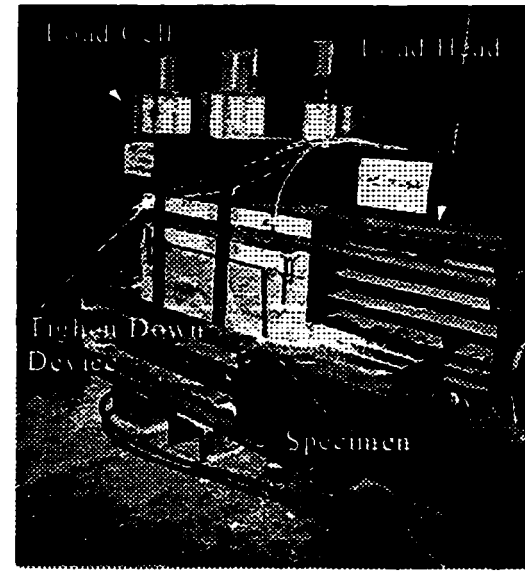

Figure 4.7 Vertical Load Device

4.2.1.6 Operation Factors

Besides the effects of the designed test variables, there were several operation related factors affecting the specimen test results. Some of the factors could not be

controlled during construction and testing. Others were unseen. In general, these factors represent the difference between ideal conditions and construction practice.

As an example of the operation factors, the closure strip concrete may not have the same consolidation as test cylinders used to evaluate concrete strength. It was obvious that air was trapped in the closure strip concrete and may have weakened the concrete at that location.

The test setup did not work effectively as it was planned to do. Difficulties in placing the specimen in the test apparatus changed the loading condition. Specimen PC-6 and PC-14 are examples which show how test results were affected by the operation errors. Specimen PC-6 was prevented by the setup from free translation along the cracked interface which resulted in very high ultimate strength and no residual strength. Specimen PC-14 was poorly grouted which resulted in a very low cracking capacity.

4.2.2 Capacity Evaluation

Because there were many factors affecting the strength of a specimen, it is impossible to develop analytical formula relating the strength to these factors. Statistical analysis was conducted to evaluate strength behavior of the closure strip specimens.

4.2.2.1 Cracking Capacity Estimate

As discussed in the previous section, cracking strength was related to the specimen dimension, strip size, shear key spacing, and panel concrete or strip grout strength. A cracking strength factor f_c was used to represent the effects of all variables.

Concrete shear strength is typically evaluated as a function of $\sqrt{f_c'}$ [5,20,35]. The shear capacity or cracking strength of a closure strip specimen is assumed to be V_n for the net gross section of shear keys along the failure interface as shown in Figure 4.8.

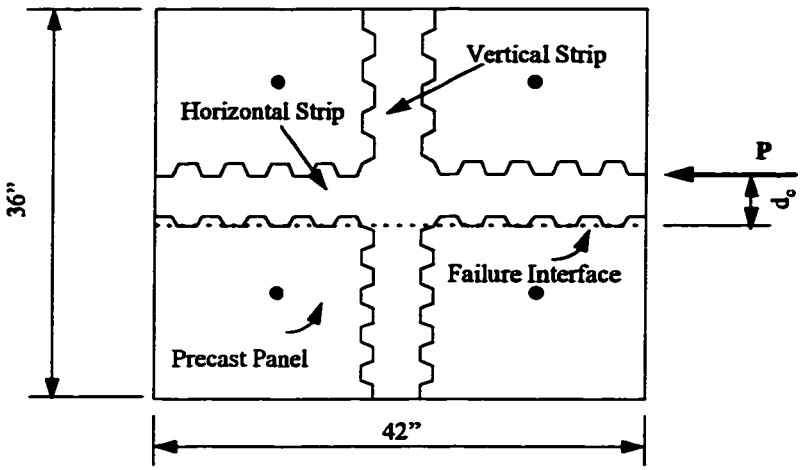

Figure 4.8 Net Shear Section on the Failure Interface

$$V_n = f_c \left(a_p \sqrt{f_{cp}'} + a_s \sqrt{f_{cs}'} \right) \tag{4-1}$$

Where f_c -------- Cracking strength factor

a_p -------- Total key section area at the interface

a_s -------- Cross section area of vertical strip

f_{cp}', f_{cs}' ------ Strength of panel & strip concrete

The nominal shear strength V_n can be calculated based on specimen dimensions and concrete strength. The measured cracking strength was denoted as P_c. By equating the measured cracking strength and calculated specimen nominal shear capacity,

$$f_c = \frac{P_c}{V_n} \tag{4-2}$$

Table 4.1 Analysis of Cracking Strength Factor Data

Specimen Number	Shear Area (in^2) Strip	Shear Area (in^2) Panel	Nominal Shear (kips)	Strength P_c (kips)	Factor f_c	Value $(f_c-f_0)^2$	ξ LN(f_c)	Value $(\xi-\xi_c)^2$
PC-1	12.00	114.00	9.159	81.0	8.843	1.182	2.1797	0.0246
PC-2	12.00	88.80	7.360	59.0	8.016	0.068	2.0815	0.0035
PC-3	12.00	114.00	9.159	69.0	7.533	0.050	2.0193	0.0000
PC-4	12.00	88.80	7.360	50.0	6.794	0.926	1.9160	0.0114
PC-5	24.00	102.00	8.371	60.0	7.168	0.346	1.9696	0.0028
PC-6	24.00	102.00	8.682	60.0	6.911	0.715	1.9331	0.0080
PC-7	24.00	102.00	6.486	40.0	6.167	2.525	1.8192	0.0414
PC-8	24.00	102.00	8.682	60.0	6.911	0.715	1.9331	0.0080
PC-9	24.00	102.00	8.682	80.0	9.214	2.127	2.2208	0.0392
PC-10	24.00	102.00	8.548	80.0	9.359	2.571	2.2364	0.0456
PC-11	24.00	102.00	8.548	84.0	9.827	4.290	2.2852	0.0689
PC-12	24.00	102.00	8.548	70.0	8.189	0.188	2.1028	0.0064
PC-13	16.00	68.00	5.861	55.0	9.383	2.648	2.2389	0.0467
PC-14	16.00	68.00	5.861	25.0	4.265	12.186	1.4505	0.3275
f_c		f_0 =	7.756	σ_f^2 =	2.349	σ_f =	1.533	
ξ		ξ_c =	2.028	σ_ξ^2 =	0.049	σ_ξ =	0.221	

The cracking strength factor f_c, a random variable, was calculated for each specimen and is listed in Table 4.1. Arranging calculated cracking strength factors in order and calculating the average frequencies, a rectangular-frequency-diagram (RFD) was obtained as shown in Figure 4.9a. This RFD indicated that the cracking strength factor f_c resembles a logarithmic-normal-distribution [32,54]. In other words, the logarithmic value of f_c,

$$\xi = \ln\left(f_c\right) \tag{4-3}$$

resembles a normal-distribution as shown in Fig. 4.9b.

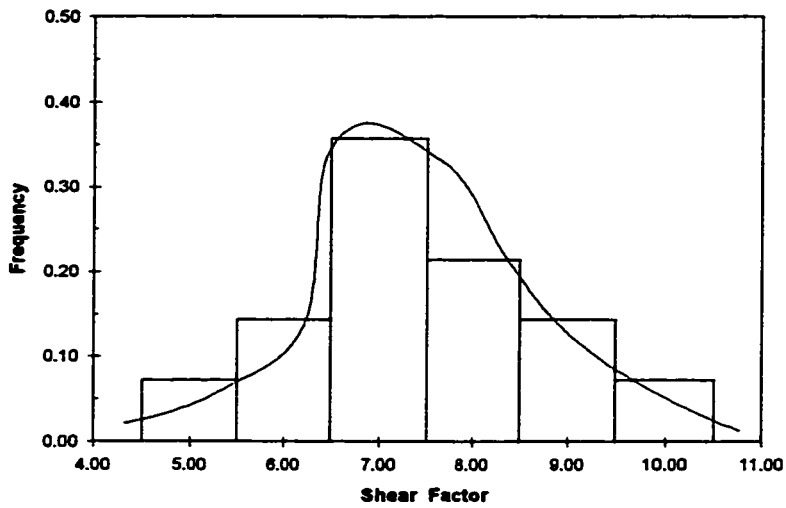

Fig. 4.9a RFD of Cracking Strength Factor f_c

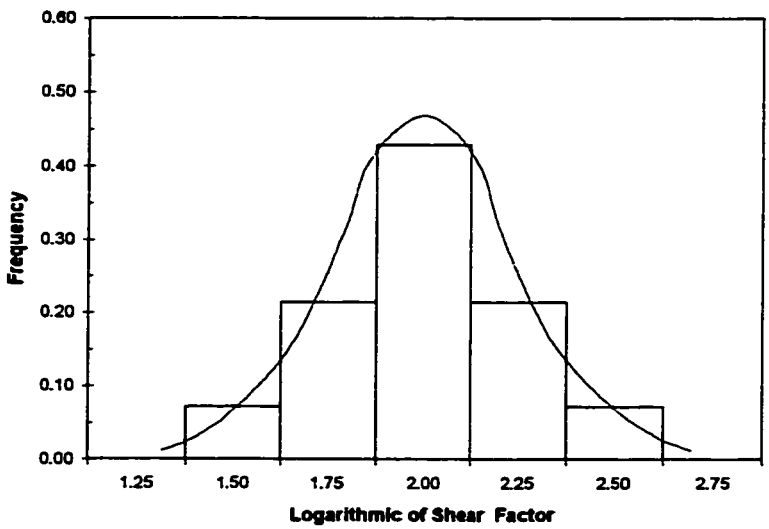

Fig. 4.9b RFD of $\xi = Ln(f_c)$

In Table 4.1, f_0 and σ_f represent the expectation and standard deviation of random variable f_c while ξ_c and σ_ξ denote the expectation and standard deviation of variable ξ, respectively. It is estimated that f_0 is 7.756 and σ_f is 1.533 while ξ_c and σ_ξ are 2.028 and 0.221 correspondingly. The probability distribution function of f_c is,

$$P(t \le x) = \begin{cases} \dfrac{1}{\sqrt{2\pi}\,\sigma_\xi t} \displaystyle\int_0^x e^{-\frac{1}{2}\left(\frac{\ln t - \xi_c}{\sigma_\xi}\right)^2} dt & x \ge 0 \\ 0 & x \le 0 \end{cases} \tag{4-3}$$

To calculate the probability of t under a specified level, substitute t with

$$\mu = \frac{\ln t - \xi_c}{\sigma_\xi} \tag{4-4}$$

Then, μ follows Standard-Normal-Distribution and the probability integration equation becomes,

$$P(t \le x) = \frac{1}{\sqrt{2\pi}} \int_{-\infty}^{\frac{\ln x - \xi_c}{\sigma_\xi}} e^{-\frac{\mu^2}{2}} d\mu \tag{4-5}$$

The probability is easily obtained for certain values of x. Table 4.2 gives the failure probabilities of cracking strength factor f_c under several estimating levels. It indicates that reliable probabilities (reliable probability = 1.0 - failure probability) for $f_c > 4.0$, $f_c > 6.0$ and $f_c > 8.0$ are greater than 99.8%, 85.5% and 40.9%, respectively. Under a probability of 99.8%, the estimated cracking strength factor f_c was estimated as 4.0 which is much greater than the shear factor used in flexural members as recommended by ACI-318. In ACI-318 the shear factor was set as 2.0 so that the

nominal shear concrete strength $V_n = 2.0\sqrt{f_c'}$ for elastic design. According to the estimated probability of 99.8%, $f_c = 4.0$ is a conservative value that was used in infill wall shear strength design for the model structure.

Table 4.2 Failure Probability of Cracking strength Factor f_C

Item	Estimate Level and Failure Probabilities							
$f_c \leq$	4.000	4.500	5.000	5.500	6.000	6.500	7.758	8.000
μ	-2.887	-2.357	-1.883	-1.454	-1.062	-0.701	0.094	0.234
P{x}	0.002	0.009	0.033	0.073	0.145	0.242	0.504	0.591

4.2.2.2 Ultimate Capacity Estimate

In the last section, it was noted that the ultimate strength is dependent on the vertical strip reinforcement ratio and is related to the moment capacity. The failure mode shown in Figure 4.5a corresponds with a failure plane along the bottom surface of the horizontal strip. A distance d_e existed between the loading plane and the failure plane. Considering a specimen as a flexural member as shown in Figure 4.10, its moment capacity can be calculated according to ACI-318.

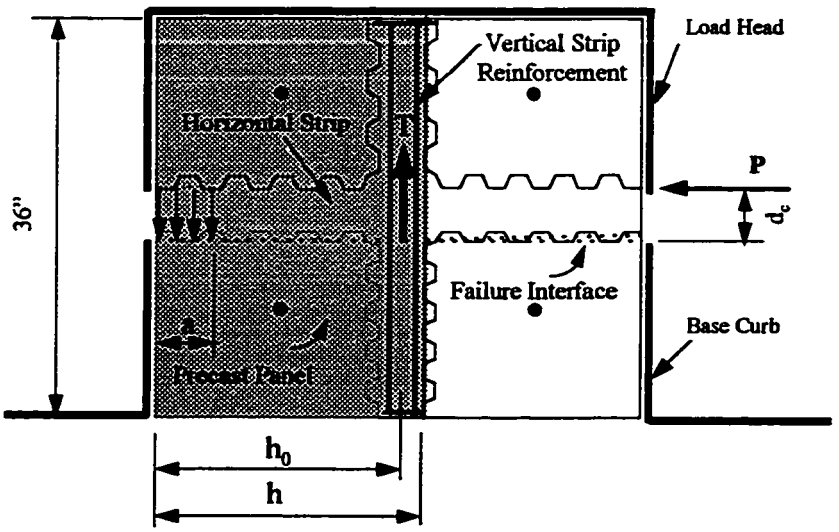

Figure 4.10 Specimen Moment Capacity (PC-5)

$$M_n = T\left(h_0 - \frac{a}{2}\right) \qquad (4\text{-}6)$$

where $T = A_s\ F_y$ ------ force of reinforcement

$h_0 = h - a'$ ------ effective height of section

$a = \dfrac{T}{0.85 f'_c\ b_c}$ ------ height of compression zone

Based on the member cross section and vertical strip reinforcement, the nominal moment was calculated for each specimen and is presented in Table 4.3. In the calculation, a steel yield strength of F_y = 70 ksi was used, and the panel or strip concrete strength whichever was lower was adopted for every specimen. Dividing the calculated nominal moment by the observed peak load (ultimate strength) P_u , a nominal moment arm was obtained:

$$d_n = \frac{M_n}{P_u} \qquad (4\text{-}7)$$

Theoretically, d_n should equal the distance d_c (5.0") between the loading and failure plane as shown in Figure 4.10. The values of d_n in Table 4.3 vary from specimen to specimen. Fortunately, d_n closely matched d_c in a range from 3.4" to 6.0" except for PC-7, PC-12 and PC-14. PC-7 had a low strip strength, and PC-12 and PC-14 had extremely high reinforcement ratios. The calculation was performed assuming that the reinforcement yielded. If the reinforcement did not yield, the value d_n obtained from the calculation should be greater than d_c. The ratio of d_c / d_n reflects the strain/stress level of the vertical strip reinforcement. In fact, the nominal moment

arm d_n that was larger than d_c indicated that the reinforcement did not yield in specimens PC-12 and PC-14.

The reinforcement strain/stress level was dependent on the reinforcement ratio and other variables as discussed in the previous section. In order to analyze the effects of variables on ultimate strength, the interior force condition of the specimen was studied. The applied external moment M_e and nominal ultimate moment capacity M_u were calculated.

$$M_e = P_u \left(3.0 + \frac{h_s}{2h_k}\right) \tag{4-8}$$

where h_s ------ height of closure strip

h_k ------ height of shear key

P_u ------ observed ultimate strength

$$M_u = T\left(c_p - \frac{a}{2}\right) \tag{4-9}$$

$$a = \frac{T}{0.85 f_c' \, b_c - \dfrac{N_p}{c_p}} \tag{4-10}$$

where c_p ------ half specimen length

N_p ------ normal (vertical) load

Considering the force T in the reinforcement as an unknown and letting,

$$\alpha = c_p - \frac{a}{2} \tag{a}$$

$$\beta = 0.85 f_c' \, b_c - \frac{N_p}{c_p} \qquad (b)$$

Then substituting equation (4-9) to (4-10),

$$\frac{T^2}{2} - \alpha\beta T + \beta M_u = 0 \qquad (4\text{-}11)$$

In order to take the tested ultimate strength into account, substitute M_u with M_e,

$$\frac{T^2}{2} - \alpha\beta T + \beta M_e = 0 \qquad (4\text{-}11_a)$$

Dividing T by the reinforcement area A_s, an effective reinforcement stress was obtained,

$$p_e = \frac{T}{A_s} \qquad (4\text{-}12)$$

Then, dividing the effective stress p_e by the yield stress F_y (70 ksi), a reinforcement efficient factor f_u was obtained.

$$f_u = \frac{p_e}{F_y} \qquad (4\text{-}13)$$

The reinforcement efficient factor f_u along with key variables used in calculating the factor are listed in Table 4.3. The efficient factor f_u indicates the vertical strip reinforcement efficiency. In other word, it provides a means for estimating the effect of vertical strip reinforcement on specimen ultimate strength.

It is seen that the value of the efficient factor is about 1.0 for most specimens having intermediate reinforcement ratios. On the other hand, a low strip (or panel)

concrete strength as in specimen PC-7 also resulted in low reinforcement efficiency as shown in Table 4.3.

Table 4.3 Reinforcement Efficient Factor and Ultimate Strength

Specimen Number	Reinforcing Ratio ρ	Nominal Moment M_n	Nominal Gap d_n (in)	Efficient Stress P_e	Efficient Factor f_e		Ultimate Strength	
					Tested	Regression	Tested P_n (k)	Estimated (k)
PC-1	0.194	289.0	3.44	81.6	1.166	1.005	84.0	72.6
PC-2	0.194	289.0	4.66	59.9	0.856	1.005	62.0	72.6
PC-3	0.194	289.0	3.91	70.7	1.010	1.005	73.0	72.6
PC-4	0.194	289.0	4.13	67.8	0.968	1.005	70.0	72.6
PC-5	0.204	272.3	3.89	90.5	1.293	1.003	70.0	54.6
PC-6 *	0.727	920.3	5.14	68.8	0.983	0.762	179.0	140.2
PC-7 **	0.727	877.4	8.60	37.5	0.536	0.762	102.0	133.7
PC-8	0.727	920.3	6.01	49.3	0.705	0.762	153.0	161.8
PC-9	0.409	534.6	5.19	67.3	0.962	0.955	103.0	102.2
PC-10 *	0.363	477.3	4.38	80.6	1.151	0.966	109.0	92.2
PC-11 *	0.409	534.6	3.41	90.7	1.295	0.955	157.0	117.9
PC-12 *	1.704	1940.0	9.60	33.8	0.482	0.658	202.0	255.2
PC-13	0.307	270.4	4.29	82.0	1.171	0.979	63.0	52.9
PC-14	1.090	890.4	12.03	27.2	0.389	0.580	74.0	103.3
Factor	ξ= 0.926		σ^2= 0.297		σ= 0.088			
f_e	Linear Regression F_u=1.048-0.229p		Parabolic regression F_u=1.313-0.931ρ+0.237 ρ^2					

* with vertical load, ** with low grout strength.

The result indicated that, in a certain range, a high reinforcement ratio results in a low efficient factor. As shown in Figure 4.11, the low reinforcement ratio in PC-1 resulted in high reinforcement strain. However, because of a very high reinforcement ratio in PC-12, the reinforcement never yielded. In fact, due to very high reinforcement ratios in specimen PC-12 and PC-14, the tested efficient factors were only 0.48 and 0.39, respectively. In other words, the reinforcement in the two specimens was stressed to only 48% and 39% of the yield strength and confirms that concrete crushing occurred instead of the reinforcement yielding due to the applied exterior moment.

The efficient factor reflected how much reinforcement can be efficiently applied in a specimen. Therefore, it can be used to estimate a reasonable

reinforcement ratio in infill and closure strip design. A relationship between reinforcement ratio and reinforcement efficiency was established based on the tested efficient factors.

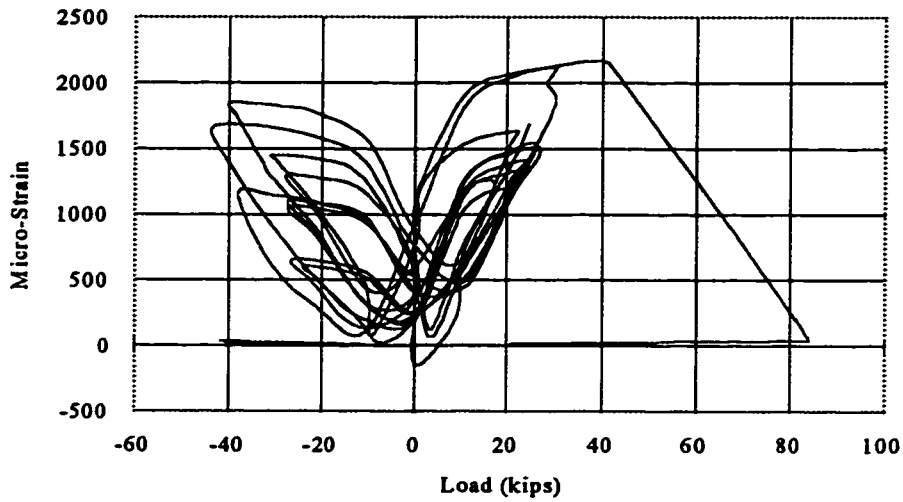

a) Reinforcement Strain with Ratio 0.19% (PC-1)

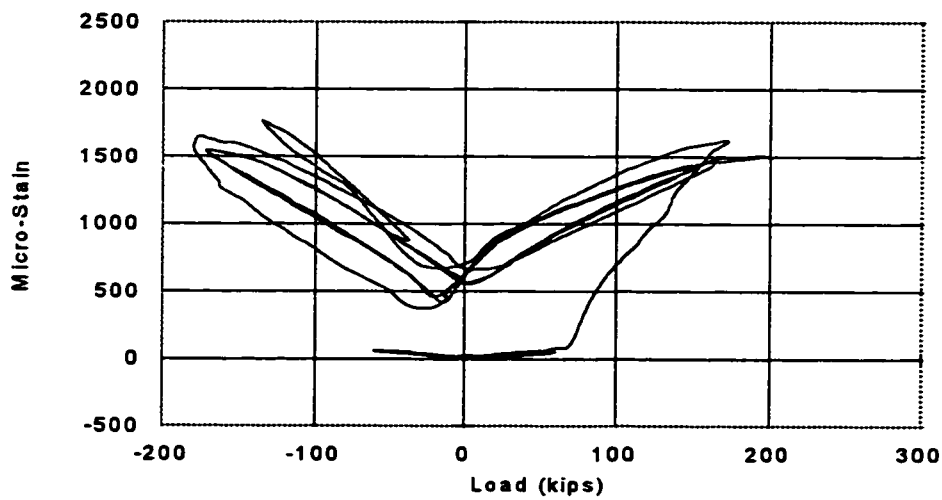

b) Reinforcement Strain with Ratio 1.7% (PC-12)

Figure 4.11 Comparison of Reinforcement strain

Linear and parabolic regressions [32,54] were performed and gave the following equations:

$$f_u^{(L)} = 1.0485 - 0.2280\rho \tag{4-14}$$

$$f_u^{(P)} = 1.3094 - 0.9180\rho + 0.2306\rho^2 \tag{4-14a}$$

The efficient factor f_u as a function of reinforcement ratio ρ is illustrated in Figure 4.12. It appears that the parabolic regression matches the experimental result more closely. Even though using an efficient factor greater than one (steel yield strength F_y greater than specified strength) is unconservative, it may be reasonable when considering strain hardening beyond the yield point. Therefore, it is recommended to apply the parabolic equation to estimate the efficient factor. However, if efficient factors less than 1.0 are desired, use of the linear equation when ρ is less than 0.425% and the parabolic equation when ρ is equal or greater than 0.425% is reasonable. The efficient factor can be used either to guide the vertical strip reinforcement design or to evaluate the specimen ultimate strength. The nominal ultimate strength for a closure strip specimen can be estimated with the equation:

$$P_u^n = \frac{f_u A_s F_y \left(c_p - \frac{a}{2}\right)}{C + \frac{h_s}{2h_k}} \tag{4-15}$$

In the equation, the variables are defined as in equations (4-8) through (4-10) while C is a constant related to the strip height and was evaluated as 3.0 for calculating the ultimate strength in this report.

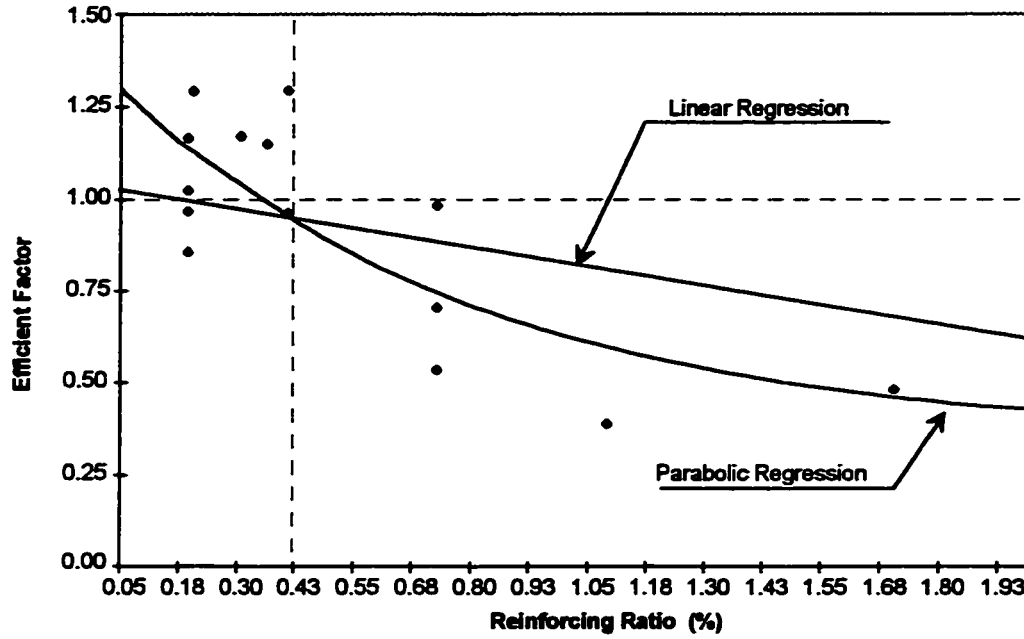

Figure 4.12 Linear and Parabolic Regression of f_u

Applying equation (4-14) for the specimens with reinforcement ratio less than 0.425% and using (4-14a) for specimens with higher reinforcement ratios, the reinforcement efficient factors were calculated for all closure strip specimens. Substituting the estimated efficient factor into equation (4-15), the ultimate strength for each specimen was calculated and presented in Table 4.3. The estimated ultimate strength matched the test results very well for all specimens except for specimens as PC-12 and PC-14 which encountered bearing failure or major operation errors. It was also seen that the vertical (normal) force made a significant contribution to the ultimate strength.

4.2.2.3 Residual Capacity Estimate

The residual strength was dependent on the panel or strip concrete strength whichever was lower, specimen dimensions, and particularly, vertical strip

reinforcement. As discussed earlier, the residual strength was developed by means of shear friction on the interface. Friction would be induced by a certain force acting normal to the interface[33,35,50]. Shear friction along the interface was basically produced by the reaction of the tension force developed in the vertical strip reinforcement. The value of tension was dependent on the area and efficiency of vertical strip reinforcement as discussed in the last section.

To estimate the tension level of the reinforcement, the efficient factor f_u computed using equation (1-14) or (4-14a) was applied in evaluating the residual strength. Equation (4-14) was used to calculate the efficient factor when the reinforcement ratio was less than 0.425% and (4-14a) was applied beyond the ratio of 0.425%. The efficient factor for each specimen is presented in Table 4.3. The reinforcement force was evaluated with the efficient factor. The nominal normal stress σ_n for a specimen was estimated as,

$$\sigma_n = \frac{1}{c_p\, b_p} \left(f_u\, A_s\, F_y + N \right) \tag{4-16}$$

The variables involved in equation (4-16) were defined earlier. Under the shear friction load (residual strength), the nominal residual shear stress for the interface is,

$$\tau_{RN} = \frac{P_R}{c_p\, b_p} \tag{4-17}$$

In order to study concrete strength effects on shear friction, the interface concrete strength was taken into account. Generally speaking, a smooth friction surface results in a lower friction coefficient and friction force. When the interface concrete experiences cracking and crushing, it is likely that a lower strength concrete

may induce a rougher surface than a higher strength concrete. Therefore, a dimensionless medium factor γ was introduced.

$$\gamma = \frac{1 \text{ ksi}}{f_c'} \tag{4-18}$$

$$\tau_R = \gamma \ \tau_{RN} \tag{4-19}$$

where τ_R ------ residual stress (ksi)

f_c' ------ concrete strength (ksi)

Generally, the friction stress is related to the normal stress on the slip surface and the relationship can be expressed with a friction factor f_R.

$$\tau_R = f_R \ \sigma_n \qquad or \tag{4-20}$$

$$f_R = \frac{\tau_R}{\sigma_n} \tag{4-20a}$$

The friction factor value f_R was calculated using equations (4-16) through (4-20a) for each specimen (except PC-6 and PC-12 for which no residual strength was obtained). The measured friction factor values were calculated and presented in Table 4.4 along with related variables. The measured friction factor f_R follows a normal distribution which is illustrated by the rectangular frequency diagram (RFD) shown in Fig. 4.13. Meanwhile, the RFD also shows that distribution of f_R concentrates to its characteristic value (expectation). In fact, the standard deviation is only 0.072 with characteristic value (expectation) of 0.322. This analysis results indicated that the friction factor f_R and the residual strength (residual stress τ_{RN}) can be closely estimated through the use of the equations discussed earlier.

Table 4.4 Closure Strip Residual Strength Friction Factor

Specimen Number	Efficient Factor f_u	Concrete Strength f_c'	Normal Stress sn	Friction Factor f_R		Residual Strength (k)		
				Tested	Regression	Estimated	Tested	ACI-318
PC-1	1.005	5100	0.129	0.379	0.371	29.2	30.0	15.5
PC-2	1.005	5100	0.129	0.366	0.371	29.2	29.0	15.5
PC-3	1.005	5100	0.129	0.341	0.371	29.2	27.0	15.5
PC-4	1.005	5100	0.129	0.353	0.371	29.2	28.0	15.5
PC-5	1.003	4000	0.128	0.436	0.379	23.3	27.0	15.5
PC-6 *	0.882	4300	0.535	-	0.279	76.9	-	55.0
PC-7	0.882	2650	0.388	0.278	0.314	63.0	58.0	55.0
PC-8	0.882	4300	0.388	0.288	0.314	63.0	54.0	55.0
PC-9	0.955	4300	0.242	0.354	0.349	43.6	45.0	30.9
PC-10	0.966	4300	0.283	0.351	0.340	49.5	45.0	27.5
PC-11	0.955	4300	0.372	0.362	0.318	61.0	60.0	30.9
PC-12 *	0.658	4300	0.616	-	0.259	82.4	-	128.8
PC-13	0.979	4500	0.187	0.294	0.361	24.2	20.0	15.5
PC-14	0.799	4500	0.513	0.127	0.278	51.4	25.0	55.0
Factor	Statistic Value		ξ =	0.322	σ^2 =	0.005	σ =	0.072
f_R	Linear Regress		f_R =	0.4078 - 0.056 (σ_v/γ)				

* No residual strength was recorded

By substituting equation (4-20) into equation (4-19) and rearranging terms, a nominal residual stress equation was obtained,

$$\tau_{RN} = \frac{\tau_R}{\gamma} = \frac{1}{\gamma} f_R \sigma_n \qquad (4\text{-}21a)$$

In equation (4-21a), σ_n and γ are to be obtained from equations (4-16) and (4-18), and only the friction factor f_R is an unknown. To estimate a specimen's residual strength, the friction factor must be determined. Analyzing the variable characteristics, a relationship of friction factor with normal stress and specimen properties has been established. It was shown that the friction factor is a function of normal stress (reaction of vertical reinforcement tension) and specimen concrete strength. Figure 4.14 illustrates the linear regression for friction factor f_R versus the variable σ_n/γ and the regression equation was listed in the bottom of Table 4.4.

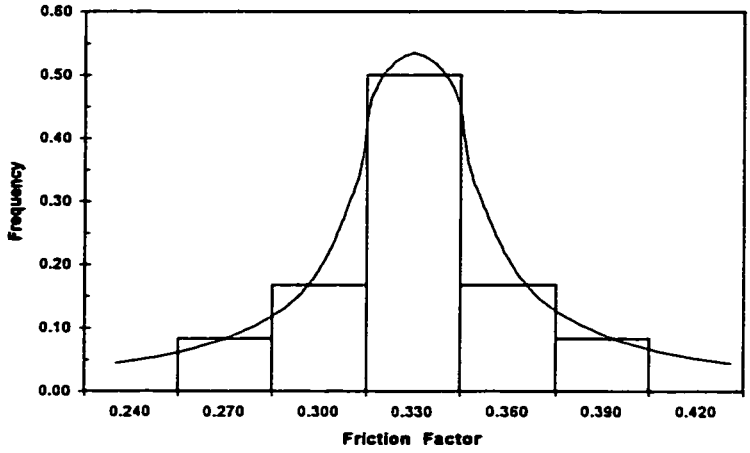

Fig. 4.13 RFD of Friction Factor f_R

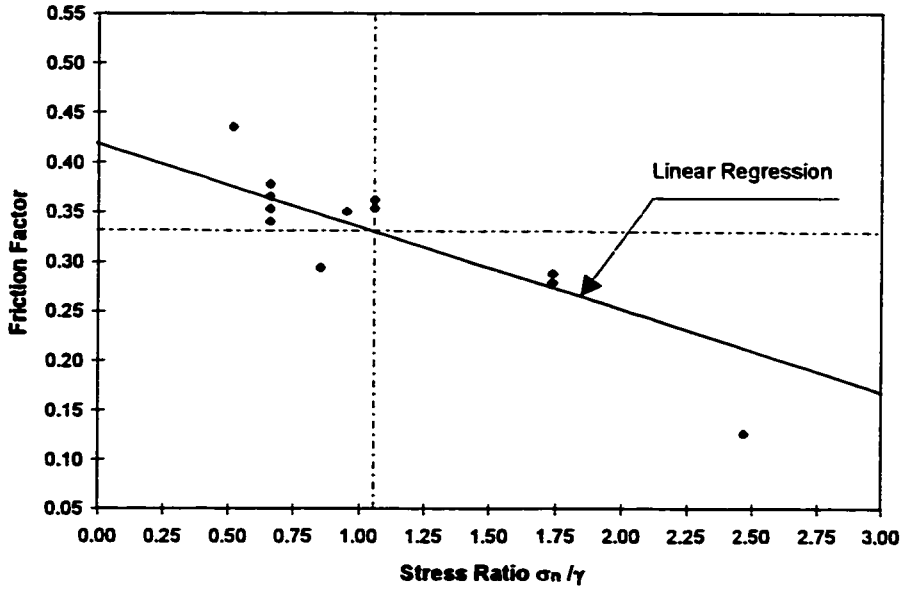

Fig. 4.14 Linear Regression of Friction factor

From Figure 4.14, it is evident that the regression results matched the test results (friction factors) very well. Applying the regression equation to calculate the friction factor, the residual strengths can be estimated as,

$$P_R = \frac{f_R}{\gamma} f_u \; A_s \; F_y \tag{4-21}$$

The residual strengths of all test specimen were estimated through the use of equation (4-21) and the values listed in Table 4.4. As expected, that the estimated residual strengths are very close to the tested results except PC-7 and PC-14 which had either lower strip strength or operation errors. It is also pointed out that both efficient factor f_u and friction factor f_R were used in the residual strength estimate. Since efficient and residual factors are derived from test results, they reflect the effects of variables on specimen strength and can be used to closely evaluate the ultimate and residual strengths for closure strip specimens.

Using equation (11-26) of ACI 318 Article 11.7.4.1, the shear friction values were also calculated and presented in Table 4.4. It was noted that ACI-318 shear friction values are close to the test results only for specimens with intermediate reinforcement ratios. Because ACI-318 equation does not reflect reinforcement ratios and concrete strength effects, the calculated shear friction values do not closely match the measured shear friction values due to the changes in reinforcement ratios or concrete strengths. The calculated shear friction value is about half of the corresponding measured residual strength for specimen PC-1 through PC-4 but more than double the measure value for specimen PC-14. It is recommended that ACI-318 equation (11-26) be modified using equation (4-21) presented in this report.

4.3 SHEAR LUG PERFORMANCE

The shear lug specimen showed different characteristics from that of a closure strip specimen. Because there were no shear keys along the edges of frame segment, the interface between the strip and frame segment cracked at a low load. When the crack occurred, the steel pipe began to resist the lateral load (shear). Because no shear keys were engaged in the interface cracking, the load inducing the shear lug specimen interface cracking was termed as **cohesion strength** to differentiate the similar event of closure strip specimen cracking strength. Ultimate and residual strengths were also observed for shear lug specimens. The steel pipe jointly worked with vertical strip reinforcement to develop the ultimate and residual strengths.

4.3.1 Variable effects

4.3.1.1 Pipe Size

As discussed in Chapter III, a steel pipe used as a shear lug was designed to have a lower yielding strength than the concrete bearing strength to prevent brittle concrete bearing failure. That is to say, an ideal pipe size would provide the specimen with a ductile behavior. If the steel pipe size is too big compared with its embedment length and the panel thickness, it could not yield. Subsequently, the specimen could fail with non-ductile behavior.

Because of suitable pipe size and embedment length, the steel pips yielded in all specimens except FC-1. In specimen FC-1, the pipe never yielded because its cross section was very large compared with its embedment length as shown in Fig. 4.14. In other words, the pipe embedment length of FC-1 was so short compared to its large cross section that yielding did not develop in the pipe.

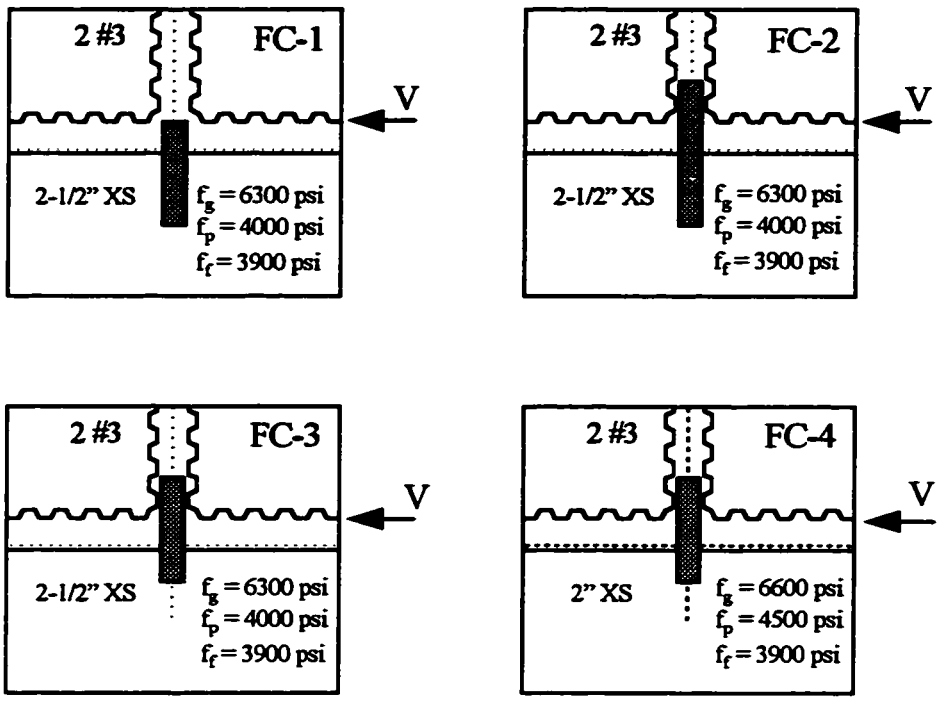

Figure 4.14 Shear Lug (Steel Pipe) Variables

4.3.1.2 Pipe Embedment Length

Change of pipe embedment length resulted in change in the failure mechanism. The pipe embedment length in the closure strip (panel) in FC-1 was equal to the height of the closure strip. As a result, the steel pipe contributed very little to the ultimate and residual strengths. After loss of cohesion, specimen FC-1 exhibited no significant difference from closure strip specimen PC-5 which had identical panel size, strip height and vertical strip reinforcement as FC-1. It indicated that the ultimate and residual strengths of FC-1 were mainly dependent on the vertical strip reinforcement.

With a pipe embedment length greater than the horizontal closure strip height, yielding developed in the pipe and the pipe contributed more to the ultimate and residual strengths. Flexural deformation of the pipe was developed as the concrete

cryshed at the points of peak bearing stress and the pipe yielded. Flexural yielding behavior was observed in the pipe of specimen FC-2 as shown in Figure 4.15a. However, if the pipe has a long embedment compared to its diameter, concrete crushing around the pipe is not likely and large flexural deformation can not be developed. The pipe with a long embedment length in FC-4 exhibited shear yielding behavior instead of flexural yielding as shown in Figure 4.15b

a) Flexure Yielding (FC-2) b) Shear Yielding (FC-4)

Figure 4.15 Steel Pipe Yielding Modes

4.3.1.3 Panel Thickness

The panel thickness coupled with vertical strip reinforcement provided moment capacity for the specimen to resist exterior load. As discussed in section 4.2.3, a higher reinforcement ratio resulted in less reinforcement efficiency in developing the ultimate strength. In fact, the reinforcement in a thin-panel specimen would provide a lower moment capacity than the same amount of reinforcement in a thick-panel specimen.

Because of reduced reinforcement efficiency (less contribution of vertical strip reinforcement) in a thin-panel specimen, the steel pipe was called on to contribute more to the specimen capacity.

On the other hand, if the precast panel is too thin compared to the pipe cross section, yielding may not develop in the vertical strip reinforcement. Specimen FC-4 was an example where the specimen thickness was relatively small compared with the pipe size. After the interface cracked, the steel pipe was called on to resist interface shear. Though the pipe cross section was relatively small, it was required to resist more of the load due to the reduced efficiency of the vertical reinforcement. Under both shear and moment actions, its shear strength was reached first as shown in Fig. 4.15b where yielding along a 45° diagonal line can be observed under very small flexural deformations.

4.3.2 Capacity Evaluation

A statistical analysis can not be used to evaluate capacities of the shear lug specimens because of the small number of test samples. However, it is not necessary to conduct statistical analysis for shear lug strength estimation because:

1) Vertical strip reinforcement effects on closure strip specimen strength have been studied and the equations derived from closure specimen tests can be used to evaluate the vertical reinforcement contribution to the shear lug specimen capacity.

2) Steel is an ideal elastic material with stable properties and the steel pipe contribution to the shear lug specimen capacity can be evaluated using steel material characteristics.

The failure mode of shear lug specimens is shown in Figure 4.16. Interface cohesion strength was first reached and then the steel pipe yielded as surrounding concrete crushed under combination of shear and moment actions produced by the lateral load.

The steel pipe in a shear lug specimen was designed to sustain part (or whole) of the interface shear. That is to say, the tested cohesion strength of a shear lug specimen is not the pure concrete cohesion capacity but the combination of concrete cohesion capacity and shear lug resistance.

Figure 4.16 Shear Lug Specimen Failure Mode

4.3.2.1 Cohesion Strength

To estimate cohesion strength of shear lug specimens, concrete rupture (cracking) strength τ_{rup}, which is specified as $6.5\sqrt{f'_c}$ in the AASHTO specification[58], may be used. The rupture strain may be estimated approximately as,

$$\varepsilon_{rup} = \tau_{rup} / G_c \qquad (4\text{-}22)$$

where G_c ------ the shear modulus of concrete.

When concrete cracked, the steel pipe was subjected to the same level of strain. Under this strain level, the pipe was subjected to a nominal shear stress:

$$\tau_n = \varepsilon_{rup} F_y / \varepsilon_y \qquad (4\text{-}23)$$

where F_y and ε_y ..... the yield stress and strain

Denoting V_p as the pipe contribution to the specimen cohesion strength V_{coh}, and V_c as concrete contribution to the specimen cohesion strength, so,

$$V_p = \tau_n A_p / \sqrt{3} \qquad (4\text{-}24)$$

where A_p ..... the pipe section area, and

$$V_c = V_{coh} - V_p \qquad (4\text{-}25)$$

Supposing concrete cohesion shear stress is proportional to the square root of concrete compressive strength, a cohesion factor can be defined as,

$$\phi_c = \frac{V_c}{\sqrt{f_c'}} \qquad (4\text{-}26)$$

Table 4.5 Shear Lug Cohesion Strength

Specimen	Pipe Contribution			Concrete Contribution			Cohesion Strength (k	
Number	Nominal (k)	Factor	Shear (k)	Shear (k)	Stress (psi)	Factor	Tested	Estimated
FC-1	71	0.159	11.2	18.8	75	1.18	30.0	32.7
FC-2	71	0.159	11.2	23.8	94	1.49	35.0	32.7
FC-3	71	0.159	11.2	18.8	75	1.18	30.0	32.7
FC-4	34	0.221	7.6	17.4	104	1.64	25.0	22.0

Using the above equations and the test results, the cohesion factor ϕ_c was calculated for each specimen and is presented in Table 4.5. The average value for the cohesion factor is approximately 1.35 which is much smaller than the cracking factor ($f_c = 4.0$) estimated in shear lug tests. This indicates that shear transfer capacity of a

keyed concrete interface is much higher than that of a smooth interface between old and new concrete.

4.3.2.2 Ultimate Strength

If no steel pipe is included, the specimen ultimate strength is mainly dependent on vertical reinforcement and can be estimated using equation (4-15) derived from the closure strip tests. Because of pipe involvement, the ultimate strength of a shear lug specimen is also dependent on shear and flexural strengths of the steel pipe.

Assuming the ultimate strength of a specimen V_u is a function of reinforcement contribution V_{ur}, pipe shear strength V_p, and pipe flexural strength M_p, then,

$$V_u = AV_{ur} + BV_p + C\frac{M_p}{d_p} \qquad (4\text{-}27)$$

where d_p ..... the nominal distance between the loading plane and specimen failure plane.

As discussed in Section 4.2, the reinforcement contribution was dependent on the ratio of vertical strip reinforcement. The shear and flexural strength contributions of the pipe were dependent on the ratio of the strip width to the pipe embedment length. Based on these observations, the following parameters were introduced.

$$\alpha = \frac{1.1\ h_s}{w_p + \frac{w_p}{w_f}} \qquad (4\text{-}28)$$

$$\beta = 1.0 - \alpha \qquad (4\text{-}29)$$

$$\gamma = \frac{1.1\ b_p}{w_p + \frac{w_f}{w_p}} \tag{4-30}$$

$$\kappa = 1.0 - \gamma \tag{4-31}$$

where h_s and b_p..... the height and width of the strip

w_p and w_f..... the pipe embedment lengths in the panel and in the frame, respectively.

The coefficients A, B and C in equation (4-27) are functions of the parameters α, β, γ and κ. To reflect reinforcement ratio and pipe embedment effects, the ultimate strength of a shear lug specimen can be estimated by,

$$V_u = a\ \alpha V_{ur} + b\ \beta \kappa V_p + \theta \beta \gamma\ \frac{M_p}{d_p} \tag{4-32}$$

Denoting parameter θ as,

$$\theta = c\ d_p + d\alpha\ d_p \tag{4-33}$$

then, equation (4-32) becomes,

$$V_u = a\ \alpha V_{ur} + b\ \beta \kappa V_p + c\ \beta \gamma\ M_p + d\ \alpha \beta \gamma\ M_p \tag{4-34}$$

In equation (4-34), only a, b, c, and d are unknowns. Substituting the measured reinforcement yield strength of 70 ksi and pipe steel strength of 54 ksi for the 2-1/2 in. diameter and 40 ksi for the 2.0 in. diameter pipes, values of V_{ur}, V_p and M_p were calculated. Substituting the measured value into equation (4-34) for V_u for each specimen, a system of four algebraic equations was established. Solving the

equations, the values of *a, b, c,* and *d* were determined to be 1.05, 2.50, 1.80, and -3.25, respectively.

Table 4.6 Shear Lug Ultimate Strength

Specimen	Reinforcement	Lug Pipe	Contribution	Ultimate Strength (k)	
Number	Contribution (k)	V_p (k)	M_p / d_p (k-in)	Tested	Estimated
FC-1	64.1	0.1	1.1	62.0	65.3
FC-2	28.5	33.4	9.9	71.0	71.8
FC-3	25.3	32.2	16.3	73.0	73.8
FC-4	23.3	27.8	4.4	55.0	55.5

The ultimate strength for each specimen was estimated using equations (4-35) and (4-34) and is presented in Table 4.6. The calculated ultimate strengths matched the test results quite well. The estimates indicated that the parameters introduced in equations (4-28) through (4-31) reasonably simulated the effects of various properties on specimen ultimate strength.

As discussed earlier, shear lug specimen FC-1 showed the same failure mode as closure strip specimen PC-5. The estimate using equation (4-34) and (4-35) accurately reflected this. From Table 4.6, it is seen that the ultimate strength of FC-1 is the strength calculated according to equation (4-15) implying the pipe made almost no contribution to the ultimate strength.

Table 4.7 Pipe Failure Behavior of FC-3 and FC-4

Specimen	Contribution of Pipe (k)		Effective	Shear Behavior (ksi)		Flexure Behavior (ksi)	
No.	Shear	Flexure	M_{ef} (K-in)	Stress τ	Strength τ_y	Stress σ	Strength F_y
FC-3	32.092	15.944	71.747	30.334	32.332	54.146	54.000
FC-4	27.730	4.295	19.328	22.931	23.094	28.425	40.000

In Table 4.7, the stresses were calculated using the plane stress formula

The flexural failure mode of FC-3 and shear failure mode of FC-4 also were indicated. Using equations (4-33) and (4-35), shear and moment contributions of the

steel pipe were calculated and presented in Table 4.7. In calculation, the distance d_p was assumed to be the strip height plus half key height. The moment-contribution termed was not a moment but a shear force. So, an effective moment on the pipe should be the moment contribution times d_p. The shear contribution, effective moment, and normal stress and shear stress in the pipe were calculated for specimen FC-3 and FC-4 and are presented in Table 4.7. Calculation results indicated that FC-4 yielded under shear stress while FC-3 yielded under normal stress (and almost yielded with shear stress as well) matching the observed test results.

4.3.2.3 Residual Strength

Applying the residual strength models derived using the closure strip specimen tests and the ultimate strength models for the shear lug specimen tests presented above, the method developed to estimate the shear lug specimen residual strength was very simple.

If there is no shear lug involvement, the specimen residual strength can be estimated with equation (4-21) derived for closure strip specimen residual strength. Replacing the reinforcement contribution V_{ur} by the residual strength V_r obtained using equation (4-21), and substituting the measured residual strength for V_u into equation (4-34), a system of four algebraic equations similar to the ultimate strength equation was established. The unknowns a, b, c, and d were obtained and are 1.45, 0.95, 1.05, and -0.70.

Applying equations (4-36) and (4-34) again considering V_u as an unknown, the residual strength for each specimen was estimated and is presented in Table 4.8. The estimates closely matched test results. It was noted that the shear lug contribution to specimen residual strength declined because of decay of embedment and loss of bond as concrete crushed around the pipe, as discussed earlier.

Table 4.8 Shear Lug Residual strength

Specimen Number	Reinforcement Contribution (k)	Lug Pipe Contribution		Residual Strength (k)	
		V_p (k)	M_p / d_p (k-in)	Tested	Estimated
FC-1	34.2	0.0	0.3	34.0	34.4
FC-2	15.2	12.7	19.8	48.0	47.7
FC-3	13.5	12.2	23.9	50.0	49.6
FC-4	14.0	10.6	6.4	31.0	31.0

The parameters α and γ defined in equations (4–28) and (4–30) properly reflected effects of pipe embedment length on specimen ultimate and residual strengths for tests presented here. These parameters may not be applied in general cases until more experiment data confirming the parameters.

4.4 DESIGN RECOMMENDATIONS

Effective connection of the PTPW system depends on proper selection of variables, and construction of closure strips and interface shear lugs. Based on connection specimen tests in Chapter III and analysis in this chapter, several key factors are recommended for PTPW system connection design.

The strength relationship developed in this chapter can be used for infill and shear lug strength design. Generally, the specified connection strength can be evaluated using the following equation,

$$P = F(\alpha f_c', \ \beta F_y) \tag{4-37}$$

where P ..... the specimen strength

$F(x, y)$ ..... a formula in previous equations.

f_c' ..... the concrete strength

F_y ..... the steel strength

α, β ..... the strength factors

Recommendations for determining strength factors α and β in equation (4-37) were presented for two categories: actual design and experimental design. In actual design, $\alpha=1.0$ and $\beta=1.0$ should be adopted for material strengths specified in design codes. In experimental design, on the other hand, $\alpha=1.3$ and $\beta=1.3$ should be applied as overstrength factors to code-specified material strengths or actual material strengths should be applied with $\alpha=1.0$ and $\beta=1.0$. Detailed design guidelines will be presented in Chapter X.

CHAPTER V

MODEL STRUCTURE TESTS

5.1 Introduction

The tests of closure strip and interface shear lug specimens provided valuable data on connection schemes, details and dimensions for pre-cast infill wall system design and construction. Using the test results and experience to design a boundary column post-tensioned pre-cast infill wall system, a PTPW system was developed for strengthening reinforced concrete moment-resisting frames. To investigate the interactions between post-tensioning and infills, and between post-tensioning and closure strips or shear lugs, a two story model frame structure was constructed and tested. In this chapter, tests of the model structure will be described.

5.2 Model Structure Design

The PTPW technique was designed for retrofitting non-ductile reinforced concrete frame structures built in the 1950's and 1960's. The model structure in the test represents a structure having non-ductile features of existing reinforced concrete frames. Design and construction of the model structure followed reinforced concrete structural design specifications of ACI 318-56 to simulate an existing frame of that period.

5.2.1 Existing Frame Simulation

Based on the reaction wall capacity and loading system available in Ferguson Structural Engineering Laboratory, a 2/3 scale was selected to model a frame having 12 ft. story heights and 20 ft. spans. The model frame specimen was designed to

represent an one-bay-frame and slab portion of an existing structural system as shown in Figure 5.1.

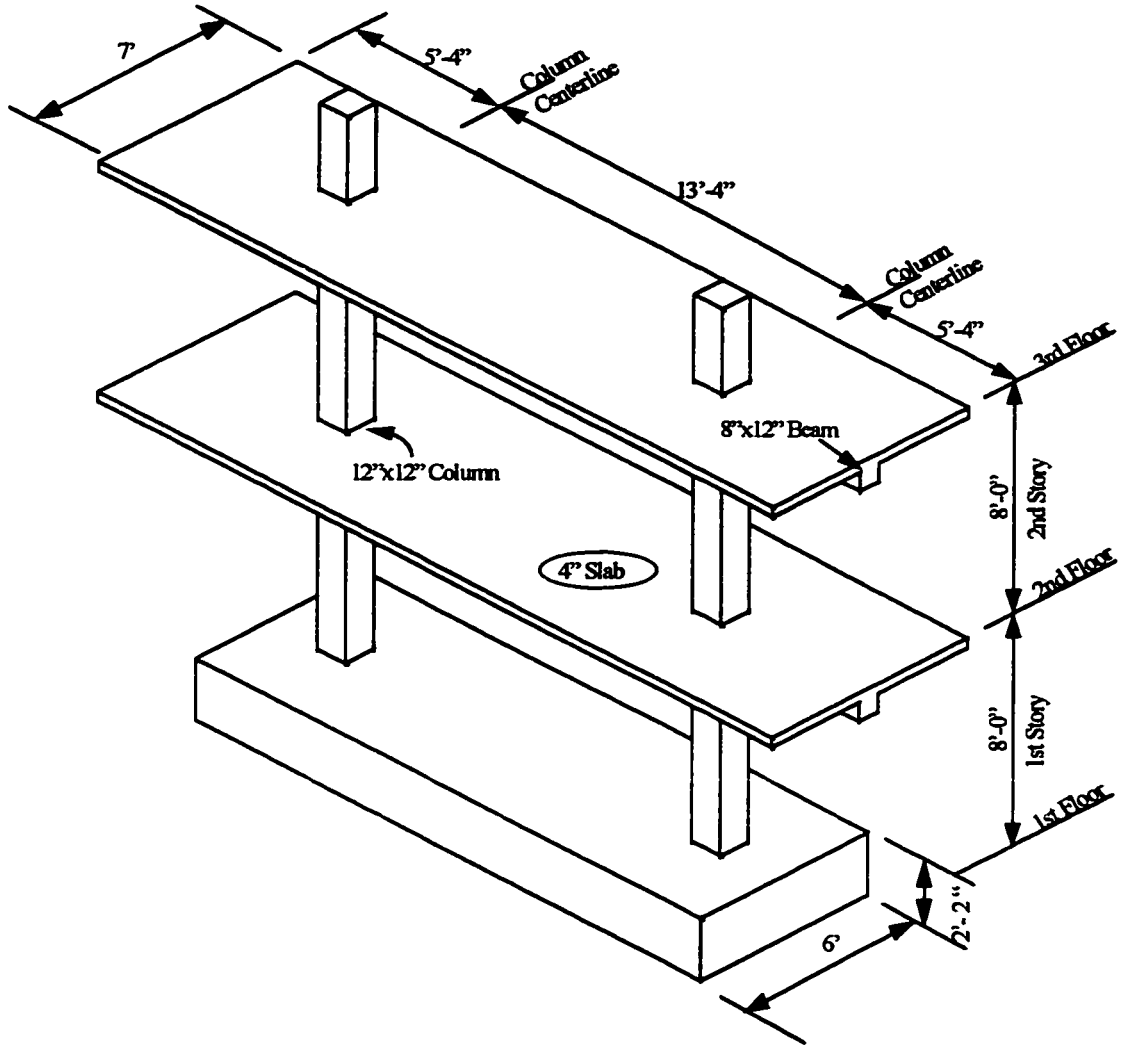

Figure 5.1 Test Specimen of One Bay Frame

The frame elements and reinforcement were typical of non-ductile existing frame structures. Some details of the model frame are presented in Table 5.1 and design drawings are shown in Appendix B.

Table 5.1 Simulated Frame Design

Story No.	Frame Column		Frame Beam			Slab Portion		Footing	Concrete
	Section	Rebar	Section	Top-Bar	Bot-Bar	Section	Fabric	Section	f_c' (psi)
First	12x12	4-#6	8x12	3-#6	3-#5	4x84	w2.9xw2.9	6' x 18'	3000
Second	12x12	4-#6	8x12	3-#6	3-#5	4x84	w2.9xw2.9	x 2'-2"	3000

Note: In the table, dimension is in inches.

5.2.1.1 Non-ductile features

The main deficiencies existing in frame structures of this period are associated with reinforcement details[1,2]. Typical reinforcement detail weak links were considered in frame design.

Beam Reinforcement: Bottom reinforcement was designed as conventional positive moment bars that were discontinuous at the beam-column joint with only a 4 in. embedment into the joint. Top reinforcement was provided in only 1/3 of the span from the column and no top rebars were provided in the middle 1/3 of the span. U-shaped stirrups were selected for the beam.

Column Reinforcement: Splices were designed as conventional compression splices with a $20d_b$ overlap. #3 ties were spaced at 12 in. with 90° hooks at the corners.

5.2.1.2 Rigid Base Mode

For construction convenience and for anchoring the post-tensioning tendons, the base of the frame was designed as a rigid footing. A solid reinforced concrete footing with 2'-2" thickness and 6'-0" x 18'-0" plan dimension was securely anchored to the laboratory floor with thirty-two 2 in. diameter threaded rods .

It should be pointed out that rigid footings or foundations rarely exist in actual structures. The rigid base footing used in the test was determined in consideration of

test demands and construction convenience. To understand foundation effects on the response of the structural system, foundation analytical models were developed and foundation performance will be discussed in Chapters VII and IX.

5.2.1.3 Lateral Loading Mode

Lateral load was applied through the slabs to simulate forces induced by floor mass during an earthquake. Magnitude of lateral load applied through each floor, as shown in Figure 5.2, followed a triangular distribution according to Static Method I for earthquake load design recommended by UBC 1994[49]. This method simulates the first vibration mode which dominates earthquake loads for most structures with intermediate or high stiffness. The triangular loading distribution was applied to the existing frame and to the retrofitted structure tests.

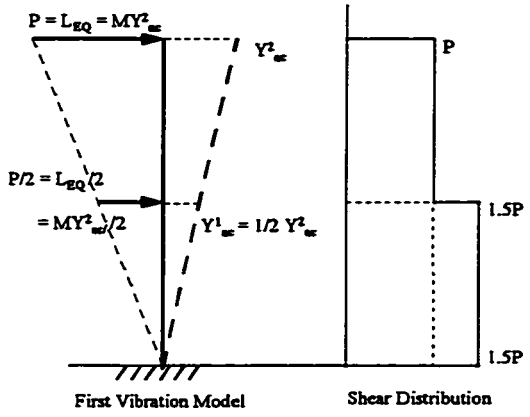

Figure 5.2 Load Distribution

5.2.2 Structural Retrofitting Simulation

Tests of the retrofitted structure focused on demonstrating the feasibility of precast infill walls and post-tensioning for strengthening a frame structural system. The test was also expected to identify precast panel, closure strip and shear lug behavior as part of a structural system under conditions that could not be realized using isolated connection specimen tests.

The retrofitting design followed the well recognized three-limit-state philosophy of structural seismic design. The limit states described in the SEAOC 1990 "Blue Book" [46] as follows:

> *Structures designed on conformance with these Recommendations should, in general, be able to:*
>
> 1. *Resist a minor level earthquake ground motion without damage (Service Limit, or Immediate Occupancy Performance);*
> 2. *Resist a moderate level of earthquake ground motion without structural damage, but possibly experience some nonstructural damage (Damage Limit, or Life Safety Performance);*
> 3. *Resist a major level of earthquake ground motion having an intensity equal to the strongest either experienced or forecast for the building site, without collapse, but possibly with some structural as well as nonstructural damage (Collapse Limit, or Collapse Prevention Performance).*

Implementing the philosophy in a PTPW system design, the retrofitted structure should have sufficient lateral capacity, stiffness and ductility to function satisfactorily in each limit state.

In the service limit state, the structure is required to have adequate strength to withstand light earthquakes. Shear capacity should be sufficient to prohibit brittle shear damage. Meanwhile, the system should also have sufficient moment capacity to function normally without flexural damage.

In the damage limit state, minor damage such as reinforcement yielding and concrete cracking are permitted under a mediate earthquake. System shear capacity

should be at such a level that flexural yielding occurs prior to brittle shear cracking. The post-tensioning tendons which provide flexural capacity to the structure should permit the structure to form plastic hinges at the wall base to develop ductility and significant deformation without element failure.

In the collapse limit state, the structure might be damaged under a major earthquake. The damaged structural system should be stable and permit to develop a mechanism that can tolerate very large deformation and still sustain certain loads, at least, the gravity load.

To reach these goals, it is required that all the infills, shear lugs and post-tension tendons work efficiently and compatibly. Basically, shear lugs are required to have shear yielding capacity that is somewhat lower than infill shear capacity to provide reliable ductility and to avoid infill shear failure. Post-tension tendons and closure strip reinforcement should be sufficient to allow the structure to continue to function in the plastic range. The connection test experiences and design recommendations presented in Chapter IV were adopted in the retrofitting design to meet the above requirements.

5.2.2.1 Closure Strip Test Application

Panel Dimension: Regarding model structure configuration and construction convenience, the infill wall for each story was made up of four pre-cast panels horizontally and two layers vertically with 32 in. x 36 in. panels as shown in Figure 5.3. Panel thickness was 6 in. for the first floor and 4 in. for the second floor. Panel dimensions and weights satisfied the requirements for construction operation convenience as described in Chapter III. Pre-cast concrete panels were reinforced with two layers of 4x4-w2.9 x w2.9 welded wire fabric as in the connection specimens.

Strip and Key Dimension: The closure strips were designed to have a height of 4.0 in. with an aligned shear keys pattern. The shear keys had a height of 1.0 in. with a one-unit spacing. It was demonstrated previously that such dimensions and arrangements are realistic in terms of placing closure strip reinforcement, embedding shear lugs, grouting closure strips and achieving overall strength characteristics.

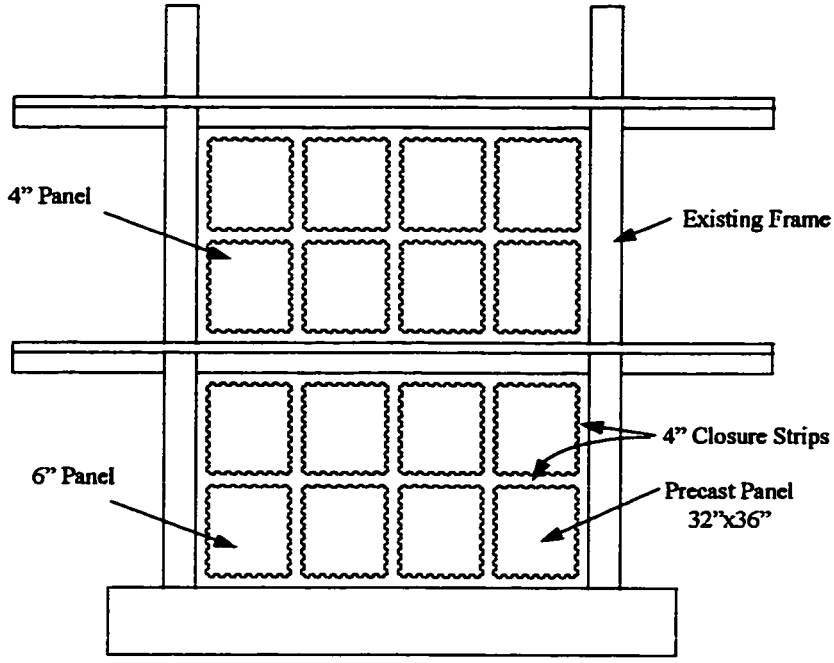

Figure 5.3 Infill Panel Arrangement

Strip Reinforcement: According to reinforcement efficient factors evaluated in Section 4.2.2.2, a ratio not less than 0.425% and not greater than 1.00% of the panel area provided optimum results. Four #4 and three #4 bars were used for vertical strip reinforcement in the first and second story, respectively. The ratios of strip vertical reinforcement were 0.46% of the infill wall. It was predicted that the vertical strip reinforcement with such ratios would yield under ultimate lateral load.

Shear Capacity Design: All panel and strip design variables are presented in Table 5.2. The infill wall shear cracking capacity was evaluated using panel and strip concrete cracking strengths. As discussed in 4.2.2.1, the concrete cracking coefficient f_c was 4.0 with a failure probability of 0.2%. It was expected that infill walls work as a monolithic wall to resist shear and moment. Therefore, when calculating infill wall cracking capacity V_n following equation (4-1), the variable a_p was taken as the full wall cross section a_w and equation (4-1) becomes,

$$V_n = 4\left(a_w\sqrt{f'_{cp}} + a_s\sqrt{f'_{cs}}\right) \tag{5-1}$$

Table 5.2 Shear Capacity Design of Infill Wall

Story	Panel Size (in.)		Strip Size (in.)		Concrete Strength (psi)			Strip Rebar		Capacity
No.	Width b_p	Thick. t_p	Strip h_s	Key h_k	$f_c'_p$	$f_c'_s$	$f_c'_f$	Rebar	Ratio (%)	V_n (kips)
First	32.0	6.0	4.0	1.0	4000	5000	3000	4-#4	0.409	228.2
Second	32.0	4.0	4.0	1.0	4000	5000	3000	3-#4	0.460	152.2

where cracking coefficient f_c = 4.0 was used for infill wall concrete shear capacity

Frame column shear cracking capacity was not counted in equation (5-1) because the infill wall was added after the columns were cracked in the existing frame test. The infill wall shear cracking capacity was predicted as 228 kips for the first story and 152 kips for the second story.

5.2.2.2 Shear Lug Test Application

To permit flexural yielding prior to brittle shear failure, shear lugs were used to provide adequate shear capacity at the interface between infills and the frame at the base. A flexural yielding mode with plastic hinges at the frame base or at beam ends was desired to permit energy dissipation and to provide structural ductility for earthquake resistance.

Pipe Number and location: Compatible with the panel and closure strip arrangement, three steel pipes were designed as horizontal shear lugs corresponding to vertical closure strip locations at the top and bottom of each infill wall for both stories as shown in Figure 5.4. One pipe was installed at the mid-height of each column as a vertical shear lug. The shear capacity of each story was estimated as the sum of the strengths of pipes at the base of the wall.

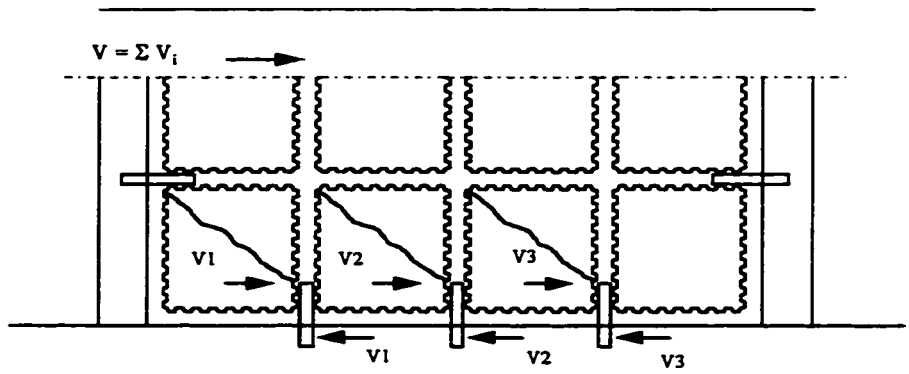

Figure 5.4 Shear Lug Arrangement

Pipe Size and Capacity: Extra strong steel pipes with nominal diameters of 2-1/2 in. and 2.0 in. were adopted for the first and second story, respectively. The nominal pipe shear strength was calculated from equation (4-27) using the tested yielding strengths of 54.6 psi for the 2-1/2 in. pipe and 40.4 psi for the 2.0 in. pipe. Total pipe yielding strength of three lugs was estimated as 209 kips at the base interface and 104 kips at the bottom of second infill wall interface.

At each story, total pipe yielding capacity was less than infill concrete cracking strength to preclude brittle failure of the wall in shear. Because of the use of post-tensioning, the column-infill interface would not be subjected to large shear but the vertical shear lugs at this interface were the same as the horizontal interface lugs in that story.

Embedment length: To prevent concrete bearing failure, pipe embedment into the frame elements was designed according to concrete bearing and pipe shear yielding strength. Bearing design followed Equation (5-2) specified in Section 10.15.1 of ACI 318. Yielding capacity was estimated using equations recommended in Chapter IV.

$$L_{em} = \frac{V_p}{\phi \left(0.85\, f_c' \sqrt{\frac{A_2}{A_1}}\right) D_o} \qquad (5\text{-}2)$$

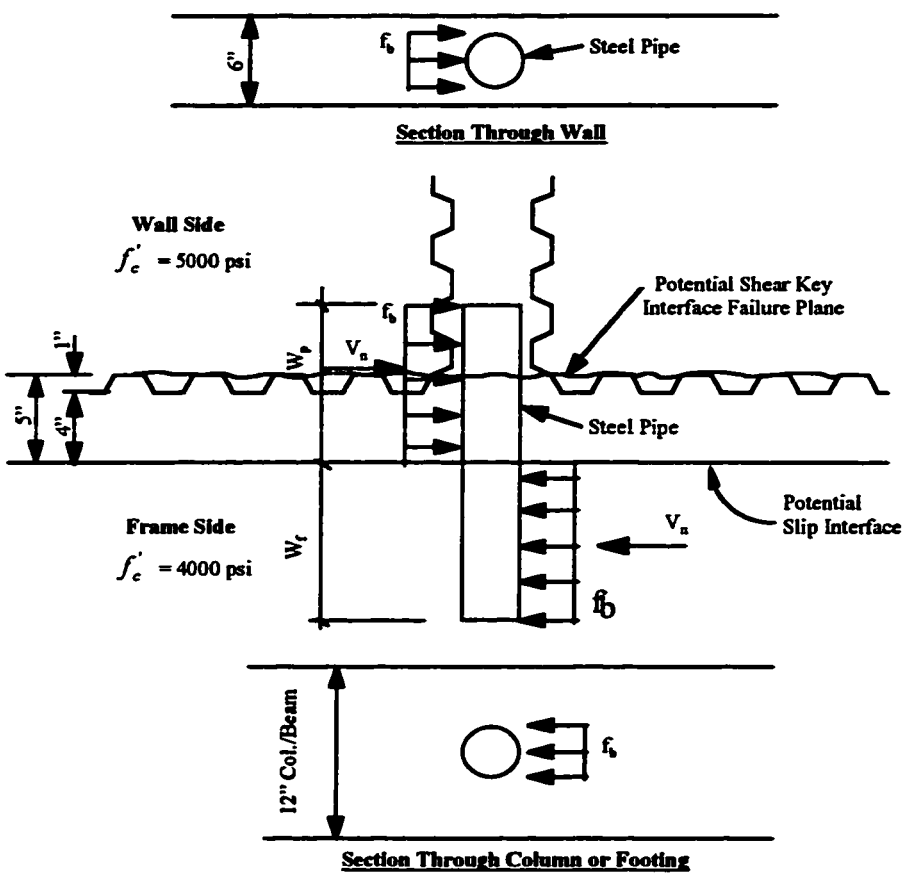

Figure 5.5 Concrete Bearing and Pipe Embedment

As shown in Figure 5.5, the embedment length into the wall was determined according to required bearing length plus the strip height. Variables including embedment length and nominal shear capacity V_p were listed in Table 5.3.

The embedment length needed to develop yielding was checked according to the recommendation in Chapter IV. The embedment length w_p into the panel was two times the closure strip height plus the shear key height. The required embedment length w_f into the frame element was calculated using equation (4-33) and (4-35) and is presented in Table 5.3 in the column labeled "yielding". The embedment length required for concrete bearing is shorter than that demanded to develop pipe shear yielding. Except for embedment into the frame at the first story, all pipe embedments satisfied the yielding requirement. The test results showed that the embedment in the frame at the first story base was not long enough and will be discussed in section 5.5.2.

Table 5.3 Pipe Embedment Length Design

Story No.	Related Element	Panel t_p (in)	Strip h_s (in)	Beam/Col. A_2 (in)	Concrete (psi) $f_c'_p$	Concrete (psi) $f_c'_f$	Pipe Embedment Length (in) Bearing	Design	Yielding	Capacity V_p (kips)
First	Wall	6.0	4.0	12.0	4000	3000	8.45	12.00	13.00	209.0
	Frame	6.0	4.0	12.0	4000	3000	6.78	6.00	9.00	
Second	Wall	4.0	4.0	12.0	4000	3000	6.22	11.00	10.00	104.0
	Frame	4.0	4.0	12.0	4000	3000	4.07	5.00	6.00	

5.2.2.3 Post -Tensioning Implementation

With an infill wall added to a frame structure, the system lateral shear capacity is greatly increased. However, if the system does not have compatible flexural capacity, it is impossible to realize the enhanced shear strength because the earthquake simultaneously induces large shear and moment on the structure and because the

infilled non-ductile frame has very low flexural capacity. An effective technique for increasing flexural capacity is boundary element (column) post-tensioning [31] .

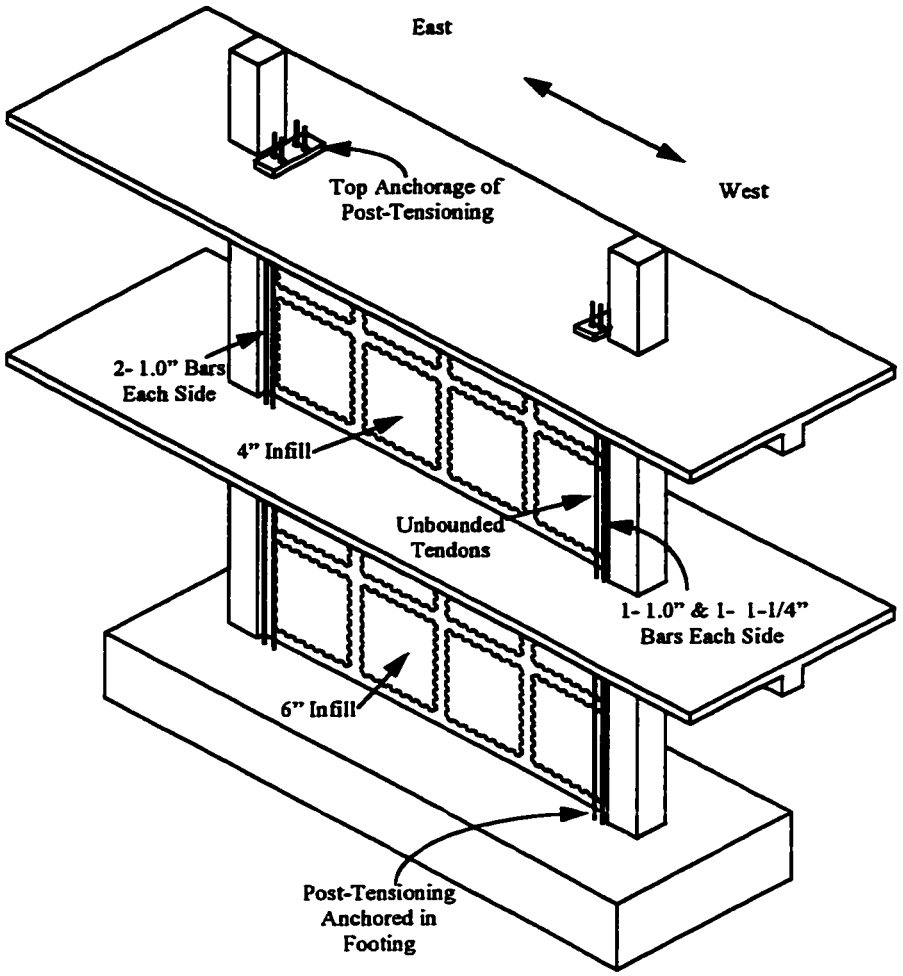

Figure 5.6 Infill With Post -Tensioning

Post-tension functions: In a PTPW system, post-tension tendons applied to boundary columns were designed to have following functions:

1) Provide adequate flexural strength compatible with infill wall shear strength.

2) *Provide prestress to column to prohibit early splice failure.*

3) *Provide a compressive stress on the infill to improve shear transfer across horizontal interfaces and to produce a system that acts as a monolithic wall.*

4) *Provide system flexural ductility to the system.*

Post-Tension Tendons: High strength Dywidag bars were adopted as post-tension tendons[31]. Based on system ultimate shear strength estimated using ACI 318, two 1.0 in. tendons were designed for both ends (boundaries of the wall) adjacent to the columns. However, it was recognized, from the connection specimen test results discussed in Chapter IV, that design following current code underestimated infill and shear lug capacities. To be compatible with actual infill wall shear capacity, larger boundary force were likely to be needed so that more tendons should be added. Therefore, two 1.0 in. tendons were added at the east end and two 1-1/4 in. tendons were added at the west end as shown in Figure 5.6. Anchorage for those tendons were embedded prior to casting the base footing so that tests under high lateral load levels (such as system shear test) could be executed to develop infill shear failure.

5.3 Model Structure Construction

5.3.1 Frame construction

5.3.1.1 Base Footing Casting

The base (footing) was cast against the laboratory floor. It was anchored to the floor with a total of forty 2.0 in. threaded rods (in which eight were reserved) through the use of PVC ducts. After the concrete cured, the rods were tightened through the use of steel plate washers and nuts as shown in Figure 5 7.

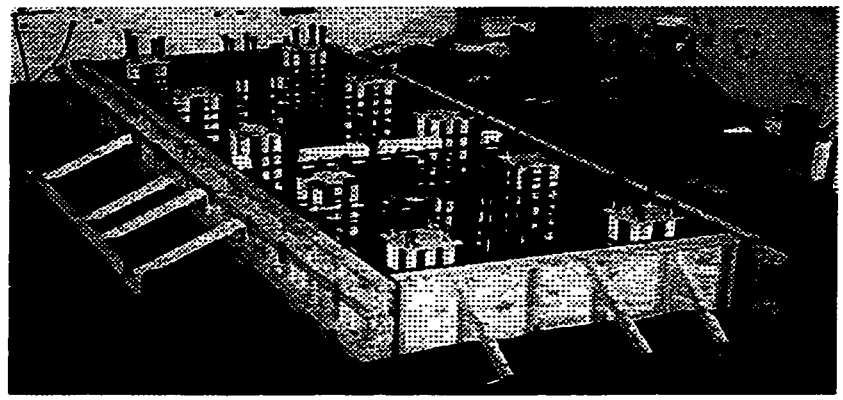

a) Footing Formwork

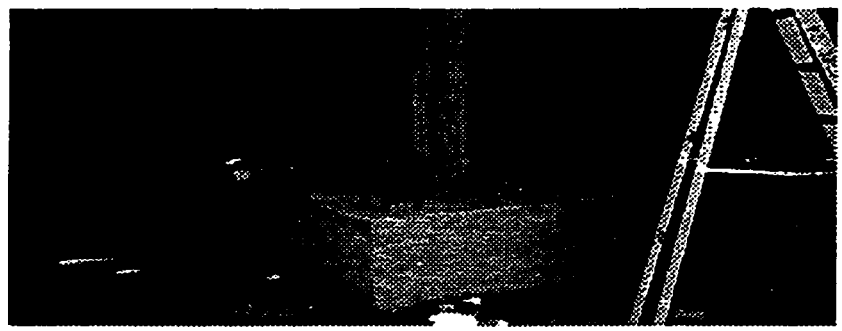

b) Cast Footing

Figure 5.7 Footing Anchorage

The post-tension tendons were installed through PVC ducts and extended to the bottom of the footing. A steel plate anchored the tendons at the footing bottom. The tendons and frame column rebars protruded out of the top surface of the footing for extension coupling and for splicing.

The holes for inserting base shear lugs were provided through the use of PVC tubes to form the holes when the footing was cast. Concrete surfaces at column locations on the footing were roughened for better shear transfer between the footing and column concretes which were cast separately.

5.3.1.2 Frame Casting

Column reinforcement were spliced to bars that projected from the footing. Each story was constructed separately. The slab, beam and columns were cast without construction joints.

The column bars projected from the first story to the second story. PVC tubes formed small ducts through the floor slabs at the position outside of the beams next to the columns for inserting post-tension tendons. Shear lug cores were also pre-formed in the footing, beams and columns with PVC tubes. Figure 5.8 shows overall frame casting and the completed frame structure. The frame was loaded to reach a level that formed cracks in columns and beams to simulate a slightly damaged frame in need of retrofitting.

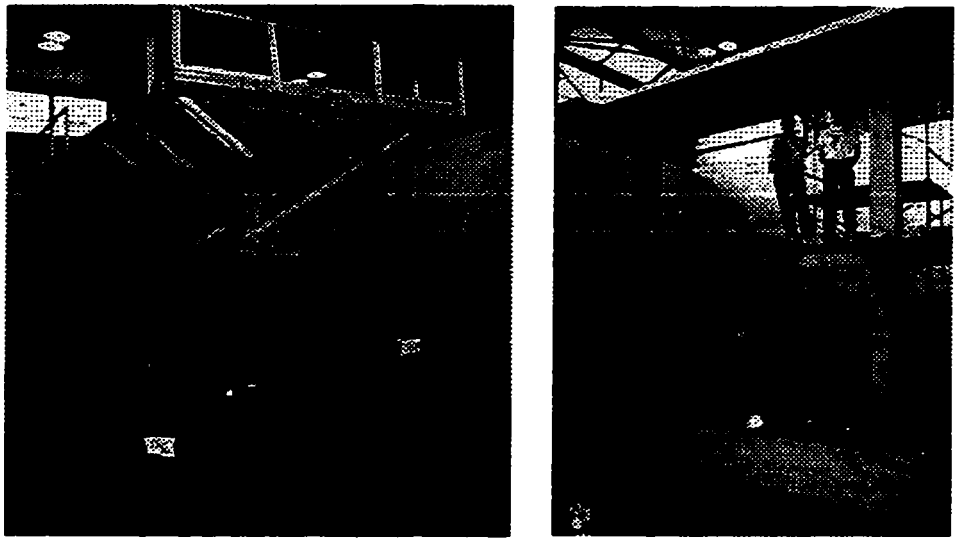

a) Frame Under Construction b) Constructed Frame

Figure 5.8 Existing Frame Construction

5.3.2 Retrofitting Construction

Retrofitting construction was conducted after the existing frame was tested. The model structure was retrofitted with pre-cast infill walls and boundary column post tensioning.

5.3.2.1 Pre-cast Panel Construction

The pre-cast reinforced concrete panels used for retrofitting are the same as the panel segment used in connection specimen tests except the size was enlarged to 32" x 36" to meet the frame dimensions. All variables for panel design were listed in Table 5.2

Direct placement of grout discussed in Chapter III worked fairly well to achieve sound consolidation of closure strip concrete. Figure 5.9 shows the panel forms and completed panels stocked prior to installation.

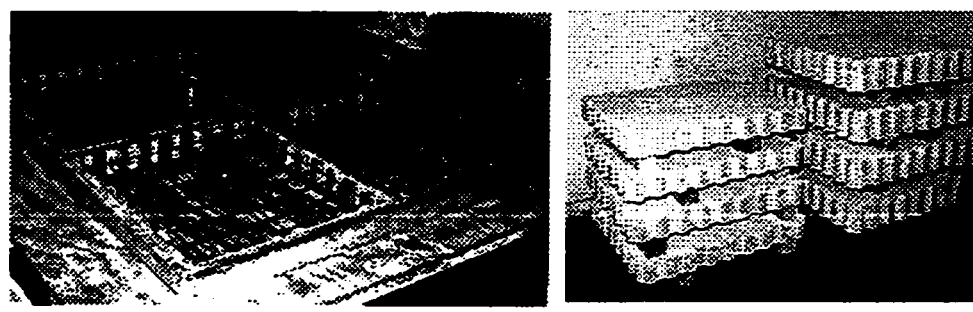

a) Infill Panel Formwork b) Piled Infill Panels

Figure 5.9 Infill Panel Construction

5.3.2.2 Panel Placing

Because it was impossible to use a forklift to place pre-cast panels on the narrow one-bay frame (model structure), the panels were positioned with a 2-ton crane after being placed on the model structure by a forklift. At the first story, a hoist was mounted on the frame beam above the infill so that a steel lifting chain could be

hung through the pre-formed shear lug insertion holes to support the hoist. For the second story infill, the crane was mounted on a scaffolding erected on the top floor. Figure 5.10 shows the lifting process. The inserts provided in panels were used for panel lifting and placement.

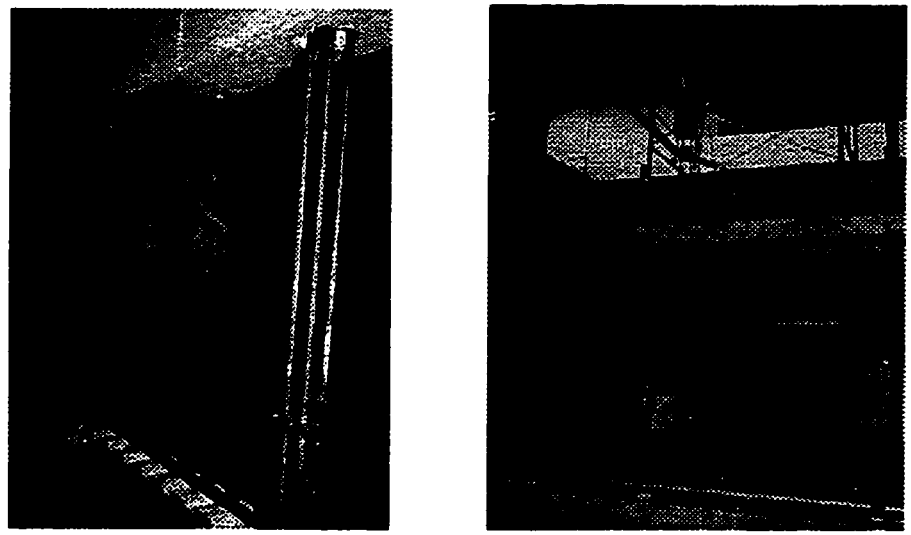

a) First Story and Close-up Hoist b) Second Story Lifting System

Figure 5.10 Panel Lifting Device

5.3.2.3 Supporting and Bracing

The panels were supported and positioned by means of lag bolts, the horizontal strip height as well as the vertical strip width was maintained with the lag bolts which were screwed into inserts provided along the panel edges as shown in Figure 5.11.

Figure 5.11 Closure Strip Lag Bolt

Lateral braces were provided on both sides of the panels to hold the panels in position. Timber 2 x 4's used as braces were secured at one end to the panel insert and at the other to the footing or floor slab as shown in Figures 5.12a and 5.12b.

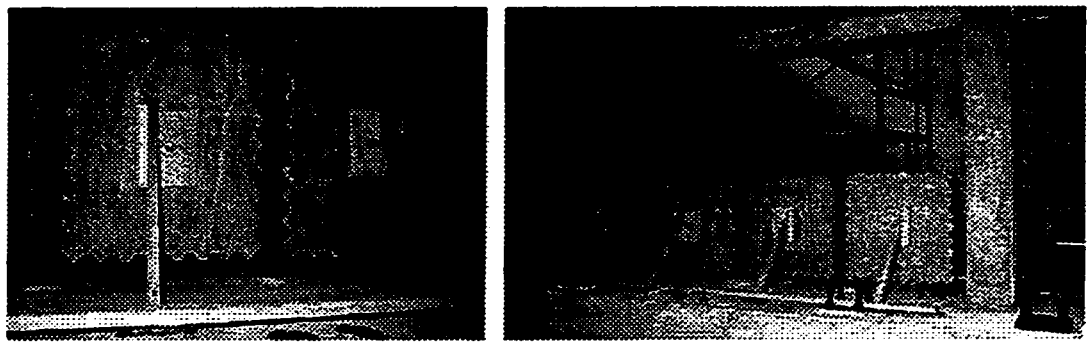

a) Panel Spacing and Support b) Panel Placement and Bracing

Figure 5.12 Panel Support and Bracing Schemes

5.3.2.4 Infill grouting

Each row of four panels, grouting was assembled and grouted in four stages: shear lug and strip reinforcement placement, closure strip formwork installation, grout placement, vibration and curing.

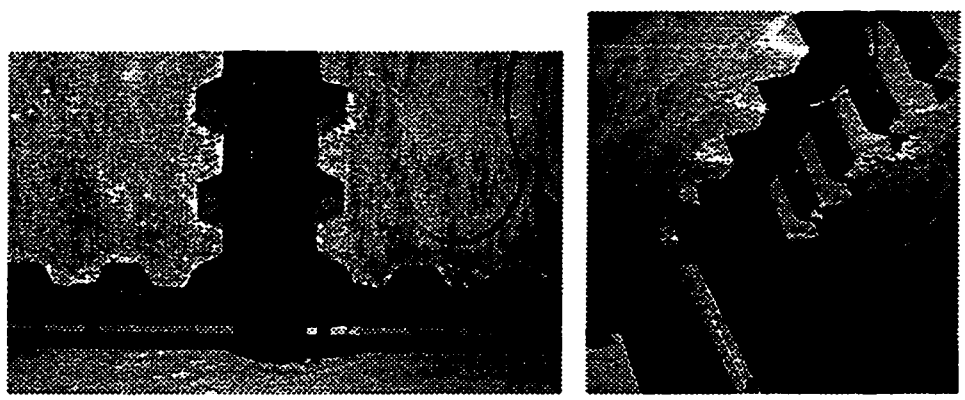

a) Base Shear Lug Insertion b) Base Lug Grouting

Figure 5.13 Base Shear Lug Insertion and Grouting

Base shear lugs were placed and grouted prior to grouting the closure strips. Grout concrete was placed from the top of the panel. Figure 5.13 shows base shear lug and closure strip construction. After the first row was grouted in each story, column shear lugs were placed along with the horizontal strip rebars as shown in Fig. 5.14. Then, the second row of strip formwork was installed as shown in Fig. 5.15. The grout concrete, at this time, was placed from the upper floor through the lug insertion cores penetrating the frame beam.

Figure 5.14 Column Lug Grouting

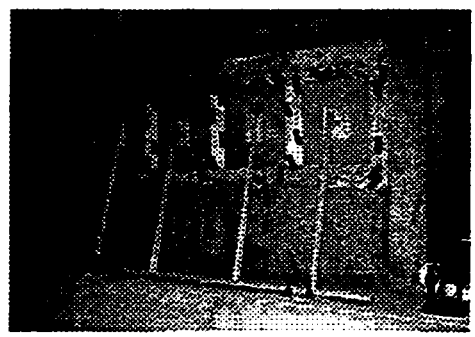

Figure 5.15 Second Row Strip

a) Simultaneous Vibration

b) Vibration Through Holes

Figure 5.16 Access Hole Method

The access hole method described in Chapter III was used for vibration. At least two holes were provided (at 4.0 ft. apart) along the horizontal strip formwork. The grout was vibrated through vertical strips from the top and simultaneously through the access holes along horizontal strips as shown in Figure 5.16. By this method, the infill could be grouted and consolidated well. Figure 5.17 shows grout quality at one corner near the column-beam joint where a small gap was noted after formwork was removed. This is the only grouting problem observed.

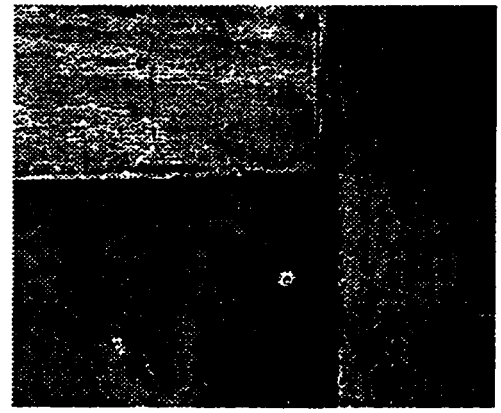

Figure 5.17 Dead Corner Grout

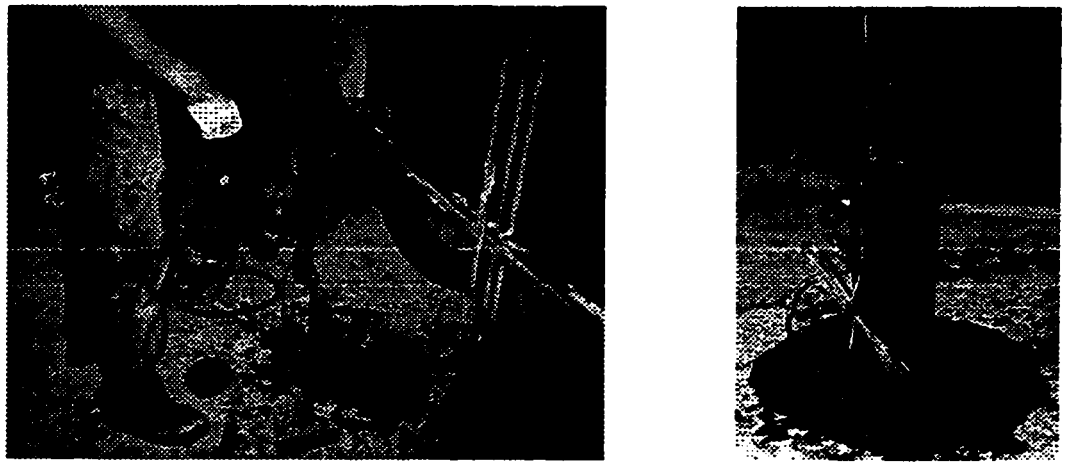

Figure 5.18 Floor/Beam Shear Lug Insertion

The later insertion process described in Chapter III was adopted to place the floor beam shear lugs as shown in Figure 5.18. At the same time, the vertical strip reinforcement was placed into the fresh grout inside the steel pipe. Figure 5.19 shows the complete frame-infill wall structure.

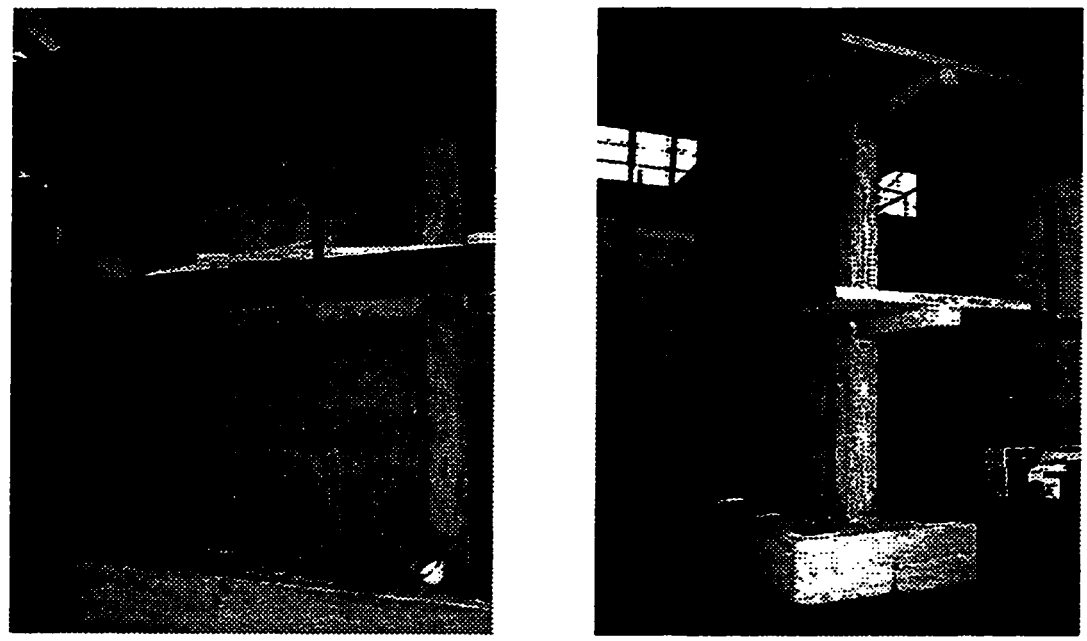

a) Grouted Infill System b) Complete PTPW System

Figure 5.19 Constructed Precast Infill Post-Tensioning System

5.3.3 Post-Tensioning Tendons

5.3.3.1 Tendons Installation

For convenience, high strength Dywidag bars were used as unbonded post-tensioning tendons. The embedded tendons protruded about one-foot above the footing surface to provide connection length for tendons extension. By means of couplers, the tendons, which have a length the same as the story height of the structure, were inserted through pre-formed ducts penetrating the slabs.

Steel anchor plates and nuts were provided on the top floor for anchoring the tendons at their upper ends. To prevent concrete bearing damage under post-tensioning force, large bearing plates were adopted. The bearing area or the bearing plate size was based on the ultimate strength of the group tendons. The bearing plates were also used to support the rams to stress the tendons as shown in Figure 5.20.

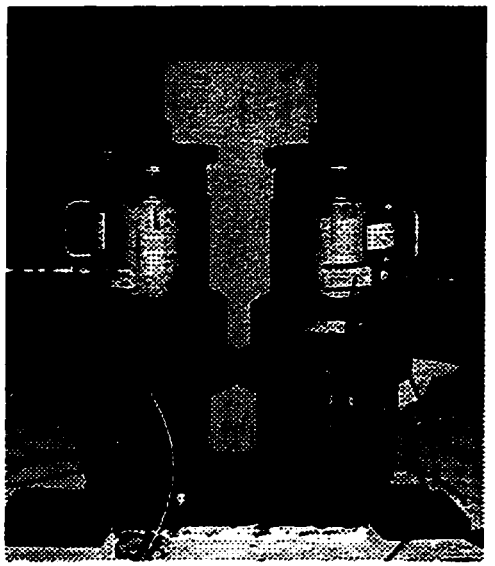

Figure 5.20 Tendons Stressing

5.3.3.2 Tendons Tensioning

Two 60-ton rams were used to stress the tendons on both sides of the beam simultaneously to prevent out-of-plane moments on the wall and column. Pressure gauges and load cells were used to monitor the tension forces. Meanwhile, strain gauges were attached to the tendons and were calibrated with load cells. Tension loads were hold at a desired level by tightening the nuts through the threaded extension bars from the top of the rams while the tendon anchorage were seated by tightening the tendon anchor nuts against the anchor plate. Strain gauge readings were calibrated to permit reduction of tension losses after release of ram loads. The completed model structure with precast infill wall and post-tensioning system is shown in Figure 5.19b prior to testing.

5.3.4 Material Demonstration

5.3.4.1 Concrete Mixture and Strength

Frame segments, panels and grouting concrete mixtures used in the connection specimen tests were adopted with only slight adjustments and the mixture variables are presented in Table 5.5.

Almost each mixture reached higher concrete strengths than the design strength. The concrete strength at the time the structure was tested are also listed in Table 5.5. Strength curves were shown in Figure 3.15

Table 5.5 Model Structure Concrete Mixture And Strength

Batch Of Mixtures	Base Footing	Frame Element	Precast Panel	Infill Wall Grout
Design Strength f'_c (psi)	3000	3000	4000	5000
Cement (pcy)	360	400	470	693
Coarse Aggregate (pcy)	184	1625	1625	1167
Fine Aggregate (pcy)	1435	1619	1655	1755
Water (pcy)	26	275	250	325
Admixture (ozcy)	10.5	12.0	20.0	27.6
Superplasticizer (ozcy)	-	-	-	25.0
Nominal Slump (in)	4.0	4.0	6.0	4.0
On Site Slump (in)	6	6	6	8
Tested Strength f'_c (psi)	4600	3600/4000	4000/5000	6000

The numbers xx/yy represent strengths of xx and yy for first and second floor respectively

5.3.4.2 Steel Strength

Steel used in the model structure test was identical to that used in connection specimen tests except for the Dywidag bars (post-tensioning tendons). The stress-strain curve for the tendons is shown in Figure 5.21. Steel strengths are presented in Table 5.6.

Table 5.6 Steel Properties in Model Structure

Steel	Beam/ Column		Strip	Shear Lugs		Dywidag Tendons	
Strength	#5 Bars	#6 Bars	#4 Bars	2" XS Pipe	2.5" XS Pipe	1" Bar	1-1/4" Bar
Yield (ksi)	61.3	61.1	63.0	40.4	53.6	152.9	146.0
Ultimate (ksi)	99.9	98.7	102.8	55.7	71.6	170.6	160.4

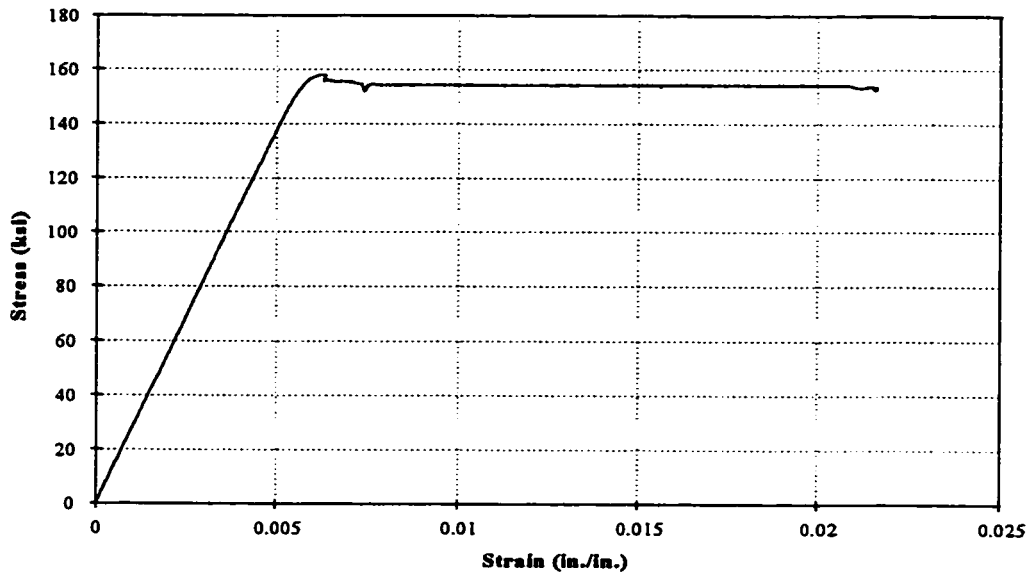

Figure 5.21 Stress-Strain Curve of Dywidag Tendons

5.4 MODEL STRUCTURE TESTS

The structure was tested first as an existing frame to provide some information on displacement and lateral capacity. Lateral load was limited to a level that it did not produce permanent damage to the frame. The retrofitted structure tests focused on investigating retrofitting efficiencies to increase shear and moment capacities by adding infill walls and post-tensioning tendons to the frame.

5.4.1 Test Setup and Instrumentation

5.4.1.1 Loading Mode and Device

The retrofitted structure was designed to have an ultimate lateral strength lower than the lateral loading capacity of the laboratory reaction wall. Cyclic lateral loads applied on the structure simulated the earthquake loads of the first vibration mode as described in Section 5.2.1.3.

Two 150-kip rams and two 100-kip rams applied horizontal loads at the second and first floor respectively. One end of the ram was mounted to the reaction wall buttress having a 300-kip lateral load capacity. The other end of the ram was connected to the structural slab through a loading transfer system shown in Figure 5.22. The loading transfer system cast in the slab was designed as steel angles attached to the slab edges longitudinally and shear studs across the slab section transversely to distribute load evenly over the slab and to prevent extreme stress concentration in the slab. Two-way rams were used to apply loads in both directions.

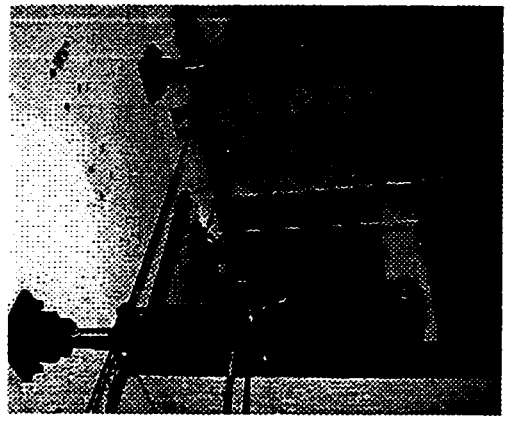

Figure 5.22 Lateral Loading System

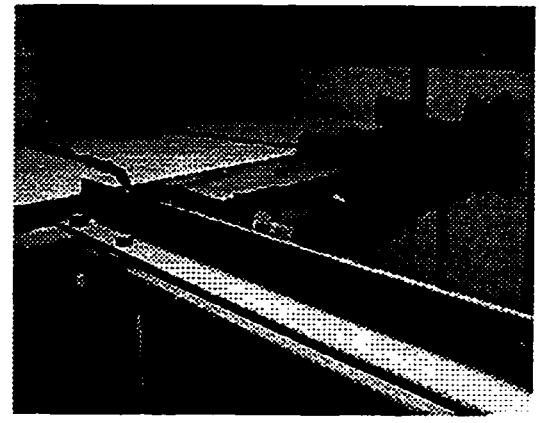

Figure 5.23 Out-of Plan Bracing

5.4.1.2 Specimen Bracing

To prevent torsion or out-of-plane moment to be induced due to uneven loads applied from rams on two sides of the structure, lateral braces were provided through another reaction wall perpendicular to the loading application wall. Steel angles used as braces, shown in Figure 5.23, were connected to the slab and reaction wall with pinned ends to allow free translation in the structural plane.

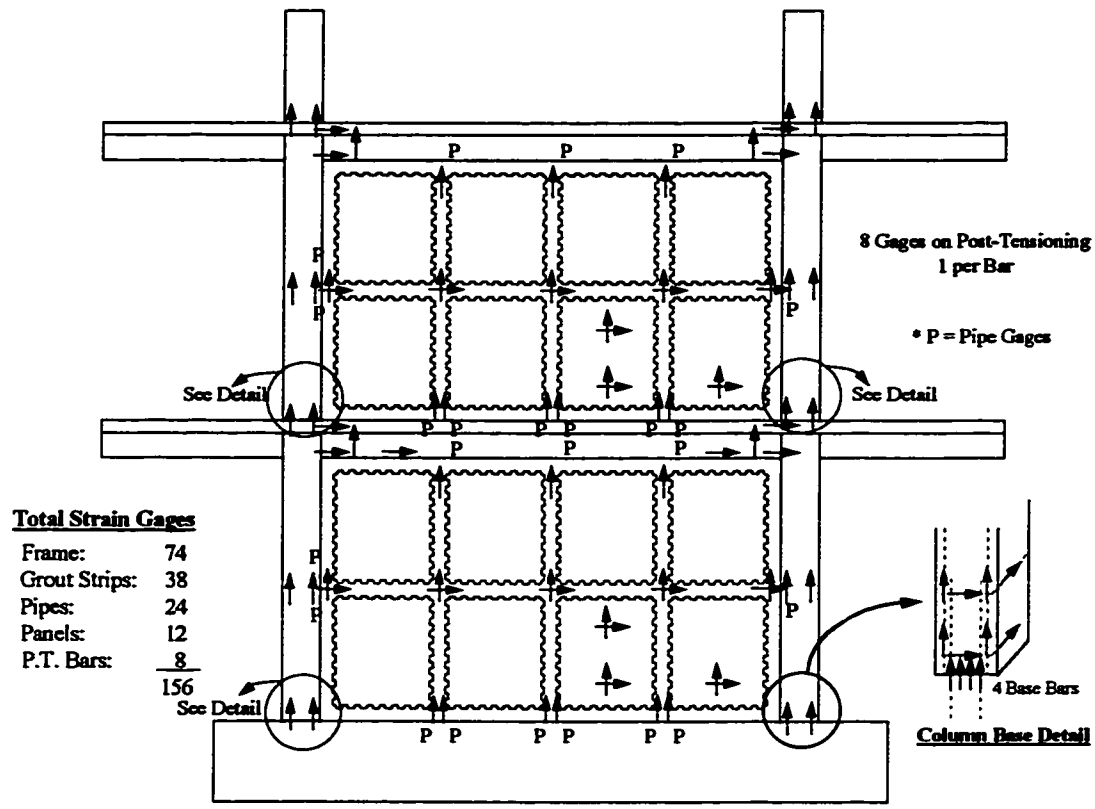

Figure 5.24 Layout of Reinforcement Strain Gauges

5.4.1.3 Instrumentation

To record and monitor structural response, the model structure specimen was well instrumented. Responses of structural elements were recorded through the use of

strain gauges attached to reinforcement in columns, beams, strips, panels, shear lugs and post tension tendons. Locations of reinforcement strain gauges are shown in Figure 5.24. Various structural displacements were monitored with displacement transducers and gauges mounted horizontally, vertically and diagonally as shown in Fig. 5.25.

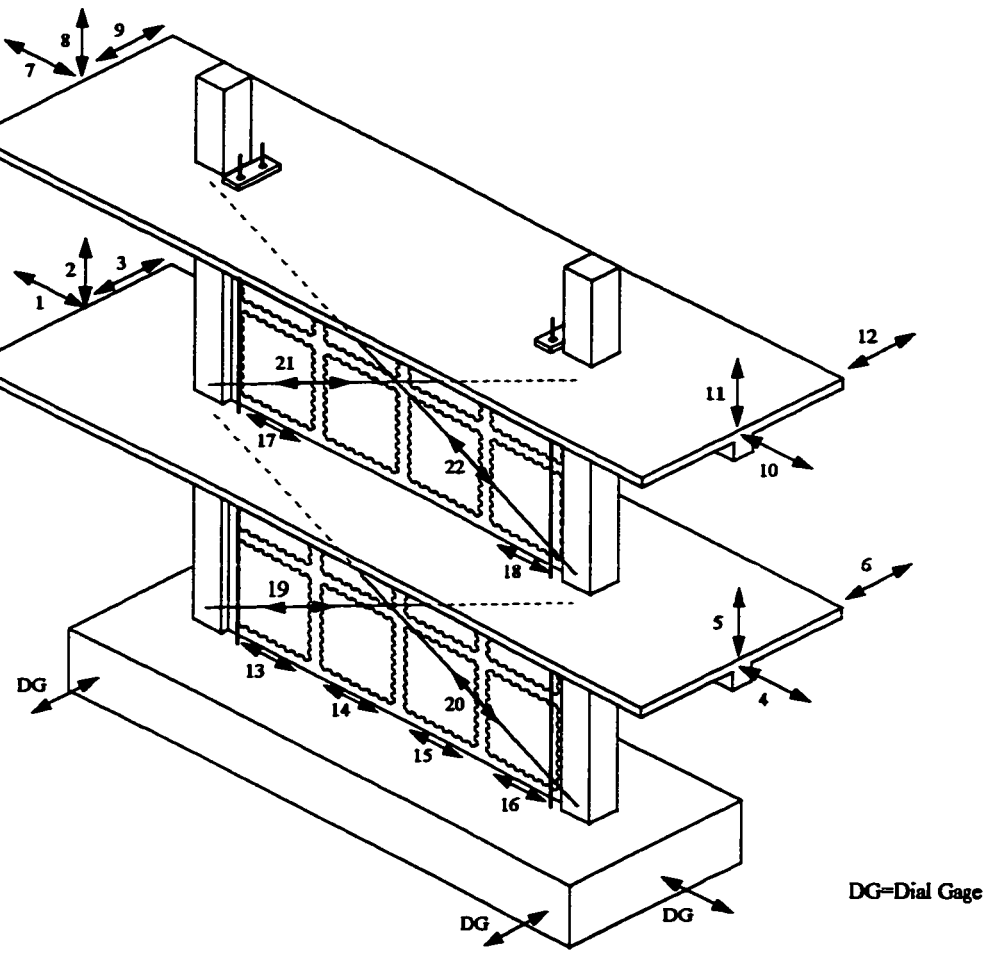

Figure 5.25 Layout of Displacement Gauges

Computer data acquisition systems were used to monitor the gauges, transducers and load cells. X-Y plotters were used to record load-displacement response. One computer and a plotter were used to record infill wall response while another computer and a plotter were used to record frame response.

Loads were controlled through the use of pressure transducers and shear pin load cells attached on both rams. Loads were also monitored through readings from the computer data acquisition systems. Loading-deformation curves were plotted by X-Y plotters. To minimize torsion effects induced by uneven loads from rams mounted on the two sides of the structure, a single pressure manifold was used to simultaneously supply the both rams at each side of the structure.

5.4.2 Frame Test

Splice failure was expected in the retrofitted model structural test. Load was limited to a level below the value corresponding to splice failure or reinforcement yielding at the bottom of columns.

Existing frame test focused on identifying the weak links and lateral capacity of the non-ductile frame structure. The test result was used to evaluate retrofitting efficiency through quantitative comparison of the lateral capacities between the non-retrofitted frame and the retrofitted PTPW system.

5.3.2.1 Test Result

Triangular distribution load mode, in a proportion of 1.0P at the second floor and 0.5P at the first floor, was used in the test. The history of the total lateral loads (base shear) applied is shown in Figure 5.26. Frame lateral displacement response to the total lateral load or base shear force is shown in Figure 5.27.

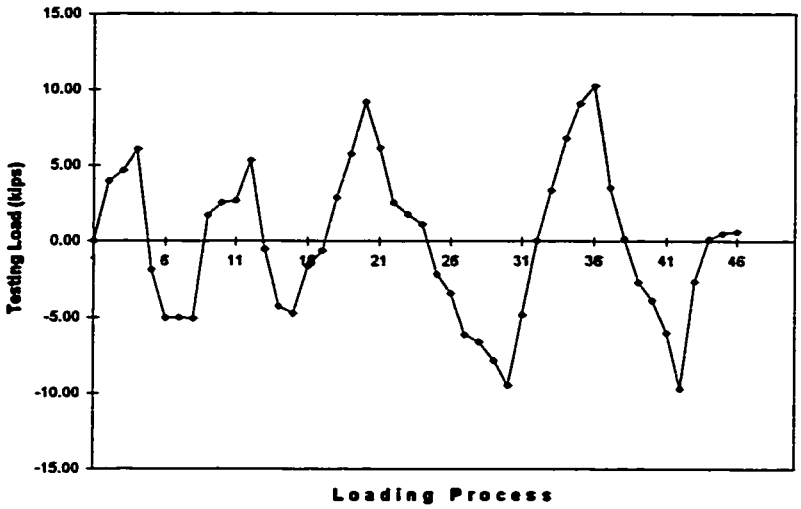

Fig. 5.26 Frame Testing load

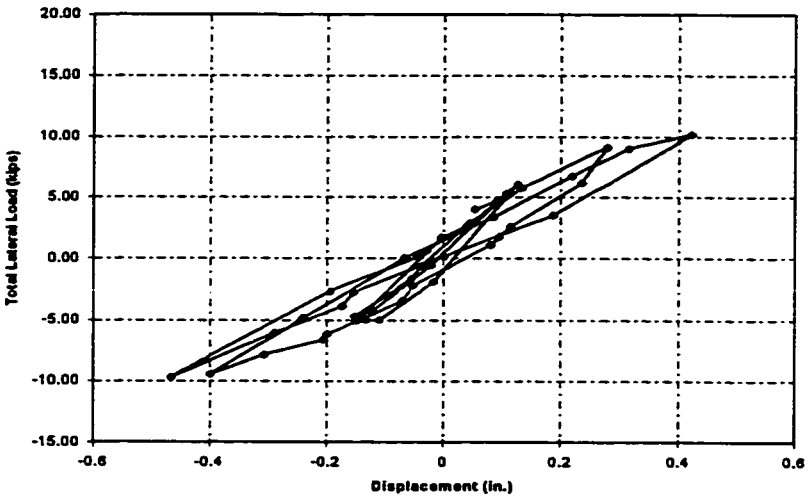

Fig 5.27 Existing Frame Test Result

Cracking first occurred at the top of first floor slab and beam, and then at the bottom of first floor columns as shown in Figure 5.28. Stress ranges in beam bottom

bars and column bars were lower than splice failure stress values calculated using Orangun [38,9] bond stress equations denoted as (5-3a) and (5-3b) respectively.

$$\mu_{bon} = \left[1.22 + 3.23\frac{C}{d_h} + 53\frac{d_h}{l_s}\right]\sqrt{f_c'} \qquad \text{(5-3a)}$$

$$\mu_{bon} = \left[1.22 + 3.23\frac{C}{d_h} + 53\frac{d_h}{l_s} + \frac{A_{tr}\, f_{yt}}{500 s d_n}\right]\sqrt{f_c'} \qquad \text{(5-3b)}$$

Structural analysis was conducted using non-linear structural analysis program IDARC to predict the frame capacity. Predicted total lateral load was 12.3 kips which was slightly greater than the applied load because the top displacement input for the IDARC analysis was slightly higher than the actual displacement. Computed reinforcement tensile stresses in columns and beams were also higher than the test results. Although cracking was observed in frame elements as shown in Figure 5.28, splice failure and plastic hinge formation did not occur.

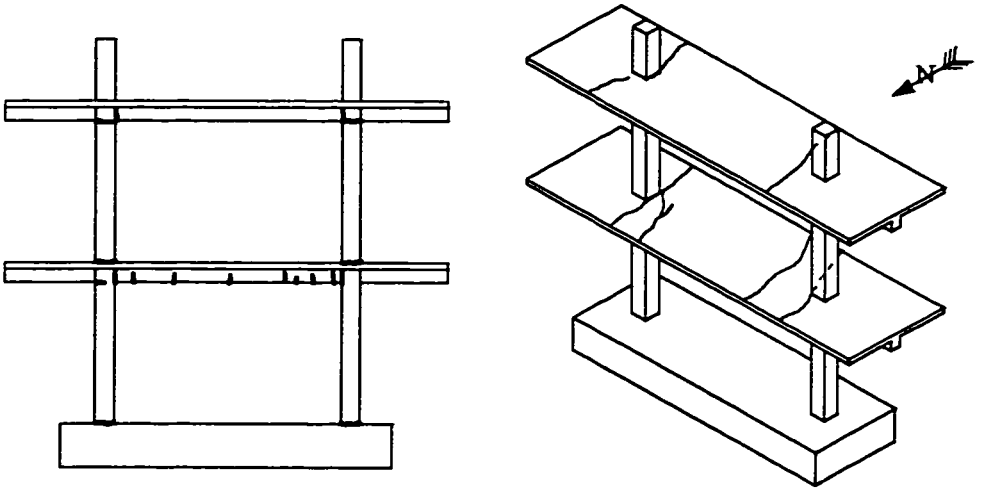

a) Beam Bottom and Column Cracking **b) Beam Top Cracking**

Figure 5.28 Element Cracking in Frame Test

5.4.3 Retrofitted Structure Tests

The PTPW system specimen was tested using the same triangular load distribution to simulate first vibration mode effects. Tests to determine both flexural and shear strength were conducted in order to confirm the evaluated connection and infill wall capacities, and to investigate post-tensioning performance and retrofitting efficiency.

5.4.3.1 Test Results

The retrofitted model structure was tested in three phases corresponding to different post-tensioning levels. Table 5.8 presented the initial post-tensioning forces and corresponding lateral loads applied in each test.

Table 5.8 Post Tension Force and Lateral Load in Model Structure Test

Test Phase	Phase I			Phase II			Phase III		
	Post Tension		Lateral	Post Tension		Lateral	Post Tension		Lateral
	West	East	Load	West	East	Load	West	East	Load
Initial	191.1	108.1	-	255.3	251.9		0.00	0.00	
Ultimate			275.0			450.0			495.0
Behavior	Flexure Dominate			Shear Dominate			Shear Dominate		

In the first phase, two 1.0 in. tendons were installed at the east column while two 1-1/4 in. tendons were installed at the west column. In the second phase, four 1.0" tendons were installed at the east, and two 1-1/4" and two 1.0" tendons were installed at the west, respectively. In the third phase, all tendons used in the second phase were retained but with zero initial stress (zero initial post-tensioning). Test results will be presented for all test phases. The test loading directions were termed as push (to the west) and pull (to the east). The test loads are presented in terms of base shear, and loading cycles were represented by the load or displacement level superscripted by the cycle number. Where 45^1 or 0.3^1 means the first cycle to 45 kips or the first cycle of 0.3 percent drift by load or displacement control, respectively.

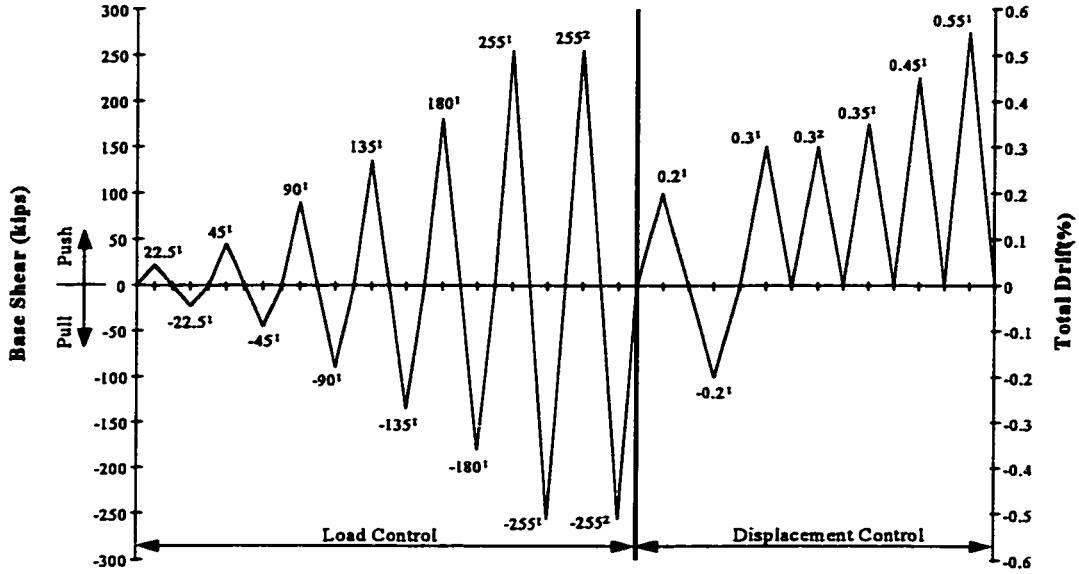

Figure 5.29 Loading History of Test I

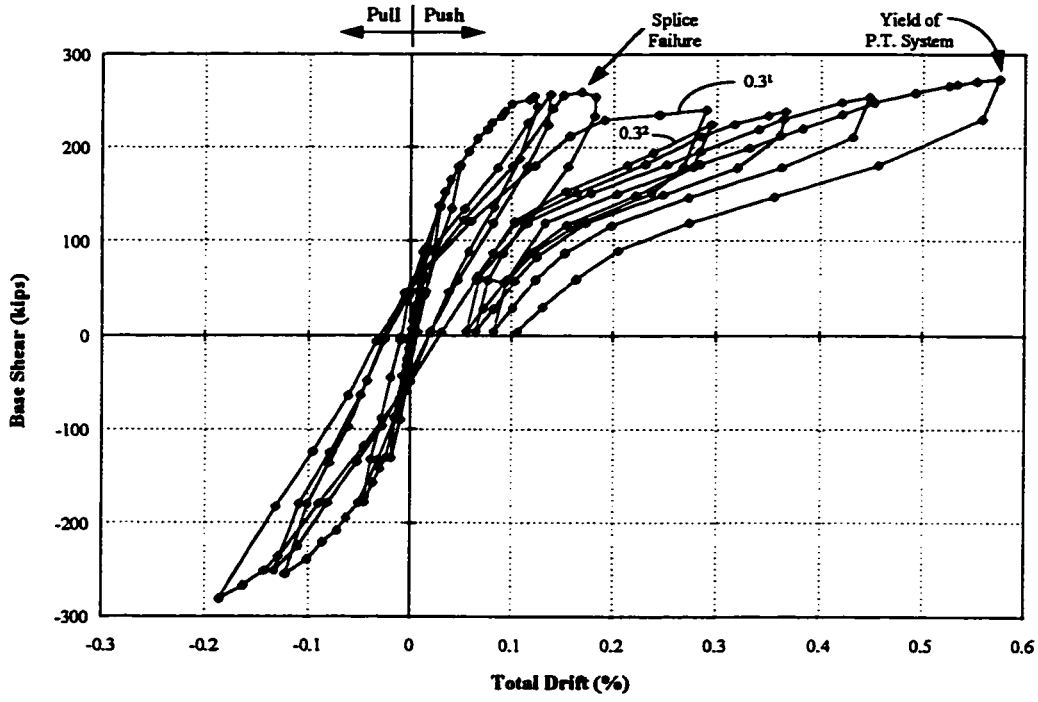

Figure 5.30 Structural Response of Test I

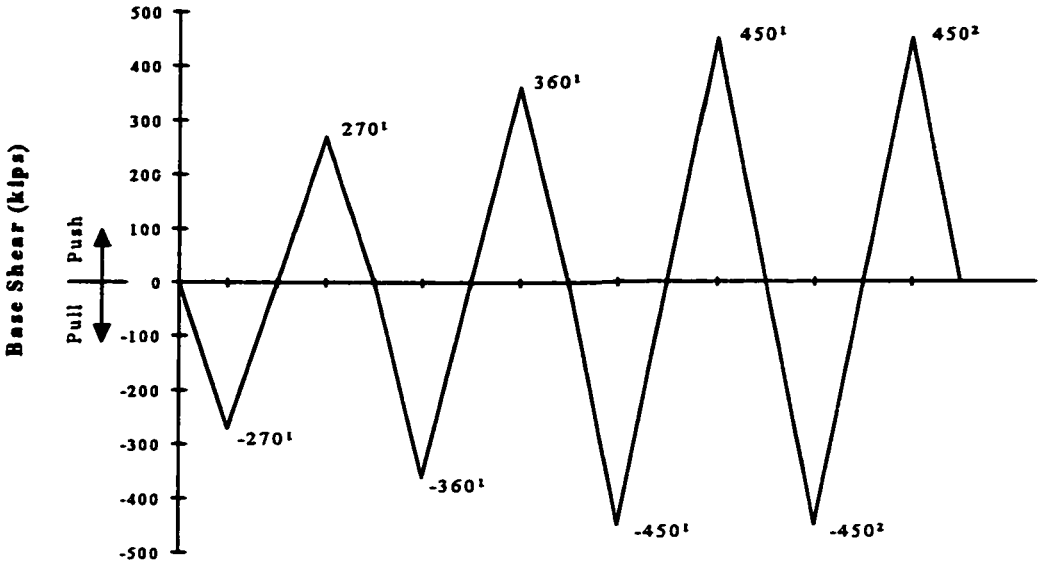

Figure 5.31 Loading History of Test II

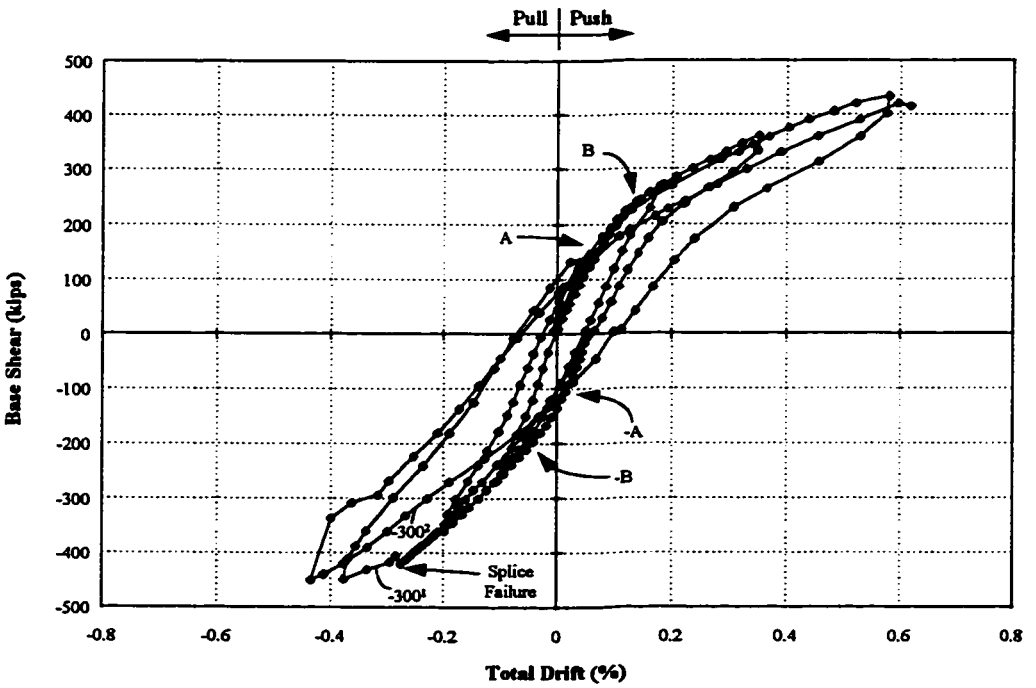

Figure 5.32 Structural Response of Test II

Test I was designed to investigate structural flexure behavior and was conducted using loading control for initial load stages. Displacement control was used when column splice failure occurred in the east column. The loading history used for phase one is shown in Figure 5.29, and the load-displacement relationship is presented in Figure 5.30.

Test II was designed to identify structural shear behavior and was conducted using loading control. Loading history is shown in Figure 5.31 and structural response is shown in Figure 5.32.

Test III was designed to reach infill wall ultimate shear strength and was conducted as a monotonic pull over test. Structural response of Test III is shown in Figure 5.33.

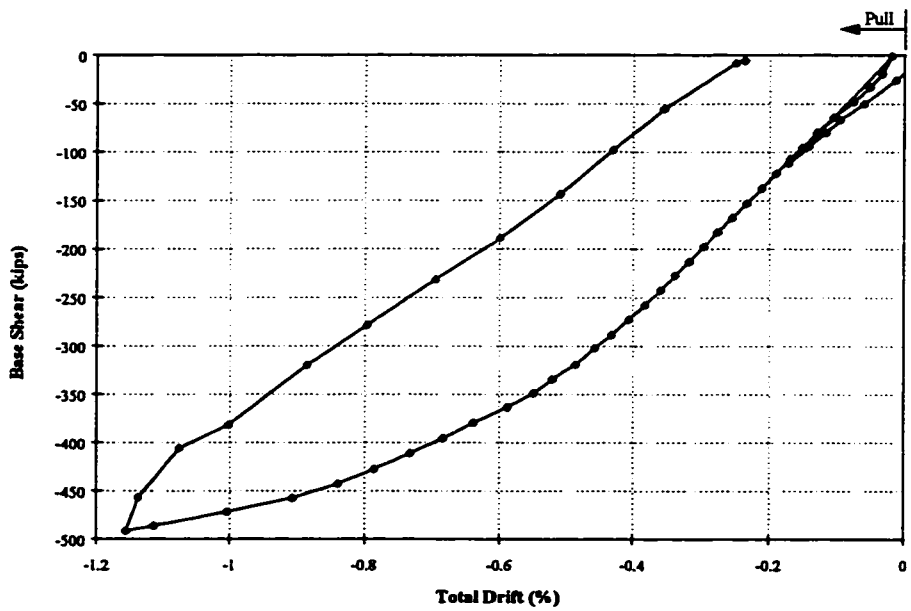

Figure 5.33 Structural Response of Test Phase III

5.5 SUMMARY

One tests was conducted for the existing frame. Three tests were performed for the PTPW system. Observed structural responses of PTPW system tests showed that: flexure dominated structural behavior in Test I; shear dominated the structural behavior in Test II; and the ultimate system shear was determined in Test III. Effects of primary variables including area of post-tensioning tendons and levels of initial post-tensioning force were investigated. Through the model structure tests, structural connection behavior observed in the first stage of the experiment was further assessed.

Performance of Infill Wall and Connections The precast infill wall performed exceptionally well as a monolithic wall system. Diagonal cracks were continuous through panels and closure strips. There was no indication of distress along grout strips. Shear cracking extended along a line from the "toe" of the wall to the top of the post-tensioning anchorage. Some cracks were concentrated around the pipe shear lugs between the wall and frame. It was demonstrated that all structural connections, closure strips and shear lugs, worked well in the PTPW system.

Performance of Post Tension Tendons The post-tensioning tendons played a significant part in the PTPW system. Tests demonstrated that splice failure of the column reinforcement at the base of the existing frame column and the PTPW system response mechanism could be controlled by selecting the amount of post-tensioning tendons and level of initial post-tensioning force.

Flexure Capacity With lower initial post-tensioning, the structural response were dominated by flexure. The flexural response developed in three stages: flexural-cracking (column cracked under tension), splice failure (column reinforcement splice failed), and post-tensioning tendon yielding. Column decompression (lose of compression provided by initial post-tensioning) was reached prior to flexural-

cracking. After column reinforcement splice failure occurred, the tendons sustained the system moment and yielded as load increased. The response could be characterized by behavior pertaining to the three stages.

Shear Capacity With more tendons and higher initial post-tensioning, the PTPW system behaved in a shear dominated mode. With different structural performance, infill-shear capacity and system-shear capacity were developed under corresponding lateral loads.

Infill-shear capacity was first reached and cracking occurred at a level close to the design shear capacity of the infill wall. Crack patterns indicated that the wall behaved as a monolithic wall even though it was constructed of multiple precast panels. It was also shown that a diagonal compression strut formed within the infill to change the structure from a frame-infill system to a braced frame system.

System-shear capacity was reached under zero initial post-tensioning. Because the compression strut formed, the system carried higher shear beyond the estimated infill shear capacity. The term "system-shear capacity" was used to represent the shear strength beyond infill wall shear capacity. System-shear capacity was reached when concrete crushed at the top of the primary compression strut. Because the system-shear capacity was higher than the infill-shear capacity, slip developed at the base of the structure. Due to slip, shear friction developed under the vertical force provided by post-tensioning tendons. Shear friction provided high shear capacity at the infill-base interface so that the system sustained a system-shear much higher than the infill-wall shear capacity.

CHAPTER VI

ANALYSIS OF MODEL STRUCTURE TEST RESULTS

6.1 INTRODUCTION

The behavior of a post-tensioned precast infill wall system is evaluated in terms of element and connection performance, structural lateral capacity, and retrofitting efficiency. Using the data, key factors and design processes are recommended for PTPW retrofitting system implementation.

6.2 STRUCTURAL RESPONSE

6.2.1 **Flexural Response** (Low Post-tensioning Force)

In Test I, structural response was elastic under load cycles up to 45^1 in both directions. Columns were in compression under initial post-tensioning. As loading increased up to 47.5 kips and 59.7 kips in the push and pull directions, decompression (zero tension stress) occurred in columns due to overturning effects of lateral load. Cracks at the column base which were initiated during the existing frame test were visible at a lateral load of 87 kips. Stiffness did not changed as load reached approximately 87 kips and 95 kips in the push and pull direction, correspondingly. The load applied to reach zero tension state or to overcome the compression in column reinforcement provided by initial post-tensioning was termed decompression load in this report. After decompression, new cracks occurred in columns as load increased. The initial stiffness K_1 was overcome at a lateral load of approximately 100 kips indicating the response changed from linear-elastic behavior. After the initial stiffness was overcome, there was a stiffness transition period until the load reached 128.0 kips. At a base shear of 128 kips, cracks were observed at the top of each infill.

A post cracking stiffness K_2 governed the response as cracks developed under load increase. This response was termed the flexural-cracking state to differentiate it from the infill cracking state in Test II.

When loading increased beyond the flexural-cracking state, more cracks developed in column splice regions and in the infills. As load in the push direction reached 240 kips within load cycle 255^1, splitting cracks along the splices were noted in the east column splice region indicating that failure was imminent. Splitting cracks did not form in the west column at the same loading level in pull direction. Several infill wall cracks extended across the infill at a load level of 248 kips indicating that infill shear strength was reached.

Because infill shear strength was reached, significant change of hysteretic response occurred in load cycle 255^2. At 0.2 percent drift, loads reached 249 kips and 270 kips in push and pull direction, respectively, and splice failure occurred in the east column as shown in Figure 6.1 and Figure 6.2. Splice failure, however, did not occur in the west column because higher initial post-tensioning resulted in a higher splice capacity.

Figure 6.1 East Column Splice Failure

After the splice failed, stiffness decreased slightly in Cycle 0.3^1 when load reached 120 kips. The hysteretic response in cycle 0.3^2 representing the post-splice failure behavior indicates that strength dropped as shown in Figure 6.3a.

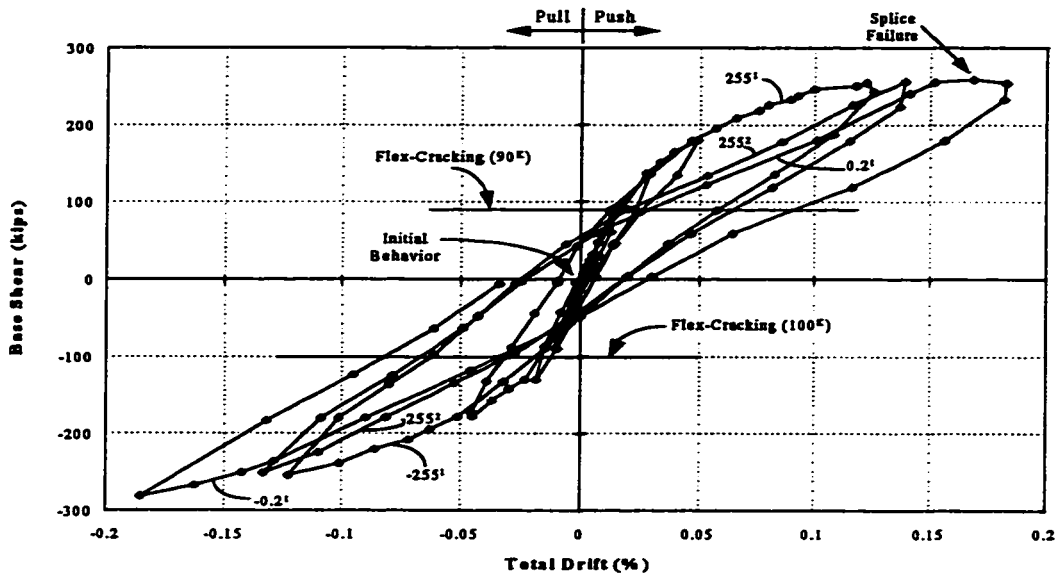

Figure 6.2 Structural Response Prior to Splice Failure (Phase I)

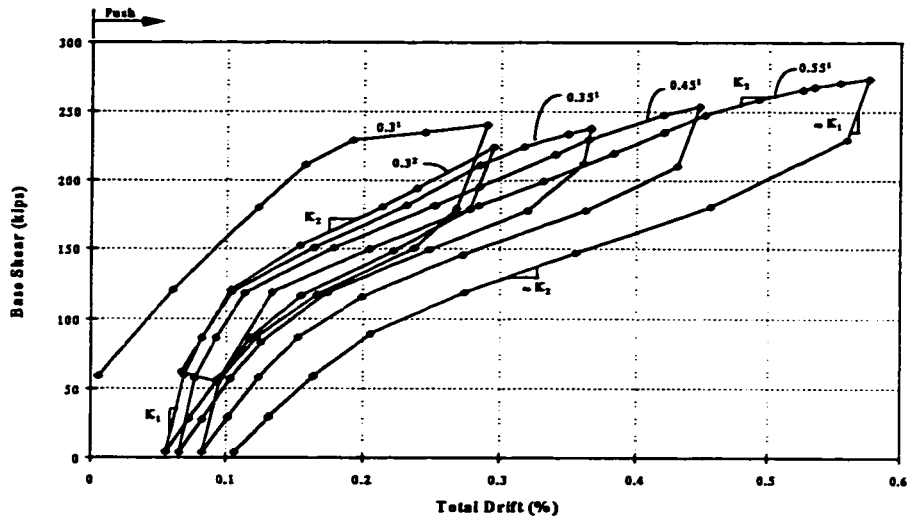

Figure 6.3a Structural Response After Splice Failure (Residual)

The structure behaved in a tri-linear fashion. The initial stiffness K_1 maintained in all cycles up to 60-kips zero tension load as shown in Figure 6.3b in which the curves have been adjusted by removing residual drifts. There was a gradual transition in stiffness between 60 and about 100 kips, after which, the response was nearly linear with a stiffness K_2. The stiffness degraded gradually to a post yielding

value K_3 at 0.50% drift when a post-tensioning tendon yielded under a lateral load of 270 kips.

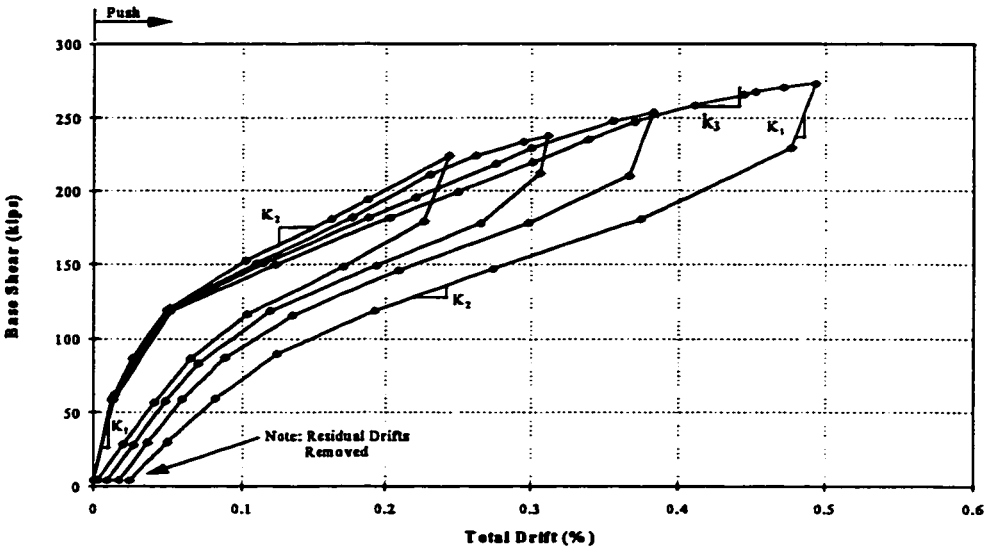

Figure 6.3b Structural Response After Splice Failure (Non-residual)

The most important characteristic of the test result is that unloading curves showed non-linear elastic behavior. Corresponding to the general pattern of the loading curves, unloading curves followed flexural-cracking stiffness K_2 with some residual deformation retained. As unloading reached the flexural-cracking load, a gradual transition was noted with the stiffness approaching a value higher than K_2 but less than K_1. The curve, then, followed approximately the initial stiffness K_1 below the zero-tension or decompression load. At zero load, the structure returned to almost its original position. Non-linear elastic behavior has been noted in other studies of post tensioned concrete structures[55]. Such behavior reflects the combination of the elastic properties of post-tensioning tendons and elasto-plastic properties of reinforced concrete elements.

Under low initial post-tensioning force, the structure's response was characterized by tri-linear hysteretic loops which showed that the structure behaved

similarly to the ordinary reinforced concrete flexural elements with good ductility. In order to make a retrofitted frame system respond as a flexure-dominated structure, an efficient ratio of post-tensioning tendons and initial post-tensioning force should be based on the frame characteristics and will be discussed in Section 6.5.

6.2.2 Infill Shear Response (High Post-Tensioning Force)

Because column splice failure occurred in the east column in Test I, Test II commenced by loading in the opposite direction. There was a very slight change in stiffness when load reached (point A) about 90.0 to 100.0 kips indicating there was still compression in the column up to this point as shown in Figure 6.4. As load increased beyond point A, there was a gradual change in stiffness up to point B (about 190 kips) where a distinct change in the load response curve was observed. As load increased beyond point B, cracking reduced the stiffness, the response following a new slop was nearly linear in both directions.

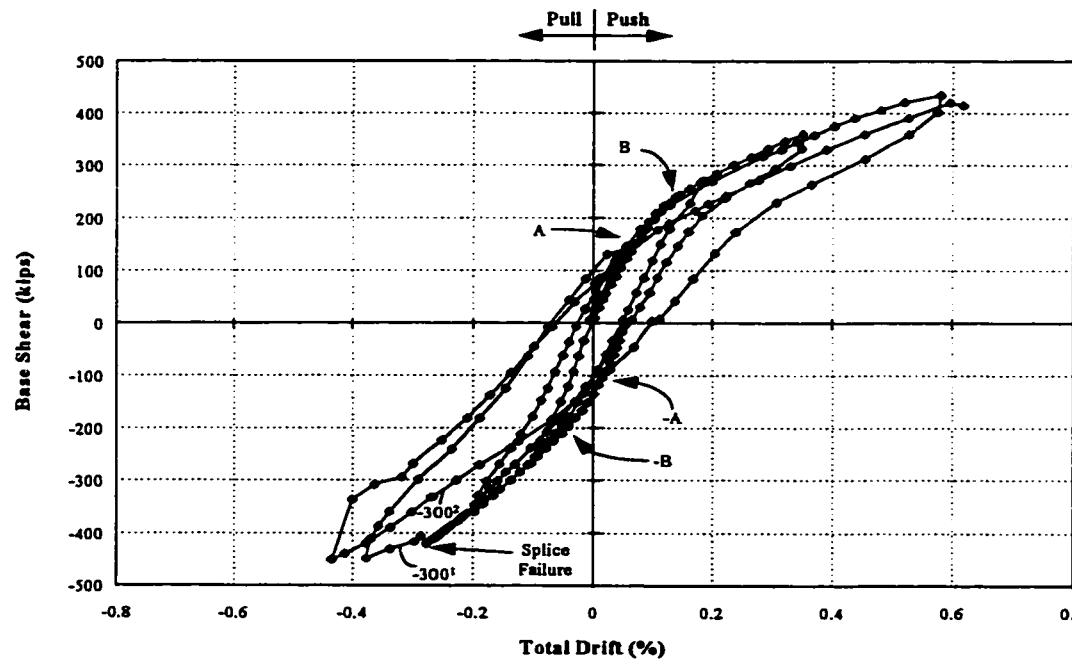

Figure 6.4 Structural Response of Test II

The specimen was stiffer in the pull direction since the number of post-tensioning tendons was larger, the initial post-tensioning force was higher, and splice failure has not occurred in the west column.

Load in the pull direction was increased until splice failure occurred in the west column at a base shear of 421 kips as shown in Figure 6.5a. After the splice failed in the west column, a distinct change in the hysteresis loops was noted in load cycle 450^2 in the pull direction which can be seen in Figure 6.4. Almost all infill wall cracks extended across the whole wall at an angle of approximately 45° as shown in Figure 6.5b.

Fig. 6.5a West Column Splice Failure

The base shear of 421.0 kips at splice failure is much higher than the designed infill shear strength of 228.0 kips and the infill was still functioning well. After the infill-shear capacity (248.0 kips) was reached in Test I, the infill sustained such a high shear load (maximum load of 459.0 kips) almost double its computed shear strength (228.0 kips).

Because of lower initial post-tensioning in Test I, the structure behaved as a cantilever beam with an "I" section in which the web (infill) sustained the shear. In Test II, on the other hand, the structural behavior was different from that of Test I because much higher initial post-tensioning was applied. The high post-tensioning force changed the flexural response and resulted in higher lateral capacity. The system

functioned like a braced frame, as shown in Figure 6.6, after infill-shear strength was reached and a diagonal strut formed. The maximum load capacity of 459.0 kips does not represent the infill wall shear capacity but the lateral load capacity of the braced frame system and, as a result, it is much higher than the infill-shear strength alone. The lateral load capacity beyond infill-shear strength in Test II was termed system-shear strength and will be discussed with the result of the Test III.

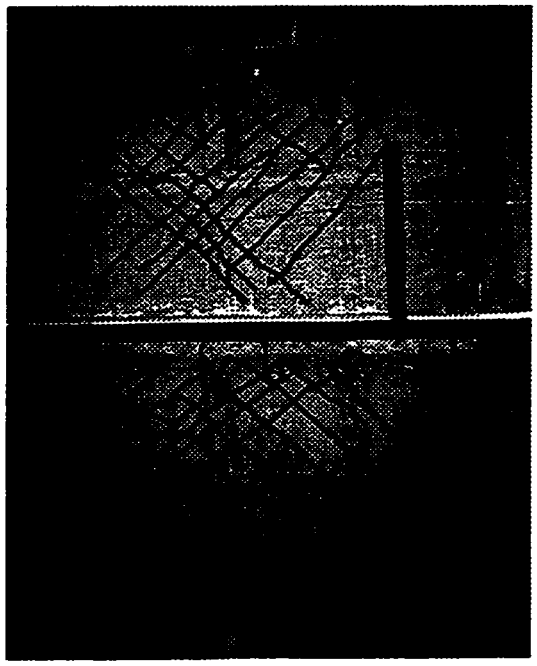

Figure 6.5b Infill Cracking Pattern

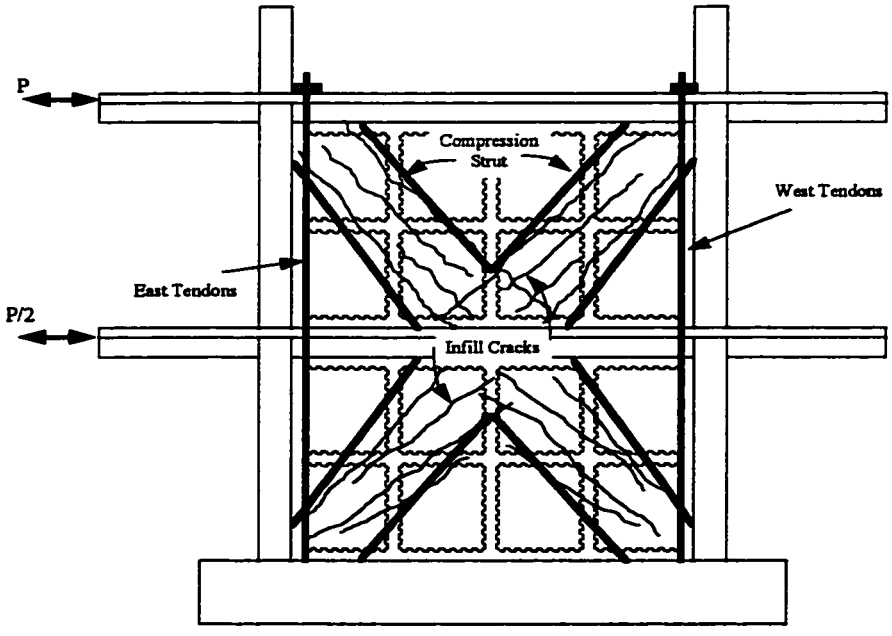

Figure 6.6 Compression Strut in Cracked Infill System

As in Test I, the structural response showed non-linear elastic behavior and was stiff because more tendons and higher initial post-tensioning forces were applied. Because of the higher initial post-tensioning force, the response was dominated by shear deformation instead of flexural deformation. Energy by infill cracking in Test II was less than that dissipated by splice failure in Test I.

The test indicated that more post-tensioning tendons and higher initial post-tensioning force resulted in a higher flexural-cracking and splice failure capacity. It must be pointed out, however, it may be unnecessary to apply such a high level of initial post-tensioning force because the foundation may not provide sufficient uplift resistance to permit high tension forces to develop in the post-tensioning tendons. Generally speaking, an effective initial post-tensioning should be determined according to foundation uplift capacity which will be discussed in Chapters VIII and IX.

6.2.3 **System Shear Response** (Zero Initial Post-Tensioning)

Test III was designed to investigate the system shear capacity defined earlier in the absence of initial post-tensioning. The same post-tensioning tendons used in Test II were maintained. Due to a localized failure of the loading system which prevented application of higher load in the push direction, load was applied monotonically in the pull direction.

Up to approximately 300 kips, the stiffness was constant. Large infill cracks developed and stiffness decreased as load increased. The trend of stiffness degradation continued until approximately 460 kips where a distinct change in the slope of the curve was noted as shown in Figure 5.36.

As discussed earlier, the system-shear strength was much higher than the infill-shear strength because of post-tensioning involvement. At 491 kips, concrete spalled in the compression strut at the top of the wall as shown in Figure 6.7. The spalling

occurred within the closure strip under the existing beam at the location of the west post-tensioning anchorage. Cracking patterns indicated that a primary compression strut had formed along a diagonal from the "toe" of the wall to the top post-tensioning anchorage. The compression strut functioned as a diagonal brace and the post-tensioning tendons at one side of the frame provided tension in the column to permit the system to work as a braced frame.

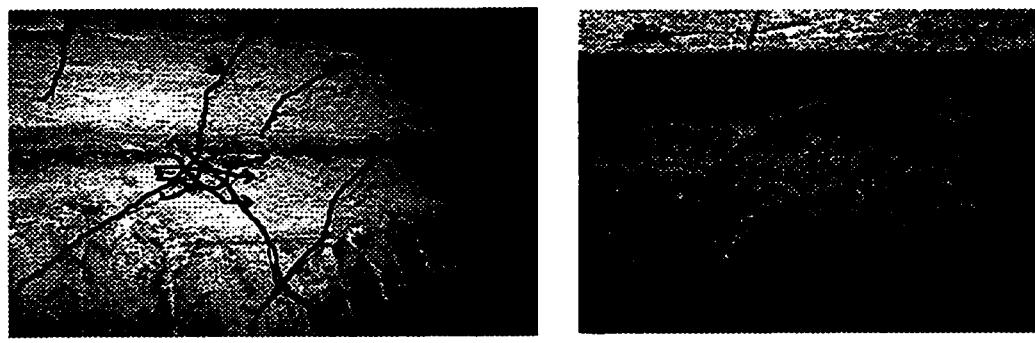

a) Spalling Location b) Detail of Concrete Spalling

Figure 6.7 Concrete Spalling within Compression Strut

Studying the cracking patterns along the strut, it was seen that the compression strut exhibited the following features as shown in Figure 6.8. It formed within the infill wall in such a way that one edge followed a 45^0 angle from the top or bottom anchor plate edge to the shear lug at the first floor beam. The other edge of the strut was bounded by the shear lugs at the first floor and at the mid-height of boundary columns.

The system-shear capacity was reached when localized spalling of concrete occurred. It is desired that the system-shear capacity should be higher than infill shear strength as in this test. Otherwise, such localized spalling failure may occur prior to reaching infill-shear strength and will reduce retrofitting efficiency.

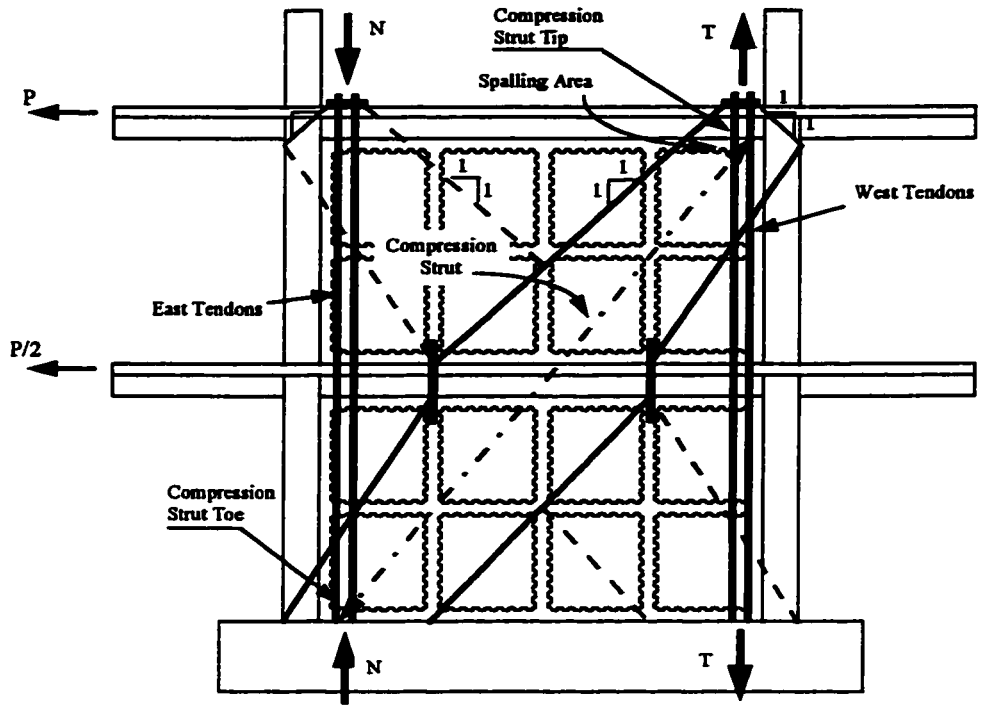

Figure 6.8 Compression Strut Formed In Infill Wall

6.3 ELEMENT PERFORMANCE

6.3.1 Column Performance

In Test I, reinforcement in the east column performed well up to a loading level of 249 kips before splice failure occurred as shown in Figure 6.9. It was noted that the reinforcement was under compression up to the decompression load of 47 kips. It remained elastic in tension prior to splice failure. After splice failure, the reinforcement did not contribute to the column tensile capacity and the post-tensioning tendon sustained all the tension needed to resist the moment as illustrated in Figure 6.10.

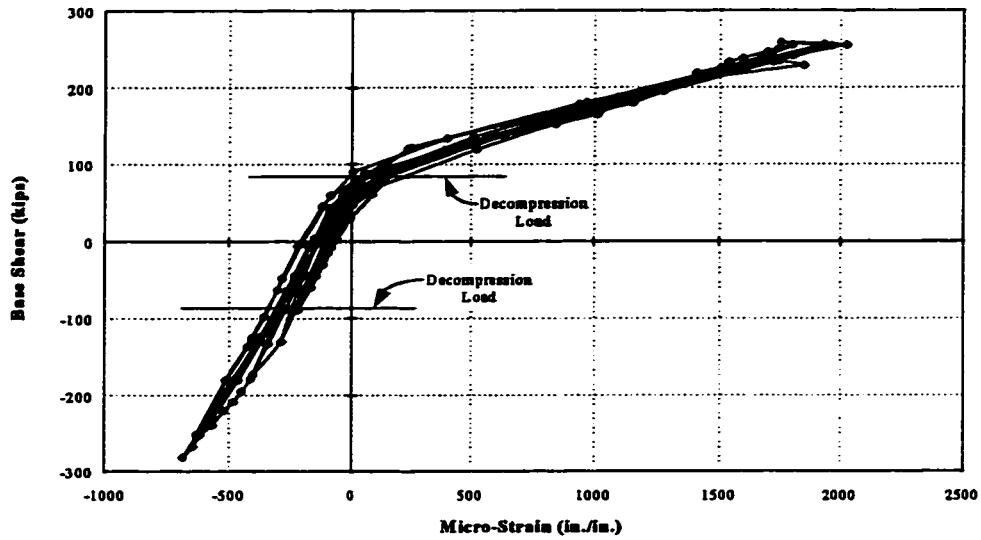

Figure 6.9 East Column Reinforcement Response (Test I)

In Test II, the west column reinforcement splice, shown in Figure 6.11, followed the same pattern as that of the east column in Test I. However, the load level at splice failure in the west column was much higher (421 kips) than the east column because there was a greater area of tendons and higher initial post-tensioning force applied in the west column in Test II.

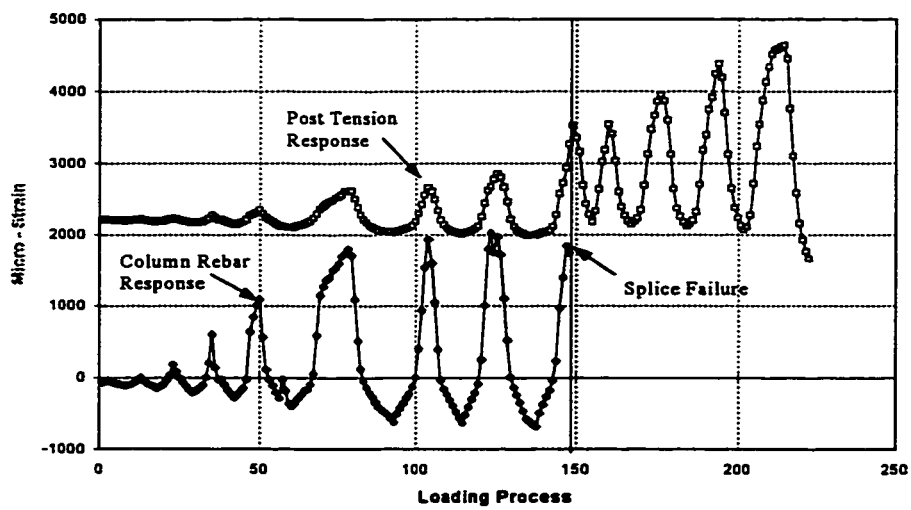

Figure 6.10 East Column Bar & Tendon Response (Test I)

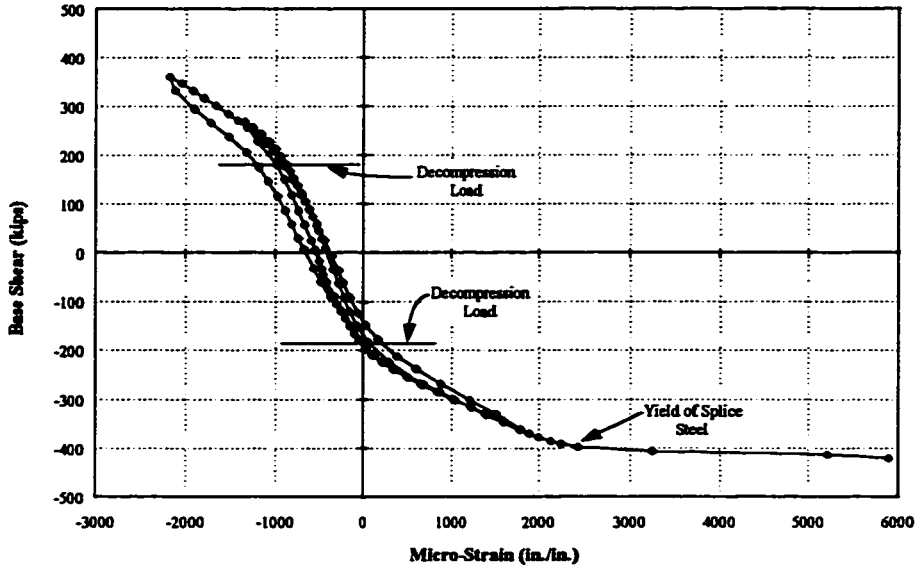

Figure 6.11 West Column Reinforcement Response (Test II)

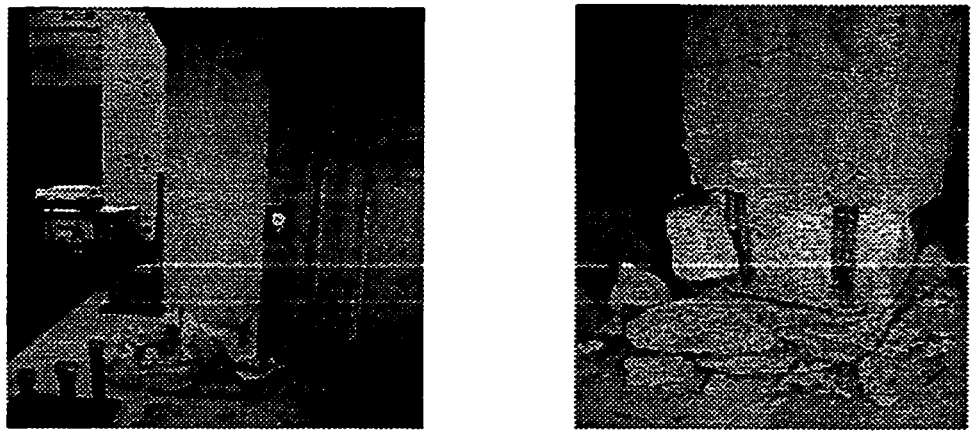

a) East Column in Test I

B) West Column in Test II

Figure 6.12 Column Concrete Crushing

Prior to splice failure, transverse cracks initiated over the splice region at the base of the column and spread upward as loading increased. Splitting (longitudinal) cracking occurred when the splice failure load was reached. Due to cracks that occurred in both directions (transverse and longitudinal), concrete at the column base

crushed as additional cycles of loading were applied as shown in Figure 6.12. Generally, splice failure is a sudden brittle action and one of the objectives of the retrofitting scheme was to prevent splice failure and to improve ductility. This objective was realized by applying post-tensioning as shown in figures 6.11.

6.3.2 Post-Tensioning Performance

In Test I, the post-tensioning force increased as lateral load increased. After splice failure, the post-tensioning force increased greatly due to loss of the column reinforcement contribution. The total strain was nearly twice the initial strain as shown in Figure 6.10. In all loading cycles up to 0.50 % drift, the post-tensioning steel remained elastic. One east (north side) post-tensioning tendon yielded as shown in Figure 6.14a. Meanwhile, the other tendons remained elastic.

In Test II, on the other hand, more tendons were applied and they responded elastically. Though the tendons were initially stressed to almost the same level (about 45% of their yielding strength) as in Test I, after splice failure, the ultimate strain level was not as high as in Test I as shown in Figure 6.13 and Figure 6.14b.

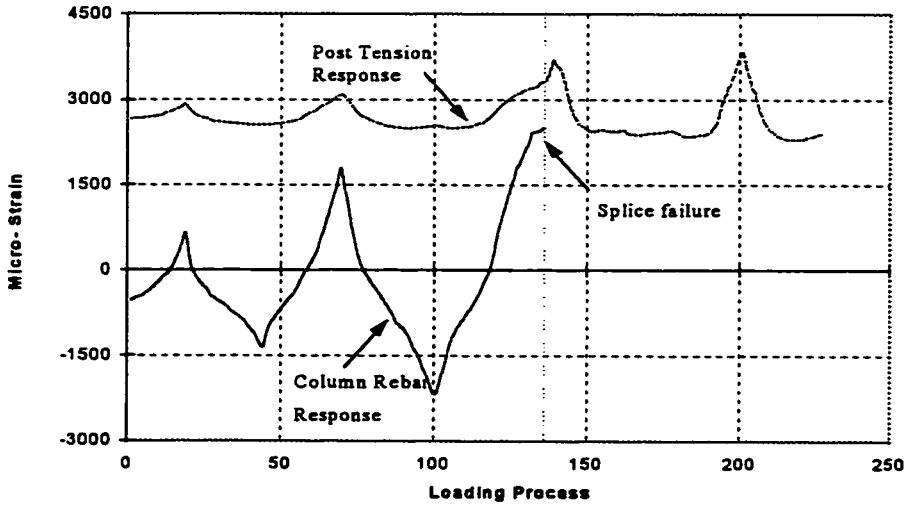

Figure 6.13 West Column Bar & Tendon Response (Test II)

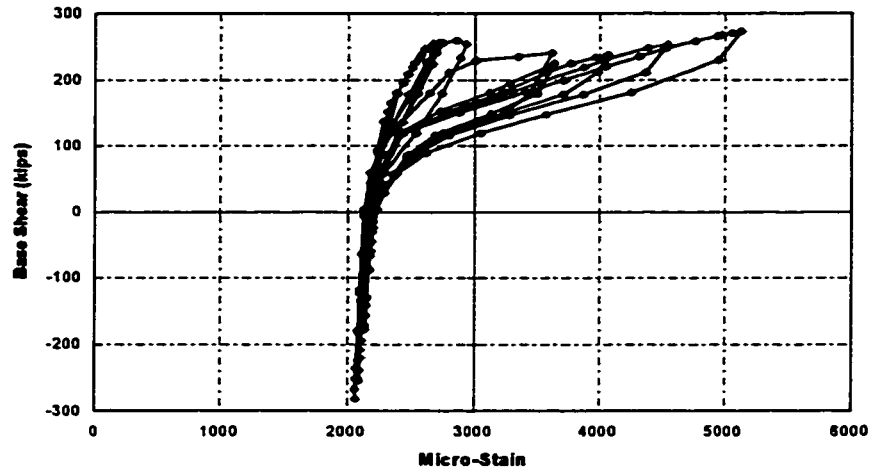

Figure 6.14a East Post-Tension Tendon Response (Test I)

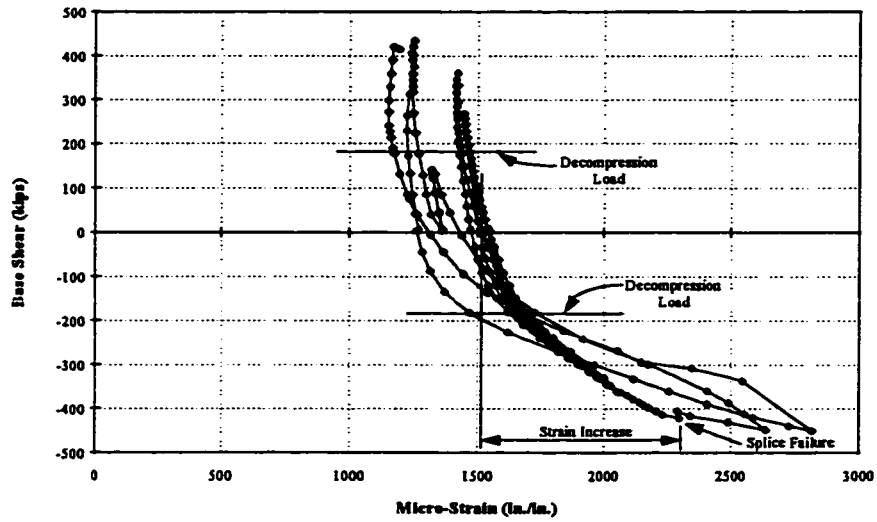

Figure 6.14b West Post-Tension Tendon Response (Test II)

The application of post-tensioning increased the moment capacity of the structure as desired. The most significant result is that the post-tensioning tendons extended the range of splice function by providing additional compression to the column. The splice failure was dependent on the initial stress level of the tendons while the flexure capacity of the system was dependent on the area of the tendons. If a

system is designed as a flexure dominated system with sufficient shear capacity to permit splice failure and tendon yielding, the post-tensioning tendons will dominate the structural retrofitting design.

6.3.3 Infill Wall Performance

Though columns cracked in Test I, the cracks did not extend into the wall due to the "jointed" nature of the wall construction. As base shear reached 158 kips, infill wall cracks were observed. The cracks then extended in later loading cycles. When splice failure occurred at base shear of 248.0 kips, infill cracks extended diagonally across the infill at approximately a 45 degree angle in the first story wall. A similar crack was also noted in the second story wall at a slightly higher load. As loading increased, additional diagonal cracks developed in the infill wall in both stories.

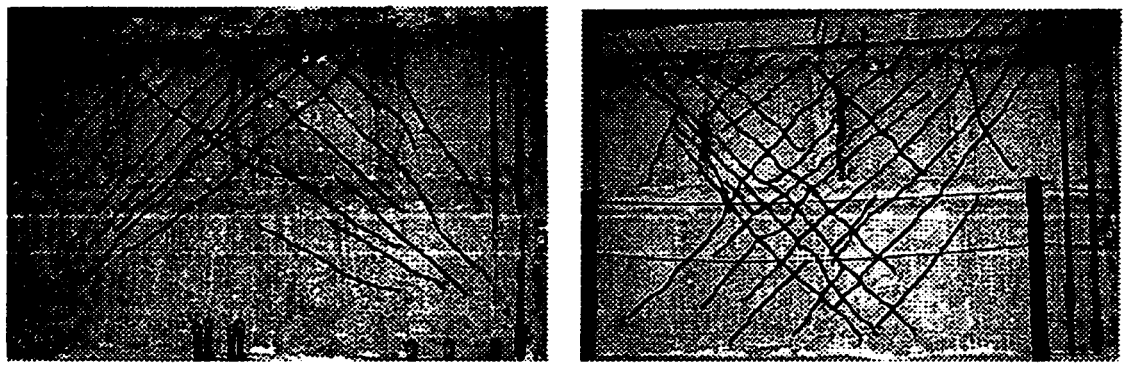

a) First Story Infill Cracking b) Second Story Infill Cracking

Figure 6.15 Infill Cracking Pattern

In Test II, the general orientation of all cracks was along a line diagonally connecting the column base to top of the other column where post-tensioning tendons were anchored. The overall cracking pattern for the structure was shown in Figure 6.5 and close up views of cracks in each story are shown in Figure 6.15.

The cracking pattern showed that the infill behaved as a monolithic wall even though it was constructed of small precast panels. The precast panels functioned as a monolithic wall. Figure 6.16a illustrates the panel reinforcement strain in Test I. The panel reinforcement remained elastic because the response was dominated by flexure as discussed earlier. In Test II, the panel reinforcement nearly yielded, as shown in Figure 6.16b, and indicated that the panels were carrying much greater shear. The large stress resulted in wide cracks (a maximum infill crack width of 0.8 mm).

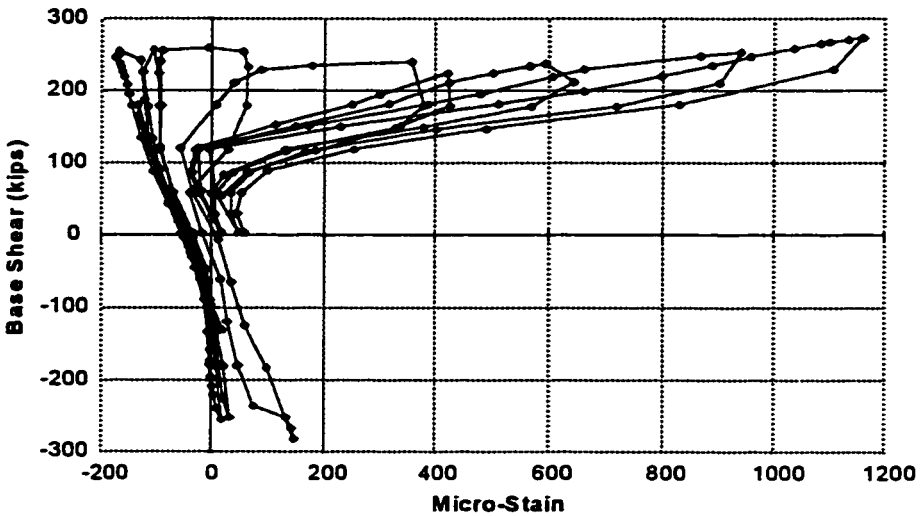

Figure 6.16a West Bottom Panel Reinforcement Response (Test I)

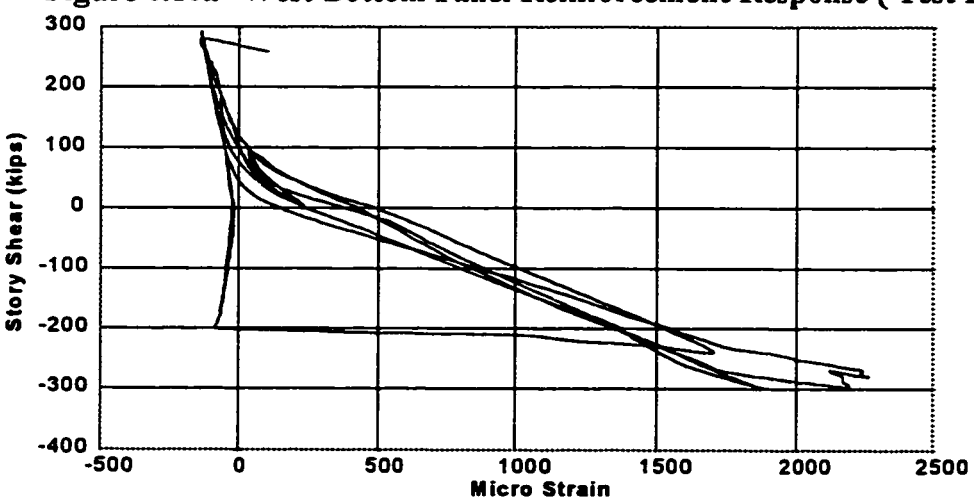

Figure 6.16b East Top Panel Reinforcement Response (II)

6.3.4 Closure Strip Performance

As shown above, infill cracks were continuous diagonally across the panels through closure strips and even the beams. There was no indication of distress along the interface of panels and closure strips.

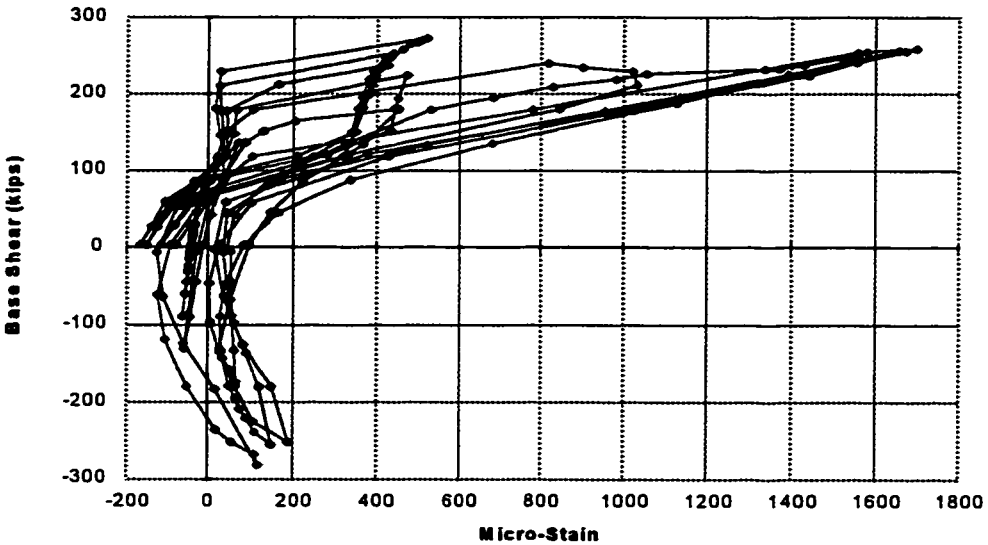

Figure 6.17a Closure Strip Reinforcement Response (Test I)

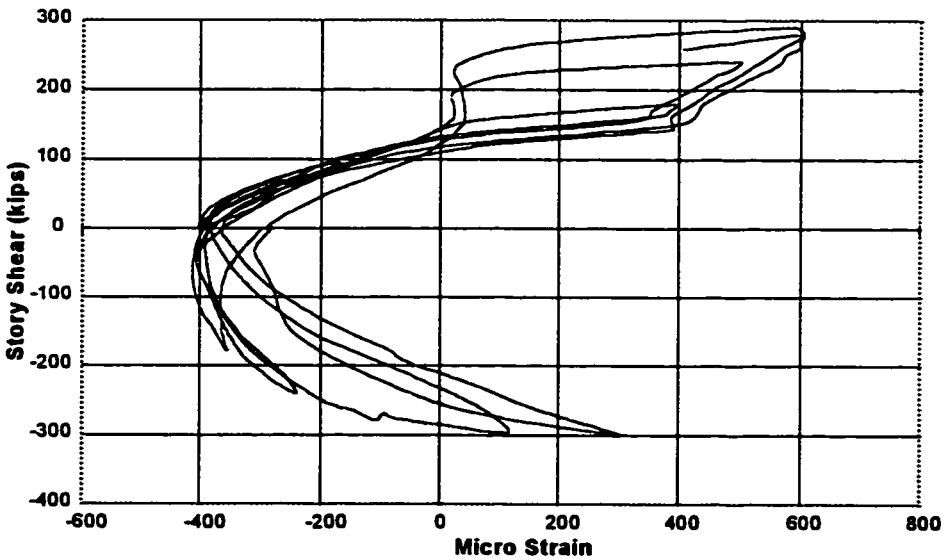

Figure 6.17b Closure Strip Reinforcement Response (Test II)

As suggested in Chapter V, the interface crack pattern observed in closure strip tests did not occur in the model structure test because direct shear was not the dominant effect. The vertical closure strip reinforcement worked very well to unite panels, to compensate for infill reinforcement discontinuity between panels, and to contribute to the system moment capacity.

Strains Response of the vertical closure strip reinforcement is shown in Figure 6.17. Figure 6.17a shows the response of the reinforcement in the second closure strip from the east column in Test I, and Figure 6.17b represents the response of reinforcement in the second closure strip from the west column in Test II. Contradictory to the panel reinforcement strain responses, closure strip reinforcement reached higher strain in Test I than in Test II which further demonstrated that flexure dominated Test I and shear dominated Test II.

The closure strip reinforcement strains exhibited response patterns similar to that of the post-tensioning tendons (shown in Figure 6.12). Because the closure strips were closer to the centroid of wall section than the tendons, the strain levels were lower than these of the tendons. For the edge closure strips, on the other hand, It was noted that the reinforcement yielded right after splice failure was reached.

6.3.5 Shear Lug Performance

The shear lugs (pipes) performed well to sustain shear between the infill and existing frame. As described in Chapter V, the base shear capacity of the PTPW system was estimated as 209 kips based on the strength of three shear lugs. In Test I, the base shear reached a higher level (270 kips) than total computed yield strength of the base lugs, but the lug pipes did not yield as shown in Figure 6.18a. In Test II, on the other hand, the strain of lug pipe reached about two times as high as in Test I approaching yield as shown in Figure 6.18b.

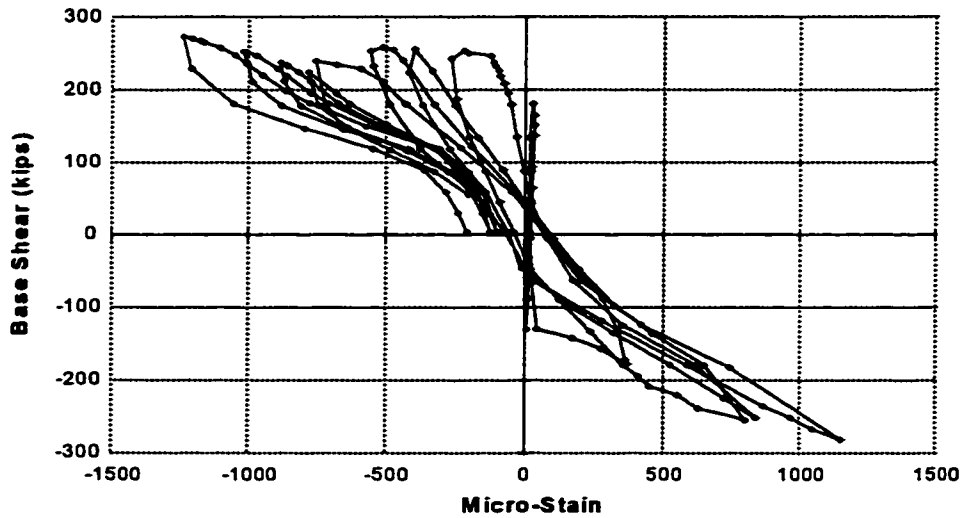

Figure 6.18a Shear Lug Response in Test I

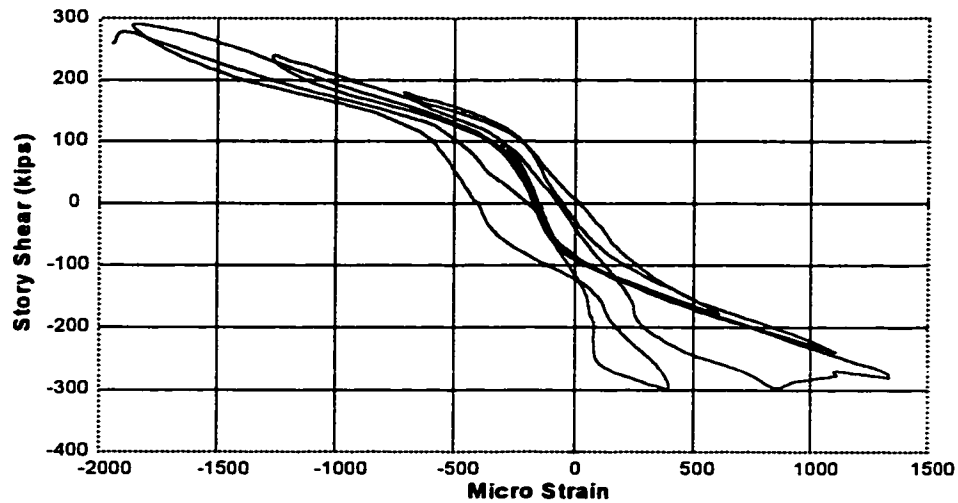

Figure 6.18b Shear Lug Response in Test II

However, a large crack developed at the base next to the column in which splice failure occurred in Test I and Test II. Since the foundation was designed as a rigid base and the post-tensioning tendons were unbonded, the tendons elongated when the splice failure occurred. The crack originated at the column due to loading beyond decompression and widened following splice failure due to the tendon

elongation as shown in Figure 6.19a. Incidentally, the joint at the wall-footing interface opened as shown in Figure 6.19b. In Test I, at initial yield of the post-tensioning bar, the maximum crack width was measured as approximately 0.75 in. as shown in Figure 6.20b. The maximum crack was smaller in Test II than that in Test I because a greater number of tendons were used.

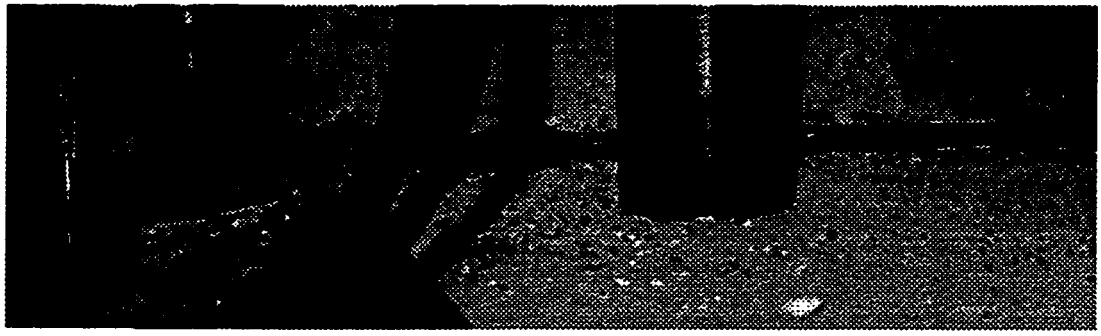

a) Crack of Column Splice Region b) Crack at Infill Base

Figure 6.19 Base Cracking Following Splice Failure

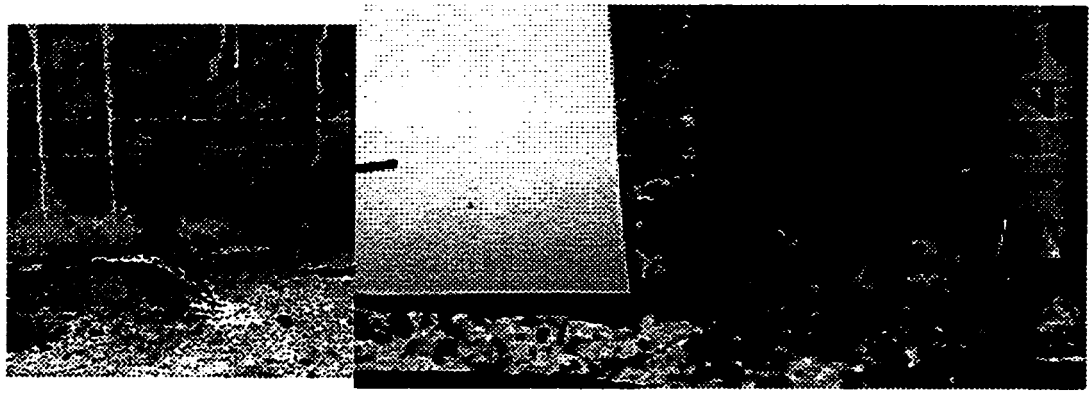

a) Footing Crack with Pipe Pull-out b) Maximum Base Crack (Test I)

Figure 6.20 Shear Lug Pull out of The Base

In Test III, though the tendons did not reach yield, the total tendon elongation was very large because no initial post-tensioning was applied. Due to the large tendon elongation and corresponding vertical displacement at the base interface, two shear

lugs were pulled out of the footing as shown in Figure 6.20a. Simultaneously, the vertical reinforcement was also pulled out since it was anchored inside the pipe.

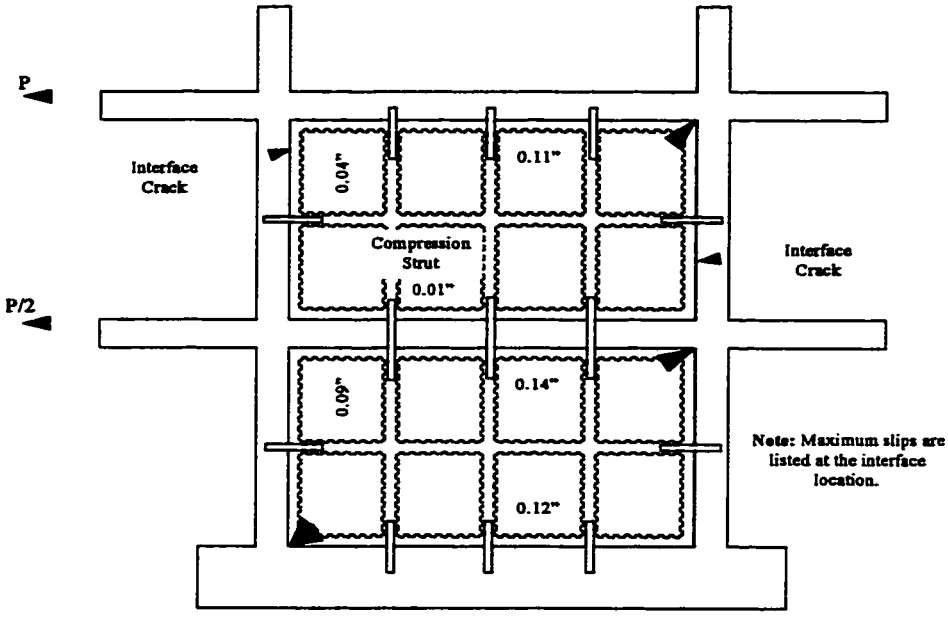

Figure 6.21 Interface Slip and Boundary Crack

Since the column splice failure occurred at the base and the post-tensioning tendons were unbonded, only one horizontal crack formed at the base of the structure. Therefore, the structure appeared to rotate as a rigid body about the "toe" of the wall and the effective shear area at the base was reduced. With the shear area reduction, a relative motion or interface slip of the wall occurred. The slip increased with the applied shear and a maximum of 0.12 in. was measured at a base shear of 491 kips as shown in Figure 6.21. A similar slip of 0.14 in. was measured at the top interface of the first story wall and the beam bottom. Extremely small interface slips of 0.01 in. were measured at the base of the second story wall. Significant slip of 0.11 in. was measured at the top of the second story wall. Due to the base slip, shear friction was

developed along the interface and the structure sustained much higher base shear than the strength of shear lugs alone.

Figure 6.21 also showed that the boundary cracking occurred along the column-wall interface and at the bottom of the beam-wall interface. Cracks were located at the corners of infill walls diagonally opposite to the direction of the compression struts. The cracks originated at the infill corners and stopped at the mid-height of the column and at about the third point of the beams where the shear lug pipes were located. The horizontal shear lugs were able to sustain vertical shears along column-wall interfaces and remained in elastic range.

6.4 STRUCTURAL CAPACITY EVALUATION

The three tests were designed to show different characteristics of structural performance. In Test I, flexure yielding occurred prior to brittle shear failure and reasonable ductility was achieved. An efficient PTPW system should be designed to have similar behavior to that of the structure in Test I. In Test II, the structure reached higher lateral strength and stiffness with limited ductility. Tests I and II showed that a precast infill constructed with closure strips and shear lugs worked very well as a monolithic wall. Higher initial post-tensioning resulted in a higher splice capacity and higher ultimate structural lateral capacity. Without initial post-tensioning, on the other hand, Test III resulted in a brittle failure mode under lateral load.

According to the structural performance in each test, structural capacity evaluation modes were studied. Flexure (flexural-cracking, splice failure, and post-tensioning tendon yielding), infill-shear, system-shear, and base shear friction capacity were estimated and will be presented in the following sections.

6.4.1 Flexure Capacity

A loading condition for the cross section of a PTPW system was shown in Figure 6.22. Before lateral load was applied, the exterior moment was zero. There was only the initial post-tensioning force T_0 in the tendons. Under the tendon force T_0, the structure was subjected to a compression load P which produced initial compression n_0 on the columns. When lateral load was applied, an exterior moment M was produced.

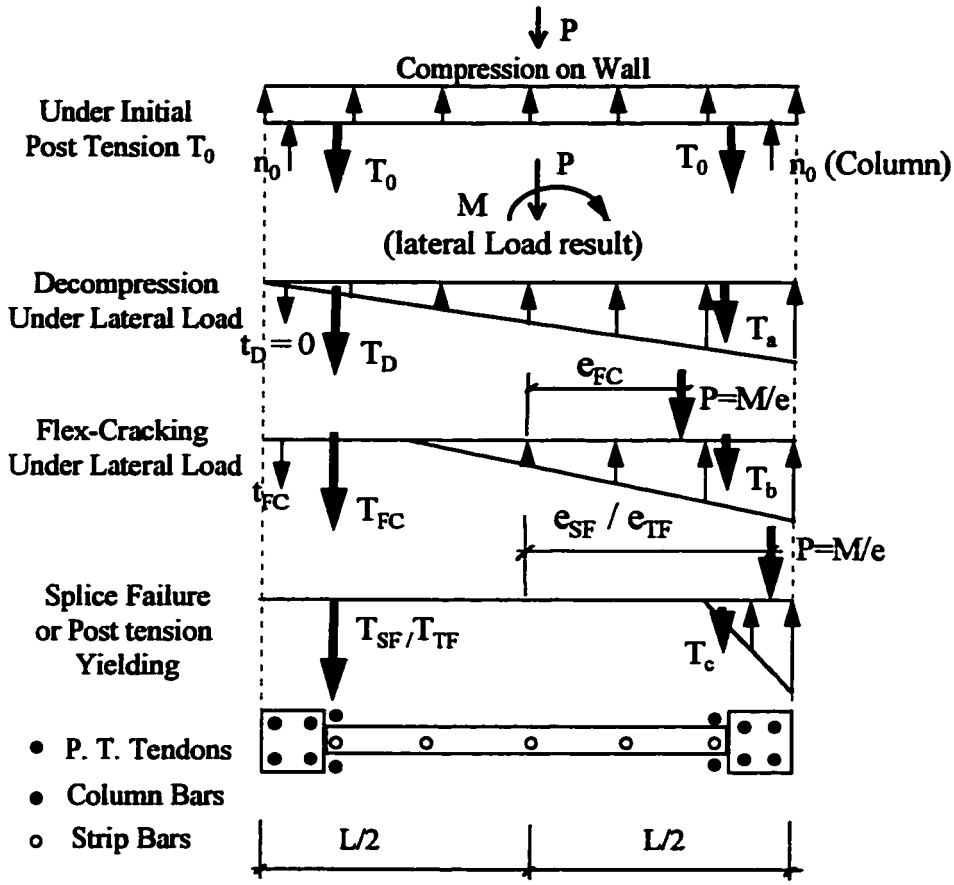

Figure 6.22 Structural Loading Condition

Under the combination of compression force P and moment M, the structure was equivalently subjected to eccentric compression with an eccentricity of e = M/P.

Compression force on one end and tension force on the other end were developed under the eccentric compression. Post-tensioning tendons, and column and strip bars at the tension side carried tension force.

With an increase in lateral load, the column carrying tension force reached the decompression or zero tension state followed by flexural-cracking, splice failure and tendon yielding states, progressively. The force in post-tensioning tendons changed at each loading state. T_{DC}, T_{FC}, T_{SF} and T_{TF} represent the tension force in the tendons pertaining to decompression, flexural-cracking, splice failure and post-tensioning tendon yielding states, respectively.

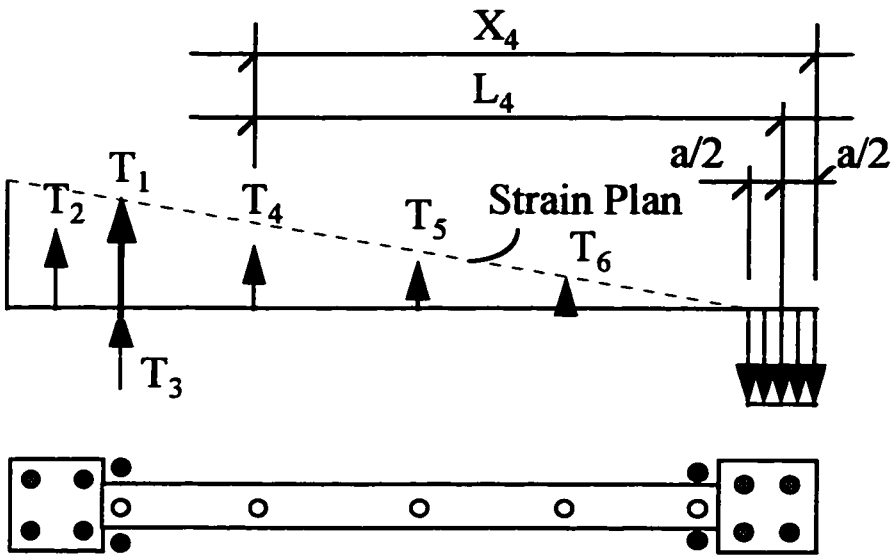

Figure 6.23 Force condition of Infill Section

Corresponding to the variation of the loading states, the strains or forces in column and strip reinforcement also changed as shown in Figure 6.23. The system moment, and forces in tendons, column and closure strip reinforcement can be

calculated using equilibrium principles. Quantitative force response for each loading state was evaluated with the following process.

Under initial post-tensioning, the compression force in column bars is dependent on the value of total compression force P, the cross section of concrete and area of column reinforcement. The compression force in column is denote as,

$$N_0 = \frac{PA_c}{2A_g} \qquad (6\text{-}1)$$

where $A_C = bh_0 + A_S E_S/E_C$ ... effective section of column

$A_G = A_C$ + half of infill section for Test I

$= A_C$ + 1/3 of infill section for Test II

The exterior and interior moments can be calculated using the following equations,

$$M_{EX} = (2 \times h_2 + h_1)V_{base}/3 \qquad (6\text{-}2)$$

$$M_{IN} = \Sigma T_i L_i \qquad (6\text{-}3)$$

$$L_i = (X_i - a/2) \qquad (6\text{-}4a)$$

$$T_i = (L_i A_i)/(L_1 A_1)T_1 \sim (X_i A_i)/(X_1 A_1)T_1 \qquad (6\text{-}4b)$$

$$a/2 = \Sigma T_i/(0.85 f_c' b_{ci}) = \eta T_1 \qquad (6\text{-}4c)$$

where $\eta = 1/(1.7 f_c' b_{c1} L_1 A_1)\ \Sigma(L_i A_i)$

Substituting (6-4) to (6-3),then,

$$M_{IN} = T_1/(X_1 A_1)\{\Sigma X_i^2 A_i - \eta T_1 (\Sigma X_i A_i)\} \qquad (6\text{-}5)$$

Replacing M_{IN} with M_{EX}, equation (6-5) can be written in a form respect to T_1,

$$\alpha T_1^2 - \beta T_1 + M_{EX} = 0 \qquad (6\text{-}6)$$

where $\alpha = \eta(\Sigma X_i A_i)/(X_1 A_1)$ (6-6a)

$$\beta = \Sigma X_i^2 A_i/(X_1 A_1) \qquad (6\text{-}6b)$$

As long as the exterior moment or the lateral load is known, tension forces in post-tensioning tendons, column bars and closure strip reinforcement can be calculated by solving equation (6-6).

Table 6.1 Frame-Infill Cross Section Analysis

	Loading State	Shear	Tendons	Moment	Column	Tendons	Column	Strip Rebars		
		V_{base}	T_0	M_{EX}	N_0	T_1	T_2	T_3	T_4	T_5
I	Initiation	0	108	0	-23	108.0	-23.5	0.0	0.0	0.0
	Zero Tension	47	108	627	-23	127.8	0.2	5.6	4.2	2.8
	Flex-Cracking	87	108	1160	-23	144.8	20.5	10.3	7.8	5.2
	Splice Failure	249	108	3320	-23	215.3	104.8	30.2	22.6	15.1
	Tendon Yield	270	108	3600	-23	245.4	-	-	29.0	19.3
II	Initiation	0	255	0	-75	255.0	-74.7	0.0	0.0	0.0
	Zero Tension	95	255	1267	-75	321.2	4.5	18.6	14.0	9.3
	Flex-Cracking	190	255	2533	-75	385.2	81.1	31.0	27.5	18.3
	Splice Failure	421	255	5613	-75	441.5	105.0	-	31.0	26.2
	Post Splice F.	459	255	6120	-75	569.2	-	-	-	-
III	System Shear	491	0	6547	0	611.3	-	-	-	-

Tension forces were estimated using equation (6-6) and are presented in Table 6.1. T_1 through T_5 represent tension forces in tendons, column and strip bars on the east end of the structure for Test I and west end of the structure for Tests II and III. Values of base shear V_{base} and moment M_{EX} were recorded, T_0 was the actual initial post-tensioning force, and N_0 was the initial compression in the boundary column provided by the initial post-tensioning. Decompression, flexural cracking, splice failure, and post-tensioning yielding states resulted in different force levels for T_1 through T_5. The estimated forces T_1 through T_5, shown in the table, matched the test results very well.

In Test I, at a base shear of 47 kips, the calculated force in column bars was about zero matching the zero tension state in the test. At a base shear of 87 kips, the estimated column bar force reached 20 kips as flex-cracking occurred. At a base shear of 249 kips, the calculated force in column bars reached 104.8 kips (which almost equals the splice strength of 105 kips evaluated using the approach of Orangun Equation[38]) and splice failure occurred. Meantime, the force in the edge closure strip reinforcement was calculated to be 30.2 kips matching its yielding strength of 30.9 kips. After splice failure, the column bar was not counted and strip bar strength remained at yield in further calculations. As load increased to a base shear of 270 kips, the calculated force in the post-tensioning tendons reached 245.3 kips matching the tendon yielding strength of 252 kips.

The estimate for Test II gave results similar to Test I. Because very high initial post-tensioning created stress concentrations and localized deformations near the column in Test II, the gross section A_G in equation (6-1) was counted as 1/3 of the infill section plus the column and column reinforcement. Under this assumption, the calculated initial compression force matched the measured force in the column bars. The calculation indicated that the maximum force in the tendons reached 569.2 kips under the maximum base shear of 459 kips. The yielding strength of tendons is 624 kips which is above the calculated value. It means that no post-tensioning tendon was yielded in Test II matching the test result. However, reinforcement yielded in all closure strips.

In Test III, with no initial post-tensioning, the column splice failed and the west end strip reinforcement was pulled out. Therefore, the system moment was sustained by the post-tensioning tendons alone. The total computed force in the west tendons was 611.3 kips which is still lower than the yielding strength of 624 kips. As discussed earlier, the system withstood the shear force by means of the compression

strut as shown in Figure 6.8. Estimate of the shear capacity of the structure including base shear strength, infill and system shear strength will be presented in the following articles.

6.4.2 Shear Capacity

6.4.2.1 Infill Shear Cracking

Shear cracking capacity of the infill wall was designed based on the cracking strength of panel and strip concrete following equation (5-1). As discussed in Article 4.2.2.1, a concrete cracking coefficient $f_c = 4.0$ was used. In the model structure design, the concrete strength was 4,000 psi. The infill wall shear cracking capacity was 228 kips for the first story and 152 kips for the second story. Based on the actual panel concrete strength of 4,500 psi and strip concrete strength of 6,000 psi, the infill shear cracking capacity was evaluated as 241 kips which closely matches the test cracking strength of 248 kips.

After the infill cracking strength was reached, the structure worked as a braced frame system and sustained much higher lateral load when the compression strut formed. The test indicated that the system shear capacity was sufficient to permit flexure yielding to occur prior to infill shear failure.

6.4.2.2 System Shear Capacity (Compression Strut)

In Test III, a system-shear strength of 491 kips was observed as the compressive strut failed at the top of the diagonal. According to the compression strut model shown in Figure 6.8, the force condition at the strut tip was studied as shown in Figure 6.24.

In the test, concrete crushed (spalled) at the tip of compression strut in the closure strip below the top floor beam. Assuming the stress in the strip concrete,

bearing the post-tensioning force, spread along a 45-degree angle from the tendon anchorage and a parabolic stress distribution was assumed across a compression region of 38.0 in.. The actual concrete strength of f_c'= *6,000* psi for the strip and f_c'= *4,500* psi for the infill were applied in the system-shear capacity evaluation. The total compression force F_c on the strip can be calculated using equation,

$$F_c = \int_{\frac{-a}{2}}^{\frac{a}{2}} t\sigma\ (x)\ d\ x = \frac{2\ at}{3}\sigma_{max} \qquad (6\text{-}7)$$

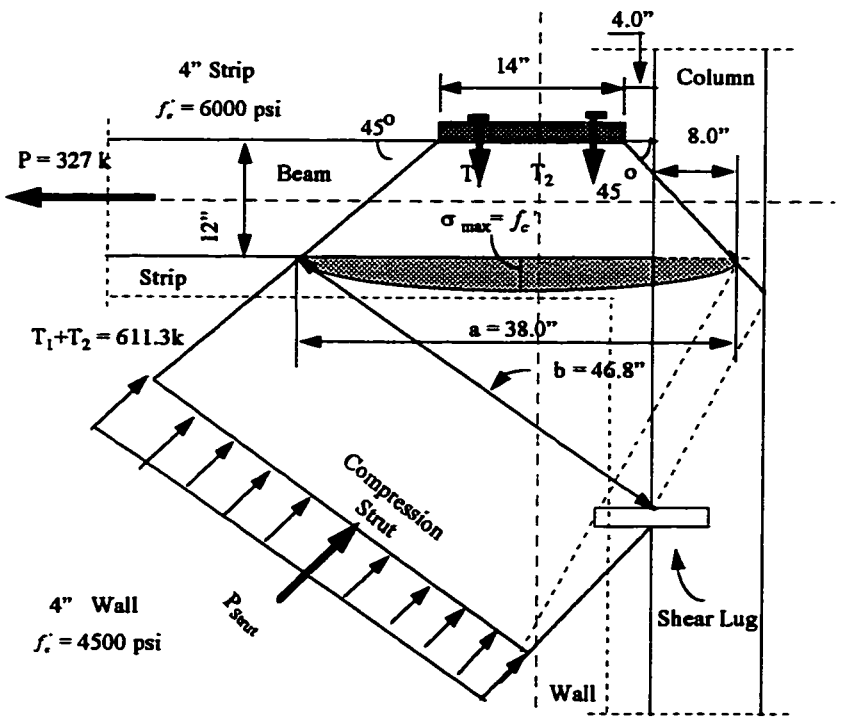

Figure 6.24 Force Condition at Compression Strut Tip

Applying strip thickness *t=4.0* in. and concrete strength f_c' = *6,000* psi. to equation (6-7), the concrete bearing capacity was evaluated as F_c = 608 kips. The bearing capacity was almost the same as the post-tensioning force of 611 kips shown

in Table 6.1. Using the computed bearing capacity, failure occurred at the tendon anchorage as the total base shear reached to 488 kips which closely matched the measured base shear of 491 kips.

The strength of the infill in the compression strut was also evaluated using the model shown in Figure 6.24. The compression force on the smallest cross section of the strut was calculated as,

$$P_{strut} = t_{wall}\ b\ f_c' \qquad (6\text{-}8)$$

Applying wall thickness $t_{wall} = 4.0$ in., compression strut width $b = 46.8$ in., and concrete strength $f_c' = 4{,}500$ psi in equation (6-8), the compression capacity of the infill strut was $P_{strut} = 824$ kips, greater than the strut force of 693 kips subjected to the base shear of 491 kips in the test. Therefore, a compression failure did not occur in the infill though the infill wall concrete strength was much lower (4,500 psi) than the strip concrete strength (6,000 psi). There was no compression or bearing failure at the compression strut "toe" because the strip and infill thickness was bigger and concrete strength was higher at the strut toe than at the strut tip.

6.4.2.3 Base Shear Capacity

Using equation (4-27), the computed yield strength of shear lugs (steel pipes) was 54.6 psi for a 2-1/2 in. pipe, and 40.4 psi for a 2.0 in. pipe. Regardless of the column shear strength, total pipe yielding strength was estimated as 209 kips at the base interface, and 104 kips at the bottom of the second-story infill wall interface. Because the column contributed shear strength and shear friction was developed along the base, a base shear strength higher than the designed value was observed.

In Test I, the base shear reached 270 kips without interface slip or concrete crushing. Shear in the lugs were not close to yielding indicating no shear friction was developed. Taking column shear strength into account, the base shear capacity was

estimated as 288 kips which was greater than the measured base shear (270 kips). When base shear was close 288 kips, interface slip was observed and shear friction was developed at the base as discussed earlier. The force in the post-tensioning tendons provided a normal force on the base interface to allow shear friction to develop. Because high post-tensioning was applied, large shear friction was developed and the base shear capacity was greatly increased. Applying the shear friction factor derived in Chapter IV (Table 4.5),

$$f_R = 0.417 - 0.083\,(\sigma_N / \lambda) \qquad (6\text{-}9)$$

Substituting the post-tensioning force T_u *for* $f_u A_s F_y$ in equation (4-21), the shear friction force is,

$$P_R = \frac{f_R}{\gamma} T_u \qquad (6.10)$$

Table 6.2 Base Shear Capacity Evaluation

Test Phase	Stress	Concrete	Factor	Factor	Tendons	Base Shear Capacity (kips)			
	σ_N	f_c'	λ	f_R	T_l	Tested	Lug	Friction	Total
II	0.726	5000	0.2	0.116	569.2	459	209	330	539
III	0.780	5000	0.2	0.094	611.3	491	209	287	496

As discussed in the last section, there was no initial post-tensioning, and two shear lugs were pulled out from the base at the tension end of the structure in Test III. Meanwhile, a larger base crack formed in Test III than that of in Test II. Based on these observations, two thirds of the infill section in Test II and one third of infill section in Test II, along with one column, was considered to be subjected to compression. Applying the maximum tendon forces in Tests II and III shown in Table 6.1, normal stress σ_N, shear friction force P_R, and total base shear strength were calculated (for tests II and III) and presented in Table 6.2. The computed base shear

capacity (496 kips), in Test III, closely matched the measured base shear (491 kips). In fact, shear friction was called on to sustain the high base shear after infill shear capacity and system shear capacity were reached.

6.4.3 Retrofitting Effective Evaluation

6.4.3.1 Frame Retrofitting

Studying the test results of the existing frame and the retrofitted model structure, retrofitting efficiency was evaluated by comparing the flexure capacity, shear strength and ductility of the two systems. Ultimate flexural capacity of the existing frame was considered as the splice failure capacity evaluated using Orangun Equation. All other values used in estimate were measured from the tests. Retrofitting efficiency was evaluated through the results of Tests I and II and is presented in Table 6.3.

Table 6.3 Frame Retrofitting Efficiency Evaluation

Test Phase		Tested Results				Ultimate Capacity		
		Splice Failure		Tendon Yield		Moment	Shear	Drift
		Load	Ductility	*Load*	Ductility	*k-f*	*kips*	%
I	Retrofitted	249.0	2.4	270.0	6.8	3600.0	270.0	0.57
	Frame	15.9	1.0	-	1.0	226.7	10.2	0.24
	Effic. Factor	15.7	2.4	-	6.8	15.9	26.5	2.39
II	Retrofitted	421.0	1.7	459.0	6.6	6120.0	459.0	0.42
	Frame	15.9	1.0	-	1.0	226.7	10.2	0.24
	Effic. Factor	24.8	1.7	-	6.6	27.0	45.0	1.76

Retrofitting efficiency was appraised by an efficient factor which is the ratio of the retrofitted structure capacity to the existing frame capacity. By means of retrofitting, the splice capacity was increased to 15.7 times and 24.8 in Tests I and II, respectively. The ultimate moment capacity and shear strength was increased respectively to 15.9 times and 26.5 times under a lower post-tensioning in Test I. The

ultimate moment capacity and shear strength increased respectively to 27 times and 45 times by higher post-tensioning in Test II.

Most significantly, the structural ductility was improved through retrofitting. Assuming the ductility factor for the existing frame was 1.0 (ultimate flexural capacity equals the splice failure capacity), ductility factor for the retrofitted structure was estimated respectively as 2.4 for splice failure, and 6.8 for tendon yielding in Test I. Incidentally, at splice failure, ductility permitted the retrofitted structure to tolerate much larger lateral drift (inelastic deformation) than the existing frame. Because of shear domination, ductility factor is lower in Test II than that in Test I which indicated that a relatively lower post-tensioning is favorable in retrofit of non-ductile frame structures by the PTPW system.

It must be pointed out, however, the retrofitting efficient factor evaluated above does not reflect the retrofitting efficiency for a structural system but a one-bay frame instead. System retrofitting efficiency should be evaluated with considerations of characteristics of structural system and behavior of earthquake excitation.

6.4.3.2 System Retrofitting

In a frame structural system, not all frames will be retrofitted with infill walls and post-tensioning. The number and locations of infills to be added are based on the moment and shear capacity of the system required by earthquake resistance. The system retrofitting efficiency was estimated with a retrofitting example.

Supposing a frame system consists of 13 frames identical to the frame tested and the retrofitted system plan is shown in Figure 6.25. Under earthquake excitation, the base shears for the existing frame system and retrofitted system were calculated

following equations (28-1) through (28-3)[49] of the static force procedure recommended by UBC-94. The following equations were used:

$$V_{base} = Z I C W / R_w \tag{6-11}$$

$$C = \frac{1.25\ S}{\sqrt[3]{T^2}} \tag{6-12}$$

$$T = C_t \sqrt[4]{H^3} \tag{6-13}$$

where C_t ..... 0.03 for existing frame structure

..... 0.02 for retrofitted PTPW system

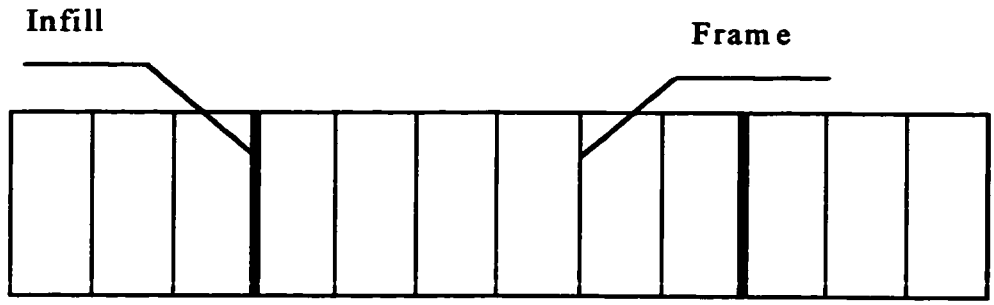

Figure 6.25 System Retrofitting Plan

The structural weight was calculated according to the dimensions of the structural elements and the coefficients were selected as shown in Table 6.4. The calculated base shear, and shear forces sustained by the frame and the infill wall are also presented in Table 6.4.

According to the calculation, each frame was required to sustain a shear of 27 kips before retrofitting. The non-ductile structure was not capable of resisting such

high lateral loads as indicated in the existing frame test. After retrofitting, two walls were added to the system, and 80% of the lateral earthquake load was supposed to be carried by the infill walls. Each infill wall sustained a shear force of 121 kips which was only a little higher than the flexural-cracking capacity but much lower than the splice capacity of the PTPW system as observed in Test I. Each frame sustained only 5 kips of shear force. Under this lower load, the frame column splice would not have failed.

Table 6.4 System Retrofitting Efficiency

Test	Site Coefficient			Structural Coefficient				Weight	Base	Element Shear (k)	
Phase	Z	I	S	C_t	C	T	R_w	W(k)	V_{base}(k)	Frame	Infill
Existing Frame	0.3	1.25	1.0	0.03	2.590	0.325	5.0	1685.0	327.3	27.3	-
Retrofitted	0.3	1.25	1.0	0.02	2.750	0.217	6.0	1763.0	303.0	5.1	121.2

The above example indicated that the retrofitting was efficient when the non-ductile frame system was converted to a frame-shear wall system to resist the earthquake load. Because of infill wall and post-tensioning involvement, the structural ductility was improved and the frame column splice was protected. The structural lateral capacity was increased and brittle shear failure was prevented.

6.5 DESIGN COMMENTS

A PTPW system can be designed as a system dominated by flexural response with three-distinct-strength behavior. Based on the three stage behavior, a PTPW system can be designed to meet the requirements of three limit states. According to the importance of structures, three stages of behavior can be classified into two categories.

A) For ordinary building structures, the flexural-cracking stage represents the service limit state, splice failure represents the damage

limit state, and post-tensioning tendon yielding represents the collapse limit state.

B) For important structures classified by UBC-94 as category I (essential facilities) and category II (hazardous facilities), the decompression (zero tension) stage represents the service limit state, the flex-cracking represents the damage limit state, and the splice failure represents the collapse limit state.

Consistent with flexure design, infill panel, closure strip and shear lugs must be designed to provide a shear capacity sufficient to prevent shear failure and to permit the development of three flexural strength stages. An efficient retrofitting design depends on the performance of the structure. To simulate the behavior of the retrofitted structure, a PTPW system design may be performed according to UBC-94.

The static equivalent force method recommended by UBC-94 can be adopted for the structural design at the service and damage limit states. Structural earthquake time-history analysis should be conducted for collapse limit state design.

The equivalent static force method was discussed for base shear capacity design in the last section. Time history analysis method will be presented in Chapter VII along with non-linear structural analysis program development for the PTPW system.

6.5.1 Flexure Capacity Design

Using equations (6-11) through (6-13), the total base shear can be calculated according to the structure behavior and earthquake coefficients as described in the last section. From the base shear, story shear can be calculated according to UBC-94 equations (28-6) through (28-8):

$$V_i = \frac{\left(V_{base} - F_t \right) W_i H_i}{\Sigma W_i H_i} \tag{6-14}$$

$$V_t = 0.07\, T\, V_{base} \tag{6-15}$$

$$\Sigma V_i + V_t = V_{base} \tag{6-16}$$

The system moment respect to story i will be calculated according to story shears,

$$M_i = \sum_{j=i}^{n} V_j (H_j - H_i) \tag{6-17}$$

The maximum moment of M_{base} can be used to calculate the tension force required in post-tensioning tendons as well as closure strip reinforcement. Because the base shear and corresponding moment were based on an elastic structure, a force reduction factor will be applied for inelastic response. The design base moment is,

$$M_{base}{}^{d} = f_d M_{base} \tag{6-18}$$

The reduction factor f_d can be determined according to the limit state and design ductility factor μ. Pertaining to the total base moment calculated for certain limit state and corresponding earthquake coefficient, the force reduction factor will be,

$$f_d = \frac{1}{\mu} \tag{6-19}$$

From the design base moment $M_{base}{}^{d}$, tension forces in the post-tensioning tendons, column bars and closure strip reinforcement can be calculated using equation (6-6). It should be noted that column bar contribution can not be included after splice failure occurred. Closure strip reinforcement will not be included when determining the ultimate tension force in the post-tensioning tendons.

The area of post-tensioning tendons can be based on the assumption that the tendon yielding capacity equals the tension force calculated using equation (6-6) from the maximum design moment at the base. The initial post-tensioning is recommended to be in the range of 30% to 50% of the tendon yielding strength. The vertical closure strip reinforcement can be designed in the ratio of 0.425% to 1.00% of the infill wall section as recommended in article 4.2.2.2.

After post-tensioning tendons and closure strip reinforcement are determined, the flexure capacity at different working stages can be estimated. Generally, decompression (zero tension), flexural-cracking and splice failure stages will be checked according to the calculated exterior moment and post-tensioning force. Initial post-tensioning can be determined following the procedure presented in Article 6.4.1.

6.5.2 Shear Capacity Design

6.5.2.1 Infill wall design

The gross section of the infill wall can be determined according to the required shear capacity. Generally, the gross section of the infill is dependent on the design base shear and concrete shear strength. To prevent brittle shear failure, the concrete shear strength may follow the specification of ACI-318 instead of the tested result discussed in article 4.2.2.1.

$$\tau_n = 2\sqrt{f_c'} \tag{6-20}$$

The base shear capacity will meet the requirement of,

$$V_{base}{}^{d} \geq f_d V_{base} \tag{6-21}$$

and the infill gross section will be,

$$A^{W}_{gross} = V_{base}{}^{d}/\tau_n \tag{6-22}$$

The infill thickness, number and locations can be selected according to the structural configuration and foundation uplift capacity which will be discussed in Chapters VIII and IV. Besides infill shear capacity design, the system shear capacity (compression strut) should be checked using a reasonable compression strut model following the procedure presented in article 6.4.2.2.

6.5.2.2 Base shear Capacity and Shear Lug Design

Corresponding to infill design, the number N_{pipe} and locations of shear lugs (steel pipe) will be determined. The gross section of the shear lugs will be determined to sustain at least the base shear estimated in the flexure design for the damage limit state.

$$A^{P}_{gross} = \frac{V_{damge}}{F_y} \tag{6-23}$$

The combined strength of shear lugs and shear friction must meet the maximum base shear requirement,

$$A^{P}_{gross} F_y + P_R \geq {V_{base}}^{d} \tag{6-24}$$

In equation (6-24), the friction shear P_R, is calculated following equation (6-9) and (6-10). Pipe embedment length must be checked to permit the development of the full strength of the shear lugs. The embedment length into the frame elements can be designed according to concrete bearing and pipe shear yielding development following equation (5-2) or written as,

$$L_{em} = \frac{V_p}{\phi \left(0.85 \, f_c' \sqrt{\frac{A_2}{A_1}} \right) D_o} \tag{6-25}$$

The embedment length into the base should be designed according to either the anchorage length of the strip reinforcement or a enlarged length of L^B_{em} whichever is greater. The enlarged embedment length in the base is recommended as,

$$L^B_{em} = 1.5\, L_{em} \qquad (6\text{-}26)$$

The strip reinforcement anchorage length for developing yield can be determined following ACI-318.

When calculating the structural strength following the above procedure and equations, concrete strength reduction factor will be applied following the specifications in ACI-318. The detailed designs of infill panels, strips, shear key and grouting were recommended in Chapter IV. Post-tensioning anchorage detail design can follow the specifications of ACI-318.

CHAPTER VII

COMPUTER SIMULATION OF SPECIMEN RESPONSE

7.1 INTRODUCTION

In the previous chapters, structural connection and model structure tests, and analysis of test results were presented which provided significant information about the behavior and performance of the PTPW system. To apply the results to structural seismic rehabilitation practice, an appropriate model must be established for analysis of the PTPW system.

To retrofit a frame structure using the PTPW system, solutions may involve different variables such as system configuration, element dimensions, material properties, reinforcement details and earthquake characteristics. To evaluate the effects of these variables on the PTPW system capacity by structural testing is time consuming and costly. Using computer simulation, the PTPW system capacity and behavior can be evaluated for various retrofitting solutions for the same structure.

To accurately simulate structural response, a suitable computer program is desired to allow designers to correctly evaluate diverse rehabilitation solutions for a given structural system. The non-linear structural analysis program IDARC-2D was modified by adding post-tensioning and non-linear elastic hysteretic response models based on the model structure test results. A new version of IDARC-2D, called IDARC-PT, was developed for PTPW system analysis and design, and calibrated using structural test results.

7.2 TIME HISTORY ANALYSIS OF STRUCTURAL RESPONSE

7.2.1 Vibration of Non-linear Systems

According to structural dynamics, the vibration of a structural system subjected to an earthquake is governed by the differential equation shown below [42] .

$$\mathbf{M}\ddot{Y} + \mathbf{C}\dot{Y} + \mathbf{K}Y = -\mathbf{M}\ddot{a} \qquad (7\text{-}1)$$

where **M, C** and **k** ... matrices of mass, damping & stiffness,

$\ddot{Y}, \dot{Y}$ and **Y** ... matrices of acceleration, velocity, and displacement, and

$\ddot{a}$ ... ground acceleration at earthquake site.

In classical dynamic response formulation, the term on the right side of equation (7-1) may be a harmonic force or other type of force that can be expressed as a function of time. Therefore, the solution of the differential equation is obtained as a function of time as shown in Figure 7.1. Earthquake actions, however, are a random process and the solution of the differential equation will be a discrete process as shown in Figure 7.2.

However, a closed-form analytical solution can not be obtained for the differential equation representing the vibration of an inelastic, non-linear structural system. Though some discrete analytical solutions have been obtained for elasto-plastic single degree of freedom systems[30] , it is difficult to apply these solutions to real complex structural systems. Other approximate methods, such as energy, discrete Fourier analysis[14] and response spectrum analysis[37] have also been used to estimate the vibration response of nonlinear systems but the solutions are not very accurate.

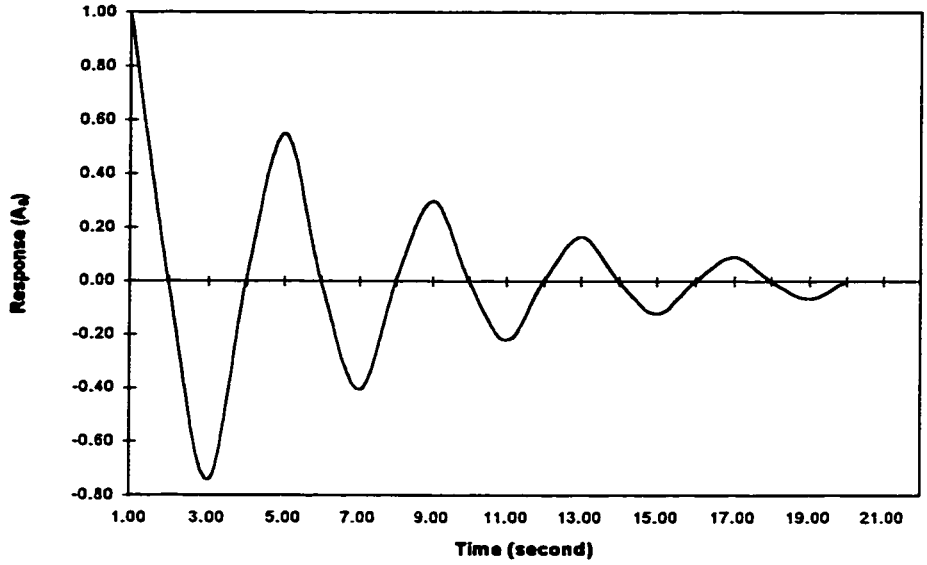

Figure 7.1 Structural Response Under Harmonic Excitation

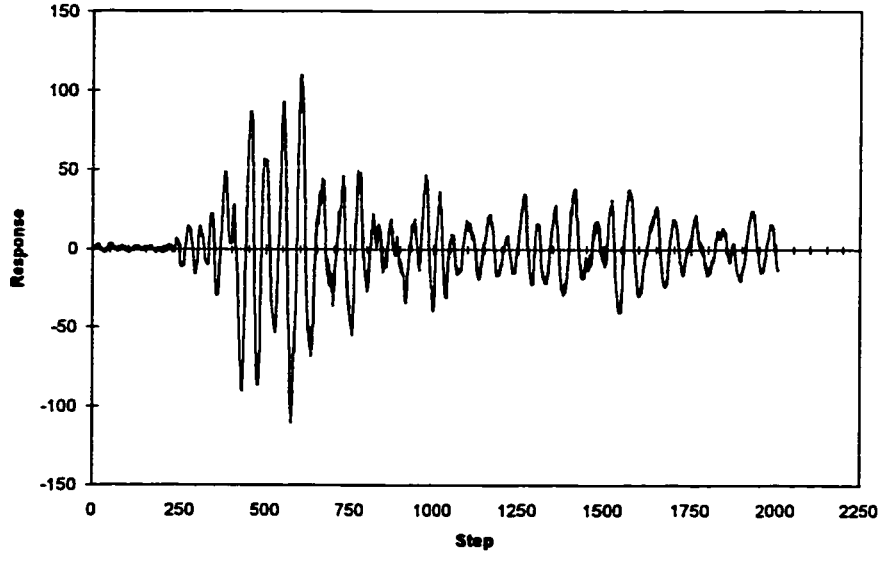

Figure 7.2 Structural Response Under Earthquake Excitation

Fortunately, the development of computer science and programming technology have made it possible to accurately analyze nonlinear structural vibration due to earthquake excitation. A step-by-step integration or time-history analysis is an efficient method for analyzing non-linear structural seismic response. The vibration of a structure is evaluated at successive time increments Δt as shown in Figure 7.3. The Constant Acceleration Method and Linear Acceleration Method are commonly used in step-by-step integration. The Linear Acceleration method has been widely used in structural time-history analysis.

7.2.2 Linear Acceleration Method

In equation (7-1), all variables except mass M are functions of time because of the behavior of earthquakes. The structural damping factor **C** and stiffness **K** are non-linear functions for an inelastic system. Due to the non-linear behavior, no closed-form analytical solution can be found for equation (7-1). However, for a small time interval, a non-linear function can be expressed as an ordinary linear function.

$$M\Delta\ddot{Y}_i + C_i\Delta\dot{Y}i + K_i\Delta Y_i = -M\Delta\ddot{a}_i \qquad (7\text{-}2)$$

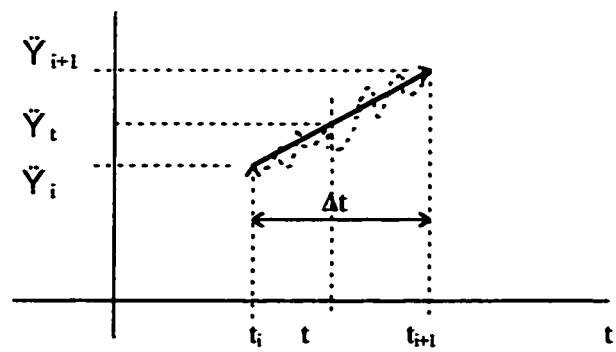

Figure 7.3 Acceleration Corresponding to Steps

The variables t_i and t_{i+1} (which equals $t_i + \Delta t$) are the designations for the time at the beginning and the end of the time interval Δt. The time interval Δt is usually

taken as a constant length for computational convenience. If Δt is sufficient small, the acceleration may be expressed by a linear function of time within the interval Δt. The properties of the system c_i and k_i over a time interval of t_i to t_{i+1} can be assumed constant. Therefore, the system coefficients **c** and **k** may include any form of nonlinearity. In this time interval, equation (7-1) may be rewritten as an incremental equation.

As shown in Figure 7.3, the acceleration may be expressed as

$$\ddot{Y}(t) = \ddot{Y}_i + \Delta\ddot{Y}_i\,(t-t_i)/\Delta t \qquad (7\text{-}3)$$

$$\text{where } \Delta\ddot{Y}_i = \ddot{Y}(t_i+\Delta t) - \ddot{Y}(t_i) \qquad (a)$$

Integrating equation (7-3) twice with respect to time between the limits t_i and t,

$$\dot{Y}_i(t) = \dot{Y}_i + \ddot{Y}_i\,(t-t_i) + \Delta\ddot{Y}_i\,(t-t_i)^2/2 \qquad (7\text{-}4)$$

$$\mathbf{Y}(t) = \mathbf{Y}_i + \dot{Y}i\,(t-t_i) + \ddot{Y}_i\,(t-t_i)^2/2 + \Delta\ddot{Y}_i\,(t-t_i)^3/(6\Delta t) \qquad (7\text{-}5)$$

The evaluation of equation (7-4) and (7-5), at time $t = t_i + \Delta t$, yields,

$$\Delta\dot{Y}i = \ddot{Y}_i\Delta t + \Delta\ddot{Y}_i\,\Delta t/2 \qquad (7\text{-}6)$$

$$\Delta\mathbf{Y}_i = \dot{Y}_i\Delta t + \ddot{Y}_i\,\Delta t^2/2 + \Delta\ddot{Y}_i\,\Delta t^2/6 \qquad (7\text{-}7)$$

$$\text{where } \Delta\dot{Y}_i = \dot{Y}(t_i+\Delta t) - \dot{Y}(t_i) \qquad (b)$$

$$\Delta\mathbf{Y}_i = \mathbf{Y}(t_i+\Delta t) - \mathbf{Y}(t_i) \qquad (c)$$

Rearranging (7-7) and substituting into (7-6), yields

$$\Delta\ddot{Y}_i = 6\Delta\mathbf{Y}_i/(\Delta t^2) - 6\dot{Y}_i/\Delta t - 3\ddot{Y}_i \qquad (7\text{-}8)$$

$$\Delta\dot{Y}_i = 3\Delta\mathbf{Y}_i/\Delta t - 3\dot{Y}_i - \ddot{Y}_i\,\Delta t/2 \qquad (7\text{-}9)$$

Substituting (7-8) and (7-9) into (7-2), the incremental equation of motion is,

$$M\{6\Delta Y_i/(\Delta t^2) - 6\dot{Y}_i/\Delta t - 3\ddot{Y}_i\}$$

$$+ C_i\{3\Delta Y_i/\Delta t - 3\dot{Y}_i - \ddot{Y}_i\,\Delta t/2\} + K_i\Delta Y_i = -M\Delta\ddot{a}_i \quad (7\text{-}10)$$

In this equation, only ΔY_i is unknown at time t_i and by rearranging (7-10), so

$$\{K_i + 6M/(\Delta t^2) + 3C_i/\Delta t\}\Delta Y_i = -M\Delta\ddot{a}_i$$

$$+ M\{6\dot{Y}_i/\Delta t + 3\ddot{Y}_i\} + C_i\{3\dot{Y}_i - \ddot{Y}_i\,\Delta t/2\} \quad (7\text{-}11)$$

For convenience, let

$$K_i^m = \{K_i + 6M/(\Delta t^2) + 3C_i/\Delta t\} \quad (d)$$

$$\Delta F_i^m = -M\Delta\ddot{a}_i + M\{6\dot{Y}_i/\Delta t + 3\ddot{Y}_i\}$$

$$+ C_i\{3\dot{Y}_i - \ddot{Y}_i\,\Delta t/2\} \quad (e)$$

Equation (7-11) can be written as a static incremental equilibrium equation

$$K_i^m\,\Delta Y_i = \Delta F_i^m \quad (7\text{-}12)$$

The problem of solving the non-linear differential equation becomes an exercise of solving the algebra equation. Once the increment ΔY_i is determined over the time interval t_i to $t_i + \Delta t$, additional increments can be evaluated using equations (7-8) and (7-9). And finally, through equation (c), (b) and (a), the system displacement, velocity and acceleration at time t_{i+1} are found as

$$Y(t_i+\Delta t) = Y(t_i) + \Delta Y_i, \text{ or } Y_{i+1} = Y_i + \Delta Y_i \quad (7\text{-}13)$$

$$\dot{Y}(t_i+\Delta t) = \dot{Y}(t_i) + \Delta\dot{Y}_i, \text{ or } \dot{Y}_{i+1} = \dot{Y}_i + \Delta\dot{Y}_i \quad (7\text{-}14)$$

$$\ddot{Y}(t_i+\Delta t) = \ddot{Y}(t_i) + \Delta\ddot{Y}_i, \text{ or } \ddot{Y}_{i+1} = \ddot{Y}_i + \Delta\ddot{Y}_i \quad (7\text{-}15)$$

Using these equations, Y_{i+2} ,....., Y_{i+m} ; $\dot{Y}_{i+2}$,..... $\dot{Y}_{i+m}$; and $\ddot{Y}_{i+2}$, ..., $\ddot{Y}_{i+m}$ can be calculated step by step. The precision of the solution changes with the length of the time interval. The smaller the time interval, Δt, the more accurate the solution.

Three variables, earthquake acceleration, system stiffness **K**, and damping coefficient **C** are involved in the integration. No matter how complicated the earthquake acceleration is, step-by step integration is applied to compute the structural response. Any non-linearities in system damping and stiffness are involved in the integration.

7.3 Non-linear Program Evaluation

Three available for non-linear structural analysis, IDARC, DRAIN-2D and REMAS (reinforced masonry) were considered. They were developed for research and each has some limitations. To apply any of these programs to the PTPW system simulation, required modification addition of new functions.

7.3.1 Calculation Model

Features of each program were studied and are outlined in Table 7.1. Each program utilizes step-by-step integration. There are some differences between the programs in applying initial force, and inputting structural data and load.

Table 7.1 Program features of calculation model

Program Name	Analysis Method	Excitation Input	Source Code	Data Input Method	Initial Force Input	Number of Frames
IDARC	Linear Acc.	Two-way	Yes	Two-way	Included	Multiple
DRAIN	Constant A.	One-way	Yes	One-way	Included	Single
REMAS	Constant A.	One-way	No	One-way	No	Single

IDARC has advantages in data input and system assembly. The structural

properties can be input as either calculated stiffness and specified hysteretic curves or element sections and reinforcement schedules. For lateral load input, IDARC allows either load control or displacement control. Moreover, IDARC can simultaneously analyze multiple frames with different properties to allow analysis of the whole structural system.

The input method used in IDARC was termed as two-way method. In contrast, the other programs, DRAIN-2D and REMAS, require input of structural strength and stiffness properties, and allow only load control. The input method for the latter two programs was described as the one-way method. In laboratory experiments, a method commonly used is load control before cracking or yielding, and displacement control after cracking or yielding. In computer simulation, it is difficult to use the load-control method because cracking, yielding and ultimate structural capacities are unknown or not can be estimated accurately. The displacement control method in IDARC can eliminate these difficulties. The system assembling function in IDARC will benefit system analysis and foundation simulation. Therefore, IDARC was selected as the program to be modified for the PTPW system.

Besides input and system assembling, a means of imposing initial force is important for a PTPW system because an initial post-tensioning force will be applied to the system. In IDARC and DRAIN-2D, initial force can be imposed on vertical elements to model the force in columns and post-tensioning tendons.

To modify a basic program or add new functions to the program for PTPW system analysis, the source code for the basic program must be available for modification. Since no source code was available for the program REMAS, it was not considered.

7.3.2 Elements involvement

Structural elements including beams, columns, and panels or walls are involved in a PTPW system. These elements are provided in IDARC and DRAIN-2D. However, there are some differences between the models in IDARC and Drain-2D. Table 7.2 shows some of the element characteristics for each program.

Table 7.2 Element Types Involved in the Programs

Program Name	Column Axial Deformation	Beam Axial Deformation	Axial Element	Infill Panel	Wall Edge Column
IDARC	Elastic	No	No	Two-Joint	Included
DRAIN-2D	Inelastic	Considered	Included	Four-Joint	No

In IDARC, no axial inelastic deformation is considered for column and beam elements, and no truss elements are provided. The panel/wall element is modeled as a two-joint, column-like member having flexural, axial and shear capacities as shown in Figure 7.4. To reflect the interaction of a wall and boundary columns, an edge column element is included with the wall element.

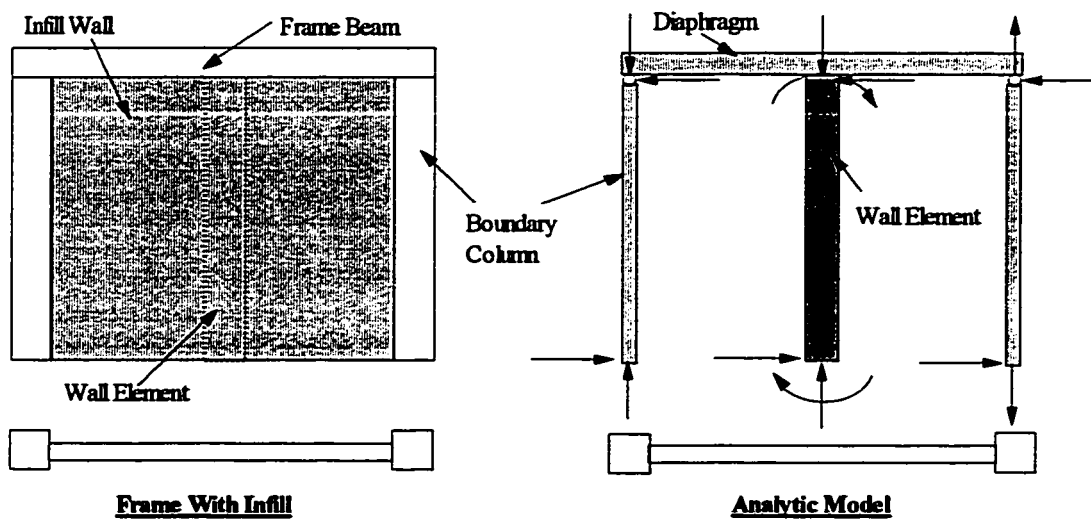

Figure 7.4 IDARC Analytic Model For Wall Elements

In DRAIN-2D, a beam or column element can be considered as an elasto-plastic element with six degrees of freedom. Truss elements are also provided in DRAIN-2D. Panel/wall elements are modeled as a four-joint element. However, only shear capacity is considered for a panel/wall element as shown in Figure 7.5. The shear model not can completely reflect the behavior of an infill wall.

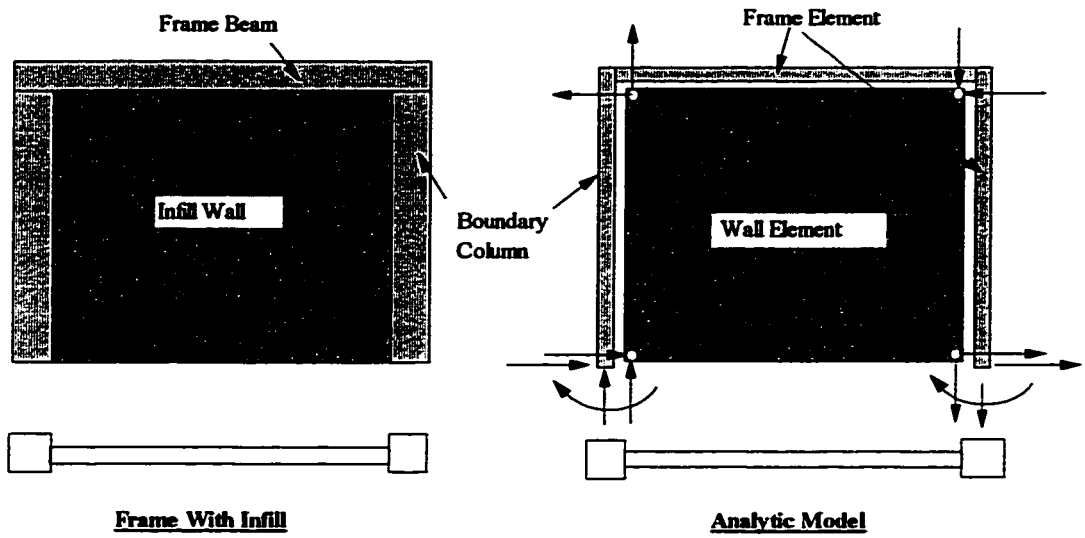

Figure 7.5 DRAIN-2D Analytic Model for Infill Wall

The beam and column models in either program meet the requirements for frame system analysis. However, applying the programs to a precast infill wall and post-tensioning system requires certain modifications. If IDARC is selected, a truss element or an axial element must be added. If DRAIN-2D is chosen, the panel/wall element must be modified so that wall members have flexural and axial capacities.

7.3.3 Mechanical Properties

Table 7.3 outlines the mechanical properties involved in the two programs. A one-degree of freedom column under cyclic load was analyzed using both IDARC and DRAIN-2D, and the layouts are shown in Figure 7.6. The result from IDARC, shown

in Figure 7.6b resembles the reinforced concrete structure/element behavior as discussed in chapter VI. Therefore, IDARC accurately reflects the behavior of reinforced concrete elements.

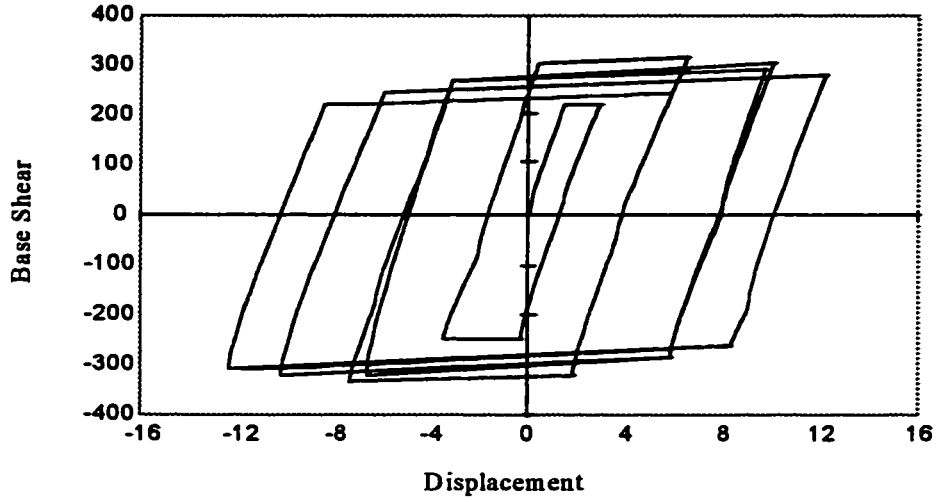

Figure 7.6a Structural Response (DRAIN-2D)

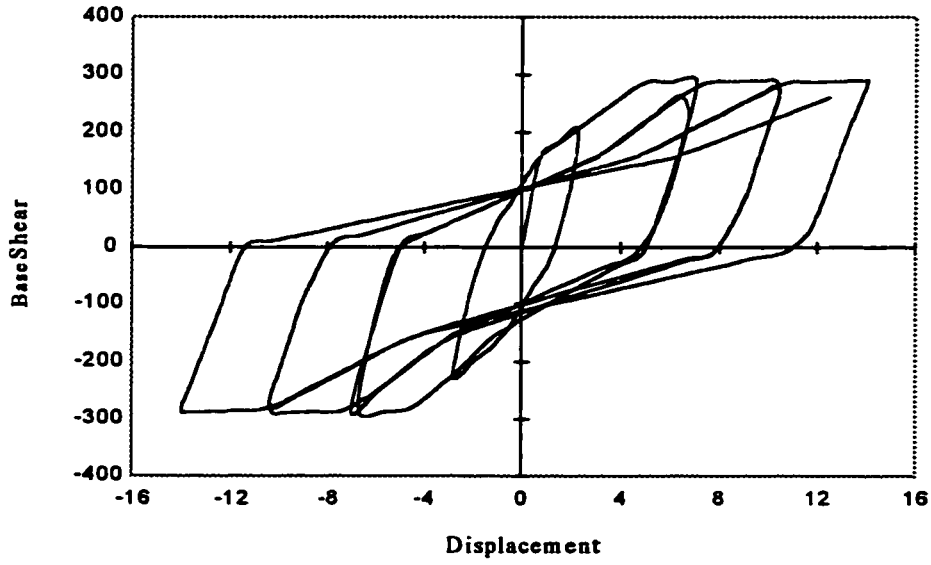

Figure 7.6b Structural Response (IDARC)

Table 7.3 Mechanical Properties Considered in Programs

Program Name	Hysteretic Response	Stiffness Behavior	Strength Behavior	Pinching Behavior	Damping Factor
IDARC	Tri-linear	Degrading	Full Degrading	Considered	Constant
DRAIN-2D	Bi-linear	No Degrading	Mini-Degrading	No	Variable

Generally, reinforced concrete structure/element response exhibits tri-linear behavior of cracking, yielding and post-yield. The hysteric response model in IDARC analysis closely simulates this behavior. Pertaining to tri-linear behavior, the structural stiffness and strength degrade in the loading cycles after yielding. Using IDARC, response of a reinforced concrete structure can be closely simulated. However, only a limited strength degradation can be simulated using DRAIN-2D. Moreover, pinching behavior observed in reinforced concrete member response can also be simulated using IDARC but is not using DRAIN-2D.

DRAIN-2D has one advantage over IDARC which involves consideration of structural damping. Structural damping can be taken as a linear combination of mass-dependent and stiffness-dependent effects as express below:

$$[C] = \alpha[M] + \beta[K] \qquad (7\text{-}16)$$

where α and β are constants depending on the structural properties of mass and stiffness.

It is obvious that the system damping factor will reduce with degradation of stiffness. Like most other non-linear structural analysis programs, a shortcoming of IDARC is that the damping factor is considered constant for a structural system. Despite the shortcoming related to the constant damping factor, IDARC has advantages related to the method of response calculation, input method, system

assembly, and especially, hysteretic response model. Therefore, IDARC was chosen as the basic program to be modified for PTPW system response simulation.

7.4 IDARC MODIFICATION AND IDARC-PT DEVELOPMENT

Through the use of example structures, program IDARC was debugged. Checking the calculation results for certain variables, and reviewing the source code, the printing, mechanical and logical mistakes in the program were detected and corrected. New calculation models were created and added into the program. A new version of IDARC, IDARC-PT, containing post-tensioning and non-linear elastic models was developed for PTPW system simulation.

7.4.1 Program Correction

For a PTPW system, a boundary column initial axial force must be applied to simulate post-tensioning force, and a wall element must be added to the system. Unfortunately, trial analyses showed that the program incorrectly predicted the response of a system with wall panels and element initial axial forces, though it correctly predicted response of frame structures consisting of beams and columns.

It was found that errors associated with initial forces were related to a DO-BLOCK in the coding for dynamic analysis. In every load cycle, the initial force was taken as the original value. By moving the initial force from the dynamic analysis DO-BLOCK and inserting it in the dead load analysis section, initial forces, such as initial post-tensioning forces were correctly simulated.

The wall element produced incorrect response because a typing mistake existed in the wall element section of the original source code. A column element variable was misused as a wall element variable. After correcting this mistake, the wall element

worked properly.

Another problem encountered in the program modification was modeling the wall element. To reflect behavior of a wall with boundary elements, wall element in IDARC is modeled as a column-like element accompanied by a special column element referred to as an edge column. Edge column response was found to be incorrect after adding the response to the output files. After studying the source code, the edge column model was observed to be very complex and difficult to correct. In order to remedy the problems associated with the edge column element, an inelastic axial spring element was added to substitute for the edge-column element.

There were other mistakes detected and corrected including inconsistencies in input methods and printing mistakes. Mistakes were detected and corrected because special features were required and new analytical models were added for PTPW systems. Without new analytical models, most mistakes in the original version of IDARC would not have been found. Though there were errors in the IDARC program, there are advantages over DRAIN-2D, as mentioned earlier. The hysteretic response was of primary concern for a PTPW system. IDARC provides a realistic model of hysteretic response for reinforced concrete structures. It was relatively easy to modify the hysteretic model in IDARC to reflect the non-linear elastic behavior of PTPW systems.

7.4.2 Addition of New Analytical Models

New analytical models were created for simulating PTPW system behavior. Program IDACR-PT was developed through addition of new analytical models to the program IDARC.

7.4.2.1 Truss Member Modeling

In the original version of IDARC, no truss elements were included. However, the program allows an element to have a hinge at one end. Revising the model to permit a column to have hinges at both ends, an axial or truss member model was introduced into the program. As long as a truss element is used as an additional member instead of a lone member at a joint in a structure, there will be no singularities in the force or displacement equations for the system.

In a PTPW system, a truss element modeled as a two-joint column is used to represent a post-tensioning tendon. The tendons are attached to the boundary columns so as not to create any singularities in the system stiffness matrix. Since the column elements in IDARC remain elastic with regard to axial deformation, truss elements based on the column element also remain in elastic. It is realistic to model post-tensioning tendons to remain elastic because the tendons will not function as desired if inelastic deformation results.

7.4.2.2 Inelastic Axial Spring Modeling

If the tendons are desired to reach yield, the truss elements not can be used to model the tendons. As an alternative, an inelastic axial spring element is recommended to represent an inelastic tendon. It can also be used as part of a boundary column element to substitute for the edge column element in IDARC to meet the requirements for PTPW system simulation.

The inelastic axial spring element was created to have the following features: it possesses cracking, yielding and post yield behavior as observed in tests. It can also be used to simulate performance of foundations with different tensile and compression behavior of the soil-structure system.

Because an inelastic rotational spring element was included in IDARC, an inelastic axial spring element was added by modifying the inelastic rotational spring element. To provide an axial spring with the features described above, an inelastic axial element was developed to follow two different backbone curves in tension and compression, as shown in Figure 7.7.

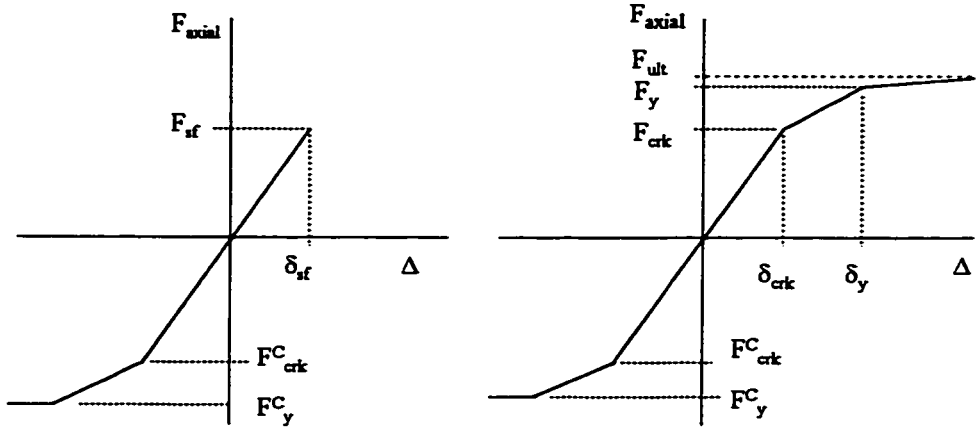

a) Splice Failure Model b) Yielding Model

Figure 7.7 Backbone Curves for Inelastic Spring

The choice of the hysteretic rule for an inelastic axial spring or a boundary column in a PTPW system depends on the reinforcement details in the boundary column. If the boundary column reinforcement splices are so short that the reinforcement yield not can be reached before splice failure, an inelastic axial spring representing the boundary column may be governed by the hysteretic rule shown in Figure 7.7a. The force level F_{sf} is the estimated splice failure strength and δ_{sf} is the corresponding axial elongation of the boundary column. Otherwise, if the column reinforcement splices are long enough that reinforcement can yield, the inelastic axial spring used as the boundary column follows the hysteretic rule shown in Figure 7.7b. For this case, a column response follows a tri-linear path in both compression and

tension.

The terms F_{crk}, F_y and F_{ult} shown in Figure 7.7b represent the cracking, yielding and ultimate strengths. Supposing the cracking occurred at the strain level of δ_{crk}[45], the cracking, yielding, and ultimate strengths of the boundary column in tension can be estimated using the following equations:

$$F_{crk} = \delta_{crk} F_c + \delta_{crk}(\varepsilon_c / \varepsilon_y) F_y \quad (7\text{-}17)$$

$$F_y = A_y f_y \quad (7\text{-}18)$$

$$F_{ult} = \gamma F_y \quad (7\text{-}19)$$

where, $F_c = A_c f'_c$ .....column concrete axial strength,

ε_c ..... concrete ultimate strain,

A_y ..... total area of reinforcement,

f_y .....yielding stress of reinforcement,

ε_y .....yielding strain of reinforcement, and

γ ..... strain hardening factor (>1.0)

In compression, regardless the reinforcement splice behavior, the micro cracking, yielding and ultimate strengths can be calculated using the following equations:

$$F^c_{crk} = \delta_{crk} F_c + \delta_{crk}(\varepsilon_c / \varepsilon_y) F_y \quad (7\text{-}20)$$

$$F^c_y = A_y f_y + (\varepsilon_y / \varepsilon_c) F_c \quad (7\text{-}21)$$

$$F^c_{ult} = \gamma F_y + F_c \quad (7\text{-}22)$$

Representing the boundary column in a PTPW system, the axial spring

elements always accompany the infill wall element. A wall and corresponding boundary columns work jointly so that the wall sustains the system shear force while the boundary columns and post-tensioning tendons resist the system moment through axial forces.

7.4.2.3 Post-Tensioning

As discussed earlier, the initial post-tensioning force is applied as an initial axial force in the tendon elements. Under lateral load, the force in a tendon develops on the basis of its effective initial force. The terms "effective initial force" and " initial force" have different meanings. The initial force defines the post-tensioning force applied on the structure by stressing the tendons. The effective initial force, on the other hand, defines the actual tendon force acting on the structure after post-tensioning losses. In other words, the initial force is the post-tensioning force input in analysis, and the effective initial force is the remaining force in the tendons accounting for post-tensioning losses.

The post-tensioning loss and effective initial force can be estimated using program IDARC-PT. In analysis, the post-tensioning force is generally imposed as a dead load action on the structure. When initial post-tensioning force is applied, the adjacent boundary column and other elements will be subjected to compression force and deformation. Simultaneously, the tension force in the tendons will be reduced due to deformation compatibility of the tendons and boundary column. After tension loss, the remaining force in the tendons is the effective initial force.

7.4.2.4 New Hysteretic Model Creation

Test results demonstrated that a PTPW system behaved almost like a nonlinear-elastic system (Chapter VI). Its loading curve is a nonlinear trace, and its

unloading curve follows a path similar to the loading curve. The residual deformation produces a gap between the two curves. The gap may be small or large depending on the energy dissipation of the system.

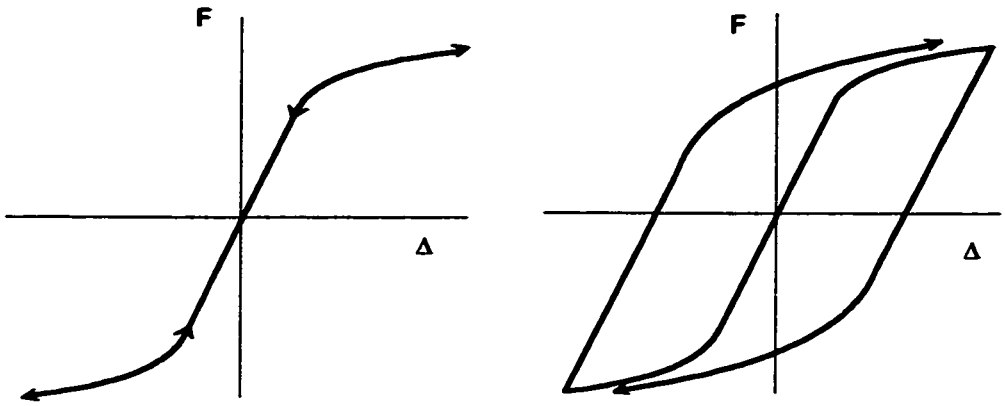

a) Elastic Nonlinear b) Inelastic Nonlinear

Figure 7.8 Elastic and Inelastic Property of Structure

Unlike either a nonlinear-elastic or nonlinear-inelastic system, the load-deformation response of a PTPW system has a shape that lies between these two systems. For a nonlinear-elastic system, unloading follows the same trace of the loading curve as shown in Figure 7.8a. For a nonlinear-inelastic system, regardless of the shape of the loading curve, unloading initially follows an elastic path with a significant residual deformation as shown in Figure 7.8b.

An ordinary reinforced concrete system will typically exhibit nonlinear-inelastic behavior with a bilinear or tri-linear loading curve, and an unloading curve with a large residual deformation as shown in Figure 7.9. In Loading process, the load-deformation response of a PTPW system resembles a non-linear trace similar to that for an ordinary reinforce concrete system. During unloading, however, the residual deformation is much smaller than that of an ordinary reinforced concrete system.

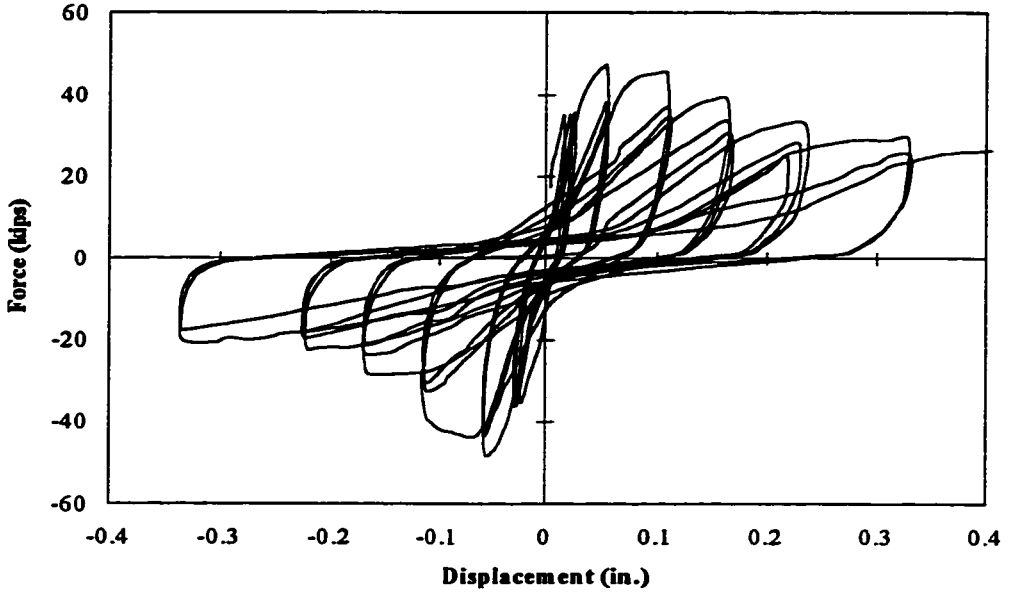

Figure 7.9 Hysteretic Behavior of Ordinary R/C Structure

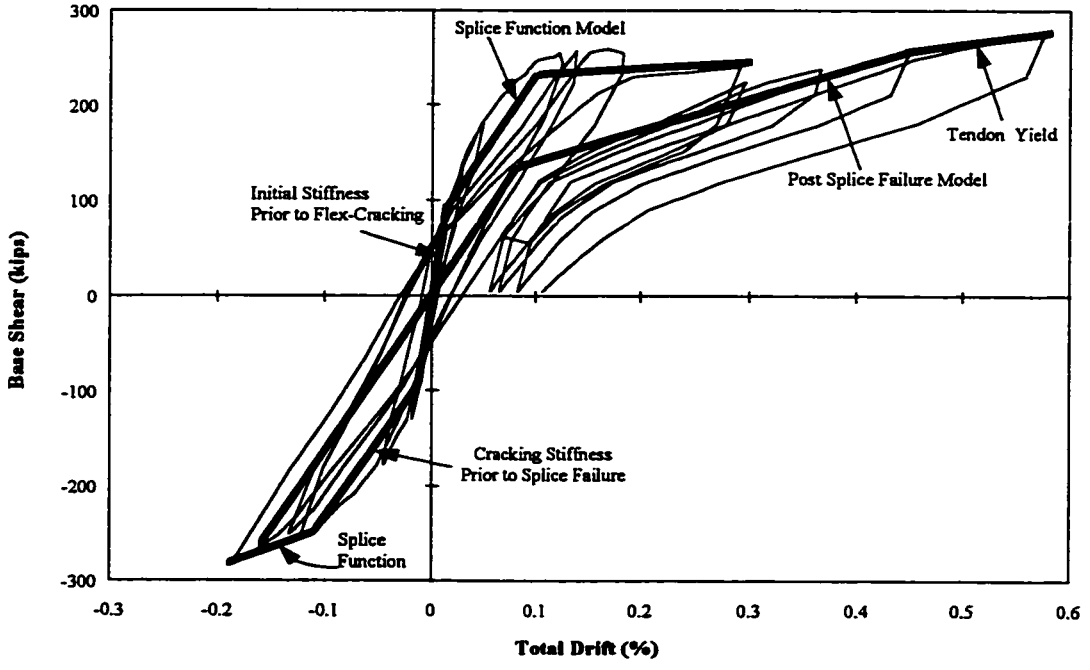

Figure 7.10 Hysteretic Behavior of Post Tensioned System

Figure 7.10 again shows the structural response of Test I to illustrate that the hysteretic behavior of a PTPW system is different from that of ordinary reinforced concrete structures. To simulate the response of the PTPW system, the hysteretic model was modified to reflect the observed response in the tests

By introducing a post-tension factor PT, and corresponding hysteretic model, the program IDARC-PT can be used to analyze PTPW systems. The shape the hysteretic model or residual deformation was controlled by the factor PT. The factor PT can be chosen between 0.0 to 1.0 according to the level of post-tensioning applied to the system.

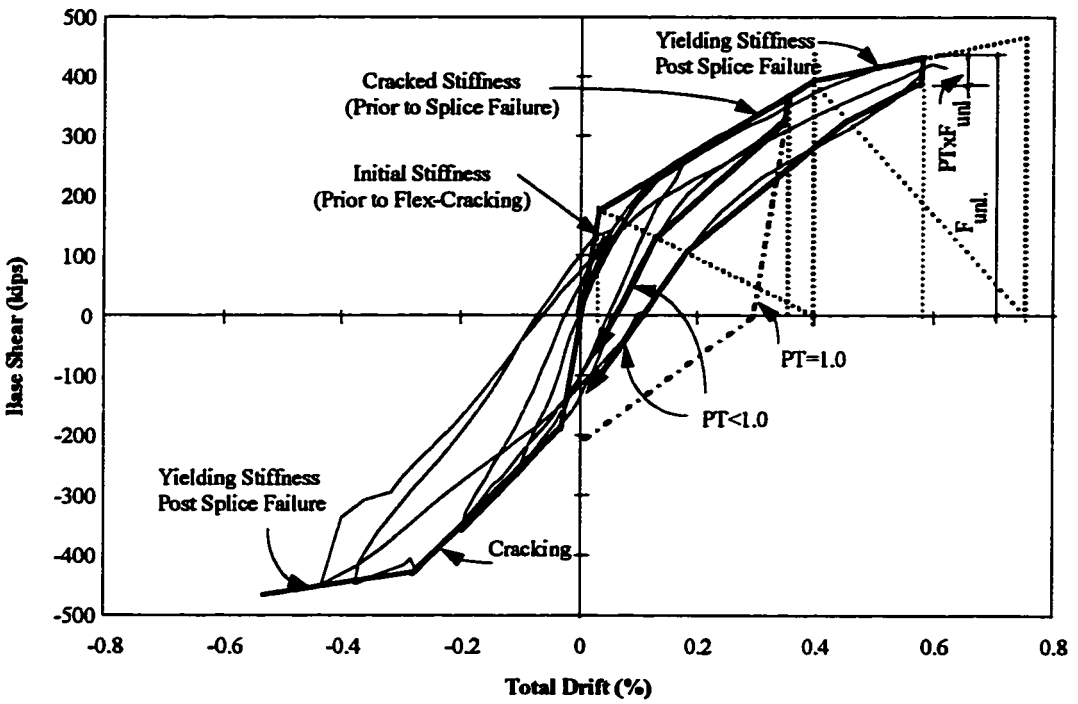

Figure 7.11 Hysteretic Model of Post Tension System

When PT = 0.0, the system is a nonlinear-elastic system in which the loading and unloading traces follow the same curve. When PT = 1.0, the system is considered

an ordinary reinforced concrete structural system. For the structural system considered here, the factor PT was always chosen between these extreme values ($0.0 < PT < 1.0$). For convenience, the program allows the user to input any value of PT. If $PT \leq 0.0$ or $PT \geq 1.0$ is inputted , a default value of 1.0 is applied. Figure 7.11 shows the influence of the post-tensioning factor on the response of a PTPW system under cyclic load.

7.4.2.5 Damping Property Modification

If a system is subject to dynamic load, its response will be affected by the system damping property. In classic linear-elastic dynamic analysis, the damping factor is constant. In order to simplify analysis, some nonlinear analysis programs, such as IDARC, set the damping factor as a constant. In fact, the damping factor is dependent on system mass and stiffness. As stiffness declines, the system damping capacity reduces.

To reflect this phenomenon, a new feature was implemented to allow the user to select either constant or variable damping for a structure. When selecting a variable damping factor, coefficients α and β in equation (7-16) are specified as input data by the user. In every time interval or step, the program will calculate the damping factor C according to the stiffness of the structure at that step so that the damping varies with stiffness change.

7.4.3 Debug of Program IDARC-PT

By correcting the existing mistakes and adding the new models and features to program IDARC-2D, a new version IDARC-PT was developed for analyzing post-tensioned pre-cast infill wall retrofitting systems. Program IDARC-PT was debugged through analyses of PTPW system examples.

7.5 SIMULATION SPECIMEN TESTS

7.5.1 Input Data Preparation

Using IDARC-PT, computer simulations were conducted for the existing-frame test and PTPW system (strengthened model structure) tests. In order to coincide with test results, realistic input data preparation was necessary. This involved hysteretic parameter selection, member capacity evaluation, post-tensioning force application, and earthquake or cyclic load input selection. Simulation results and input data selection for each test are discussed in the following articles.

7.5.2 Simulation of Existing Frame Test

As described in Chapter V, the existing frame structure was loaded to first cracking in the test. The existing frame test was simulated using both IDARC-2D and IDARC-PT.

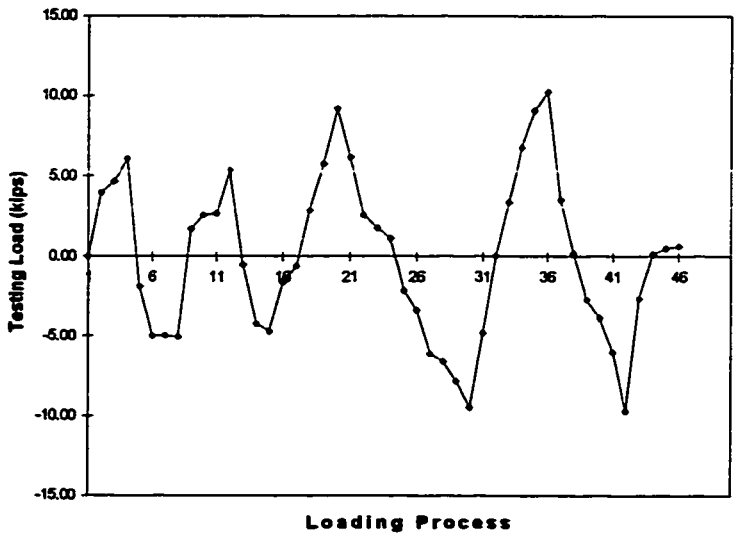

Fig. 7.12 Load Input for Frame Test

In the frame test, lateral cyclic loads were applied at each story as described in Chapter V. Total lateral load or base shear applied to the frame test is shown in Fig. 7.12. The simulation input, for IDARC-PT, was the top displacement history (displacement control) as shown in Fig. 7.13.

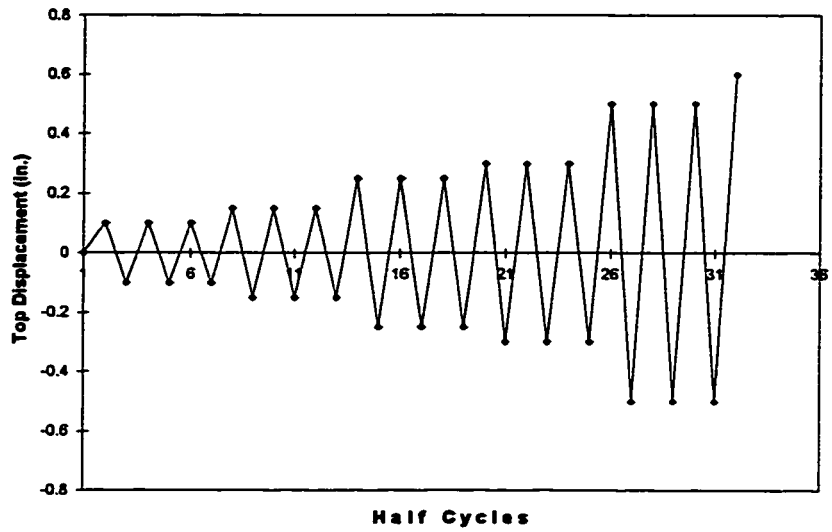

Fig. 7.13 Displacement Input for Analysis Using IDARC-PT

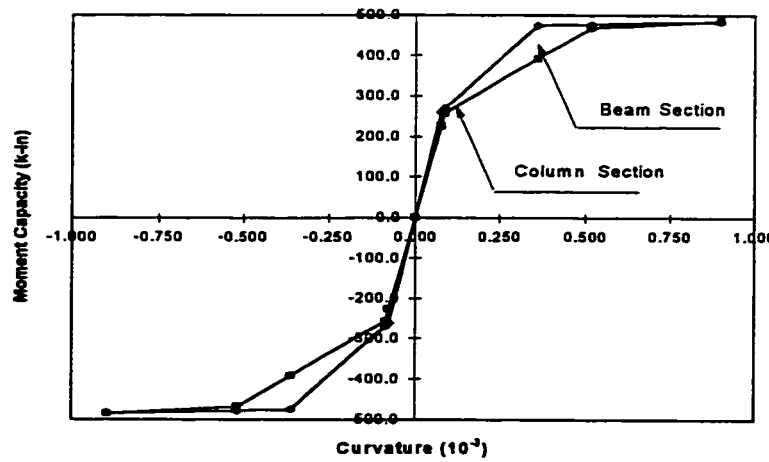

Fig 7.14 Moment-Curvature Relationship for Frame Elements

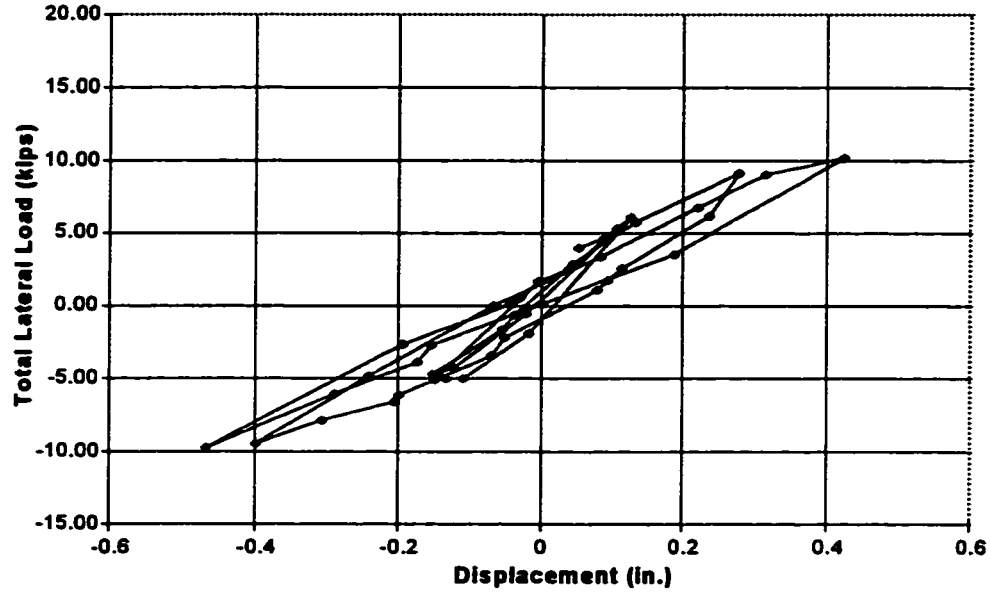

Fig 7.15 Existing Frame Test Response

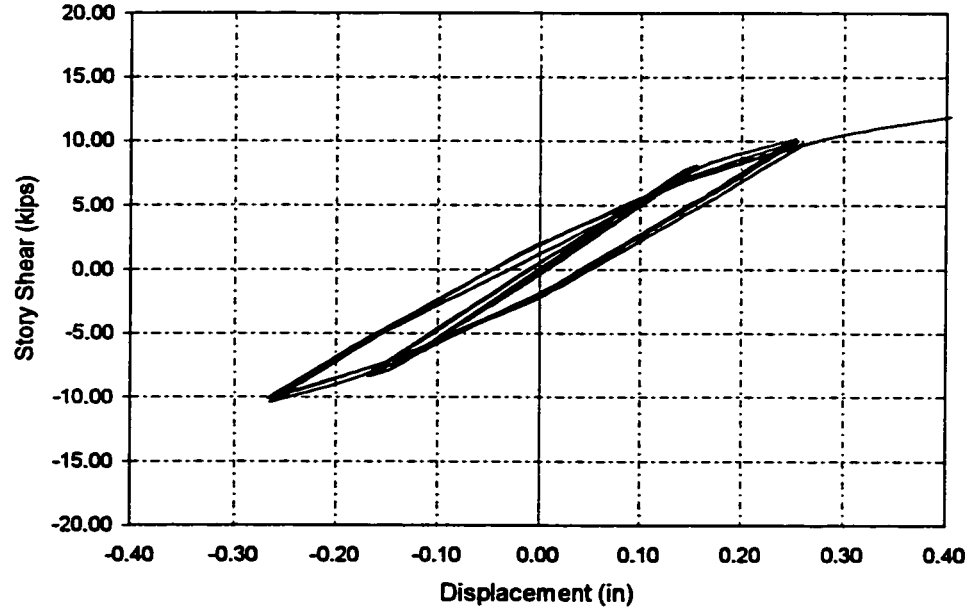

Fig 5.16 Frame Test Simulation Response

The frame characteristics such as original, cracking and post-cracking stiffness, and corresponding strength can be calculated either by the program or by the user. In the simulation, the frame configuration, element dimensions and reinforcement details were input directly. Based on a concrete strength of 4,000 psi and modulus of elasticity of $57000\sqrt{f_c'}$, moment-curvature relationships, as shown in Fig. 7.14, were calculated. The hysteretic parameters [45] were selected as shown in Table 7.4.

Table 7.4 Hysteretic Parameters Used in Frame Test Simulation

Structural Member	Stiffness Degrading	Strength Degrading		Pinching Behavior	ost Tensio Parameter
		Ductile	Energy		
Flexure	5.00	0.10	0.10	0.50	1.00
Shear	2.00	0.10	0.10	0.50	1.00

The computed structural response matched the test response reasonably well as shown in Figure 7.15 and Figure 7.16, which implies that the parameters [45] listed in Table 7.4 are reasonable.

7.5.3 Computed Response of Retrofitted Model Structure

The main features of IDARC-PT are the new model for post tensioned elements and corresponding hysteresis model. Because the wall element in IDARC is modeled as a column-like member instead of a solid element, the structure was represented as shown in Figure 7.17 within IDARC-PT.

The most important variable is the infill wall stiffness. Because the infill wall in the PTPW system is made up of pre-cast panels and connected to the frame with shear lugs, the wall initial stiffness may not be as the same as a monolithic wall element. In addition, the wall stiffness in Test I was different from that of Test II because cracking occurred in Test I. These factors were considered in wall stiffness and strength calculations for the computer model.

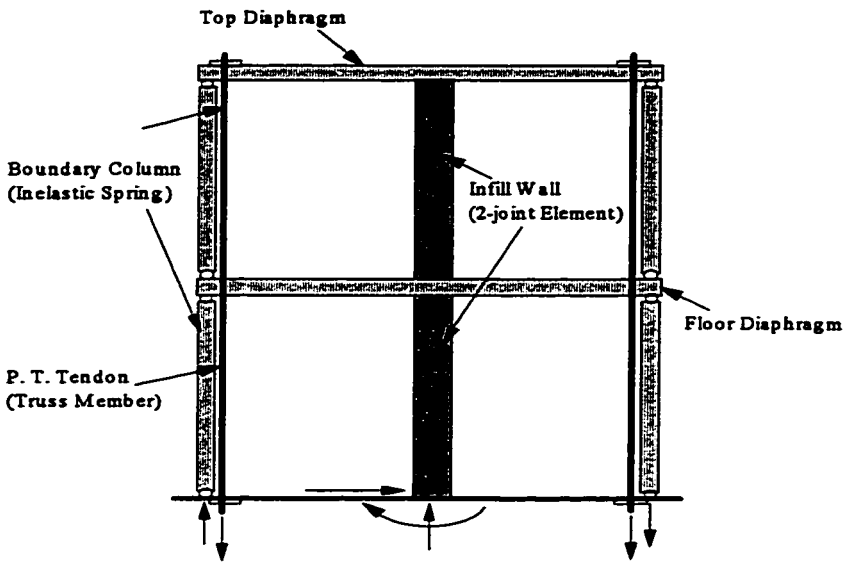

Figure 7.17 Analytic Model Of Retrofitted Frame Test

7.5.3.1 Simulation of Test I (Flexure Model)

For simulating flexural response of the infill wall system, truss members were adopted to model the post-tensioning tendons, inelastic spring elements were used to represent the boundary column elements and the diaphragm was represented by a deep beam element with large stiffness and strength. In modeling the infill wall, the full wall section and one boundary column were considered for determining the wall stiffness and strength.

Load input in the IDARC-PT analysis followed the cyclic test loading history. The recorded actual initial post-tensioning force applied in the test was adopted as the initial force in the inelastic spring elements used to model the post-tensioning tendons. Actual dead load was applied according to the self-weight of the model structure.

Tested concrete and steel properties were used in the simulation. A 4,000 psi

concrete was used for the column element (truss member). Concrete strength of 5,000 psi was used for infill walls. Yield strengths of 70,000 psi and 150,000 psi were used for the reinforcement and post-tensioning tendons, respectively. Stiffness and strength degrading parameters and other hysteresis coefficients are listed in Table 7.5. Tri-linear moment-curvature relationships were used for all elements except the post-tensioned tendons. Figure 7.18 illustrates the column and beam (diaphragm) relationships and Figure 7.19 presents the moment-curvature and shear-shear deformation relationships for the infill wall.

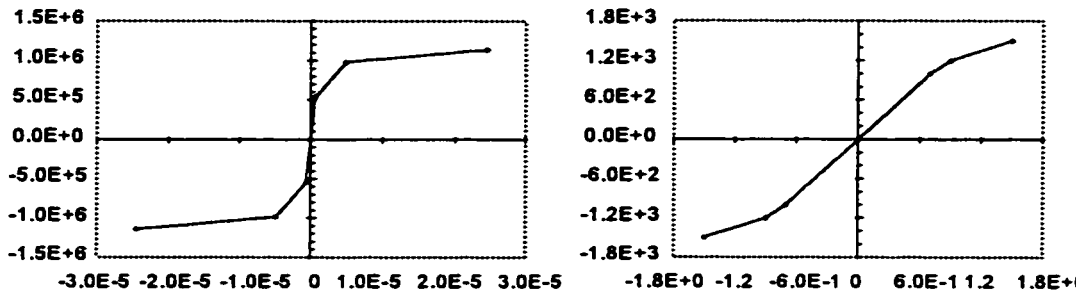

a) Beam Moment-Curvature b) Column Moment-Curvature

Figure 7.18 Moment-Curvature Envelops for Frame Elements

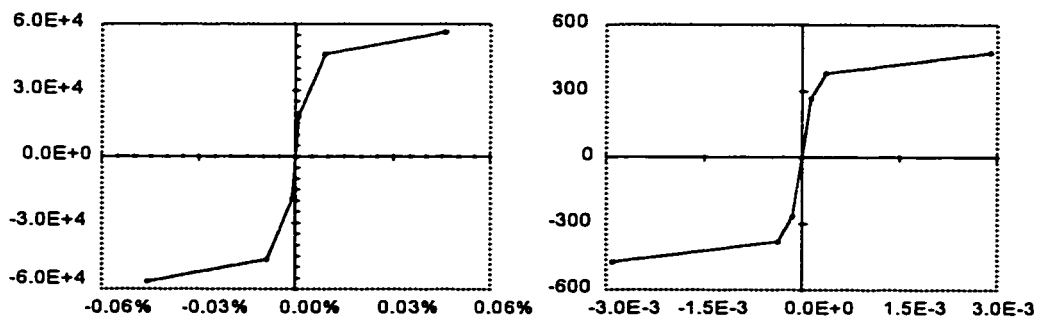

a) Moment-Curvature b) Shear-Angle

Figure 7.19 Infill Wall Force-Deformation Relationships (Test I)

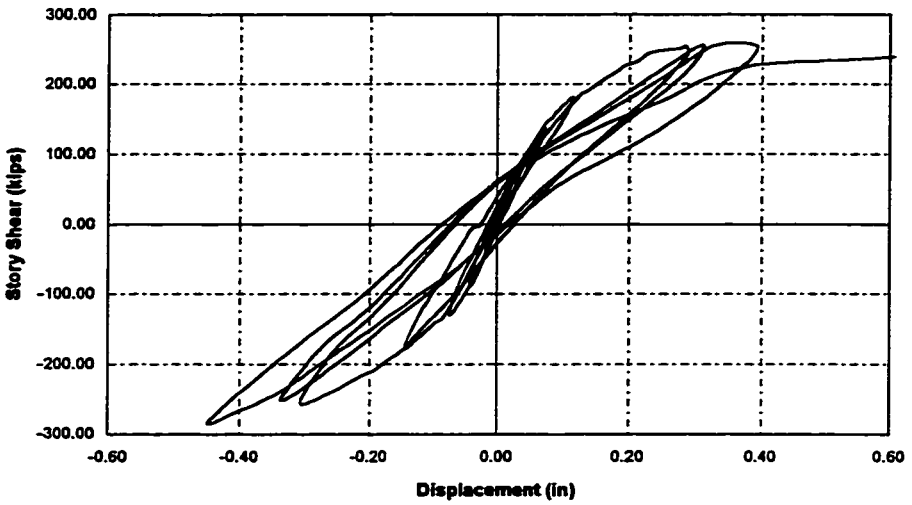

Figure 7.20 Measured Response of Test I

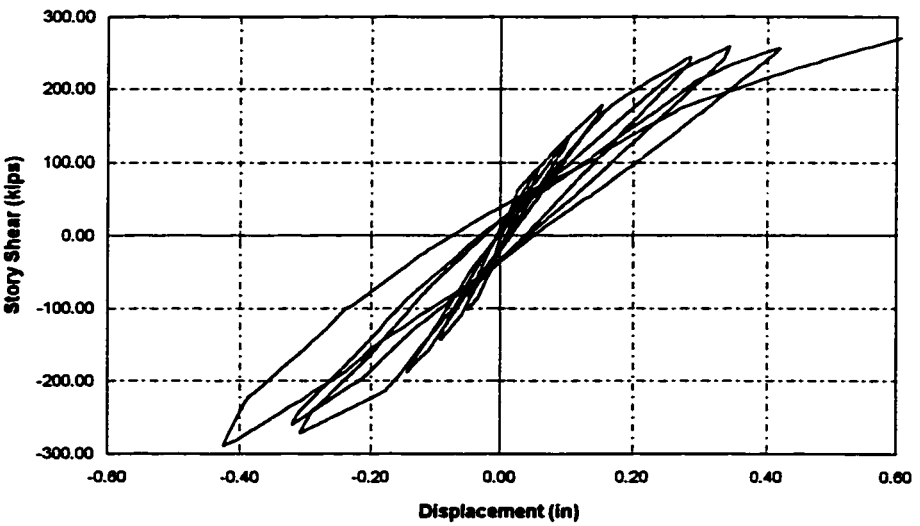

Figure 7.21 Computed Response of Test I

Table 7.5 Hysteretic Parameters for Flexure Test Simulation

Structural Member	Stiffness Degradation	Strength Degradation		Pinching Behavior	Post Tension Parameter
		Ductile	Energy		
Column & Beam	9.00	default	0.00	0.20	1.00
Wall (Shear)	0.25	0.10	0.15	0.15	0.90
Wall (Flexure)	9.00	default	0.05	1.00	0.20

The computed response of Test I is presented in Figure 7.21, and the measured response is shown in Figure 7.20. The computed response matched the test result quite well. However, it must be pointed out that the selections of hysteresis coefficients, especially the post-tensioning coefficient PT, were calibrated to match the test response.

7.5.3.2 Simulation of Test II (Shear Model)

Except for the infill wall element, all other members were modeled as for the flexural test. The infill wall was considered to be a cracked wall element because it was cracked during Test I. Due to cracking, the infill flexural stiffness was greatly reduced but shear capacity was retained.

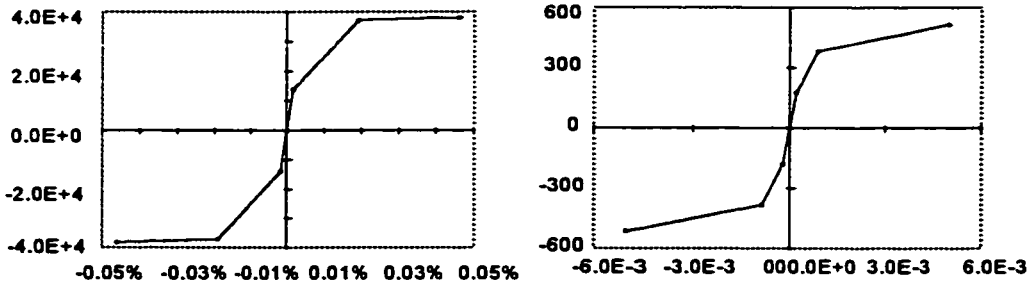

a) Moment-Curvature b) Shear-Angle

Figure 7.22 Infill Wall Force-Deformation Relationship (Test II)

Two-thirds of the infill wall section and one boundary column were taken as the effective portion of the infill wall for stiffness computation. This assumption is

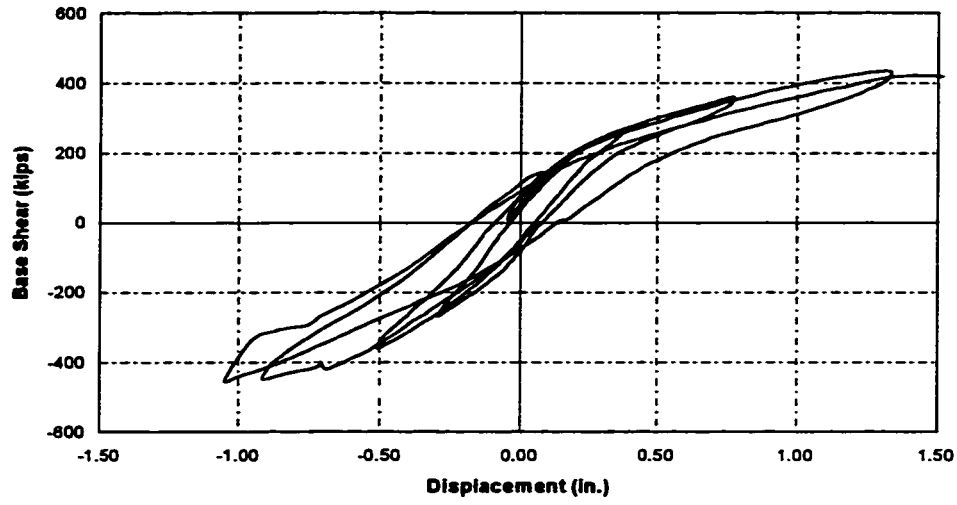

Figure 7.23 Measured Response of Test II (Shear Test)

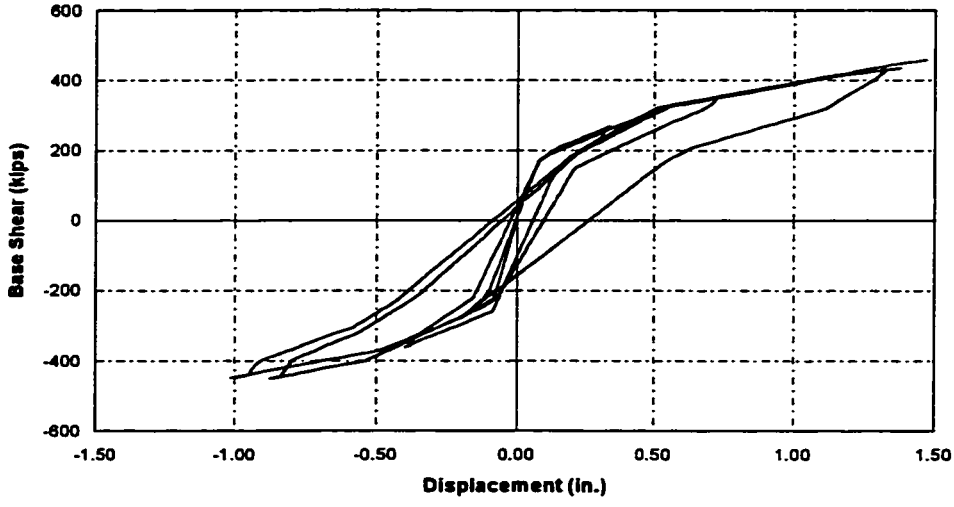

Figure 7.24 Computed Response of Test II

consistent with the effective shear section of a cracked infill wall adopted in the shear friction evaluation discussed in 6.4.2.3. Based on the effective section, the flexure and shear stiffness and strength of the infill wall were calculated for input into the analysis program. Figure 7.22 presents the force-deformation relationship for the infill wall.

Table 7.6 Hysteretic Parameters for Shear Test Simulation

Structural Member	Stiffness Degrading	Strength Degrading		Pinching Behavior	ost Tensio Parameter
		Ductile	Energy		
Column & Beam	9.00	default	default	0.20	1.00
Wall (Shear)	0.25	default	0.05	1.00	0.20
Wall (Flexure)	9.00	default	0.05	1.00	0.20

As for Test I, material strengths and initial post-tensioning force recorded in Test II were input for the computer model. Load input in the IDARC-PT analysis simulated the test loading records. The stiffness and strength-degrading parameters and other hysteresis coefficients are listed in Table 7.6.

The computed response is presented in Figure 7.24 and the measured response in the test is shown in Figure 7.23. The computed response matched the test result quite well. However, it should be noted that the effective wall sections was based on a cracked infill wall. In general, for analysis of PTPW systems, original infill wall section should be used in force-deformation response computation.

7.6 SUMMARY

By means of adding new analytical models including a truss member, inelastic spring and non-linear elastic hysteretic model to the existing non-linear structural analysis program IDARC-2D, program IDARC-PT was developed for analyses of post-tensioned precast infill wall systems. Through structural analysis of the model

structures using program IDARC-PT, the behavior of PTPW systems could be simulated.

For analysis of a PTPW system with IDARC-PT, the key factor is the post-tensioning parameter PT for non-linear elastic hysteretic response. However, because test results were limited, a general relationship for the parameter PT can be established in this project. The parameter PT is a function of the ratio of post-tensioning tendon area to infill wall cross section area, the ratio of initial post-tensioning force to tendon capacity, and the ratio of infill wall width to structure height. If infill walls and post-tensioning are properly applied in a PTPW system, a parameter PT ranging from 0.1 to 0.5 may be selected for the system analysis using IDARC-PT. However, more experimental data and analysis are desired to establish a quantitative relationship for parameter PT.

It is also recommended that a small integration time step be adopted in PTPW system analysis using IDARC-PT. The smaller the step length, the more accurate the computed results. A time step of 0.001 second was used in this study.

IDARC-PT appears to be a valuable tool for PTPW system simulation and analysis. When a PTPW system retrofit design requires time-history analysis as recommended in Chapter VI, IDARC-PT can be used. Designs of the infill wall section, post-tensioned tendons, and initial post-tensioning can be evaluated using program IDARC-PT.

CHAPTER VIII

ANALYTICAL MODEL OF FOUNDATION

8.1 INTRODUCTION

In Chapter VII, the model structure test simulations demonstrated the reliability of computer program IDARC-PT for analyzing a post-tensioned precast infill wall (PTPW) system. Using this program, effects of different variables can be studied by computer analysis instead of laboratory tests, and PTPW system rehabilitation designs can also be evaluated. However, neither the experiments nor the computer simulations, presented in the previous chapters, considered foundation effects. It is desirable to determine how the foundation affects the implementation of a PTPW rehabilitation system. In this Chapter, foundation analytical model is developed. In the following chapter, foundation performance and post-tensioning force and foundation interaction will be studied through the use of computer the program IDARC-PT.

The foundation and soil supporting a structural system will have a given period, stiffness, and bearing capacity. Under earthquake excitation, the response of a structure is affected by the foundation properties[29,51]. The bearing capacity is the principal property routinely considered in foundation design. Structural vibration introduces uneven pressure distribution and differential deformation or settlement of the foundation soil. Severe differential foundation settlement may damage a structure. Figure 8.1 shows an example of such damage. If the foundation is a saturated soil with very low strength, soil liquefaction can occur under a long duration earthquake, and the structure can collapse or overturn due to foundation failure as shown in Figure 8.2. The stiffness of the foundation can also play an important role in structural

response. If the foundation is considered as part of a structural system, a low soil stiffness may soften the whole structural system and can reduce or increase the earthquake load depending on the predominant period of the earthquake. On the other hand, a soft foundation may also result in a long period and increase lateral displacement of the structure. The large displacement could produce large secondary forces and aggravate P-Δ effects and on the structure. The period of the foundation can greatly influence the response of the structure under earthquake excitation. The most severe case is when the basic structural period coincides with the foundation period and resonance results.

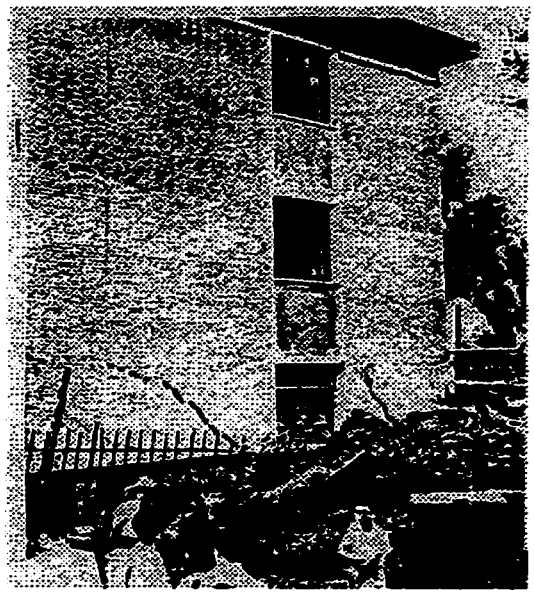

Figure 8.1 Building Damage Due to Differential Foundation Settlement

Figure 8.2 Structural Collapse Due to Soil Liquefaction

In order to avoid these problems, a suitable structural system and reasonable foundation should be selected. The selection of structural systems and foundation types are beyond the scope of this project. In this project, it is supposed that the foundation system will not be strengthened or renovated for the purpose of PTPW system application. In structural rehabilitation, generally speaking, static load bearing capacity of the foundation would not be a problem because only 3 to 5% more weight will be added to the structure for common retrofitting cases. The main concern in this study is the effect of foundations on dynamic response, and possibilities for mitigating or eliminating those effects with a PTPW system.

It is obvious that soil provides only compression strength and not can sustain tension. Except for a pile foundation structure, the uplift force induced by an earthquake can be resisted only by structural dead load and soil weight overlying the foundation. In most reinforced concrete frame structures, tension or uplift effects are seldom considered for foundations, especially if earthquake forces are not a design requirement. Earthquake reports show that foundation pull-out failure is rarely a problem. However, the PTPW rehabilitation system is a new technique for earthquake retrofitting. There are no reported earthquake observations or examples coupling structural system performance with foundation effects for a PTPW system.

With addition of infill walls in several frames and addition of post-tensioning tendons at the corresponding boundary columns, the behavior of the existing frame structural system is changed. A considerable amount of earthquake energy will be absorbed by bays where frames are retrofitted with infill walls and post-tensioning tendons. In other words, the earthquake load will be sustained mainly by the strengthened bays as discussed in Chapter II and Chapter VI. Consequently, foundations or parts of foundation of these frames would be required to support the extra compression and tension loads induced by the earthquake. Particularly, because

the post-tensioning tendons are to be anchored to the foundation, it must be determined if the post-tensioning can work properly without simultaneously strengthening the foundation structure, and, if the foundation can sustain the uplift force created by the post-tensioning tendons and earthquake excitation.

To answer these questions, the best method is to conduct experiments to investigate the foundation performance for PTPW systems. Unfortunately, due to budget and time limitations, such experiments could not be performed as part of this project. In fact, the post-tensioning tendons were anchored to a firm foundation in the model structure. Therefore, the post-tensioning performance coupled with foundation effects could not be evaluated through the model structure test. In order to investigate the foundation effects, a computer simulation was conducted. Applying the modified non-linear structural analysis program IDARC-PT, simulations were performed to analyze example structures with and without foundation involvement. Foundation effects and post-tensioning performance were studied by comparing the simulation results of different foundation models for a diverse set of earthquake ground motions.

Through foundation simulation analysis, post-tensioning-foundation interaction behavior of the PTPW system was evaluated. Different solutions for retrofitting the same frame system were also studied for reducing or eliminating foundation effects. Based on the simulations, general guidelines were proposed for preventing severe foundation problems with application of PTPW rehabilitation systems.

8.2 ANALYTICAL MODEL OF FOUNDATION

The targets of the simulation were foundations or parts of foundations that are coupled with infill walls and post-tensioning tendons. In a PTPW system, post-

tensioning may be ineffective if the foundation is not able to sustain the uplift force at the boundary of the infill wall. Generally, the post-tensioning force is a local internal force and never produces tension in the overall structure and foundations. In effect, the post-tensioning force the foundation is called on to sustain is only the anchorage force from the tendons. However, an external tension force from the structure producing uplift at the foundation base-soil interface may be developed. The anchorage methods for post-tensioning tendons will not be discussed. It is supposed that the tendons are firmly anchored to the foundation with reliable methods according to the structural type and base condition of the foundation.

Based on the above assumption, foundation behavior as a function of soil condition and foundation type was investigated. According to different foundation and soil behavior, foundation capacities were evaluated, analytical models of foundation response were established, and different earthquake excitations were used for foundation performance simulation.

8.2.1 Foundation Types

A type foundation system has to be selected depending on the structural and/or architectural configuration and the foundation soil condition. Generally speaking, five types of foundation systems are commonly used for building structures as well as for reinforced concrete frame structures. They are pile or pier foundation, box foundation, mat or raft foundation, strip foundation, individual footings, or a combination of two or more types of these foundations as shown in Figure 8.3.

Pile and box foundations have advantages in sustaining earthquake forces imported by the PTPW rehabilitation system. The foundation piles with long or intermediate length can withstand a larger uplift force by means of friction. The box foundation, on the other hand, mobilizes a large reaction mass to offset the uplift force

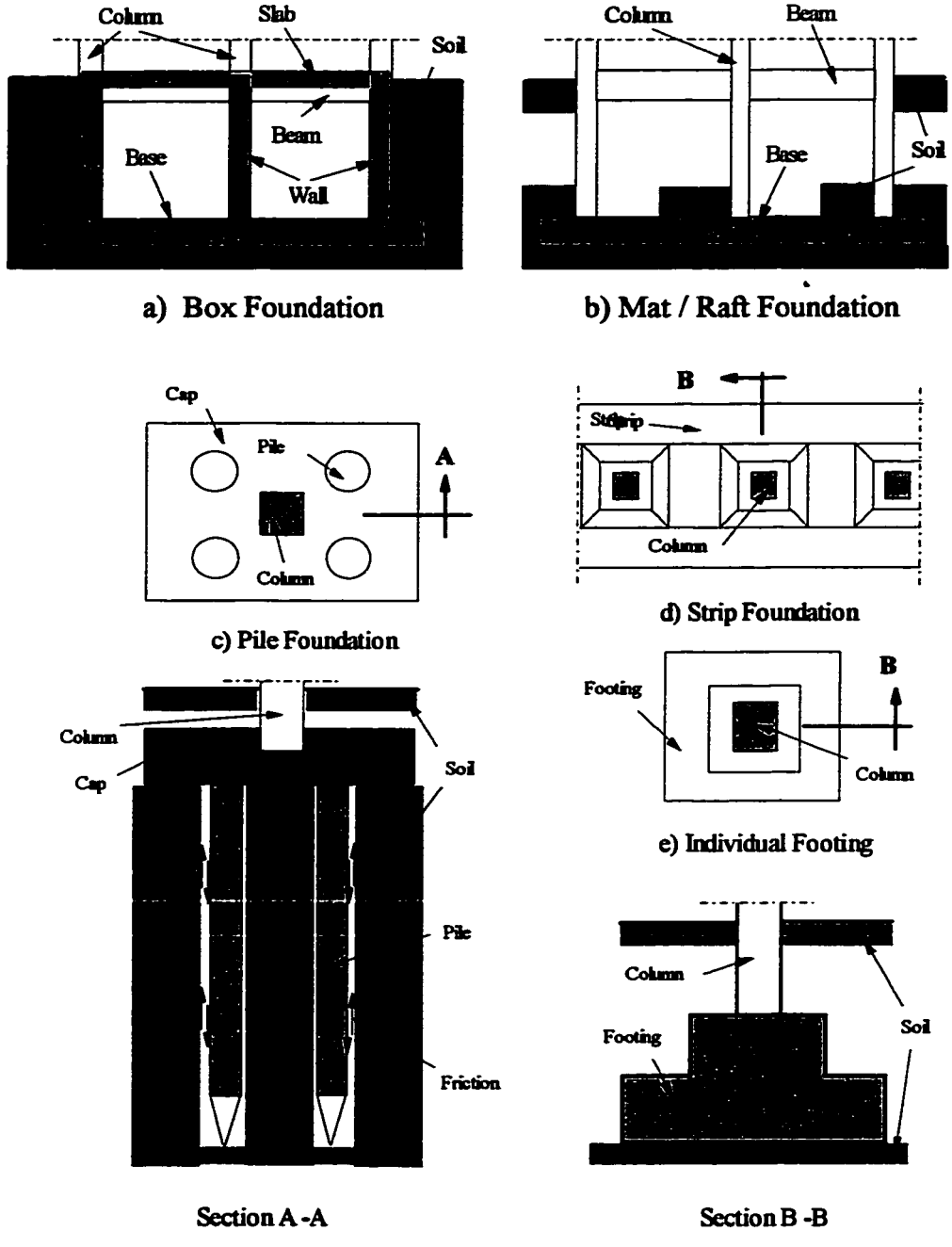

Figure 8.3 Commonly Used Foundation Types

induced by an earthquake. It is intended to work as a monolithic unit to prevent local failure induced by the individual frames that are retrofitted with infills and post-

tensioning tendons. As a result, these two foundation types are not targets in this study. The mat foundation has characteristics similar to a box foundation despite having a relatively lower structural stiffness. Strip or individual footings do not have the advantages of the former three types. For any individual frames retrofitted with the PTPW system built on a strip foundation, the overlying soil weight is much less than a box foundation because of its small plan area. Also, it could not work as a monolithic structural block because of its low stiffness. The situation is much worse for an individual footing foundation. The weight that could be counted on to offset uplift effects due to an earthquake is the frame dead load and soil weight overlying the footing. An individual footing works independently without significant interaction from neighboring footings. So, the individual footing foundation represents the worst foundation type for the PTPW system.

Unfortunately, most foundations for reinforced concrete frame structures are the latter two types. Particularly, individual footings are commonly used for non-ductile reinforced concrete frame structures that have less than five stories. So, our studies of foundation effects on PTPW system response and foundation-post-tensioning interaction focused on the structures with individual footing foundations.

8.2.2 Uplift Resistance Capacity

The foundation and soil resist compressive forces transmitted from the superstructure. However, tension or uplift capacity may be required for foundations when using a PTPW system to retrofit frame structures. In PTPW systems, the principal function of the post-tensioning tendons is to restore the tension capacity in boundary columns and to provide moment capacity for the infilled frames to sustain earthquake loads. The earthquake load induces tension force in the post-tensioned boundary columns and eventually to the supporting foundations or footings as shown

in Figure 8.4. This tension force, which is termed an "uplift force" in this report, may damage or even pull the foundation out from the soil. It may benefit the structural lateral strength if the foundation provides uplift resistance which combines with the structural dead loads to resist the uplift force induced by earthquake excitation.

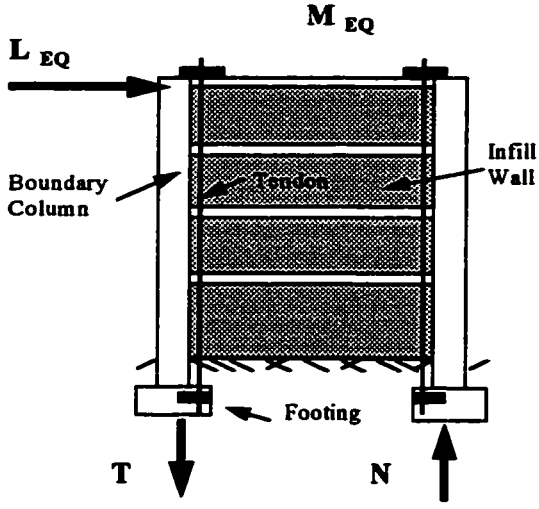

Figure 8.4 Tensile Force On Footing

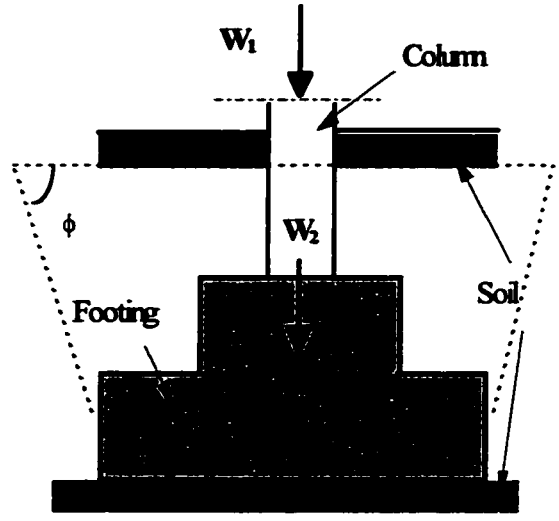

Figure 8.5 Dead Loads On Footing

8.2.2.1 Static Loads On Footing

Without foundation retrofitting, as mentioned, external static loads acting on the foundation are the main forces resisting the uplift force. For an individual footing of a frame boundary column under post-tensioning, two kinds of static loads are developed to resist the uplift force as shown in Figure 8.5. First, the dead load W_1 represents the weight of the superstructure transferred to the footing. Secondly, the dead load W_2 represents the total weight of the foundation system and weight of soil overlying the footing from ground level to the effective footing depth as shown in Figure 8.5 within the dashed lines corresponding to an angle ϕ ranging from 45° to 90°.

For the uplift force to pull the foundation out from the soil, it must overcome the vertical static loads. In structural analysis, the static load W_1 is often considered to be the dead load of the superstructure. Dead load W_2 can be taken into account to evaluate the uplift resistance capacity of the foundation. In this project, the foundation's **"initial capacity"** for uplift resistance is denoted as F_0 and equals W_2. In addition to loads W_1 and W_2, other factors to be considered in evaluating the foundation capacity to resist uplift include soil shear or friction capacity along the soil rupture surface and the adjacent foundation assistance or interaction through deformation compatibility of the superstructure.

8.2.2.2 Shear Capacity Of Soil

If the uplift force generated by an earthquake is sufficient large and the column tensile strength is sufficient, the footing may be pulled out from the soil base. During the failure process, soil rupture will occur along a inclined surface as shown in Figure 8.6. Shear or friction stresses will be developed along the rupture surface to resist soil movement.

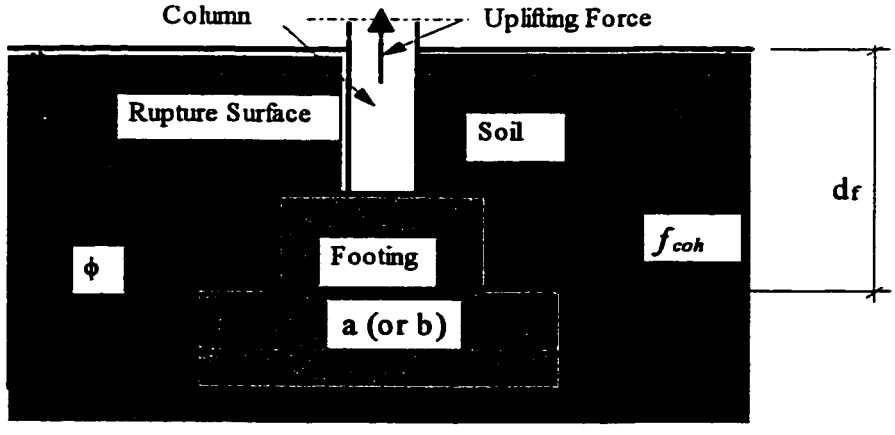

Figure 8.6 Shear Force on The Soil Rupture Surface

Soil cohesive strength f_{coh} representing shear or friction strength was used to evaluate the soil rupture capacity. The cohesion stress on the soil rupture surface is defined as the nominal shear strength of the soil. The uplift resistance due to soil rupture is evaluated as a function of nominal soil shear strength, rupture angle ϕ and depth d_f for an individual footing. The rupture angle ϕ may lie in the range of 45° to 90° depending on the type of soil. According to soil nominal shear strength, rupture angle, and footing depth, a vertical component of force can be calculated over the rupture surface for an individual footing. This vertical force is defined as the soil **rupture capacity** for resisting uplift force and is given by:

$$F_R = A_R f_{coh} \sin \phi \qquad (8\text{-}1)$$

where $A_R = 2d_f(a + b + 2d_f \cot \phi)$

---- total rupture surface area

f_{coh} ---- soil cohesive strength

$a,\ b$ ---- edge lengths of the footing plane, and

d_f ---- the effective depth of the footing.

To develop soil rupture along the surface, as shown in Figure 8.6, the uplift force must be greater than the footing initial capacity F_0 defined earlier and the soil rupture capacity F_R, thus,

$$F_t = F_0 + F_R \qquad (8\text{-}2)$$

The force F_t is defined as the footing's nominal **individual uplift strength** to resist uplift force. In the following section, this nominal uplift strength will be used to establish the mechanical model for footing simulation.

8.2.2.3 Neighboring Footing Assistance

The assistance provided by neighboring footings is dependent on the flexural stiffness of the linking members/beams of the superstructure and the difference in uplift forces on footings between retrofitted and non-retrofitted neighboring frames. The mechanism of neighboring footing interaction is illustrated in Figure 8.7. It shows the columns of an orthogonal edge frame viewed from one end of the retrofitted frame. Column C_3 is the post-tensioned boundary column of the retrofitted frame and the rest are the boundary columns of non-retrofitted neighboring frames. Because most of the earthquake load is resisted by the frame retrofitted with an infill wall and post-tensioning, the uplift force on the footing of that boundary column is much higher than that on the non-retrofitted frame footings. It is assumed that the footings in every frame are the same size, have the same ultimate uplift capacity, and the column tensile capacity is greater than the footing's individual uplift strength. Its ultimate capacity can be evaluated with consideration of neighboring footing assistance.

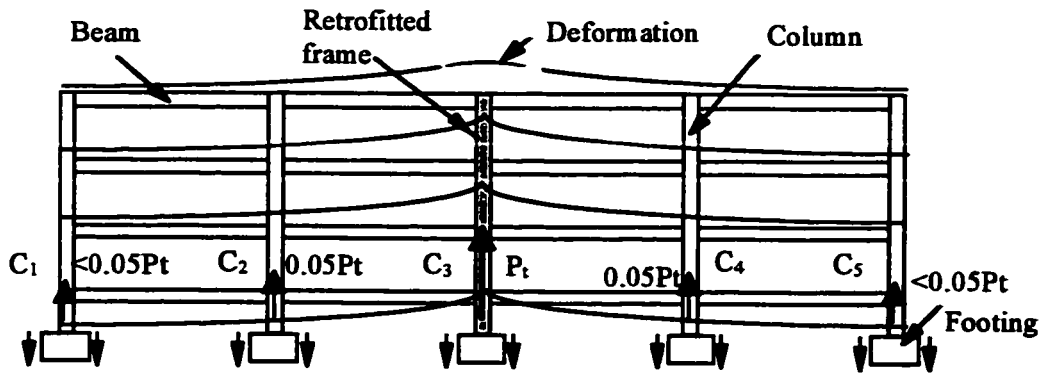

Figure 8.7 Interaction of Neighboring Footings

As shown in Figure 8.7, supposing an uplift force P_t acts on the post-tensioned column C_3. For simplification, a smaller tension force which is taken as $0.05P_t$ acts on the columns next to the retrofitted frame, and a force less than $0.05P_t$ acts on the other columns. When the large tension force P_t of the post-tensioned column appears

to pull its footing from the base soil, the small tension on the other columns does not result in uplift. The link-beams will resist the uplift and transfer force to neighboring footings. Thus, some of the large tension from the retrofitted frame footing is distributed to other footings and is a function of the linking element properties.

Under these conditions, two extreme cases may occur when the retrofitted frame footing uplifts. The first is that the overall stiffness and strength of the structure are capable of making all footings work as a unit, and the uplift force is high enough to cause uplift of all the footings in the orthogonal frame. Such response is unlikely because earthquake reconnaissance has not produced such observations. The second case is that the members linking retrofitted and non-retrofitted frames reach ultimate capacity and the retrofitted frame footings are pulled out from the foundation base independently. Such response is also unlikely because these linking members maintain a certain strength and stiffness after reaching ultimate capacity. Response is likely to lie somewhere between the two extreme cases.

After reaching nominal individual uplift strength and before failure of the linking members, the footing beneath the post-tensioned column acquires additional uplift capacity from neighboring footings which is denoted as F_a. The footing's **ultimate uplift strength** can be expressed as,

$$F_u = F_t + F_a = F_0 + F_R + F_a \qquad (8\text{-}4)$$

Corresponding to the trilinear hysteretic response model used in IDARC-PT, the uplift capacity of the foundation may also be exhibit trilinear behavior. To represent the footing behavior based on a trilinear response envelop, initial strength, individual uplift strength and ultimate strength have been derived for an individual footing:

1) **Initial uplift strength F_0** (dead load W_2) corresponds to the cracking strength of the IDARC-PT input;

2) **Individual uplift strength F_t** (F_0 plus soil rupture strength F_R) corresponds to the yield strength of IDARC-PT input;

3) **Ultimate uplift strength F_u** (F_t plus neighboring footing assistance F_a) corresponds to post-yielding strength of IDARC-PT input.

8.2.3 Stiffness And Mechanical Model

Considering a footing as an inelastic spring element possessing different capacities in tension and compression, a mechanical model of the footing can be represented by an envelop as shown in Figure 8.8. The compression strength and stiffness of the footing are evaluated based on soil properties. The tensile strength properties are evaluated as the initial, individual and ultimate uplift resistance capacity as discussed earlier. The footing stiffness will be described in the following.

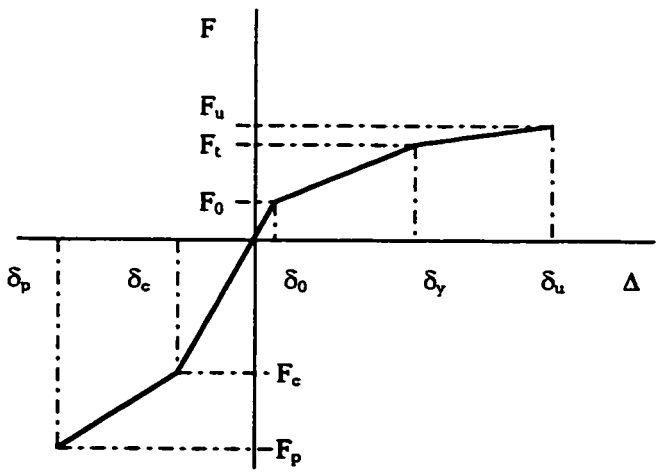

Figure 8.8 Response Envelop for Footing

8.2.3.1 Compression Capacity

The compression capacity of soil is dependent on soil density, ratio of voids, and water content[27, 44]. The modulus of elasticity of a soil stratum is also related to its properties. For a soil stratum *i*, the modulus of elasticity E_i is determined from soil mechanics[27,44]. An allowable compressive strength σ_c is also determined according to properties of multiple soil strata. Based on the allowable compressive strength σ_c, the compression loading capacity F_c of the foundation base is determined as,

$$F_c = A_c \sigma_c = a\, b\, \sigma_c \tag{8-5}$$

where A_c ---- compression area of the footing.

Under load F_c, the level of stress acting on different soil layers reduces as the depth increases as shown in Figure 8.9. Supposing the average stress in stratum *i* is $\sigma_i = \alpha_i \sigma_c$, where $\alpha_i \leq 1.0$, the accumulated footing settlement will be,

$$\delta_c = \sum \frac{\sigma_c\, \alpha_i\, h_i}{E_i} \tag{8-6}$$

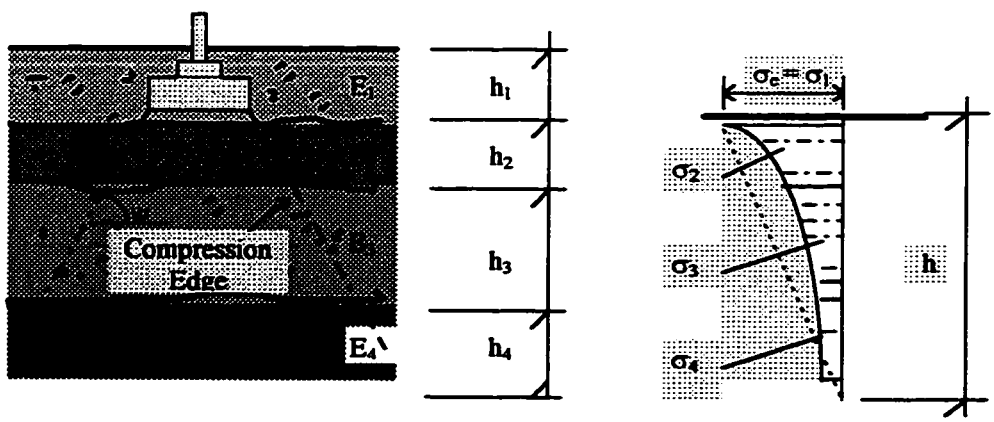

a) Soil Strata and Modulus b) Stress Distribution

Figure 8.9 Modulus and Stress on Soil Strata

The effective soil depth is evaluated according to the stress spreading angle ψ. The angel ψ may be assumed in a range of 45 to 90 degrees, and the effective depth ***h*** may be evaluated to the depth where compression stress is reduced to 5% or less of the maximum stress σ_c. Once the effective depth ***h*** is estimated, a comprehensive modulus E_c can be evaluated as,

$$E_c = \frac{\sigma_c}{\delta_c} = \frac{1}{\sum \frac{\alpha_i \, h_i}{E_i}} \tag{8-7}$$

Meanwhile, the accumulated footing settlement δ_c can also be calculated using this equation. The footing bearing capacity F_c and displacement (settlement) δ_c are defined as the **basic compressive strength** and **basic compressive displacement** of the inelastic spring representing the footing as shown in Figure 8.8.

For convenience, the estimation of the modulus may be simplified. Based on the modulus E_i of each soil stratum under a footing, the comprehensive modulus E_c can be replaced by a weighted average modulus value for multiple soil strata using,

$$E'_c = \frac{\sum h_i \, E_i}{\sum h_i} \tag{8-8}$$

The stress may be considered as a linear distribution as shown in Figure 8.9b. This simplification would not significantly affect foundation simulation because the compression capacity of soil is often sufficient and the soil remains in the elastic range. According to the above simplification, the inelastic spring basic compressive displacement will be,

$$\delta_c = \frac{\sigma_c \, h}{2 \, E'_c} \tag{8-9}$$

The ultimate compression capacity F_p of the footing spring is evaluated as the ultimate compression strength of the column or the compression strength of the footing whichever is smaller. The ultimate displacement of the spring δ_p can be evaluated based on the property of the soil within the effective depth h.

8.2.3.2 Tension Capacity

In order to establish a tension-deformation relationship for a footing spring, three levels of uplift resistance were derived as presented in 8.2.2. The footing spring tension-deformation curve should be compatible with the input schemes of program IDARC-PT. Simulation of foundation performance and foundation-post-tensioning interaction requires input of footing spring properties using a trilinear response envelope curve. The footing spring uplift (tensile) stiffness corresponding to the three strength levels needs to be derived.

Initial Uplift Strength Initial strength F_0 was defined as the static dead load W_2 or the overlying soil weight on the footing. Generally speaking, the initial stiffness in tension is different from the original stiffness in compression. Nevertheless, in order to simplify analysis and to comply with the hysteresis model in IDARC-PT, the footing spring initial tensile or uplift stiffness was taken to be the same as the original compression stiffness. This simplification is practical because the value F_0 is often so small that it should not affect foundation simulation significantly.

Corresponding to the footing initial uplift strength, the initial displacement δ_0 can be calculated using equation (8-6) or (8-9) when δ_c is replaced by δ_0. The initial stress σ_0 is calculated by the equation,

$$\sigma_0 = \frac{F_0}{A_c} \tag{8-10}$$

where A_C ..... the compression area of the footing

and the initial displacement is,

$$\delta_0 = \sum \frac{\sigma_0 \alpha_i \, h_i}{E_i} \tag{8-11}$$

or,
$$\delta_0 = \frac{\sigma_0 \, h}{2 \, E'_c} \tag{8-12}$$

Individual Uplift Strength The nominal individual uplift strength was derived from the soil shear capacity of the rupture surface and the nominal individual uplift stiffness should also be the shear stiffness of the rupture surface. The stiffness can be simply expressed as:

$$S_t = G A_R \tag{8-13}$$

where $G = \frac{E}{2(1-\mu)}$ --- the shear modulus of soil

A_R --- the total area of rupture surface defined earlier

For a specific type of soil, the shear modulus is determined according to soil mechanics[27,44]. To evaluate the soil shear stiffness, the shear modulus is derived from its Young's modulus of elasticity E_i and Poisson's ratio μ (ranging from 0.35 to 0.45). Young's modulus E_i of a soil stratum is determined according to the soil properties or standard penetration procedures as discussed earlier, and the comprehensive modulus E_c can be represented by either E_c or E'_c from equation (8-7) or (8-8), respectively.

Supposing soil cohesion stress is uniformly distributed, then ,the vertical component of relative deformation or displacement along the rupture surface is the displacement corresponding to the footing's individual uplift strength F_R and,

$$\delta_R = \frac{f_{coh}}{G} d_t \sin\phi \qquad (8\text{-}14)$$

Therefore, the footing's individual displacement (corresponding to individual uplift strength) is,

$$\delta_t = \delta_0 + \delta_R \qquad (8\text{-}15)$$

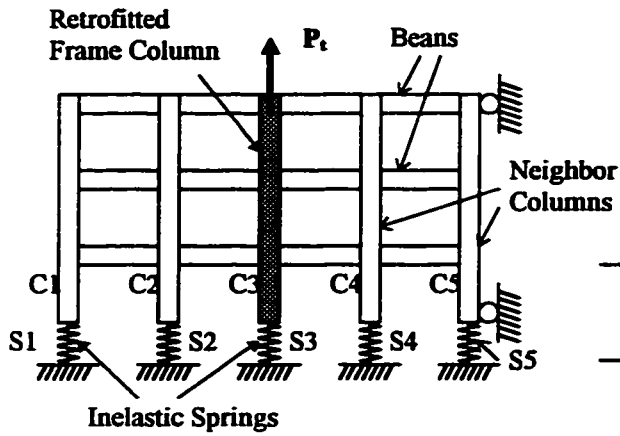

Figure 8.10 Edge Frame Model

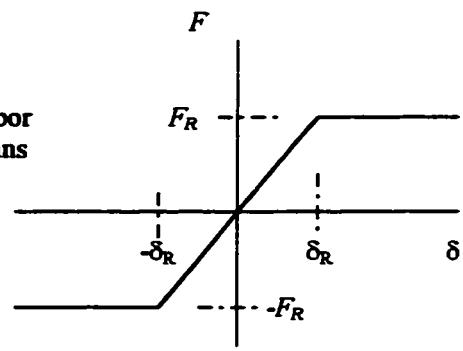

Figure 8.11 Spring Property

Ultimate Uplift Strength The footing's ultimate uplift capacity can be determined by analyzing the edge frame under a tension force at the retrofitted frame as shown in Figure 8.10. The individual footings are represented by inelastic springs for which the tension-deformation relationship behaves in an elastic-perfectly plastic manner, as shown in Figure 8.11. The link-beams and columns, which are flexure members, are also modeled with elastic-perfectly-plastic behavior. The value of load $\mathbf{P_t}$ that induces failure of link-beams is recognized as the ultimate capacity for the retrofitted column footing.

According to the edge frame model, the footing ultimate uplift strength can be determined either by manual calculation or computer program analysis. With

monotonic lateral load analysis, IDARC-PT provides a convenient way to evaluate the footing's ultimate uplift capacity. Converting the structure in Figure 8.10 to a lateral loading system shown in Figure 8.12 for using IDARC-PT, a load-displacement curve can be obtained by analyzing the structure under monotonic lateral load P_t.

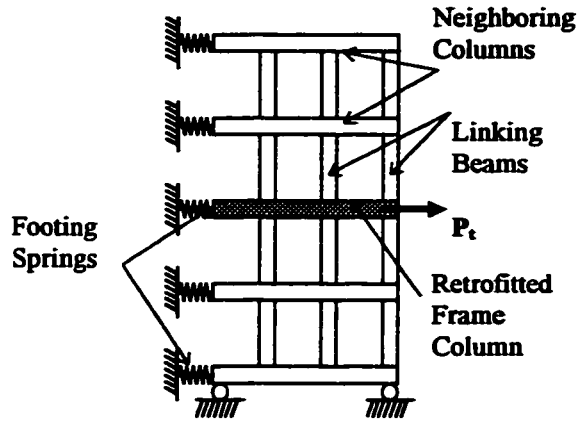

Figure 8.12 Monotonic Loading Model

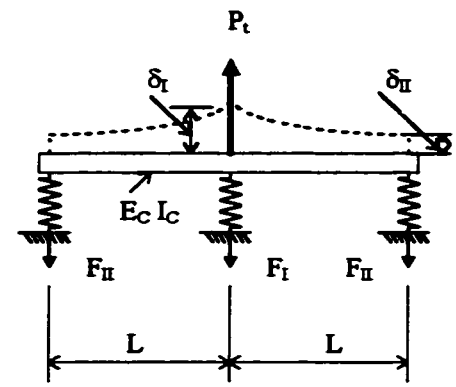

Figure 8.13 Simple Footing Model

To simplify analysis for hand calculations, a footing interaction system with three footings as shown in Figure 8.13 is considered to substitute for the edge frame in Figure 8.10. In the simplified model, columns were eliminated and three-story beams were represented by one beam which has a flexural stiffness $E_b I_b$ equivalent to the stiffness summation of beams over upper stories. By increasing load P_t, the middle spring representing the footing where the frame was retrofitted will be elongated. When its elongation reaches $\delta_I = \delta_R$, the spring force will be $F_I = F_R$ and load $P_t = P_R$. The force in adjacent springs representing the footings where frames were not retrofitted will be,

$$F_{II} = \frac{1}{2}(P_R - F_R) \tag{8-16}$$

From equation (8-1), the stress over the rupture surface of adjacent footings is,

$$\sigma_{II} = \frac{F_{II}}{A_R \sin\phi} \tag{8-17}$$

From equations (8-14) and (8-17), the displacement δ_{II} is,

$$\delta_{II} = \frac{F_{II}}{GA_R} d_t \tag{8-18}$$

On the other hand, considering displacement compatibility, the differential displacement between the middle and adjacent springs should be,

$$\delta_d = \delta_I - \delta_{II} = \frac{F_{II}\ L^3}{3E_b\ I_b} \tag{8-19}$$

Substituting equation (8-18) into (8-19) and rearranging the variables, yields,

$$F_{II} = \frac{\eta}{\xi}\delta_I \tag{8-20a}$$

where $\eta = 3E_b I_b GA_R$

$$\xi = GA_R L^3 + 3E_b I_b d_t$$

F_{II} represents extra uplift capacity provided by interaction of one neighboring footing. Considering interaction of two adjacent footings, the neighboring footing assistance F_a is,

$$F_a = 2F_{II} \tag{8-21a}$$

If considering interaction of four neighboring footings, then,

$$F_a = 2F_{II} + 2F_{III} \tag{8-21b}$$

In equation (8-21b), F_{III} represents the assisting capacity from footings S_1 and S_5 shown in Figure 8.10. Approximately, F_{III} can also be determined using equation (8-20a) when with δ_{II} is substituted for δ_I and,

$$F_{III} = \frac{\eta}{\xi}\delta_{II} \qquad (8\text{-}20b)$$

It is noted from equation (8-20a) that the neighboring footing assistance F_a is a function of soil properties, footing dimension and link-beam stiffness. For any specific frame structure with given footings, the value of F_{II} is determined corresponding to the value of δ_I. When calculating F_a, δ_I should be taken greater than δ_R and less than the value that induces link-beam flexural yielding. It is reasonable to consider link-beam yielding as the upper limit that δ_I will reach. The link-beam yield moment M_y^b is equal to $F_{II}L$. Substituting $M_y^b = F_{II}L$ into equations (8-18) and (8-19) and then combining, results in,

$$\delta_I = \delta'_u = \left(\frac{L^2}{3E_c I_c} + \frac{d_t}{GA_R L} \right) M_y^b \qquad (8\text{-}22)$$

Once the upper limit of $\delta_I = \delta'_u$ is determined, the upper limit of F_{II} is obtained following equation (8-20a), δ_{II} is determined following equation (8-18) and F_{III} can also be determined following equation (8-20b). Eventually, the total neighboring footing assistance is determined using equation (8-21b). The footing ultimate uplift resistance is,

$$F_u = P_t + F_0 = F_R + F_a + F_0 = F_0 + F_R + 2F_{II} + 2F_{III} \qquad (8\text{-}23)$$

Corresponding to F_u, the ultimate displacement δ_u can also be determined,

$$\delta_u = \delta_0 + \delta'_u \qquad (8\text{-}24)$$

As an example, supposing a footing built on an intermediate soft soil is a reinforced concrete element with a plan dimension of 4.5-foot x 4.5-foot and underlies at a depth of

3.5 feet. It is assumed that the soil cohesive strength is 3.12 psi, the soil shear modulus is 896 psi, and the soil rupture angle is 60 degrees. It is also assumed that a three story edge frame has link-beams with a cross section of 12 in. x 22 in. and length of 20 feet; the retrofitted column has a 12 in. x 12 in. section with the same concrete strength as the link-beams. The concrete strength is 4,000 psi and two #7 grade 60 reinforcing bars are used in the columns and link-beams. Uplift force levels for the footing can be calculated following the equations derived earlier. Table 8.1 shows the calculation results for uplift resistance of the footing, while Figure 8.14 illustrates the load-deformation curve for the footing spring.

Table 8.1 Uplift Resistance Capacity of Footing

Items	Vertical Forces On Footings					Displacements Of Footings				
	F_0 (k)	Fr (k)	F_{II}^r (k)	F_{III}^r (k)	F (k)	δ_0 (in)	δ_I (in)	δ_{II}^r (in)	δ_{III}^r (in)	δ (in)
Individual	24.5	41.016	2.938	0.211	71.782	0.0162	0.12665	0.0091	0.0007	0.1428
Ultimate	24.5	41.016	27.985	2.005	125.463	0.0162	1.20621	0.0864	0.0062	1.2224
Property	M_y^0= 1343.3 k-in				$E_b I_b$= 1.15E+08 k-in^2			A_R= 15180 in^2		

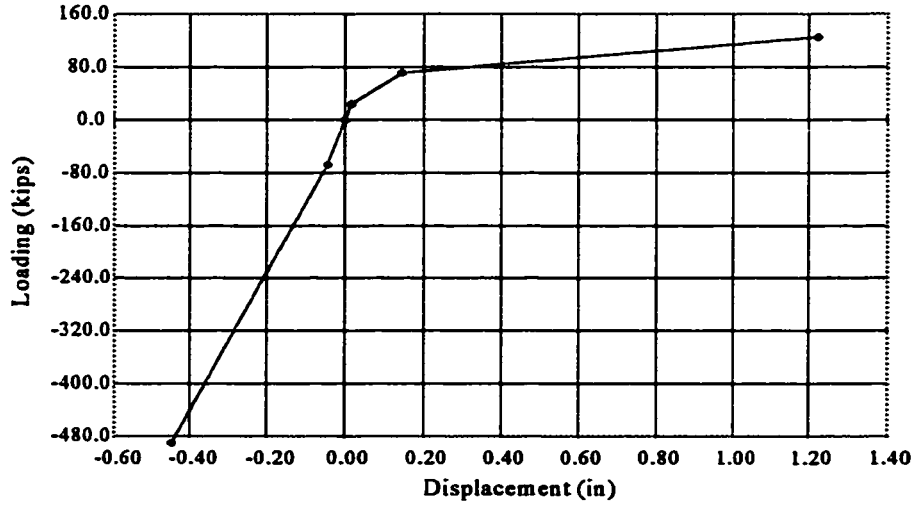

Figure 8.14 Example of Footing Spring Deformation Curve

According to earlier analysis, it can be seen that the neighboring footing interaction is mainly dependent on the ratio of shear stiffness of the soil rupture surface

to the flexural stiffness of link-beams. The higher the link-beam stiffness in the edge frame, the greater the contribution from neighboring footings. However, using the simple footing model shown in Figure 8.13 may underestimate the footing interaction because simplifications were made in the analysis. Though it is conservative to use the simplified model, monotonic loading analysis using IDARC-PT is recommended for practical footing simulation and PTPW system retrofitting design.

When conducting IDARC-PT analysis to determine the footing spring deformation curve, the displacement input method should be used[45]. Applying the displacement δ_3 conforming to spring S_3 in the edge frame shown in Figure 8.10, the converted model shown in Figure 8.12 will be analyzed for a monotonic load input. The maximum value of δ_3 is limited to such a level that flexural yielding is reached in the link-beams connected to column C_3. A footing spring deformation curve can be obtained from separate IDARC-PT analysis for the structure shown in Figure 8.12. It should be remembered that initial strength F_0 and δ_0 must be considered adding respectively to the maximum strength P_t and δ_1 obtained from IDARC-PT analysis.

8.2.4 Structural Model of Foundation

In the simulation, the column-foundation or footing joint was recognized as a structural joint. Like other structural joints, the foundation joint should generally be modeled with three degrees of freedom. Foundation involvement is represented by inelastic spring elements as shown in Figure 8.15.

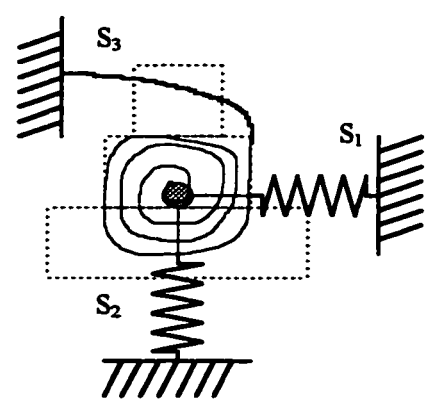

Figure 8.15 Footing Joint

Spring S_1 represents the horizontal property of the foundation soil; spring S_2 represents the vertical property; and spring S_3 represents the rotation property of the foundation.

To simplify the foundation model, some assumptions were made based on experience. Because foundation rotation capacity of an individual footing is very low in comparison with overall structural rotation capacity, the rotation spring was eliminated from the foundation model. A horizontal failure is not likely in a foundation under earthquake excitation; the axial spring representing foundation horizontal capacity can be modeled as working in the elastic range in both compression and tension. With these simplifications, the spring representing foundation vertical compression and tension capacities is left as the only one to consider.

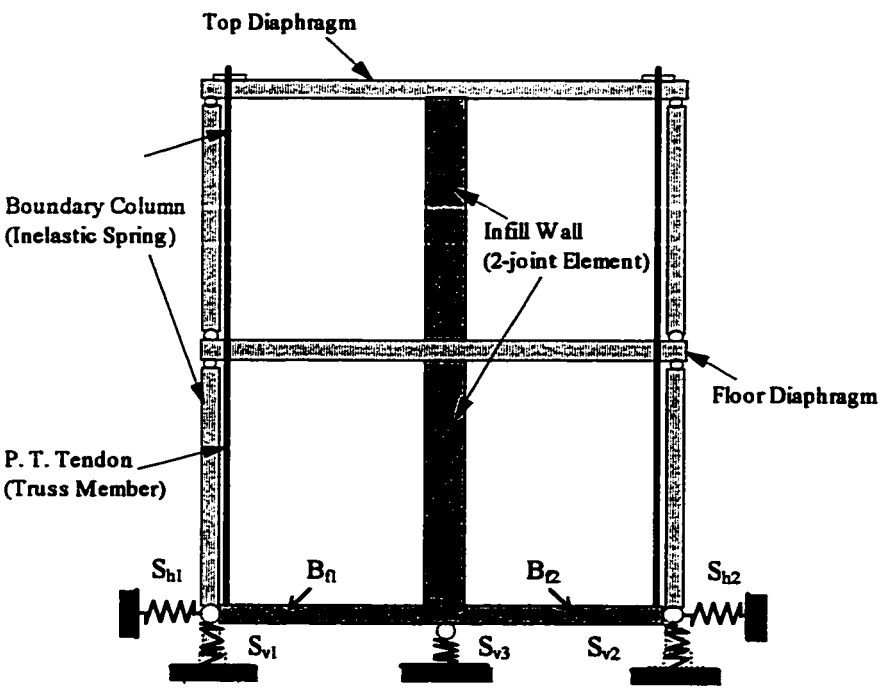

Figure 8.16 Structural Model of Footings With Frame

8.3 SUMMARY

Uplift resistance capacity of individual-footing foundations was studied by analyzing rupture behavior of soil around the footing. Based on the structural and foundation soil behavior, envelope curve for the footing spring was determined and a structural model was established as shown in Figure 8.16. Applying this model with a foundation-infill connection model to a PTPW system, foundation performance simulations were conducted and will be discussed in the next chapter.

CHAPTER IX

FOUNDATION SIMULATION

9.1 INTRODUCTION

The structural modeling for a PTPW system has been described and structural test simulation with program IDARC-PT was presented in Chapter VII. Applying the foundation analytical model developed in Chapter VIII to the structural system used in Chapter VII, a PTPW system coupled with a foundation model was established as shown in Figure 8.16. Analyzing this structural system, structural earthquake response or foundation simulation was conducted and foundation performance was evaluated under different conditions. The variables that could influence foundation performance and structural response were included in foundation simulations. Table 9.1 presents the simulated structural systems possessing different foundation soil properties, earthquake ground motions, levels of initial post-tensioning, and retrofitting plans.

Adopting a superstructure identical to the structural system used in Chapter VIII (or the model structure in Chapter V), five basic structural systems were modeled with different foundation soil properties and classified as Systems **0, A, B, C** and **D**. System **0** is the structure used in the flexure test simulation in Chapter VII to represent a structure setting on a rigid foundation. A rigid foundation in this study means that the foundation does not deform and the superstructure is connected to the foundation with fixed joints. Systems **A** through **D** are structures supported with foundations modeled as shown in Figure 8.16. The first symbol α in the system notation Sys-$\alpha\beta\gamma\eta$, denotes a soil type where "A" represents a foundation of stiff or firm soil, "B" represents a soft soil, "C" represents a very soft soil and "D" represents an extremely (extra) soft soil.

Table 9.1 Foundation Simulation Variables For Different Systems

System	Earthquake Ground Motion					Initial Post - Tensioning				Retrofitting Plan		Foundation
	TAFT (T)	Mexico -2D (2)		Mexico -9S (9)		High	No	Zero	Low	Infill Number		Soil
ID	0.33g	0.33g	0.22g	0.33g	0.22g	250 (k)	Tendon	Tension	110 (k)	Two	Three	Properties
Sys-0TGF	X					X				X		Rigid (0)
Sys-ATGF	X					X				X		Firm (A)
Sys-BTGF	X					X				X		
Sys-BTNF	X						X			X		
Sys-BTZF	X							X		X		
Sys-BTLF	X								X	X		Soft (B)
Sys-B2GF		X				X				X		
Sys-B2SF			X			X				X		
Sys-B9GF				X		X				X		
Sys-B9SF					X	X				X		
Sys-CTGF	X					X				X		
Sys-C2GF		X				X				X		Very
Sys-C2SF			X			X				X		Soft
Sys-C9GF				X		X				X		(C)
Sys-C9SF					X	X				X		
Sys-DTGF	X					X				X		
Sys-D2GF		X				X				X		
Sys-D2SF			X			X				X		Extra
Sys-D2SM			X			X					X	Soft
Sys-D9GF				X		X				X		(D)
Sys-D9SF					X	X				X		
Sys-D9SM					X	X					X	

Three basic earthquake ground motions were used as earthquake excitation in foundation simulations. They were the TAFT, Mexico-2D and Mexico-9S ground motions. The second symbol β in the system notation Sys-αβγη denotes an earthquake ground motion where "T" represents the TAFT earthquake ground motion, "2" represents the Mexico-2D ground motion, and "9" represents the Mexico-9S ground motion. The peak acceleration was normalized to 0.33g for each ground motions.

Meanwhile, a normalized peak acceleration of 0.22g was also used for the Mexico-2D and Mexico-9S ground motions. Therefore, a total of five different ground motions were used in simulations. For Mexico-2D and Mexico-9S, the third symbol γ in the system notation Sys-αβγη denotes a normalized peak acceleration where "G" represents a General peak acceleration of 0.33g and "L" represents a Low peak acceleration of 0.22g.

However, for structures subjected to the TAFT ground motion, the peak acceleration did not change and the symbol γ denotes the level of initial post-tensioning. Different levels of initial post-tensioning were selected only for System B subjected to the TAFT ground motion with a peak acceleration of 0.33g. "G" represents a General (high) level of initial post-tensioning identical to the flexure test (Test I) presented in Chapter V. "N" means N post-tensioning tendons were applied to the structure. "Z" represents Zero initial post-tensioning for the same post-tensioning tendons as Sys-TBGη. "L" represents Low initial post-tensioning for the same post-tensioning tendons as Sys-TBGη.

The retrofitting plan was to add different number of infill walls to the same structure. The fourth symbol η in the system notation Sys-αβγη denotes the number of infill walls where "F" represents Fewer (two) and "M" represent More (three) infills.

Using program, IDARC-PT, a total of 22 structural systems modeled with different variables were analyzed. Foundation performance, foundation effects, foundation-post-tensioning and foundation-infill interaction were studied. Foundation simulation will be presented in detail in the following sections,.

9.2 FOOTING-INFILL CONNECTION SCHEME

Footing modeling was discussed in the last chapter. Another important issue involved in foundation simulation is how to link the infill wall with the footing model. It has been mentioned that the foundation would not be strengthened in conjunction with superstructure retrofitting. The infill-wall added to a frame is supported on the existing footings. There may be two ways to place and connect the infills and post-tensioning tendons to the footings. One method is to place the infills at the ground level and the other is to set the infills at the same depth as the footing cap as shown in Figure 9.1. To reflect the mechanical behavior for the two cases, different foundation-infill link models have to be determined.

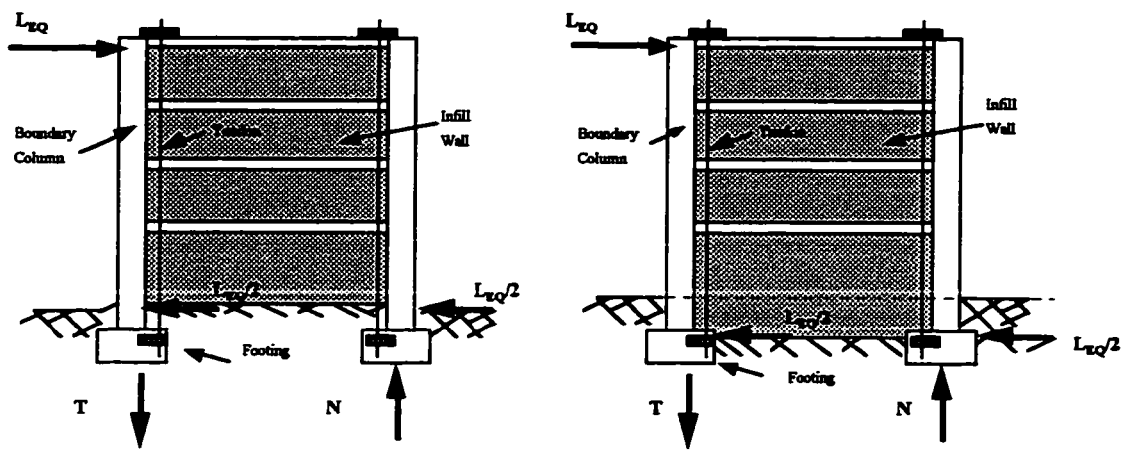

a) Infill at Ground Level b) Infill at Footing Level

Figure 9.1 Different Method of Infill Setting

The first method may be convenient for retrofitting construction but may not make optimum use of the PTPW system. If the infill is set on the ground level, the soil wall interface might not provide much restraint to the horizontal movement of the structure. Meanwhile, the large earthquake shear force $L_{EQ}/2$ shown in Figure 9.1 would have to be

transferred through each of the frame columns as shown in Figure 9.1a. In such a case, column shear failures would likely. In addition, the infill flexure strength would not be efficient in providing system moment capacity at the base because the system moment capacity is provided by means of tension-compression forces in the boundary columns. Consequently, it may be incorrect to assume that horizontal foundation failure is not likely, and the horizontal spring may not be modeled as working in the elastic range. In fact, the horizontal loading capacity at the base is as low as the shear capacity of the frame boundary columns. Therefore, it is always preferable to place the infill wall directly on the footing in a PTPW system.

As discussed in Chapter VII, a wall member was modeled as a column-like element with wall member capacities in shear and flexure. The foundation-infill linking characteristics for the infill wall supported directly on the footing was modeled as in the system shown in Figure 8.16. The horizontal springs S_{h1} and S_{h2} represent foundation resistance to the structural horizontal movement. The vertical springs S_{v1} ,S_{v2} and S_{v3} represent the foundation strength and deformation characteristics under vertical load. The link-beams B_{f1} and B_{f2} represent the foundation rotation deformation characteristics for the wall member.

9.3 FOUNDATION PERFORMANCE

Foundation performance was investigated using non-linear time-history analysis for a frame structure strengthened by the PTPW system with a plan shown in Figure 9.2a. The frame retrofitted with the infill wall and post-tensioning was identical to the large-scale model structure presented in Chapter V. The foundation properties are shown in Figure 9.2b. For the TAFT ground motion, shown in Figure 9.3 with normalized peak acceleration of 0.33g and system damping coefficient of 5%, the

earthquake response analysis was conducted for the structure Sys-BTGF. The time-history response for roof displacement is shown in Figure 9.4a.

In order to study the response difference between the structures with and without foundation involvement, time-history analyses were also conducted under identical earthquake excitation for the same structure without foundation involvement. This structure denoted as Sys-0TGF was modeled with neither foundation spring elements nor foundation rotation beam elements. It was assumed that the structure was founded on a non-deformed rigid foundation with fixed supports. The time-history response for top displacement is shown in Figure 9.4b.

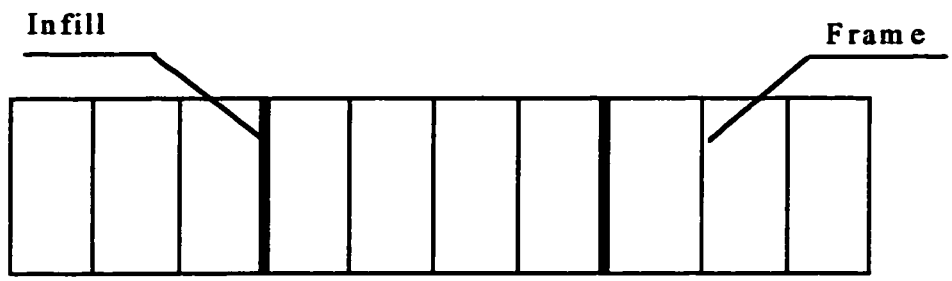

a) Retrofit Plan for Structure System B

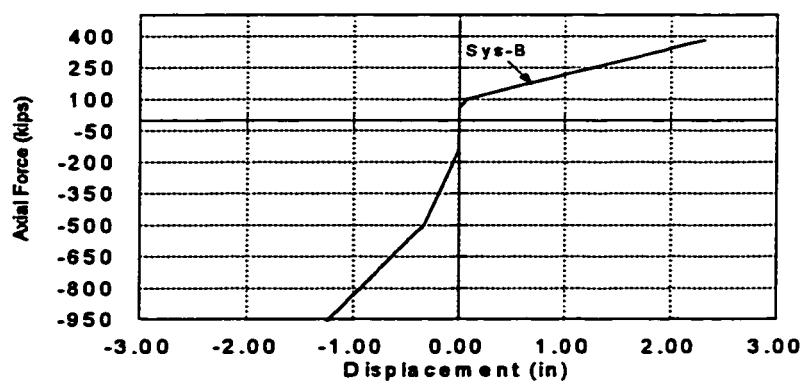

b) Foundation Spring Property (soft soil)

Figure 9.2 Retrofit Plan and Foundation Properties of Sys-BTGF

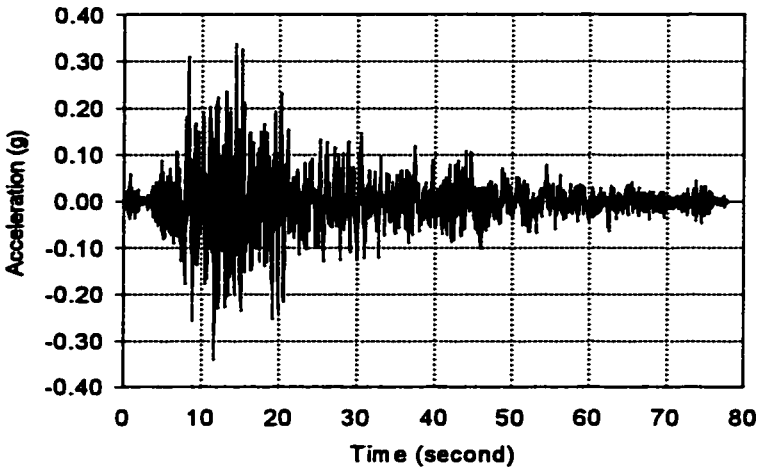

Figure 9.3 TAFT Ground Motion with Normalized Peak Acceleration of 0.33g

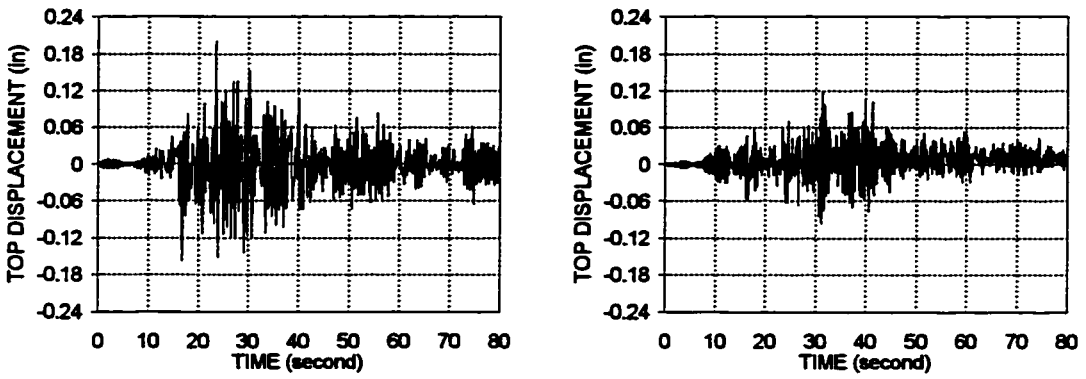

a) Sys-BTGF (soft soil) b) Sys-0TGF (rigid foundation)

Figure 9.4 Top Floor Drift Responses of Sys-BTGF & Sys-0TGF (0.33g TAFT)

Comparison of the acceleration and displacement responses of the two structures shows noticeable differences. For Sys-BTGF, the soft foundation softened the structural system. A soft system would be expected to respond with lower accelerations and frequencies but larger displacements. The time-history analyses showed this to be true.

Expanded responses show that, under the same earthquake ground motion, the period of Sys-BTGF with foundation involvement is longer than that of Sys-0TGF without

foundation involvement. The structural acceleration response of Sys-BTGF is much lower and the displacement response is much larger than that of Sys-0TGF, shown in Figures 9.5 and 9.4, respectively. The displacement of Sys-BTGF is about 1.75 times that of Sys-0TGF and, the peak acceleration of Sys-0TGF is about 1.5 times that of Sys-BTGF.

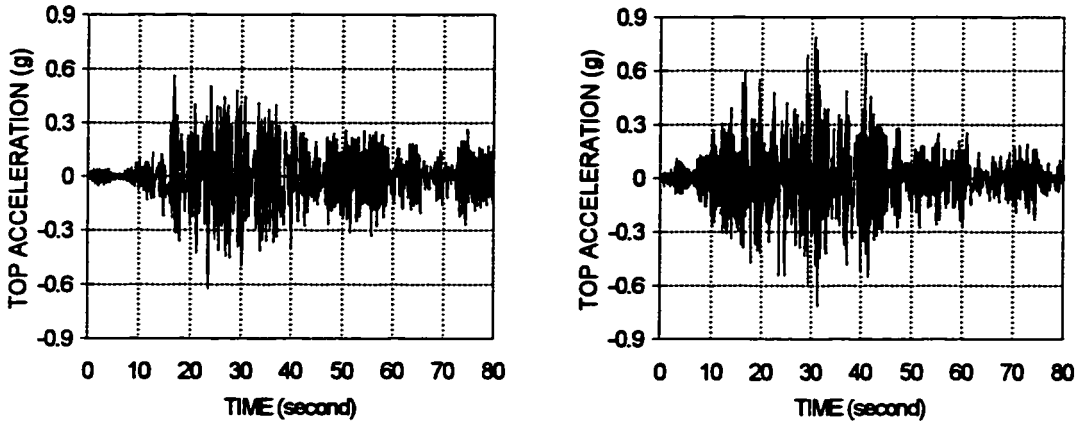

a) Sys-BTGF (soft soil) b) Sys-0TGF (rigid Foundation)

Figure 9.5 Roof Acceleration Response of Sys-BTGF & Sys-0TGF (0.33g TAFT)

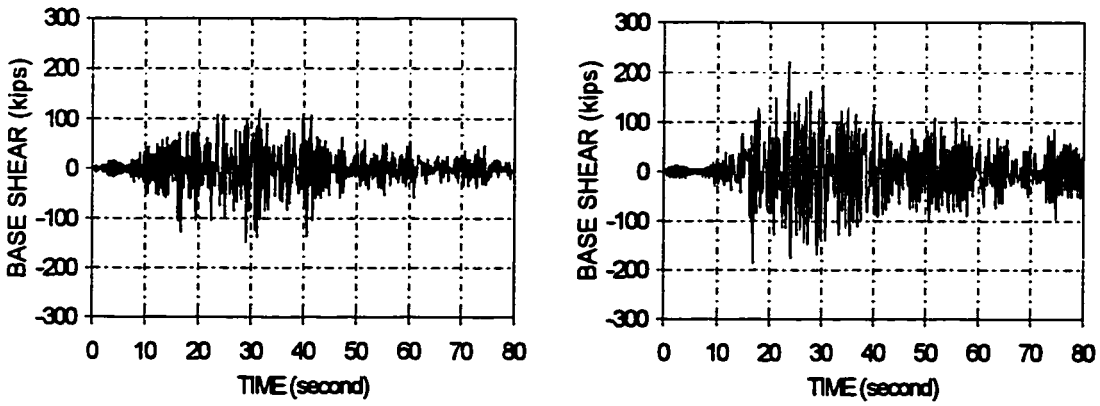

a) Sys-0TGF (rigid foundation) b) Sys-BTGF (soft soil)

Figure 9.6 Base Shear Response (0.33g TAFT)

Comparing the responses of Sys-A and Sys-B subjected to the TAFT ground motion, the softer the foundation, the larger the displacements and the lower the accelerations. Consequently, the lower the acceleration, the smaller the earthquake loads on the structure. On the other hand, the larger the displacements, the higher the internal forces induced in the elements. The earthquake load induced in the structure is dependent not only on the earthquake properties but also the foundation strength and stiffness properties. Specifically, the lateral loading on Sys-BTGF is greater than that on Sys-0TGF which is clear from the total base shear values shown in Figure 9.6. It shows that the total earthquake load on Sys-BTGF is about two times that on Sys-0TGF. Soil property effects on structural response were further investigated with the following simulations.

9.4 SOIL PROPERTY EFFECTS

The simulation indicated that foundation involvement could jeopardize structures retrofitted with the PTPW system. In order to comprehensively understand foundation effects, different variables such as base soil properties and earthquake ground motions affecting structural responses were also studied.

To study soil effects, four soil types were considered through selection of different properties of vertical springs in the foundation model. The first condition considered was a foundation with very high stiffness and strength. The fourth condition was selected as an extremely soft soil with very low stiffness and strength. The second and third types were intermediate conditions with stiffness and strength between those of the first and the fourth. Figure 9.7 shows the spring mechanical behaviors for all foundation types. It is pointed out that all soft soil types considered in this report, except the first soil type, conform to the "soft soil" specified in UBC-94 in which only two soil types were specified: firm soil and soft soil.

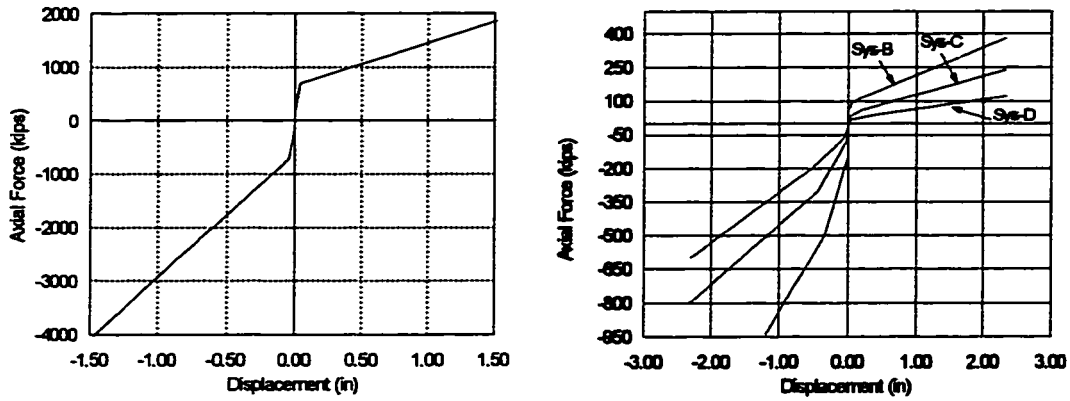

a) System A with Firm Soil b) Systems B, C and D with Soft Soil

Figure 9.7 Foundation Spring Properties of Structures

Table 9.2 Structural Response for Different Soil Conditions

Ground Motion	Foundation Soil	System ID	Top Floor Drift (%)	Top Floor Acc. (g)	Base Shear (k)
TAFT	Rigid	Sys-0TGF	0.062	0.78	122
	Firm	Sys-ATGF	0.068	0.82	176
	Soft	Sys-BTGF	0.105	0.56	223
	Very Soft	Sys-CTGF	0.383	0.45	135
	Extra Soft	Sys-DTGF	0.764	0.33	109
Mexico-2D	Soft	Sys-B2GF	0.064	0.44	159
	Very Soft	Sys-C2GF	0.454	0.52	191
	Extra Soft	Sys-D2GF	3.643	0.57	298
Mexico-9S	Soft	Sys-B9GF	0.064	0.38	172
	Very Soft	Sys-C9GF	0.416	0.44	192
	Extra Soft	Sys-D9GF	7.193	1.07	403

Through the application of each of the four different foundation springs to an identical frame structure, four different structural systems, Sys-ATGF, Sys-BTGF (Sys-BTGF was analyzed earlier), Sys-CTGF and Sys-DTGF, were investigated using TAFT ground motion with a normalized peak acceleration of 0.33g. A structural damping

coefficient of 5% was used for both the superstructure and footing springs, and time-history analyses (foundation simulations) were conducted for all four structures. Table 9.2 outlines the top floor acceleration, base shear and top floor displacement responses for the structures. Responses subjected to the Mexico earthquake ground motions for the soft soil conditions are also included in Table 9.2 and will be discussed in the next section. Base shear response for each structure is presented In Figure 9.8.

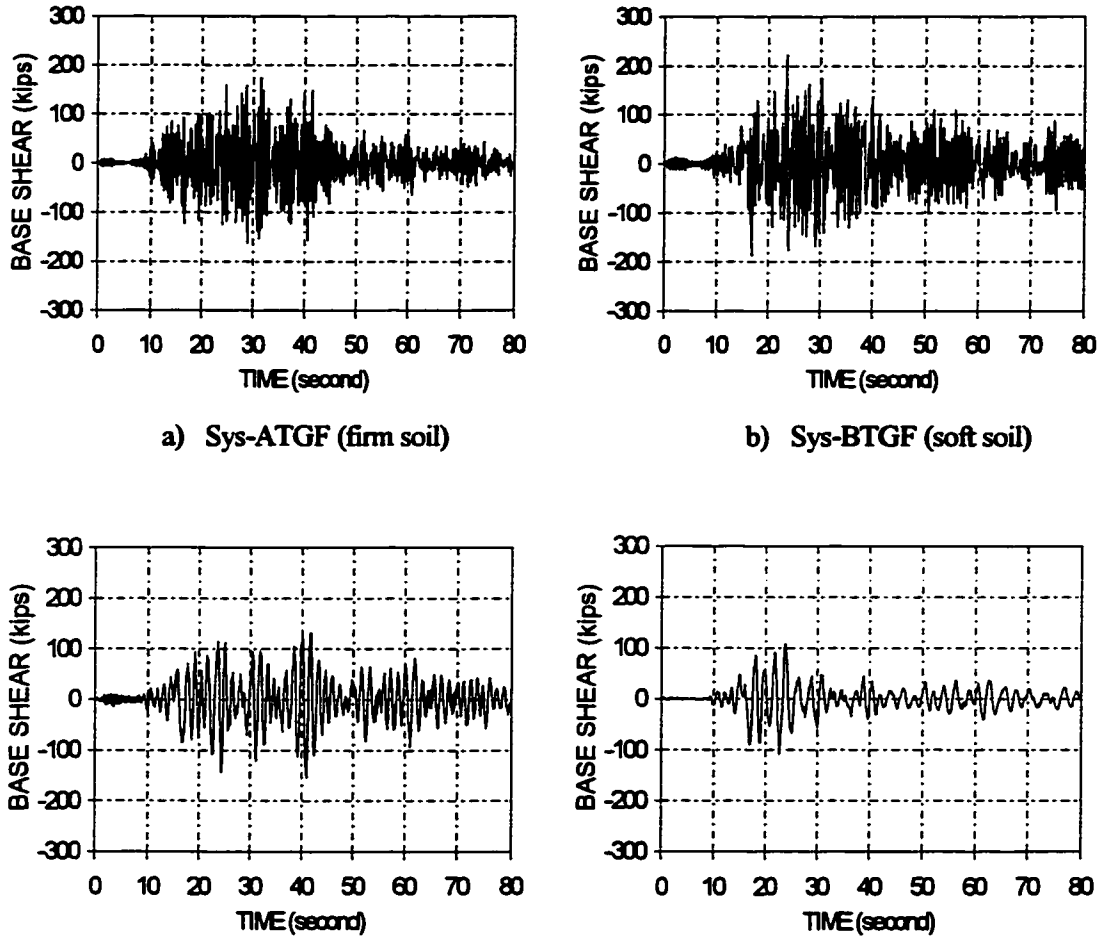

a) Sys-ATGF (firm soil)

b) Sys-BTGF (soft soil)

c) Sys-CTGF (very soft soil)

d) Sys-DTGF (extra soft soil)

Figure 9.8 Structural Base Shear Response for Different Soil Types

The simulation results indicated that soil effects on structural acceleration and displacement responses discussed in Section 9.3 are true for these structures subjected to the TAFT earthquake. However, base shear response increased as soil type changed from rigid to soft soil, and then, dropped as soil type changed from soft soil to extra soft soil.

Previous simulations were conducted with identical earthquake ground motion applied to structures with different foundation or soil conditions. Though it is necessary to study one factor while keeping other variables constant, using the same earthquake ground motion for various soil zones does not realistically reflect real earthquake behavior in a specific zone. In fact, soft soil zones often transmit earthquake waves with long periods and low accelerations. Generally speaking, the softer the soil zone, the longer the period and the lower the acceleration of earthquake waves transferred through the soil. For structures located in particular soil zones, earthquake ground motion consistent with soil properties should be selected as input in the structural seismic analysis. To understand earthquake behavior effects on PTPW systems, simulations were also conducted with variables related to earthquake ground motions and are presented in Section 9.5.

9.5 EARTHQUAKE BEHAVIOR EFFECTS

9.5.1 Long Period Earthquake with Higher Peak Acceleration

For the structures modeled with different soft soils, System B, System C and System D, simulations were also conducted using Mexico city earthquake records (Mexico-9S and Mexico-2D). For consistency with cases considering the TAFT ground motion, the same retrofitting plan (two infills) was adopted, and the peak acceleration for the Mexico city ground motions was also normalized to 0.33g. Six structural systems were studied in which Sys-B2GF, Sys-C2GF and Sys-D2GF were analyzed using the Mexico-2D ground motion, and Sys-B9GF, Sys-C9GF and Sys-D9GF were analyzed using the

Mexico-9S ground motion. Figure 9.9 shows the acceleration time-histories for Mexico-9S and Mexico-2D. The structural responses were presented in Table 9.2. Simulation results indicate that for the Mexico earthquake records with the same peak acceleration as TAFT, the structural responses possess significant differences from that discussed in the last section.

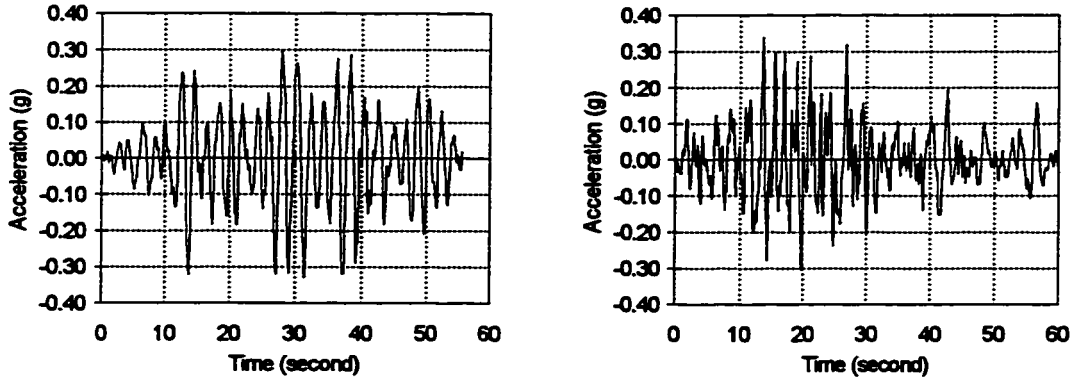

a) Mexico-9S b) Mexico-2D

Figure 9.9 Acceleration Histories for Mexico City Earthquake Ground Motions

For the Mexico city ground motions, the structural responses exhibited longer periods than corresponding structures responding to the TAFT ground motion. As shown in Figure 9.10, as foundation stiffness and strength decreases or softens, the acceleration response decreases, while the base shear response increases and then decreases for the TAFT ground motion. For the Mexico city ground motions, however, as the foundation softens, the acceleration and base shear response increases. The Mexico city ground motion induced much higher base shears and larger displacements than the TAFT ground motion did for Systems C and D with very soft and extra soft soil foundations.

It can be concluded that a longer-period ground motion can result in more severe response of a PTPW system built on softer soils. In fact, the extremely large displacements

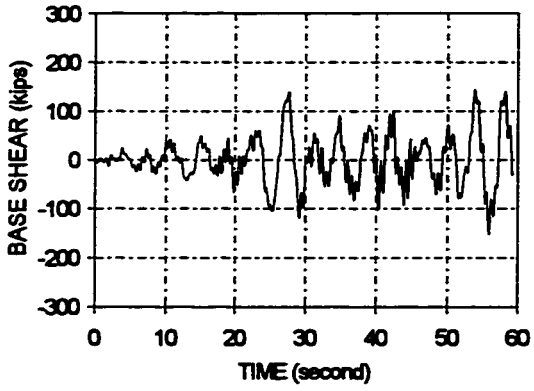

a) Sys-B9GF (soft soil)

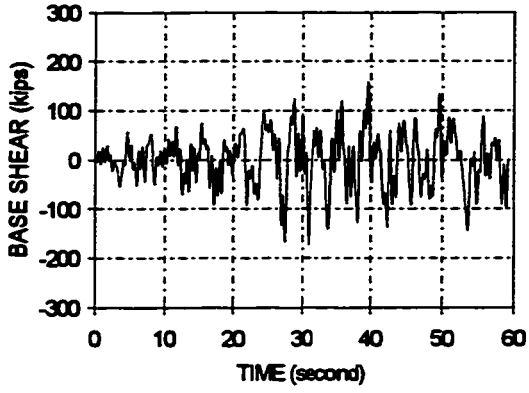

b) Sys-B2GF (soft soil)

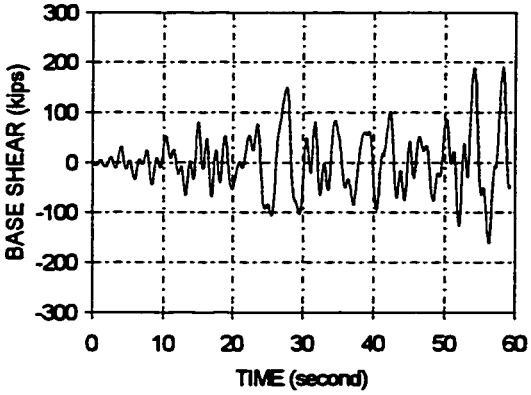

c) Sys-C9GF (very soft soil)

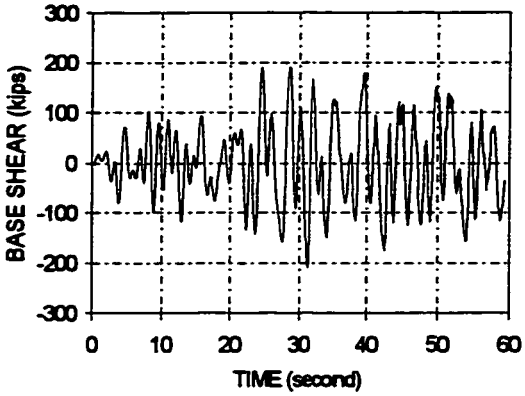

d) Sys-C2GF (very soft soil)

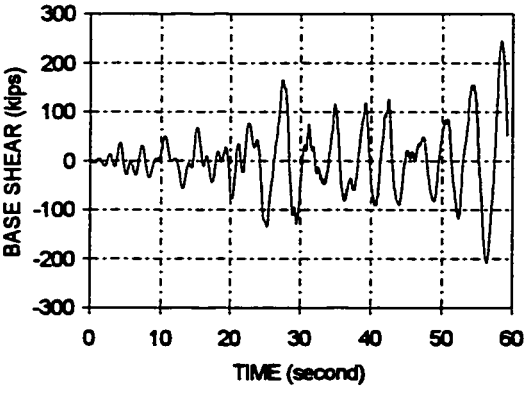

e) Sys-D9GF (extra soft soil)

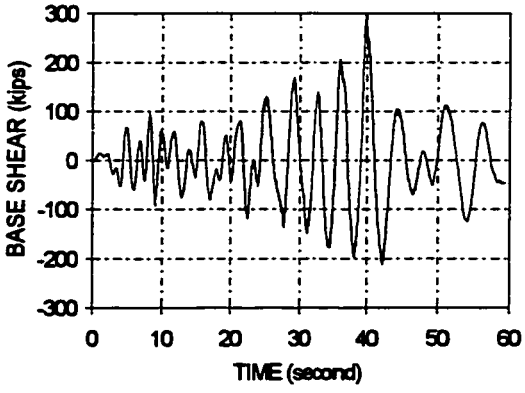

f) Sys-D2GF (extra soft soil)

Figure 9.10 Structural Base Shear Responses for Different Earthquakes

of Sys-D2GF indicated that the structure failed at approximately 40 seconds for the Mexico-2D excitation.

The simulation reveals that if a structure located on a soft soil is subjected to an earthquake containing predominantly a long periods and large peak accelerations, the structure will be subjected to extremely high earthquake forces which may cause collapse of the structure. Unfortunately, as mentioned previously, long period earthquakes typically happen in soft soil zones. If an earthquake has both long period and high peak accelerations, it is likely to be a severely destructive event for structures.

The above simulations and discussions were based on normalizing long and short period earthquakes to have the same peak acceleration. This is not commonly true for earthquakes. Generally, longer period earthquakes often possess lower peak accelerations. For example, it was evident, from Figure 9.3 and Figure 9.9, that the peak acceleration for the short-period TAFT earthquake is much higher than that for the long period 1985 Mexico City earthquake. This property should be considered when selecting earthquake records for foundation simulation.

9.5.2 Long Period Earthquake with Lower Peak Acceleration

In previous simulations, the peak acceleration for the TAFT ground motion was normalized to 0.33g which amplified the original peak acceleration of 0.04g by 8.6 times. For consistency, it was initially reasonable to amplify the 1985 Mexico city ground motion with the same factor. Responses were computed for Systems C, and D subject to the Mexico-2D and Mexico-9S ground motions with a normalized peak acceleration of 0.22g. Four systems denoted as Sys-C2SF, Sys-D2SF, Sys-C9SF and Sys-D9SF were analyzed.

The peak responses of systems Sys-C2SF, Sys-D2SF, Sys-C9SF and Sys-D9SF along with those of Sys-C2GF, Sys-D2GF, Sys-C9GF and Sys-D9GF are presented in Table 9.3. The base shear responses of the systems Sys-C2SF and Sys-D2SF are

illustrated in Figure 9.11 and are compared with the responses of systems Sys-C2GF and Sys-D2GF. The base shear, and top floor displacement are still large for Sys-D2SF but have been greatly reduced with the decrease in the peak ground acceleration from 0.33g to 0.22g.

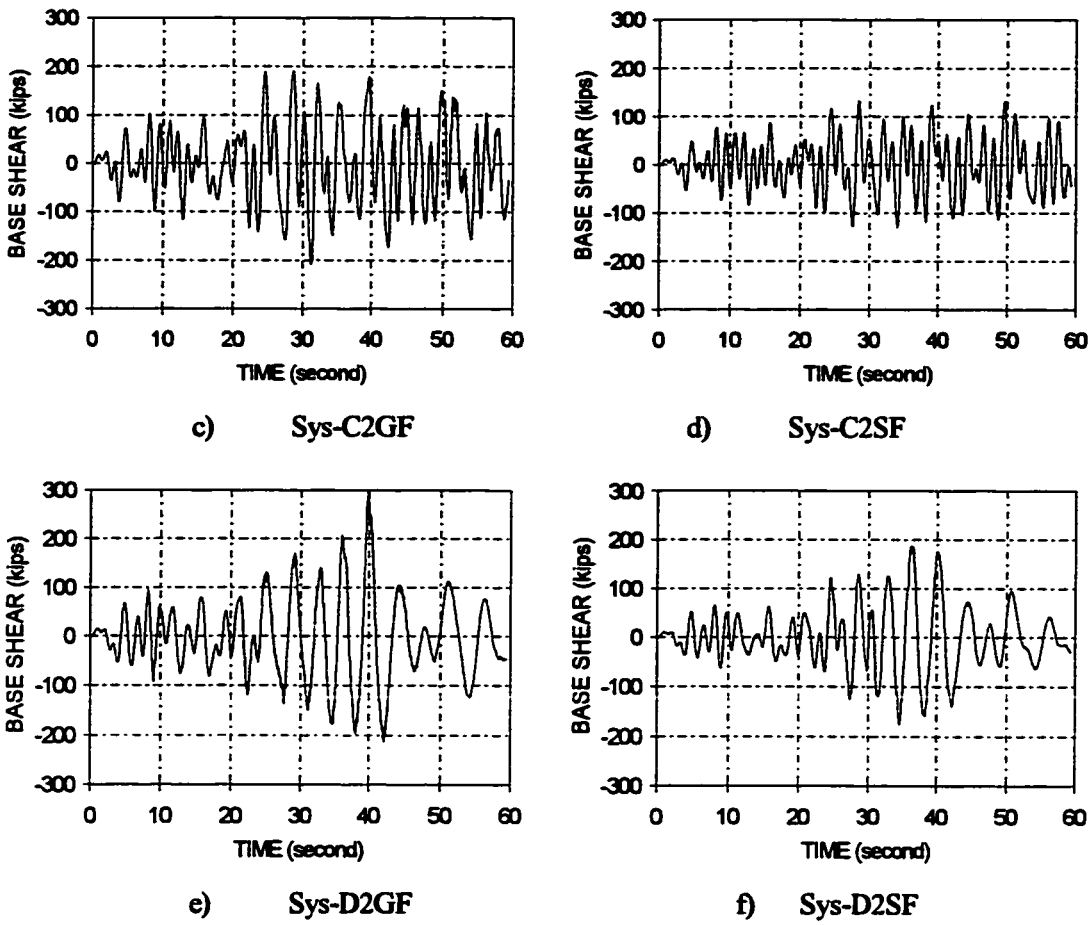

Figure 9.11 Base Shear Response for Different Peak Ground Acceleration

For structures built on soft soil, if an earthquake has a lower peak acceleration, foundation effects may not be very severe as long as the foundation soil is not extremely soft as illustrated by Sys-C2SF response. However, if a long period earthquake has a high peak acceleration, severe foundation effects on the structure may occur as indicated by

computed responses for Sys-C2GF and Sys-D2GF. Commonly, the foundation effects on a structure are dependent on soil properties (stiffness or period), earthquake period, and peak acceleration. Foundation simulation is strongly recommended for structures built on soft soil, especially, when a long period earthquake is likely to occur.

Table 9.3 Structural Responses for Different Peak Ground Accelerations

Ground Motion		System	Top Floor	Top Floor	Base
Records	Peak Acc.	ID	Drift (%)	Acc. (g)	Shear (k)
Mexico-2D	0.33g	Sys-C2GF	0.454	0.524	191
	0.22g	Sys-C2SF	0.238	0.361	134
	0.33g	Sys-D2GF	3.643	0.571	298
	0.22g	Sys-D2SF	2.873	0.564	188
Mexico-9S	0.33g	Sys-C9GF	0.416	0.435	192
	0.22g	Sys-C9SF	0.241	0.317	140
	0.33g	Sys-D9GF	7.193	1.073	403
	0.22g	Sys-D9SF	2.266	0.533	175

9.5.3 General Effects of Soil and Earthquake Properties

The effects of soil and earthquake period on structural response can be evaluated through structural base shear responses. Base on the simulations, base shear responses can be illustrated with the structural response spectra shown in Figure 9.12. In the response spectra, T_A, T_B, T_C and T_D represent the periods of structural Systems A, B, C and D respectively. For the short period TAFT earthquake ground motion (with a peak acceleration of 0.33g), the base shear response increases as the soil softens or the structural period increases from Sys-ATGF to Sys-BTGF. As the soil further softens or the structural period increases beyond the earthquake period, the base shear reduces from Sys-BTGF to Sys-DTGF.

For the long period Mexico-2D ground motion (with a peak acceleration of 0.33g), the base shear increases as the soil softens or the structural period increases from Sys-B2GF to Sys-D2GF. If the peak acceleration of Mexico-2D is reduced to 0.22g, the base

shear reduces though the spectra shows a pattern similar to that for the same ground motion with a high peak acceleration of 0.33g.

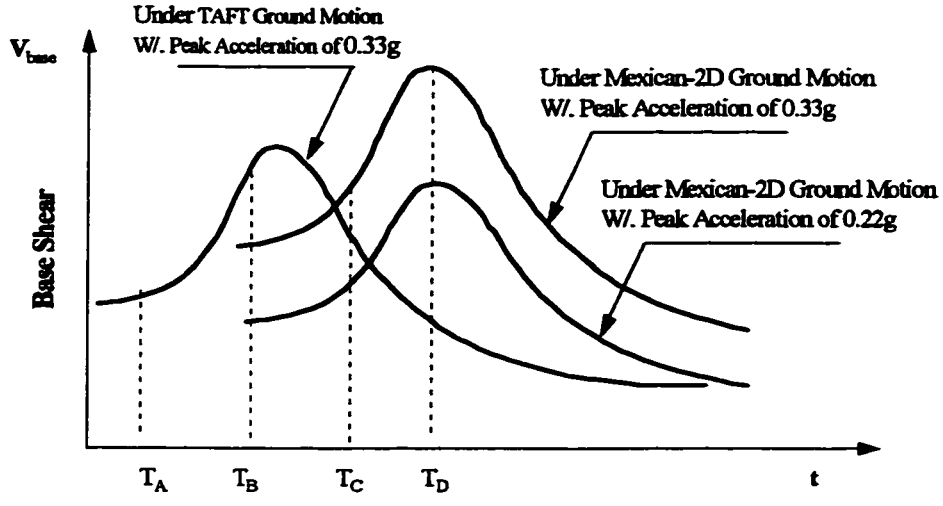

Figure 9.12 Base Shear Response Spectra

9.6 INTERACTION ANALYSIS

In previous sections, discussions were limited to foundation effects on the structural system response. The principal thought for using a PTPW system to retrofit a reinforced concrete frame structure is to take advantage of the high shear capacity of infills and high moment capacity provided by post-tensioned boundary columns to sustain the lateral earthquake load. If the foundation effects jeopardize the function of the post-tensioning or the infill wall, the overall capacities of infills and post-tensioning tendons may not influence the response, and advantages of the PTPW system will not be realized. It is important to investigate interaction between the foundation and post-tensioning tendons as well as infills.

9.6.1 Foundation Response

Foundation simulations focused on studying foundation performance and effects on retrofitted structures. Under earthquake excitation, foundation response is dependent on soil properties and superstructure characteristics. Figure 9.13 illustrates foundation responses for Systems B through D for the TAFT and Mexico-2D earthquake ground motions.

Except for structures Sys-DTGF and Sys-D2GF, all other structures modeled with "soft" and "very soft" soils performed satisfactorily according to the simulation results. Simulation indicated that vertical foundation springs responded in compression and tension cyclically as shown in Figures 9.13a through 9.13d. However, foundation springs of structures Sys-DTGF and Sys-D2GF, which modeled "extremely soft soil" conditions, responded in tension only after 20 and 40 seconds respectively as shown in Figures 9.13e and 9.13f. Such responses indicated that the foundations of Sys-DTGF and Sys-D2GF failed or were severely damaged.

Failure of foundations in Sys-DTGF and Sys-D2GF was caused by the extra soft soil. The results indicated that very high uplift forces were induced on the footings of the frame retrofitted with infills because fewer infill walls (two) were added to the system, and the footings could not sustain the uplift forces. That is to say, the retrofitting plan (two walls) could not provide the structures Sys-DTGF and Sys-D2GF with sufficient capacity to resist the input earthquakes, and therefore this was not a feasible retrofitting plan.

If a retrofitting plan appears reasonable for a structure, the foundation effects should be considered to determine if under earthquake load, the lateral displacements are consistent with levels the foundation can sustain. It is possible that the foundation will lift off its supporting soil without severe structural or foundation damage. The whole structural system may rock, in which case the PTPW system provides a stiff structure

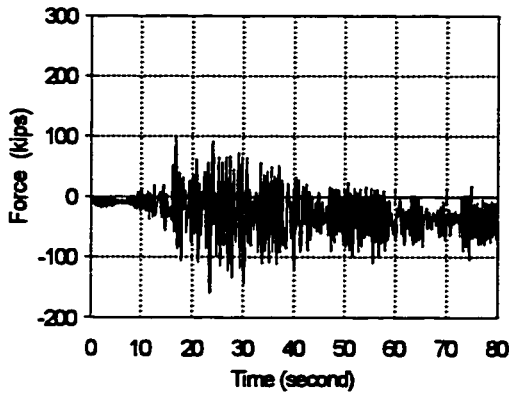

a) Sys-BTGF

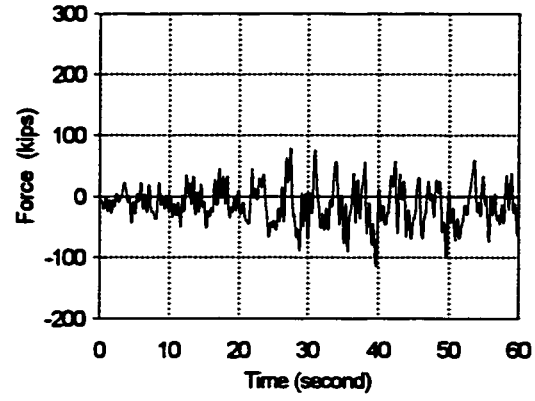

b) Sys-B2GF

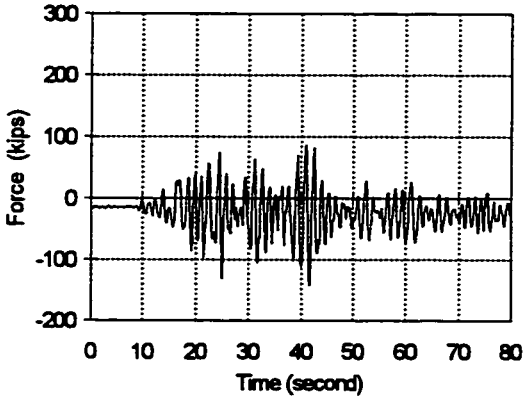

c) Sys-CTGF

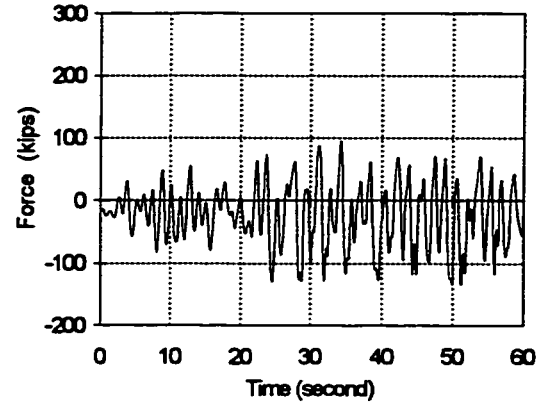

d) Sys-C2GF

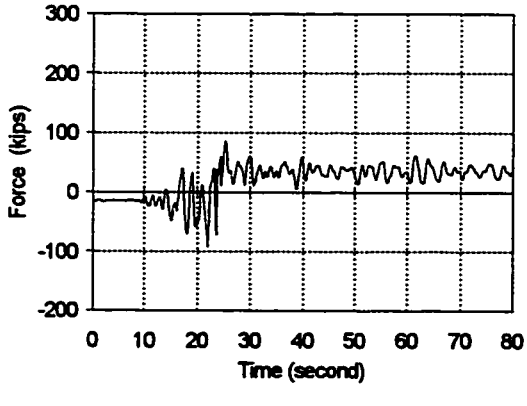

e) Sys-DTGF

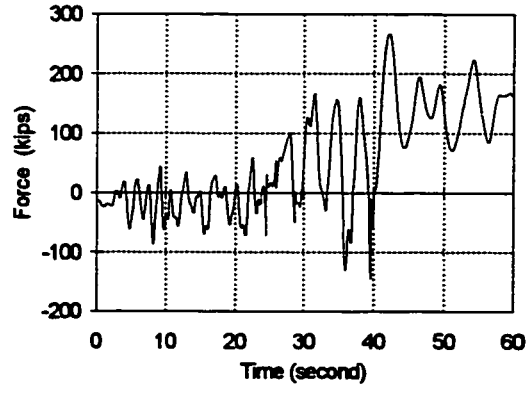

f) Sys-D2GF

Figure 9.13 Foundation Spring Responses

capable of sustaining such deformation. The structural rocking behavior may be an acceptable solution for a PTPW system on soft soil. Further studies will show that structural rocking is an acceptable option for a properly retrofitted structure with a PTPW system.

9.6.2 Foundation / Post-tensioning Interaction

If a structure retrofitted with a PTPW system tends to rock on a soft soil base, the structural system should, logically, behave relatively like a rigid body. Internal forces in elements would vary in a relatively small range under cyclic or earthquake load. Post-tensioned tendons in simulations displayed this response.

9.6.2.1 Tendon Force Versus Foundation Property

In previous simulations, initial post-tensioning force was at the same level as in the model structure. The tendon force changed as the structure vibrated during earthquake excitation. In structure Sys-0TGF which represents a structure fixed on a rigid foundation (without foundation involvement), the axial forces in the post-tensioning tendons ranged from 230 kips to 320 kips. The tendons in Sys-0TGF sustained the large moment induced by the earthquake on the PTPW system. By examining various foundation conditions, the range of post-tensioning forces was reduced with lower foundation stiffness as shown in Figure 9.14. The softer the foundation, the less the force change in the tendons.

For Sys-DTGF and Sys-D2GF in which the foundation is an extremely soft soil, the tendon forces showed almost no change during the earthquake, as shown in Figure 9.15. Moreover, the post-tensioning tended to relax or decrease slightly during the earthquake as shown in Figure 9.15b.

The reduction in post-tensioning force in tendons further indicates that the PTPW retrofitting system tends to rock about a soft soil base. If the system rocks, the post-

tensioning tendons do not need to resist high moments in the system. The maximum moment generated is limited by the level at which the foundation lifts. Therefore, it should be questioned whether post-tensioning is necessary in a PTPW system on soft soil. More simulations were conducted with different initial post-tensioning levels and without post-tensioning tendons, and will be discussed in the following section.

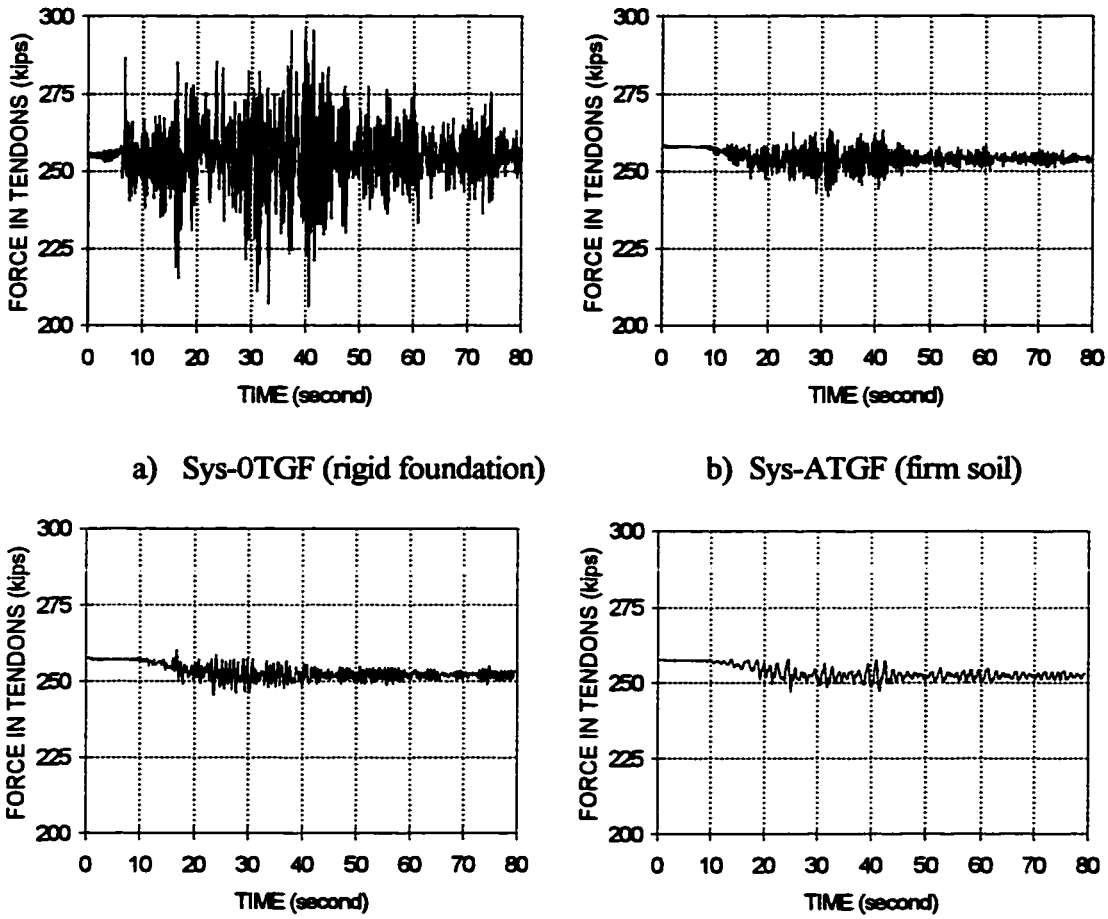

a) Sys-0TGF (rigid foundation)

b) Sys-ATGF (firm soil)

c) Sys-BTGF (soft soil)

d) Sys-CTGF (very soft soil)

Figure 9.14 Tendon Force Response Versus Foundation Stiffness

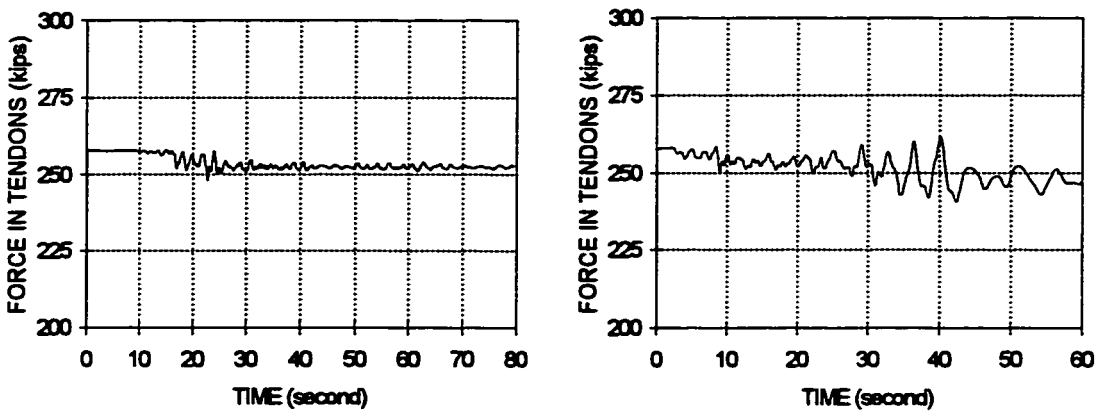

a) Sys-DTGF (extra soft soil) b) Sys-D2GF (extra soft soil)

Figure 9.15 Tendon Force Response for Soft Soil Conditions

9.6.2.2 Effect of Initial Tendon Force and No Tendons

A primary reason for applying post-tensioning was to prevent splice failure of boundary columns. Post-tensioning makes the system effectively more stiff and enables it to rock as a rigid body about its base. It is likely that post-tensioning will sustain system moments without column splice failure regardless of the changes of tendon force.

However, if there are no post-tensioning tendons or the tendons are not post-tensioned, the result may be different. Without boundary column modification, the existing column will be subjected to larger tension forces. The large tension forces will produce early splice failure in columns because existing column reinforcement was detailed with insufficient lap lengths or ties in the splice region. Once the boundary column splice fails, the infill wall will solely sustain the system moment in the absence of tendons. Because the infill wall has a very low flexural capacity, the system may fail under earthquake excitation.

With different post-tensioning levels or no tendons, simulation was conducted for the structure System B and the responses are presented in Table 9.4. The structural system denoted as Sys-BTNF was modeled identical to Sys-BTGF but without post-tensioning tendons.

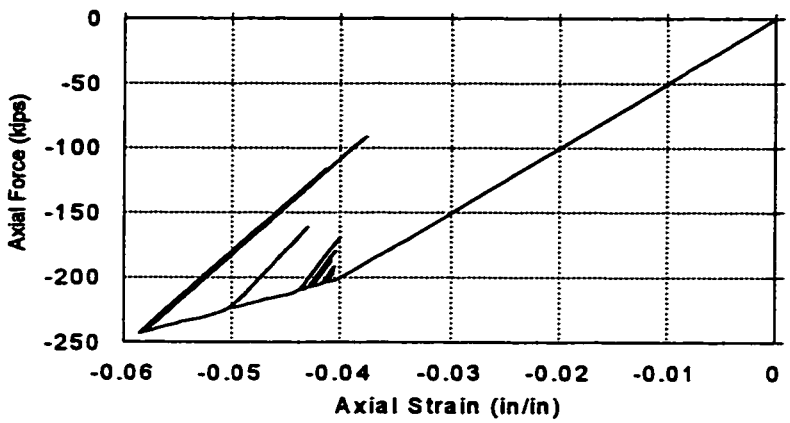

a) Sys-BTGF (high post-tensioning)

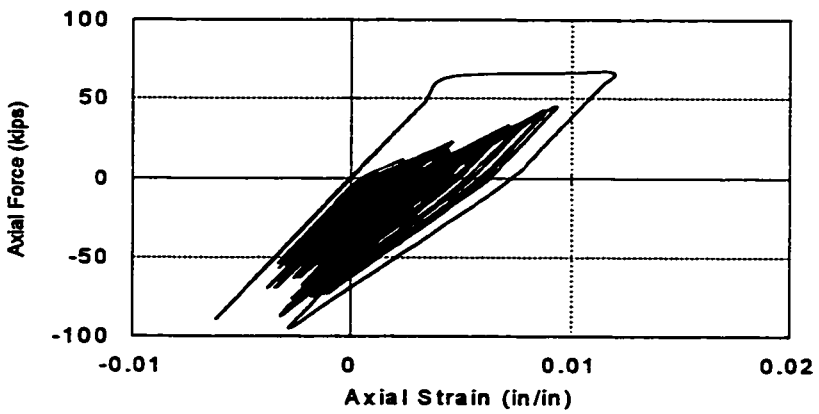

b) Sys-BTNF (without Post-tensioning Tendon)

Figure 9.16 Post-Tensioning Effect on Column Splice

Simulations were also conducted for the same structure System B with post-tensioning tendons at different initial tension levels. Sys-BTZF represents a system

with zero initial post-tensioning force, and Sys-BTLF represents a system with less than a half of the initial post-tensioning force applied in Sys-BTGF.

The column was yielded in Sys-BTNF as shown in Figure 9.16b which indicates that splice failure occurred because the splice was too short to develop reinforcement yielding. It can also be seen from Table 9.4 that the tension force in the column of Sys-BTNF reached the level at which the splice fails. However, as shown in Figure 9.16a, the boundary column in Sys-BTGF worked in compression and splice failure never occurred because a high post-tensioning force was applied. To prevent column splice failure and system flexural failure, post-tensioning is absolutely necessary for efficient use of the infill wall retrofitting technique.

However, the post-tensioning force level for structures on a soft soil may not need to be as high as for structures on a firm foundation. The post-tensioning force must be designed at a level that allows the boundary column to work with little or no tension to prevent splice failure.

The boundary column axial force responses for structures Sys-BTZF, and Sys-BTLF are shown in Figure 9.17. These indicate that as long as post-tensioning tendons are used, the boundary column splice is protected, as shown in Figure 9.17a, even though there is no initial post-tensioning applied. Furthermore, with a reasonable level of initial post-tensioning applied, the boundary column in Sys-BTLF remains in compression as shown in Figure 9.17b.

Table 9.4 Post-Tensioning Effects on Structural System B

Ground Motion	Initial Post Tensioning	System ID	Axial Force In Column (k)	Top Floor Drift (%)	Top Floor Acc. (g)	Base Shear (k)
TAFT	High (250 k)	Sys-BTGF	-91	0.105	0.565	223
	No Tendon	Sys-BTNF	73	0.103	0.567	249
	Zero	Sys-BTZF	66	0.103	0.560	223
	Low (110 k)	Sys-BTLF	-28	0.104	0.562	223

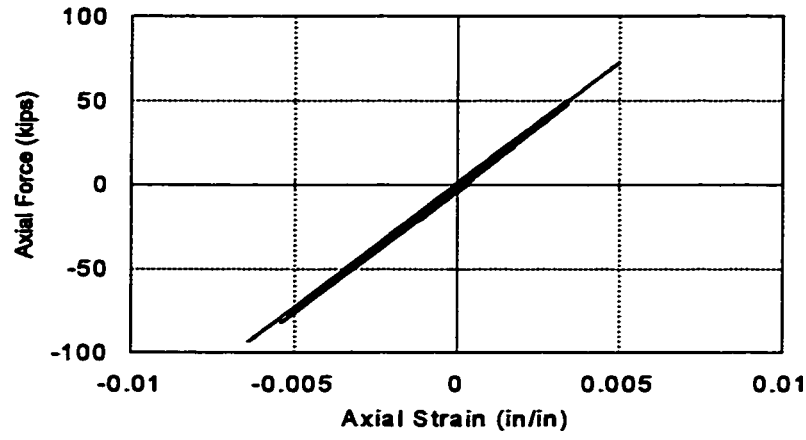

a) Sys-BTZF (zero post-tensioning)

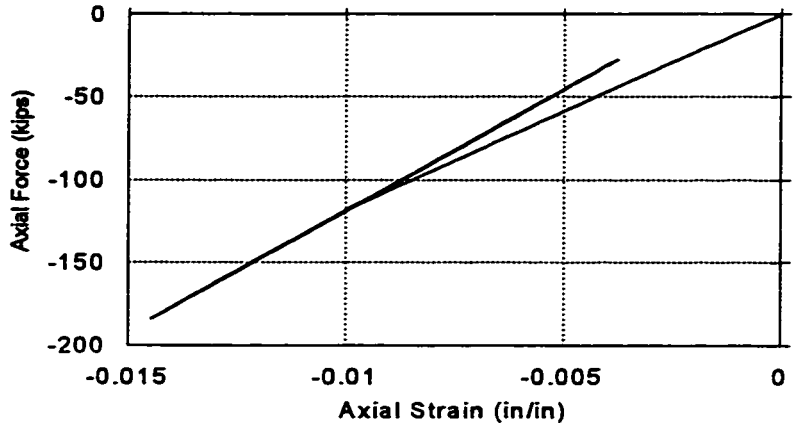

b) Sys-BTLF (low post-tensioning)

Figure 9.17 Column Response Versus Post-tensioning

9.6.3 Foundation - Infill Wall Interaction

The infills in a PTPW system were designed primarily to sustain shear in the structural system because moment capacity of the precast infills is low. As discussed in Chapter VI, it is required that post-tensioning tendon capacity is high enough to sustain overturning moment in the system. If the post-tensioning tendon capacity is

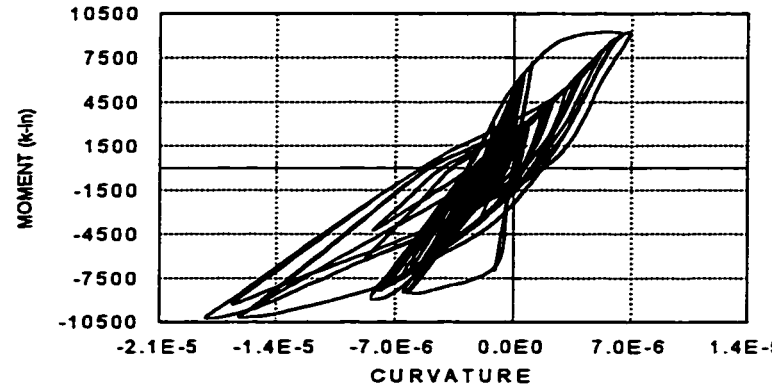

a) Sys-ATGF (firm soil)

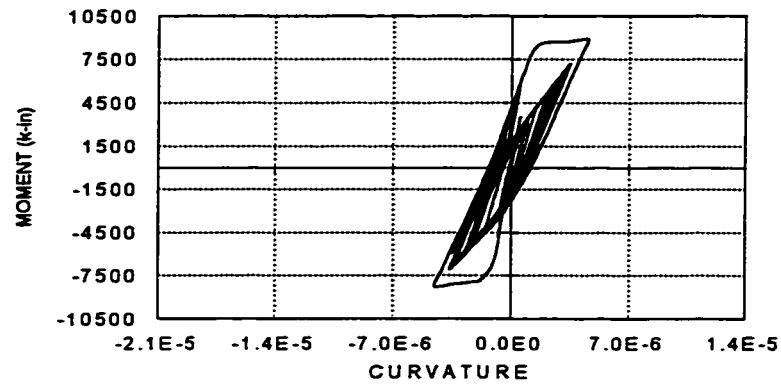

b) Sys-BTGF (soft soil)

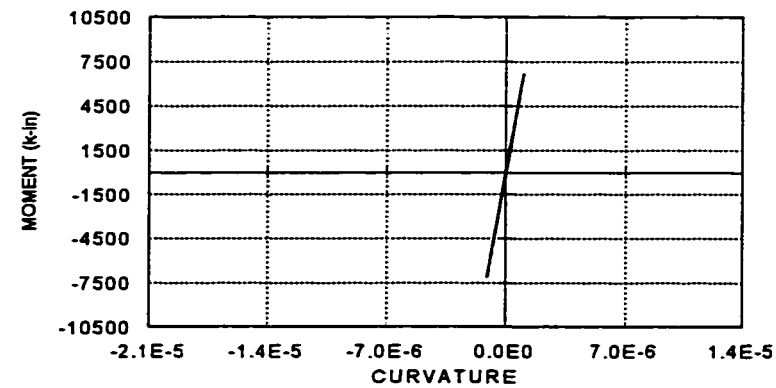

c) Sys-CTGF (very soft soil)

Figure 9.18 Moment Response at Base of Infill Walls (TAFT)

lower than that required to carry the system moment, infills will be called on to resist the system moment and flexural failure will occur before shear failure occurs. Shear failure and flexural failure mechanism were discussed in Chapters VI and VII. In foundation simulations, foundation-infill interaction was also investigated.

9.6.3.1 Interaction With Soil Base

Because of foundation involvement, infill wall behavior is different from that of the model structure built on a rigid foundation. For structures subjected to the TAFT ground motion, the base shear decreased and post-tensioning efficiency declined as softer soils were considered. As shown in Figure 9.18 a) and b), the infill wall flexural deformation (curvature) of structure Sys-BTGF was much smaller than that of Sys-ATGF. It was also noted that softer soil results in much lower flexural response of the infill wall. In fact, infills in Sys-CTGF (Sys-DTGF as well) remained in the elastic range as shown in Figure 9.18c indicating that the infill wall was rocking about its base.

9.6.3.2 Interaction with Earthquake Period

For structures subjected to the longer-period Mexico earthquake, the lateral earthquake force (base shear) increased as softer soils were considered (as shown in Figure 9.10). Particularly, because post-tensioning efficiency declines as the foundation becomes softer, the infill flexural response increases. Under the same soil condition, the long-period earthquake produced greater infill deformation in Sys-D2GF than the short period earthquake did in Sys-DTGF, as shown in Figure 9.19.

All infill walls in Sys-BTGF, Sys-CTGF, Sys-B2GF, Sys-C2GF and Sys-D2GF reached inelastic stages. However, with softer soil, infill wall inelastic deformations reduced for structures subjected to the TAFT ground motion but increased for structures subjected to the Mexico ground motion.

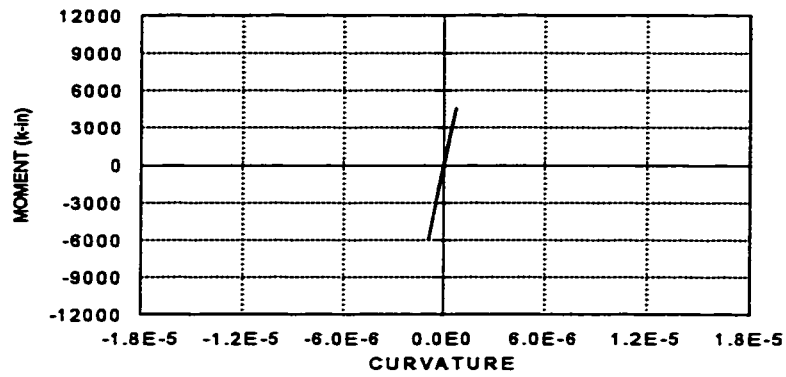

a) Sys-DTGF (extra soft soil / TAFT)

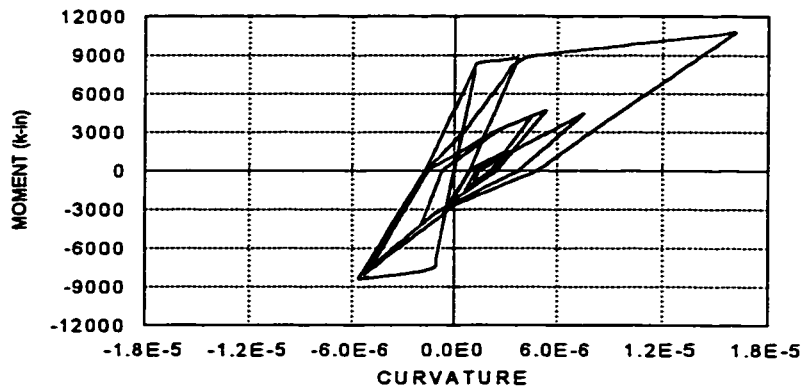

b) Sys-D2GF (extra soft soil / Mexico-2D)

Figure 9.19 Moment Response at Base of Infill Walls

9.6.3.3 Interaction With Post -Tensioning

Different levels of post-tensioning also lead to different responses of the foundation-infill wall interaction. As discussed earlier, boundary column splices failed when no post-tensioning tendons were provided, as in Sys-BTNF. Consequently, the infill wall was the only element available to sustain system moments, and large deformations occurred as shown in Figure 9.20a.

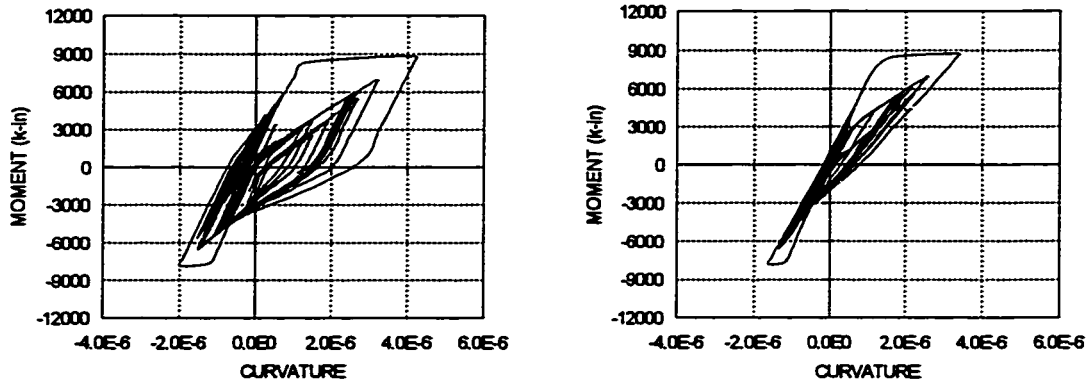

a) Sys-BTNF (no tendons) b) Sys-BTZF (zero post-tensioning)

Figure 9.20 Wall Moments for Different Post-Tensioning

With post-tensioning tendons provided, infill flexural failure can be eliminated and the retrofitting system will behave properly. Even with zero initial post-tensioning, the system flexural response was satisfactory as shown in Figure 9.20b. In Sys-BTZF, the infill is required to sustain only a very small part of the system moment. It demonstrates how important the post-tensioning tendon is for the precast infill wall retrofitting technique.

9.7 DESIGN COMMENTS

Through foundation simulations, foundation performance and foundation-structure interaction were studied and foundation (soil) effects on PTPW system response were evaluated. Based on foundation simulations, design comments are developed with regard to reducing or eliminating foundation effects on PTPW system response so as to efficiently use PTPW retrofitting techniques in reinforced concrete frame rehabilitation. Some key issues are included in the comments and will be presented.

9.7.1 Proper Location of Infills

The PTPW retrofitting system focuses on correcting non-ductile structural defects and weak links. When applying a PTPW system, weak links have to be corrected and new weak links must not be created as a result of the retrofitting plan. With a PTPW system design, foundation effects should be evaluated by means of foundation simulation as presented in the previous sections.

Corner footings would be most likely to uplift due to lack of neighboring footing interaction and low dead load. If the end frame is to be retrofitted with an infill wall, large earthquake loads will concentrate at the end frame, and the corner footing may be required to resist large uplift force. Though retrofitting an end frame may be convenient for construction and less disruption to building use, it should be discouraged for PTPW systems. If that is the only choice, foundation simulation must be conducted to verify that foundation effects are not likely to jeopardize retrofitting.

Applying PTPW to a multiple-bay, multiple-frame system, only a few bays need to be retrofitted with infills and post-tensioning. The location and configuration of the infills in the structural plan must be studied to prevent torsion effects. As discussed in Chapter II, severe torsion response occurs due to eccentricity between the centroids of structural mass and lateral resisting stiffness. To prevent such torsion response, the gross section of the infills in the structural plan should be distributed to correspond with the total structural mass. Improper location and distribution of infill walls may not only induce severe torsion response but may also lead to foundation damage or failure, and severe foundation-structure interaction. In infill retrofit plan design, foundation effects may be demonstrated by means of foundation simulation.

9.7.2 Adding More Infills

To reduce or eliminate severe foundation effects or interaction, an efficient method is to reduce the uplift force induced by earthquakes. A large uplift force is concentrated at the edge column footing in the frame which is retrofitted with infill walls. By reducing the cross section of each individual infill and retrofitting more frames, the concentrated uplift force can be reduced for an individual footing and severe foundation effects will be reduced.

Simulations were conducted for System D with more infills than that added in Sys-D2SF and Sys-D9SF, respectively, as shown in Figure 9.2a. Except for more (three) infills, as shown in Figure 9.21, added to the new systems denoted as Sys-D2SM and Sys-D9SM, all other variables are the same as in Sys-D2SF and Sys-D9SF, respectively. Structural responses of systems Sys-D2SM and Sys-D9SM were presented in Table 9.5 and are illustrated in Figures 9.21 and 9.22.

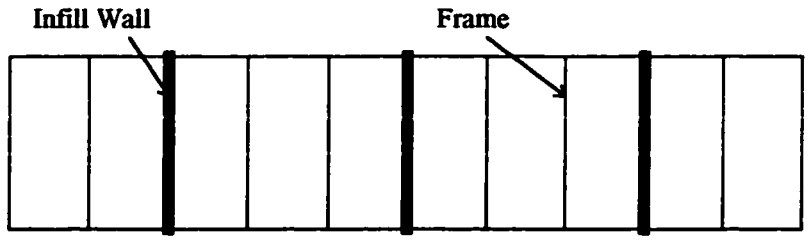

Figure 9.21 Retrofitting Plan of More Infills

Table 9.5 Infill Effects to Structural Response for System D (0.22g)

Ground Motion	Retrofitting Plan	System ID	Max Moment In Wall (k-in)	Top Floor Drift (%)	Top Floor Acc. (g)	Base Shear (k)
Mexico-2D	Two Walls	Sys-D2SF	8476	2.873	0.564	188
	Three Walls	Sys-D2SM	3518	0.233	0.329	81
Mexico-9S	Two Walls	Sys-D9SF	8396	2.266	0.533	175
	Three Walls	Sys-D9SM	3507	0.228	0.273	83

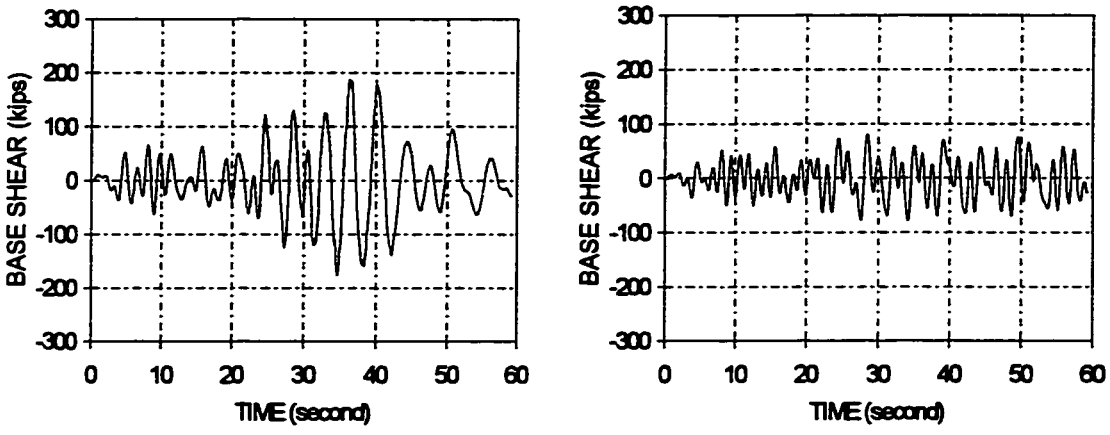

a) Sys-D2SF (two walls) b) Sys-D2SM (three walls)

Figure 9.22 Base Shear Responses of Sys-D2SF & Sys-D2SM

From Figure 9.22, which provides a comparison of base shear responses for Sys-D2SF and Sys-D2SM, the earthquake load was greatly reduced by adding only one more infill wall to the same structure. The peak shear response in Sys-D2SM is less than one third of that of Sys-D2SF. It must be pointed out that large differences between the two does not mean that the system stiffness of Sys-D2SM is greatly increased but that the foundation effect was greatly reduced. In fact the stiffness of Sys-D2SM is increased by half that of Sys-D2SF even though it efficiently eliminates severe foundation effects.

The efficiency can be visualized more clearly from Figure 9.23 which shows the foundation spring responses of both structures. The footing spring response of Sys-D2SF demonstrates that the foundation failed under the Mexico-2D earthquake. The same footing spring in Sys-D2SM worked perfectly in the elastic range for very small uplift loads. In other words, the foundation of Sys-D2SM worked principally in compression. Conclusively, by adding more infills to a structural system with proper

arrangement, severe foundation effects and foundation-structure interaction can be successfully eliminated or reduced.

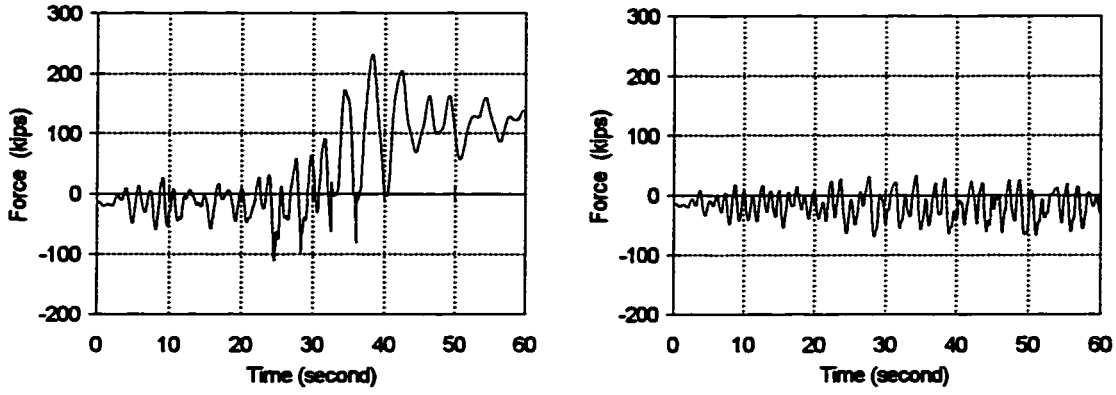

a) Sys-D2SF (two walls) b) Sys-D2SM (three walls)

Figure 9.23 Footing Spring Responses for Sys-D2SF & Sys-D2SM

To prevent and eliminate foundation-structure interaction and to successfully apply PTPW retrofitting systems in structural seismic rehabilitation, it is strongly recommended that foundation simulation be conducted in PTPW system design to determine the number of infill walls, to arrange infill wall locations, and to control structural lateral stiffness distribution. The foundation simulation of Sys-D2SM is a good example of the PTPW system design.

9.7.3 Enhancing Infill Wall Flexural Capacity

As discussed earlier, severe interaction of the foundation and infill wall may occur depending on the soil and earthquake properties. The Sys-ATGF response shown in Figure 9.18a, with a relatively short-period earthquake and firm foundation indicated that severe infill flexure response will occur even though higher post-tensioning is applied. Similar interaction may also occur for structures subjected to a

longer-period earthquake and with a very soft foundation as shown for Sys-D2GF in Figure 9.19b.

To prevent damage of the infill as a result of flexural response, foundation simulation should be conducted to check the infill flexural capacity in PTPW system design. Adding more infills has been proven to be an efficient scheme to eliminate severe foundation effects. When it is difficult or impossible to add more infills, and damage to the infill is indicated from foundation simulation, infill flexural capacity can be increased.

To increase infill flexural capacity, vertical closure strips may be widened and more vertical reinforcement may added in the closure strips. However, widening strips and increasing strip reinforcement may not modify the effective flexural capacity of the infill. Because the weak link of the infill is at the base, without secure and sufficient connection of the strip reinforcement to the foundation, infill flexural capacity not can be significantly increased.

By placing the infill walls deeper into the soil base, and increasing infill section and reinforcement at the base level, the flexural capacity of the wall at the base level could be increased. The most efficient way to increase infill flexural capacity is to anchor vertical strip reinforcement securely to the foundation. Infill flexural capacity is an important issue associated with foundation-structure interaction which must be checked and for which potential problems must be solved in PTPW system design.

9.8 SUMMARY

In this Chapter, seismic analyses of structures with foundation involvement are presented. The foundation effects on structural response and interaction of the

foundation with post-tensioning, with boundary columns and with infill walls was investigated. The foundation system modeled as a part of the structure affects structural response in several aspects that are summarized below.

9.8.1 Soil and Earthquake Effects

If a structure is founded on a soft soil, the soft soil effectively softens the entire structural system. A soft system responds in a long-period mode and is sensitive to long-period earthquakes. When the period of the structure is close to that of the earthquake, large response and severe structural damage may result. Soft soil may reduce the efficiency of the PTPW retrofitting technique.

Through foundation simulations, soil and earthquake effects on structural seismic response were investigated. The simulation results showed that soil and earthquake effects on structural response can be concluded as follows:

a) *The softer the soil base, the longer the period of structural response.*

b) *The softer the soil base, the smaller the structural acceleration to a short-period earthquake or the larger the structural acceleration to a long-period earthquake.*

c) *The softer the soil base, the larger the structural displacement.*

d) *The softer the soil base, the higher the base shear resulted from a long-period earthquake or the lower the base shear resulted from a short- period earthquake.*

It is obvious that large structural displacements and earthquake lateral load would impose high interior It is obvious that large structural displacement and earthquake lateral load would impose high interior forces on the structural elements. These high forces may damage structural elements and eventually cause collapse of the

structure. When designing a PTPW system located on a soft soil, foundation simulation is needed to understand soil effects for selecting a reasonable retrofitting plan to prevent severe foundation-structure interaction. Severe foundation effects could jeopardize the effectiveness of a PTPW system. Retrofitting strategies were studied to prevent or eliminate severe foundation-structure interaction which will be discussed in the following sections.

9.8.2 Soil / Post -Tensioning Interaction

Soft soil, a weak joint at the base of the structure, reduces the sensitivity of vertical post-tensioning tendons to ground motions. In other words, soft soil reduces the effectiveness of post-tensioning. However, the vertical post-tensioning tendons stiffen the superstructure which tends to rock as a relatively rigid body on the soft soil during earthquakes. If no vertical post-tensioning tendons are applied, a splice failure in the boundary columns may occur and the superstructure will no longer respond in the same manner rocking as a relatively rigid body.

Boundary column splice failure may lead to flexural failure in the infill walls and moment capacity loss in the structural system. It is necessary to apply vertical post-tensioning tendons to protect the boundary column splices, to provide the system with sufficient moment capacity and to permit the superstructure to rock as a relatively rigid body on the soft soil. The level of initial post-tensioning required in a PTPW retrofitting system is dependent on the retrofitting plan and foundation (soil) uplift capacity. To design the post-tensioning for a PTPW system, foundation models and structural seismic analysis and are needed.

9.8.3 Soil / Infill Interaction

The number, location, and gross section of infill walls are key issues in the retrofitting plan of a PTPW system. An ill-considered retrofitting plan may result in

severe foundation effects and soil-infill interaction. However, severe foundation effects on structural response can be reduced or eliminated with an effective retrofitting plan. An effective scheme to reduce foundation effects is to decrease uplift forces on footings of the retrofitted frames by adding more infill walls to the structural system to distribute uplift load to more footings. Through foundation simulation, effectiveness of the retrofitting plan can be evaluated and a desirable retrofitting solution can be reached to reduce severe foundation effects and soil-structure interaction for a PTPW system.

Comprehensive studies on foundation simulation detected foundation effects and problems associated with PTPW system application. These effects and problems also exist in ordinary structural systems. However, foundation effects and interaction simulation have not been widely used in structural seismic analysis and design. Foundation effects on structural seismic response and structural capacity design are often ignored in design and selection of lateral force resisting schemes.

By the current design approach, structural seismic forces generally are reduced (underestimated) without considering possible damage due to foundation effects for both new designs and seismic retrofitting. The study reported here is a departure from typical practice and the research will benefit ordinary structural seismic design. It is recommended that the results of the foundation simulation be used for any kind of structural system in seismic design and retrofitting. For an individual footing foundation, the model developed in this project can be used directly in general structural seismic analysis. For other types of foundations, using soil cohesive strength and the soil rupture mechanism developed in this project, reasonable and feasible

models can be established through further research which was recommended as the next research topic and will be further discussed in Chapter X.

CHAPTER X

DESIGN GUIDELINES

10.1 INTRODUCTION

To strengthen non-ductile reinforced concrete frame structures using a post-tensioned precast infill wall (PTPW) system, seismic retrofitting design guidelines have been developed. The guidelines were developed based on the structural connection and model structure tests, test result analyses and computer simulations. The guidelines will be presented through a discussion of retrofitting principles and structural retrofitting design procedures.

10.2 PRINCIPLE OF RETROFITTING

It has been discussed, in Chapter VI, that a vertically post-tensioned precast infill wall (PTPW) system is an efficient seismic retrofitting technique for non-ductile reinforced concrete frame rehabilitation. Seismic retrofit of an existing frame structure should meet desired structural seismic behavior and lateral resistance requirements. Retrofitting is recommended to meet three limit states or three performances[56] for structural seismic design.

10.2.1 Philosophy of Seismic Design

These well accepted limit states for structural seismic design were discussed in Chapter II and in general, structures should be designed to:

1. Resist a minor earthquake ground motion without damage (Service limit, or Immediate Occupancy Performance);
2. Resist a moderate earthquake ground motion without structural damage, but possibly experience some nonstructural damage (Damage limit, or Life Safety Performance);
3. Resist a major earthquake ground motion having an intensity equal to the strongest either experienced or forecast for the building site, without collapse, but possibly with structural as well as nonstructural damage (Collapse limit, or Collapse Prevention Performance).

Corresponding to these limit states and tri-linear hysteretic behavior of PTPW systems, the following failure stages are proposed for two structural categories.

A) Ordinary Building Structures

   1) Flexural-cracking stage represents the service limit state.
   2) Splice failure stage represents the damage limit state.
   3) Yielding of post-tensioning tendons represents the collapse limit state.

B) Important Structures (Classified by UBC-94 as category I-essential facilities and category II - hazardous facilities)

   1) Decompression (zero tension) stage represents the service limit state.
   2) Flex-cracking stage represents the damage limit state.
   3) Splice failure stage represents the collapse limit state.

10.2.2 Targets Of Retrofitting

Seismic retrofitting focuses on correcting structural defects or structural weak links and enhancing structural lateral capacities to withstand earthquake excitation. Structural lateral loading capacities to be increased include strength, stiffness, and deformation tolerance or ductility.

10.2.2.1 Increasing Structural Strength

If a structure built in a seismic zone does not have sufficient strength to sustain earthquake lateral loads, it must be retrofitted or strengthened. Structural seismic loads will be first estimated following the current design codes. Structural retrofitting may be considered to increase flexural and shear capacities to satisfy earthquake resistance in any limit state.

$$P_{STR} > P_{EQ} \qquad (10\text{-}1)$$

where P_{STR} ..... the structural / member capacity

P_{EQ} ..... the expected the force during an earthquake.

Besides structural loading capacity, the structural stiffness may need to be enhanced to limit the structural lateral drift within a reasonable range to prevent severe damage of elements or collapse of the structure.

$$\delta_{EQ} < \delta_{STR} \qquad (10\text{-}2)$$

where δ_{STR} ..... the limit ratio of the top level drift to the structure height, and

δ_{EQ} ..... the drift ratio resulting from the earthquake.

In design, it may be accepted that the largest drift ratio δ_{EQ} is limited to 1/300 for the service limit state, 1/200 for the damage limit state, and 1/100 for the collapse limit state, respectively.

10.2.2.2 Providing Ductility

Although the non-ductile behavior of existing frame structures is related to element detailing inadequacies, the PTPW retrofitting technique is intended to bypass the detailing inadequacies to improve structural ductility. Ductility of the retrofitted structure is provided by the boundary column post-tensioning tendons.

The tendons and initial post-tensioning force are designed to increase flexural capacity and to limit axial tension force in the existing column so that the column splice does not fail prematurely. To realize this goal, tendon area and initial post-tensioning level must be designed to provide adequate tensile capacity and to produce necessary pre-compression to the column in accordance with specified design limit states.

The infill wall, precast panel connection (closure strips) and frame-infill connection (shear lugs) must be designed to have sufficient shear capacity and to permit structural flexural capacity development and to avoid brittle failure. Detailed design procedures will be presented in the next section.

10.2.2.3 Correcting Structural Defects

Besides strength and detail problems, most structures possess structural system defects such as discontinuities, irregularity, and lack of redundancy as discussed in Chapter-II. The system defects create weak links in the structure. The weak links jeopardize the earthquake resistance and may lead to severe structural damage or may

trigger collapse. An important target in structural retrofitting is to eliminate the system weak links.

An overall structural system retrofit plan including location and dimension of infill walls and corresponding post-tensioning must focus on,

1) Correcting structural discontinuities,

2) Correcting structural irregularities, and

3) Increasing structural redundancy.

10.2.2.4 Preventing New Defects

To retrofit a structure, some new elements are added to the structural system. Generally speaking, the addition of a new element to a structure will increase the structural capacity. However, it may also create new problems or weak links. Addition of new elements may also create foundation problems, especially for PTPW systems since only a few infill walls are added to selected frames in a structural system, earthquake generated forces will concentrate in these frames and corresponding foundations. The large concentrated loads may induce foundation failure as discussed in Chapter VIII.

Design of structural lateral capacity, existing system defect correction, location, and dimensions of infill walls and corresponding post-tensioning must be comprehensively planned to prevent new potential problems from being created.

10.2.3 Strategy of PTPW System Design

10.2.3.1 Retrofitting Schemes

Retrofitting a non-ductile structural system to an acceptable earthquake resistant system is much cheaper than rebuilding a structure because existing structural

elements are used and continue to function. In a PTPW system, since post-tensioning is provided, the existing boundary columns function well at least prior to splice failure. Existing slab and beams of the structure still function as diaphragms in the retrofitted structure. So, a PTPW system provides a technique protecting existing elements and improving system performance.

Like other retrofitting techniques, the PTPW system involves adding new elements to the structure. Precast infill wall and post-tensioning tendons are added to a few frames of the structural system to convert the frame structure to a wall dominated system. New added precast infill walls and post-tensioning tendons must be securely connected to the existing frame structure by means of closure strips and shear lugs. Connection detailing will be discussed in Section 10.4.

10.2.3.2 Mechanical behavior

It is necessary that a PTPW system possess sufficient lateral shear capacity so that flexural capacity is developed before shear failure occurs. This can be realized through proportioning of the infill wall section and the post-tensioning tendons to permit flexural-cracking, splice failure and post-tensioning yielding to be developed in accordance with service, damage and collapse limit states.

10.3 STRUCTURAL CAPACITY DESIGN

For the structures of category A in service and damage limit states and the structures of category B in service limit state, the static equivalent force method recommended by UBC-94 can be used to determine capacity requirements. In accordance with the static force method, a different earthquake zone coefficient, as listed in Table 10.1, may be used for each limit state.

Table 10.1 Earthquake Zone Coefficient for Each Limit State

Structural Category	Service Limit State (Immediate Occupancy)	Damage Limit State (Life Safety)	Collapse Limit State (Collapse Prevention)
A	0.1	0.2	0.3
B	0.15	0.25	0.4

To retrofit a non-ductile frame structure, a solution can be based on estimated structural period, soil condition, earthquake zone, and engineering judgment. According to the retrofitting solution, the total base shear of the structural system can be determined from static forces recommended by UBC-94 as presented in Chapter VI.

$$V_{base} = Z I C W / R_w \qquad (10\text{-}3)$$

$$\text{where } C = \frac{1.25\ S}{\sqrt[3]{T^2}}$$

$$T = C_t \sqrt[4]{H^3}$$

For category B structures at damage and collapse limit states, and category A structures at collapse limit state, time-history analysis can be conducted using program IDARC-PT.

10.3.1 Foundation Uplift Capacity Evaluation

As discussed in Chapter IX, the foundation of a frame retrofitted with a PTPW will sustain large uplift force. So, the ultimate tensile capacity design of post-tensioning tendons and number and location of infill walls will be affected by uplift capacity of the foundation.

In PTPW system design, foundation uplift capacity of the frame, in which infill wall and post-tensioning tendons are added, should be evaluated. The foundation uplift

capacity evaluation is based on the foundation type, base soil property and foundation dimension as discussed in Chapter IX. For an individual footing, its uplift capacity can be calculated following the procedure and equation presented in 8.2.3.

$$F_t = 2d_f x\,(a + b + 2d_f \tan\phi)\, x f_{ch} = 2d_f x\, A\, x f_{ch} \quad (10\text{-}4)$$

where f_{ch} ---- the soil cohesive strength,

a, b ---- the footing bottom plan edge, lengths in both directions,

d_f ---- footing depth, and

$A = a + b + 2\, d_f \tan\phi$ ---- the total area of rupture surface.

For other types of foundations, calculation modes may be determined according to soil cohesive strength and foundation characteristics. In any circumstance, foundation uplift capacity F_t should be determined prior to structural system capacity design.

10.3.2 Flexural Capacity Design

10.3.2.1 Overall Structural Flexural Capacity

Using equations (6-11) through (6-13), the total base shear can be determined following equation (10-3). Pertaining to the base shear, story shear can be calculated using equations (28-6) through (28-8) from UBC-94, which were written as,

$$V_i = \frac{\left(V_{base} - F_t \right) W_i\, H_i}{\sum W_i\, H_i} \quad (10\text{-}5)$$

$$V_t = 0.07\, T\, V_{base} \quad (10\text{-}6)$$

$$\Sigma V_i + V_t = V_{base} \tag{10-7}$$

Moment with respect to story i will be computed based on story shears.

$$M_i = \sum_{j=i}^{n} V_j (H_j - H_i) \tag{10-8}$$

The maximum moment at the base M_{base} can be obtained and will be used to calculate the maximum tension force in the post-tensioning tendons. Since the base shear and moment were calculated on an elastic basis, a force reduction factor will be applied for inelastic response to determine the design base moment M_{base}^{d}.

$$M_{base}^{d} = \phi_d M_{base} \tag{10-9}$$

The reduction factor ϕ_d is dependent on the limit state and designed structural ductility factor μ. Generally, the force reduction factor may be determined using the equation below.

$$\phi_d = \frac{1}{\mu} \tag{10-10}$$

where μ = 1.0 for service limit state
2.0 for damage limit state
4.0 for collapse limit state

According to base design moment M_{base}^{d}, total tension forces in post-tensioning tendons, column bars and closure strip reinforcement can be calculated following the procedure and equation presented in Section 6.4.1.

$$\alpha T_1^2 - \beta T_1 + M_{base}^{d} = 0 \tag{10-11}$$

where $\alpha = \eta (\Sigma X_i A_i) / (X_1 A_1)$

$$\beta = \Sigma X_i^2 A_i / (X_1 A_1)$$

It is noted that column bars make no contribution to system flexural capacity after splice failure. The closure strip reinforcement does not contribute to system moment when determining the ultimate tension force in post-tensioning tendons.

Total area of post-tensioning tendons is based on equilibrium that the tendon yielding capacity equals the ultimate tension force calculated from equation (10-11). So, the total tendon area A_{pt} can be determined.

$$A_{pt} = T_1 / F_y^{pt} \qquad (10\text{-}12)$$

where F_y^{pt} ..... the tendon yield strength.

It is recommended that initial post-tensioning be in a range of 30 to 50% of the tendon yield strength. Vertical closure strip reinforcement may be designed for a ratio of 0.425 to 1.00% of infill panel section as recommended in 4.2.2.2.

10.3.2.2 Infill Number And Location Determination

After tendon area is determined, flexural capacity of the retrofit solution will be rechecked, and the number and location of infill wall will be determined. The infill walls number N_{wall} is basically determined according to the foundation uplift capacity F_t following equation:

$$N_{wall} = T_1 / (\phi F_t) \qquad (10\text{-}13)$$

where ϕ ..... the foundation performance factor.

Conservatively, the factor ϕ may be chosen as 1.0 to design foundation uplift capacity to equal the tendon ultimate capacity. It can also be chosen greater than 1.0 if foundation damage and rocking of the structure are expected. If foundation damage is not permitted, ϕ may be selected less than 1.0.

After the infill wall number is determined, infill locations and section will be designed depending on the retrofitting principle presented in Section 10.2 and the total base shear and story shear obtained with equations (10-3) and (10-5).

Structure flexural capacity for different working stages will be estimated. Generally, decompression, flexural-cracking and splice failure stages will be checked according to exterior moment and tendon force following the procedure presented in Section 6.4.1 and 6.5.1.

10.3.3 Shear Capacity Design

10.3.3.1 Infill Wall Design

Gross section of the total infill walls will be determined base on the shear capacity requirement. Generally, the infill gross section will be designed based on the base shear and concrete shear strength. To prevent brittle shear failure, concrete shear strength recommended by ACI-318, instead of that estimated in section 4.2.2.1, will be used.

$$\tau_n = 2\sqrt{f_c'} \tag{10-14}$$

Since the design base shear is,

$$V_{base}{}^{d} = \phi_d V_{base} \tag{10-15}$$

the infill gross section may be designed as,

$$A^{W}_{gross} = V_{base}{}^{d}/\tau_n \tag{10-16}$$

10.3.3.2 System Shear Strength

It is very important that the system-shear capacity be checked. After infill wall section post-tensioning tendons are determined, a compression strut model of the

system may be developed for evaluating system-shear capacity using the procedure presented in Section 6.4.2.2.

10.3.3.3 Base Shear Capacity and Shear Lug Design

Corresponding to infill design, the number of shear lug number N_{pipe} and location will be determined. The gross area of shear lugs A^P_{gross} is designed to sustain at least the base shear for the damage limit state estimated in flexural design.

$$A^P_{gross} = \frac{V_{damge}}{\frac{F_y}{\sqrt{3}}} \tag{10-17}$$

The total shear strength of shear lugs ($A^P_{gross} F_y$) and shear friction (P_R) should be greater than the maximum base shear.

$$A^P_{gross} F_y + P_R \geq V_{base}{}^d \tag{10-18}$$

According to the shear lug gross area and closure strips in the infill wall, the number and diameter of shear lugs can be determined.

To prevent concrete shear failure prior to yield developed in the shear lugs, total pipe yield capacity at each story should be less than the infill concrete cracking strength.

10.4 STRUCTURAL DETAIL

10.4.1 Infill wall

10.4.1.1 Precast Panel

According to forklift capability and building accessibility, acceptable panel size and panel weight can be determined. The thickness of precast infill wall panels is

decided by infill wall capacity design presented in Section 10.3. In any circumstance, the least panel thickness should be greater than 4.0". It is recommended that the longest dimension of a precast panel be not longer than 5 feet and its weight not greater than 1,000 pounds.

Shear keys along panel edges are strongly recommended for interpanel shear transfer. An aligned shear key pattern is recommended for key arrangement. It is also recommended that a ratio of key height to base width should be not greater than 0.5, and the base angle of the key should not be less than 45 °. Two layers of welded wire fabric are required for panel reinforcement. The reinforcement ratio should meet the minimum requirement of the current design codes.

10.4.1.2 Closure Strip

Closure strip detail design should be designed to have the following functions.

1) unite the precast reinforced concrete panels as a solid wall,

2) provide enough reinforcement within the closure strip to compensate for the reinforcement discontinuity between pre-cast reinforced concrete panels,

3) provide space for embedding shear lugs (dowels) between infill walls and existing frame elements,

4) provide out-of-plane resistance for the infill wall system, and

5) provide access for grouting closure strips through shear lug holes across the frame beams between stories .

A closure strip must be designed to have adequate size. Practically, the height of the closure strip must be greater than 4.0 in. to provide room for reinforcement placement and grout consolidation.

Reinforcement for closure strips should at least compensate for reinforcement discontinuity between panels, connect the infill to the existing frame structure, and keep the infill wall from out-of-plane swaying.

According to the reinforcement efficiency factor estimated in Section 4.2.2.2, a ratio of reinforcement to the panel section should not be less than 0.425% and not greater than 1.00%. The strength ratio of closure strip grout and panel concrete should not be less than 0.7 nor greater than 1.5.

10.4.2 Shear Lug

It is recommended that shear lug size be not greater than the infill thickness minus 2.0 in., and not be greater than 40% of the frame beam width. Total shear capacity of shear lugs in an infill wall should not be greater than the concrete cracking capacity of the infill wall.

Pipe embedment length is an important factor to permit shear lug strength development. The embedment length to the frame elements may be designed according to concrete bearing and pipe shear yield capacity following equation (5-2), which is,

$$L_{em} = \frac{V_p}{\phi \left(0.85\, f_c' \sqrt{\frac{A_2}{A_1}}\right) D_o} \qquad (10\text{-}19)$$

The embedment length for the base, on the other hand, will be designed to be either the strip reinforcement anchorage length or the factored embedment length L_{Beam} whichever is greater. The strip reinforcement anchorage required to develop yielding

will be determined according to ACI-318. The factored embedment length L_{Beam} is recommended as,

$$L_{Beam} = 1.5\, L_{em} \qquad (10\text{-}20)$$

10.4.3 Post-Tensioning Details

Post-tensioning tendons applied to boundary columns were designed to perform the following functions:

1) *Provide adequate flexural strength compatible with infill wall shear strength.*

2) *Provide prestress to column to prohibit premature splice failure.*

3) *Provide a net compressive stress on the infill to improve shear transfer across the horizontal interface, and to produce a system acting as a monolithic wall.*

4) *Permit flexural yielding to occur before a brittle failure occurs.*

5) *Provide system flexural ductility to the system.*

High-strength Dywidag steel or other high-strength steel is recommended for use as post-tensioning tendons. Tendons must be securely anchored to the structural foundation and the structure. At tendon anchorages, concrete bearing capacity must be checked according to ACI-318.

Post-tensioning tendons may be applied either continuously or segmentally. A connection coupler may be adopted when segment tendons are used. Tendons may be applied in different quantities between higher and lower story heights according to tensile force required for system flexural capacity design presented in Section 10.3.

10.5 SUMMARY

Design guidelines were developed according to structural performance of PTPW systems. All analytical models and equations were established based on connection specimen and model structure test results and theoretical analyses. The guidelines presented in this Chapter outline the research results of this project. For PTPW system retrofitting design following the guidelines, detailed analytical models and equations are provided in the previous chapters.

CHAPTER XI
CONCLUSIONS

11.1 INTRODUCTION

In seismic zones, many reinforced concrete moment-resisting frame structures are non-ductile systems. They do not have sufficient strength and deformation tolerance capacity to sustain earthquake loads. As discussed in Chapter II, several seismic rehabilitation techniques have proven to be constructible and feasible for many structures. However, the cost of such rehabilitation projects remains a major problem for many owners. The costs may involve not only the actual construction, but the expenses associated with relocation of operations and loss of rental revenue or production during the period of construction.

A post-tensioned precast infill wall (PTPW) system was developed that takes advantage of the shear strength of an infill wall to increase the shear capacity and the tensile strength of post-tensioning tendons to increase the flexural capacity of the frame systems. Through the use of precast wall panels to build infill walls, PTPW rehabilitation facilitates construction and eliminates time and space consuming procedures required for cast-in-place construction. Using PTPW retrofitting techniques will correct defects and weak links in a nonductile frame system, simplify the construction process, reduce the inconvenience of construction, and eliminate obstructions keeping the structure functioning during construction.

The project focused on studying the feasibility and methodology of PTPW system implementation and involved three phases of research: experimental investigation, computer analysis program modification and development, and foundation simulation.

Based on experimental results and computer simulation analysis, design and detailing guidelines were developed for PTPW retrofitting systems.

The first phase, experimental research, consisted of two stages of laboratory tests. In the first stage, structural connection tests, the behavior of closure strips and shear lugs were investigated. In the second stage, model structure tests, the overall behavior of a PTPW system and connection details and schemes developed in the first stage were assessed.

The second phase, computer program development, included program modification of a non-linear structural analysis program and computer simulation of structural experiments. Special analytic models for post-tensioning tendons and non-linear elastic hysteresis response models were developed for PTPW system analysis and design. A computer program IDARC-PT was developed for PTPW systems and it was demonstrated through simulation of structural experiments.

The third phase, foundation simulation, investigated the foundation performance and effects on PTPW systems. A mechanical model of the foundation was established to simulate the behavior of foundations subjected to uplift force subject to earthquakes. A structural model of the foundation was also developed for use with program IDARC-PT to simulate foundation effects on structural response and foundation-structure interaction. Effects of different foundation soil properties and earthquake excitations were studied through foundation simulations. Foundation/post-tensioning and foundation/infill wall interactions were also investigated by selecting different post-tensioning levels in the simulations.

Design procedures and various schemes for PTPW system implementation were studied through structural retrofit examples. Guidelines were developed for PTPW system design. Further topics were recommended for studies related to the PTPW retrofitting technique.

11.2 EXPERIMENTAL INVESTIGATION

11.2.1 Structural Connection Tests

11.2.1.2 Panel-Panel Connection (Closure Strip)

Fourteen specimens were tested to investigate behavior of the connection between adjacent precast panels. The specimens, representatives of interior wall joints, were tested by applying cyclic shear across the connection interface. In general, the response of a closure strip specimen could be categorized through three loading stages, cracking, yielding to ultimate, and residual strength. The cracking capacity depended on the concrete strength of the grout or the panel, whichever was the lower, and the cross section area of the specimen. The ultimate capacity was a function of the concrete strength and the amount of vertical reinforcement crossing the shear plane. After ultimate capacity was reached, there was a transition to a lower load plateau or residual capacity that was maintained through large slip levels. The residual capacity was maintained by shear friction which was directly dependent on the amount of vertical reinforcement, concrete strength and area of the section. The following conclusions were drawn from the test results:

1. Cracking originated at horizontal grout interfaces of the shear keys due to a reduction in effective shear section of the specimens.

2. The shear key configuration (alignment and spacing) had no significant effect on shear capacity at the interface.

3. The shear key size had insignificant effect on specimen behavior.

4. The strip height did not affect the specimen capacity but had a significant effect on reinforcing placement and closure strip fabrication.

5. The grout and panel concrete strength, whichever was lower, controlled the specimen capacity and failure surface location.

6. The peak and residual capacity of the specimen increased directly with the wall thickness.

7. The ratio of the vertical reinforcement controlled both the peak and residual capacities of the specimens.

Among the three stages of specimen capacity, cracking and residual are significant for the strength design of PTPW systems. The residual capacity could be determined using shear friction theory. Based on the studies, however, a revision of the shear friction provision of ACI-318 was recommended. The peak capacity could be evaluated as a function of the vertical strip reinforcement. The cracking capacity was determined using the effective section of shear keys.

11.2.1.2 Infill- Frame Connection (Shear Lug)

Four specimens were tested to investigate the connection between the precast infill wall panels to the existing frame elements. The specimens, representative of the wall boundary joints, were tested by applying cyclic shear along the frame boundary interface.

Like in closure strip specimen tests, response of the shear lug specimens was also categorized into three stages: cohesion, yielding to ultimate, and residual or friction strength at large deformations. However, the shear lug specimens behaved differently from closure strip specimens because the shear keys were replaced by a steel pipe embedded into the elements on both sides of the closure strip. Unlike cracking in closure strip specimens, cohesive failure occurred much earlier with lower loading capacity along the closure strip-frame interface. After reaching a peak capacity, there was a transition to a lower load plateau or residual capacity that was maintained at a nearly constant level to extremely large slips. Conclusions were made as following:

1. Cohesive strength of the connection is dependent on the concrete strength of the grout and the cross section of the shear lug (steel pie) at the interface.

2. Ultimate strength of the connection was dependent on pipe cross section, pipe embedment length, and vertical strip reinforcement.

3. Residual strength of the connection specimen was also dependent on the vertical strip reinforcement, the steel pipe section and pipe embedment length.

4. The pipe embedment length contributed significantly to the specimen strength development.

The cohesive strength was estimated using a procedure developed in Chapter IV. The peak and residual strengths of frame-infill connections were primarily dependent on the pipe cross section. However, proper embedment was required to develop shear yielding of

the pipe. Lack of embedment can result in flexural failure of the pipe that may reduce the capacity of the connection. Pipe embedment lengths should be determined on the basis of concrete bearing and development of pipe shear yielding.

11.2.2 Model Structural Test

A two-story nonductile frame was constructed and rehabilitated with the precast infill wall and post-tensioning system developed in this research. The model structure was constructed with typical details of 1950's and 60's construction. The model structure had two columns spaced at 13 ft. - 4 in. and floor heights of 8 ft. which corresponded with a 2/3 scale for typical moment-frame buildings investigated. Infill walls of 6 in. and 4 in. thickness were provided in the first and second story respectively.

11.2.2.1 Existing Frame

The existing frame was tested to determine its overall behavior and to produce cracking at critical sections in the frame elements to simulate conditions likely prior to rehabilitation. The structure was loaded with an inverted triangular distribution simulating earthquake effects, and behaved as predicted by analytical modeling. Analysis and testing demonstrated that the structure had low lateral resistance and was nonductile. Therefore, structural rehabilitation was required to upgrade the structure to provide sufficient lateral capacity.

11.2.2.2 Model Structure

To evaluate the behavior of the precast infill wall and the post-tensioning system used to restore column tensile strength and system lateral capacity, three tests were

conducted. In Test I, flexure dominated structural behavior. In Test II, shear dominated the structural behavior. In Test III, the ultimate system shear was determined. Loads were cyclically applied to the floor slabs in an inverted triangular distribution to simulate earthquake effects. Effects of primary variables including the amount of post-tensioning tendons and initial post-tensioning loads were investigated. Through the model structure tests, structural connection behavior observed in the first stage of the experiment was further verified and the performance of closure strips, shear lugs and precast panels in a PTPW system was investigated.

Performance of Infill Wall and Connections The precast infill wall performed exceptionally well practically like a monolithic wall system. Diagonal cracks were continuous through panels and closure strips. There was no indication of distress along grout strips. Shear cracking extended along a line from the "toe" of the wall to the top post-tensioning anchorage. There was some cracking concentrated around the pipe shear lugs between the wall and frame. It was demonstrated that all structural connections, closure strips and shear lugs, worked exceptionally well in the PTPW system.

Performance of Post-Tensioning Tendons The post-tensioning tendons played a significant part in the PTPW system. Testing demonstrated that splice failure of the column reinforcement at the base of the existing frame column could be controlled by selecting the number of post-tensioning tendons and initial post-tensioning force. By varying the number of post-tensioning tendons and the level of initial post-tensioning, the PTPW system response mechanism could also be controlled or changed.

Flexural Capacity Under relatively low initial post-tensioning, the structural response was dominated by flexure. The flexural response developed in three stages:

flexural-cracking, splice failure, and yielding of the post-tensioning tendons. Column decompression (loss of compression under initial post-tensioning) was reached prior to flexural-cracking. After column reinforcement splice failure occurred, the tendons sustained the system moment and yielded as load increased. The response could be characterized by behavior pertaining to the three stages discussed.

It was recommended that PTPW system flexural capacity design follow the three limit state design philosophy corresponding to the three stages of behavior. Equations were developed for design of infill walls, selection of post-tensioning tendons and initial post-tensioning force for each stage of behavior.

Shear Capacity With more tendons and higher initial post-tensioning, the structure behaved in a shear-dominated mode. With different structural performance, infill shear and system shear were developed under lateral loads.

Infill shear capacity was first reached and cracking occurred at a level close to the design shear capacity of the infill wall. Crack patterns indicated that the wall behaved as a monolithic wall even though it was constructed of multiple precast panels. It was also shown that a diagonal compression strut was formed within the infill. The structure was changed from a frame-infill system to a braced frame system after infill wall shear strength was reached and the compression strut formed.

System shear capacity was reached under zero initial post-tensioning. Because a compression strut formed, the system carried higher shear beyond the estimated infill shear capacity. The term "system shear capacity" was used to represent the shear strength beyond infill shear capacity. Under further load, system shear capacity was reached when concrete crushed at the top of the primary compression strut. Because the system shear capacity was

higher than the infill shear capacity, slip developed at the base of the structure. Due to slip, shear friction developed under vertical force provided by post-tensioning tendons. Shear friction provided high shear capacity at the infill-base interface so that the system sustained a system shear much higher than the infill shear capacity.

Equations were developed for infill and system shear capacity evaluation. The shear friction equation developed in Chapter VI was successfully used to evaluate infill wall shear capacity at the infill-base interface by including post-tensioning tendons as vertical reinforcement. The system shear capacity model was established using the compression strut geometry and loading and boundary conditions.

11.3. IDARC-PT DEVELOPMENT AND TEST SIMULATION

11.3.1 Analytic Model of PTPW System

To reflect the real behavior of the PTPW system in test simulations or system rehabilitation design calculations, a non-linear structural analysis program was needed for the PTPW system. Because of advantages in input schemes, system assembly, and incorporation of hysteresis response models, program IDARC was chosen to be modified for PTPW system analysis.

Mistakes in program IDARC were detected and corrected. To meet the special analysis requirements for PTPW systems, new analytic models for structural elements and hysteresis models were established and added to IDARC to produce IDARC-PT. The new analytical models include:

1. A special truss member to simulate post-tensioning tendons which can be initially post-tensioned.

2. An inelastic spring element to simulate the frame boundary column which can behave with different stiffness and capacity in compression and tension, and is subject to potential splice failure.

3. Non-linear elastic hysteresis model to reflect post-tensioning effects and ductile behavior of PTPW systems that can simulate characteristics of the model test structure.

4 Variable damping to simulate changing damping characteristics of a non-linear structural system.

The capabilities of IDARC-PT were demonstrated with structural examples.

11.3.2 Structural Test Simulation

Using program IDARC-PT, model structural test simulations were conducted. The simulations included the existing frame test, and model structural flexural test and shear test. The simulation results of IDARC-PT matched the experiment results quite well for every test. This demonstrated that the non-linear structural analysis program IDARC-PT is a valuable tool by which a PTPW system behavior can be correctly evaluated and the structural seismic response can be accurately calculated. IDARC-PT is recommended for use in performing damage limit state and collapse limit state analysis, and design of PTPW systems.

In analyzing a PTPW system using IDARC-PT, the key factor is the post-tensioning parameter PT for non-linear elastic response simulation. Generally speaking, the parameter PT is a function of the ratio of the post-tensioning tendons to the infill wall section, ratio of initial post-tensioning force to the tendon capacity, and the ratio of infill wall width to the structure height. In other words, the non-linear hysteretic response of a PTPW system is dependent on the strain energy conservation in the post-tensioning tendons and strain energy dissipation in the concrete infill walls. A value of 0.1 to 0.5 is recommended as the post-tensioning parameter PT. It is also recommended that a small integration time step be used in PTPW system analysis using program IDARC-PT.

11.4. FOUNDATION SIMULATION

11.4.1 Analytical Model of Foundation

Because large post-tensioning forces act on the foundation of the frame in which the infill wall is added, the foundation may uplift. To simulate foundation response, an analytical foundation model was established using soil properties and foundation behavior under uplift forces. A foundation response curve was modeled as an inelastic spring which has different tensile and compression capacities. Foundation tensile capacity was simulated with the following steps:

1. Initial capacity includes both foundation weight and soil overlaying on the foundation. Foundation stiffness in compression was used for initial stiffness in both compression and tension.

2. Uplift capacity of soil was developed using a soil rupture mechanism and the soil cohesive strength around the foundation. The shear stiffness was adopted as rupture stiffness over the rupture surface.

3. Nominal ultimate capacity of the foundation was estimated as its rupture capacity plus the assistance from neighboring footings. The ultimate stiffness was also obtained from neighboring footing interaction.

By adding a foundation model to a PTPW system, structural analysis including foundation properties could be conducted. The structural model coupled with the foundation model was used to study foundation / structural interaction.

11.4.2 Foundation Effects

Four different foundation types (firm, soft, very soft and extremely soft soil bases) were studied with an identical superstructure retrofitted with the PTPW technique. The simulation results indicated that:

1. The softer the soil base, the longer the period of structural response;

2. The softer the soil base, the smaller the structural acceleration under relatively short-period earthquakes or the larger the structural acceleration under relatively longer-period earthquakes;

3. The softer the soil base, the larger the structural displacement;

4. The softer the soil base, the higher the base shear for structures subjected to long-period earthquakes, or the lower the base shear subjected to short-period earthquakes.

5. The softer the soil base, the less effective the post-tensioning.

Three earthquake records, the TAFT ground motion, and the 1985 Mexico city ground motions Mexican-2D and Mexican-9S were applied to an identical superstructure on four different soil types. Peak accelerations of earthquake records were normalized as either 0.33g or 0.22g.

Post-tensioning effects were also studied by applying different levels/conditions of post-tensioning to an identical structure on an identical soil base. In the first condition, no post-tensioning tendons were applied. Three conditions simulated different initial post-tensioning levels with identical post-tensioning tendons. The results indicated that post-tensioning was required to maintain boundary column capacity and to prevent splice failure. However, the post-tensioning efficiency declined as the soil base softened.

Different retrofitting arrangements were also studied for the same frame system to investigate methods for reducing or eliminating foundation effects. By arranging the infill wall location or distributing infill shear wall over the system plan, foundation effects can be reduced or eliminated.

According to foundation simulation, general comments were proposed and foundation effect simulation was recommended in the design guidelines for PTPW system retrofitting analysis and design.

11.5 DESIGN GUIDELINE DEVELOPMENT

Design and detailing guidelines for precast infill wall systems were developed to provide designers with a design scheme and procedure for retrofitting reinforced concrete frames using PTPW systems.

The guidelines presented in Chapter X consist of discussions on design philosophy, strategy, targets and schemes. The most useful part of the guidelines is the capacity design for PTPW systems which includes:

1. Precast panel design and infill wall shear capacity design.
2. Structural connection design consisting of closure strips and shear lugs.
3. PTPW system flexural strength design including evaluating the load capacity at flexural-cracking, splice failure and post-tensioning yielding.
4. PTPW system shear strength design consisting of infill shear, system shear and base shear friction capacity determination.
5. Design of post-tensioning tendons and corresponding initial post-tensioning in accordance with structural system and foundation properties.
6. Simulation of structural response considering foundation involvement with foundation mechanical and structural analytical models.

The guidelines developed from test results and analytical studies provided a comprehensive scheme and design procedure for PTPW systems. Analytical models, equations and computer program IDARC-PT can be used in the design process. Following the design guidelines, a PTPW system can be analyzed and designed properly.

11.6 FUTURE RESEARCH

The research presented in this report was developed for retrofitting nonductile concrete moment-frame structures since they are identified as a threat to life safety. Due to time and cost limitation, some topics related to PTPW system implementation have not been studied. In order to successfully apply PTPW retrofitting techniques and widen the use of research results of this project, some topics are recommended for further study.

11.6.1 Post-Tensioning Tendon Anchorage

In this project, research was conducted based on the assumption that the post-tensioning tendons were securely anchored to the structural foundation. How or by what schemes the tendons are anchored to the foundation has not been studied. As discussed in Chapter IX, post-tensioning is required for a PTPW retrofitting system. However, without secure anchorage, post-tensioning tendons not can provide the system with increased moment capacity and, consequently, the retrofit fails.

Applying post-tensioning to a frame infill wall system, the tendons must be securely anchored to the foundation. How to anchor the post-tensioning tendons to the foundation is an important topic to be studied. Anchorage construction schemes, details, materials and capacity evaluation are concrete targets in the study.

11.6.2 Upgrade Post-Tensioning Model

Though PTPW system analysis can be performed through the use of non-linear structural analysis program IDARC-PT developed in this project, the non-linear elastic model of structural response has not been comprehensively studied due to time and budget limitations. The experiment simulation was conducted through the use of a post-tensioning

factor PT which was selected and calibrated according to model structural test results. Without test results, the post-tensioning factor may be determined based on engineering judgment. Improper engineering judgment or unreasonable use of a post-tensioning factor will result in incorrect simulation results. Determining a post-tensioning factor based on actual structural behavior and upgrading the non-linear elastic model is necessary.

As mentioned in Chapter VII, the non-linear elastic behavior of PTPW system response was caused by the combination of elastic properties of the post-tensioning tendons and the hysteretic behavior of the reinforced concrete elements. The value of post-tensioning factor PT is dependent on the ratio of the total energy dissipation of concrete elements and the total energy conservation of post-tensioning tendons in the process of energy transformation from structural vibration to element deformation.

To realistically model the hysteretic response of a PTPW system, a relationship between the post-tensioning parameter PT and energy dissipation in reinforced concrete members and energy conservation in the post-tensioning tendons should be studied. Once the relationship is established, the non-linear elastic hysteretic response model can be upgraded.

11.6.3 Application of Post-Tensioning Model

The hysteretic model of PTPW system analysis can also be applied to a prestressed reinforced concrete structural system because prestressing has the same function as post-tensioning to restore energy in a structural system. Post-tensioning or prestress effects on the structural non-linear elastic behavior is a valuable topic to be studied.

The study will benefit structural analysis and design not only for PTPW systems but also for any structural system including post-tensioning or prestressed elements. Studies on the hysteretic behavior of a prestressed reinforced concrete structural system can be conducted if the post-tensioning model is upgraded. The study may be conducted theoretically to establish the energy conservation and dissipation relations between prestressed tendons and concrete elements. Some structural experiments may be necessary to verify the analytical results.

11.6.3 Application of Foundation Simulation

Foundation simulations conducted in this project indicated that the foundation properties significantly affect structural seismic response. However, structural seismic analysis is generally based on the assumption that structures are built on a rigid foundation. This is neither correct nor conservative. In fact, a soft soil base tends to amplify the structural response. By assuming a rigid foundation, analytical results greatly underestimate the structural response or potential structural danger due to earthquakes.

To realistically analyze seismic response, foundation effects must be considered. It is recommended that a foundation model be established and included in structural seismic analysis. The model of the footing foundation established in this project can be adapted to a structural system regardless of post-tensioning involvement.

Research should be conducted to establish foundation analytical models for any other types of foundation structures. Soil cohesive strength and soil rupture mechanisms developed in this project can be used for other types of foundations. It is recommended

that structural analysis programs include with foundation models for general earthquake response analysis and structural design.

11.7 CONCLUSION

The post-tensioned precast infill wall (PTPW) system studied in this research project may eliminate many of the costly and time-consuming procedures currently used in cast-in-place infill wall construction. PTPW systems can reduce overall costs[57] in rehabilitating existing structures and allow the rehabilitation to be tailored to the requirements of the owner. Furthermore, the system can be used to decrease nonstructural damage and costs associated with damage and to increase life safety.

Through structural experiments and computer simulations, a PTPW retrofitting technique was developed. This technique provides structural professionals with a valuable scheme that offers the potential to correct many structural defects and weak links associated with existing non-earthquake resistance structures. Design guidelines developed provide engineers with a procedure and method to analyze and design a PTPW system.

The recommendations for further research are based on the research and problems associated with the PTPW system in this project. Structural engineering and technology has been developing through valuable scientific research and engineering practice. It is hoped that the recommended research topics will be undertaken and the mentioned problems listed will be solved in the near future.

APPENDIX A

STRUCTURAL CONNECTION TEST DATA

A.1 CLOSURE STRIP SPECIMENS

A.1.1 Variables of Closure Strip Specimens

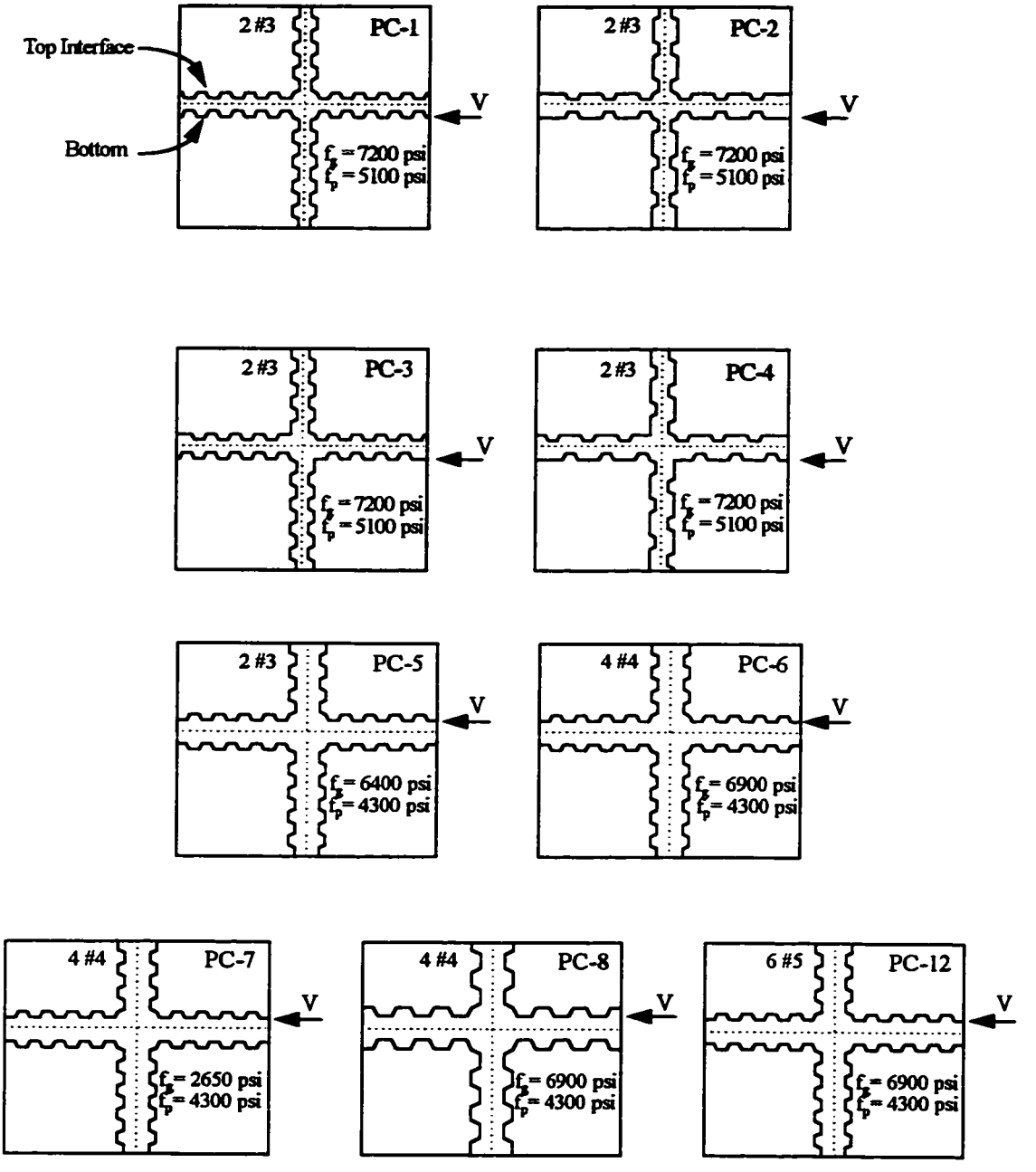

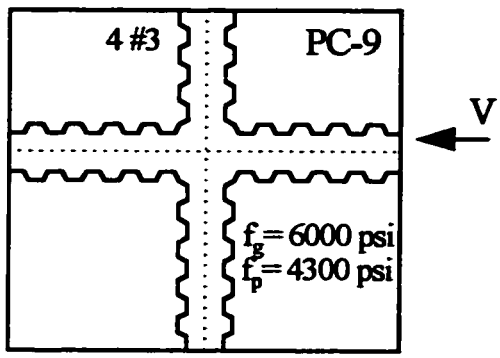
4 #3
PC-9
V
f_g = 6000 psi
f_p = 4300 psi

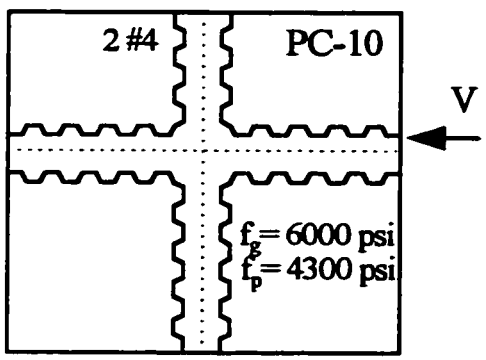
2 #4
PC-10
V
f_g = 6000 psi
f_p = 4300 psi

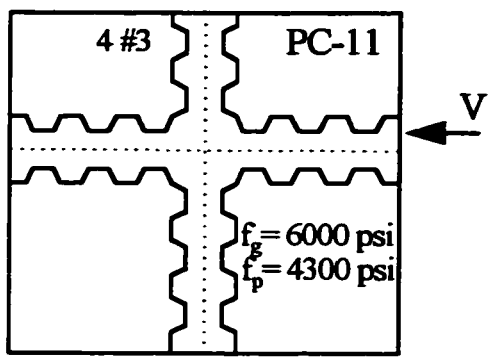
4 #3
PC-11
V
f_g = 6000 psi
f_p = 4300 psi

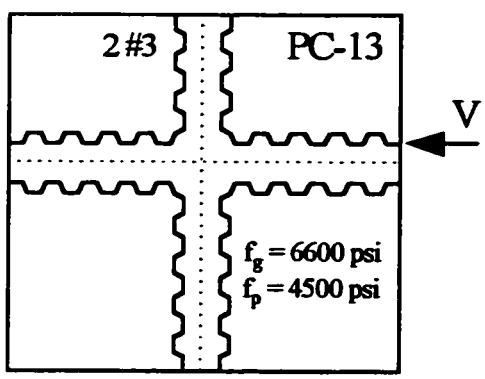
2 #3
PC-13
V
f_g = 6600 psi
f_p = 4500 psi

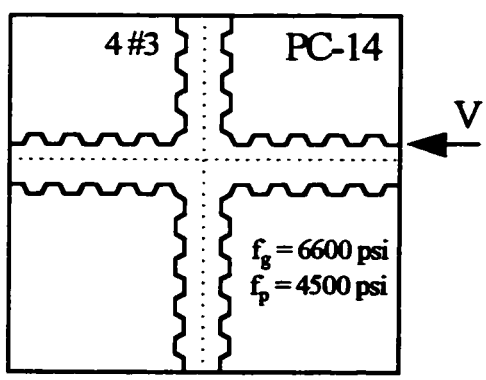
4 #3
PC-14
V
f_g = 6600 psi
f_p = 4500 psi

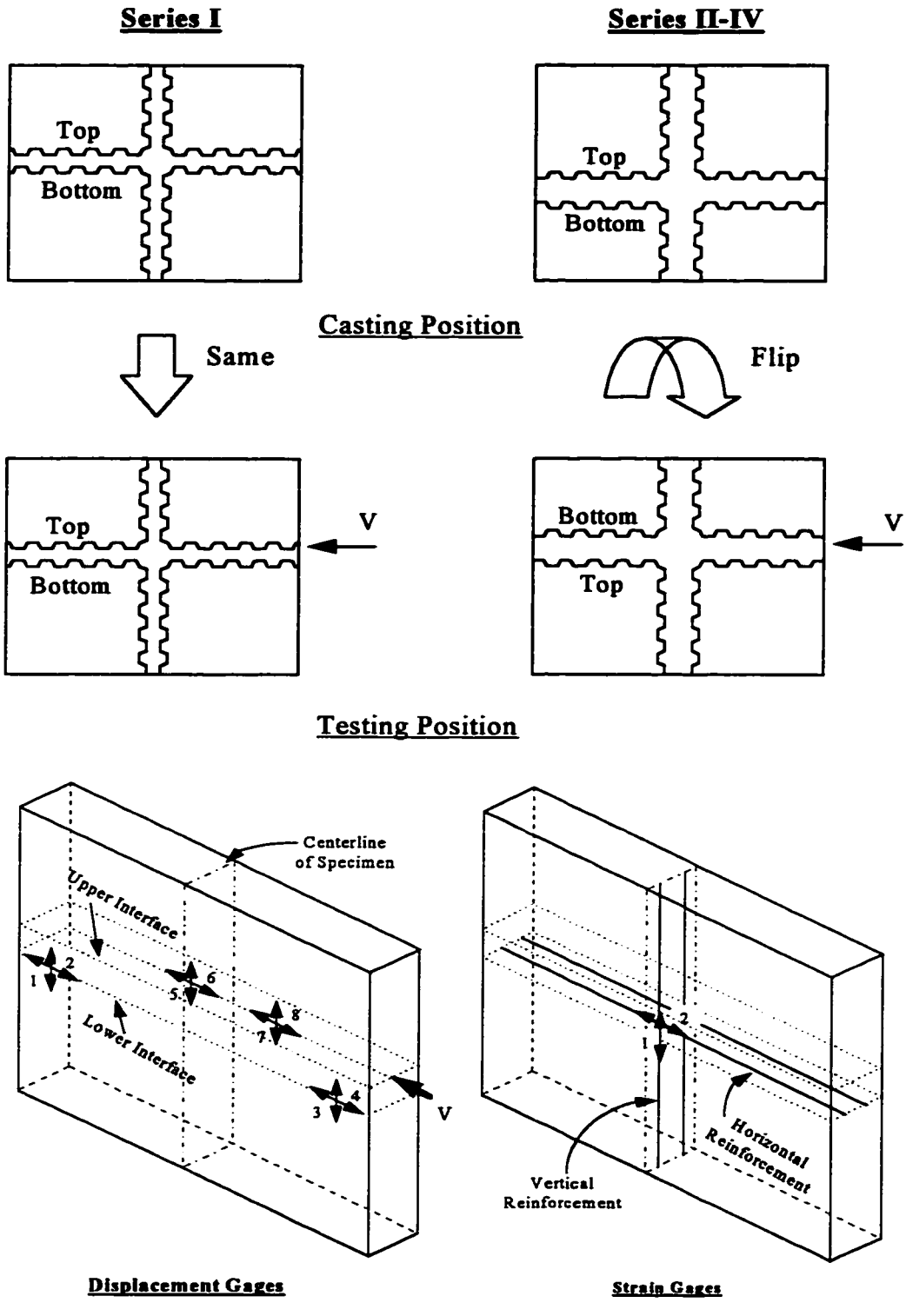
Series I
Series II-IV
Top
Bottom
Top
Bottom
Casting Position
Same
Flip
Top
Bottom
V
Bottom
Top
V
Testing Position
Centerline of Specimen
Upper Interface
Lower Interface
1
2
3
4
5
6
7
8
V
1
2
Horizontal Reinforcement
Vertical Reinforcement
Displacement Gages
Strain Gages

A.1.2 Test Results of Closure Strip Specimens

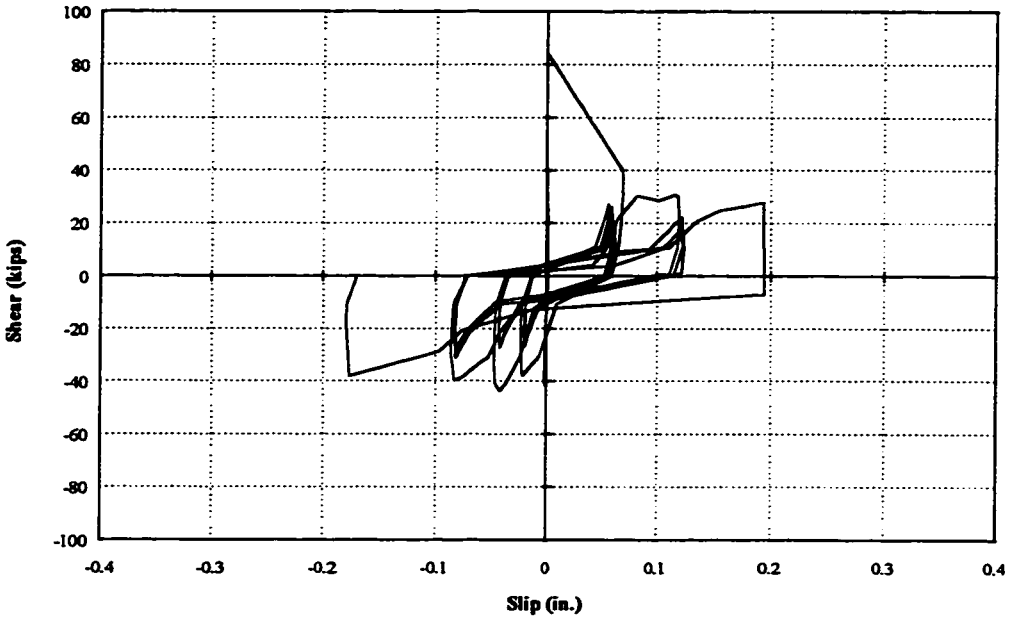

Figure A-1.1 Test Result of PC-1

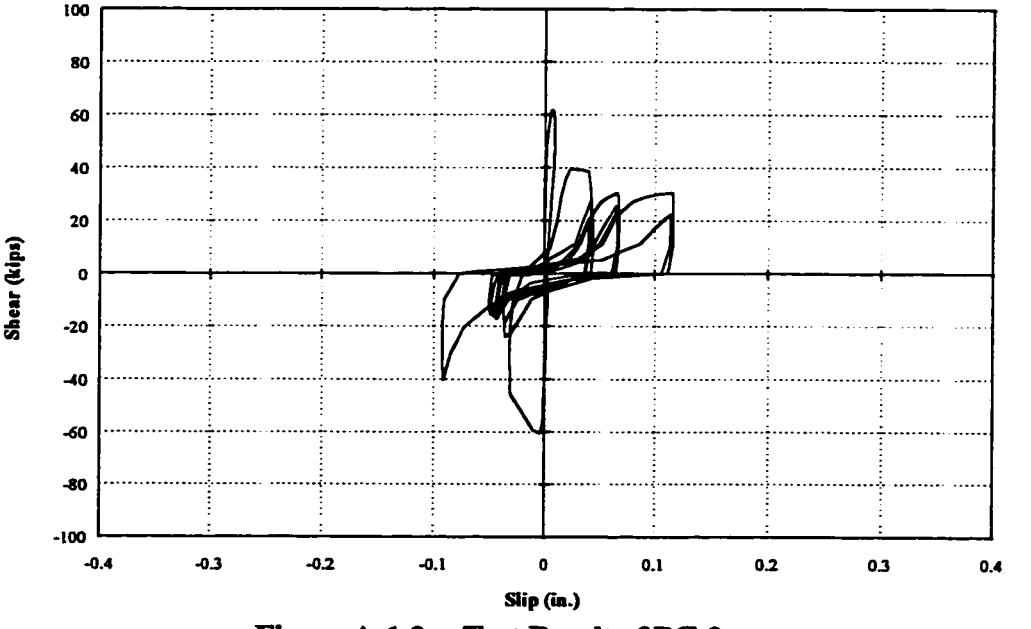

Figure A-1.2 Test Result of PC-2

Figure A-1.3 Test Result of PC-3

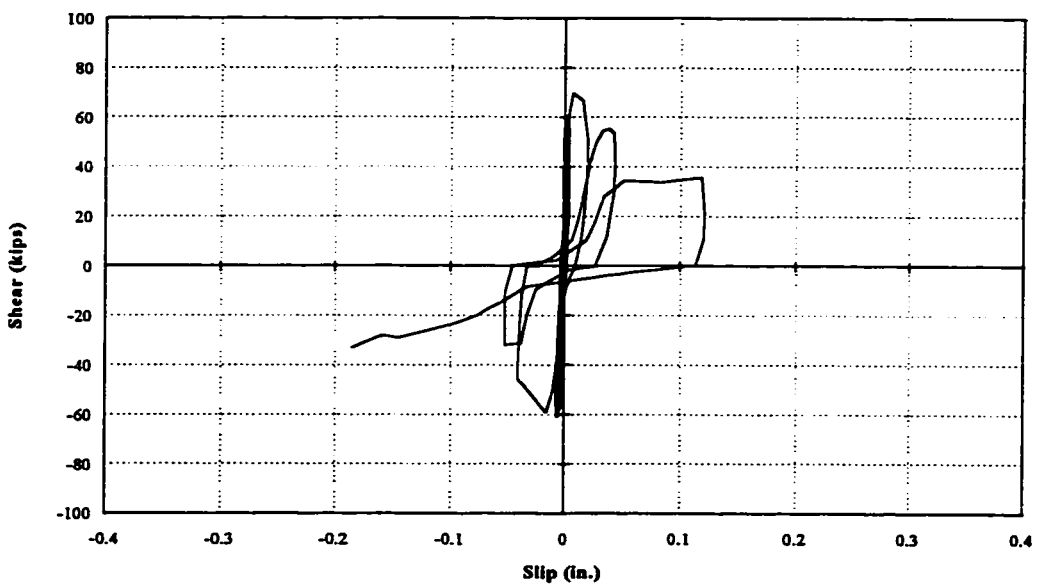

Figure A-1.4 Test Result of PC-4

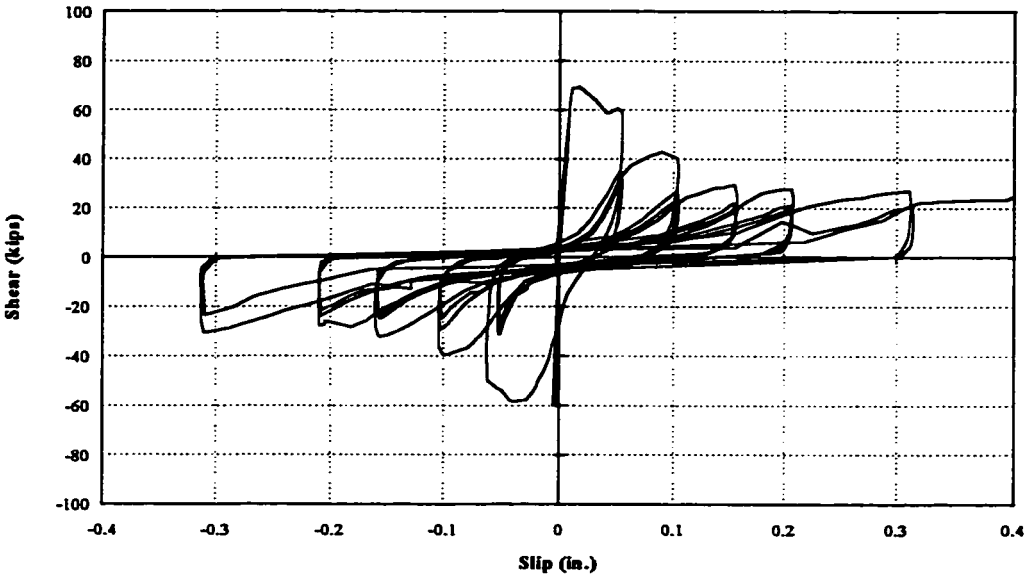

Figure A-1.5 Test Result of PC-5

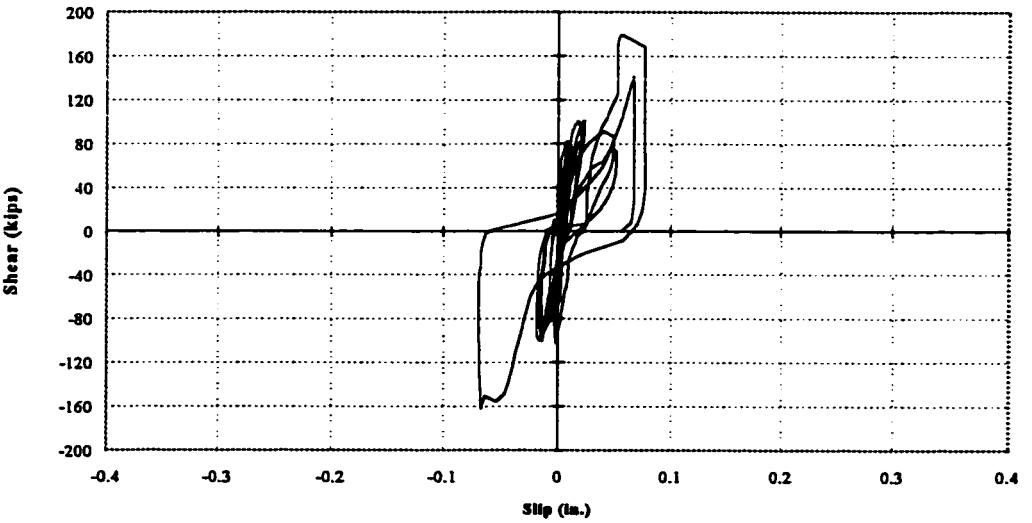

Figure A-1.6 Test Result of PC-6

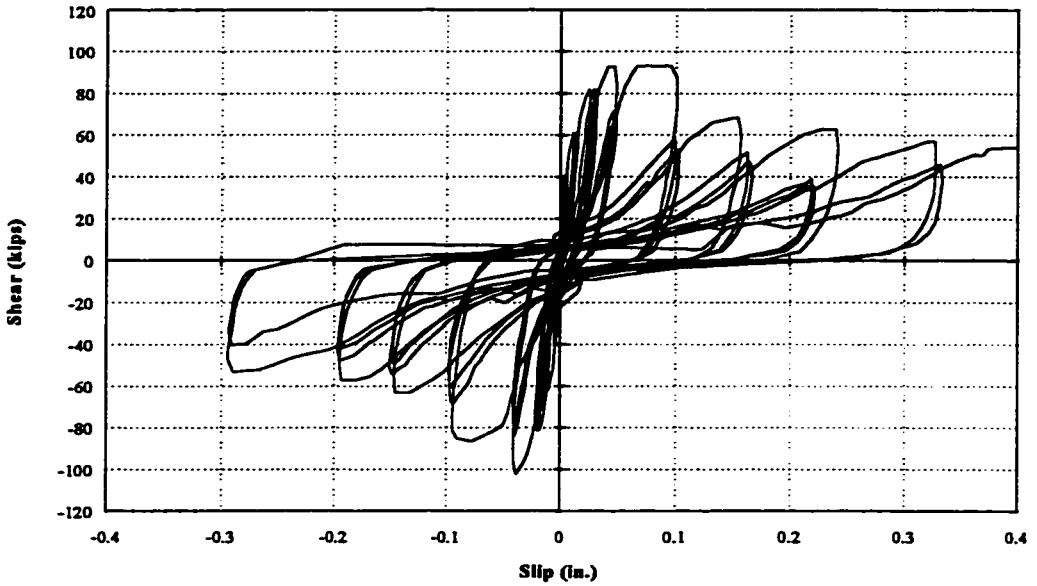

Figure A-1.7 Test Result of PC-7

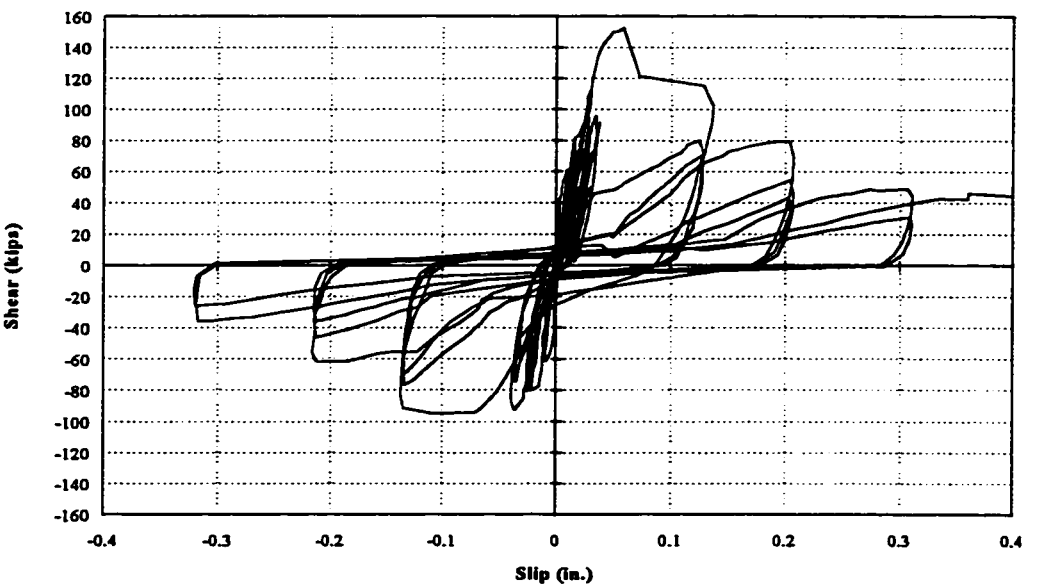

Figure A-1.8 Test Result of PC-8

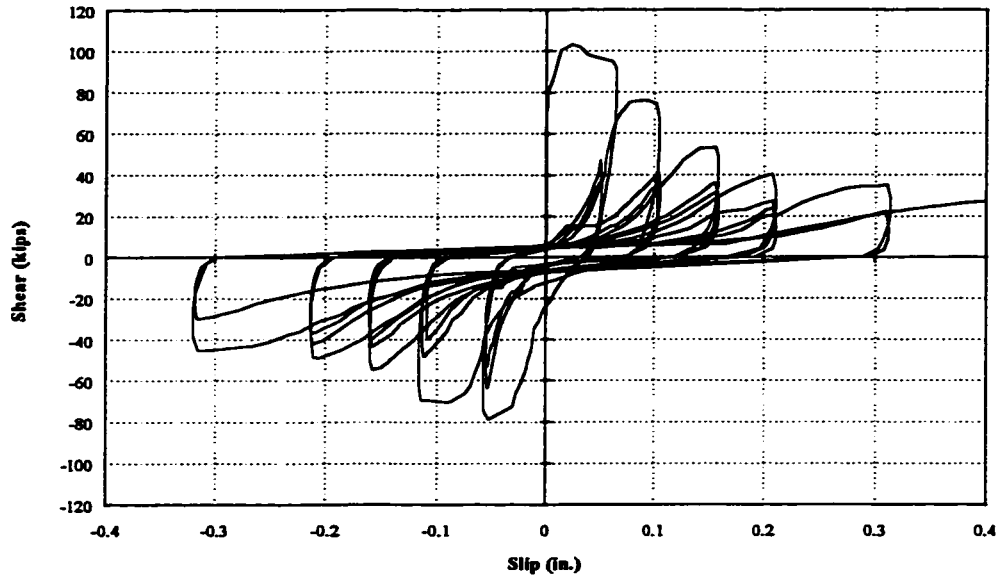

Figure A-1.9 Test Result of PC-9

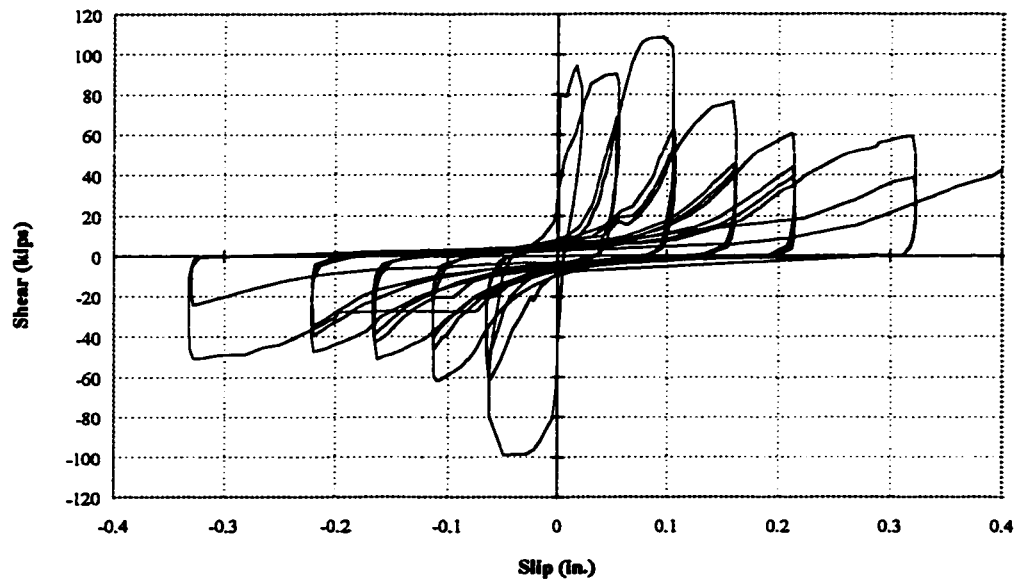

Figure A-1.10 Test Result of PC-10

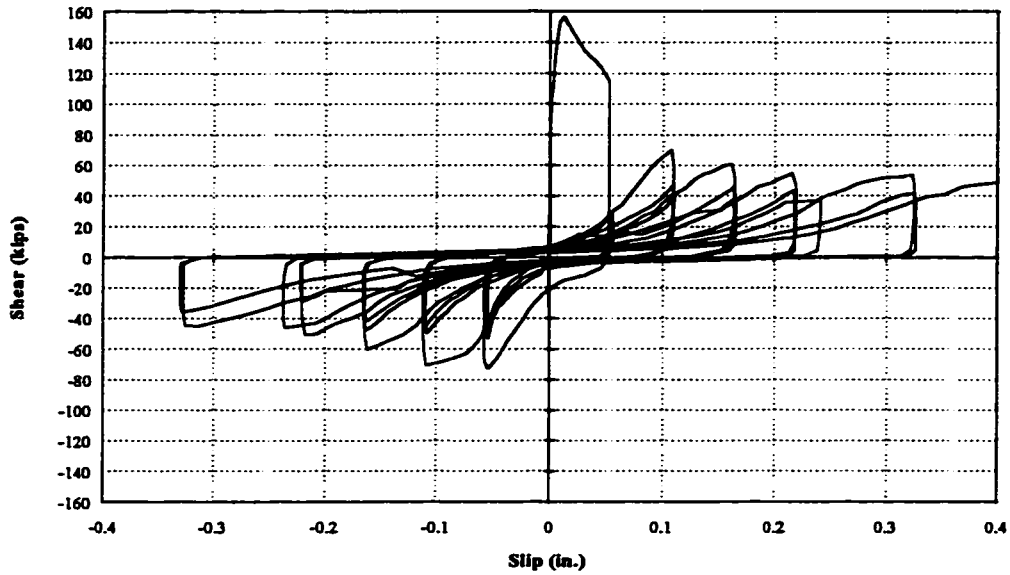

Figure A-1.11 Test Result of PC-11

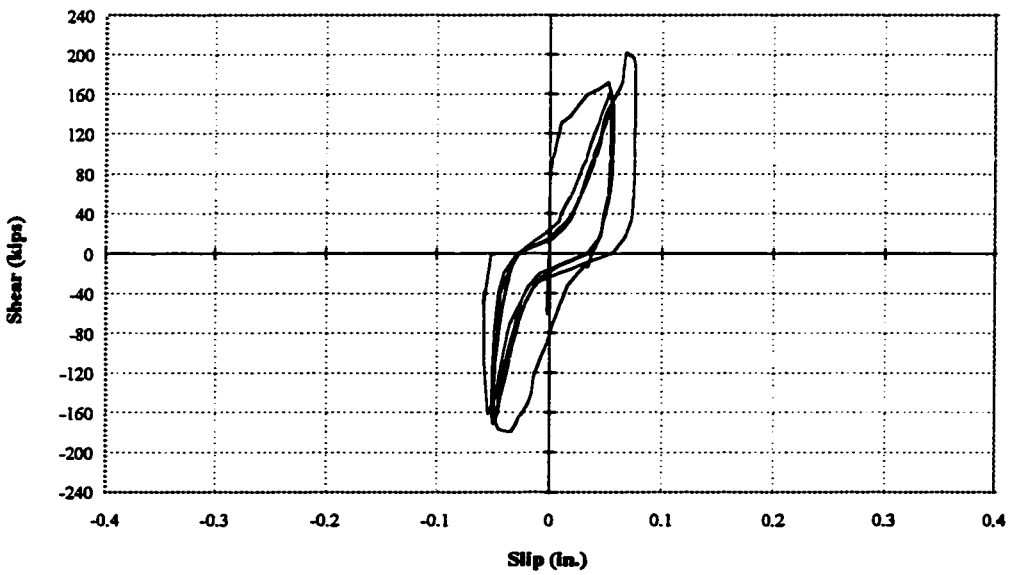

Figure A-1.12 Test Result of PC-12

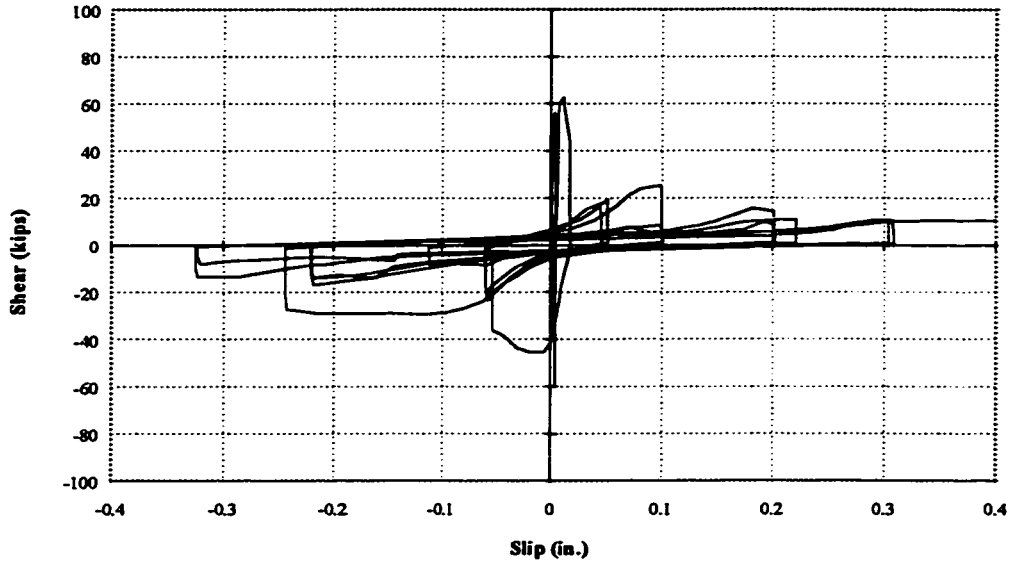

Figure A-1.13 Test Result of PC-13

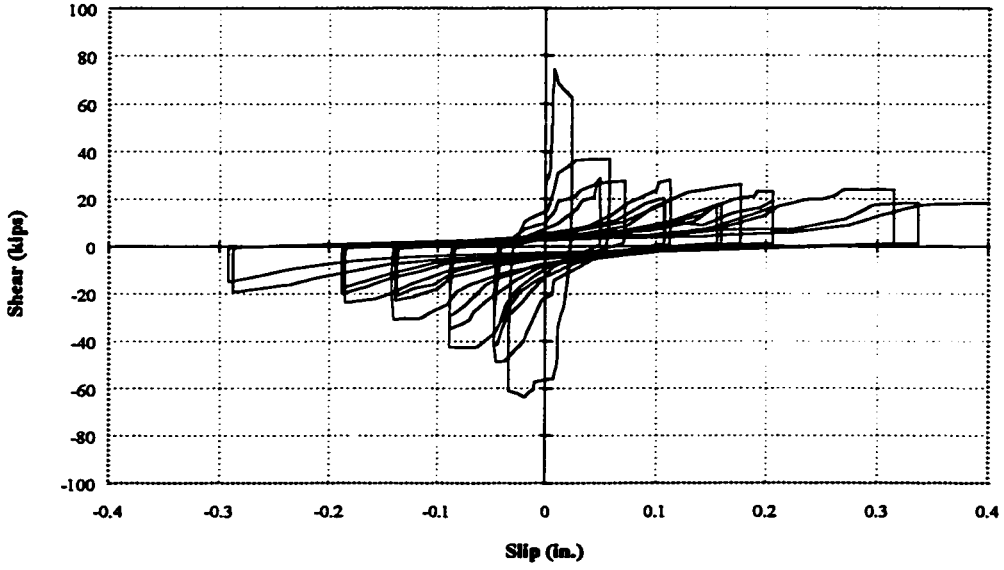

Figure A-1.14 Test Result of PC-14

A.2 SHEAR LUG SPECIMENS

A.2.1 Variables of Shear Lug Specimens

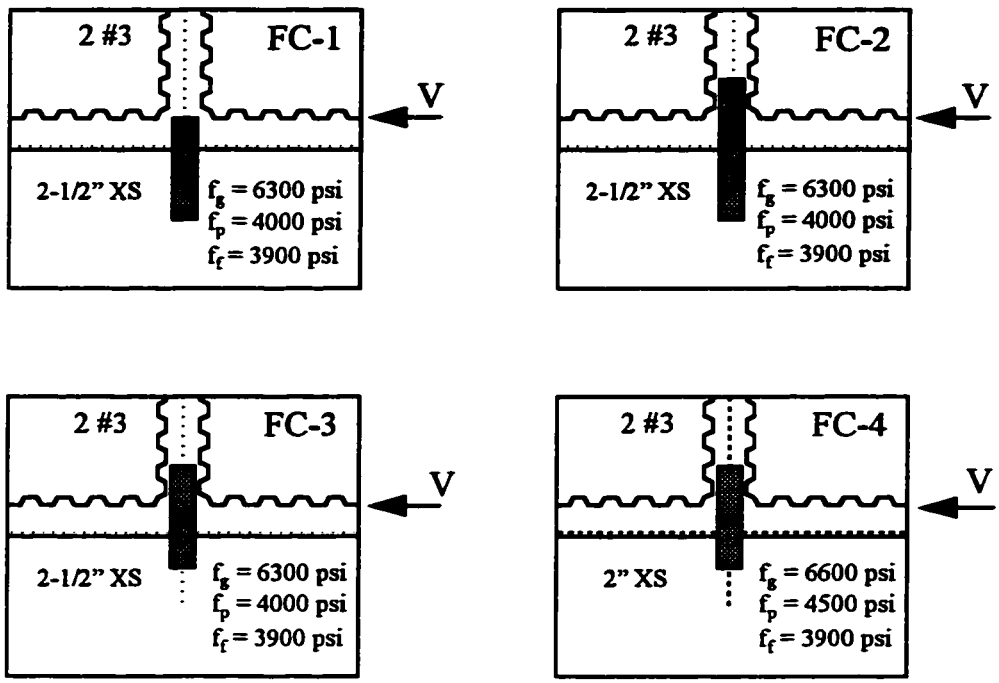

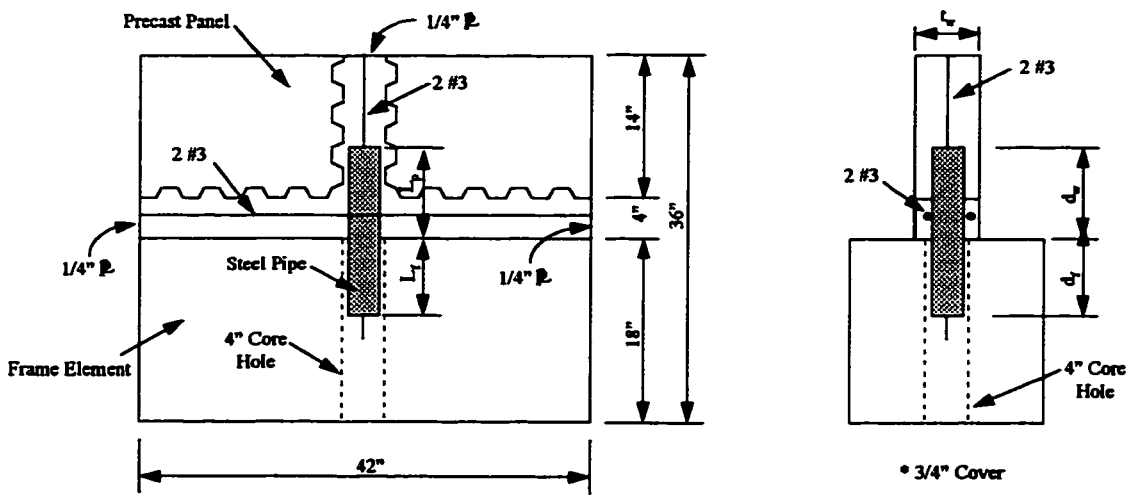

A.2.2 Test Results of Shear Lug Specimens

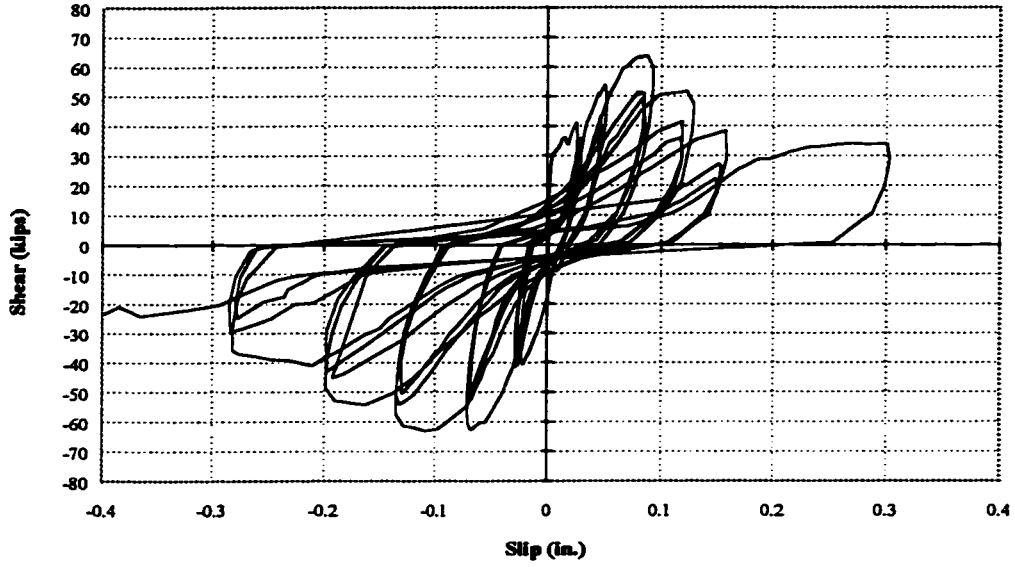

Figure A-1.15 Test Result of FC-1

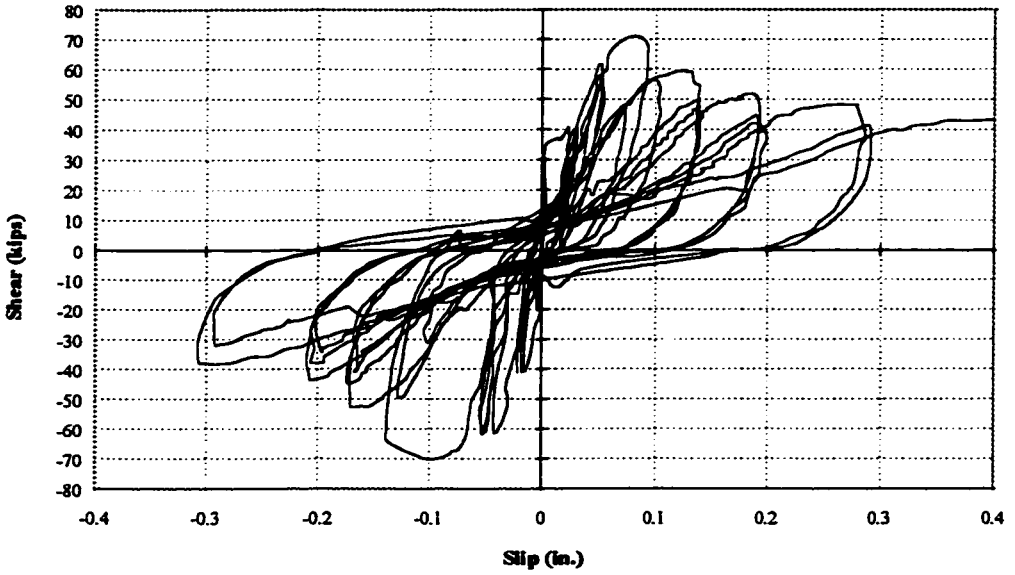

Figure A-1.16 Test Result of FC-2

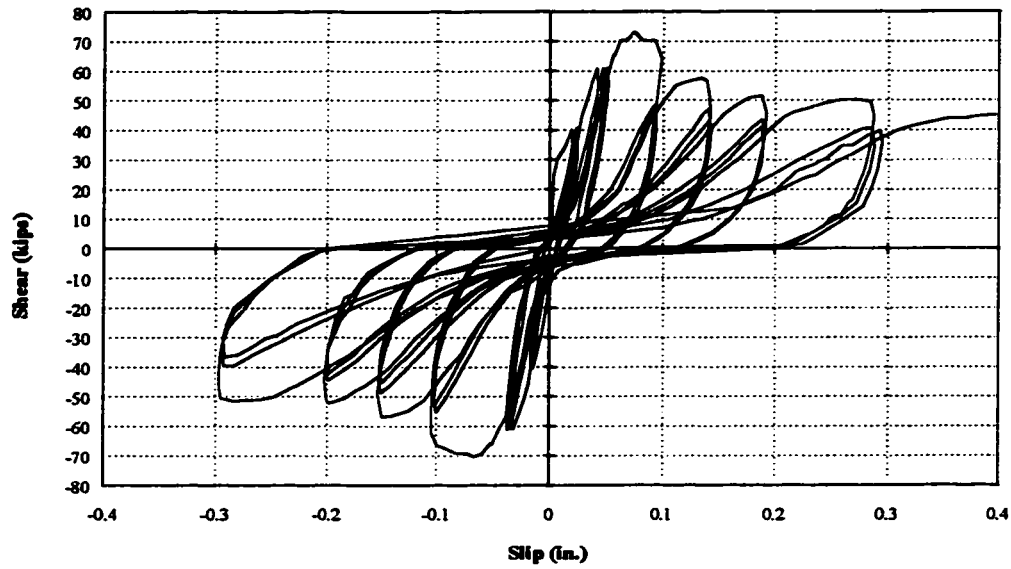

Figure A-1.17 Test Result of FC-3

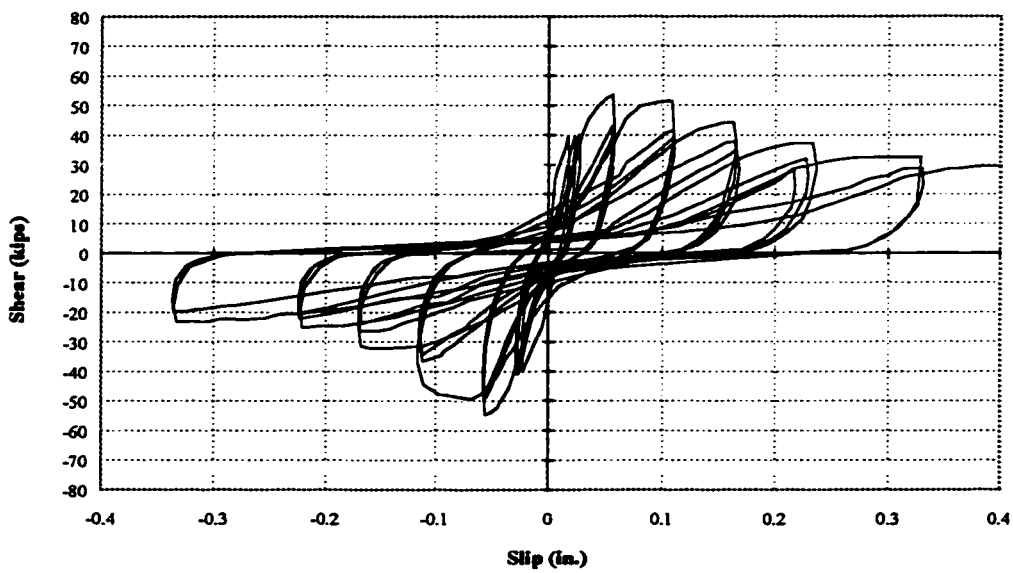

Figure A-1.18 Test Result of FC-4

APPENDIX B

MODEL STRUCTURE TEST DATA

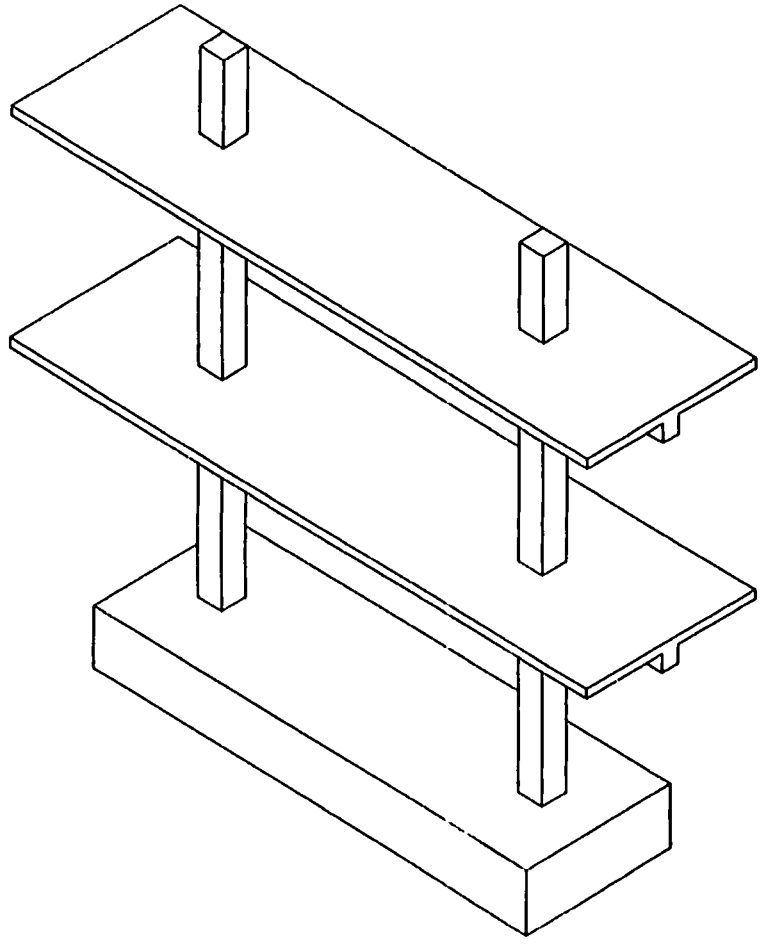

GENERAL NOTES

1. All concrete work shall be in accordance with ACI standard specifications for concrete and reinforced concrete.
2. All concrete shall be normal weight and shall test 3000 psi at 28 days.
3. Reinforcing steel shall be A.S.T.M. Grade 60 deformed bars. Reinforcing steel for the second and third floor slabs shall consist of 4x4-W2.9xW2.9 welded wire fabric with a yield strength of 60,000 psi.
   Detail Reinforcing steel in accordance with the A.C.I. Manual of Standard Practice for Detailing Reinforced Concrete Structures.
4. All structural steel shall be ASTM A572-Grade 50
5. All structural steel shall be manufactured and fabricated in accordance with the latest A.I.S.C. specifications.
6. All welds shall be with E70XX Electrodes.
7. Footing and slabs designed in accordance with ACI 318-89.
   Building frame designed in accordance with ACI 318-56.
8. Design loads:
   Loads in addition to structural weight include the following:

Frame	DL:	Partitions	20psf
		Clg/finish	10psf
		Services	5psf
		Miscellaneous	7psf
	LL:	50psf	
Slab	LL:	50psf	
Footing	400k lateral.		

Existing Nonductile Frame Isometric View	
Project Title: RC Frame Systems	
Dwg: STR-1	Sheet 1 of 10
Ferguson Structural Engineering Laboratory University of Texas at Austin	

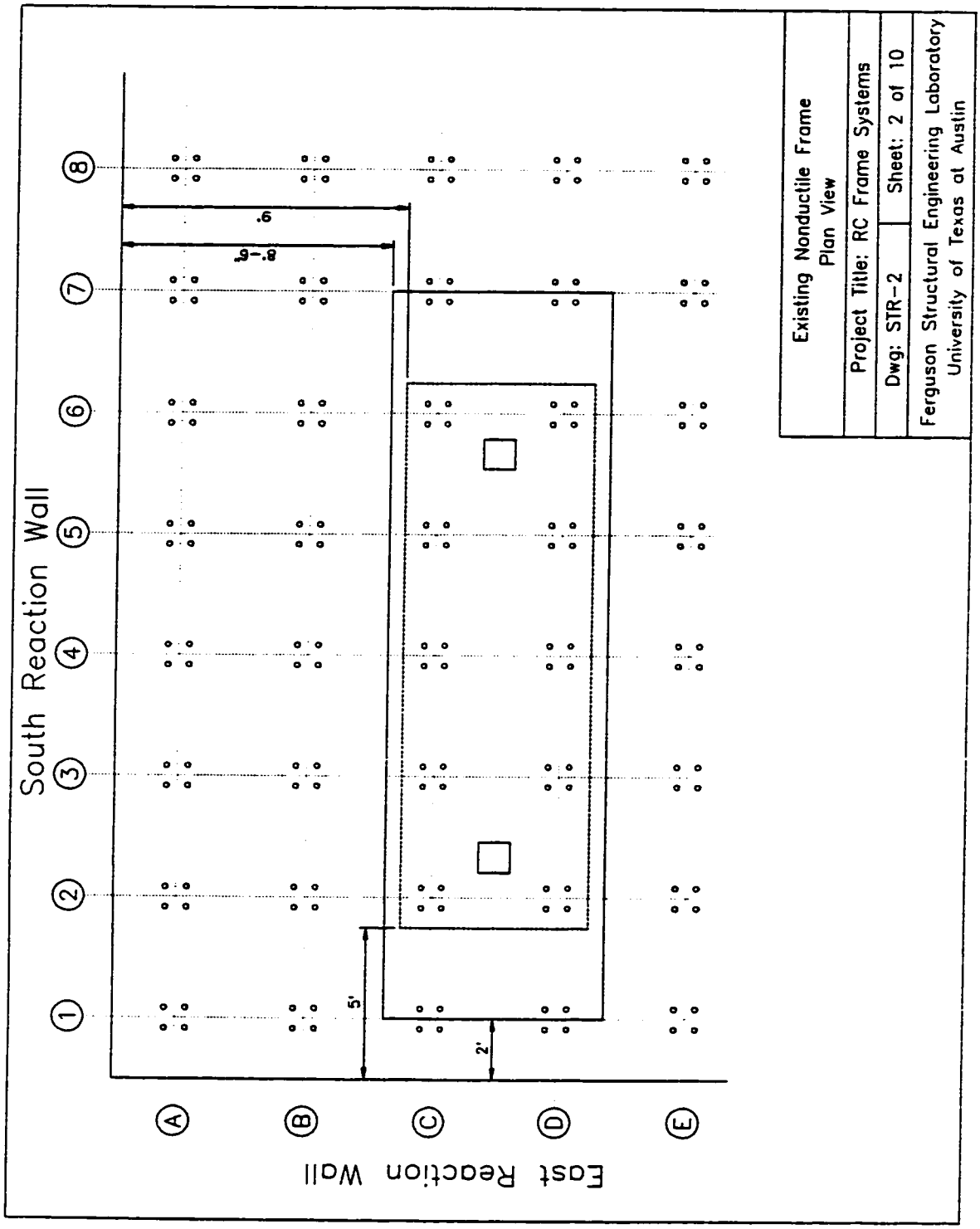
South Reaction Wall
East Reaction Wall
1
2
3
4
5
6
7
8
A
B
C
D
E
9'
8'-6"
5'
2'
Existing Nonductile Frame
Plan View
Project Title: RC Frame Systems
Dwg: STR-2
Sheet: 2 of 10
Ferguson Structural Engineering Laboratory
University of Texas at Austin

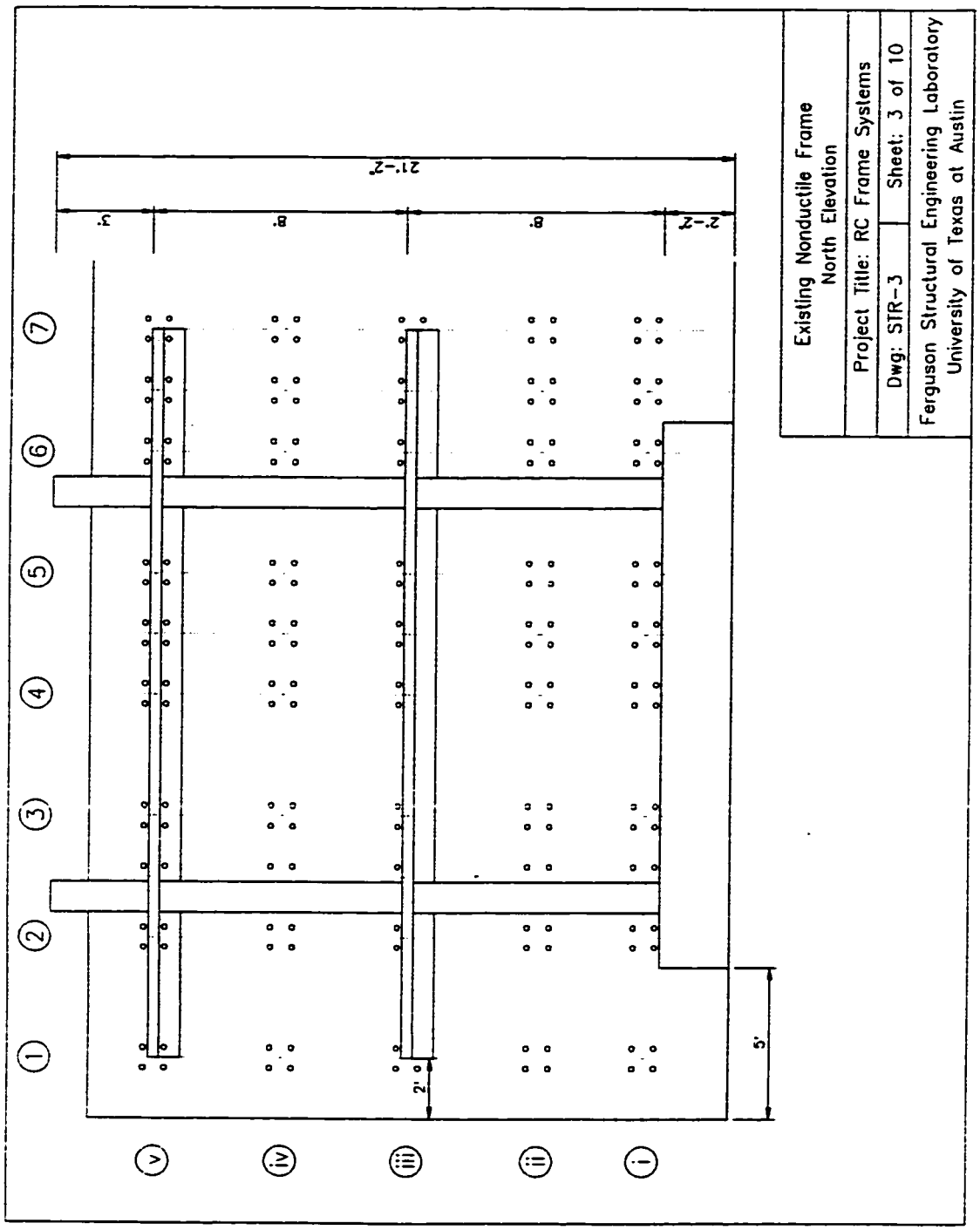
Existing Nonductile Frame
North Elevation
Project Title: RC Frame Systems
Dwg: STR-3
Sheet: 3 of 10
Ferguson Structural Engineering Laboratory
University of Texas at Austin
21'-2"
2'-2"
8'
8'
5'
2'
1
2
3
4
5
6
7
i
ii
iii
iv
v

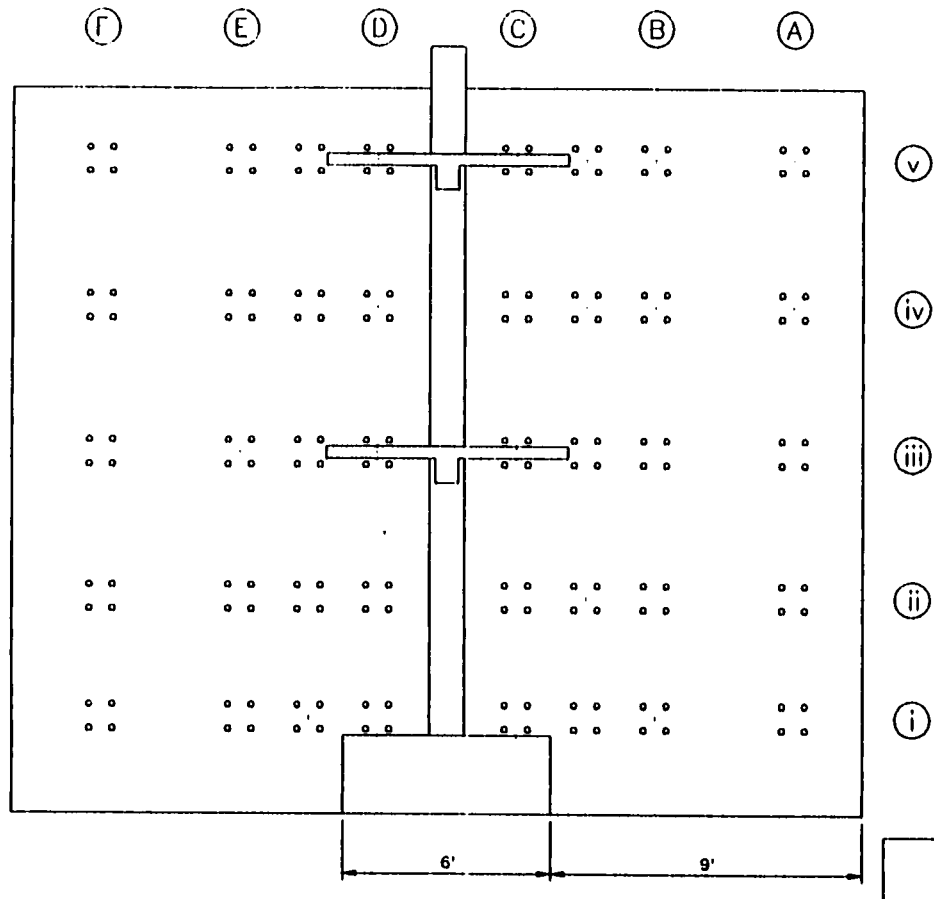

Existing Nonductile Frame West Elevation	
Project Title: RC Frame Systems	
Dwg: STR-4	Sheet: 4 of 10
Ferguson Structural Engineering Laboratory University of Texas at Austin	

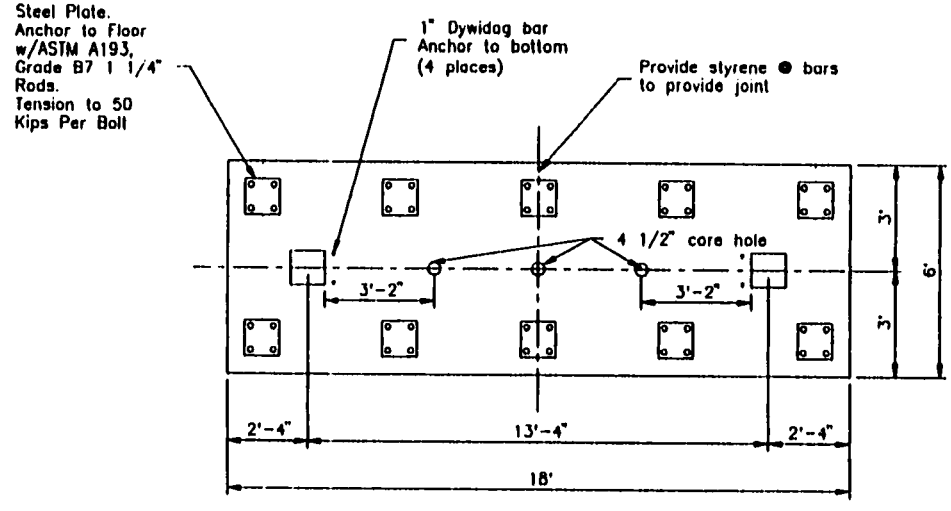

Top of footing ● El 2'-2"

Existing Nonductile Frame Footing Plan	
Project Title: RC Frame Systems	
Dwg: STR-5	Sheet: 5 of 10
Ferguson Structural Engineering Laboratory University of Texas at Austin	

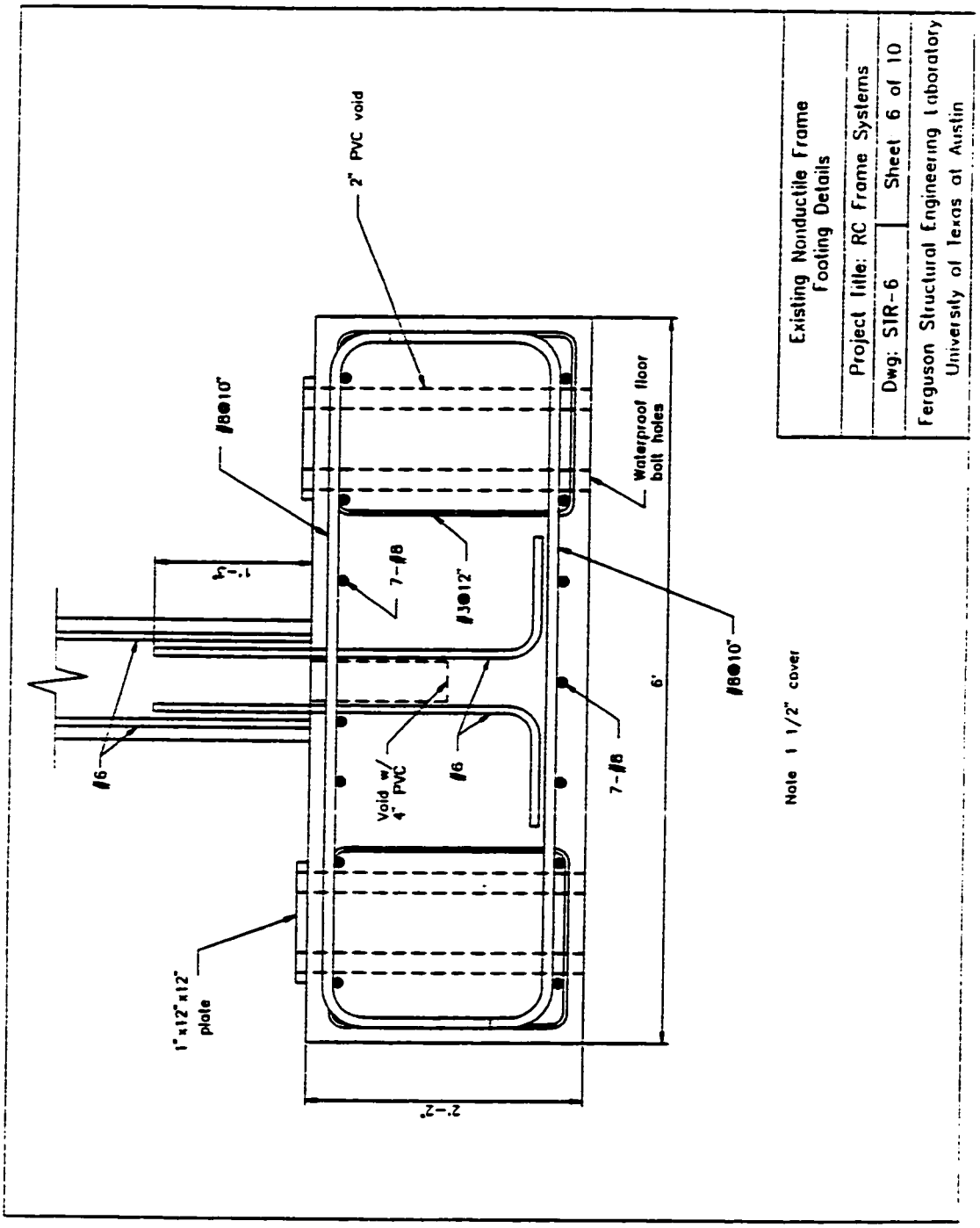
2" PVC void
#8@10"
Waterproof floor bolt holes
7-#8
#3@12"
#6
Void w/ 4" PVC
#6
7-#8
#8@10"
6'
2'-2"
1"x12"x12" plate
Note 1 1/2" cover
Existing Nonductile Frame Footing Details
Project title: RC Frame Systems
Dwg: SIR-6
Sheet 6 of 10
Ferguson Structural Engineering Laboratory
University of Texas at Austin

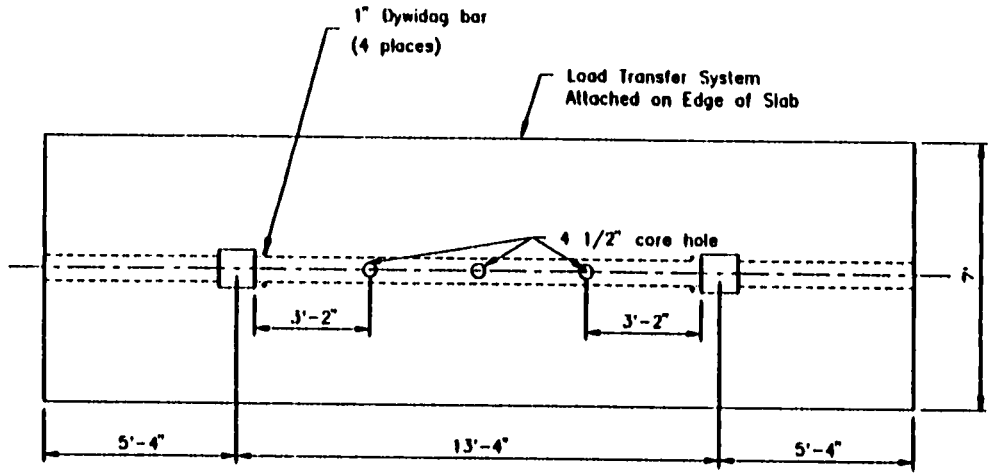

Top of second floor ● El 10-2"
Top of third floor ● El 18'-2"

Existing Nonductile Frame Floor Plan	
Project Title: RC Frame Systems	
Dwg: STR-7	Sheet: 7 of 10
Ferguson Structural Engineering Laboratory University of Texas at Austin	

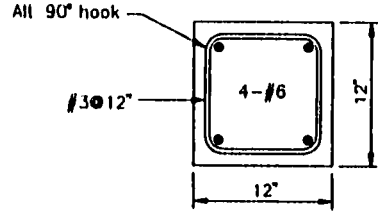

Column Detail

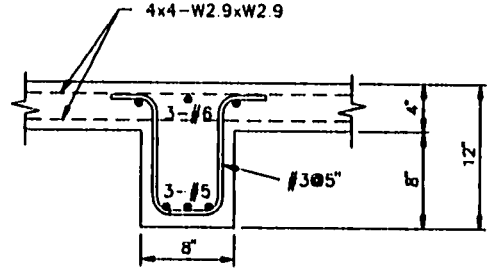

Beam Detail

Note: 1" cover

Existing Nonductile Frame Column and Beam Details	
Project Title: RC Frame Systems	
Dwg: STR-8	Sheet: 8 of 10
Ferguson Structural Engineering Laboratory University of Texas at Austin	

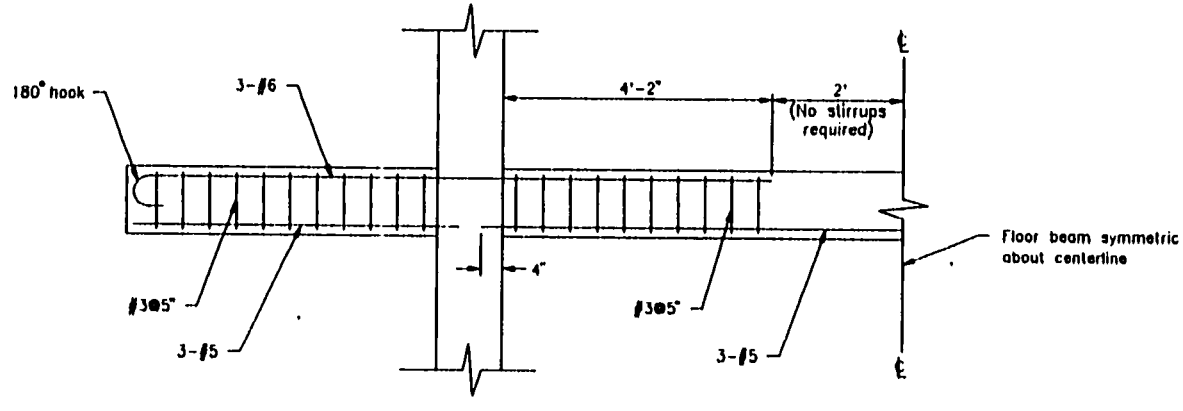

Existing Nonductile Frame Floor Beam Reinforcement Detail	
Project Title: RC Frame Systems	
Dwg: STR-9	Sheet: 9 of 10
Ferguson Structural Engineering Laboratory University of Texas at Austin	

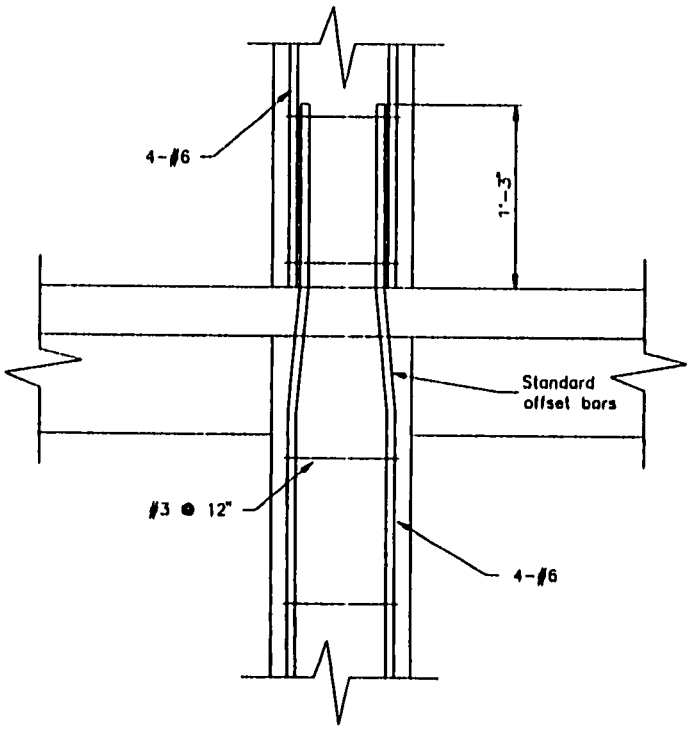

Existing Nonductile Frame Column Splices	
Project Title: RC Frame Systems	
Dwg: STR-10	Sheet: 10 of 10
Ferguson Structural Engineering Laboratory University of Texas at Austin	

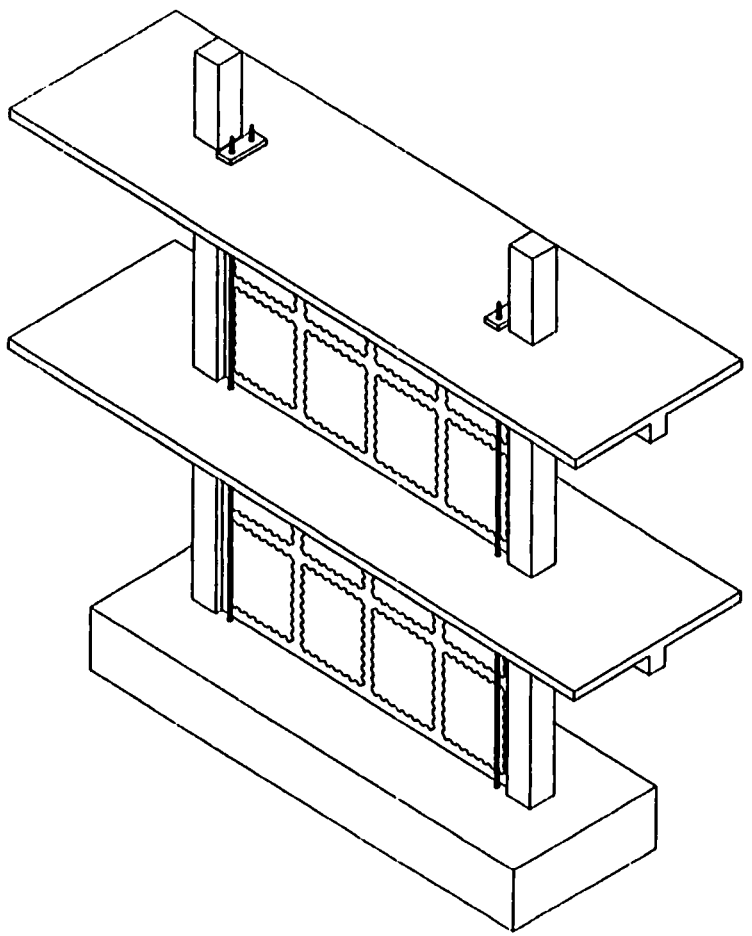

GENERAL NOTES

1. All concrete work shall be in accordance with ACI standard specifications for concrete and reinforced concrete.
2. All precast panel concrete shall be normal weight and shall test 4000 psi at 28 days.
3. All grout used in closure strips shall be normal weight and shall test 5000 psi at 28 days.
4. Reinforcing steel shall be A.S.T.M. Grade 60 deformed bars. Reinforcing steel for the precast panels shall consist of 4x4-W2.9xW2.9 welded wire fabric with a yield strength of 60,000 psi.

   Detail Reinforcing steel in accordance with the A.C.I. Manual of Standard Practice for Detailing Reinforced Concrete Structures.
5. Post-Tensioning steel shall be DYWIDAG Grade 150.

Infilled Building Frame Isometric View	
Project Title: RC Frame Systems	
Dwg: INF-1	Sheet 1 of 3
Ferguson Structural Engineering Laboratory University of Texas at Austin	

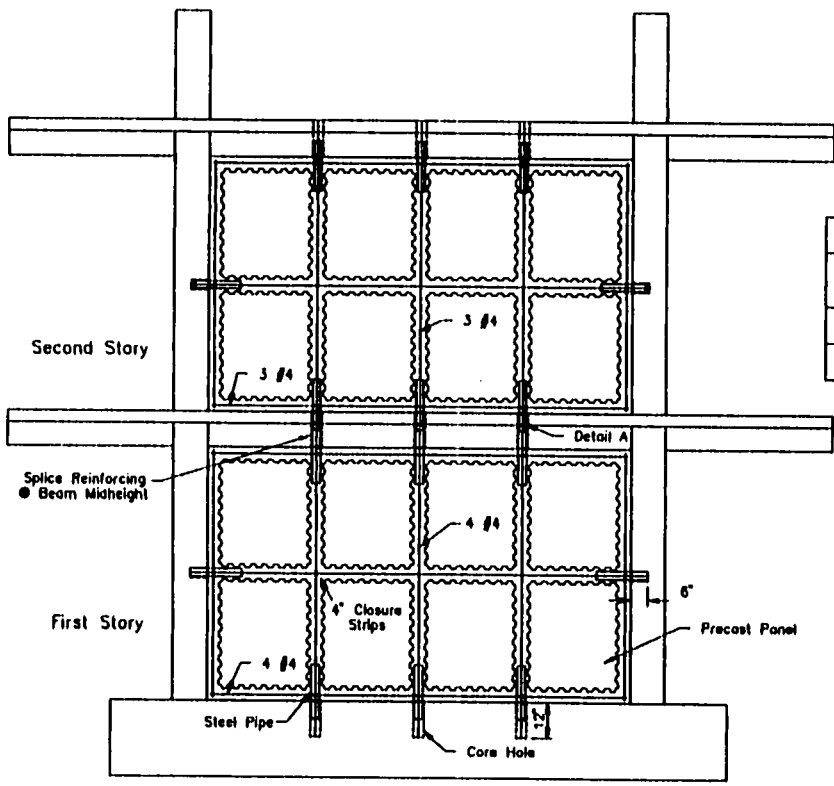

Pipe Schedule			
Story	Pipe	Embedment	
		Frame Side	Wall Side
First	2-1/2" XS	6"	12"
Second	2" XS	5"	11"

Closure Strip Reinforcing Schedule	
Story	Reinforcing
First	4 #4
Second	3 #4

Infilled Building Frame
Infill Wall Details

Project Title: RC Frame Systems

Dwg: INF-2 | Sheet: 2 of 3

Ferguson Structural Engineering Laboratory
University of Texas at Austin

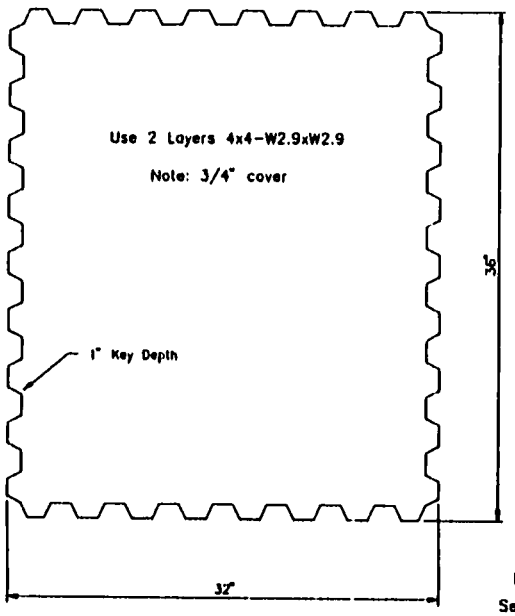

First Story: 6" Panel
Second Story: 4" Panel

Precast Panel

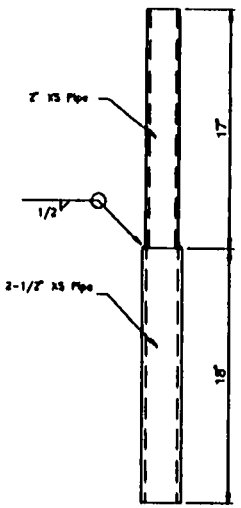

Pipe Detail A

Infilled Building Frame Panel and Pipe Details	
Project Title: RC Frame Systems	
Dwg: Inf-3	Sheet: 3 of 3
Ferguson Structural Engineering Laboratory University of Texas at Austin	

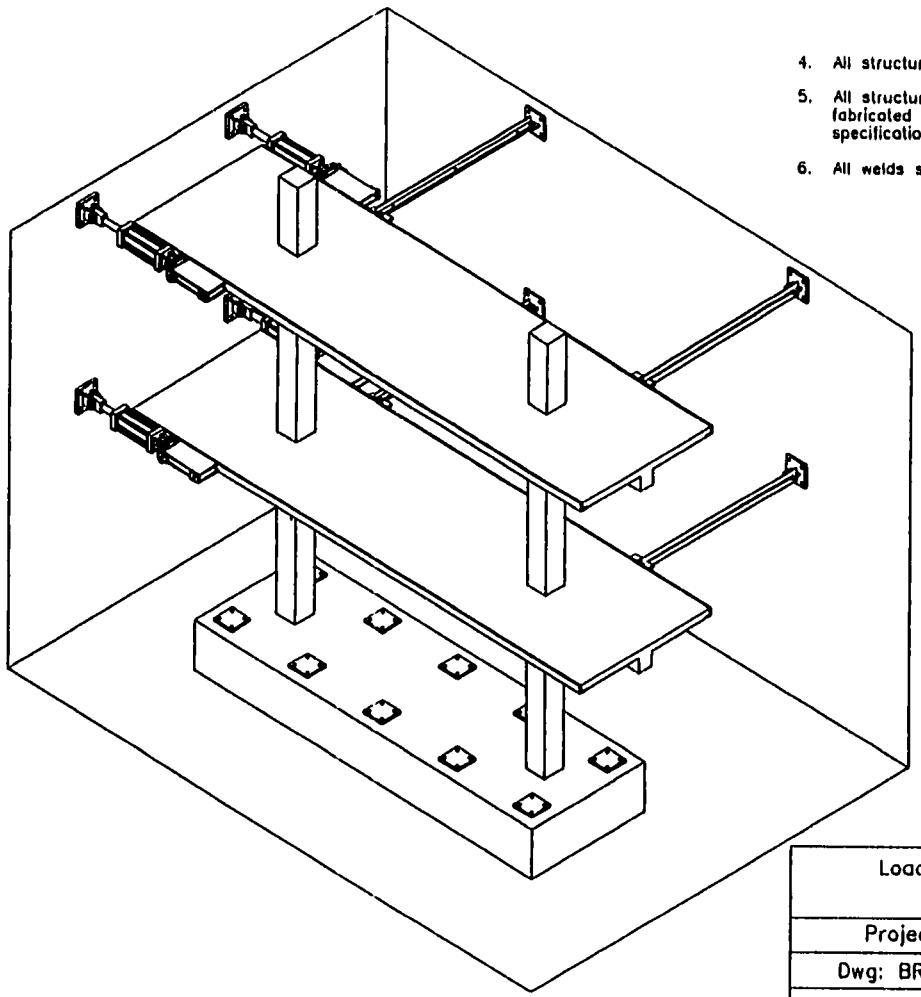

GENERAL NOTES

4. All structural steel shall be ASTM A572–Grade 50.
5. All structural steel shall be manufactured and fabricated in accordance with the latest A.I.S.C. specifications.
6. All welds shall be with E70XX Electrodes.

Loading and Bracing System Isometric View	
Project Title: RC Frame Systems	
Dwg: BRAC–1	Sheet: 1 of 14
Ferguson Structural Engineering Laboratory University of Texas at Austin	

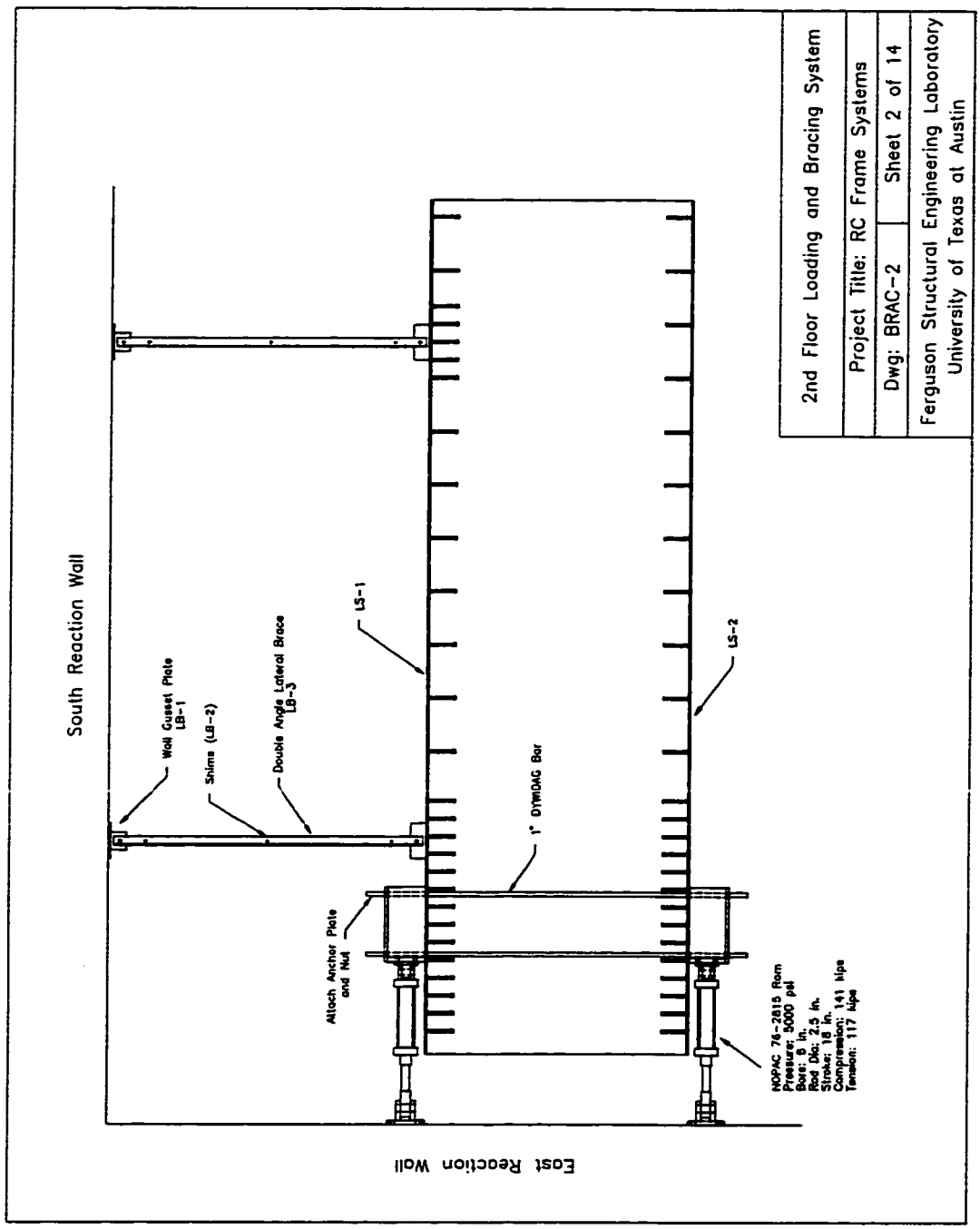
South Reaction Wall
East Reaction Wall
Wall Gusset Plate LB-1
Shims (LB-2)
Double Angle Lateral Brace LB-3
LS-1
LS-2
1" DYWIDAG Bar
Attach Anchor Plate and Nut
NOPAC 74-2815 Rom
Pressure: 3000 psi
Bore: 6 in.
Rod Dia: 2.5 in.
Stroke: 18 in.
Compression: 141 kips
Tension: 117 kips
2nd Floor Loading and Bracing System
Project Title: RC Frame Systems
Dwg: BRAC-2
Sheet 2 of 14
Ferguson Structural Engineering Laboratory
University of Texas at Austin

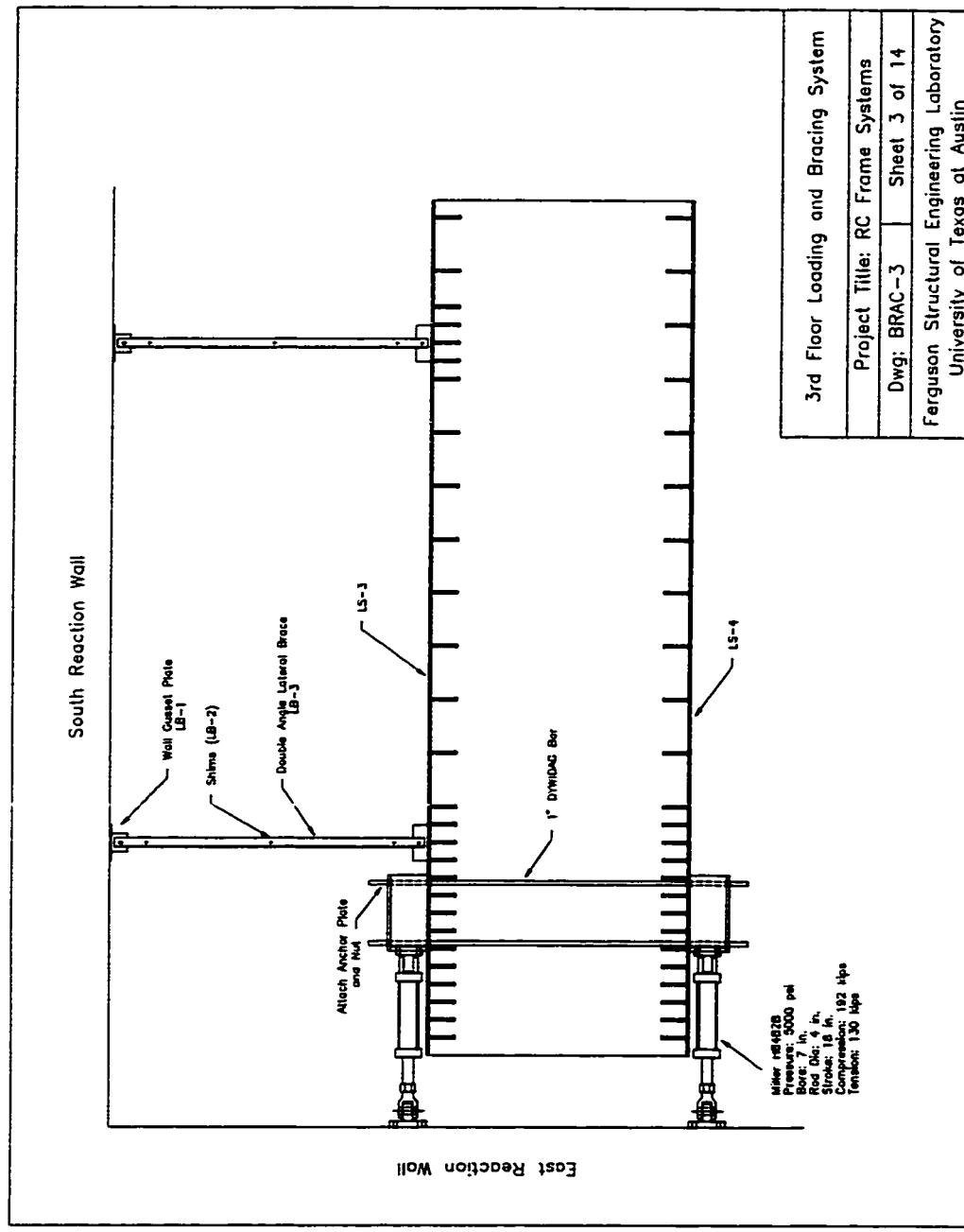
South Reaction Wall
East Reaction Wall
Wall Gusset Plate LB-1
Shims (LB-2)
Double Angle Lateral Brace LB-3
LS-3
LS-4
1" DYWIDAG Bar
Attach Anchor Plate and Nut
Miller mBH628
Pressure: 5000 psi
Bore: 7 in.
Rod Dia: 4 in.
Stroke: 18 in.
Compression: 192 kips
Tension: 130 kips
3rd Floor Loading and Bracing System
Project Title: RC Frame Systems
Dwg: BRAC-3
Sheet 3 of 14
Ferguson Structural Engineering Laboratory
University of Texas at Austin

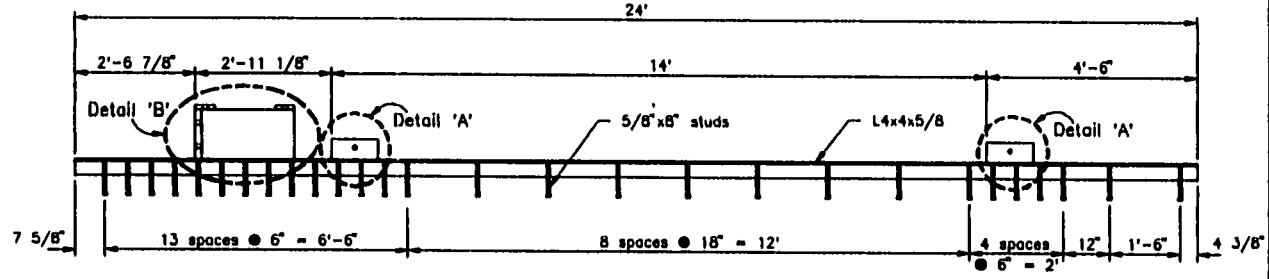

LS-1

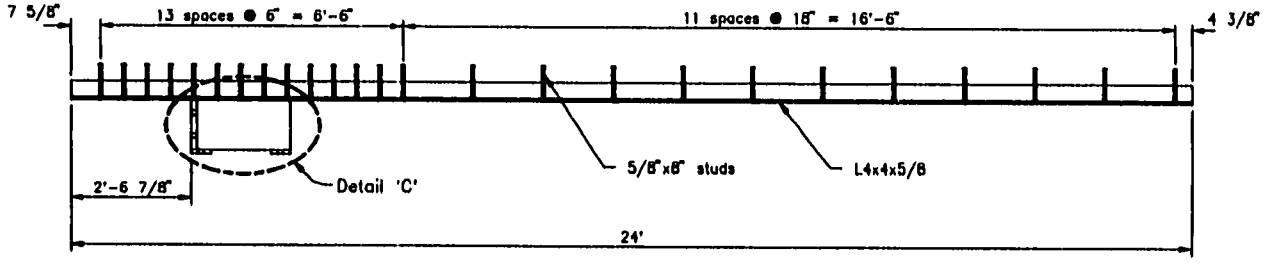

LS-2

Part Number	Number Required
LS-1	1
LS-2	1

Structural Steel Shop Drawings
2nd Floor Load Transfer System

Project Title: RC Frame Systems

Dwg: SH-1 | Sheet: 4 of 14

Ferguson Structural Engineering Laboratory
University of Texas at Austin

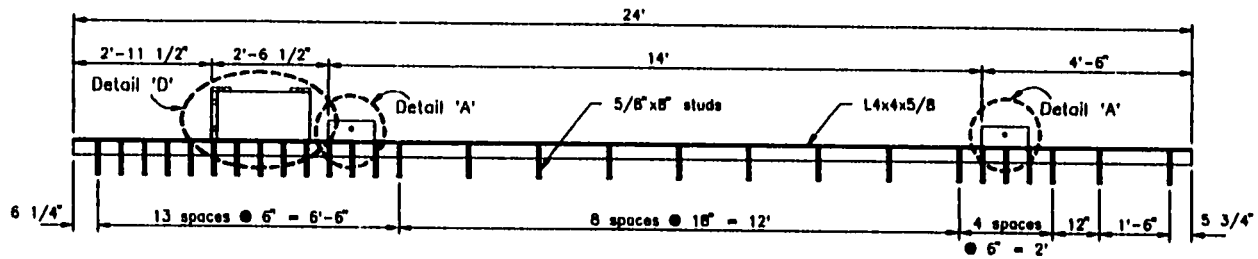

LS-3

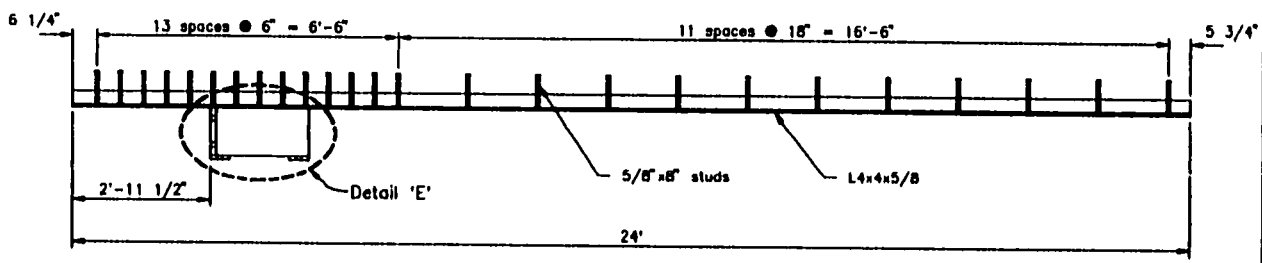

LS-4

Part Number	Number Required
LS-3	1
LS-4	1

Structural Steel Shop Drawings 3rd Floor Load Transfer System	
Project Title: RC Frame Systems	
Dwg: SH-2	Sheet: 5 of 14
Ferguson Structural Engineering Laboratory University of Texas at Austin	

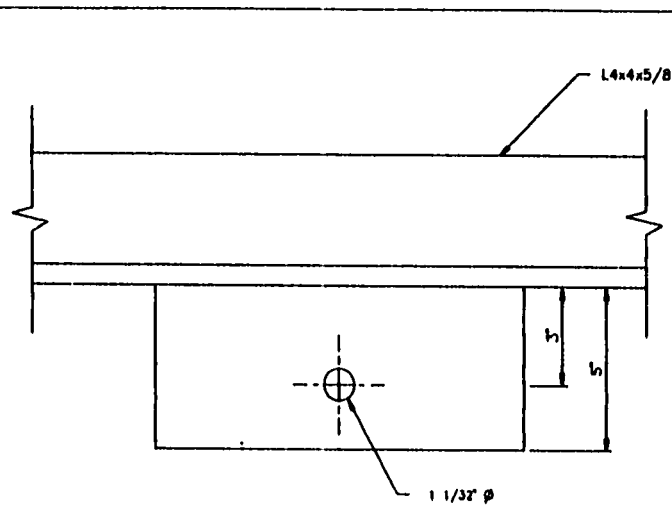

Detail 'A'

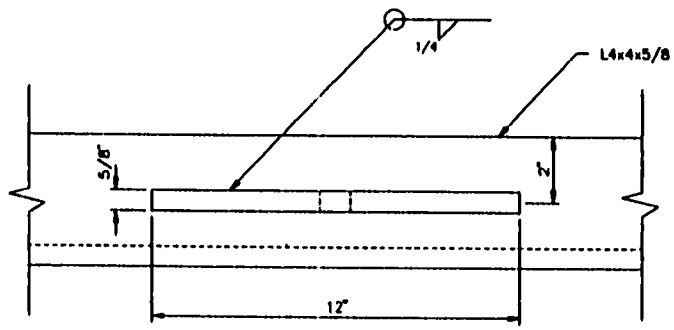

Structural Steel Shop Drawings Detail 'A'	
Project Title: RC Frame Systems	
Dwg: SH-3	Sheet: 6 of 14
Ferguson Structural Engineering Laboratory University of Texas at Austin	

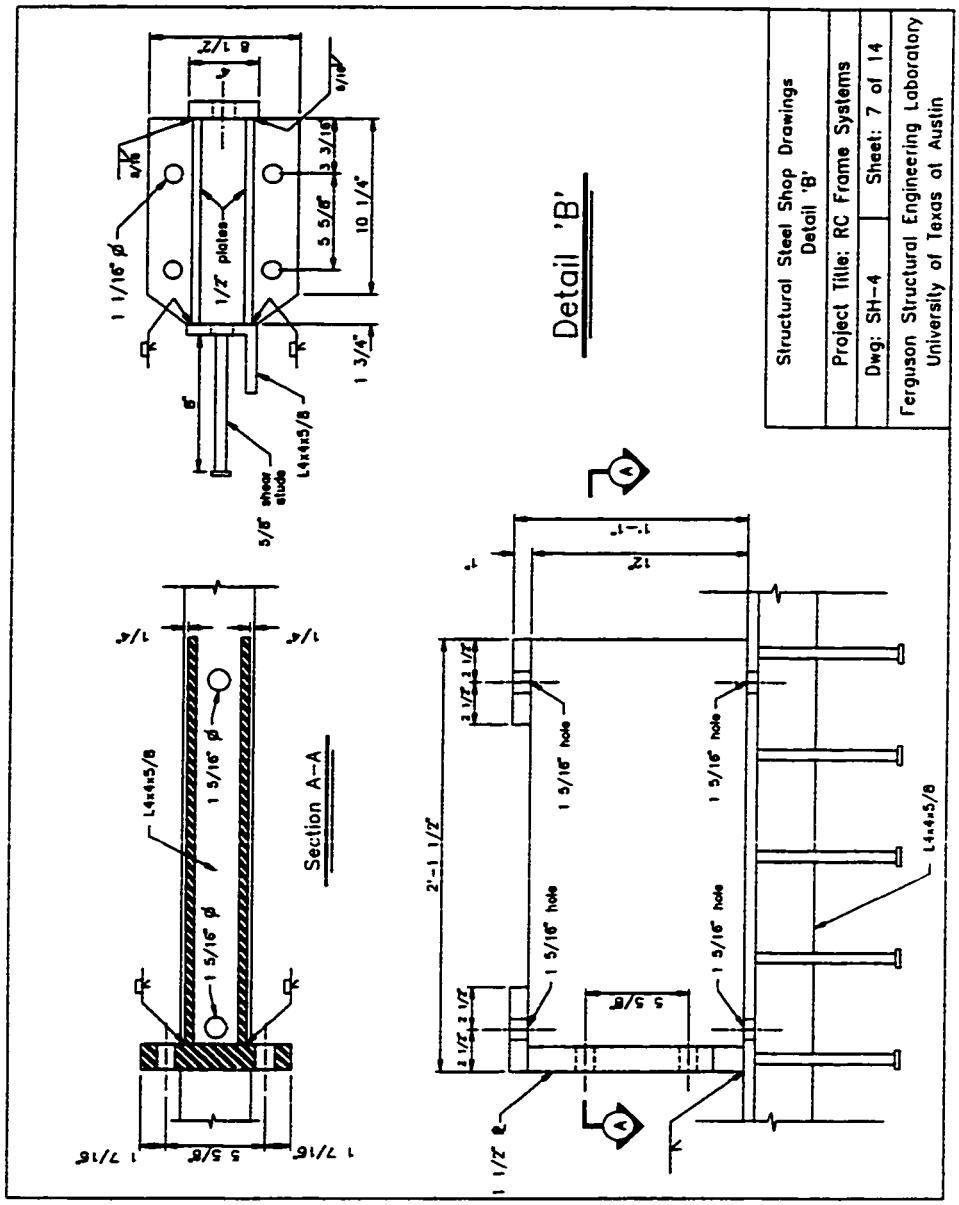
Structural Steel Shop Drawings
Detail 'B'
Project Title: RC Frame Systems
Dwg: SH-4
Sheet: 7 of 14
Ferguson Structural Engineering Laboratory
University of Texas at Austin
Detail 'B'
Section A-A
L4x4x5/8
1 5/16" hole
1 1/2"
2'-1 1/2"
5 5/8"
1 7/16"
1/4"
1/2" plates
1 1/16" ø
5/8" shear studs
10 1/4"
5 5/8"
3 3/16"
1 3/4"

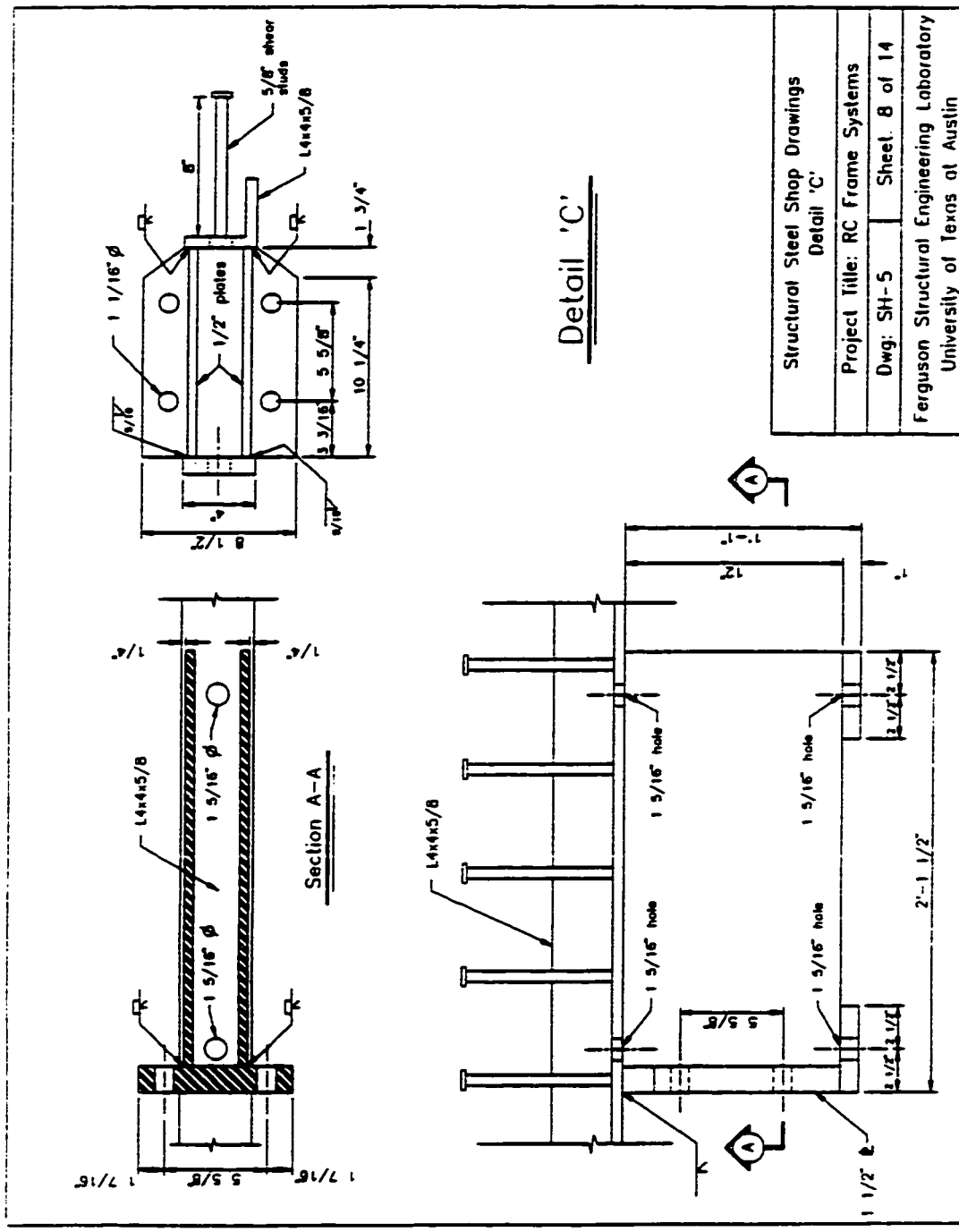
Structural Steel Shop Drawings
Detail 'C'
Project Title: RC Frame Systems
Dwg: SH-5
Sheet 8 of 14
Ferguson Structural Engineering Laboratory
University of Texas at Austin
Detail 'C'
Section A-A
L4x4x5/8
1 5/16" hole
2'-1 1/2"
1 1/2"
1 1/16" ø
1/2" plates
5/8" shear studs
1 3/4"
5 5/8"
10 1/4"
8 1/2"
5 5/8"

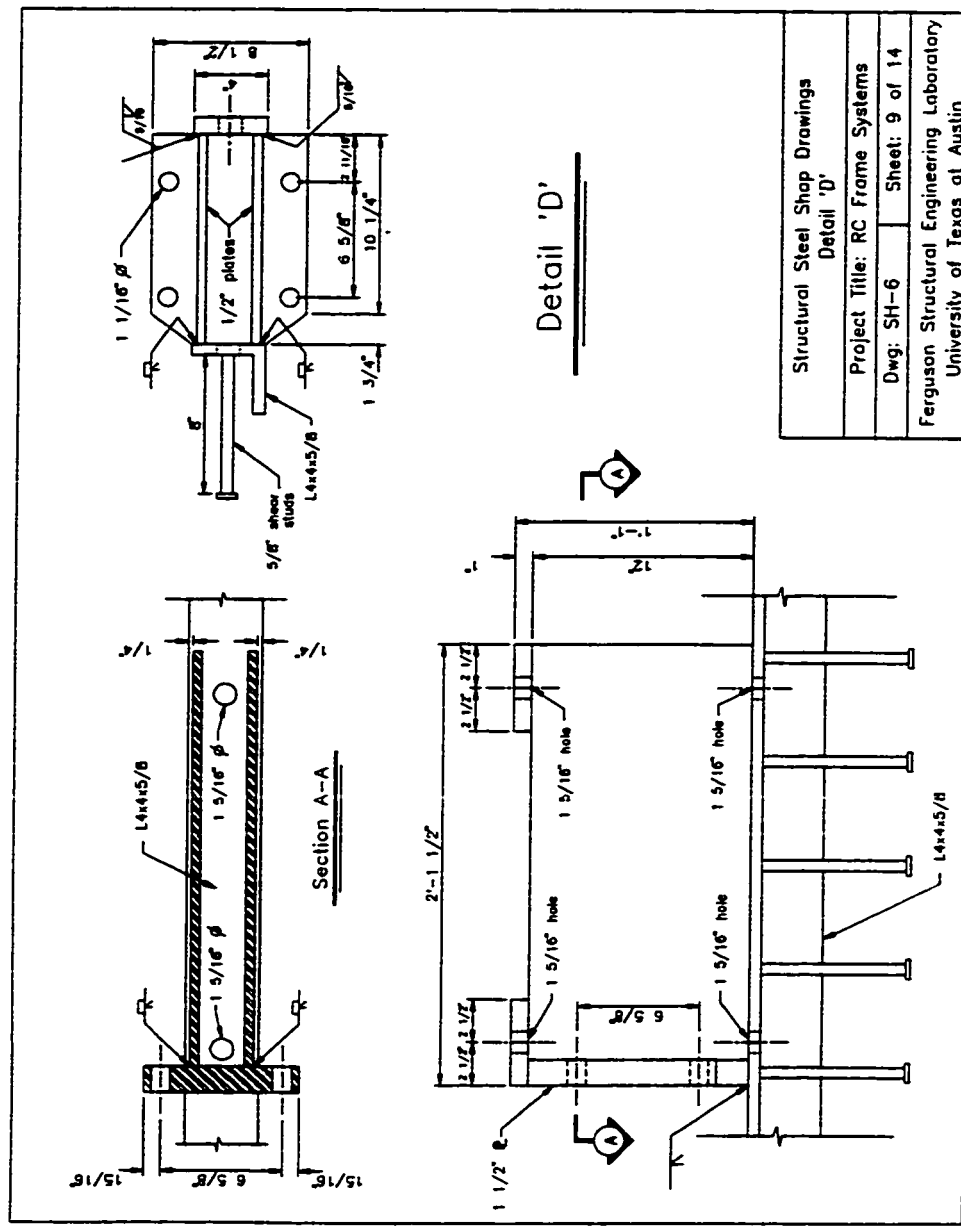
Structural Steel Shop Drawings
Detail 'D'
Project Title: RC Frame Systems
Dwg: SH-6
Sheet: 9 of 14
Ferguson Structural Engineering Laboratory
University of Texas at Austin
Detail 'D'
Section A-A
1/2" plates
L4x4x5/8
5/8" shear studs
1 5/16" hole
6 5/8"
15/16"
1 1/2"
2'-1 1/2"

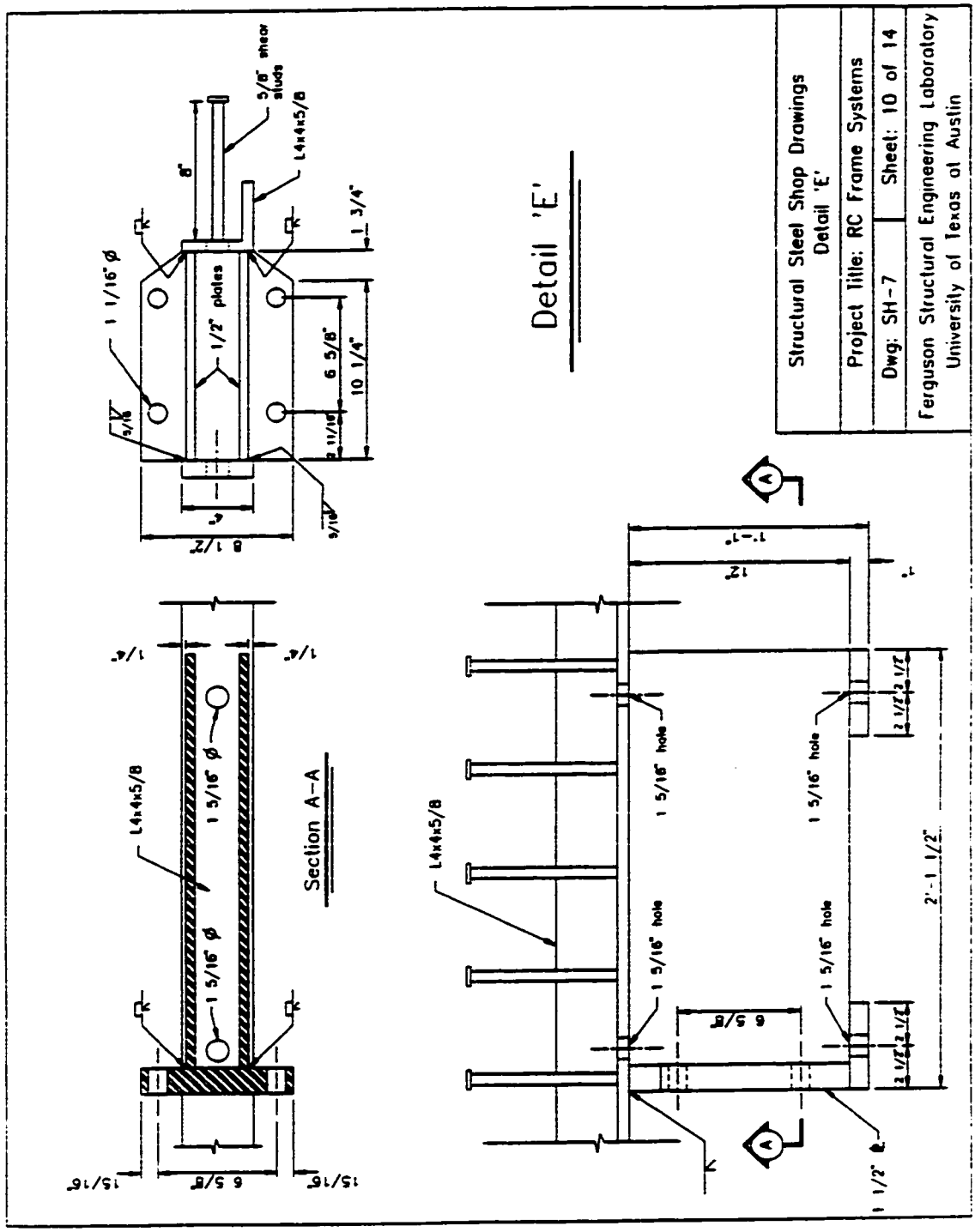
Structural Steel Shop Drawings
Detail 'E'
Project Title: RC Frame Systems
Dwg: SH-7
Sheet: 10 of 14
Ferguson Structural Engineering Laboratory
University of Texas at Austin
Detail 'E'
Section A-A
L4x4x5/8
1 5/16" hole
2'-1 1/2"
1 1/2"
1/2" plates
5/8" shear studs
1 1/16" ø
1 3/4"
6 5/8"
10 1/4"
8 1/2"
15/16"

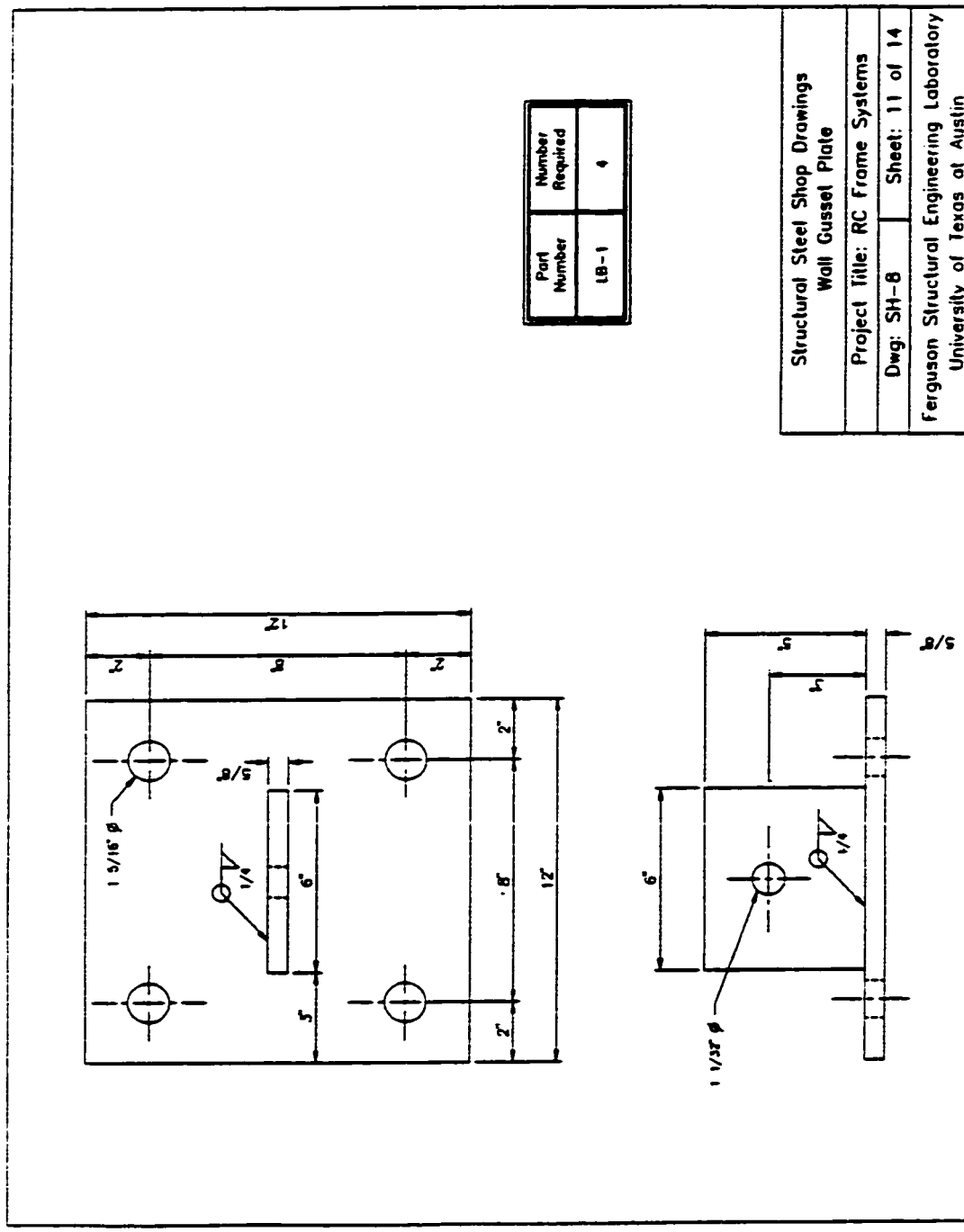
Structural Steel Shop Drawings
Wall Gussel Plate
Project Title: RC Frame Systems
Dwg: SH-8
Sheet: 11 of 14
Ferguson Structural Engineering Laboratory
University of Texas at Austin
Part Number
Number Required
LB-1
4
12"
2"
8"
2"
5"
6"
1/4
15/16"
1 5/16" ø
1 1/32" ø
1/4
6"
5/8"

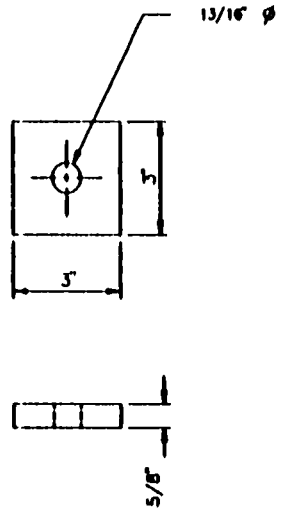

Part Number	Number Required
LB-2	12

Structural Steel Shop Drawings Angle Connection Shims	
Project Title: RC Frame Systems	
Dwg: SH-9	Sheet. 12 of 14
Ferguson Structural Engineering Laboratory University of Texas at Austin	

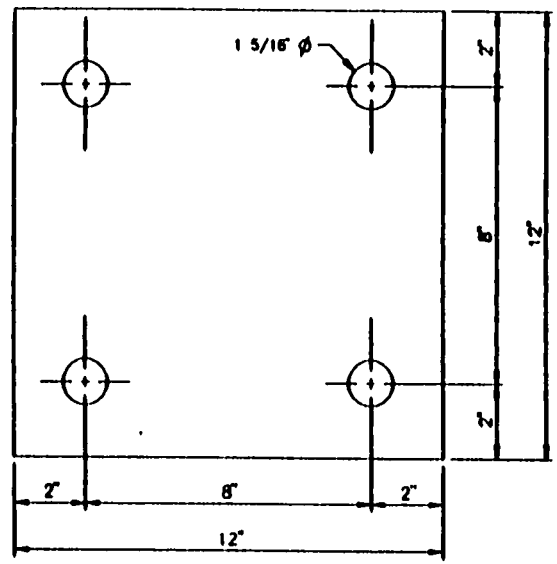

Part Number	t	Number Required
FP-1	1"	10
LS-5	2"	2

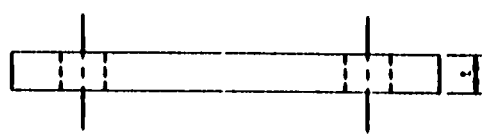

Structural Steel Shop Drawings Bearing Plate	
Project Title: RC Frame Systems	
Dwg: SH-10	Sheet: 13 of 14
Ferguson Structural Engineering Laboratory University of Texas at Austin	

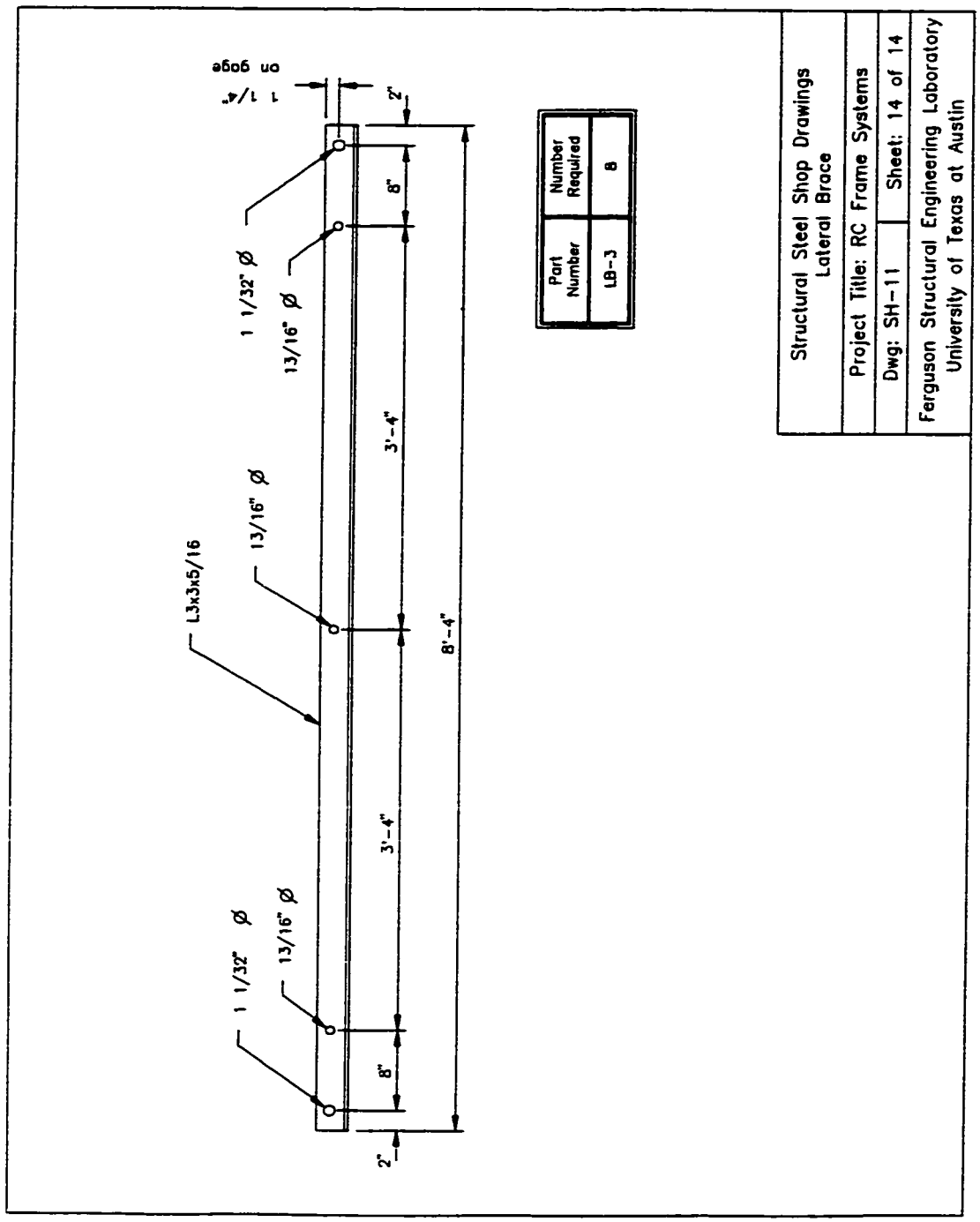
Structural Steel Shop Drawings
Lateral Brace
Project Title: RC Frame Systems
Dwg: SH-11
Sheet: 14 of 14
Ferguson Structural Engineering Laboratory
University of Texas at Austin
Part Number
Number Required
LB-3
8
L3x3x5/16
1 1/32" Ø
13/16" Ø
1 1/32" Ø
13/16" Ø
13/16" Ø
1 1/4" on gage
2"
8"
3'-4"
8'-4"
3'-4"
8"
2"

APPENDIX C

MANUAL FOR COMPUTER PROGRAM IDARC-PT

C.1 USER'S MANUAL OF PROGRAM IDARC-PT

Input Format

A free format is used to read all input data. Standard FORTRAN variable format is used to distinguish integers and floating point numbers.

Provision is made for a line of text between each data files accompanying this Manual. No blank lines are to be input. A blank input will result in program default values, where applicable.

Data Set A General Information

TITLE OF PROBLEM

TITLE Alpha-numeric title, up to 80 characters

CONTROL DATA (SEE IDARC FIGURE III.1)
USER-TEXT Reference information up to 80 characters

NCO,NFR, NCON, NSTL, NPDE, NPST, NFUD

NCO =	Number of stories	
NFR =	Number of typical frames (non-identical)	
NCON =	Number of concrete properties	
NSTL =	Number of steel properties	
NPDT =	0;	ignore P-Delta effected
	1;	include P-Delta effects
NPST =	0;	no prestressed members
	1;	post/prestress member included
NFUD =	0;	no foundation effects
	1;	foundation effects included

ELEMENT TYPES (SEE IDARC FIGURE III.1)

USER-TEXT Reference information up to 80 characters

MCOL, MBEM, MWAL, MEDG, MTEN, MTRN, MRSPR, MASPR

MCOL= Number of column types
MTEN= Number of tendon types
MBEM = Number of beam types
MWAL = Number of wall types
MEDG= Number of edge column types
MTRN= Number of transverse beam types
MRSPR= Number of rotation spring types
MASPR= Number of axial spring types

ELEMENT DATA

USER-TEXT Reference information up to 80 characters

NCOL, NBEM, NWAL, NEDG, NTEN, NTRN, NRSP, NASP, NMR

NCOL = Number of columns
NTEN = Number of tendons
NBEM= Number of beams
NWAL= Number of walls
NEDG= Number of edge columns
NTRN = Number of transverse beams
NRSP = Number of rotation springs
NASP = Number of axial springs
NMR = Number of moment release

UNIT SYSTEM

USER-TEXT Reference information up to 80 characters

IU Unit system =0, Default: inch,kips
=1, inch, kips
=2, mm, KN

FLOOR ELEVATION (SEE IDARC FIGURE III.2)

USER-TEXT Reference information up to 80 characters

HIGT(1) HIGT(2), ... HIGT(NCO)

Elevation of each story from the base to roof, beginning with the first story height.

DESCRIPTION OF IDENTICAL FRAMES
USER-TEXT Reference information up to 80 characters

NDUP(1), NDUP(2), ...NDUP(NFR)

Description
Number of duplicates of each typical(non-identical) frame. Total of NFR typical frames

PLAN CONFIGURATION
USER-TEXT Reference information up to 80 characters

NVLN(1), NVLN(2), ... NVLN(NFR)

Description Number of column lines (or J-locator points) in each frame

NODAL WEIGHTS (SEE IDARC FIGURE III.2)
USER-TEXT Reference information up to 80 characters

LEVL,IFR(1), WVT(1), ... WVT(NVLN(1))
IFR(2), WVT(2), ... WVT(NVLN(2))
.....
IFR(NFR),WVT(NFR), ... WVT(NVLN(NFR))

Description LEVL = Story level
IFR(J) = Frame number
WVT(k) = NODAL WEIGHT
(NEXT LEVEL)
Repeat for NCO levels

ENVELOPE GENERATION OPTION
USER-TEXT Reference information up to 80 characters

IUSER Code for specification of user properties
=0, requires IDARC-PT generated envelopes for at least one element

=1, Complete moment-curvature envelope data to be provided by user

DATA SET B **CONCRETE PROPERTIES** (SEE IDARC FIGURE III.3)
(Skip this input if NCON equal 0)
USER-TEXT Reference information up to 80 characters

IM, FC, EC, EPS0, FT, EPSU, ZF

IM	=	Concrete type number
FC	=	Unconfined compressive strength
EC	=	Initial Young's modulus
EPS0	=	Strain at maximum strength (%)
FT	=	Stress at tension cracking
EPSU	=	Ultimate compressive strain (%)
ZF	=	Slope parameter of failing branch

Repeat for each of the NCON concrete type

Default Values:

EC=57*(FC*1000)^0.5 ksi;
EPS0=0.2%; FT=0.12*FC
EPSU & ZF can be derived based on other data

DATA SET C **REINFORCEMENT PROPERTIES** (SEE IDARC FIGURE III.4)
(SKIP THIS INPUT IF NSTL EQUAL TO 0)

USER-TEXT Reference information up to 80 characters

IM, FS, FSU, ES, ESH, EPSH

IM	=	Steel type number
FS	=	Yield strength
FSU	=	Ultimate strength
ES	=	Modulus of elasticity
ESH	=	Modulus of strain hardening
EPSH	=	Stain at start of hardening(%)

Repeat for each of the NSTL steel types

Default Values:

FSU=1.4FS; ES=29,000 ksi;
ESH=(ES/60) ksi; EPSH = 3.0%

DATA SET D: HYSTERETIC RESPONSE MODELING
(SEE IDARC FIGURE III.5, AND FIGURE C-1 IN THIS MANUAL)

USER-TEXT Reference information up to 80 characters
NHYS Number of types of hysteretic rules

HYSTERETIC MODEL PARAMETERS

IR,HC,HBD,HBE,HS, PT

IR	=	Parameter set number
HC	=	Stiffness degrading parameter
HBD	=	Ductility related strength decay
HBE	=	Energy related strength decay
HS	=	Target slip/crack-closing factor
PT	=	Post tension effect parameter

Repeat for each NHYS set of hysteretic response rules

Default Values:

HC=2.0; HBD=0.0; HBE=0.1; HS=1.0; PT=1.0
Input only if HC,HBE,HBD & HS are not zero

DATA SET E COLUMN PROPERTIES
(SKIP THIS INPUT IF THERE IS NO COLUMN ELEMENT)

USER-TEXT Reference information up to 80 characters

IUCOL Type of column input
=0, Input section and reinforcement data
=1, Input moment-curvature data

IF IUCOL=1, GO TO SET E3

USER-TEXT Reference information up to 80 characters

For each column type, input the following:

ICTYPE — Type of column
=1, rectangular section
=2, circular section

IF ITCTYPE =2, GO TO SET E2

SET E1: ICTYOE=1; rectangular COLUMN (SEE IDARC FIGURE III.6)

General data — KC, IMC,IMS,AMLC, RAMC1 RAMC2,ANLDC
Bottom section — KHYSC,D,B,DC,AT,HBD,HBS,CEF

Top section — If KHYSC for bottom section is input with negative sign, section is symmetrical, hence, do not input top section data. Else, repeat as above, starting with KHSYC

KC = Column type number
IMC = Concrete type number
IMS = Steel type number
AMLC = Center-to center column height
RAMC1 = Rigid zone length at bottom
RAMC2 = Rigid zone length at top
ANLDC = Initial axial force

Column data for bottom section

KHYSC = Hysteretic rule number
D = Depth of section
B = Width of section
DC = Concrete cover of reinforcement
AT = Reinforcement area on one side
HBD = Hoop bar diameter
HBS = Hoop bar spacing
CEF = Effective of confinement

Column data for top section

Similar to bottom if KHYSC is positive
Skip top input if KHUSC is negative

Return to input of ICTYPE. When done, go to SET F

SET E2: ICTYOE=2; CIRCULAR COLUMN (SEE IDARC FIGURE III.7)

KC, IMP,IFS,KHYSC,AMLC, RAMC1 RAMC2,ANLDC
DO,CVR,DST,NBAR,BDIA,HBD,HBS

KC	=	Column type number
IMP	=	Concrete type number
IFS	=	Steel type number
KHYSC	=	Hysteretic rule number
AMLC	=	Center-to center column height
RAMC1	=	Rigid zone length at bottom
RAMC2	=	Rigid zone length at top
ANLDC	=	Initial axial force
DO	=	Outside diameter
CVR	=	Cover to center of hoop bar
DST	=	Clear diameter between rebars
NBAR	=	Number of longitudinal bars
BDIA	=	Diameter of longitudinal bars
HBD	=	Hoop bar diameter
HBS	=	Hoop bar spacing

Return to input of ICTYPE. When done, go to SET F

SET E3: USER INPUT PROPERTIES (IDARC FIGURE III.8)

USER-TEXT	Reference information up to 80 characters
General data	KC, AMLC, RAMC1 RAMC2, ANLDC
Bottom section	KHYSC,EI,EA,GA, PCP,PYP,UYP,UUP,EI3P PCN,PYN,UYN,UUN,EI3N
Top section	If KHYSC for bottom section is input with negative sign, section is symmetrical, hence,do not input top section data. Else, repeat as above, starting with KHSYC

General data

KC = Column type number
AMLC = Center-to center column height
RAMC1= Rigid zone length at bottom
RAMC2= Rigid zone length at top
ANLDC= Initial axial force

Column data for bottom section

KHYSC= Hysteretic rule number
EI = Initial flexural rigidity
EA = Axial stiffness
GA = Shear stiffness

Positive properties

PCP = Cracking Moment (+)
PYP = Yield Moment (+)
UYP = Yield Curvature (+)
UUP = Ultimate Curvature (+)
EI3P = Post yield stiffness (+)

Negative properties

PCN = Cracking Moment (-)
PYN = Yield Moment (-)
UYN = Yield Curvature (-)
UUN = Ultimate Curvature (-)
EI3N = Post yield stiffness (-)

Column data for top section

Similar to bottom if KHYSC is positive
Skip top input if KHUSC is negative

Repeat for each column, starting with general data (E3)

SET F: TENDON ELEMENT PROPERTIES
(SKIP THIS INPUT IF THERE IS NO TENDON MEMBERS)
USER-TEXT Reference information up to 80 characters

IUTEN Type of tendon input
=0, Input tendon area
=1, Input force-elongation data

If IUTEN =1, go to SET F2

SET F1 IUTEN=0, Input tendon area
USER-TEXT Reference information up to 80 characters

KTEN, IMP,IFS,AMLT, ANLDT,KHYST,AT,CEF,ITCL

KTEN = Tendon type number
IMP = Concrete type number
IFS = Steel type number
AMLT = Center-to center tendon length
ANLDT= Initial axial force
KHYST= Hysteretic rule number
AT = Area of tendon
CEF = Effective of confinement
ITCL = Tendon classification number
= 1; Stress at Anchorage (post- tension)
= 2; Stress at end of seating loss zone (post tension)
= 3; Lower-relaxation (pre-tension)
= 4; Stress-relieved (pre- tension)

Repeat input with total NTRU tendones, starting with general data.
When done, go to SET G

SET F2 USER INPUT PROPERTIES
USER-TEXT Reference information up to 80 characters

General data KTEN, AMLT, ANLDT
KHYST,EA, PYP,UYP,UUP,EA3P
PYN,UYN,UUN,EA3N

General data
KTEN = Tendon type number
AMLT = Center-to center tendon length
ANLDT= Initial axial force
KHYST= Hysteretic rule number
EA = Axial stiffness
Positive properties
PYP = Yield force (+)
UYP = Yield elongation (+)
UUP = Ultimate elongation (+)
EA3P = Post yield stiffness (+)

Negative properties

PYN	=	Yield force (-)
UYN	=	Yield elongation (-)
UUN	=	Ultimate elongation (-)
EA3N	=	Post yield stiffness (-)

Repeat for each tendon, starting with general data (F2)

DATA SET G: BEAM PROPERTIES
(SKIP THIS INPUT IF THERE IS NO BEAM ELEMENT)

USER-TEXT Reference information up to 80 characters

IUBEM Type of beam input
=0, Input section and reinforcement data
=1, Input moment-curvature data

IF IUBEM =1, GO TO SET G2

SET G1: SECTION / REINFORCEMENT INPUT (IDARC FIGURE III.9)
USER-TEXT Reference information up to 80 characters

General data KB, IMC,MS,AMLB, RAMB1,RAMB2 ANLDB

Left Section KHYSB,D,B,BSL,TSL,BC,AT1,AT2,HBD,HBS

Right Section If KHYSB for left section is input with negative sign, section is symmetrical, hence,do not input right section data.
Else, repeat as above, starting with KHSYB

KB	=	Beam type number
IMC	=	Concrete type number
IMS	=	Steel type number
AMLB	=	member length
RAMB1	=	Rigid zone length at left
RAMB2	=	Rigid zone length at right
ANLDB	=	Initial axial force

Beam data for LEFT section

KHYSB=		Hysteretic rule number
D	=	Depth of section
B	=	Width of section
BSL	=	Concrete cover of reinforcement
TSL	=	Reinforcement area on one side
BC	=	Cover to centroid of bars
AT1	=	Area of bottom bars
AT2	=	Area of top bars
HBD	=	Hoop bar diameter
HBS	=	Hoop bar spacing
CEF	=	Effective of confinement

Beam data for RIGHT section

Similar to left KHYSB is positive Skip RIGHT section input if KHUSB is negative.

Repeat for each beam type starting with general data (G1) When done, go to SET H

SET G2: **USER INPUT PROPERTIES** (SEE IDARC FIGURE III.8)

USER-TEXT Reference information up to 80 characters

General data KB, AMLB, RAMB1 RAMB2, ANLDB

LEFT section KHYSB,EI,EA,GA PCP,PYP,UYP,UUP,EI3P
PCN,PYN,UYN,UUN,EI3N

RIGHT section If KHYSB for LEFT section is input with negative sign, section is symmetrical, hence,do not input RIGHT section data.
Else, repeat as above, starting with KHSYB

General data

KB	=	Beam type number
AMLB=		Member length
RAMB1=		Rigid zone length at bottom
RAMB2=		Rigid zone length at top
ANLDB=		Initial axial force

Beam data for left section

KHYSB=		Hysteretic rule number
EI	=	Initial flexural rigidity
EA	=	Axial stiffness
GA	=	Shear stiffness

Positive properties

PCP	=	Cracking Moment (+)
PYP	=	Yield Moment (+)
UYP	=	Yield Curvature (+)
UUP	=	Ultimate Curvature (+)
EI3P	=	Post yield stiffness (+)

Negative properties

PCN	=	Cracking Moment (-)
PYN	=	Yield Moment (-)
UYN	=	Yield Curvature (-)
UUN	=	Ultimate Curvature (-)
EI3N	=	Post yield stiffness (-)

Beam data for right section

Similar to left if KHYSC is positive
Skip right input if KHUSC is negative

Repeat for each beam, starting with general data (SET G2)

SET H: SHEAR WALL PROPERTIES (SEE IDARC FIGURES III.10 & 11)
Skip this input if there is no wall element

USER-TEXT — Reference information up to 80 characters

IUWAL — Type of wall Input
=0; In put section and reinforcement data
=1; Input moment-curvature data

IF IUWAL = 1, GO TO SET H2

SET H1: SECTION AND REINFORCEMENT SPECIFICATIONS

USER-TEXT — Reference information up to 80 characters

General data: KW, IMC, IMS, KHYSW(1), KHYSW(2), KHYSW(3),AMLW, NSECT, ANLDW

KW	=	Shear wall type number
IMC	=	Concrete type number
KHYSW(1)	=	Hysteretic rule number (bottom)

KHYSW(2)= Hysteretic rule number (Top)
KHYSW(3)= Hysteretic rule number (Shear)
AMLW = Height f shear wall
NSECT= Number of sections
ANLDW= Initial axial force

For each of the NSECT section, Input the following:

KS,IMS,DWAL,BWAL, PV,PH

KS = Section number
IMS = Steel type number
DWAL= Depth of the section
BWAL = Width of the wall section
RV = Vertical reinforcement ratio (%)
RH = Horizontal reinforcement ratio

Repeat NSECT times

Repeat for each wall type starting with General Data.
When done, go to SET I.

SET H2: USER INPUT PROPERTIES(SEE IDARC FIGURE III.8)
USER-TEXT Reference information up to 80 characters

General Data: KW,AMLW,EAW

Flexure (Bot): KHYSW, EI, PCP,PYP,UYP,UUP,EI3P
PCN,PYN.UCN,UUN,EI3N

Flexure (Top): If KHYSW (1) for the bottom section is negative, section is symmetric, hence, do not input top section property.
Else, repeat as above,starting with KHYSW(2)

Shear: KHYSW(3),GA,ANLDW, PCP,PYP,UYP,UUP,GA3P
PCN,PYN.UCN,UUN,GA3N

Variable description

KW = Wall type Number
AMLW = Wall length
EAW = Axial Stiffness

Flexural properties

Data for wall bottom section

KHYSW(1)= Hysteretic rule number
EI = Initial Flexural stiffness
ANLDW= Initial axial force

Positive properties

PCP = Cracking Moment (+)
PYP = Yield Moment (+)
UYP = Yield Curvature (+)
UUP = Ultimate Curvature (+)
EI3P = Post yield stiffness (+)

Negative properties

PCN = Cracking Moment (-)
PYN = Yield Moment (-)
UYN = Yield Curvature (-)
UUN = Ultimate Curvature (-)
EI3N = Post yield stiffness (-)

Data for wall top section

Input similar data to bottom section if KHYSW(1) is positive.
Else, skip top section input if KHYSW(1) is negative.

Shear Properties

KHYSW(3)= Hysteretic rule number for shear
GA = Initial shear stiffness

Positive properties

PCP = Cracking Moment (+)
PYP = Yield Moment (+)
UYP = Yield Curvature (+)
UUP = Ultimate Curvature (+)
GA3P = Post yield shear stiffness

Negative properties

PCN = Cracking Moment (-)
PYN = Yield Moment (-)
UYN = Yield Curvature (-)
UUN = Ultimate Curvature (-)
GA3N = Post yield shear stiffness

Return to start of General Data (SET H2).
Repeat for each wall type.

SET I: EDGE COLUMN PROPERTIES (IDARC-2D MANUAL)
THIS SECTION IS SKIP IN THIS MANUAL

SET J: TRANSVERSE BEAM PROPERTIES (IDARC-2D MANUAL)
THIS SECTION IS SKIP IN THIS MANUAL

SET K: INELASTIC SPRING PROPERTIES (IDARC FIGURE III.8)
(SKIP THIS INPUT IF THERE IS NO SPRING ELEMENT)

USER-TEXT Reference information up to 80 characters

ISPRT Classification number of inelastic spring
=0; inelastic rotation spring
=1; Inelastic axial spring

IF ISPRT = 1, GO TO SET K2

Default value ISPRT =0

SET K1: INELASTIC ROTATION SPRING (SEE IDARC FIGURE III.8)

USER-TEXT Reference information up to 80 characters

General Data: KRS,KHYRS EI, PCP,PYP,UYP,UUP,EI3P
PCN,PYN,UYN,UUN,EI3N

KRS = Rotation spring type number
KHYRS= Hysteretic rule number
EI = Initial rotation stiffness (M/q)

Positive properties
PCP = Cracking Moment (+)
PYP = Yield Moment (+)
UYP = Yield Rotation (+ radian)
UUP = Ultimate Rotation (+radian)
EI3P = Post yield stiffness ratio (+)

Negative properties
PCN = Cracking Moment (-)
PYN = Yield Moment (-)
UYN = Yield Rotation (- radian)
UUN = Ultimate Rotation (- radian)
EA3N = Post yield stiffness ratio (-)

Repeat for each rotation spring element type
When done, go to SET L

SET K2: INELASTIC AXIAL SPRING (SEE IDARC FIGURE III.8)
USER-TEXT Reference information up to 80 characters

General Data: KS,ANLDS,KHYAS EAL, PCP,PYP,UYP,UUP,EA3P
PCN,PYN,UYN,UUN,EA3N

Description

KS = Axial spring type number
ANLDS= Initial axial force
KHYAS= Hysteretic rule number
EAL = Initial AXIAL stiffness (EA/L)

Positive properties

PCP = Cracking axial Force (+)
PYP = Yield axial Force (+)
UYP = Yield elongation (+)
UUP = Ultimate elongation (+)
EA3P = Post yield stiffness (+)

Negative properties

PCN = Cracking axial Force (-)
PYN = Yield axial Force (-)
UYN = Yield elongation (-)
UUN = Ultimate elongation(-)
EA3N = Post yield stiffness (-)

Repeat for each axial spring element type

ELEMENT CONNECTIVITY INPUT

SET L: COLUMN CONNECTIVITY (SEE IDARC FIGURE III.13)
Skip This Input If There Is No Column Element
USER-TEXT Reference information up to 80 characters

MC,ITC,IC,JC,LBC,LTC

Description

MC = Column number
ITC = Column type number
IC = Frame number

JC = Column line number
LBC = Story level at column bottom
LTC = Story level at column top

(NCOL lines of data)
Input is required for each of the NCOL columns

SET M: TENDON CONNECTIVITY (SEE IDARC FIGURE III. 12)
USER-TEXT Reference information up to 80 characters

MT,ITENd,ITS,JTS,LTS,KTSL

Description

MT = Tendon number
ITEND= Tendon type number
ITS = Frame number
JTS = Column line number for vertical tendon; or, story level for horizontal tendon
LTS = Story level at the bottom of vertical tendon; or,column line number at the left end of horizontal tendon
KTSL = Story level at top of vertical tendon; or, column line at right end of horizontal tendon

(NASPR lines of data)
Input is required for each of the NTEN tendons

SET N: BEAM CONNECTIVITY (SEE IDARC FIGURE III.13)
SKIP THIS INPUT IF THERE IS NO BEAM ELEMENT
USER-TEXT Reference information up to 80 characters

MB,ITB,LB,IB,JBB,JTB

Description

MB = beam number
ITB = beam type number
LB = story level
IB = frame number
JBB = column line at left end
JTB = column line at right end

(NBEM lines of data)

Input id required for each of the NBEM beams

SET Q: SHEAR WALL CONNECTIVITY (SEE FIGUre AC.13)
Skip This Input If There Is No Wall Element
USER-TEXT Reference information up to 80 characters

M,ITW,IW,JW,LBW,LTW

Description

M	=	wall number
ITW	=	wall type number
IW	=	frame number
JW	=	column line number
LBW	=	story level at wall bottom
LTW	=	story level at wall top

(NWAL lines of data)
Input id required for each of the NWAL walls

SET P: EDGE COLUMN CONNECTIVITY (IDARC-2D MANUAL)
EDGE COLUMN IS SKIPPED IN THIS MANUAL

SET Q: TRANSVERSE BEAM CONNECTIVITY (IDARC-2D MANUAL)
TRANSVERSE BEAM ELEMENT IS SKIPPED IN THIS MANUAL

SET R: INELASTIC SPRING CONNECTIVITY (FIGURE AC.13)
Skip This Input If There Is No Spring Element

USER-TEXT Reference information up to 80 characters

MSPT, ISPRT

MSPT =	Inelastic spring number
ISPRT=	Classification number of spring

If input axial spring connectivity, GO TO SET R2

SET R1: ROTATION SPRING
USER-TEXT Reference information up to 80 characters

ITRS,ISPRT,IS,JS,LBS,KRSL

ITRS	=	Element type number
IRS	=	Frame number
JRS	=	Column line number
LRS	=	Story level
KRSL	=	Relative spring location code
	=1;	Spring on beam, left of joint
	=2;	Spring on column, top joint
	=3;	Spring on beam, right of joint
	=4;	Spring on column, bottom joint

(NRSPR lines of data)
Repeat each rotation spring, start with spring number (R) When done, return to SET R, if there is axial spring, else, go to SET S.

SET R2: AXIAL SPRING CONNECTIVITY (SEE IDARC FIGURE III.13)
USER-TEXT Reference information up to 80 characters

ITAS,IAS,JAS,LAS,KASL

ITAS	=	Element type number
IAS	=	Frame number
JAS	=	Column line number for vertical spring; or, story level for horizontal spring
LAS	=	Story level at the bottom of vertical spring; or,column line number at the left end of horizontal spring
KASL	=	Story level at the top of vertical spring; or, column line at the right end of horizontal spring

(NASPR lines of data)
Repeat each axial spring, start with spring number (R) When done, return to SET R, if there is rotation spring, else, go to SET S.

SET S MOMENT RELEASE SPECIFICATION (IDARC FIGURE AC.15)
Skip This Input If Moment Release Are Not Required(Nmr=0)

USER-TEXT Reference information up to 80 characters

IDM,IHTY,INUM,IREG

IDM	=	Moment release ID number
IHTY	=	Element type code
	=1;	column
	=2;	beam
	=3;	wall
INUM	=	Column, beam or wall number
IREG	=	Hinge/moment release location
	=1;	bottom of column/wall, or left of beam
	=2;	top of column/wall, or right of beam

Repeat NMR lines

SET T: POST TENSION MEMBER SPECIFICATION
SKIP THIS INPUT IF THERE IS NO POST TENSIONING (NPST=0)

USER-TEXT Reference information up to 80 characters

IPST,MPSTP,NPSTM NPSTC

IPST	=	Post tension ID number
MPSTP	=	Element type code
	=1;	column
	=2;	beam
	=3;	wall
	=4;	edge column
	=5;	axial spring
MPSTM	=	Element number
NPSTC	=	Post tension hysteretic code

Repeat for NPST times

SET U ANALYSIS OPTION

USER-TEXT Reference information up to 80 characters

IOPT Option for continuing analysis
- =0; STOP (data check only)
- =1; Inelastic analysis with incremental static load
- =2; Monotonic (pushover) analysis including static load when specified
- =3; Inelastic dynamic analysis with earthquake motion including static load
- =4; quasi-static cyclic load analysis including static load

SET U1: LONG-TERM LOADING SPECIFICATION (STATIC LOADS)

Control information

USER-TEXT Reference information up to 80 characters

NLU,NLJ,NLM,NLC

- NLU = No. of UNIFORMLY LOADED BEAMS
- NLJ = No. of lateral loaded joints
- NLM = No. of specified nodal moments
- NLC = No. of concentrated vertical loads

IF NLU=NLJ=NLM=NLC=0 AND IOPT=2,CONTINUE TO SET U2
IF NLU=NLJ=NLM=NLC=0 AND IOPT=3,CONTINUE TO SET U3
IF NLU=NLJ=NLM=NLC=0 AND IOPT=4,CONTINUE TO SET U4

Next data set:

JSTP,IOCRI

- JSTP = No.OF INCREMENTAL STEPS to apply the static loads (default=1)
- IOICRL= Steps between printing output
  - =0; only final results will be printed
  - ="N"; printout will result every N steps and so on

Uniformly loaded beam data

Skip this input if there is no uniformly loaded beams (NLU=0)

USER-TEXT	Reference information up to 80 characters		
IL,IBN,FU	IL	=	Load number
	IBN	=	Beam number
	FU	=	Magnitude of load (FORCE/length)

NLU lines of data required in this section

Laterally loaded joints
Skip this input if there is no joint load (NLJ=0)

USER-TEXT	Reference information up to 80 characters		
IL,LF,IF,FL	IL	=	Load number
	LF	=	Story number
	IF	=	Frame number
	FL	=	Magnitude of load

NLJ lines of data required in this section

Nodal Moment Data
SKIP THIS INPUT IF THERE IS NO NODAL MOMENT (NLM=0)

USER-TEXT	Reference information up to 80 characters		
IL,IBM,FM1,FM2	IL	=	Load number
	IBM	=	Beam number
	FM1	=	Nodal moment (left)
	FM2	=	Nodal Moment (right)

NLM lines of data required in this section
Moment sign convention refer to IDARC Figure III.1

Data for Concentrated Vertical Loads
SKIP THIS INPUT IF THERE IS NO CONCENTRATED LOAD

USER-TEXT	Reference information up to 80 characters

IL,IFV,LV,JV,FV

IL	=	Load number
IFV	=	Frame number
LV	=	Story level number
JV	=	Column line number
FV	=	Magnitude of load

NLC lines of data required in this section

IF IOPT =2; CONTINUE TO SET U2
IF IOPT =3; CONTINUE TO SET U3
IF IOPT =4, CONTINUE TO SET U4

SET U2: MONOTONIC PUSHOVER ANALYSIS (IOPT=2)
USER-TEXT Reference information up to 80 characters

JOPT Pushover Option
=1; Force control
=2; DISPLACEMENT CONTROL

FOR JOPT =2, GO TO SET U2.2

SET U2.1 FORCE CONTROL SPECIFICATION
USER-TEXT Reference information up to 80 characters

ITYP Control Code
=1; Linear (inverted triangle)
=2; Uniform
=3; Step-step updated
(based on story shear for the previous step)
=4; User input option

For ITYp =4, go to SET U2.2
PMAX,MSTEPS,DRFLIM

PMAX=	Target ultimate base shear coefficient
MSTEPS=	Number of steps to reach PMAX
DRFLIM=	Upper limit for displacement of structure top-story (percentage of building height)

Continue to SET V

SET U2.2 DISPLACEMENT CONTROL SPECIFICATION

NLDED	Number of loaded stories	
NSTLD(I)	I=1,NLDED	List of loaded stories
PX(I)	I=1,NLDED	List of maximum forces or displacement applied at loaded stories
MSTEPS,DRFLIM		
	MSTEPS=	Number of steps to reach each ultimate story force or displacement
	DRFLIM=	Upper limit for displacement of structure top story (percent of building height)

Continue to set V

SET U3: DYNAMIC ANALYSIS CONTROL PARAMETERS (IOPT=3)

USER-TEXT Reference information up to 80 characters

GMAXH,GMAXV,DTCAL,TDUR,DAMP

GMAXM=	Peak horizontal acceleration (g's)
GMAXV=	Peak vertical acceleration (g's)
DTCAL=	Time step of response analysis (second)
TDUR =	Total duration of analysis (s)
DAMP =	Damping coefficient (% of critical)

Input seismic wave (earthquake record)

USER-TEXT Reference information up to 80 characters

IWV,NDATA,DTINP

IWV =0;	Vertical compoment of acceleration not include
=1;	Vertical component acceleration is included
NDATA=	Number of points in wave files
DTINP=	Time interval of input waves

Wave Title

NAMEW — Name of file (with extension) from which to read horizontal components of earthquake records

WINPH(I), I=1,NDATA — Horizontal components of eartquake wave file with total of NDATA poins

Wave data for vertical component

SKIP THIS INPUT IF IWV=0

File name for horizontal component

WVFILE — Name of file (with extension) from which to read vertical components of earthquake recrd

INPV(I),I=1,NDATA — Vertical component of erthquake wave file with total NDATA points

GO TO DATA SET V

SET R4: QUASI-STATIC CYCLIC ANALYSIS (IOPT=4 ONYL)

USER-TEXT — Reference information up to 80 characters

ICNTRL — Cyclic analysis option
=0; force control input
=1; displacement control input

NLDED — Number of story levels at which the force or displacement is applied

NSTLD(I),I=1,NLDED — List of story levels at which the force or displacement is applied

NPTS — Number of points to be read in force or displacement history

F(I,1),I=1,NPTS — First data set(NPTS) at story level NSTLD(1)

F(I,2),I=1,NPTS — Next data set(NPTS) at story level NSTLD(2)

.

.

F(i,k),I=1,NPTS — Repeat till last set, where K=NSTLD(NLDED)

DTCAL — Analysis step (fraction of input steps)

SET V Global Output control

USER-TEXT Reference information up to 80 characters

NSOUT,DTOUT,ISO(I),I=1,NSOUT

NSOUT= No. of output histories
DTOUT= Output time interval,for earthquake wave output point =TDUR/DTOUT
ISO(I)= output story numbers

FNAMES(1) Filename to store time history output for story number ISO(1)
FNAMES(2) Filename to store time history output for story number ISO(2)
.
.
FNAMES(NSOUT) Filename to store time history output for story number ISO(NSOUT)

IF IOPT=2, STOP HERE

SET W: ELEMENT HYSTERESIS OUTPUT
USER-TEXT Reference information up to 80 characters

KCOUT,KBOUT,KWOUT,KPOUT,KSOUT,KAOUT

KCOUT= Number of COLUMNS for which hysteresis output is required
KPOUT= Number of TENDONS for which hysteresis output is required
KBOUT= Number of BEAMS for which hysteresis output is required
KWOUT= Number of WALLS for which hysteresis output is required
KROUT= Number of ROTATION SPRINGS for which hysteresis output is needed
KAOUT= Number of AXIAL SPRINGS for which hysteresis output is required

COLUMN output Specification
SKIP THIS INPUT IF KCOUT =0

USER-TEXT Reference information up to 80 characters

ICLIST(I),I=1,KCOUT List of column numbers moment-curvature hysteresis is output

TENDON output Specification
SKIP THIS INPUT IF KPPOUT =0
USER-TEXT Reference information up to 80 characters

IPLIST(I),I=1,KPOUT List of TENDONS numbers FORCE-ELONGATION hysteresis is output

BEAM output Specification
SKIP THIS INPUT IF KBOUT =0
USER-TEXT Reference information up to 80 characters

IBLIST(I),I=1,KBOUT List of BEAM numbers moment-curvature hysteresis is output

WALL output Specification
SKIP THIS INPUT IF KWOUT =0
USER-TEXT Reference information up to 80 characters

IWLIST(I),I=1,KWOUT List of WALL numbers moment-curvature hysteresis is output

ROTATION SPRING Output Specification
SKIP THIS INPUT IF KROUT =0
USER-TEXT Reference information up to 80 characters

IRLIST(I),I=1,KROUT List of ROTATION SPRING numbers moment-curvature hysteresis is output

AXIAL SPRING Output Specification
SKIP THIS INPUT IF KAOUT =0
USER-TEXT Reference information up to 80 characters

IALIST(I),I=1,KAOUT List of AXIAL SPRING numbers FORCE-ELONGATION hysteresis is output.

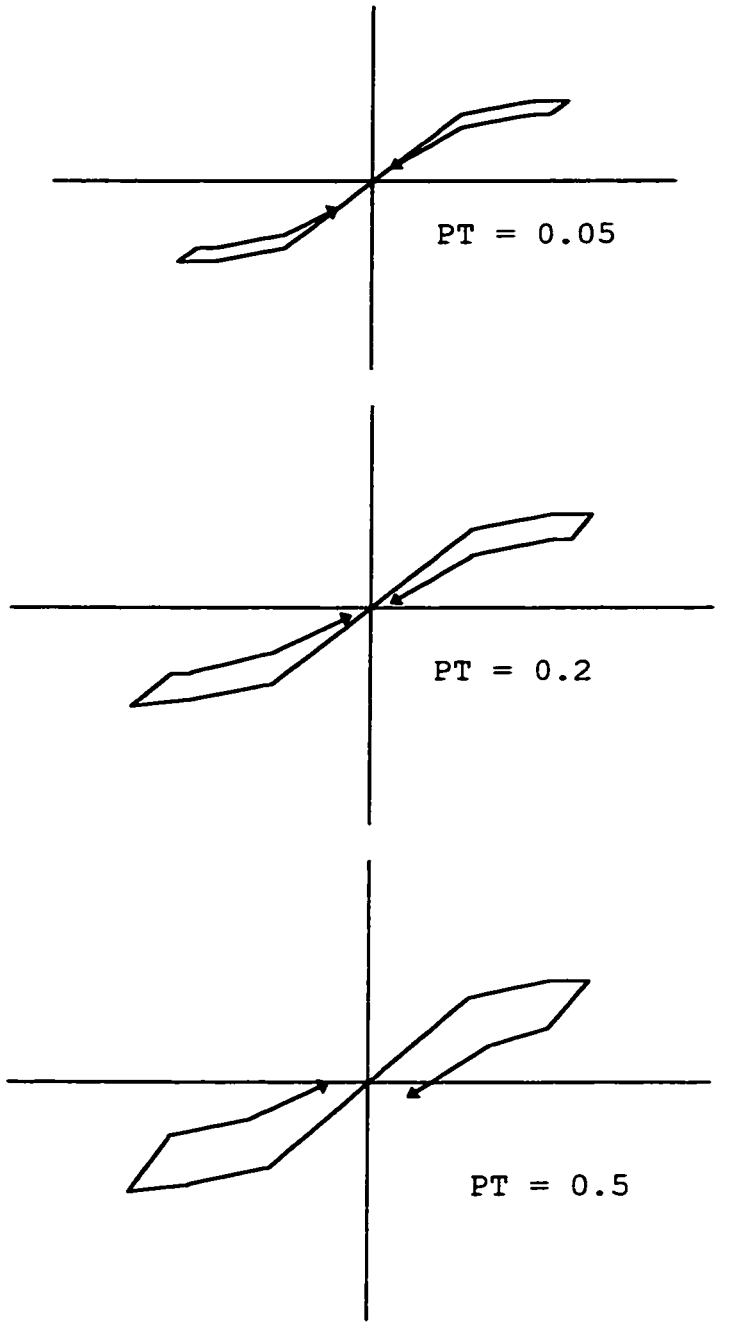

Figure C-1 Post-Tensioning Parameter PT Effects

C.2 EXPERIMENTAL SIMULATION RESULTS USING IDARC-PT

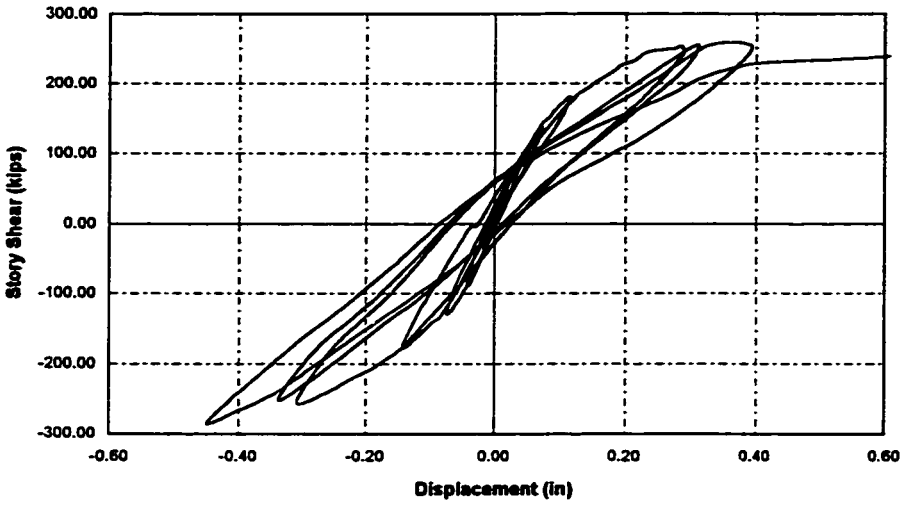

Figure C-2 Measured Response of Test I

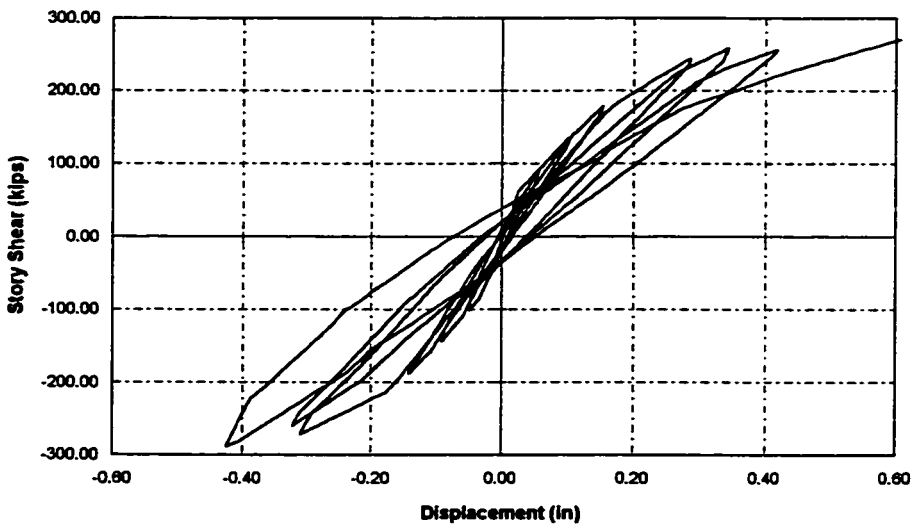

Figure C-3 Computed Response of Test I

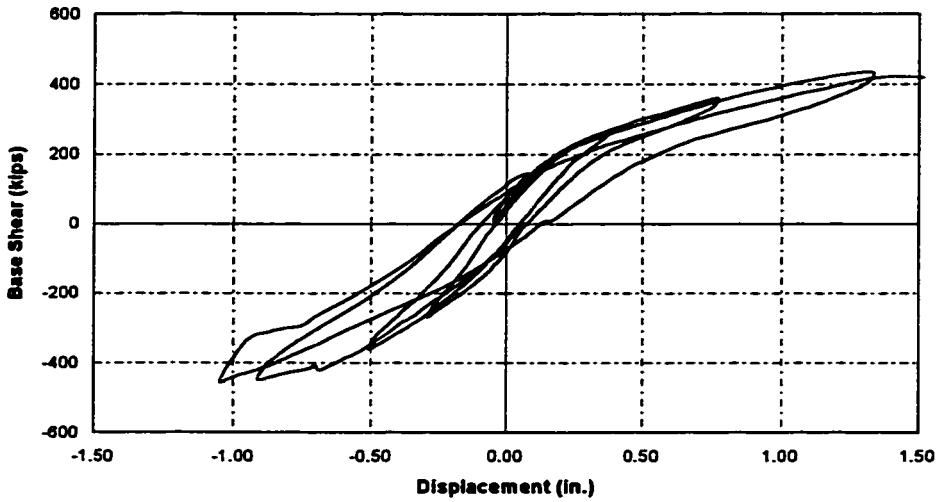

Figure C-4 Measured Response of Test II (Shear Test)

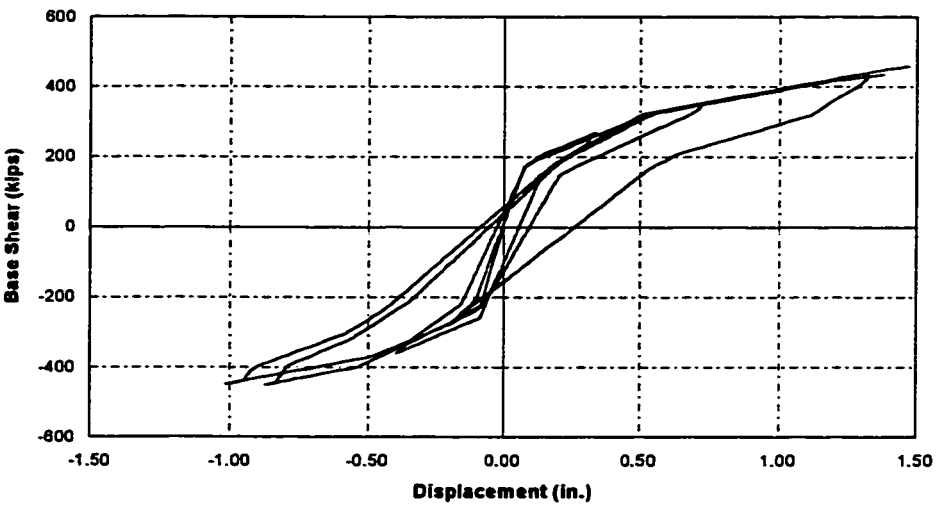

Figure C-5 Computed Response of Test II

APPENDIX D

FOUNDATION SIMULATION DATA

D.1 STRUCTURAL MODEL OF FOUNDATION

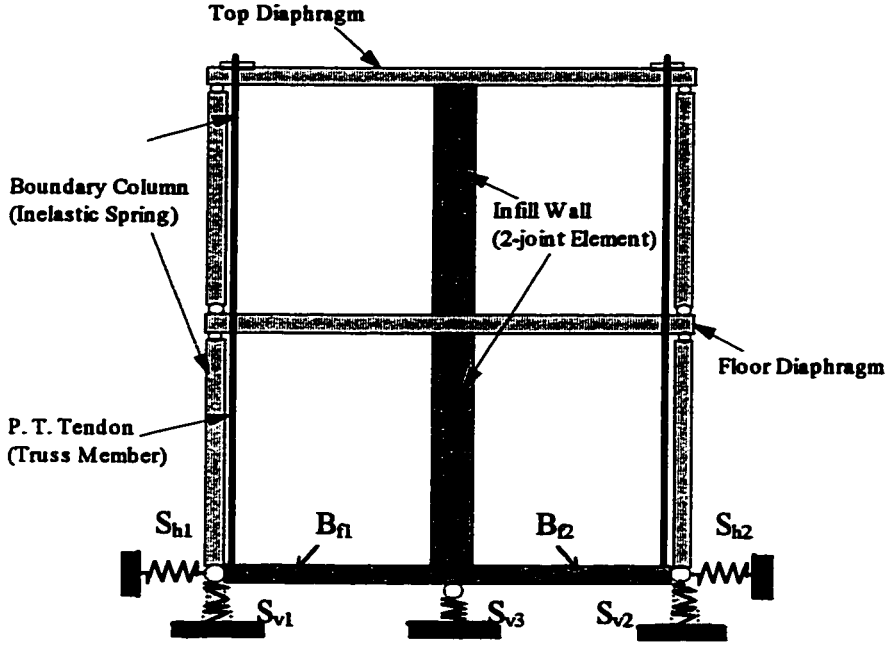

D.2 DIFFERENT RETROFITTING PLANS

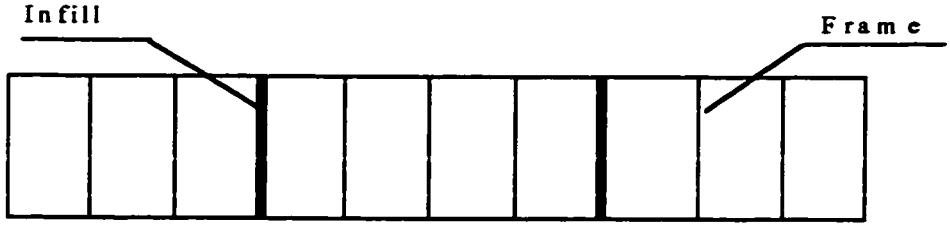

a) Plan One - Few Infill Walls

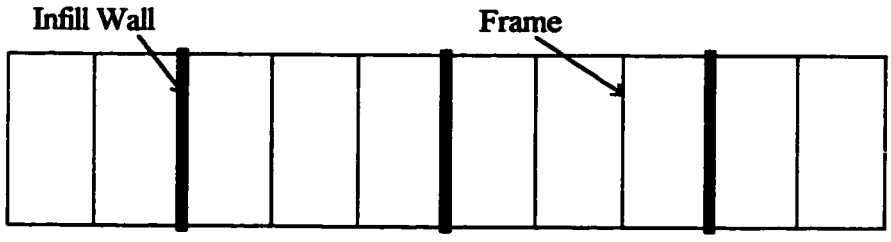

b) Plan Two - More Infill Walls

D.3 DIFFERENT EARTHQUAKE INPUTS

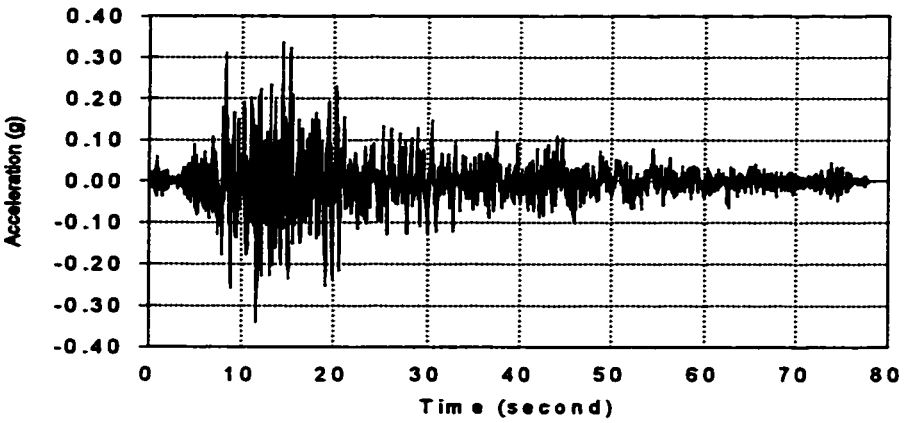

TAFT Ground Earthquake Record (Peak Acceleration of 0.33g)

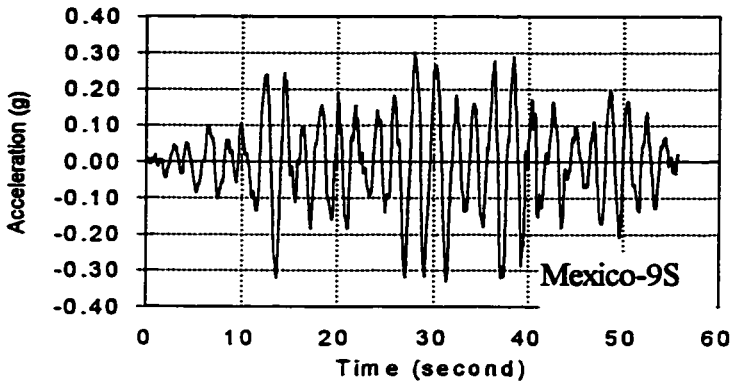

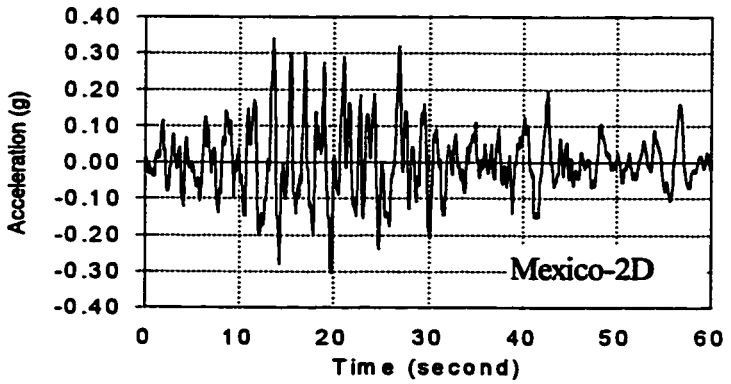

Mexico City Earthquake Records (Peak Acceleration of 0.33g)

D.4 DIFFERENT SOIL PROPERTIES

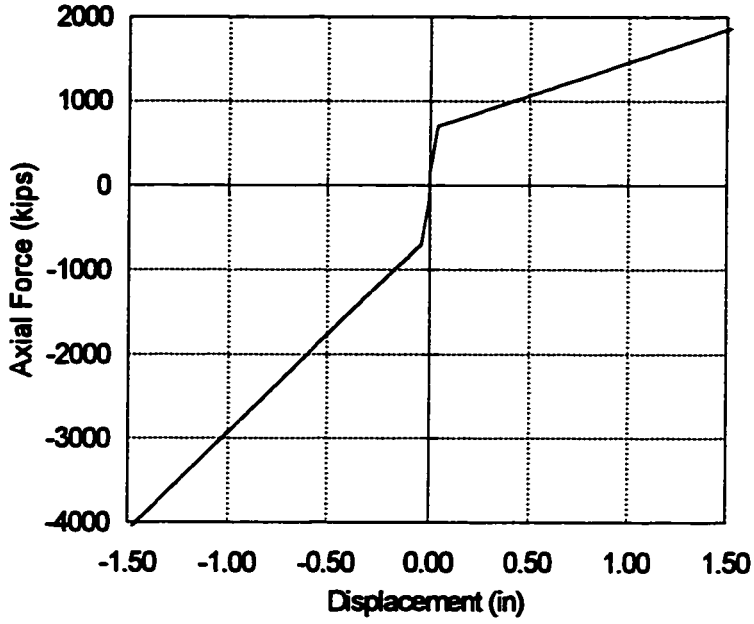

a) System A with Firm Soil

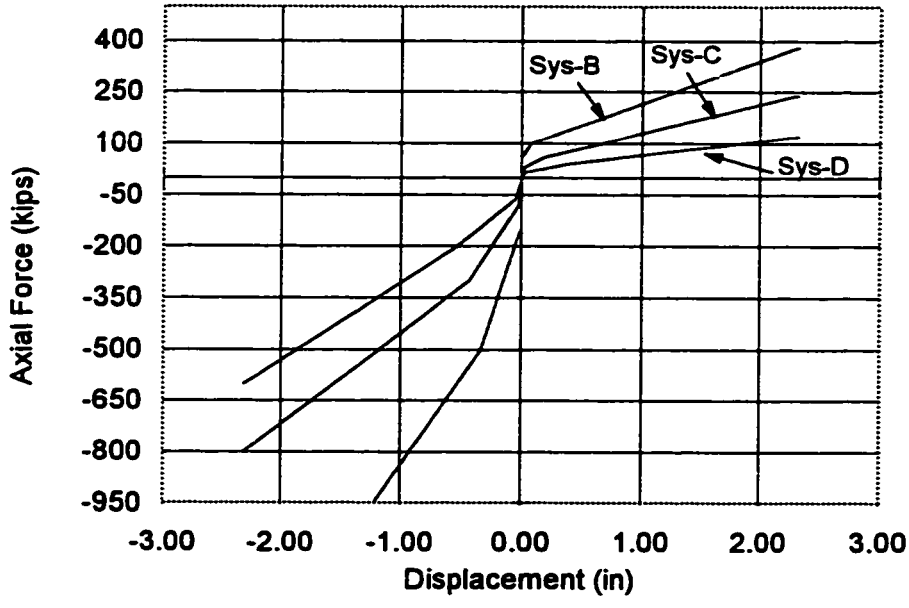

b) Systems B, C and D with Soft Soil

Table 9.1 Foundation Simulation Variables For Different Systems

System	Earthquake Ground Motion					Initial PostTensioning				Retrofitting Plan		Foundation
	TAFT (T)	Mexico-2D (2)		Mexico-9S (9)		High	No	Zero	Low	Infill Number		Soil
ID	0.33g	0.33g	0.22g	0.33g	0.22g	250 (k)	Tendon	Tension	110 (k)	Two	Three	Properties
Sys-0TGF	X					X				X		Rigid (0)
Sys-ATGF	X					X				X		Firm (A)
Sys-BTGF	X					X				X		Soft (B)
Sys-BTNF	X						X			X		
Sys-BTZF	X							X		X		
Sys-BTLF	X								X	X		
Sys-B2GF		X				X				X		
Sys-B2SF			X			X				X		
Sys-B9GF				X		X				X		
Sys-B9SF					X	X				X		
Sys-CTGF	X					X				X		Very Soft (C)
Sys-C2GF		X				X				X		
Sys-C2SF			X			X				X		
Sys-C9GF				X		X				X		
Sys-C9SF					X	X				X		
Sys-DTGF	X					X				X		Extra Soft (D)
Sys-D2GF		X				X				X		
Sys-D2SF			X			X				X		
Sys-D2SM			X			X					X	
Sys-D9GF				X		X				X		
Sys-D9SF					X	X				X		
Sys-D9SM					X	X					X	

D.6 FOUNDATION SIMULATION

D.6.1 Foundation Effects

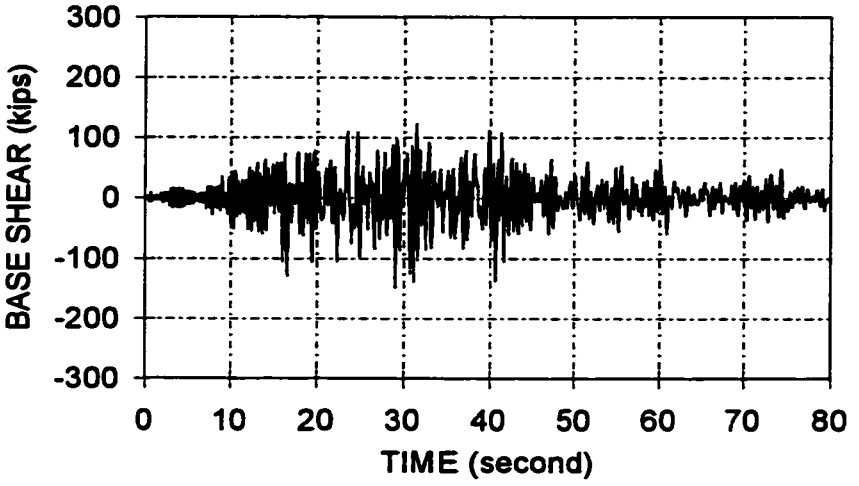

a) Sys-0TGF (rigid foundation)

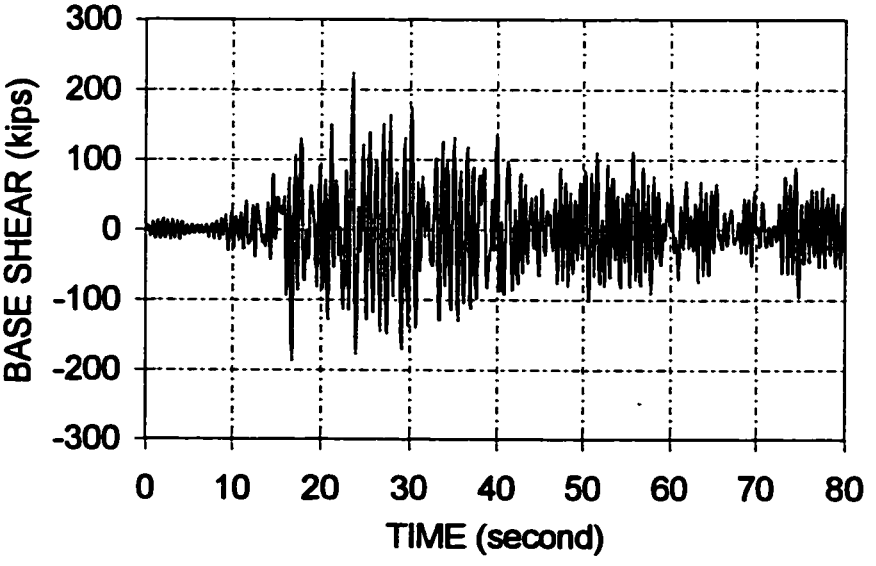

b) Sys-BTGF (soft soil)

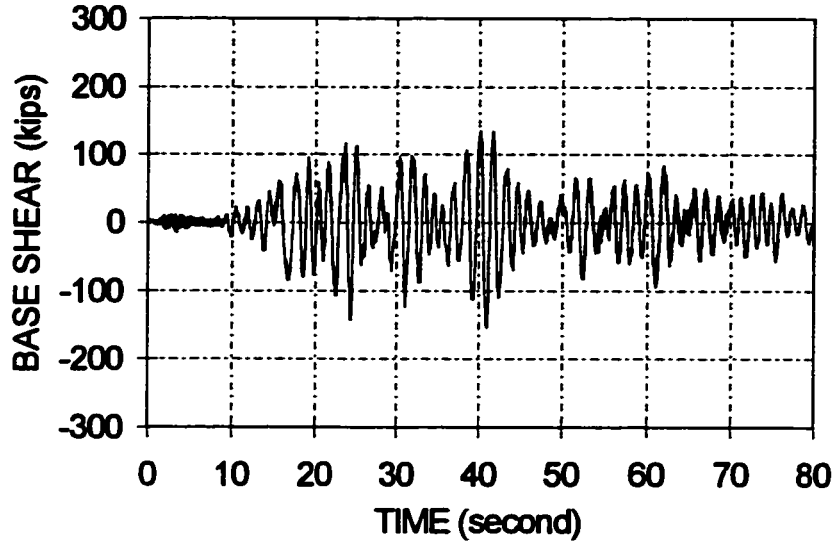

c) Sys-CTGF (soft soil)

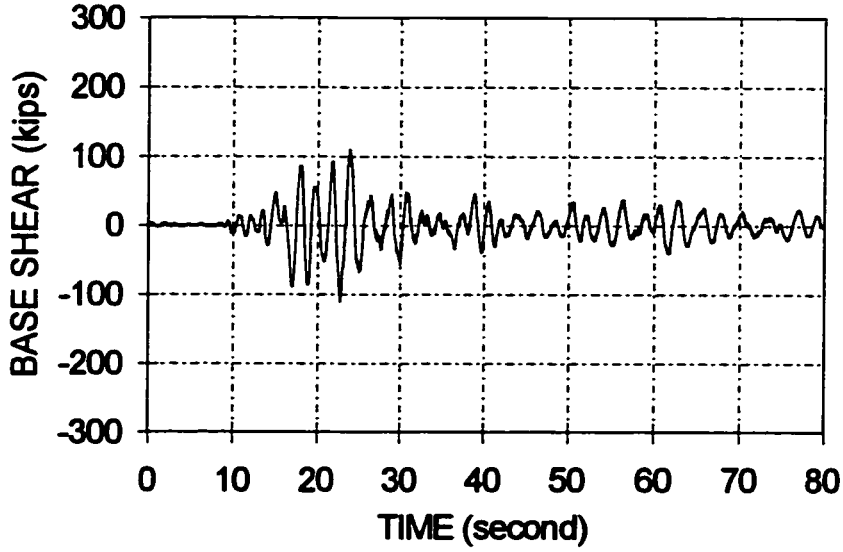

d) Sys-DTGF (soft soil)

D.6.2 Earthquake Effects

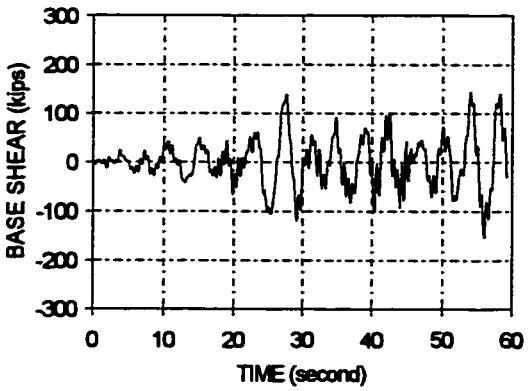

a) Sys-B9GF (soft soil)

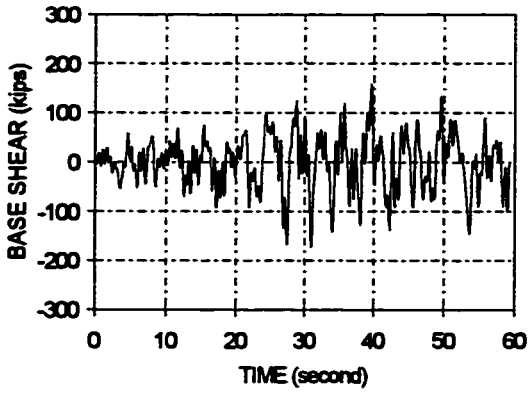

b) Sys-B2GF (soft soil)

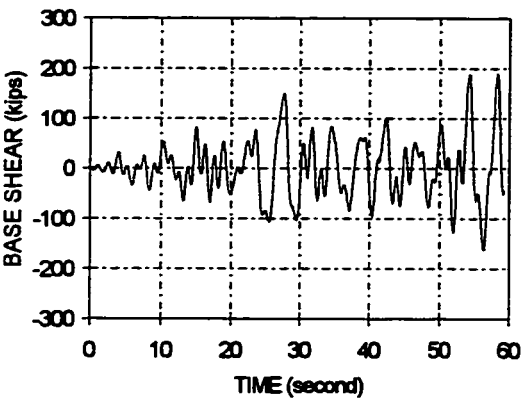

c) Sys-C9GF (very soft soil)

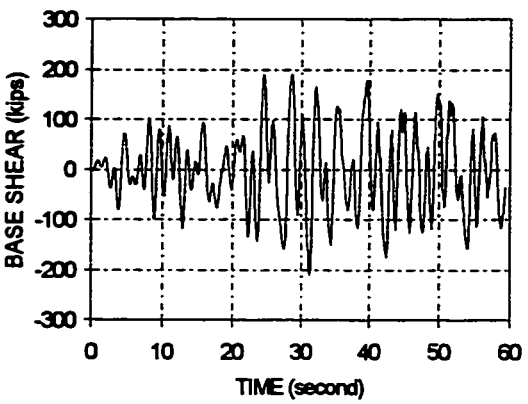

d) Sys-C2GF (very soft soil)

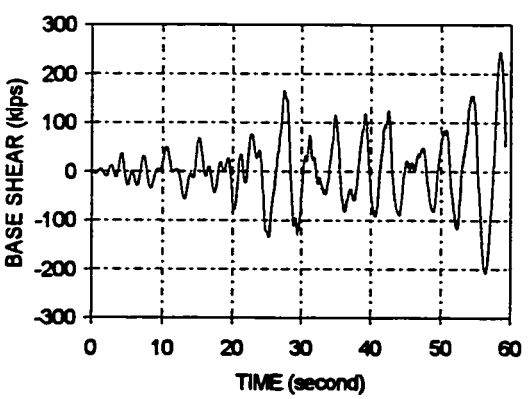

e) Sys-D9GF (extra soft soil)

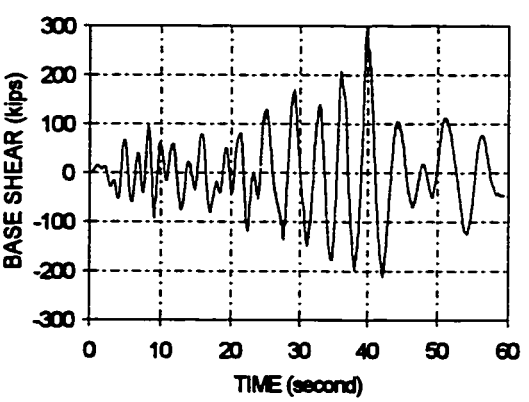

f) Sys-D2GF (extra soft soil)

D.6.3 EARTHQUAKE ACCELERATION EFFECTS

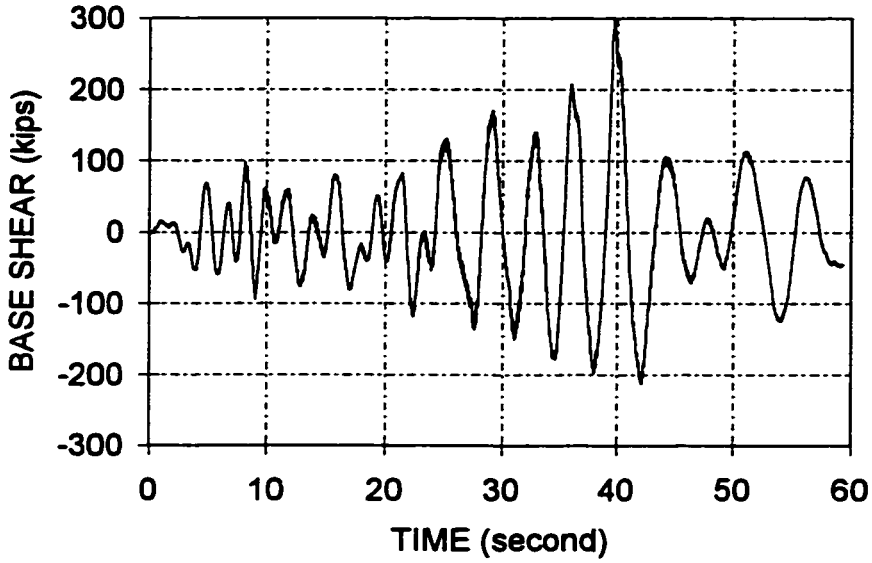

a) Sys-D2GF (high acceleration)

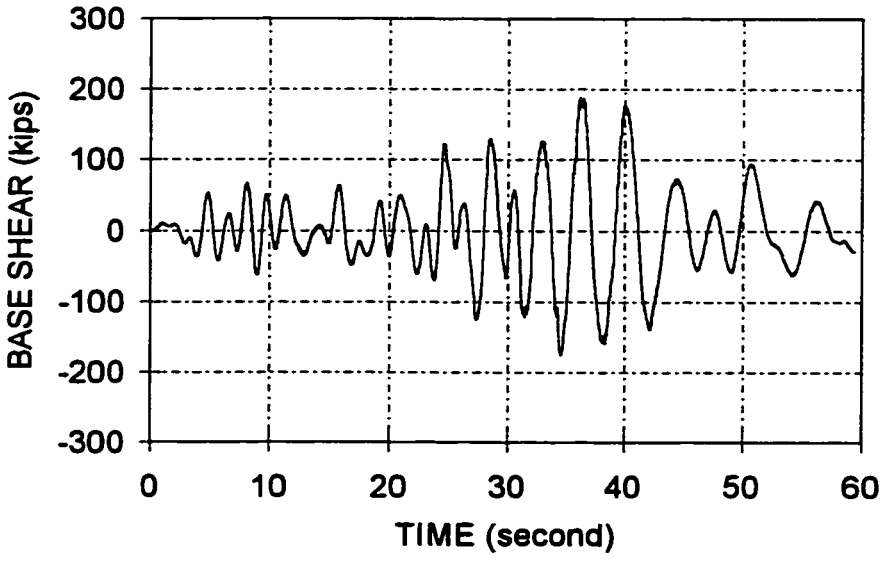

B) Sys-D2SF (low acceleration)

D.6.4 SUMMARY OF SOIL/EARTHQUAKE EFFECTS

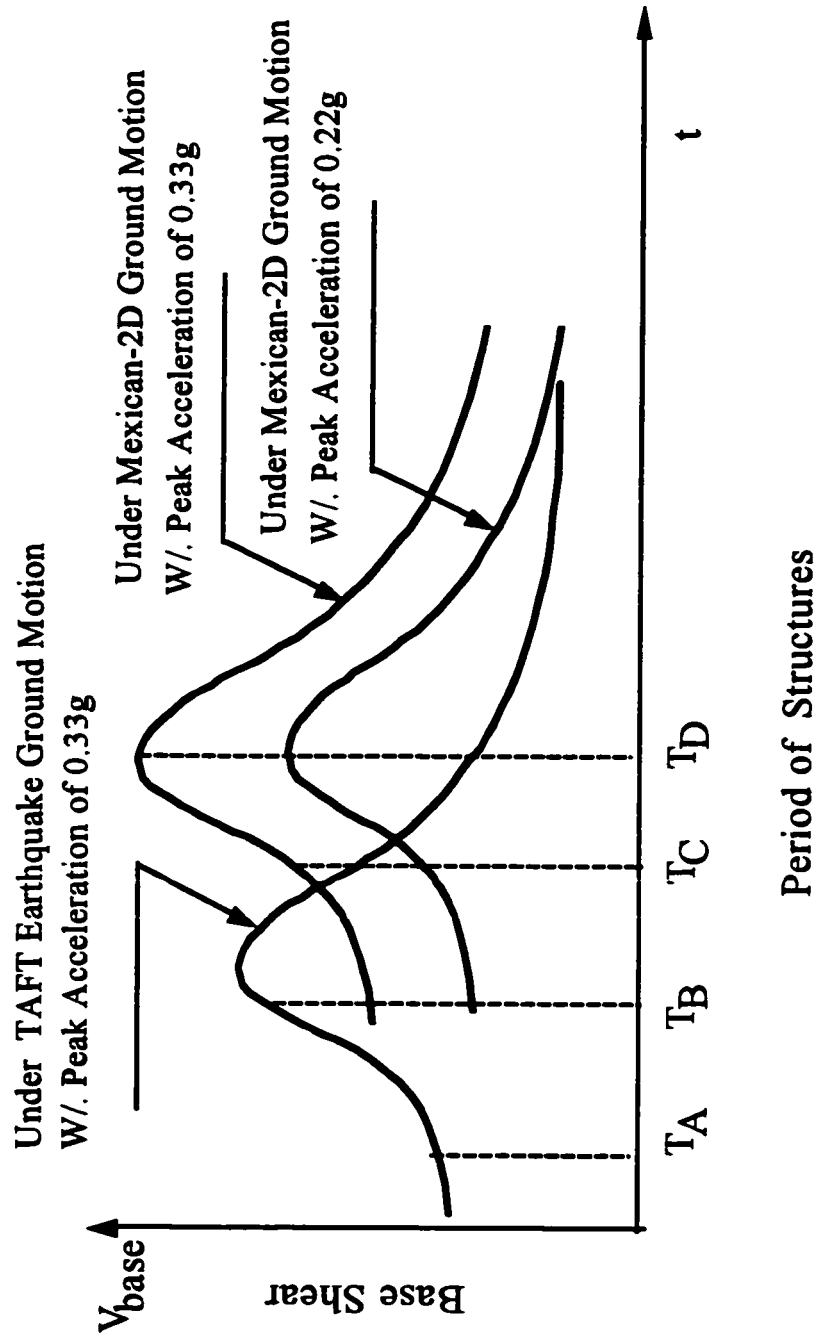

D.7 FOUNDATION /S STRUCTURAL INTERACTION

D.7.1 Foundation Spring Response

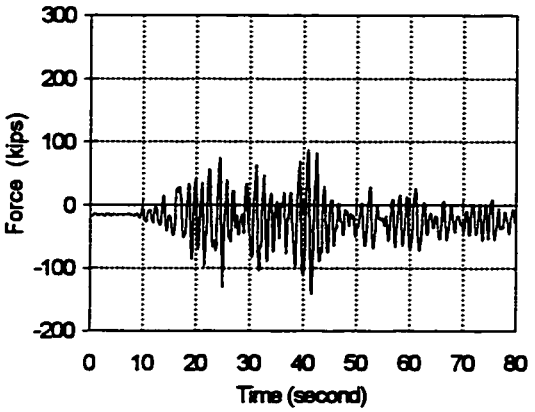

c) Sys-CTGF

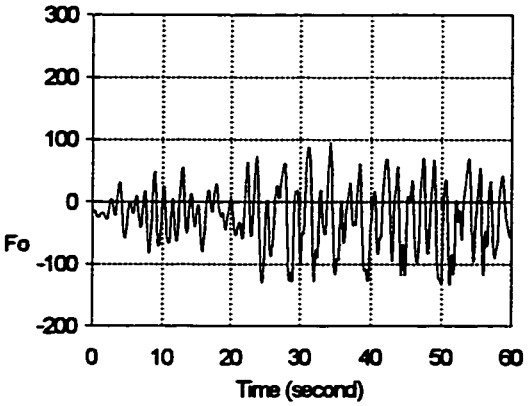

d) Sys-C2GF

Foundation Spring Responses for Very-Soft Soil

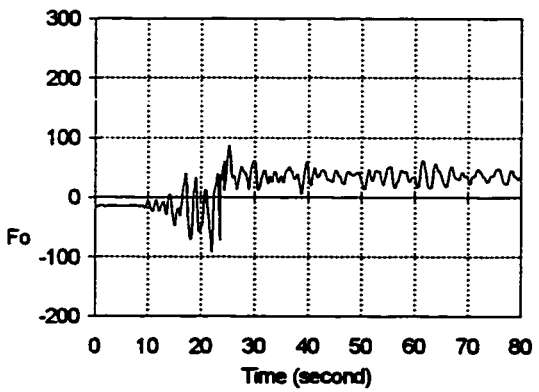

e) Sys-DTGF

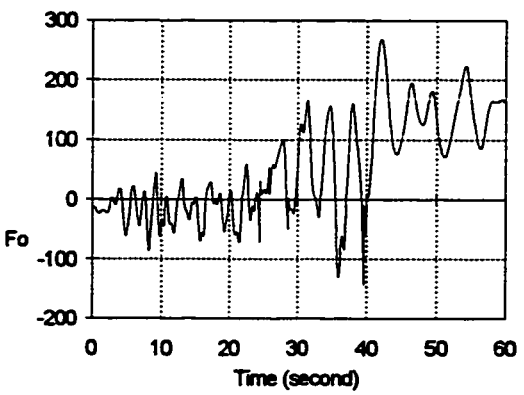

f) Sys-D2GF

Foundation Spring Responses for Extra-Soft Soil

D.7.2 Post-Tensioning Tendon Response

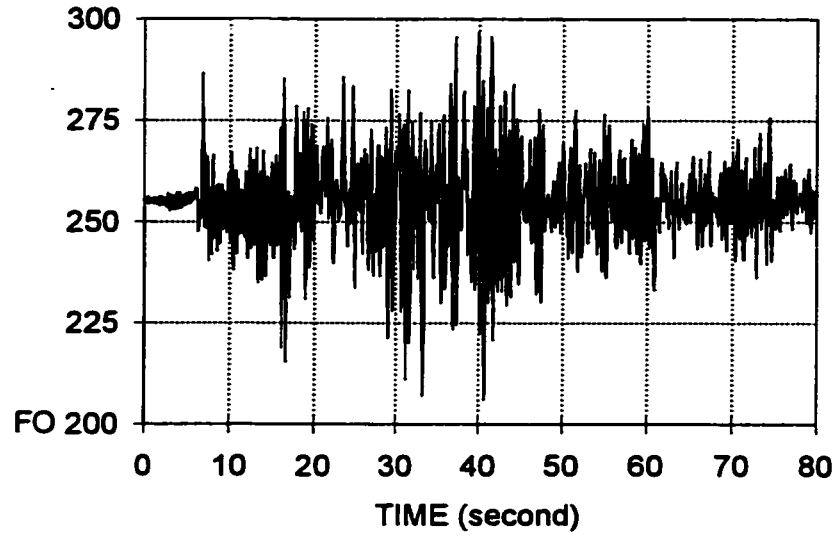

a) Sys-0TGF (rigid foundation)

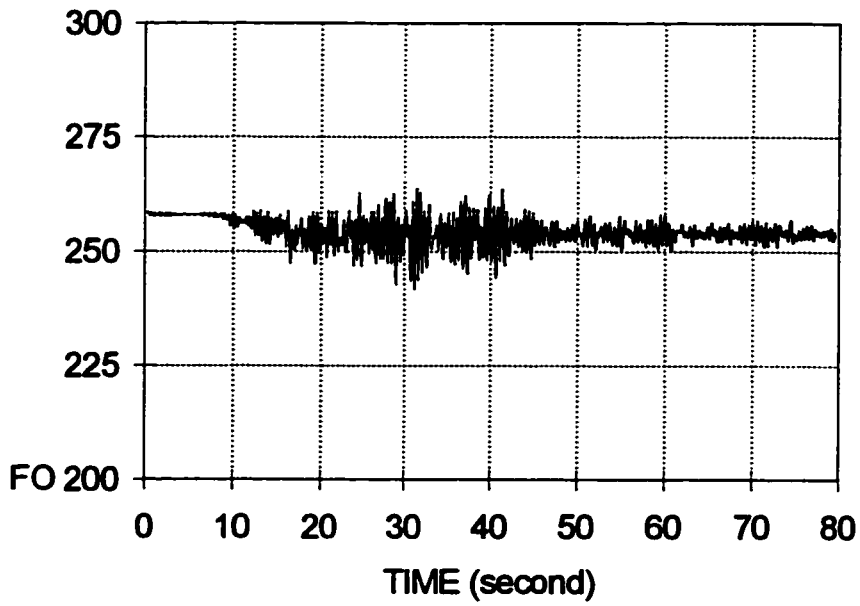

b) Sys-ATGF (firm soil)

D.7.3 Column Splice Response

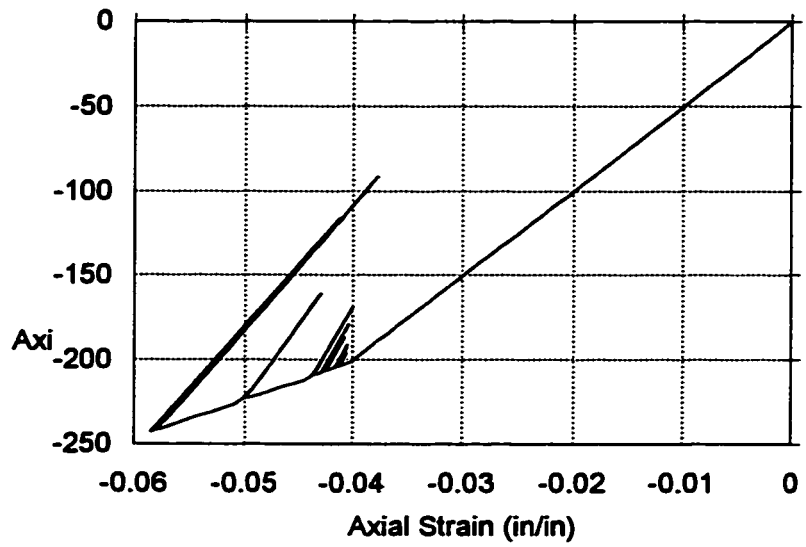

a) Sys-BTGF (high post-tensioning)

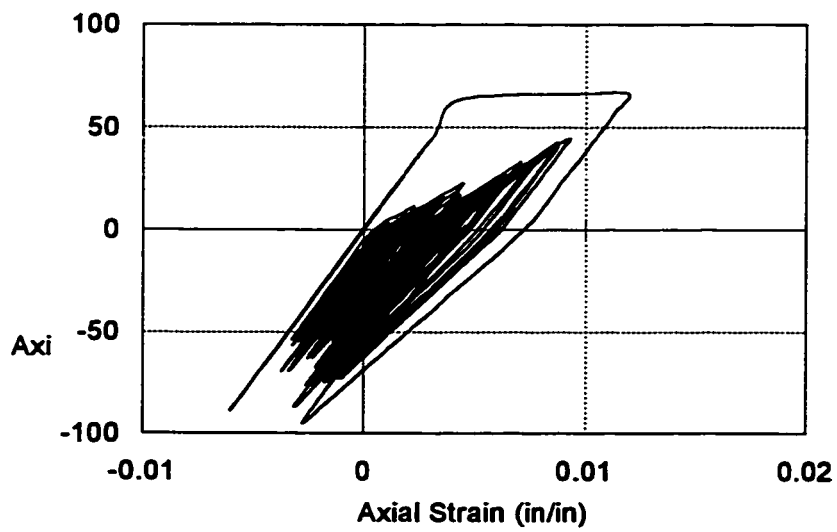

b) Sys-BTNF (without Post-tensioning Tendon)

D.7.4 Infill Wall Response

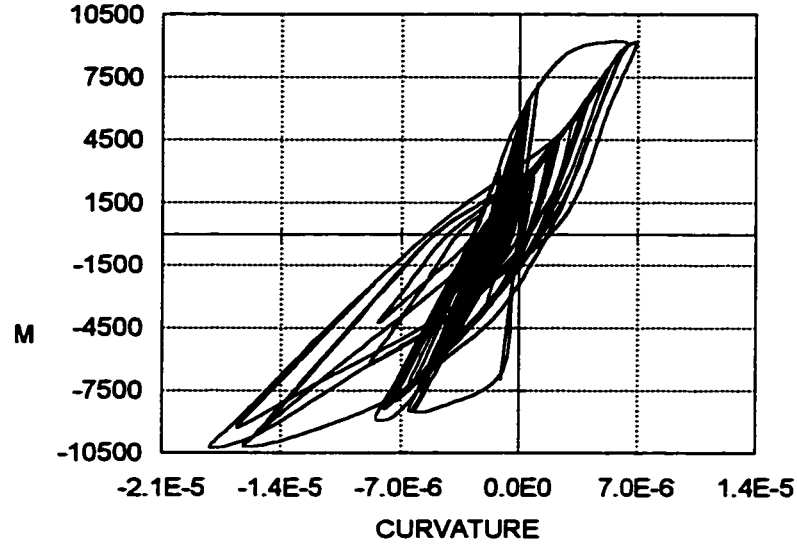

a) Sys-ATGF (firm soil)

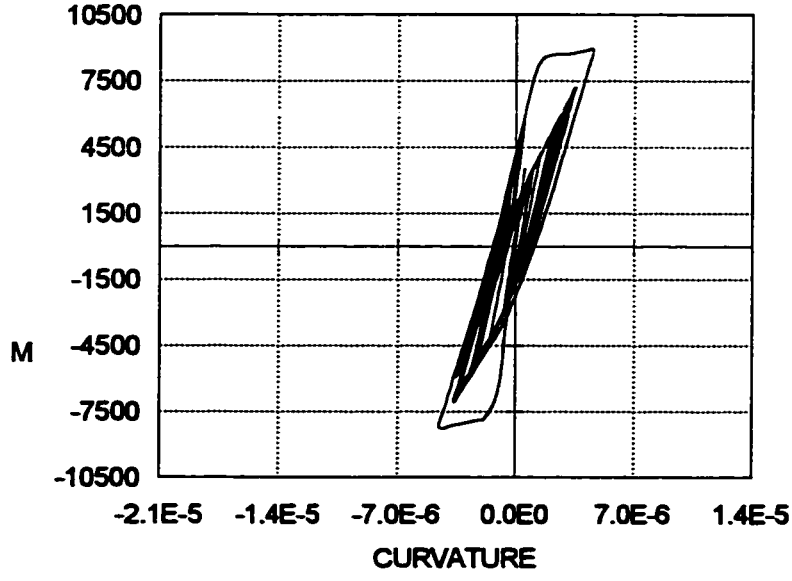

b) Sys-BTGF (soft soil)

D.8 FOUNDATION EFFECTS REDUCTION

D.8.1 Reducing Earthquake Load

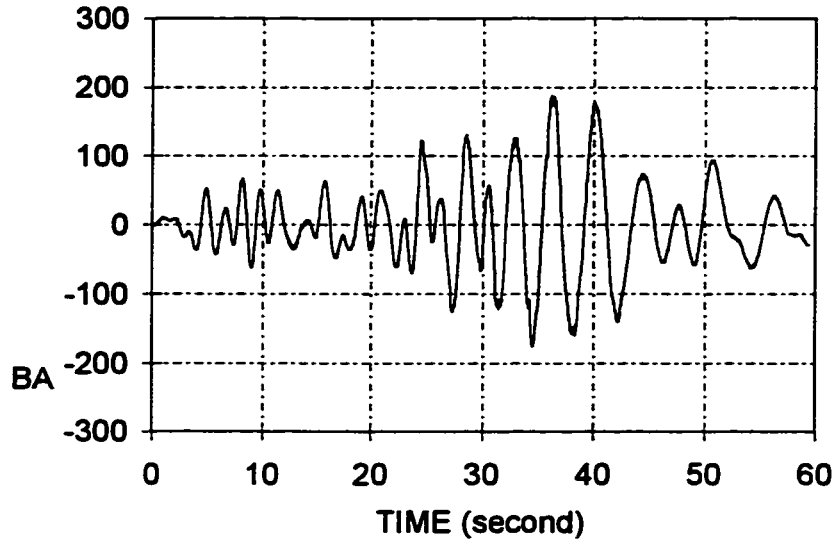

a) Sys-D2SF (two walls)

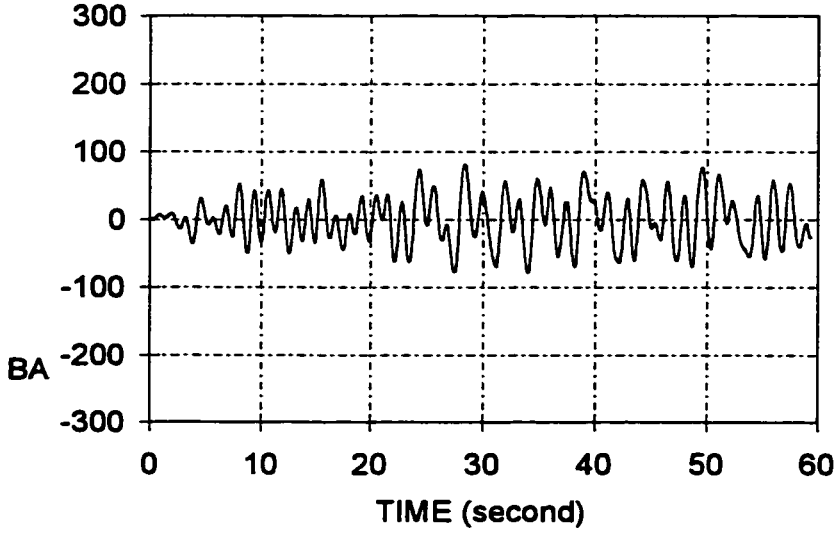

b) Sys-D2SM (three walls)

D.8.2 Reducing Foundation Spring Response

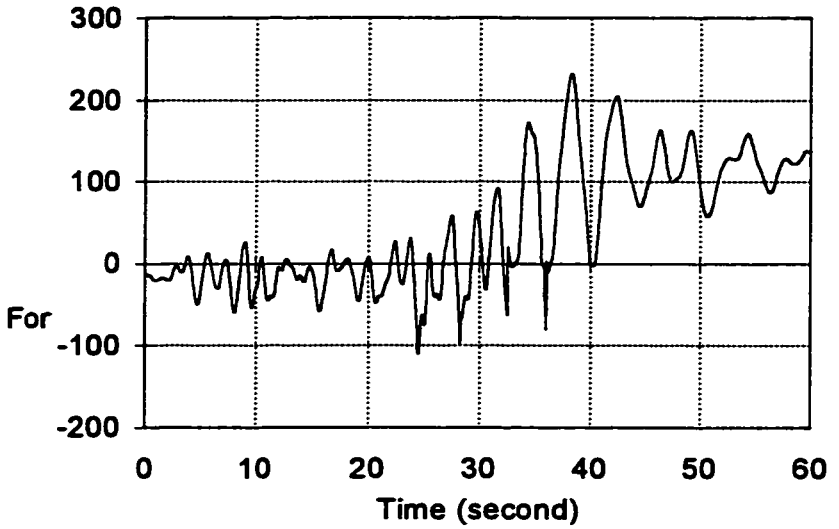

a) Sys-D2SF (two walls)

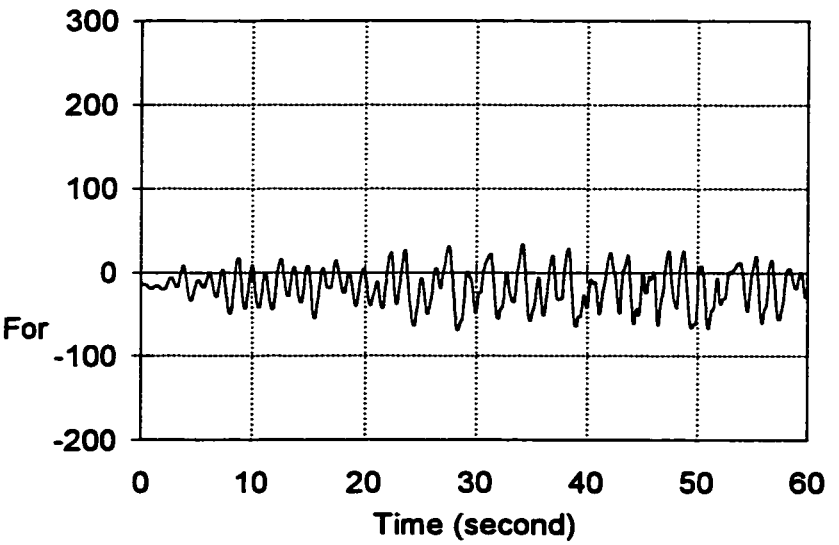

b) Sys-D2SM (three walls)

BIBLIOGRAPHY

1. ACI Committee 318, "Building Code Requirements for Reinforced Concrete," ACI 318-56, American Concrete Institute, Detroit, 1956.

2. ACI Committee 318, "Building Code Requirements for Reinforced Concrete," ACI 318-63, American Concrete Institute, Detroit, 1963.

3. ACI Committee 318, "Building Code Requirements for Reinforced Concrete and Commentary," ACI 318-89, American Concrete Institute, Detroit, 1989.

4. AISC, "Manual of Steel Construction -Load & Resistance Factor Design," American Institute of Steel Construction, Inc., Chicago, Ill, 1986.

5. Bass, R. A., Carrasquillo, R.L., and Jirsa, J.O., "Interface Shear Capacity of Concrete Surfaces Used in Strengthening Structures," *PMFSEL Report No. 85-4*, University of Texas, Austin, Dec. 1985, 82 pp.

6. Bass. R.A., Carrasquillo, R.L., and Jirsa, J.O, "Shear Transfer across New and Existing Concrete Interfaces," *ACI Structural Journal*, V. 86, No. 4, July-Aug. 1989, pp.383-393.

7. Becker, J.M., and Llorente, C., "Seismic Design of Precast Concrete Panel Buildings," *Proceedings of a Workshop on Earthquake Resistant Reinforced Concrete Building Construction*, Vol. 3, U.C. Berkeley, July 1977.

8. Berg, G.V., Seismic Design Codes and Procedures, Earthquake Engineering Research Institute, 1982.

9. Bergmeister, K., Breen, J.E., Jirsa, J.O., and Kreger, M.E., "Detailing for Structural Concrete," *PMFSEL Report No. 1127-3F*, University of Texas at Austin, May 1993, 300 pp.

10. Birkeland, P.W., and Birkeland, H.W., "Connections in Precast Concrete Construction," ACI Journal, *Proceedings*, Vol. 63, No. 3, Mar. 1966, pp. 345-368.

11. Bush, T., Jones, E., and Jirsa, J. O., "Behavior of an RC Frame Strengthened Using Structural Steel Bracing", Journal of Structural Engineering, ASCE, Vol. 117, No.4, April, 1991.

12. Bush, T., Wyllie, L. A., and Jirsa, J. O., "Observations on Two Seismic Strengthening Schemes for Concrete Frames", Earthquake Spectra, Journal of Earthquake Engineering Research Institute.

13. Cholewicki, A., "Loadbearing Capacity and Deformability of Vertical Joints in Structural Walls of Large Panel Buildings," *Building Science*, Vol. 6, 1971, pp. 163-184.

14. Cooley, J. W., Lewis, P. A. W. and Welch, P. D., The Fast Fourier Transformation and Its Applications", IEEE Transaction and Education, Vol.12, No. 1, PP 27-34, 1969.

15. Davis, H.E., Troxell, G.E., and Hauck, G.F.W., The Testing of Engineering Materials, McGraw-Hill, Inc., 1982.

16. FEMA-172, *NEHRP Handbook for Seismic Rehabilitation of Existing Buildings*, Building Seismic Safety Council, Washington, D.C., 1992.

17. FEMA-178, *NEHRP Handbook for the Seismic Evaluation of Existing Buildings*, Building Seismic Safety Council, Washington, D.C., 1992.

18. FEMA-222, *NEHRP Recommended Provisions for the Development of Seismic Regulations for New Buildings*, Building Seismic Safety Council, Washington, D.C., 1991.

19. Gaynor, P.J. "The Effect of Openings on the Cyclic Behavior of Shear Walls," *M.S. Thesis*, The University of Texas at Austin, May 1988, 245 pp.

20. Hofbeck, J.A., Ibraham, I.O., and Mattock, Alan H., "Shear Transfer in Reinforced Concrete," *ACI Journal*, Vol. 66, No. 2, Feb. 1969, pp. 119-128.

21. Hurd, M.K., Formwork for Concrete, SP-4, Fifth Edition, American Concrete Institute, Detroit, 1989.

22. Jimenez, L.R., "Strengthening of RC Frames Using an Eccentric Wall," *M.S. Thesis*, The University of Texas at Austin, May 1989, 67 pp.

23. Kiureghian, A. D., "A Spectrum Method for Random Vibration" Report No. UCB/EERC-80/15, Earthquake Engineering Research Center, University of California, Berkeley,

24. Klingner, "Earthquake Engineering" , Graduate Course CE-384L, University of Texas at Austin, 1994.

25. Kosmatka, S.H. and Panarese, W.C., Design and Control of Concrete Mixtures, Portland Cement Association, 1988.

26. Koseki, K., and Breen, J.E., "Exploratory Study of Shear Strength of Joints for Precast Segmental Bridges," *PMFSEL Report No. 248-1*, University of Texas at Austin, Sept. 1983, 94 pp.

27. Lambe, T.W., and Whitman, R. V., "Soil Mechanics", John Wiley & Sons, New York,1969.

28. Li, W., Lun, Q., and He, J., "Torsional Seismic Response Behavior of Theatrical Building Structures Due to Stiffness Discontinuity and System Irregularly", *Academic Report of CABR, Vol. 31, 1989.*

29. Li, W., Wei, L., and Qun, L., "Foundation Settlement Effects on Structural Seismic Capacity, Retrofitting Example -- Beijing Railroad Station", *A Handbook for Structural Seismic Retrofitting, Beijing, April 1989.*

30. Li, W., and Wei, L., "Stable Analysis of Stochastic Vibration of Elasto-plastic Structural Systems" *World Conference of Earthquake Engineering, The 10th Anniversary of Tangshan Earthquake, Tangshan, PRC, July, 1986.*

31. Lin, T.Y., and Burns, N.H., Design of Prestressed Concrete Structures, John Wiley & Sons, Inc., New York, 1981.

32. Mao, S. S., and Wang, L. L., "Reliability Statistics" Normal University of East China, Shanghai, 1984

33. Mast, R.F., "Auxiliary Reinforcement in Concrete Connections," *Proceedings*, ASCE, Vol. 94, ST6, June 1968, pp. 1485-1504.

34. Mattock, A.H., "Shear Transfer in Concrete Having Reinforcement at an Angle to the Shear Plane," *Shear in Reinforced Concrete, SP-42*, American Concrete Institute, Detroit, 1974, pp. 17-42.

35. Mattock, A.H., and Hawkings, N.M., "Shear Transfer in Reinforced Concrete - Recent Research," Journal, *Prestressed Concrete Institute*, V. 17, No. 2, Mar-Apr. 1972, pp.55-75.

36. Mindess, S., and Young, J.F., Concrete, Prentice Hall, Inc., Engelwood Cliffs, New Jersey, 1981.

37. Newmark, N. M., and Riddell, R. "Inelastic Spectra for Seismic Design", proceedings of 7th World Conference on Earthquake Engineering, Istanbul, Turkey, 1980

38. Orangun, C.O., Jirsa, J.O., and Breen, J.E., "A Reevaluation of Test Data on Development Length and Splices," *ACI Journal*, March 1977, pp. 114-122.

39. Paulay, T., and Loeber, P.J., "Shear Transfer by Aggregate Interlock," *SP 42-1*, American Concrete Institute, Detroit, 1974, pp. 1-14.

40. Paulay, T., Park, R., and Phillips, M.H., "Horizontal Construction Joints In Cast-In-Place Reinforced Concrete," *SP 42-27*, American Concrete Institute, Detroit, 1974, pp. 599-616.

41. Paulay, T. and Preistley, M.J.N., Seismic Design of Reinforced Concrete and Masonry Buildings, John Wiley & Sons, Inc., New York, 1992.

42. Pas, M., "Structural Dynamics ---Theory and Computation" Van Norstrand Reinhold, New York, 1991.

43. Popov, E.P., Mechanics of Materials, Prentice-Hall, Inc. Englewood Cliffs, New Jersey, 1976.

44. Prakash, S., "Soil Dynamics", McGraw-Hill Book Company, New York, 1981

45. Sashi K. Kunnath, and Andrei M. Reinhorn, "Inelastic Damage Analysis of RC Building Structures, IDARC2D, V.3.1, University of Central Florida, University of New York at Buffalo, Sept., 1994

46. SEAOC, *Recommended Lateral Force Requirements and Commentary ("Blue Book")*, Seismology Committee, Structural Engineers Association of California, Sacramento, CA, 1990.

47. Shah, S.N., "Evaluation of Infill Wall Strengthening Schemes for Non-Ductile RC Buildings," *M.S. Thesis*, The University of Texas at Austin, May 1989, 68 pp.

48. Steinbrugge, k. v. "Earthquake damage and Structural Performance in The United States", Earthquake Engineering, Prentice-Hall, Englewood Cliffs, NJ

49. UBC, *Uniform Building Code*, International Conference of Building Officials, Whittier, CA, 1991.

50. Valluvan, R., "Issues Involved In Seismic Retrofit of Reinforced Concrete Frames Using Infilled Walls," *Ph.D. Dissertation*, The University of Texas at Austin, December 1993, 293 pp.

51. Wei, Lian, "Structural Seismic Analysis and Design of High-rise Buildings", Industrial Publication, Beijing, 1989.

52. Wei, Lian, "Strengthening Existing Building Structures", *Academic Report of CABR, Vol. 22, 1984.*

53. Zeck, U. "Joints in Large Panel Precast Concrete Structures," *M.S. Thesis*, Department of Civil Engineering, Mass. Inst. of Tech., Cambridge, MA, 1976.

54. Zheng, S. L. , Wu, L. D., Tao, Z. Y., and Wang, J. G., " Probability and Statistics" Shanghai Technology, Shanghai, 1978

55. Priestley, M. J. Nigel, "Precast Frame Connected with Unbonded Prestressing Tendons", ACI '95 Spring Convention, Salt Lake City, March, 1995.

56. Drewry, Julia Mae, "Cost and Construction Factor for Seismic Strengthening Schemes Using Precast Concrete Panel Infill Walls", Master Degree Thesis, University of Texas, Austin, May 1994.

57. FEMA 274, NEHRP Commentary on the Guidelines for the Seismic Rehabilitation of Buildings, (Ballot Version), Sept., 1996

58. AASHTO , 6th Edition, 1996, American Association of State Highway and Transportation Officials

VITA

Wanzhi Li was born in Luanxian, Hebei Province, China, on November 1, 1952, the third son of Guoxiang Li and Zhenling Duan. After graduating from Railroad Engineering Technical School, Tianjin, China, in 1974, he worked in The Third Institute of Railroad Engineering as an Assistant Engineer in Tianjin. After surviving the Tangshan Earthquake in 1976, he made up his mind to dedicate himself to Earthquake Engineering. In February, 1978, he entered Tianjin University, Tianjin, China, and graduated in January, 1982, receiving the degree of Bachelor of Science in Engineering. As valedictorian of the university, he was admitted as a graduate by famous specialists Dr. He Guangqian and Prof. Wei Lian, China Academy of Building Research (CABR). He worked on Structural Seismic Engineering and graduated in December, 1984, receiving the degree of Master of Science in Engineering. He continued working on earthquake engineering as a Research Engineer and Head of The Special Structural Department, The Institute of Earthquake Engineering, CABR, from December, 1984 to May, 1991. He was the Chief Engineer, in cooperation with architects in P&T Company in Hong Kong, and responsible for the structural design of the high-rise building, Liangmahe Complex built in Beijing. After completing the project for retrofit of Beijing Railroad Station Structure, one of the Ten Most Important National Buildings in Beijing, he begun to study foundation impacts on structural seismic response. His research projects, Structural Seismic Behavior of High-rise Steel Towers under Multiple Dimensional Earthquakes, and Structural Seismic Design Strategies for Theatrical/Auditorium Buildings, were funded by China National Administration of Earthquake Engineering. He entered The University of Texas, as a Ph.D. graduate, at Arlington Campus in May, 1991 and transferred to Austin Campus in August, 1992. He worked as a Teaching Assistant at Arlington Campus and as a Graduate Research Assistant at Austin Campus. He published 18 research papers on Structural

Seismic Engineering since 1985. He has been working for Maxim Technologies, Inc. as a Structural Engineer. He will continue his career with Maxim Technologies.

Permanent Address:

Laoli Zhuang, Xinglong Xiang
Luanxian, Hebei 063704
The People's Republic of China

This dissertation was typed by the author.

TEST TARGET (QA-3)

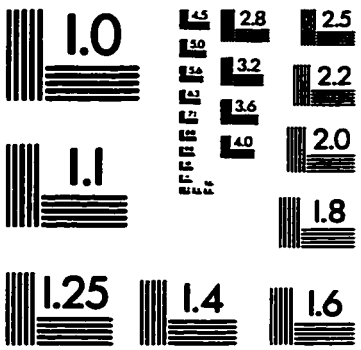

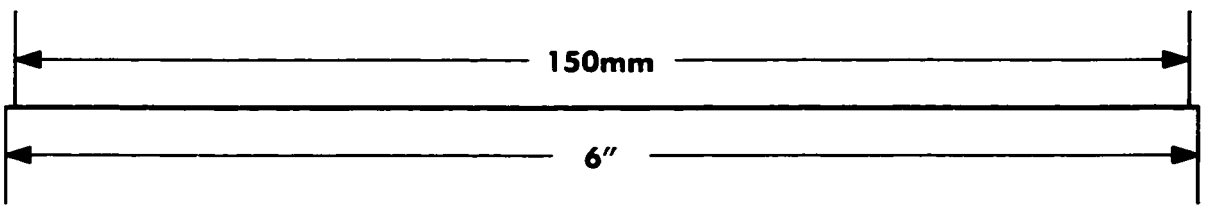

APPLIED IMAGE, Inc
1653 East Main Street
Rochester, NY 14609 USA
Phone: 716/482-0300
Fax: 716/288-5989